CRANFIELD UNIVERSITY

S. F. Ali

TWO PHASE FLOW IN LARGE DIAMETER VERTICAL RISER

SCHOOL OF ENGINEERING

PHD THESIS

CRANFIELD UNIVERSITY

School of Engineering
Department of Process and Systems Engineering

PHD THESIS

Academic Year 2008 - 2009

Shazia Farman Ali

Two phase flow in large diameter vertical riser

Supervisor: Dr. H. Yeung

February 2009

This thesis is submitted in partial fulfilment of the requirements for the degree of Doctor of Philosophy

Abstract

The rapid depletion of hydrocarbon fields around the world has led the industry to search for these resources in ever increasing water depths. In this context, the large diameter (D > 100mm) vertical riser has become a subject of great interest.

In this research work, a major investigation was undertaken to determine the two phase flow hydrodynamics in a 254mm vertical riser. Two types of experiments were performed for range of air-water superficial velocities. The first experimental campaign addresses the issue of the two gas injector's performances (conventional vs. novel design gas injector) in the large diameter vertical riser. The experimental results show that the novel design gas injector should be the preferential choice.

The second set of the experimental work investigates the two phase flow hydrodynamics in the vertical riser in detail. The two phase flow patterns and their transitions were identified by combination of visual observations and statistical features. Based on the results, the experimental flow regime map was developed and compared with the existing vertical upflow regime maps/models. None of the flow regime transition models adequately predicted the flow regimes transitions in large diameter vertical risers as a whole. In this regard, the Taitel *et al.* (1980) bubble to slug flow transition model has been modified for large diameter vertical upflow conditions, based on the physical mechanism observed. The general trends of modified criteria agreed well with the current and other large diameter experimental results.

The effect of upstream conditions on the vertical riser flow behaviour was also investigated in detail by two different inlet configurations (i) near riser base injection and (ii) upstream flowline injection. It was found that no significant differences exist in flow behaviour at low air-water superficial velocities for both the inlet configuration, at high air-water superficial velocities, the intermittent flow behavior in flowline influences the riser flow pattern characteristics and thereby controls the riser dynamics. It is found that liquid slugs from the flowline naturally dissipate to some extent in the riser as a consequence of compression of succeeding bubble that rapidly expands and break through the liquid slug preceding it when it enters the riser. The experimental work corroborates the general consensus that slug flow does not exist in large diameter vertical upflow condition.

Experimental data has been further compared to increase the confidence on the existing two phase flow knowledge on large diameter vertical riser: (a) by comparing with other experimental studies on large diameter vertical upflow in which generally, a good agreement was found, (b) by assessing the predictive capability of void fraction correlations/pressure gradient methods. The important implication of this assessment is that the mechanistic approach based on specific flow regime in determining the void fraction and pressure gradient is more successful than conventional empirical based approaches. The assessment also proposes a proposed set a of flow regime specific correlations that recommends void fraction correlations based on their performances in the individual flow regimes.

Finally, a numerical model to study the hydrodynamic behaviour in the large diameter horizontal flowline-vertical riser system is developed using multiphase flow simulator OLGA. The simulated results show satisfactory agreement for the stable flows while discrepancies were noted for highly intermittent flows. The real time boundary application was partially successful in qualitatively reproducing the trends. The discrepancies between the predicted results and experimental data are likely to be related to the incorrect closure relations used based on incorrect flow regimes predictions. The existence of the multiple roots in the OLGA code is also reported for the first time.

Keywords: *air-water flow, comparison, drift flux, flow pattern, flow pattern transitions, large diameter, numerical simulation, flowline-riser, OLGA, vertical pipe, two phase, void fraction, correlations.*

Acknowledgements

First of all I want to express my thanks to my supervisor Dr. Hoi Yeung for his guidance and support throughout the duration of this work.

A lot of thanks to Prof. Chris Thompson, head of PASE department for his warm encouragement when it was most needed.

I gratefully acknowledge the financial support provided by the Department of Process and Systems Engineering.

I wish to express thanks to the entire Process and Systems Engineering Group, all of you have been very helpful, especially I wish to thanks, Mrs. Linda Whitfield, Mrs. Sam Skears, Mr. Flemming Nielsen, Mr. John Knopp and all my fellow students.

The assistance received from the staff of Kings Norton Library especially Ms. Anita Beal and staff of Cranfield Computer Centre during the course of this work is greatly appreciated.

A special thanks to Mr. Tim Lockett of Scandpower Technology for answering my OLGA questions.

I would also like to thank Mrs Zoë Hersov, founder of Anne Marie Schimmel Scholarship, all my teachers at school, college and universities and many many others who have been a constant source of encouragements.

My deepest gratitude to my husband Nadeem for his love and support and very very special love thanks to my son Humd, for his cheerful face has been a constant source of motivation and delight.

Last but not the least, I would like to thank both my parents, brothers and sister who have been the greatest inspiration through their nobility and fortitude.

To all of you, I humbly dedicate this thesis.

Table of Contents

List of Figures

List of Tables

Nomenclature

A. Symbols

Symbol	*Units*	*Description*
A	[m^2]	Area
C	[-]	Flooding constant (C=1)
C_l	[-]	Blasius Constant (C_l=0.046)
Co	[-]	Distribution/concentration parameter
D	[m]	Diameter
D_h	[m]	Hydraulic Diameter
E	[J/kg]	Internal energy per unit mass
e	[volts]	Final voltage being measured by the sensing device.
e_o	[volts]	Voltage measured at zero value of physical variable.
f_{sp}	[-]	Single phase friction factor
f_{Tp}	[-]	Two phase friction factor
G	[kg/m^2-s]	Mass flux
G´	[kg/s]	Mass source in OLGA
g	[m/s^2]	Acceleration due to gravity
h_L	[m]	Liquid height
$\hat{h}_L$	[-]	Dimensionless liquid height
H_L	[-]	Holdup
H_s	[J/kg]	Enthalpy
j_a	[m/s]	Superficial air velocity
$j_{a,inj}$	[m/s]	Superficial air velocity injected in riser base
j_g	[m/s]	Superficial gas velocity injected in riser base
j_l	[m/s]	Superficial liquid velocity
j_w	[m/s]	Superficial water velocity
j_m	[m/s]	Total volumetric flux (mixture velocity)
k	[-]	Gain
K_A	[-]	Armand Constant
K	[-]	Slip constant
L	[m]	Length
l_ε	[m]	Entrance length
m	[kg/s]	Mass flow rate
$N_{\mu f}$	[-]	Viscosity number
n	[-]	Blasius constant
P	[bar]	Pressure
ΔP	[bar]	Differential Pressure
Q_g	[m^3/s]	Volumetric gas flow rate
Q_l	[m^3/s]	Volumetric liquid flow rate
R	[m]	Radius
R_D	[-]	Distribution slip ratio
R_s	[-]	Gas mass fraction
S	[m]	Wetted perimeter

s	[-]	Slip
T	[ºC]	Temperature
t	[s]	Time
U_{bs}	[m/s]	Taylor bubble velocity
U_{fs}	[m/s]	Liquid film velocity
U_{gj}	[m/s]	Drift flux velocity
u_g	[m/s]	Mean gas velocity
u_l	[m/s]	Mean liquid velocity
V	[-]	Volume fraction
v_{OD}	[m/s]	Fall velocity of droplet
v_r	[m/s]	Relative velocity
v_g	[m/s]	Mean gas velocity
v_l	[m/s]	Mean liquid velocity
v_D	[m/s]	Droplet velocity
x	[-]	quality of gas phase
X	[-]	Physical variable being measured (e.g. flow rate)
X_{tt}	[-]	Lockhart and Martinelli parameter
z	[m]	Height

B. Greek Symbols

Symbol	*Units*	*Description*
α	[-]	Void fraction
α_c	[-]	Critical void fraction
β	[-]	Gas volumetric ratio
δ	[m]	Liquid film thickness
ε	[-]	Pipe roughness
θ	[-]	Inclination angle
λ	[-]	Friction coefficient
μ_g	[Pa-s]	Dynamic Gas viscosity
μ_l	[Pa-s]	Dynamic Liquid viscosity
ν_l	[m^2/s]	Kinematic Liquid viscosity
ρ_g	[kg/m^3]	Gas density
ρ_l	[kg/m^3]	Liquid density
ρ_m	[kg/m^3]	Mixture density
ρ_{TP}	[kg/m^3]	Two phase density
$\Delta\rho$	[kg/m^3]	Density difference between the two phases
σ	[N/m]	Surface tension
ϕ_l	[-]	Liquid Friction multiplier
Φ	[-]	Two phase multiplier
ψ_g	[-]	Mass transfer rate between phases
ψ_e	[-]	Entrainment rate
ψ_D	[-]	Deposition rate

C. Subscripts

a	Air
b	Bubble
D	Droplet
f	Film
g	Gas
go	Gas only
i	Interface
l	Liquid
lo	Liquid only
m	Mixture
SP	Single phase
TP	Two phase
w	Water

D. Acronyms

Acronym	*meaning*
AB	Agitated bubbly flow
AECL	Atomic Energy of Canada limited
BU	Bubbly flow
BWR	Boiling water reactor
C	Churn/froth flow
CANDU	Canada Deuterium Uranium
CAPEX	Capital expenditures
CFL	Courant-Friedreich-Levy criteria
DAQ	Data Acquisition
DC	Direct Current
DP	Differential pressure transducer
Eo	Eotvos number
FAD	Free air delivery
FIC	Automatic controller controlling flowrate of air flow meters
FL	Flowline
Fr	Froude number
FT	Air flow meters of three phase facility
GOR	Gas/Oil ratio (ratio of the produced gas to produced oil)
GOM	Gulf of Mexico
GF	Gas Volume Fraction
H	Horizontal flow line air injection (no injectors)
HRA /HRT	Horizontal flowline air injection with riser base injection from injector
HEM	Homogenous Equilibrium Model
HVF	Homogenous Void Fraction
HVFM	Homogenous Void Fraction Model
LNG	Liquid Nitrogen Gas
LPG	Liquefied Petroleum Gas
L/D	Length to Diameter ratio

LWR	Light water reactor
Max	Maximum
Min	Minimum
MRBL	Multiple Riser base Lift
NEL	National Engineering Laboratory
N_2	Nitrogen gas
NRA	Natural lift by riser air injection from Annular sleeve injector
NRT	Natural lift by riser air injection from Tee injector
OLGA	OiL and GAs
OPEX	Operational expenditure
P3	Pump
PDF	Probability density function
PMF	Probability mass function
PL	Plug flow
PT	Riser base/top transducers
PWR	Pressurized water reactor
PVC	Polyvinyl chloride
PVT	Pressure-Volume Temperature
R	Riser injection cases
RA /RT	Riser air injection by Annular sleeve injector / Tee injector
RBP	Riser base pressure
RBGL	Riser base gas lift
Re	Reynolds number
RTP	Riser top pressure
SL	Slug flow
SS1	Severe slugging class 1
SS	Severe slugging class 2
ST	Stratified flow
T	Temperature sensor
TOPFLOW	Transient Two Phase Flow
US	Unstable slug flow
USB	Universal Serial Bus
VA	Valve for air controlling
VF	Void Fraction
VF1	Sectional void fraction at 5m
VF1	Sectional void fraction at 8m
VI	Virtual instrument of LABVIEW software
VW	Valve for water controlling
We	Weber number
WFM	Water flow meter
X_{tt}	Martinelli Parameter

Chapter 1

Introduction

1.1 Background

The research work in this thesis is motivated by the need to better understand the hydrodynamic behaviour of two phase flow in large diameter (D > 100mm) vertical pipes (often referred as "risers"). Such large diameter vertical risers are now increasingly being chosen for future developments in various fields due to increase in production demand. This demand is further enhanced by the economical push (Pickering *et al.*, 2001) and safety considerations (Khartabil *et al.*, 1995 and Shoukri *et al.*, 2000) involved, which implies the use of larger diameter.

Large diameter vertical risers are frequently encountered in the oil and gas industry in transferring the crude products from the reservoir to the processing facilities, especially in deep seas, where the recovered hydrocarbon is transported from subsea wells, through a network of flowlines and riser, to the topside floating platform or receiving and processing vessel. The fast depletion of near-shore fields employing risers with modest diameters (typically 75mm) have increased the necessity to recover hydrocarbons more efficiently and economically whilst moving much deeper into the sea of harsher and remote environments. This has led to the major challenge of the development of riser diameters that are much larger than previously used by the oil and gas industry in order to maximize the hydrocarbon recovery, at an acceptable cost. Many of these deep offshore developments are located in water depths exceeding 1km (e.g. BP's Greater Plutonio (block-18) at 1258m with riser diameter of 304.8mm, Elf's Girassol at 1300m with riser diameter of 203.2mm and Petrobras' Roncador at 1500-2000m with riser diameter of 244.475mm) (Pickering *et al.*, 2001). The installation and operation of a riser system in such an environment become a technical challenge and, a major part of the field development costs. Up to 2005, the costs for such a riser system was quoted to be around US$70 million i.e. 20% of estimated US$35 billion investment (Matar *et al.*, 2008). With such high expenditures involved, the prediction of the internal hydrodynamic performance of such riser systems is of vital importance and needs to be determined beforehand.

The use of large diameter vertical risers is not just confined to the oil and gas industry but, is also relevant to the nuclear industry. In the actual nuclear reactor system, large pipe sizes (D_H = 0.01 to 1m) are also found and the length of this piping also has a

wide range (Ohnuki and Akimoto, 2000). In the nuclear industry, such risers are used either in normal operating piping network or in the safety systems, in injecting coolant in the reactor or heat removal systems in cooling the hot coolant from the reactor. Also, some new applications such as advance reactors are employing passive cooling systems which consists of large diameter horizontal and vertical piping networks e.g. the advanced CANDU-6 design includes a large diameter vertical riser and horizontal pipe connecting the calandria vessel to an external heat sink (heat exchanger) (Khartabil *et al.*, 1995 and Shoukri *et al.*, 2000). As the safety requirements are critical in the operation of nuclear reactors, the requirement of accurate prediction of thermal hydraulic behaviour in large diameter vertical risers is essential.

Although, the field of the multiphase flows has received much attention in the past, it is surprising that most of this research was confined to predicting the flow behaviour in pipe diameter less than 100mm, and the results were tenuously extrapolated to the larger diameters. Many studies examining the above extrapolations, indicates that the results obtained are significantly in error, due to the complexity arising from interaction of the phases and are the result of lack of detailed knowledge of flow behaviour in large diameter vertical pipes (Kataoka and Ishii, 1987; Ohnuki *et al.*, 1995 and Pickering *et al.*, 2001). Such studies have led the investigators to question the accuracy and recommend that additional research to be conducted with larger diameters.

The vertical liquid flows are generally dominated by hydrostatic head, under the above conditions, if gas phase is introduced near the downhole, vertical two phase flow with a decrease in hydrostatic head results. This gas-liquid transport mechanism is well established technique known as gas lift and widely applied in various above applications of vertical riser. The application varies from oil industry where it is used for lifting fluids from deep onshore/offshore wells to nuclear industry where gaslift principle is envisaged to enhance coolant circulation needed for heat removal capabilities.

Although this work is motivated by need to understand the two phase gas-liquid flow in large diameter vertical riser, the effectiveness of gas injectors in the large diameter riser is the focus of the research with particular relevance to oil industry.

In the oil industry, the gas lift is utilized because of its twofold benefits; firstly, achieving enhance production of oil by injecting gas in the pipe thereby lowering the downhole pressure to enable more inflow of oil (Guet *et al.*, 2003), secondly to stabilize upward unstable (pulsating/cyclic) multiphase flow from deep sea underwater risers. The later situation corresponds to the conditions, such as low gas-liquid flowrates, flowline geometry, startup, pigging etc. resulting in reduction in production and damaging the installation. Generally in these cases, large amplitude, long duration cyclic pressure and flow rate fluctuations are set up in the system that result in liquid slugs that are much longer than steady state slug and are problematic for the downstream facility. Researchers have defined the previous as severe slugging and the later as hydrodynamic slugging. In above conditions, gas lift serves the

purpose of mitigating the unstable (pulsating/cyclic) multiphase flow by providing enhanced circulation and stabilizing the upward flow. Although various methods are available to mitigate the above mentioned slugging, among all the methods, gas lift is the most widely applied method. In gas lifting, to avoid slugging, the external gas is injected into the riser base (Riser Base Gas Lift or RBGL) to reduce the hydrostatic head in the riser. This gas injection in the base vicinity not only results in continuous lifting of liquid from the accumulated area but it also prevents the further build-up of liquid and succeeding blockage to the gas flow.

In the early eighties at the BP research centre (London), a Tee gas injector design was tested to mitigate slugging in the riser. The injector showed successful reduction in both types of slugging and based on this result, RBGL tests were performed in the S.E Forties field. The gas injector design successfully reduced the extent of severe slugging although large amount of gas was used (Hill, 1989). Thus the gas lift applicability for managing the flow line/riser instability was established, facilitating the use of the technique for similar future projects. In 2004, when BP's Angola Block 18 Greater Plutonio project team decided to install the longest ever (1258m-tall) single large diameter (304.8mm) riser tower in the world (Figure 1.1), the applicability of the conventional Tee gas injector posed questions on its performance (Fairhurst, 2004). Many new designs were considered on small scale and finally a novel annular sleeve design was selected with the intention of comparing the hydrodynamic performance with conventional Tee injector.

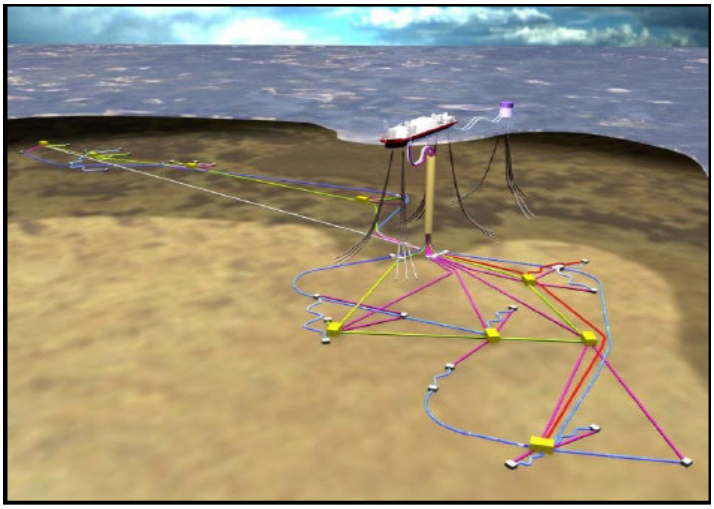

Figure 1.1 Schematic diagram of the Greater Plutonio Development: host FPSO vessel, riser, flowlines and wellheads (BP Angola, 2004).

The department of Process and Systems Engineering, Cranfield University, with the financial support of British Petroleum-Exploration group set up a large diameter (254mm) two phase flow vertical riser-horizontal flowline experimental facility, the first of its kind in UK. The idea behind this is to elucidate the flow behaviour in the

large diameter vertical pipes, with emphasis on studying the effect of the two gas injector designs, as a background for performance evaluation for above proposed riser tower system.

In last decade, experimental studies with intermediate diameter sizes ($100< D \leq 200$mm) (Cheng *et al.*, 1998; Hibiki and Ishii, 2003; Hills, 1976; Hills, 1992; Hirao *et al.*,1986; Oddie *et al.*, 2003; Ohnuki and Akimoto, 2000; Omebere-Iyari *et al.*, 2007; Omebere-Iyari *et al.*, 2008; Prasser *et al.*, 2002; Shen *et al.*, 2003; Shoukri *et al.*, 2000 and Sun *et al.*, 2002) and higher diameter sizes ($300 < D \geq 500$mm) (Hashemi *et al.*,1986, Ohnuki and Akimoto, 1996 and Shipley, 1984) have emerged. Although these studies have contributed to the topic of the large diameter vertical risers, majority of the work was performed on isolated risers i.e. the gas-liquid introduction in the vertical pipe base (Cheng *et al.*,1998; Hibiki and Ishii, 2003; Hills, 1976; Hills, 1992; Hirao *et al.*,1986; Oddie *et al.*, 2003; Ohnuki and Akimoto, 2000; Omebere-Iyari *et al.*, 2007; Omebere-Iyari *et al.*, 2008; Prasser *et al.*, 2002; Shen *et al.*, 2006; Shoukri *et al.*, 2000 and Sun *et al.*, 2002). This situation may not represent the real conditions such as the one encountered in current work, as the entrance effects on the flow behaviour in such cases are not explicitly included. Likewise, others studies (Shipley, 1984; Hashemi *et al.*, 1986 and Ohnuki *et al.*, 1995) have mostly been confined to very small length-to-diameter ratio ($L/D <12$), which may also not depict the true two phase flow behaviour in a longer vertical riser. Moreover in the above studies, it is also noted that either, the way two phases are introduced in the vertical pipe were given in the vague way, if not entirely omitted or the gas distributor configurations (porous plates, perforated plates/rings, porous tubes multiple/single-orifice plates, nozzle, shower caps discs or porous sinter walls etc.) were entirely different than the configurations encountered in industrial conditions. Hence these studies do not include the industrial effect of the flow path which is typical for applications like flowline-riser system (or hot leg of a nuclear reactor or once through steam generator that have a certain inlet pipe/configuration connected to a vertical pipe).

While the major impediment to the application of large diameter vertical risers had been the lack of the experimental data, there exists only one published work on the hydrodynamic performance of the gas injectors in vertical pipe flow, the study of Guet *et al.* (2003). The study has been conducted at low gas-liquid flow rates in a 72mm diameter vertical pipe with (a) a horizontal porous ring plate around circumference, (b) long porous vertical inlet (1cm×10cm) fixed parallel to pipe wall and (c) a nozzle type configuration (see Figure 1.2) that aimed towards enhancing the oil production in the deep oil wells. For the conditions such as the one studied in this thesis, above gas inlet designs may be unsuitable as the configuration of (a) and (b) might block the vertical pipe base thereby restricting the flow passage and also making the pigging operation difficult. Moreover the porous material has the diameter of about 10μm that are likely to be clogged easily. Even if above factors are overcome, the differences seen in the flow behaviour of the conventional small diameter and large diameter vertical pipes, the conditions derived from the above small scale study may not be valid for large diameter vertical pipes.

Thus, in spite of the extensive two phase flow research in various industries, little information was available on both the above topics. Therefore, the research work described in this thesis can be considered as an important contribution to the topic of two phase flow in large diameter vertical riser as it presents the detail effect of different flow configuration, commonly found in actual field conditions. Moreover, it can be considered to be a bridge between the two ends of large diameter vertical pipe work (work on diameter less than 200mm and greater than 300mm), thus not only filling up the knowledge gap but also strengthening the basic foundations of the subject of multiphase flows in vertical pipes.

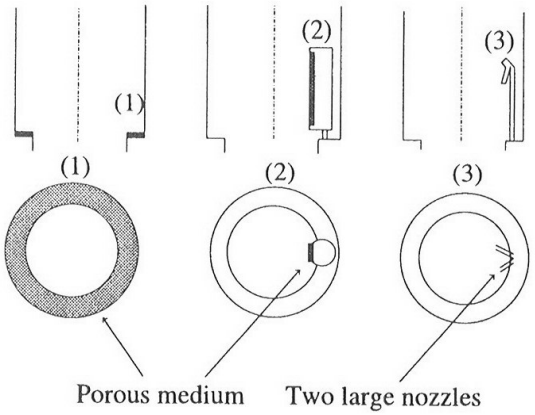

Figure 1.2 The top and side views of three gas injector inlets (porous annular, porous slot and nozzle) used by Guet *et al.* (2003) to study the gaslift efficiency.

1.2 Objectives

The objective of this research is to add to the fundamental knowledge on the hydrodynamic flow behaviour in large diameter vertical risers by:

1. Literature review on the topic of large diameter (D ≥ 100 mm) vertical pipe upflow conditions.
2. Design, selection and calibration of the measurement equipments and operation of two phase flow large diameter riser facility.
3. Study the riser base gas lift performance in large diameter vertical riser with a conventional (Tee) and a novel design gas (Annular sleeve) injector.
4. Undertake the experimental data collection of the hydrodynamic flow behaviour in large diameter vertical riser for a variety of two phase flow conditions.
    - To investigate the flow patterns and flow regime transitions in 254mm diameter vertical riser.
    - To validate the claim of non existence of slug flow for this size of riser.

- Development of experimental flow regime map and its comparison with existing flow regime maps.

5. Investigate the effects of the upstream conditions on the flow behaviour in the vertical riser.
6. Compare the current experimental data with other large diameter vertical upflow experimental studies where appropriate.
7. Compare and analyze the collected data to increase the confidence on the existing two phase flow phase pressure gradient and void fraction prediction methods.
8. Development of a numerical model of the large diameter horizontal flowline-vertical riser using multiphase flow simulator OLGA.
   - Steady state and transient modelling.
   - Comparison of the results from both numerical and experimental work for flow patterns, riser base pressure, average void fraction and pressure drop.

The facility employs air-water as the working fluid because it's easier to build and operate the setup when using air-water than other working fluids that may require special handling. Furthermore, initial small scale visual studies of gas injectors are available for reference, apart from the available air-water two phase flow literature, in which case, the use of air-water as test fluids can lead to more representative results for comparison. In this research, a horizontal flowline topology is adopted, contrary to implementing some terrain affect in the flowline that could produce the effect of sea floor (e.g. inclination at riser base and/or upstream), terminating to a vertical riser. This has been done to ignore the geometrical inclination effect on the flow behaviour in the riser while concentrating on the influence of diameter alone. However, the large diameter riser facility is built with enough flexibility so that various parametric effects (refer to section 7.2) could be studied in future by modifying the setup.

1.3 Thesis outline

This dissertation is divided in seven chapters and four appendices. The content of each chapter is summarized below.

Chapter 1 Introduction - This chapter outlines a brief discussion of the background for this dissertation and outlines the objectives.

Chapter 2 Literature Review - This chapter provides relevant fundamentals of two phase flow, review on experimental studies on large diameter vertical pipes, and a state of art review on the application of the OLGA code.

Chapter 3 Experimental facility, Instrumentation, and Data acquisition - This chapter describes specifically designed and build experimental facility and also outlines the instrumentation used, data acquisition and processing, installation and calibration. Finally, the details of the experimental campaign are presented.

Chapter 4 Experimental Results - The chapter presents riser base gas lifts performance results obtained from the large diameter riser facility. The flow pattern identification, flow regime transitions, and flow pattern map are given, and the effects of the inlet conditions on the two-phase flow in the large diameter vertical pipe upflow are presented. Finally, the experimental data is compared with other large diameter vertical pipe studies and with those of existing models.

Chapter 5 Performance Assessment Study of the existing Void Fraction Correlations and Pressure Gradient Models with experimental results from Large Diameter Vertical Riser - This chapter evaluates some of the commonly used void fraction correlations and pressure gradient methods against the experimental data obtained.

Chapter 6 Numerical Simulation of Large diameter horizontal flowline-vertical riser -In this chapter, large diameter horizontal flowline-vertical riser system has been numerically simulated. A major commercial simulator OLGA has been explored for computing hydrodynamic characteristics. The code's version 5.1 was used to predict the hydrodynamic behaviour, though some difficult cases were also tried with version 5.2 and 5.3.

Chapter 7 Conclusions and Recommendations - This final chapter presents the conclusions and outlines the future research

Nomenclature is provided at the beginning while references are provided at the end of Chapter 7, followed by the Appendices presenting relevant information in more detail.

Chapter 2

Literature Review

The first part of this chapter outlines the relevant fundamentals of two phase flow. Next an extensive literature survey was performed on the topic of two phase flow in vertical pipes. However here, the main topics of interest are only presented, a literature review of experimental studies on large diameter vertical pipe flow along with a theory on OLGA code and a state of art review on the application of the OLGA code.

2.1 Fundamentals of Two phase flows

In this section some basic definitions describing the two phase gas-liquid flows are presented.

2.1.1 Void fraction - The Definition

An important term known as "hold-up or fraction" is often used in two phase flows representing the ratio of the volume of either phase to that of total volume of the pipe. However, usually the term holdup represents the liquid fraction while the term void fraction is used to represents the gas volume fraction. Both the terms are interchangeably used throughout the two phase flow studies depending upon the requirement. These terms are perhaps the most important parameters that relate the two phases and thus provide necessary information of the combined two phase behaviour. Below are the mathematical definitions of the two terms:

$$\alpha = \frac{V_g}{V} = \frac{A_g}{A} \qquad 2.1$$

$$H_L = \frac{V_l}{V} = \frac{A_l}{A} = 1 - \alpha \qquad 2.2$$

Here α is the void fraction and H_L is the liquid fraction or the hold-up. V_g, V_l and V are the volume of gas, volume of liquid and total volume respectively. A is the total pipe cross sectional area, while A_g and A_l are the area occupied by the two phases respectively.

2.1.2 Pressure gradient - The Definition

In this work, the term pressure gradient (dp/dz) is defined as the rate of change of pressure with distance along the pipe. The pressure gradient is considered as a sum of three components; namely frictional, gravitational, and acceleration pressure gradients. Sometimes, it is also referred as "total pressure gradient" (ESDU, 2004). Mathematically it is represented as:

$$-\left(\frac{\mathrm{dp}}{\mathrm{dz}}\right) = -\left(\frac{dp_f}{dz} + \frac{dp_s}{dz} + \frac{dp_a}{dz}\right) \qquad 2.3$$

For adiabatic flows in both horizontal and vertical pipes, the third component of pressure gradient (the acceleration pressure gradient) is often very small typically less than 1% of the total pressure gradient (ESDU, 2004). Thus dp_a/dz is neglected leaving only the frictional and gravitational to be considered. In this work also the acceleration term is neglected.

2.1.3 Gas-Liquid flow pattern

The gas-liquid flows in a conduit can adopt various physical distributions knows as flow patterns (or flow regimes). These flow patterns can be detected by various methods, however they can be classified into traditional methods (direct observation or photography in transparent pipe) or objective indicator methods (void fraction fluctuations, pressure fluctuations, x-rays, gamma-rays, fluorescent light, tomography etc).

2.1.3.1 Flow pattern in vertical pipes

For the vertical upward flows, four typical flow patterns may be distinguished namely; bubbly, slug, churn and annular flow (Hewitt and Roberts, 1969; Matsui, 1984; Mishima and Ishii, 1984 and Spedding and Nguyen, 1980), however many researchers further differentiate between these categories. Flow patterns observed in vertical upward, co-current flow at different gas-liquid superficial velocities are shown in Figure 2.1. The sequence defined is that which would normally be seen as the gas superficial velocity is increased.

a) ***Bubbly flow:*** In this flow, gas is dispersed in the continuous liquid phase. Various researchers have further classified this flow pattern as: dispersed bubbly flow and low liquid input bubbly flow (Taitel *et al.*, 1980; Weisman and Kang, 1981; McQuillan and Whalley, 1985; Barnea and Brauner, 1986 and Barnea 1987)

- Dispersed bubbly flow: This type of flow is realised over whole pipe diameter range and inclination (Barnea, 1987). The gas phase is dispersed as small discrete bubbles in continuous liquid phase.
- Low liquid input bubbly flow: At low liquid superficial velocity, gas bubble of

approximately same sizes will exist and are evenly distributed in the liquid phase with some occasional coalescence in the core (Taitel *et al.*, 1980).

It is to be noted that many other researchers (Mishima and Ishii, 1984; Kokal and Stanislav, 1989; Weisman and Kang, 1981) do not delineate any exact distinction between the above two flows.

b) ***Slug flow:*** For this flow as the gas superficial velocity is increased, the gas bubble will begin to coalesce and form long smooth bubble with front having cap/bullet shape (also called nose). These bubbles are referred as Taylor bubbles are of equivalent cross section as that of the tube, being separated from the wall by a thin liquid film. The two consecutive Taylor bubbles are separated by a liquid slug that may contain small air bubbles that are being shed from the tail of the leading Taylor bubble.

c) ***Churn/ froth flow:*** As the gas superficial velocity is increased in slug flow regime, the Taylor bubble becomes more distorted at liquid-gas interface. The distorted bubble travels in churning motion giving rise to irregular shaped portions of gas and liquid. This flow is also called froth slug, dispersed slug, churn-turbulent flow, and pulsating annular (Brauner and Barnea, 1986). Many researchers (e.g. Mao and Dukler, 1993) do not consider churn/froth flow as a separate flow regime and treat this flow under the slug flow regime (Hewitt and Jayanti, 1993).

d) ***Annular flow:*** In this flow, the gas phase exists in the core while liquid exists as film around the periphery of the tube. The liquid will also exist as entrainment (drops) in the core. There are two variation of this flow namely (Hewitt, 1982);

- Wispy annular flow: Here entrained liquid is present as relatively large drops and liquid film will contain gas bubbles.

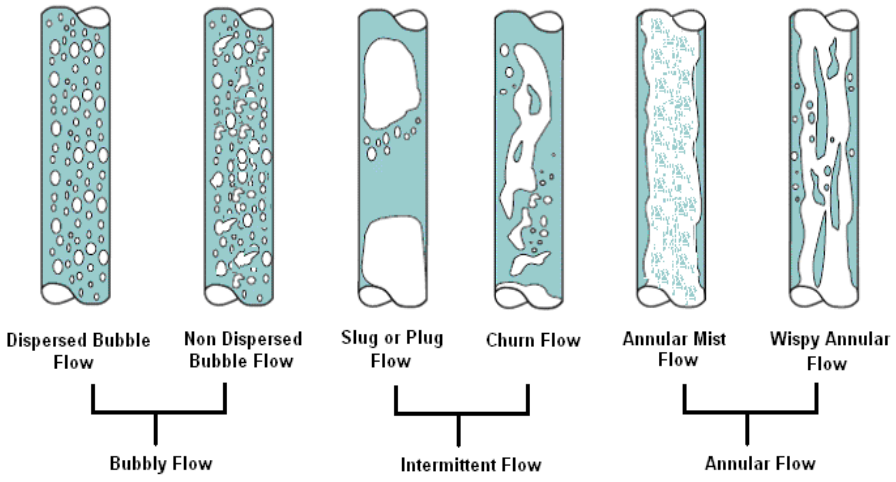

Figure 2.1 Flow regimes in vertical gas-liquid upflow.

- Annular mist flow: In this flow gas occupies the centre of the core while liquid flows along the periphery. The core gas will contain the liquid entrainment but the drops size is not large.

2.1.3.2 Flow pattern in horizontal pipes

Although this work basically deals with flow patterns in vertical pipe, however later in the thesis effect of inlet conditions to vertical pipes has been studied and where flow in horizontal flowline will be discussed. The common flow patterns for horizontal flow in a round tube are illustrated in Figure 2.2. Here due to the asymmetry caused by gravity the two phases tends to separate out, flow patterns observed are:

a) ***Bubbly flow:*** In horizontal flow the gas bubbles tends to congregate and flow at the top of the tube. At higher liquid velocities bubbles may become uniformly distributed and appear as froth.

b) ***Plug flow:*** As the gas superficial velocity is increased bubbles become larger and coalesce to form, long bubbles known as plugs, still moving along the top of the tube.

c) ***Stratified flow***: At still higher gas superficial velocity but with definite low liquid flow rate, the gas phase separates out and flows separately with liquid flowing at the bottom and gas phase being lighter flowing on the top. There exist two variation of these flows namely;

- Stratified smooth flow - in which liquid-gas interface is smooth.
- Stratified wavy - in which the liquid wave amplitude increases (forming ripples and rolls) as gas superficial velocity is increased so that smooth interface transforms into waves.

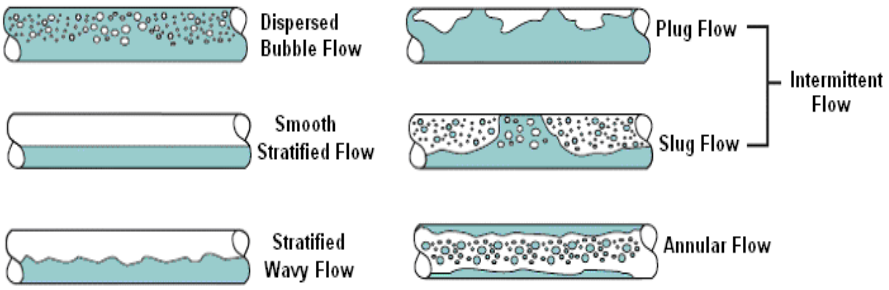

Figure 2.2 Flow regimes in horizontal gas-liquid flows.

d) ***Slug flow:*** Here the wave amplitude have become so large that the wave touches the top of the tube forming pockets of the gas in the pipe that are smooth from

front but keeps on shedding gas bubble from the tail area while flowing.

e) ***Annular flow:*** When the gas superficial velocity have increased to an extent that liquid is taken away in the same direction by high velocity travelling gas, annular flow said to exist. The core is occupied by gas while liquid exist as film around the whole periphery of the pipe. There also exists liquid entrainment in form drops in the core.

2.1.4 Flow regime maps

Development of the co-current gas-liquid flow models to predict two phase flow behaviour requires information of flow patterns in the pipe. For such information flow regime maps have been developed.

2.1.4.1 Well known flow pattern maps

Although many methods exist to identify the flow pattern but commonly used method of identification of the flows patterns is through visual observation in experiments and locating them on the flow map. A wide variety of two flow pattern maps in pipes exits in literature. Most of these maps have gas-liquid superficial velocities as dimensional coordinates, however there exists various other flow maps in literature with coordinate's parameter other than superficial velocities such as of Hewitt and Roberts (1969) and Baker (1954). Earlier, most flow maps were based on empirical correlations generated from experimental data and had limited applicability. Taitel *et al.* (1976) put forward first mechanistic flow map for horizontal flows based on physical transitions mechanism of each flow regime. Taitel *et al.* (1980) modified the flow map of Dukler and Taitel (1977) for vertical upward air-water flow at 25 °C and 0.1 MPa in 25 and 50mm tubes. Weisman and Kang (1981) and McQuillan and Whalley (1985) also presented modified vertical flow pattern maps for two-phase vertical upflow. Mishima and Ishii (1984) like Taitel *et al.* (1980) also presented a mechanistic flow regime transition for upward two phase flow in vertical pipes that is in good agreement with other vertical flow maps. A unified model for whole range of pipe inclination including the vertical and horizontal was presented Barnea (1987). Figure 2.3 to 2.5 shows some commonly encountered flow regime maps for horizontal and vertical flows.

2.1.4.2 Flow pattern transitions and mechanisms

The knowledge of which flow pattern is occurring under which condition is very important as each flow pattern results in different hydrodynamic characteristics. These characteristics further influences the properties like pressure drop and heat and mass transfer capabilities. Hence the identification of flow pattern and their transitions are very important. The flow regime transitions depends upon many factors such as gas-liquid velocities, fluid properties, orientation of conduit, tube diameter (D) and operating conditions. While the most popular method of flow pattern identification is off course experimental but empirical and mechanistic models are also used to identify the flow regime transitions. The later category is quite successful in explaining the flow regime transitions as it explains the mechanism that governs the transition from one flow pattern to another. Taitel *et al.* (1980), Mishima

& Ishii (1984), McQuillan & Whalley (1985) and Barnea (1987) are some well known names that provided mechanistic modelling of commonly encountered vertical flow patterns. However there are some others that provided the specific models for particular flow pattern like transition from bubbly to dispersed bubbly flow (Chen *et al.*, 1997) and slug to churn flow (Brauner and Barnea, 1986; Jayanti & Hewitt, 1992; Mao & Dukler, 1993). Many past investigations has been made on the flow regime transitions collectively for all flow regimes or individually, however they have been mainly performed for conventional pipe sizes (D < 100mm). It is beyond the scope of this thesis to review all this work, below only the popular work has been exemplified.

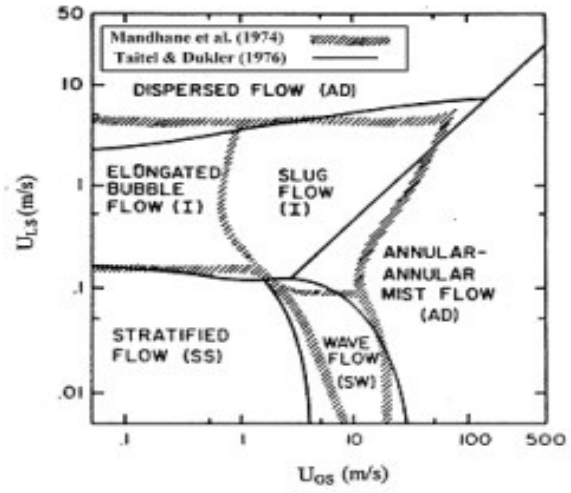

Figure 2.3 Flow regime map for horizontal flow showing Mandhane *et al.* (1974) and Taitel *et al*. (1976) transitions (Brennen, 2005).

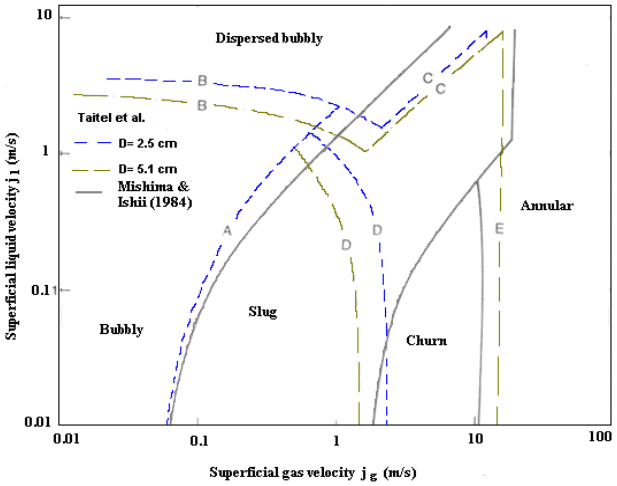

Figure 2.4 Flow regimes map for vertical upflow showing Taitel *et al.* (1980) and Mishima and Ishii (1984) transitions (Mishima and Ishii, 1984).

Transition from Bubbly to Slug flow

According to McQuillan and Whalley (1985) and Mishima and Ishii (1984), the bubbly flow is observed at low gas superficial velocities, irrespective of the liquid flow rate. In this work non-dispersed bubbly flow or low liquid input bubble flow is simply referred as bubbly flow.

The agglomeration and coalescence of bubbles was proposed as cause of flow transition from bubbly to slug flow. In general, as the gas superficial velocity is increased, more bubbles are generated and hence the bubble density increases causing the distance between them to decrease to extent that they results in coalesce.

Cheng et al. (1998) quote in his paper, Radovcich and Moissis (1962) qualitatively showed that probability of coalescences becomes very large at 0.3 and they inferred this as the flow regime transition. Dukler and Taitel (1977) too proposed the value of 0.3 as the critical void fraction responsible for transition. Taitel *et al.* (1980) work also attribute the gradually coalesce of sufficient quantity of bubbles into large Taylor bubble. Taitel *et al.* (1980) found that this transition from bubbly to slug flow occurs around the critical void fraction (α_c) of 25% of the pipe volume (line A on the Figure 2.4).

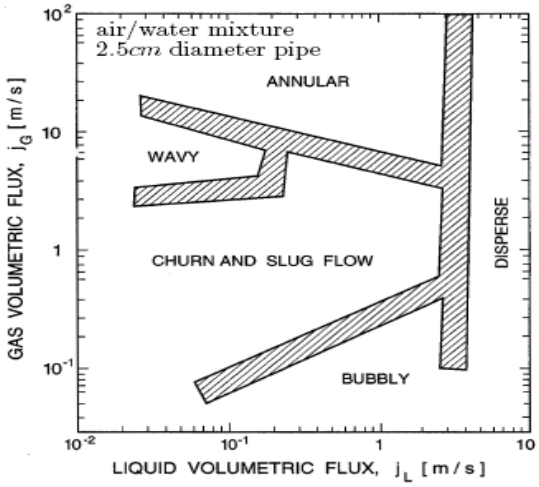

Figure 2.5 Flow regimes map of Weisman and Kang (1981) for vertical upflow (Brennen, 2005).

$$j_l = \left(\frac{1-\alpha_c}{\alpha_c}\right)\cdot j_g - (1-\alpha_c)\cdot U_o \qquad 2.4a$$

$$j_l = 3j_g - 1.15\left[\frac{\sigma\cdot g(\rho_l-\rho_g)}{\rho_l^{\,2}}\right]^{1/4} \qquad 2.4b$$

Where, j_g and j_l are gas and liquid superficial velocities, U_o is the terminal riser velocity of the gas phase, α_c is the critical void fraction, σ is surface tension, ρ_l and ρ_g are gas and liquid densities respectively and g is the acceleration due to gravity. From the equation 2.4a, it can be noted that the equation is independent of the diameter of the pipe.

Weisman and Kang (1981) classified the slug/plug and churn flow as intermittent flow and modified Taitel and Dukler (1977) transition criteria between bubbly and intermittent flow. Since their experimental data suggested that transition between bubble and intermittent flow is governed by the Froude number, they proposed that a simple relationship exists between the Froude number of gas and the Froude number based on total volumetric flow. Thus the modified expression becomes as:

$$\frac{j_g}{\sqrt{g \cdot D}} = 0.45 \left(\frac{j_m}{\sqrt{g \cdot D}} \right)^{0.78} \qquad 2.5$$

Where, j_g and j_m are gas and total mixture superficial velocities, σ is surface tension, D is the diameter, ρ_l and ρ_g are gas and liquid densities respectively and g is the acceleration due to gravity. This line represented as line "A" in the Figure 2.5.

Mishima and Ishii (1984) suggested that the bubbly to slug flow transition occurs due to the coalescences/ agglomerations of smaller bubbles into large bubbles. Once these large bubbles are formed, they will further promote coalescences in their wake region. They further provided a mathematical explanation of using a critical void fraction value of 0.30 for this transition, which upon substitution yielded the following equation:

$$j_l = \left(\frac{3.33}{C_o} - 1 \right) j_g - \frac{0.76}{C_o} \left(\frac{\sigma \cdot g (\rho_l - \rho_g)}{\rho_l^{\,2}} \right)^{1/4} \qquad 2.6$$

$$\text{and} \qquad C_o = 1.2 - 0.2 \sqrt{\frac{\rho_g}{\rho_l}} \qquad 2.7$$

Where, j_g and j_l are gas and liquid superficial velocities, σ is surface tension, ρ_l and ρ_g are gas and liquid densities, g is the acceleration due to gravity and C_o is the distribution parameter. Unlike the equation 2.4, this equation indirectly takes into account of variation of void fraction across the diameter via C_o, see Figure 2.4.

From above and few other studies on the topic of transition from bubbly to slug flow (Song *et al.*, 1995, Cheng *et al.*, 1998 and Guet *et al.*, 2003), it can be found that the critical void fraction and initial bubble size are the important factors in determining the bubbly to slug flow transition. All the above studies propose that the bubbly to slug flow transition is influenced by initial bubble size resulting in different

interaction and hence affecting the behaviour of flow. Hence it's the bubble size that will ultimately determine the bubble to slug flow transition.

Transition from Bubbly to Dispersed Bubbly or Dispersed Bubbly to Slug /Churn

While non-dispersed bubbly flow or bubbly is said to occur at low liquid input, the dispersed bubbly flow is said to exist at higher (j_l > 3m/s) liquid superficial velocities only (Taitel *et al.*, 1980). This transition between the two bubbly flows based on stability of bubble i.e. a force balance between agglomeration of bubble and breakup of bubble (Taitel *et al.*, 1980). In case of low liquid input the coalescence will dominate while at higher liquid superficial velocities, the turbulence in the liquid will govern to break up the larger bubbles into smaller spherical bubbles and/or suppress the formation of larger bubbles.

Taitel *et al.* (1980) based their work on Hinze (1955) theory of breakup of fluid phases by turbulent forces and used the homogeneous mixture flow theory to calculate the void fraction. At high enough liquid flow rates once the turbulent fluctuations are enough to initiate breakup, agglomeration phenomena will be suppressed, even though the critical void fraction could be higher than 25%. Based on this assumption Taitel *et al.* (1980) derived an expression at which turbulent dispersion took place below. This relation outlines the expression relating fluid properties and pipe size at which turbulent induced dispersion takes place.

$$j_l = 4\left\{\frac{D^{0.429}\cdot\left(\frac{\sigma}{\rho_l}\right)^{0.089}}{\nu_l^{0.072}}\cdot\left[\frac{g(\rho_l-\rho_g)}{\rho_l}\right]^{0.446}\right\} - j_g \qquad 2.8$$

Where, j_g and j_l are gas and liquid superficial velocities, D is the diameter of the conduit, σ is surface tension, ν_l is the liquid kinematic viscosity, ρ_l and ρ_g are gas and liquid densities and g is the acceleration due to gravity. The above expression is represented as curve B in Figure 2.4.

Mishima and Ishii (1984) did not classify the bubbly flow as dispersed bubble flow and non-dispersed bubble flow. McQuillan and Whalley (1985) adopted the empirically modified expression by Taitel and Dukler (1976) for flow in horizontal tubes. The transition assumes that at the higher liquid velocities, there is negligible slip between the two phases, so bulk liquid turbulence is only cause of bubble break, moreover there is no tube inclination effect. The bubbly to dispersed bubbly correlation is valid for vertical orientation and is independent of the gas superficial velocity. The dispersed bubble flow is said to exist if:

$$j_l \geq \frac{6.8}{\rho_l^{0.444}} \cdot \left\{ g \cdot \sigma \cdot \left(\rho_l - \rho_g \right) \right\}^{0.278} \cdot \left(\frac{D}{\mu_l} \right)^{0.112} \qquad 2.9$$

Where, j_g and j_l are gas and liquid superficial velocities, D is the diameter of the conduit, σ is surface tension, μ_l is the liquid dynamic viscosity, ρ_l and ρ_g are gas and liquid densities, g is the acceleration due to gravity.

Barnea (1987) while acknowledged the bubbly flow classification stated that the distinction between the two flows is not always clearly visible. Nevertheless, the dispersed bubble flow is observed over the whole range of pipe inclinations, while the bubbly flow pattern is observed only in vertical and off-vertical flows in relatively large diameter tubes. They modified Taitel *et al.* (1980) transition criteria to account for pipe inclination from bubbly to dispersed bubble, stating that at high liquid rates dispersed bubble can exist for even when $\alpha > 0.25$ because the turbulence causes the bubble to break and suppress coalescence and thus slug flow cannot take place. The mathematical expression for above is:

$$2\left[\frac{0.4 \cdot \sigma}{g \cdot \left(\rho_l - \rho_g \right)} \right]^{1/2} \cdot \left(\frac{\rho_l}{\sigma} \right)^{3/5} \left[\frac{2}{D} \cdot C_l \cdot \left(\frac{D}{\nu_l} \right)^{-n} \right]^{2/5} \cdot j_m^{\,2(3-n)/5} = 0.725 + 4.15\alpha^{0.5} \qquad 2.10$$

Where j_g and j_l are gas and liquid superficial velocities, D is the diameter of the conduit, σ is surface tension, ν_l is the liquid kinematic viscosity, ρ_l and ρ_g are gas and liquid densities respectively, α is the gas void fraction, C_L and n are coefficients in the Blasius correlation of the friction factor ($C_l = 0.046$, $n = 0.2$). This transition is valid for $0 \leq \alpha \leq 0.52$.

Chen *et al.* (1997) transition criterion to dispersed bubbly flow defines that the dispersed bubbly flow will only exist if the turbulent kinetic energy of the liquid phase is greater than the surface free energy of dispersed spherical bubbles. It was further suggested that Taitel *et al.* (1980) criterion for dispersed bubbly flow shows an incorrect trend of this transition (a straight line with a slope of -1.0) when plotted in a j_l vs. j_g for a given pipe size and gas-liquid mixture. It was noted that the critical threshold for dispersed bubbly flow to occur i.e. transition liquid superficial velocity increases monotonically with an increase in gas superficial velocity.

Where j_g and j_l are gas and liquid superficial velocities, D_H is the diameter of the conduit, σ is surface tension, ν_l is the liquid kinematic viscosity, ρ_l and ρ_g are gas and liquid densities respectively, C_l and n are coefficients in the Blasius correlation of the friction factor ($C_l = 0.046$, $n = 0.2$).

$$\frac{j_l}{j_g} = 12.65 \frac{Y_L}{E_o^{1/2}} \qquad 2.11$$

$$E_o = \frac{g \cdot (\rho_l - \rho_g) \cdot D_H^{\,2}}{\sigma} \qquad 2.12$$

$$Y_L = \frac{g \cdot (\rho_l - \rho_g)}{\frac{4C_l}{D}\left(\frac{D_H \cdot j_l}{\nu_l}\right)^{-n} \cdot \frac{\rho_l \cdot j_l^{\,2}}{2}} \qquad 2.13$$

Weisman and Kang (1981) classified the dispersed bubbly and bubbly flow and used the equation suggested by Husain and Weisman (1978). The original equation was suggested for horizontal flows, however Weisman and Kang (1981) suggested that the orientation of the pipe has little effect on this flow as the dispersed bubbly flow transition occurs when turbulent forces are sufficient to breakup the bubbles and these turbulent forces can be related to pressure drop. The correlation is independent of gas superficial velocity and takes into account of diameter and surface tension effects.

$$\left(\frac{\left(\frac{dp}{dx}\right)^{sp}}{\Delta\rho \cdot g} \right)^{1/2} \cdot \left(\frac{\sigma}{\Delta\rho D^{2} g} \right)^{-1/4} = 9.7 \qquad 2.14$$

Investigators who have considered the bubbly flow classification into dispersed and non-dispersed had further defined the transition criteria to/or from dispersed bubbly flow to slug/churn flow. In these studies it has been assumed that when the gas phase concentration gets high enough so that maximum packing density (spherical bubbles arranged in a cubic lattice) is reached, agglomeration into large bubble will occur even in the presence of turbulent liquid flow. Taitel *et al.* (1980) took a value of 0.52 for this maximum gas void fraction for dispersed bubble; see Figure 2.4 defining line C which also delimit the curve B.

$$j_l = j_g \frac{1-\alpha}{\alpha} \qquad 2.15$$

Where j_g and j_l are gas and liquid superficial velocities, α is the gas void fraction equal to 0.52.

Transition from Slug to churn flow

Some previous investigations have defined churn flow as a transition state occurring between the slug flow and annular flow (Mao and Dukler, 1993) and therefore considering it to be the part of slug flow, there are others who have defined this flow

as separate flow regime (Hewitt and Hall-Taylor 1970, Jayanti and Hewitt, 1993). The flow itself is characterized by chaotic flow pattern where the conventional slugs are destroyed by the high gas superficial velocity. Transition to churn is said to approach when the ratio of the length of Taylor bubble to that of liquid slug decreases with an increase in gas superficial velocity to the extent that aeration within the slug destroys it (Chen *et al.*, 1997). Due to the complex nature of the flow, several mechanisms had been proposed to model this transition. However below are four major approaches used:

1. Entrance effect mechanism
2. Wake effect mechanism
3. Bubble coalescence mechanism
4. Flooding mechanism

Taitel *et al.* (1980) as well as Dukler and Taitel (1986) and Mao and Dukler (1993) regarded the churn flow as an entrance phenomenon that leads to stable slug flow some distance downstream from the pipe entrance if the length of the pipe is long enough. This further means that near the entrance, the liquid slug separating the two consecutive Taylor bubble are so short that the wake behind the Taylor bubble destroys this liquid slug bridging and hence churn flow is observed. This criterion is given by line D on Taitel *et al.* (1980) flow regime map (see Figure 2.4) and gives the number of pipe diameters downstream from the pipe entrance where churn flow is likely to be observed. An expression to evaluate the entrance length, l_ε, required to form stable slugs in a given flow condition was also given by Dukler and Taitel (1986):

$$\frac{l_\varepsilon}{D} = 42.6\left(\frac{j_g + j_l}{\sqrt{gD}} + 0.29\right) \qquad 2.16$$

Where l_ε is the estimated entrance length, j_g and j_l are gas and liquid superficial velocities, g is the acceleration due to gravity, and D is the tube inner diameter. If the length of the pipe is less than calculated l_ε, using equation above, then churn flow is observed in the entire pipe and if not than otherwise slug flow will prevail.

Mishima and Ishii (1984) proposed that the churn flow is the result of collapse of liquid slugs due to the wake effect of the Taylor bubbles. In detail they assumed that at the point of transition the liquid slugs are so short that the wake of the Taylor bubble is enough to destabilize the liquid slug and dissipate it. Mathematically this transition occurs when the mean void fraction of the Taylor bubble region becomes equal the average void fraction in the pipe.

$$\alpha_{avg} = \frac{j_g}{C_o j_m + 0.35\sqrt{\frac{Dg\left(\rho_l - \rho_g\right)}{\rho_l}}} \qquad 2.17$$

$$\alpha_b = 1 - 0.813\left[\frac{(C_o - 1)(j_g + j_l) + 0.35\sqrt{\frac{Dg(\rho_l - \rho_g)}{\rho_l}}}{j_m + 0.75\sqrt{\frac{Dg(\rho_l - \rho_g)}{\rho_l}}\left(\frac{(\rho_l - \rho_g)D^3\rho_l}{\mu_l^2}\right)^{1/18}}\right] \quad 2.18$$

Where j_m is the volumetric flux and is a sum of j_g and j_l, j_g and j_l are gas and liquid superficial velocities, g is the acceleration due to gravity, D is the tube inner diameter μ_l is the liquid kinematic viscosity, α_{avg} is the gas void fraction, α_b is the mean gas void fraction of Taylor bubble, ρ_l and ρ_g are gas and liquid densities respectively.

Brauner and Barnea (1986) proposed that the slug to churn flow transition takes place due to increase in aeration within liquid slugs. It was postulated that when the average gas void fraction within the liquid slug reaches the maximum bubble cubic volumetric packing (0.52), local coalescence of bubbles occurs within the liquid slugs, destroying the liquid bridge and hence churn flow occurs. Thus the transition from the slug flow to churn will be reached when the gas void fraction is greater than 0.52. The expression for this transition assumes that near the transition gas phase in liquid slugs behaves as dispersed bubbles developed by Barnea and Brauner (1985) for predicting the liquid holdup in the slug.

$$\alpha_b = 0.058\left[d_c \cdot \left(\frac{2 f_m j_m^{\,3}}{D}\right)^{0.4} \cdot \left(\frac{\rho_l}{\sigma}\right)^{0.6} - 0.725\right]^2 \quad 2.19$$

$$d_c = 2\sqrt{\frac{0.4 \cdot \sigma}{g(\rho_l - \rho_g)}} \quad 2.20$$

$$f_m = \frac{16}{\mathrm{Re}} \qquad \textit{if } Re \le 2100 \quad 2.21$$

$$f_m = 0.046\,\mathrm{Re}^{-0.2} \qquad \textit{if } Re > 2100 \quad 2.22$$

In above set of equations j_m is the volumetric flux and is equal to sum of j_g and j_l, d_c is the characteristics bubble size, σ is the liquid surface tension, α_s is the mean gas void fraction of Taylor bubble, ρ_l and ρ_g are gas and liquid densities respectively, f_m is friction factor based on mixture velocity and g is the acceleration due to gravity. The above model though was in agreement with Dukler and Taitel (1986) for L/D ratio of 250-50, Jayanti and Hewitt (1992) in their assessment showed a poor performance at low liquid flow rate.

The last mechanism proposed for the transition from slug to churn flow is onset of flooding in liquid film surrounding Taylor bubble in slug flow. The mechanism was first proposed by Nicklin and Davidson (1962) and later improved by Wallis (1969), McQuillan and Whalley (1985) and Jayanti and Hewitt (1992). The flooding is defined as the breakdown of the liquid film due to the formation of large interfacial waves formed on it in counter current flow of gas and liquid. In case of flooding around Taylor bubble, a liquid film falling downward is taken upward by the gas velocity forming waves that lead to the collapse of slugs between the large bubbles. Below is the semi-empirical expression for predicting the flooding proposed by Wallis (1961) and Hewitt & Wallis (1963).

$$\sqrt{j_g^*} + \sqrt{j_l^*} = C \qquad 2.23$$

$$j_g^* = j_g \frac{\sqrt{\rho_g}}{\sqrt{g \cdot D(\rho_l - \rho_g)}} \qquad j_l^* = j_l \frac{\sqrt{\rho_l}}{\sqrt{g \cdot D(\rho_l - \rho_g)}} \qquad 2.24 \text{ (a \& b)}$$

In above equations j_g^* and j_l^* are dimensionless gas and liquid superficial velocities, j_g and j_l are gas and liquid superficial velocities, D is the diameter of the conduit, ρ_l and ρ_g are gas and liquid densities respectively and C is flooding constant.

McQuillan and Whalley (1985) proposed that in above equation 2.24 (a-b) the phase superficial velocities should be replaced by the Taylor bubble superficial (U_{BS}) and the liquid film superficial (U_s) as the flooding occurs in this region, hence the equation 2.24 should be instead written as:

$$U_{bs}^* = U_{bs} \frac{\sqrt{\rho_g}}{\sqrt{gD(\rho_l - \rho_g)}} \qquad U_{fs}^* = U_{fs} \frac{\sqrt{\rho_l}}{\sqrt{gD(\rho_l - \rho_g)}} \qquad 2.25 \text{ (a-b)}$$

$$U_{bs} = \left(1 - 4\frac{\delta}{D}\right)\left(1.2 j_m + 0.35\sqrt{\frac{g.D(\rho_l - \rho_g)}{\rho_l}}\right) \qquad 2.26$$

$$U_{fs} = U_{bs} - j_m \qquad 2.27$$

$$\delta = \left[\frac{3 \cdot U_{fs} D \mu_l}{4g(\rho_l - \rho_g)}\right]^{1/3} \qquad 2.28$$

U_{bs} can be determined by equation 2.27, Nussle's expression for a laminar falling film, δ is the liquid film thickness in the Taylor bubble region, j_m is the volumetric flux and is equal to sum of j_g and j_l, ρ_l and ρ_g are gas and liquid densities, g is the

acceleration due to gravity and D is the tube inner diameter, μ_l is the liquid kinematic viscosity. In equation 2.25, constant C depends upon many factors but has been observed to lie near unity.

Jayanti and Hewitt (1992) experimentally identified flooding of falling liquid film around a rising gas slug and made an assessment of the above four different approaches (*Entrance effect mechanism, Flooding mechanism, Wake effect mechanism and Bubble coalescence mechanism*). Through their assessment they showed that churn flow is still predicted in the region where Taitel *et al.* (1980) predicted the slug flow. Using the Owen (1986) data of fully developed vertical upflow in pipe, they proposed an improvement in flooding model by accounting for the effect of the Taylor bubble length and overall length of the pipe. Using Broz (1954) empirical correlation that is applicable over a wide range of liquid film Reynolds numbers, they calculated the liquid film velocity and also accounted for the effect of the length of the falling liquid film on the flooding velocity.

$$U_{bs} = \alpha_b \left(1.2 j_m + 0.35 \sqrt{\frac{g.D\left(\rho_l - \rho_g\right)}{\rho_l}} \right) \qquad 2.29$$

$$\delta \left[\frac{g\Delta\rho}{\nu_l^{\,2}\rho_l} \right]^{1/3} = 0.1719\,\mathrm{Re}_l^{\,2/3} \qquad 2.30$$

$$U_{fs} = 9.9196\left(1-\alpha_b\right)\sqrt{\frac{gD\Delta\rho\left(1-\sqrt{\alpha_b}\right)}{\rho_l}} \qquad 2.31$$

$$\alpha_b = 1 - 4\frac{\delta}{D} \qquad 2.32$$

$$\sqrt{j_g^{\,*}} + m \cdot \sqrt{j_l^{\,*}} = C \qquad 2.33$$

$$m' = 0.1928 + 0.01089\left(\frac{L}{D}\right) - 3.754\times10^{-5}\left(\frac{L}{D}\right)^2 \quad \textit{if } L/D \le 120 \qquad 2.34\text{ (a-b)}$$

$$m' = 0.96 \approx 1 \quad \textit{if } L/D > 120$$

In above sets of equations, U_{bs} and U_s are superficial Taylor bubble and liquid film superficial velocities, δ is the liquid film thickness in the Taylor bubble region, j_m is the volumetric flux and is equal to sum of j_g and j_l, ρ_l and ρ_g are gas and liquid densities, g is the acceleration due to gravity, D is the tube inner diameter, ν_l is the liquid kinematic viscosity and Re is the Reynolds number. The constant C attains a value of unity for smooth inlet and outlet conditions, a value of 0.75 for sharp flanges into the tube and a value of 0.88 for rounded flanges.

Lastly the transition model by Tengesdal *et al.* (1999) is presented. The model is based on drift flux approach with transition global void fraction. This global void fraction is presented by drift flux equation for slug flow

$$\frac{j_g}{\alpha} = 1.2 j_m + U_s \tag{2.35}$$

$$j_g = 12.19(1.2 j_l + U_s) \tag{2.36}$$

$$U_s = (0.35 \cdot \sin\theta + 0.54 \cdot \cos\theta) \cdot \sqrt{\frac{g \cdot D(\rho_l - \rho_g)}{\rho_l}} \tag{2.37}$$

$$j_g = 12.19\left[1.2 j_l + (0.35 \cdot \sin\theta + 0.54 \cdot \cos\theta) \cdot \sqrt{\frac{g \cdot D(\rho_l - \rho_g)}{\rho_l}}\right] \tag{2.38}$$

Where j_g is gas superficial velocity, j_m is the volumetric flux and is equal to sum of j_g and j_l, α is the global gas void fraction, θ inclination angle and U_s is rise velocity of Taylor bubble. Tengesdal *et al.* (1999) used the global void fraction of 0.78, taken from the Owen (1986) experimental data and Bendiksen *et al.* (1984) relation for rise velocity of Taylor bubble in inclined tubes to define the slug-churn boundary as:

Transition from Churn to Annular flow

Most of the previous investigators have modelled this transition from churn to annular flow as the point where the gas superficial velocity is sufficiently high to prevent liquid droplets from falling. Thus the liquid film flows upward adjacent to the wall by high velocity gas that also carries the entrained liquid droplets in the centre of the tube. The high velocity gas while travelling upward may create wavy interface that are torn away by incoming gas phase from film surface as droplets. Thus liquid moves on periphery or wall of the conduit as well as droplets within the core via interfacial shear and drag forces.

Taitel *et al.* (1980) applied the force balance between the gravity and drag forces to determine the minimum gas velocity required to suspend a droplet. Thus the velocity below which annular flow would not exist is given by:

$$j_g = \frac{K_v}{\sqrt{\rho_g}}\left[\sigma \cdot g(\rho_l - \rho_g)\right]^{1/4} \tag{2.39}$$

In above equation Taitel *et al.* (1980) suggested a value of $K_v = 3.1$, where as ρ_l and ρ_g are gas and liquid densities, g is the acceleration due to gravity and σ is surface

tension. Pushkina and Sorokin (1969) suggested a similar equation as that of Taitel *et al.* (1980) to predict the transition between churn and annular flow by using K=3.2.

Mishima and Ishii (1984) suggested the transition from churn to annular as the instability of the up flowing liquid. They postulated that this transition is possible by two different mechanisms (a) by a flow reversal/flooding in the liquid film flowing alongside of large bubbles and, (b) when liquid slugs or large wave are the destroyed by entrainment or deformation. The criterion for the first mechanism is presented by equation 2.39 and second by equation 2.41. The equation 2.40 should satisfy the condition given by equation 2.16. In above equations, ρ_l and ρ_g are gas and liquid densities; g is the acceleration due to gravity, σ is surface tension and D is the diameter of the conduit.

$$j_g = \sqrt{\frac{g \cdot D(\rho_l - \rho_g)}{\rho_g}} \cdot (\alpha - 0.11) \qquad \textit{for } \alpha_{avg} > \alpha_m \textit{ \& for small D} \tag{2.40}$$

$$j_g \geq \left(\frac{g \cdot \sigma \cdot (\rho_l - \rho_g)}{\rho_g^{\,2}} \right)^{1/4} \cdot N_{\mu l}^{\,-0.2} \qquad \textit{for large D} \tag{2.41}$$

$$N_{\mu l} = \frac{\mu_l}{\left[\rho_l \cdot \sigma \sqrt{\frac{\sigma}{g \cdot (\rho_l - \rho_g)}} \right]^{1/2}} \qquad D > \frac{\sqrt{\sigma / \Delta\rho \cdot g} \cdot N_{\mu l}^{\,-0.4}}{\left[(1 - 0.11 C_o) / C_o \right]^2} \tag{2.42}$$

By using the McQuillan and Whalley (1985) flooding velocity expression with zero liquid superficial velocities relating the gas-liquid superficial velocities at the flooding point by equation 2.25, the above equations can be retreated. In above churn to annular transition it is interesting to note that Taitel *et al.* (1980) is independent of diameter and liquid superficial velocity while Wallis (1969), Mishima and Ishii (1984) and McQuillan and Whalley (1985) expressions shows dependency on diameter of conduit but independent of liquid superficial velocity.

2.1.6 Void phase distribution characteristics in the vertical pipe

Most of the sophisticated two phase modelling tools require constitutive equations in order to close the basic equations for both gas and liquid phases. It is these equations that require local flow characteristics (void phase distribution, bubble sizes, and frequency etc.) in order to accurately predict the flow behaviour in two phase flows. The void phase distribution varies dramatically throughout the flow regimes and its magnitude is found to depend on many factors like superficial gas velocity, gas inlet method, bubble size distribution, pipe diameter, nature of the gas-liquid systems and

operating conditions. Many past investigations (Serizawa *et al.*, 1975; Herringe and Davis, 1976 and Liu, 1993) are concerned with the phase distribution in vertical pipe flow. It is to be noted, that earlier such detail studies were performed with conventional pipe diameter vertical up flow conditions and the sophisticated codes mostly employed these empirical data.

Many of the above investigators observed wall peaking in their experiments while others observed a peak in the pipe centre. The literature review showed that in small diameter pipes (typically < 75mm), at high gas and low liquid superficial velocities (i.e. high mean void fraction) the void profile is centrally peaked (core peak or parabolic) but at low gas and high liquid superficial velocities (bubbly flow) the profile exhibits a peak near the wall region (saddle like distribution) with central minimum. As the gas superficial velocities increases the wall peak becomes much less pronounced showing what is knows as intermediate peak. Among all the above researchers, it was Serizawa and Kataoka (1987), who summarised above phase distribution trends in 30mm diameter pipe into four major void distribution profiles namely wall peaked, intermediate peak (also referred as broad wall peak), transition (two peaks, one at walls and other at center) and core peak on the flow regime map, refer to Figure 2.6. It was emphasized that the phase distribution of the void fraction is a strong function of the flow pattern and changes from a wall peak to a core peak distribution as the gas superficial velocity increases at constant liquid superficial velocity. The wall peak distribution corresponds to bubbly flow, and a core peak to the slug flow in conventional pipe sizes.

Many investigators from their small pipe experiments have concluded that radial void profile are not only effected by gas and liquid velocities but by positions of the gas inlets (i.e. centreline or through the walls), its distance upstream of the measurement position, by the mean bubble diameter and operating conditions (Serizawa *et al.*, 1975; Herringe and Davis, 1976; Sekouchi *et al.*, 1980; Liu, 1993 & Hibiki and Ishii, 2002).

Herringe and Davis (1976) investigated the three different gas inlet systems in 51mm vertical pipe involving porous sinter through the wall, a drilled hole copper mixer and central jet. At low gas and high liquid velocities, the profile from nozzle and porous sinter gradually turned to slightly wall peaked around 108D while drilled hole mixer showed a core peak from 8D to 108D. In the other experiments at still lower liquid but increased gas superficial velocities, all the three injectors showed the same core peak profile. Subbotin *et al.* (1975) also measured radial void profiles in 21mm diameter tube with air injected through mixer of 0.5-0.8 mm holes in the centre and on walls and observed that centre injection gave central peak while later gave a wall peak in appropriate ranges of flows rates (Hills, 1993).

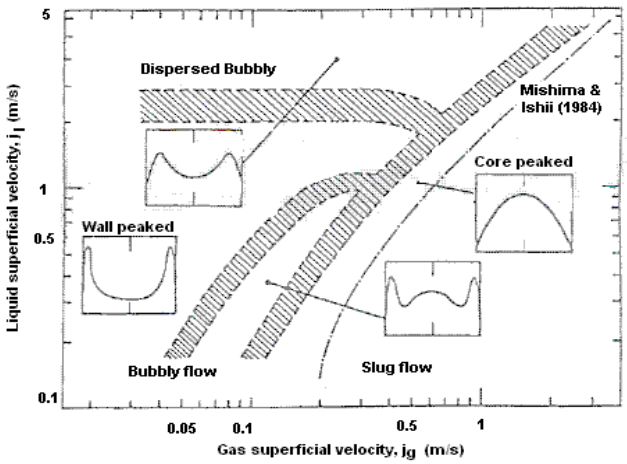

Figure 2.6 Phase Distribution according to flow regimes in 30mm internal diameter pipe by Serizawa and Kataoka (1987).

Sekouchi *et al.* (1980) observed core peak profile for centreline injection and wall peak for porous wall injection even after a mixing length of 140D under same flow conditions in the test section with different air-water velocities. Van der Welle (1985) found a core peak void distribution in vertical pipe air-water flows with specially designed mixer containing 600 ferrules for air flow. Hills (1993) found no sign of wall peaking even under high liquid-low gas conditions in a 150mm tube instead a core peak was observed in all cases, with little variation in shape as gas and liquid rates varied. This behaviour was attributed to the large bubble sizes produced by the gas distributor in the center of the column base.

The void phase distribution or radial profiles are the result of the non-drag force, acting perpendicularly to the flow direction that is caused by the liquid shear flow in the tube. Zun (1988) reported that the non drag forced called lift force acts into wall direction in a vertical tube upwards flow. Tomiyama *et al.* (1998) found that this lift force changes sign depending on the diameter of the bubble. In case of air-water system under ambient conditions, this crossover occurs at a bubble diameter of about 5.8mm. Bubbles with a diameter less than 5.8mm were found preferably near the wall and larger bubbles in the pipe centre (Tomiyama, 1998).

Although the early studies claim that phase distribution variation was solely due to the gas and liquid phase velocities, Serizawa *et al.* (1975), Tomiyama *et al.* (1998) and Liu (1993) all concluded that by changing the initial bubble size, the void phase distribution may change even under the fixed gas-liquid velocities and this phenomenon is especially pronounced under low liquid velocity condition. Serizawa *et al.* (1975) investigated the effect of initial bubble size by using nozzle with varying bubble diameters. They performed measurement as far as 83D from the inlet and found that as bubble size increased, the wall peak diminished to be replaced by a central peak for the largest bubbles of more than about 5mm diameter. Similarly,

Sekoguchi *et al.* (1980) observed the behaviours of isolated bubbles through a single nozzle in vertical rectangular channel (25mm×50mm). It was found that the distorted ellipsoidal bubbles diameter less than 5mm tended to migrate toward the walls while the bubbles with diameter larger than 5mm preferably flow in the core region. An extensive review on the bubble behaviours is given by Serizawa and Kataoka (1988) where they suspected that bubble size might be the key factor which caused discrepancies in the phase distribution and flow pattern under similar experimental conditions because the bubble frequency follows a similar profile like void phase distribution. According to Liu (1993) the size of the bubble can vary for different type of injectors used which seems to affect the void fraction profile also. In case the air bubbles from the injectors are small than they will migrate towards the wall and contribute in the wall peak and when coalescence starts to place and they grow they will move towards the pipe centre to contribute to core peaking. The critical bubble diameter causing this inversion was fund to be about 5-6mm by most of the above investigations.

Hibiki and Ishii (2002) states that the bubble size governs the void phase distribution and hence in turn affects the distribution parameter (C_o). This distribution parameter is an important parameter utilized by many drift flux based codes. When turbulence due to liquid is dominant, the small bubbles are pushed towards the wall and concentration of bubbles is smaller in the centerline in such case a wall peaking profile exist ($C_o < 1$). When the coalescing starts, there is an increase in diameter of bubbles causing a migration of large bubbles towards the center of the core. In presence of these large bubbles, the so called core peaking occurs, where the distribution of bubbles at the centerline is higher than near the wall ($C_o > 1$). For uniform distribution of void across the diameter, the distribution parameter is near to unity since centerline velocity and the average velocity are same ($C_o \approx 1$).

Guet *et al.* (2003) suggested that size of bubble influence the transitions from bubbly to slug flow. The test performed with three different gas inlet configurations, a cone injector (with 4mm holes) produced large diameter bubbles (between 1-20mm) showed an early bubble-to-slug transition than the other two porous injectors where due to smaller bubble sizes (mean size of 3.5 or 4mm) the transitions was delayed. It was further found that the size of the bubble generated also influence the lifting of fluid, see Figure 2.7. Smaller bubbles have lower rise velocity in the liquid than larger one and hence average void fraction in the pipe is higher for smaller bubble than for larger bubbles at the same gas injection flow rate. The concept was proposed for designing the well gas injectors to enhance the oil production from the well.

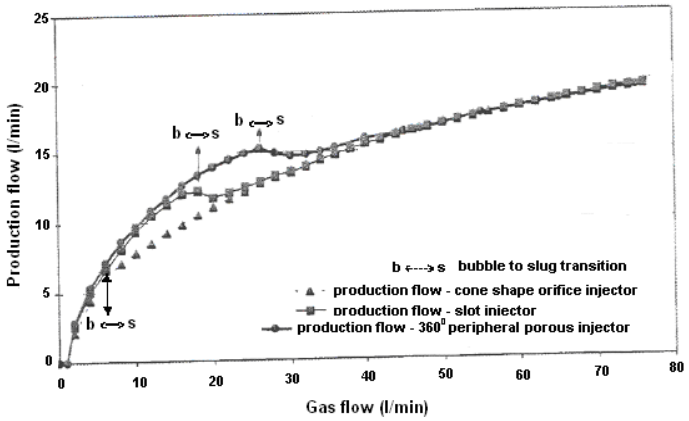

Figure 2.7 Comparison of the injection devices in 72mm diameter pipe (Guet *et al.*, 2003).

Hewitt (1982) observed that physical properties and operating conditions also greatly affect the two phase flow behaviour especially the void fraction and flow pattern via viscosity, surface tension and system pressure. Generally, it has been observed that the pressure of the system not only changes the void fraction but it also changes the void fraction profiles. At higher pressures smaller bubbles are formed increasing the overall void fraction with more uniform/flat void phase distribution. However research on the effects of physical properties and operating conditions are rare especially concerning the void phase distribution.

2.2 Literature Review on the Large Diameter (D ≥ 100mm) Studies in the Past

This section summarizes the studies that have been undertaken on the topic of large diameter vertical pipe in last few decades. General outline of the experiment conducted and the parameters involved are mentioned in Table 2.1. Further on these studies outcome can be found in later sections.

The oldest work on the topic large diameter was by Hills (1976) on recirculating column of 150mm. The typical bubbly flow and churn/froth flow was noticed in experiments. It was found that the experimental data did not collapse on straight line of drift flux relation, hence two drift flux relation were proposed, same form as Zuber and Findlay, valid for $j_l \leq 0.3$m/s and $j_l > 0.3$m/s based on the experimental data.

Table 2.1 Literature survey conducted on large diameter vertical upflow pipes

Researcher	Year	Fluid system	Pipe diameter (mm)	L/D	$j_{g\ max}$ (m/s)	$j_{l\ max}$ (m/s)	Systems Pressure (MPa)	Bubble Injection Method	Flow regime observed
Hills	1976	Air - water	150.0	70.0	0.62-3.5	0.5 - 2.6	0.1	Vertical pipe at the center of test section at the base	Bubbly, Large bubbles with froth and Churn
Shipley	1984	Air - water	457.0	12.34	5.0	2.0	0.1	Cross shaped sparger	Bubbly
Clark and Flemmer	1986	Air - water	100	10	-	-	0.1	-	Bubbly, Large cap bubbles
Hashemi *et al.*	1986	Air - water	305.0	9.41	1.16	0.06	0.1	Air injection before elbow in horizontal run	Bubbly, Large bubbles, Churn and Annular
Hirao *et al.*	1986	Steam- water	102.3	-	1.0	4.0	0.5,1.0 and 1.5	Sintered metal tube	Bubbly, Large bubbles with froth and Churn
Ohnuki and Akimoto	1996	Air - water	480	4.2	0.02 - 0.87	0.01 - 0.2	0.1	Sinter inlet and Nozzle at inlet	Uniform bubbly, Agitated Bubbly, some Cap bubbles and Churn
Cheng *et al.*	1998	Air - water	150.0	70.0	1.113	1.25	0.1	Sparger cap at the base of Riser	Bubbly, occasional Cap bubbles, and Churn
Hibiki and Ishii	2000	Nitrogen - water	102.0	53.9	0.286	0.387	0.1	No horizontal section	Bubbly, occasional Cap bubbles, and Churn
Ohnuki and Akimoto	2000	Air - water	200.0	61.5	4.7	1.06	0.1	Porous sintered tube cap	Uniform bubbly, Agitated Bubbly, Churn-bubbly, Churn-slug and Churn-froth
Shoukri *et al.*	2000	Air - water	100 and 200	43.0	0.02 - 15.5	0 - 1.8	0.1	Circular disc of shower head geometry	Bubbly , Churn and Annular
Hibiki and Ishii	2001	Nitrogen - water	102.0	53.9	0.146	0.198	0.1	With horizontal section	Bubbly, occasional Cap bubbles, and Churn
Prasser *et al.*	2002	Air - water	200 mm	-	0.037 - 1.30	1.0	0.1	Conical perforated head	Uniform/ agitated bubbly and Churn
Sun *et al.*	2002	Air - water	112.5	106.7	0.122	0.011 and 0.15	0.1	-	Bubbly, Distorted cap bubbly and Churn
Oddie *et al.*	2003	Nitrogen - water	150.0	73.33	1.57	1.57	-	through pipe in inlet plenum	Bubbly, elongated bubbles and Churn
Sun *et al.*	2003	Air - water	101.6	40.0	0.502	0.058 - 1.03	0.1	Three Sintered spargers units	Bubbly, occasional Cap bubbles, and Churn
Omebere *et al.* (VERTIGAL)	2004	Nitrogen - Naphtha	189.0	264.5	4.0	15.0	2.0 and 9.0	Vertical pipe in the center of the base & pipe in base with side outlet only	Bubble, Churn and Annular
Our Experiment -1	2004	Air - water	254.0	46.0	4.44	3.0	0.1	Tee and Annular sleeve	-

Shipley (1984) performed two phase experiments in 457mm in diameter and 5.64m high Perspex vertical pipe of. The rig was operated with air-water at superficial velocities of 5 and 2m/s respectively. The air was introduced into the riser by cross-shaped sparger to give uniform distribution. Void fraction measurements were made and drift flux correlation was proposed. Although flow regimes were not reported, some recirculation details were put forward where large bubbles were being carried upward while small were carried downward by the liquid near the wall. Since the length-to-diameter ratio (L/D) of the rig was small, it is likely that the data included the end effects and may not be true representative of the actual conditions.

Van der Welle (1985) conducted experiments at atmospheric condition for air-water in 100mm internal diameter test section. The air was injected into the vertical pipe with some 600 ferrules. The data set consisted of void fraction ranging between 0.25 - 0.75 combined with 5 set of liquid superficial velocities i.e. 0.9, 1.3, 1.7, 2.1 and 2.5 m/s. The local measurements of bubble diameters, void fraction and bubble velocity were done by using resistivity probe. Core peak void fraction (parabolic) profile was found in the investigation for above set of conditions. Bubble diameters were measured and some of the results indicated the presence of large bubbles however the paper does not provide any information regarding the flow patterns observed in the experiments.

Clark and Flemmer (1986) performed experiments in vertical pipe of internal diameter 100mm with mixture volumetric fluxes from 0.7 to 2.7 m/s. The work was performed on air-water system. The experimental work reports bubbles of various sizes ranged between 1.5 to 5mm in diameter with occasional large cap bubbles forming in the pipe. They found severe discrepancies of distribution parameter when comparing with literature and reported that traditional drift flux model do not apply on the large diameter vertical pipe upflow and hence proposed two drift flux relations.

In the same year, Hirao *et al.* (1986) also published their experimental work using a 102.3mm diameter vertical pipe. The experiments were conducted with the steam-water to simulate the thermal hydraulic transient's behaviour of PWR. Similar to Shipley (1984) and Clark and Flemmer (1986), a clear linear relationship of drift flux was not observed in their analysis, which probably also the reason of proposing three separate drift flux relations. They further reported that with steam as gas phase no typical slug flow was observed but rather distorted and frothy flow including many small bubbles was observed because of the reduced effects of surface tension.

Hashemi *et al.* (1986) studied the effects of diameter on the two phase flow regimes and liquid carryover in model of PWR using air-water has working fluid. The tests were to investigate the two phase flow characterization in PWR, performed at atmospheric pressure, using air-water flow in 305mm diameter and 3m high vertical pipe (L/D = 9.8). At lower air-water flow rates the flow was mainly bubbly with occasional large bubbles causing local recirculation. At higher flow rates, flow progressed to churn flow rather than slug flow found in smaller diameter tubes at same mass fluxes. Their results were in reasonably good agreement with Zuber-Findlay correlation for void fraction prediction.

Next study on the large diameter preformed by Hills (1993) on the same set as in 1976. The gas and liquid superficial velocity were in the range 0.07-3.5 m/s and 0-2.7 m/s. The primary aim of this work was to measure the void phase distribution, thus two air injection devices; an open ended pipe in the middle of the base and a sparger cap (with 60 × 3.1mm holes) were used to introduce the air in liquid flow up the column. The phase distribution was found to be core peak in all cases, with little variation in shape as gas and liquid rates vary. This was attributed to the large bubble sizes produced by the gas distributor. No sign of wall peaking, even under high liquid-low gas conditions was observed. Further to above, bubbly flow with large bubbles in core at low j_g and churn turbulent flow at high j_g was observed and the presence of liquid recirculation near the wall below $j_l < 0.5$m/s was also reported. This recirculation of liquid caused some of the bubbles to circulate near the wall causing the uniform bubbly flow to transform into agitated bubbly. It was further suggested that wall peaking may be less pronounce in larger diameter pipes with even small bubbles because of the weak liquid velocity gradients.

Ohnuki *et al.* (1995) performed experiments on vertical pipe of 480mm diameter with (L/D = 4.16) using air-water as working fluid. The air was injected through porous sinter rectangular section in the base of the vertical pipe. The experimental data consisted of the visual flow observations, void phase distribution and local liquid velocity measurements. Although the length-to-diameter ratio (L/D) for these experiments is small to consider the flow to be fully developed but even under small L/D, the void fraction distribution was rather flat profile for uniform bubbly flow while a core peak was observed for other cases. In the experimental range of air-water superficial velocities bubbly flow, agitated bubbly flow and churn bubbly flow were observed. No slug flow was reported in these experiments.

In 1996, Ohnuki and Akimoto studied the flow structure of developing flow by using two injection methods, a nozzle injection and porous sinter method in the same setup. Similar to previous study uniform bubbly, agitated bubbly and churn bubbly were reported on a flow pattern map, see Figure 2.8. No slug flow was realised in the experiments regardless of the air injection method and the agitated bubbly flow observed due to the consequences of the downward motion of the liquid as this liquid flowing downward was almost negligible in the uniform bubbly flow. A distorted phase distribution was found near the base of the test section of both injectors due to the location of the air injection devices, however a clear core peak was found at the middle and the top irrespective of the air injection methods. The main drawback of this study is that data collected was sparse in the region of transition from bubbly to agitated bubbly flow regime.

Hasanein *et al.* (1997) experimental results are for steam-water two phase flows in large diameter vertical pipe of 508mm diameter and 4m height at elevated pressure of 2.8MPa (230°C) and 6.4MPa (280°C). Similar to Ohnuki and Akimoto (1995 and 1996) agitated bubbly, churn bubbly and annular flows were reported. The slug flow was never observed in either of the pressure conditions. Void fraction measurements preformed in the study were satisfactorily compared with the drift flux model for large diameter pipes proposed by Kataoka and Ishii (1987).

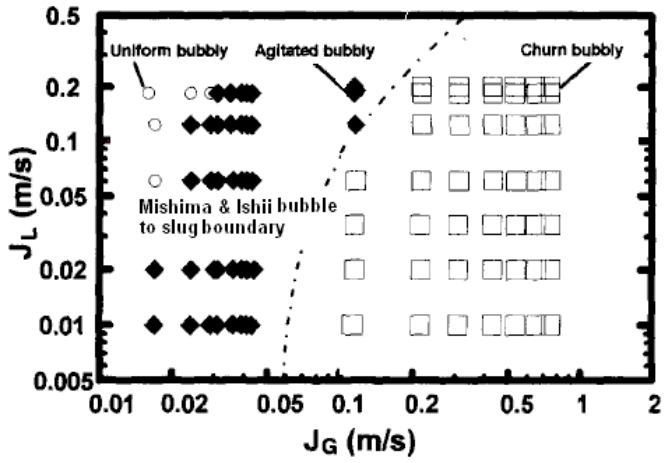

Figure 2.8 Ohnuki and Akimoto (1996) data on Mishima and Ishii (1984) flow map.

Cheng *et al.* (1998) performed experiments with a view to investigate the internal flow structure of upward air-water flow especially near the bubble to slug transition. The experiments was performed on same setup as used by Hills (1976 and 1993) and compared with 28.9mm diameter column. Absence of traditional slug flow and transition from bubbly into churn flow via occasional cap bubbles with liquid near the wall moving randomly upward and downward was reported. It was further noted that in 150mm experiments, the flow regime transition from bubbly to churn flow was smoother in comparison to bubble to slug flow transition in 28.9mm column, where a sudden transition was observed, suggesting that the transition was associated with void fraction wave instabilities.

Ohnuki and Akimoto (2000) experimental study was based on the transitions of flow patterns, void phase distribution and bubble sizes in upward air-water two phase flow in 200mm diameter, 12.3m height vertical setup. The slug flow was never observed rather undisturbed bubbly, agitated bubbly, churn bubbly, churn-slug and churn flows were reported from visual observation, see Figure 2.9. It was found that the bubbly flow in large diameter pipe is likely to be agitated and the area of so called wall peak distribution on Serizawa and Kataoka void distribution map is higher and narrower for the experimental boundary for 200mm diameter pipe locates under lower j_g and higher j_l than for smaller scale pipes. The distribution can be seen in the Figure 2.10(a) for the large diameter pipe. It was also observed that the transition of void phase distribution is due to the change of flow pattern with core peak profile occurring at high j_g and wall peak at low j_g. The wall peak was not pronounced as observed in small diameter pipes due to the larger turbulent dispersion force and lower radial velocity gradient of water. From Figure 2.10(b), it can be seen that void fraction near the wall in the large diameter (200mm) pipe has not exceeded over 0.1

and the transition from wall peak has started and core peak is attained under j_g of 0.26 m/s. On the other hand the void fraction near the wall in the small diameter (38mm) pipe is over 0.3 and the wall peak is maintained under almost the same flow rates as for the core peak case in large diameter pipe.

Shoukri *et al.* (2000 and 2003) in collaboration with AECL Canada performed experiments in support of a new passive emergency cooling system design in CANDU reactors. The cooling system consisted of large diameter vertical pipes thus requiring detail assessment. The test section consisted of two transparent risers of 100 and 200mm diameter and with 5.5m and 10m height. The study presented the flow patterns, phase distribution, bubbles sizes and interfacial area concentration results. Taitel *et al.* (1980) flow regime map was found to predict their experimental flow patterns transitions satisfactorily. In their experimental condition slug flow was never observed. The area-averaged void fraction data were correlated using the drift-flux model. Shoukri *et al.* (2003) validated the Ohnuki and Akimoto (2000) phase distribution results while performing experiments on 100 mm and 200 mm diameter pipes. For low area averaged void fraction ($\alpha < 0.04$) in both vertical pipes, the wall peak was typically encountered in comparison to small diameter pipes. As the gas flow rate was increased the profile changed gradually to core peak. In all churn flow tests the observed phase distribution was core peak in nature with peak at the centre increasing with increasing the average void fraction. The values for the interfacial area concentration were higher in large diameter pipes when compared with data obtained under the same flow conditions in small pipes.

Sun *et al.* (2002) performed studies on 112.5mm diameter vertical pipe of 12m in height. By analysing the void fraction waves and its instability they proposed that slug is formed due to increase in void fraction waves by coalescence of bubbles clusters from unstable bubbly flow. The slug formation is associated with certain critical frequencies that rapidly increase the void fraction waves causing merger of bubble clusters into slugs. The study further explained that at high volume fluxes, slug formation is suppressed due to the intense turbulence and formation vortex in the liquid phase. This intense turbulence is associated with boundary condition and hence do not exist in smaller diameter pipe due to the restraint of the walls.

Next validation study was conducted by Hibiki and Ishii (2003) for the drift flux model application in nuclear-reactor transients and accidents. It was found that due to diameter effect, liquid recirculation present causes the drift velocity and the distribution parameter to be different in comparison to the small diameter pipe. Two types of inlet-flow-regime dependent drift–flux correlations at low mixture volumetric flux were proposed. At high mixture volumetric flux, Kataoka and Ishii (1987) and Ishii (1977) correlations were recommended. Hibiki and Ishii (2003) also found that no Taylor bubble existed and explained that large Taylor slug bubble can not be sustained due to interfacial instability and thus disintegrates into smaller bubbles.

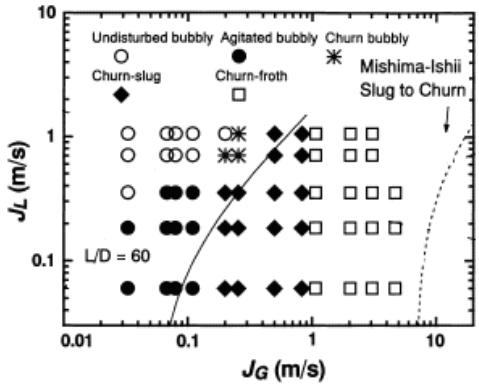

Figure 2.9 Ohnuki and Akimoto (2000) data on Mishima and Ishii (1984) flow map.

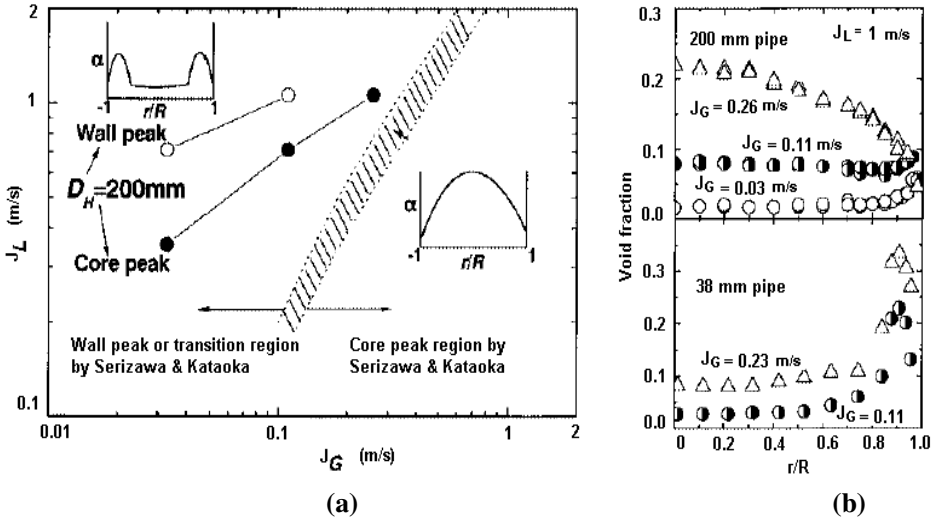

(a) **(b)**

Figure 2.10 Comparison of phase distribution according to flow regimes in 38 mm and 200 mm diameter pipe (Ohnuki and Akimoto, 2001).

Sun *et al.* (2003) performed experiments in 101.6mm diameter pipe reported that no slug bubbles was observed, instead a flow regime in which large cap bubbles with chaotic motions was noticed. These bubbles were formed around average void fraction of around 0.18-0.20.

Oddie *et al.* (2003) performed the steady state and transient experiments with kerosene oil/tap water and nitrogen in a 150mm diameter and 11m long transparent inclinable test section. The tests were conducted with large number of varying flow rates and inclinable positions measuring hold-up and visually observing the flow patterns. For vertical orientation only bubbly and large elongated bubbles with distorted surfaces and irregular shapes were reported. The work aimed at providing

the data for improving the drift flux model for large diameter pipe application in multiphase simulator Eclipse.

Prasser *et al* (2002) of Institute of Safety Research, Rossendorf (Germany) performed experiments at their TwO Phase FLOW (TOPFLOW) Test Facility consisting of a vertical test section of 9m height and 194mm inner diameter. A non conventional bend of perforated conical head in the vertical pipe base was used for air was injection. This study provided information of bubble size distribution and advanced visualization of the flow structure by use of wire mesh sensor (tomography). The bubble size investigations with air-water flows were compared with 51.2mm diameter vertical upflow. Only two flow patterns bubbly and churn turbulent flow was reported, it was found that with increasing superficial gas velocity, large bubbles appeared in the flow that grew rapidly gaining irregular structure. The Figure 2.11 compares the flows encountered in large diameter pipe (200mm) with smaller diameter (51.2mm) pipe. The figure is constructed from wire mesh tomography and indicates the various flow regimes encountered with an increase in air superficial velocities at constant water superficial velocity of 1m/s.

The Figure 2.12 shows the high spatial and temporal resolution analysis of air-water in 194mm diameter pipe. The use of the novel wire mesh technique allowed the large deformed bubble in highly turbulent core to be visualized for the first time that was otherwise obstructed by irregular swarms of small bubbles in periphery. The figure also shows that there is no similarity of these large distorted bubbles with traditional smooth Taylor bubbles. Their shape was analyzed by separating individual bubbles from the three-dimensional measuring information of the wire-mesh sensors (Figure 2.12b & c). At the given high air flow rate (Figure 2.11, case b), the bubble was found to be about 0.66m tall.

The study done by Prasser *et al.* (2002) further indicates that the bubble size distribution in the pipe of D = 200mm is similar to the bubble size distribution in pipe of D = 50mm showing a bimodal distribution. The Figure 2.13 shows that for smaller diameter pipe, a second peak appears that corresponds to slug flow region (presence of Taylor bubbles) where the large bubble fraction shows equivalent diameters which are greater than the pipe diameters. At similar gas velocities where slug flow is seen in smaller diameter pipe, large diameter (D = 200mm) pipe shows bubbles of the much larger than the smaller pipe while their contribution to the overall all gas fraction (peak height) is smaller and appearing much broader. This implies that in large diameter pipes, large bubble of equivalent size of diameter does exit but due to the obstructed view by small bubble swarm around periphery and high turbulence at their interface they are not clearly visible

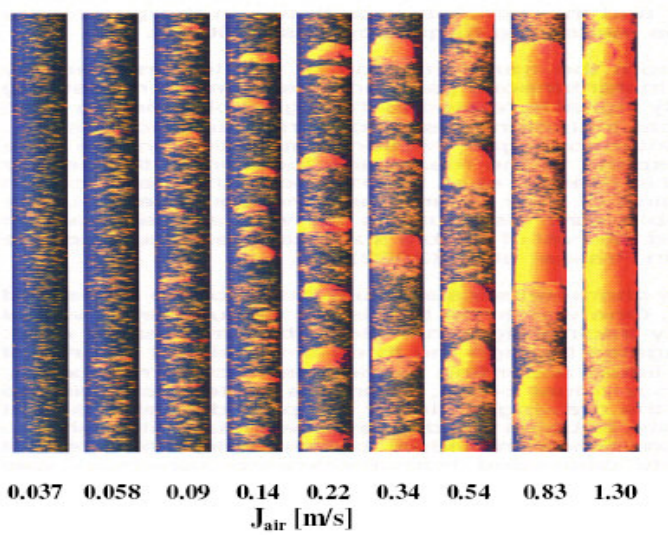

(a)

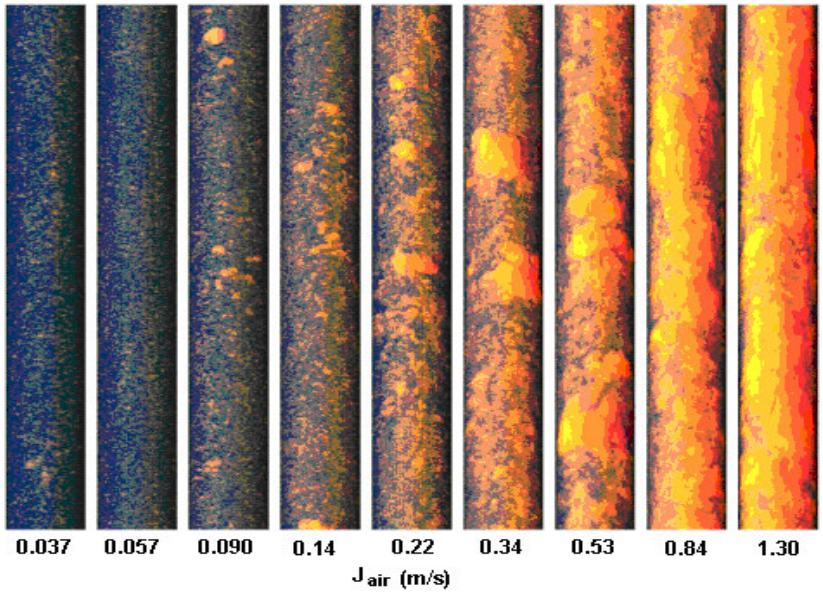

(b)

Figure 2.11 The flow patterns in (a) 51.2mm and (b) 200mm diameter pipe taken with wire mesh tomography (Prasser *et al.*, 2002).

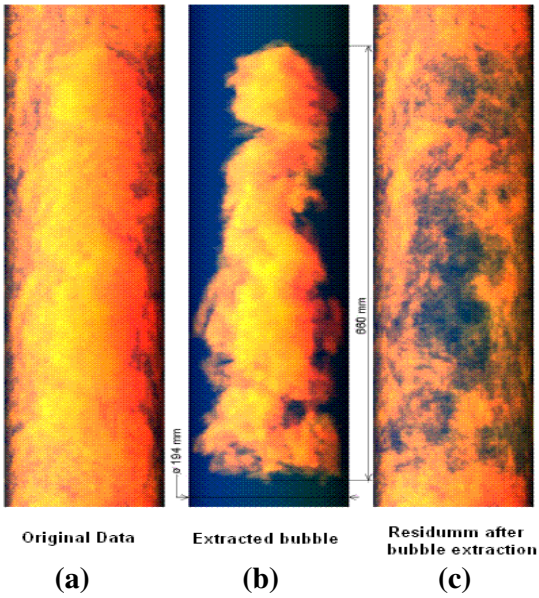

Figure 2.12 The extraction of a large bubble from the signal of the wire-mesh sensor at j_g = 1.3 m/s and j_w = 1 m/s (Prasser *et al.*, 2002).

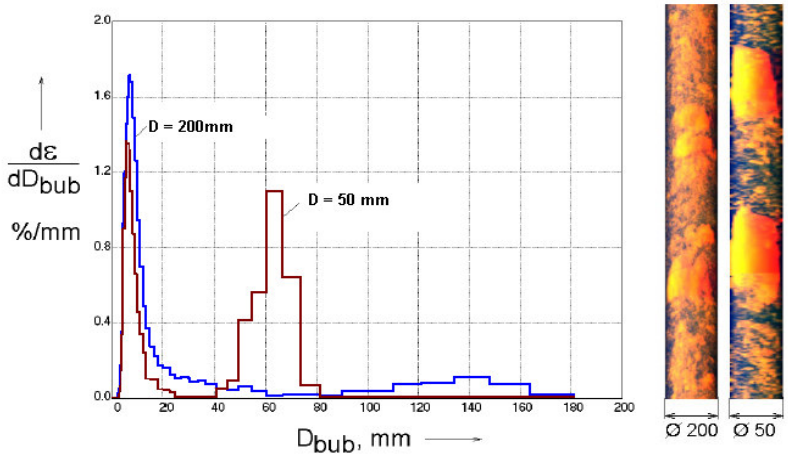

Figure 2.13 Comparison of bubble size distribution in 200 mm and 50 mm diameter pipe at j_g of air = 0.53m/s and j_l = 1m/s (Prasser *et al.*, 2002).

The evolution of the gas-liquid structure in a large vertical pipe of 194mm diameter was presented Prasser *et al.* (2007). This work allowed the study of bubble coalescence and break-up due to the evolution of bubble size distributions. Significant differences in the lateral migration of bubbles of different size were observed with measured bubble size resolved radial gas fraction. The influence of the physical

properties of the fluid was studied by comparing steam-water tests at 65bar with air-water experiments. It was found that the steam-water flow at high pressure produces smaller size bubbles than air-water at ambient conditions. However a bimodal bubble-size distribution was still observed characterizing larger bubble and small bubble sizes with narrower distribution than seen with air-water.

Shen *et al.* (2006) characterize the flow patterns and phase distribution patterns under the same setup as Ohnuki and Akimoto (2000) for various flow conditions. The flow regimes in this work were categorized into undisturbed bubbly, agitated bubbly, churn bubbly, churn slug and churn froth by visual observations. The two phase void phase distribution characteristics were identified as either core peaked or wall peaked. It was found that for most of the above flow regimes the void phase distribution was core peak and only for the undisturbed bubbly flow, a wall peak was found. The concept of skewness was used to quantitatively distinguish the two-phase distribution patterns, apart from proposing an empirical correlation. It was found that the measured void fraction profiles, bubble sizes, their frequencies and interfacial area concentration, all follow same distribution. With changes in flow regime, the bubbles lengths and their sizes also changes causing a larger bubble size distribution.

Recently, Omebere-Iyari *et al.* (2007) performed experiments at SINTEF facility, Trondheim (Norway) on 189mm diameter and 50m high riser with nitrogen-naphtha at 20 and 90bar. As the system is high pressure facility, visual observation of flow pattern was not possible and had to be deduced from objective indicator method of probability density function of void fraction. The flow patterns deduce for above ranges of velocities were bubbly, intermittent, semi annular and annular flows. The comparison of experimental flow pattern transition with existing models failed to yield satisfactory predictions, see Figure 2.14(a). The Figure 2.14(b) shows the proposed modification to the Taitel *et al.* (1980) bubble to slug transition model, however it should be noted that above modification still could not predict the transition accurately below $j_l < 0.1$m/s. The slug flow characterized by twin peaks in PDFs corresponding to liquid slug and the Taylor bubble at low to intermediate void fraction was not observed. Instead, a sharp twin peak existed at mean void fraction greater than 0.58, this was classified by them as intermittent flow not slug flow. However, Matsui (1984) found similar twin peaks of void fraction in their smaller diameter pipe experiments and suggested this behaviour due to liquid dominant portion or aerated slug longer than the gas dominant portion. It should be noted that the working fluids employed, were used to simulate the offshore oil and gas as the surface tension of naphtha and nitrogen is fairly close to that of crude oil-natural gas at above pressures (Fuchs and Brandt, 1989). It is due to reduce surface tension and high gas density effect the two phases will exhibit a bubblier flow and transition from bubbly flow will be delayed. This effect may partly explain the observed behaviour of twin peak behaviour at higher void fraction in comparison to that observed with air-water. Moreover, as the bubble coalescence could not be suppressed for long, ultimately transition will take place and hence large bubble will be formed, however the small bubble population will remain high thus a high peak (lower void fraction) corresponds to highly aerated liquid slug (of small bubbles) and the small peak due the comparatively low in number coalesced bubbles at higher void fraction.

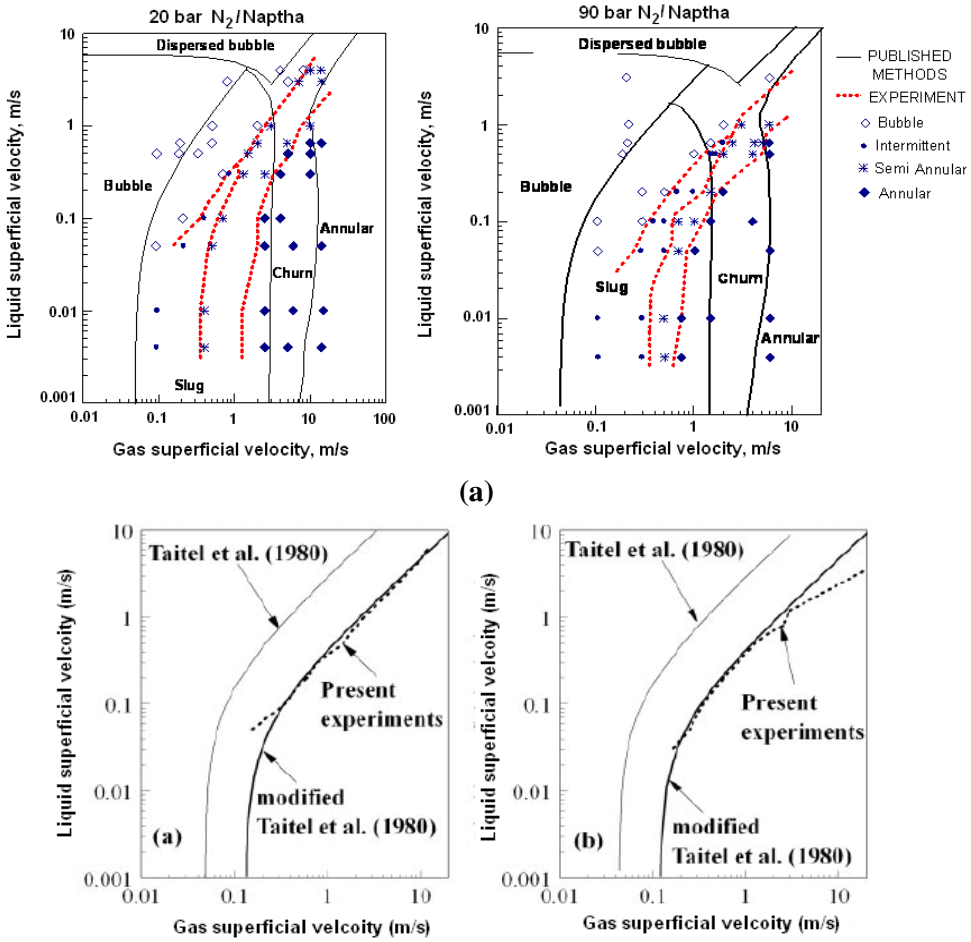

Figure 2.14 Omebere-Iyari *et al.* (2007) data on (a) Taitel *et al.* (1980) flow map and (b) modified bubble to slug transition.

Lastly, Omebere-Iyari *et al.* (2008) work is based on comparison between the results from the above 189mm diameter (SINTEF facility) nitrogen-naphtha data and 194mm diameter (TOPFLOW) steam-water results. The work compares the flow patterns, phase distribution etc. under the same physical properties and phase velocities. In 194mm steam-water experiments, bubbly flow and churn turbulent flow was reported while for nitrogen-naphtha bubbly, intermittent and annular flows were found. The average void fraction with nitrogen-naphtha was found to be higher due to the difference in physical properties of the liquid phase than that of the steam-water. The void phase distribution comparison indicated a core peak signifying the presence of large distribution of bubble sizes for the steam-water while flat void phase distribution profiles representing more uniform and narrow bubble size distribution was analytically deduced for the nitrogen-naphtha. The Figure 2.15 shows the flow pattern map for 194mm diameter vertical pipe showing bubbly to churn turbulent transition prediction by Taitel *et al.* (1980) and modified Taitel *et al.* (1980) model.

Note that former model bubbly to slug flow criteria could not define the experimental transitions. The modified criteria of critical void fraction = 0.38 (from steam-water experiments) was only able to define the transition at higher liquid superficial velocities.

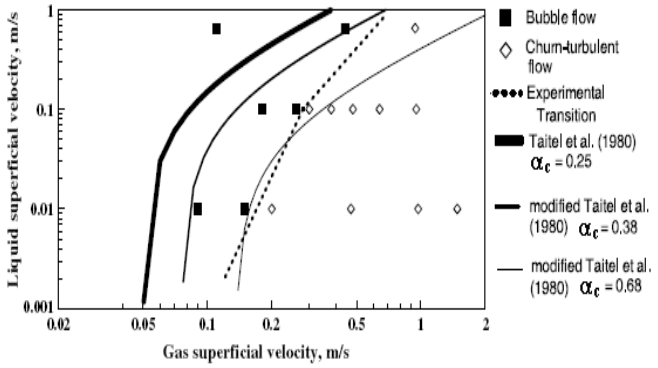

Figure 2.15 Omebere-Iyari *et al.* (2008) data on Taitel *et al.* (1980) flow map.

2.3 Application of Vertical Pipe in Offshore Flowline-Riser system

Multiphase phase flows application in vertical, horizontal and inclined pipes is not just confined to land but is also widely used in oil and gas exploration in sea where the recovered hydrocarbon fluids flow through a well to the top facility. In many of these remote offshore areas the oil & gas from different deep sea wells are combined through many flow lines and than transported via a single pipe or a set of pipelines (vertical or slightly inclined) frequently called the riser(s) to main topside facility (Schmidt *et al.*, 1981). As the last section of the piping network is essentially a riser, it needs to be positioned in such a way that it can stabilize itself as it is the main coupling between the topside and subsea facilities. And it is the need of this stabilization that has resulted in different riser configurations, refer to Figure 2.16. Thus the selection of the particular riser type is dictated by the depth and nature of water current gradients (Yeung and Montgomery, 2002). Deep sea currents along with substantial motion of the vessel/floating facility can induce vibrations of different intensity that can aggravate the hydrodynamic behaviour in the riser system. Moreover with large riser height, temperature variation along the height becomes larger resulting in wax/hydrate formation. To complex the situation more, the reservoir itself is likely to experience changes in flow rates, GOR and water cut during the operating life (Yeung and Montgomery, 2002). Thus during this path from deep sea well to topside facility, the fluid will experience geometry changes, inclination, compositional and temperature variation etc. that will affect the flow pattern and flow characteristics (Kang *et al.*, 2000). All above changes will affect the performance of the offshore production system resulting in considerably higher

CAPEX and OPEX. Hasanein and Fairhurst (1998) estimated a riser cost to be around US$20 to US$30 million in North sea water depths of 350 to 500m whereas in 2005, the costs for a riser system in deep seas was quoted to be around $70 million (Matar *et al.*, 2008). This means that riser system cost will increase with depth, severe environment, reservoir characteristics, number of risers and vessel motions.

Among all the above issues faced by the industry, prediction of the internal hydrodynamic behaviour of the flowline-riser is the most challenging task as it needs to be constantly addressed throughout the lifetime of the field. In particular, the most significant issue of hydrodynamic behaviour to be dealt is the unsteady cyclic flow phenomenon that results in large amplitude and long duration instabilities causing serious detrimental effects like reduction in production and damaging the topside facility. The problem has been observed from the beginning of near-shore exploration days but has aggravated over the time for longer flowlines and risers at greater water depths.

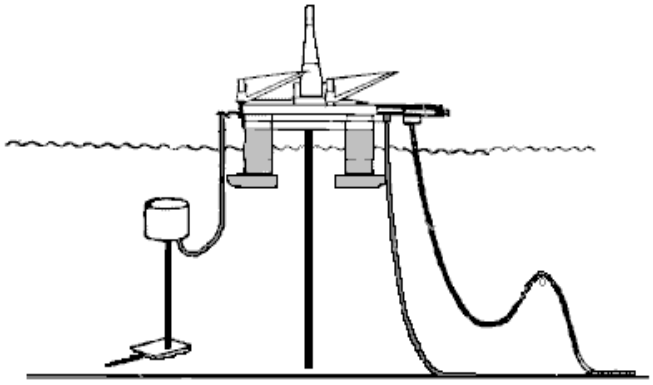

Figure 2.16 Figure depicting some of the deep water riser shapes.

2.3.1 Unstable cyclic flow

Usually the unstable/cyclic instabilities arise because of the configurations at the riser base (downward inclined or undulating pipe or complex riser shape) and production flow hydrodynamics like at start-up of the system or at the end of the well life; when system experiences flow fluctuations resulting from normal and or low flowrate production conditions. These instabilities arising in the flowline-riser system can be classified as either severe slugging (also called terrain induced slugging) or hydrodynamic slugging (normal slugging).

Different definitions are given by researchers to define severe slugging (Schmidt *et al.*, 1985; Taitel, 1990; Fabre *et al.*, 1991), however mainly the severe slugging is defined as the slugging set in the system when liquid accumulates at low points in the flowlines or in riser base due to downward inclination or complex riser shape. This

scenario sets up the cyclic production of liquid slugs that are either equal or longer than riser height with large amount of liquid and gas delivery in the separator. However, the severe slugging generally occurs at low liquid and gas flow rates and requires the flow pattern to be stratified in flowline that leads to undesirable cyclic operation. All riser types experience severe slugging; however generally the phenomenon is explained with respect to the vertical riser (Schmidt *et al.*, 1985; Taitel, 1986; Fabre *et al.*, 1991), for severe slugging in various riser types, refer to (Tin, 1991; Jansen *et al.*, 1996 and Yeung and Montgomery, 2002).

The Figure 2.17 explains the severe slugging phenomenon with respect to downward inclined flowline-vertical riser. According to the Pickering *et al.* (2001), the phenomenon becomes evident with pressure fluctuations becoming cyclic in nature along with alternate arrival of gas-liquid production at the topside facility. It was further explained that the "first phase of the cycle called slug formation takes when the base of the riser become blocked with liquid preventing free passage of gas. The pressure in the pipeline then increases as more liquid runs down to the base of the pipeline increasing the size of the liquid slug. The system remains 'stable' until the pressure has built sufficiently to overcome the gravitational head associated with the liquid slug. The system is then hydrodynamically unstable and the liquid slug is discharge rapidly up the riser followed immediately by a gas surge as the pipeline blows down. The pressure in the pipeline then returns to a low value, leading to insufficient gas velocities to carry the liquids up the riser, and the whole process is repeated".

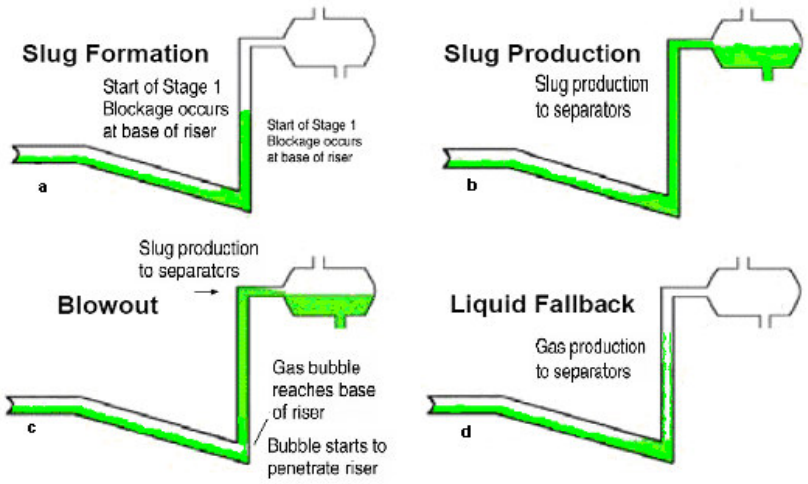

Figure 2.17 Schematic of Severe Slugging in Flowline Riser Systems (Pickering *et al.*, 2001)

The slugging characterized as hydrodynamic slugging is because of the slug formation in the flowline that travels up the riser. Under this flow condition, liquid slugs generated in the flowline flow almost unchanged through the riser pipe (Schmidt *et al.*, 1981), which in turn prevents the generation of a liquid slug at the base of the riser pipe. However, analysis of two phase flow tests in large diameter flowlines of (304.8 and 406.4mm) at Prudhoe Bay field demonstrated that normal slug flow in large and very long flowlines can yields liquid slugs that are longer than expected from normal slugging or transition to slugging i.e. almost longer than a riser pipe height (Brill *et al.*, 1981). Although these slugs lack the spontaneous vigorous blowout that is characteristic of severe slugging, they can be problematic of upstream processing facilities as they also results in unstable cyclic pressure and flow rate fluctuations.

Whether its severe slugging or hydrodynamic slugging in case of long and large flowlines, these unstable cyclic flow conditions will cause periods of no gas and liquid production in the topside separator with cyclic arrival of high liquid and gas flow rates. Such cyclic fluctuation in pressure and flowrates causes the topside separator to over flow and shutdown, reducing the production from the field while gas arrival surges can make flaring operation difficult (Pots *et al.*, 1985; Jansen *et al.*, 1994; Jansen *et al.*, 1996).

In conclusion, a great economical potential can be achieved if above cyclic flow instabilities can be eliminated or reduced. Thus in order to mitigate the harmful effects that these unstable cyclic flow causes to subsea oil production, a number of solutions have been proposed.

2.3.2 Methods to eliminate/ reduce unstable cyclic flows

Although many alternatives exist to avoid/reduce the flow related instabilities, generally accepted criterion is to mitigate severe slugging. Several methods have been suggested to mitigate severe slugging by various investigators which are summarised by Sarica and Tengesdal (2000) namely; Back pressure increase, Choking, Gas lift, Splitting of flow into dual or multiple streams, Use of mixing devices at the riser base, Subsea separation, External bypass line, Coiled tube packers in the pipeline and Foaming. According to Montgomery (2002) many of techniques seek to prevent severe slugging either by preventing liquid accumulation or fall back at the riser base or imposing stable flow in the riser through the application of back pressure from the separator. Here in this report the emphasis is on gas lift technique. Before discussing the gas lift technique in detail in reminder of the work a brief overview of all other the techniques are given below.

Back pressure increase method was found to eliminate the severe slugging by increasing the system pressure, however, this was accompanied by the reduction in the production capacity. Yocum (1973) has reported that flow capacity reduction of up to 50% have been observed in order to minimise slugging on offshore platforms. This is due to the increase in the back pressure of the systems until a flow regime was

reached in which slugging and pressure fluctuations were reduced to level that can be handled by topside facility.

Choking was found to be effective in increasing the back pressure, as it resulted in increasing the velocities in the riser. This action prevents the spontaneous blow out of the liquid column from the riser by increasing the pressure drop through the riser (Montgomery, 2002). However, Schmidt *et al.* (1980) outlined that a careful choking is needed in order to minimize the backpressure. For deep water systems the back pressure increase could be even more important due to potential production losses (Sarica and Tengesdal, 2000).

Johal *et al.* (1997) suggested that RBGL apart from being expensive due to high CAPEX may also pose additional problems due to Joule Thompson cooling of injected gas at control valves and thereby encouraging wax and hydrate formation and thus requiring hydrate inhibition. Therefore Multiple Riser base Lift (MRBL) was more suitable choice. MRBL is based on diverting the stable multiphase flow stream to the nearest pipeline riser system experiencing severe slugging. The study claimed a considerable savings in CAPEX alone compared to RBGL.

Use of mixing devices such as helices or impact mixing barrel at the riser base was also put forward by Yocum (1973) for temporary mixing the partially stratified flow at the entrance to the riser.

Song and Koba (2000) suggested the subsea separation of phases thereby eliminating the severe slugging. The limitation of the technique is requirement of two separate flow lines and a liquid pump to over come the hydrostatic head to pump the liquid to the surface.

Tengesdal *et al.* (2003) suggested a self lifting slug-elimination technique by having an external bypass line. The purpose of this external bypass line was to transfer the flowline gas to a point above the riser that will result in not only reducing the flowline pressure but also reducing the hydrostatic head in the riser, thus decreasing the severity or mitigating the severe slugging by maintaining the a stable two phase flow in the riser.

Fairhurst (2004) suggested the use of coiled tube within the production tubing as an option for mitigating severe slugging. This arrangement will result in closer contact with the incoming fluid, thus the temperature difference between injected gas and production fluid will be small thereby reducing flow assurance problems. Moreover coiled tube could be used to inject the gas at various chosen depth typically near the riser base. The tube could be removed for pigging operations. However this option is still not being applied for practical situation.

Hasanein and Fairhurst (1998) suggested foaming as an option for mitigating severe slugging but this idea requires foaming agents. Fairhurst (2004) further suggested that foam lift by injecting foams at or near the base of the riser concept will allow more

efficient lifting to produced fluids as well as provide high compressibility regions in the flow that will help in dissipating the slug energy.

Apart from above methods and devices offering mitigation of unstable flows, several feedback control strategies are developed allowing the system to operate at stable production rate when within the unstable production region. This includes the small scale display of Schmidt *et al.* (1979) and large scale demonstration of Hedne and Linga (1990) using topside choking to control the pressure at the riser base with a simple PI feedback control scheme. Nowadays several companies like Shell and ABB have developed more sophisticated slug control systems (S^3 system and SlugCon etc.) for handling unstable flows especially slug flow control.

In above, the Shell Severe Slugging Suppression (S^3) system looks extremely useful for mitigating the surging experienced as it combines the principle of a slug catcher with active control. Shell Global Solutions licensed the S^3 to Dril-Quip, which holds the rights to marketing, manufacture and sale of the product. In this patented slug control system, the multiphase flow is separated to gas and liquid in a mini separator. The gas and liquid flows out of the mini separator separately in a controlled manner. The mini separator level and pressure are automatically controlled with fast response separate gas and liquid valves. This method has demonstrated to suppress several kinds of slug flow. The system was initially tested on an air-water test loop consisting of a 100m pipeline and a 15m riser and been shown to reduce severe slugging. After these preliminary tests, the system has been successfully deployed under field conditions on the Shell (UK) Gannet-Alpha platform (Central North Sea) also. The recent installations of this slug suppression system include the GOM (Na Kika). The Na Kika field is the deepest subsea cluster in the world for oil and gas production in the GOM in the water depths range from 1,770m to 2,360m. The field consists of the two loops namely, the North production loop and the South loop employing steel catenary risers (Fairhurst, 2004). The production systems feature an advanced slug control (gas lift, surface slug suppression device, automated process controls, dynamic modelling), a coiled tubing gas lift for start-up and production enhancement and an enhanced produced water treatment. The production from the field began in December 2003 (Offshore Technology, 2009).

2.3.3 Gas lifting

Although various methods are available for elimination of flow instabilities, usually combination of various methods are employed. These include combination of gas lift and choking via properly developed control schemes. The technique originated from gas lift in wells where the gas is injected to increase the production flow and thereby reducing the back pressure (Montgomery, 2002). In gas lifting for severe slugging, gas is injected either into the flowline or at the riser base that results in lowering the riser base pressure and hence reducing the hydrostatic head in the riser and liquid fall back. A steady flow is generally achieved when very large amounts gas has been injected. This in turn will stabilize the unstable production and minimise the slug sizes arriving on topside.

With the above benefits, gas lifting also possesses limitations i.e. for deep waters there is an increased frictional pressure loss and Joule-Thompson cooling. Both these potential problems are the direct result of high injection gas flow rates (Tengesdal *et al.*, 2003). Additionally gas lifting requires a large space on the platform for associated equipment and a large amount of gas (Pots *et al.*, 1985). Yocum (1974) and Schmidt *et al.* (1985) also emphasised that the operational cost of gas lifting can be very significant. In fact, Yocum (1973) suggested that the gas stream from the separator can be re-injected at the base of the riser to increase the velocity and create a uniform bubbly flow solely in the riser resulting in considerable savings.

Pots *et al.* (1985) showed the influence of riser base supplementary gas lift with the help of small scale experiments. It was concluded from the experiments that the quantity of gas required for stabilizing still remains either equal or greater than the amount supplied from flowline inlet gas supply. Apparently this near riser base injection is still not able to eliminate the severe slugging but the injected gas simply broke the long liquid slug into manageable pieces. Results for gas injection in the riser further indicated that with 300% of flowline inlet gas, the cyclic behaviour of liquid slugs still persisted.

For gas lifting, two possibilities exist for gas injection location: gas can be injected into the base of the riser, or it can be injected into the flowline. Among all the alternatives for gas injection position Riser Base Gas Lift (RBGL) has become more popular as method for elimination of riser flow instabilities, reduction of well head pressure and for the start-up (Jansen *et al.*, 1994). A RBGL system is normally incorporated within subsea field development to (1) minimise unstable pressure and flow fluctuations resulting from normal and or low flow rate production conditions (2) minimise severe slugging due to a domination of riser configuration and production flow hydrodynamics (3) minimise back pressure on wells through the reduction of static pressure head and start-ups instability.

Hill (1990) performed a detailed analysis on the effects of gas injection on severe slugging. The tests were conducted on a 50m long flowline with 50mm diameter, inclined by 2º downward towards the riser base ending on a 15m high vertical riser with air and water as the working fluid. From the work, it was found that only after injecting large amount of gas, the severity of severe slugging reduced. However, for continuous lift of liquid from the base, the flow regime had to be brought to annular flow in the riser. It was also shown that gas injection for lifting at riser base will allow smooth start-up of the systems that have shut down along with more continuous production.

Jansen *et al.* (1994) verified the results of Hills (1990) with comments that a large amount of injected gas (several times larger than gas inlet rates) is needed to completely stabilize the system as compared to the flowrate of gas in the flowline. The experimental worked indicated that gas lift only provides stability when the flow pattern in the riser is brought to annular flow, only small degree of the stability was achieved along the liquid superficial liquid velocity.

2.4 OLGA – *the multiphase flow simulator*

2.4.1 Introduction

As oil and gas field development moves further and further into deep seas, maximizing hydrocarbon recovery at an acceptable cost is one of the greatest challenges facing the industry today. Thus the design and operation of deep offshore recovery systems are therefore crucial in terms of CAPEX and OPEX. For such critical application, much optimised designs are needed; therefore use of the transient multiphase flow simulators plays an important role. These simulators are not only used for the designing of recovery systems and prediction of their expected operational behaviour, but are also used for flow assurance in existing facilities.

Nowadays many transient multiphase flow simulators like OLGA, PROFES and TACITE are commercially available for the oil and gas industry. However, over the time it is observed that these codes fall short in predicting the correct behaviour of larger diameter piping system (Pickering *et al.*, 2001). This may be firstly, due to the computer codes being based on empirical data and phenomenological information derived from small diameter pipe observations and secondly, the scarcity of the field and experimental data of large diameter vertical riser system.

In this work, OLGA multiphase simulator will be reviewed as among all the above simulators, OLGA is claimed to have been developed for flows in large diameter (189mm) risers.

2.4.2 OLGA – The code

OLGA (OiL' and 'GAs') is an extensively used multiphase simulation tool that has jointly been developed by IFE and SINTEF. All most all of the work involving OLGA simulator has been focused on the field applications e.g. oil and natural gas flowlines or transportation lines, wet gas or condensate pipelines, well stream from a reservoir, LNG/ LPG pipelines, dense phase pipelines, network of merging and diverging pipelines, artificial lift and other mass source injections, pipelines with process equipment, topside process systems. The simulator is broadly applied to design stages as well as to simulate various scenarios of above industries like start-up and shutdown transients, terrain slugging, variable production rates, pigging, artificial lift etc. The initial data for code development and validation came from small diameter SINTEF flow loop (OLGA-1983) but for later versions the data was collected from the 189mm SINTEF flow loop which includes a 500m flowline and 52m high riser. Later the simulator was also verified from the experimental work done in Tulsa University, USA on a 30m long flowline and 15m high riser (Bendiksen *et al*, 1991; Schmidt *et al.*, 1980).

The OLGA simulator is available as OLGAS and OLGA version5.3. The OLGA-S incorporates only steady state processor while OLGA-5 is the complete one-dimensional, extended two-fluid model transient computational code with full

functionality available for above scenarios. OLGAS is a steady state mechanistic flow model that has been developed alongside with the standard OLGA. The steady state model is developed on the basis of the test data supplied by operating companies over a number of years and calculates flow patterns, void fraction/liquid hold-up along with pressure gradients at a particular section of pipe. The code is extensively used in a number of leading commercial steady state simulators such as PIPEPHASE, PIPESIM, Pipeflow, NetSim, METTE, UniSim and HYSYS (OLGA, 2007).

The OLGA code is of propriety nature and hence not much detail regarding the mathematical equations and closure relations are available in public domain. Only paper presenting the overview of the code is of Bendiksen *et al.* (1991), below are the mathematical formulations of equations taken from the publication.

2.4.2.1 The Equations

The OLGA solves seven (7) equations; three (3) separate continuity equations for bulk liquid, gas and liquid droplets in gas, two (2) momentum equations with one for liquid and one for combined gas and liquid droplets in gas, lastly a (1) combine mixture energy conservation equation. All of the above equations are related to each other with closure relationship to friction factors and/or wetted parameters depending upon the flow regime.

Continuity Equations

- The gas phase equation:

$$\frac{\partial}{\partial t}\left(V_g \rho_g\right) = -\frac{1}{A}\frac{\partial}{\partial t}\left(A V_g \rho_g v_g\right) + \psi_g + G'_g \qquad 2.43$$

- The bulk liquid phase equation:

$$\frac{\partial}{\partial t}\left(V_l \rho_l\right) = -\frac{1}{A}\frac{\partial}{\partial t}\left(A V_l \rho_l v_l\right) - \psi_g \frac{V_l}{V_l + V_g} - \psi_e + \psi_d + G'_l \qquad 2.44$$

- And equation for the liquid droplet within gas phase:

$$\frac{\partial}{\partial t}\left(V_D \rho_l\right) = -\frac{1}{A}\frac{\partial}{\partial t}\left(A V_D \rho_l v_D\right) - \psi_g \frac{V_D}{V_l + V_D} + \psi_e - \psi_d + G'_D \qquad 2.45$$

In the above equations V_g, V_l, and V_D are the volume fraction of gas (subscript as g), liquid (subscript as l) and liquid droplets (subscript as D), A is the pipe cross sectional area, ψ_g is the mass transfer between the phases, ψ_e and ψ_D are entrainment and deposition rates and G' is the mass source.

Momentum Equations

- The gas phase equation:

$$\frac{\partial}{\partial t}\left(V_g \rho_g v_g\right) = -V_g\left(\frac{\partial P}{\partial z}\right) - \frac{1}{A}\frac{\partial}{\partial z}\left(AV_g \rho_g v^2{}_g\right) - \lambda_g \frac{1}{2}\rho_g |v_g| v_g \cdot \frac{S_g}{4A} \qquad 2.46$$
$$+ \lambda_i \frac{1}{2}\rho_g |v_r| v_r \cdot \frac{S_i}{4A} + V_g \rho_g \cos\theta + \psi_g v_a - F_D$$

- Equation for the liquid droplets is:

$$\frac{\partial}{\partial t}\left(V_D \rho_l v_D\right) = -V_D\left(\frac{\partial P}{\partial z}\right) - \frac{1}{A}\frac{\partial}{\partial z}\left(AV_D \rho_l v^2{}_D\right) + V_D \rho_l g \cos\theta \qquad 2.47$$
$$- \psi_g \frac{V_D}{V_D + V_l} v_a + \psi_e v_i - \psi_d v_D + F_D$$

- Equation for the liquid at the wall:

$$\frac{\partial}{\partial t}\left(V_l \rho_l v_l\right) = -V_l\left(\frac{\partial P}{\partial z}\right) - \frac{1}{A}\frac{\partial}{\partial z}\left(AV_l \rho_l v^2{}_l\right) - \lambda_l \frac{1}{2}\rho_l |v_l| v_l \cdot \frac{S_l}{4A}$$
$$+ \lambda_i \frac{1}{2}\rho_g |v_r| v_r \cdot \frac{S_i}{4A} + V_l \rho_l g \cos\theta - \psi_g \frac{V_l}{V_l + V_D} v_a - \psi_e v_i + \psi_d v_D \qquad 2.48$$
$$- V_l d(\rho_l - \rho_g) g \frac{\partial V_l}{\partial z} \sin\theta$$

Combining equation 2.45 and 2.46 cancels the term gas/droplet drag term and equation becomes:

$$\frac{\partial}{\partial t}\left(V_g \rho_g v_g + V_D \rho_l v_D\right) = -\left(V_l + V_D\right)\left(\frac{\partial P}{\partial z}\right) - \frac{1}{A}\frac{\partial}{\partial z}\left(AV_g \rho_g v^2{}_g + AV_D \rho_l v^2{}_D\right)$$
$$- \lambda_g \frac{1}{2}\rho_g |v_g| v_g \cdot \frac{S_g}{4A} - \lambda_i \frac{1}{2}\rho_g |v_r| v_r \cdot \frac{S_i}{4A} + \left(V_g \rho_g + V_D \rho_l\right) g \cos\theta \qquad 2.49$$
$$+ \psi_g \frac{V_D}{V_l + V_D} v_a + \psi_e v_i - \psi_d v_D$$

In above equations 2.46 to 2.48, θ is the angle of the inclination from the vertical, P is the pressure, d is the droplet deposition, S is the wetted perimeter, v_r is the relative velocity, λ is the friction coefficient for gas (g), liquid (l) and interface (i). Here an

assumption is made that internal source G'_f is assumed to enter at 90º angle to the pipe and hence does not carry any net momentum, so that:

- When $\psi_g > 0$, the evaporation from the liquid film gives $\nu_a = \nu_l$, and
- When $\psi_g > 0$, the evaporation from the liquid droplets gives $\nu_a = \nu_D$.
- For $\psi_g < 0$, the condensation gives $\nu_a = \nu_g$.

The conservation equations can be applied to all possible flow regimes; with certain terms dropping out from above equation for certain flow regimes. Next slip equation defined that consists of relative velocity, ν_r:

$$\nu_g = R_D(\nu_l + \nu_r) \qquad 2.50$$

In above equation R_D is the distribution slip ratio caused by an uneven distribution of the phases and velocities across the pipe cross section. Like wise above equation for the droplet velocity is defines as:

$$\nu_D = \nu_g - \nu_{OD} \qquad 2.51$$

Here ν_{oD} is the fall velocity of the droplets. Next before discretizing the equation in the differential form, OLGA reformulates it obtain the pressure equation, thus solving this equation with momentum equations and allowing the stepwise time integration.

Equations 2.42-2.44 are expanded with respect to pressure, temperature and composition assuming the densities is function of $\rho_f = \rho_f$ (p, T, R_s). Where R_s is gas mass fraction and is given by:

$$R_s = \frac{m_g}{m_g + m_l + m_D} \qquad 2.52$$

Now expanding the equation 2.42-2.44 and dividing them with the phase densities and summing them up together and applying $V_g + V_l + V_D = 1$ yields single equation for pressure and phase fluxes.

$$\left[\frac{V_g}{\rho_g}\left(\frac{\partial \rho_g}{\partial p}\right)_{T,Rs}+\frac{1-V_g}{\rho_l}\left(\frac{\partial \rho_l}{\partial p}\right)_{T,Rs}\right]\frac{\partial p}{\partial t}=-\frac{1}{A\rho_g}\frac{\partial\left(AV_g\rho_g v_g\right)}{\partial z}$$
$$-\frac{1}{A\rho_l}\frac{\partial\left(AV_l\rho_l v_l\right)}{\partial z}-\frac{1}{A\rho_l}\frac{\partial\left(AV_D\rho_D v_D\right)}{\partial z}+\psi_g\left(\frac{1}{\rho_g}-\frac{1}{\rho_l}\right)+G_g\frac{1}{\rho_g} \qquad 2.53$$
$$+G_l\frac{1}{\rho_l}+G_D\frac{1}{\rho_l}$$

In above equation (2.52), the phase mass transfer term ψ, if taken as function of pressure, temperature and composition, then can be obtained from expansion by Taylor series, so $\psi_f = \psi_f$ (p, T, R_s), where R_s is gas mass fraction given by equation 2.54.

Energy Equation

In equation (2.53) below, E is the internal energy per unit mass, H_s is the enthalpy from the mass source, U is the heat transfer from the pipe walls and m=v.ρ.

$$\frac{\partial}{\partial t}\left[m_g\left(E_g+\frac{1}{2}v_g^2+gh\right)+m_l\left(E_l+\frac{1}{2}v_l^2+gh\right)+m_D\left(E_D+\frac{1}{2}v_D^2+gh\right)\right]=$$
$$-\frac{\partial}{\partial z}\left[\begin{array}{l} m_g v_g\left(H_g+\frac{1}{2}v_g^2+gh\right)+m_l v_l\left(H_l+\frac{1}{2}v_l^2+gh\right) \\ +m_D v_D\left(H_D+\frac{1}{2}v_D^2+gh\right)\end{array}\right]+H_s+U \qquad 2.54$$

To close the above set of the equations closure relation are needed i.e. liquid wave height, interfacial friction, liquid wall friction, gas wall friction, droplet entrainment, droplet deposition, droplet velocity, slug bubble velocity, gas fraction in the liquid slugs and the distribution slip in slugs. All these closure relations are propriety nature so no information is available about them.

From above, a set of coupled first order, nonlinear, 1D partial differential equations with complex coefficients is obtained. The concept of control volume (or mesh cell) approach is used to solve the staggered spatial mesh where pressure, energies, and void fraction are defined at the cell center and velocities are defined on the cell boundaries. First momentum equations are solved together with pressure equation with masses and temperatures from previous time step. Next mass equations are solved with above new pressure and velocities and finally energy equation is solved for the mixture temperature.

2.4.2.2 Flow regime and its transitions

Flow regimes in OLGA are defined as distributed and separated flows. Distributed flows are that contains bubble and slug flow and separated flows contains stratified

and annular mist flow. The criterion for existence of particular flow regime e.g. like separated flow is based on wave height calculation. For wave height it is assumed that if the wave height is less then certain value the flow is stratified smooth otherwise it is stratified wavy. For the transition between stratified or annular, if the wetted perimeter of the liquid film becomes equal to film inner circumference, then its annular flow regime else it's stratified. For distributed flow it is assumed that wave height needs to be greater then the liquid film thickness such that surface tension is then unable to maintain wave stability and breaks into droplets leading into dispersed flows.

In OLGA the friction factor and wetted perimeters depends upon the flow regime while transition between the distributed and separated flow regime are based on the assumption of continuous average void fraction and is determined according to a minimum slip concept i.e. the flow regime yielding minimum gas velocity is chosen (Bendiksen *et al.*, 1991). It is to be noted here that OLGA predicts the flow in terms of numeric values that correspond to the different flow regimes namely Stratified Flow = 1, Annular Flow = 2, Slug Flow = 3 and Bubbly Flow = 4.

2.4.2.3 Fluid Properties

OLGA code uses a tabular form fluid property file generated in PVTSim software which is generated before OLGA is run. The actual values in time and space are calculated by OLGA through interpolation. The mixture composition is assumed constant in time along the pipeline allowing the gas and liquid composition to change with pressure and temperature as result interfacial mass transfer.

2.4.2.4 Slug tracking module

OLGA code has also recently added a module of slug tracking that is activated as restart file after slug flow regime is identified in flowline. The module provides statistics of slug i.e. number of slugs, length, positions etc. However in current work, this module is not explored as the objective was to determine the applicability of OLGA code to distinguish the flow regimes and to be able to predict the riser base behaviour satisfactorily.

2.4.3 Literature Review on OLGA

OLGA ('OiL' & 'GAs') code is jointly been developed by IFE and SINTEF, Norway. The simulator is widely applied to design and operational problems e.g. start-up and shutdown transients, terrain slugging, variable production rates, pigging, gaslift etc. The code is based on 1D, extended two-fluid model and is available as steady state point model (OLGAS) and, as complete transient computational code (OLGA). The basic mathematical formulation of the code can be found in Bendiksen *et al.* (1991). Although the use of OLGA since its commercialization in 1983 has been continuously expanding, very limited publications can be found in open access discussing its performance, below is a brief literature review available on code.

Bendiksen *et al.* (1980) benchmarked the code against the published data of flow regimes by Barnea *et al.* (1980) and terrain slugging predictions from Schmidt (1979) experimental data. The code was validated with some 3500 experiments from the 189mm SINTEF Two-Phase Flow pressurised loop (20 to 90bar) with naphtha/diesel/lube oil and nitrogen between 1983 and 1986 (Bendiksen *et al.*, 1986). The code predicted both types of terrain slugging as well as the boundary to stable flow of these benchmark experiments closely. Klemp (1988) presented the practical design experience with the OLGA code demonstrating the steady state versus dynamic simulation results, terrain slugging, shut-in and start-up operations and temperature transients, by using actual field data. Bendiksen *et al.* (1986) provided a case study of terrain slugging and its successful elimination by choking at the riser outlet. Bendiksen *et al.* (1991) compared the code with SINTEFF data, Vic Bilh-Lacq field data and Schmidt *et al.* (1980) data. While the former two field case simulations predicted the trends successfully, in the latter, an over prediction of flowline and under prediction of riser base pressures was seen in the simulations, see Figure 2.18. Note in the figure that OLGA over predicted the flowline pressure cycle but under predicts the riser pressure.

Burke *et al.* (1992) compared the field results of a North Sea oil flowline with the OLGA. A good match between the OLGA and the field data was found after fine tuning the fluid and heat transfer properties. Straume *et al.* (1992) compared the standard code performance with the slug tracking option in the standard code for severe slugging flowline-riser systems case. A large deviation in the prediction of liquid holdup in the riser base was reported for the standard code in comparison to the latter. Vigneron *et al.* (1995) compared his data with the predictions of the three leading codes OLGA, PLAC and TUFFP. The codes did not yielded satisfactory results indicating that further work was needed to obtain better predictions. Dhulesia and Lopez (1996) critically evaluated five mechanistic models including OLGA using 5952 data from four separate experimental facilities with pressures to 90bars, with real hydrocarbon fluid. The results indicated that TACITE, another famous drift flux based simulator performed better than OLGA. Burke and Kashou (1996) provided a study of field case with OLGA simulation, however the model was fine tuned to obtain closer match. Kashou (1996) simulated the severe slugging trends in S-shaped and catenary riser from the data of the BHRG facility. Although the OLGA did simulate the general severe slugging trends in S-shaped or catenary riser like flow regime, cycle times and slug lengths, the code did not predicted well the steady state production, peak production and pressure cycling characteristic. Xu (1997) demonstrated the successful prevention of severe slugging in Dubar-Alwyn flowline and controlling of hydrodynamic slugging from Hudson field to Tern platform. In another performance assessment performed by Lopez and Suchaux (1998) OLGA and TACITE were assessed with TUFFP data and Bekapai-Senipah pipeline field data. Both the codes successfully simulated the steady state behaviour but the transient behaviour associated with flow rates changes was underestimated by the codes. Song and Kouba (2000) used OLGA for deepwater severe slugging simulation in conventional and S-shaped risers with hypothetical field data.

Yeung and Montgomery (2001) compared the results from three leading transient multiphase flow codes OLGA, PLAC and TACITE with data obtained from S-shaped riser. Many discrepancies were highlighted between the simulated results and the experiments. Putra (2002) simulated the East Java gas pipeline with OLGA. A fine tuning of pipeline flow parameters was performed in simulation to match the field data. Postvoll *et al.* (2002) simulations on Huldra-Heimdal flowline with OLGA real time analysis predicted the pressure drop within 10% of field data after tuning the pipe roughness but the liquid holdup predictions indicated fairly large inaccuracies. Yeung *et al.* (2003) investigated the causes of the deviation of OLGA simulation from experimental results of Yeung and Montgomery (2001). They verified from the experimental data that the code did not predict the details characteristics correctly as the liquid holdup and gas blowdown are over predicted by the code. The code also dissipates slugs much quicker than experimentally observed value.

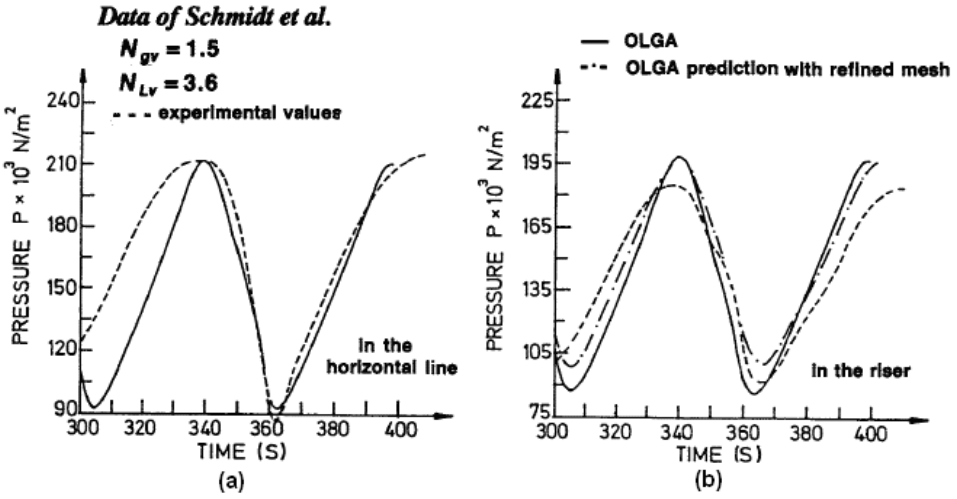

Figure 2.18 Pressure oscillations of severe slugging in horizontal flowline-vertical riser system taken from Schmidt *et al.* (1980) data along with OLGA predictions.

Irfansyah *et al.* (2005) compared Bekapai-Senipah and TCP-CPA 304.8mm diameter pipelines field data with OLGA. The result showed the steady state pressure drop prediction within +8% of the measured value; however, discrepancies in transient simulation of OLGA were noted. Eidsmoen *et al.* (2005) highlighted the modelling aspect of steady state and transient simulation of gas-condensate pipelines. Heskestad (2005) compared the North Sea field results with OLGA. The code highly underestimated the pressure drop and the transients cases also did not perform well. Mehrdad *et al.* (2006) work emphasized the use of OLGA code in the control design phase for reduction or elimination of slugging. A dynamic OLGA model of the SINTEF's Tiller loop was developed and tested against the experimental data. Several control strategies were implemented on the model to suppress the slug generation in the flowline however the application of just controller did not suppress the slug

generation and indeed a combination of choke followed by feedback controller from riser base pressure achieved the slug suppression target. Mokhatab (2007) reported the OLGA2000 simulated results for 10.5 m high, 108.2 mm internal diameter catenary-shaped riser. The work highlighted the severe slugging in a catenary riser, the SS1 was generally predicted but discrepancies were noted between simulated results and experiments for SS2 and slug flow. Also the detailed characteristics of the observed classical severe slugging were also not accurately predicted.

Following aspects are noted from the detailed literature survey aimed to summarise the OLGA code application available in public domain:

- The survey indicates that there are many field examples where the code has been able to produce desired results. However in these works, many available parameters in the code were calibrated to match the results and this has been expressed as the code predictions being satisfactorily.
- The study also indicates that very limited work is available with regard to the code's application in the experimental loops (Schmidt *et al.*, 1980; Kashou, 1996; Yeung and Montgomery, 2001; Yeung *et al.*, 2003 and Mokhatab, 2007). It further indicates that apart from the SINTEFF loop, on which the OLGA validation is based on, the code was unable to demonstrate satisfactory performance (Kashou, 1996, Montgomery, 2002 and Yeung *et al.*, 2003).

2.4.4 Literature review on horizontal flowline-vertical riser

Among earlier researcher, Schmidt *et al.* (1980) work included the experiments on the 30.5m long horizontal flowline with 15.24m high vertical riser having 50.8mm diameter using air-kerosene as working fluid. The experiments were performed in the superficial velocity range of 0.015 to 3.048m/s for liquid with 0.106 to 12.192m/s for gas. Based on the experimental work they also proposed the flow regime maps (±2, ±5 and 0º) using the Duns & Ros dimensionless gas and liquid velocity numbers, see Figure 2.19 for horizontal pipeline-vertical riser system.

Schmidt *et al.* (1980) did not observed severe slugging in horizontal or positively inclined flowline and it was postulated that this phenomena is typical for negative pipeline inclinations only. It further postulated from the experimental work that in order for severe slugging to occur, the flow in the flowline prior to the riser has to be stratified flow. Additionally severe slugging may also occur at the condition of lowest gas flow rate to a liquid rate where slugs are riser generated slugs but of course are of shorter length than riser. It is to be noted that Bendiksen *et al.* (1991) while using Schmidt *et al.* (1980) data to validate the OLGA code illustrates the pressure oscillations of severe slugging typical for horizontal-vertical riser system (see Figure 2.18). Moreover, Brill *et al.* (1981) while experimenting at large diameter flowlines (304.8 and 406.4mm) at Prudhoe Bay field found that slugs formed were longer than expected from normal slugging or transition to slugging. From the behaviour it was

inferred that in case of large diameter flowlines, normal slugs formed could be longer than riser pipe height.

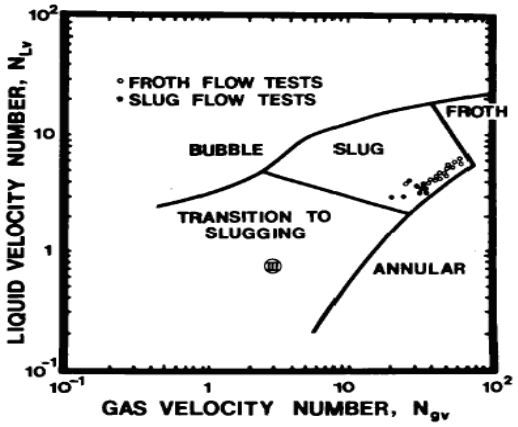

Figure 2.19 Schmidt *et al.* (1980) vertical flow regime map for horizontal flowline-vertical riser system (*Brill et al.*, 1981).

Pots *et al.* (1987) performed experiments on horizontal pipeline-vertical riser system did not found severe slugging with long period cycle at the small scale setup verifying the observation of Schmidt *et al.* (1980) work. However they did observe the irregular severe slugging at the lowest gas-liquid flow rates and attributed this as the failure to keep a complete horizontal flowline topology during the experiments conducted. The flow regime map developed for horizontal-vertical riser is given in Figure 2.20 below.

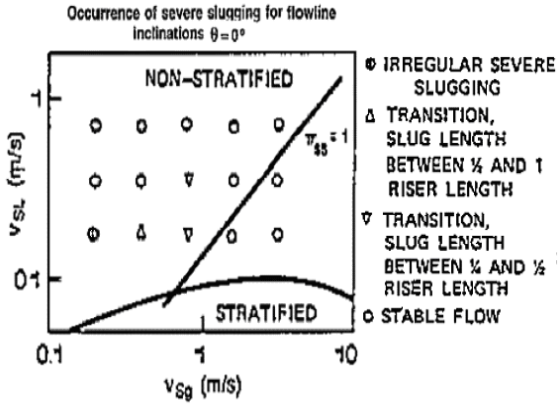

Figure 2.20 Pots *et al.* (1987) flow regime map for horizontal flowline-vertical riser system.

Fabre *et al.* (1990) also performed air-water experiments on a horizontal flowline-vertical riser setup of 25m long flowline and 13.5m high vertical riser, both of 53mm diameters each. Contrary to Schmidt *et al.* (1980) and Pots *et al.* (1987) work, Fabre *et al.* (1990) found severe slugging in the horizontal flowline, refer to Figure 2.21 for the flowline pressure response. Also they did not agree to the definition of severe slugging defined by Schmidt *et al.* (1980) and proposed a broader definition to severe slugging by defining the whole process due to the variations in the flow pattern and in the liquid level of the riser that influences the flowline in setting up these large long period cyclic instabilities. These instabilities have larger amplitude in case of downward inclined pipe then in horizontal pipes with their occurrence corresponding to the stratified flow domain defined by Taitel and Dukler (1976). They concluded that for horizontal orientation, the instabilities occurred below 0.2m/s of liquid superficial velocities while for negative pipe slope it occurred at higher liquid superficial velocity corresponding to a more extended stratified flow regime. Additionally they also inferred that while slug build-up, gas blowdown and liquid fall back does occur in horizontal flowline, the slug production does not exist.

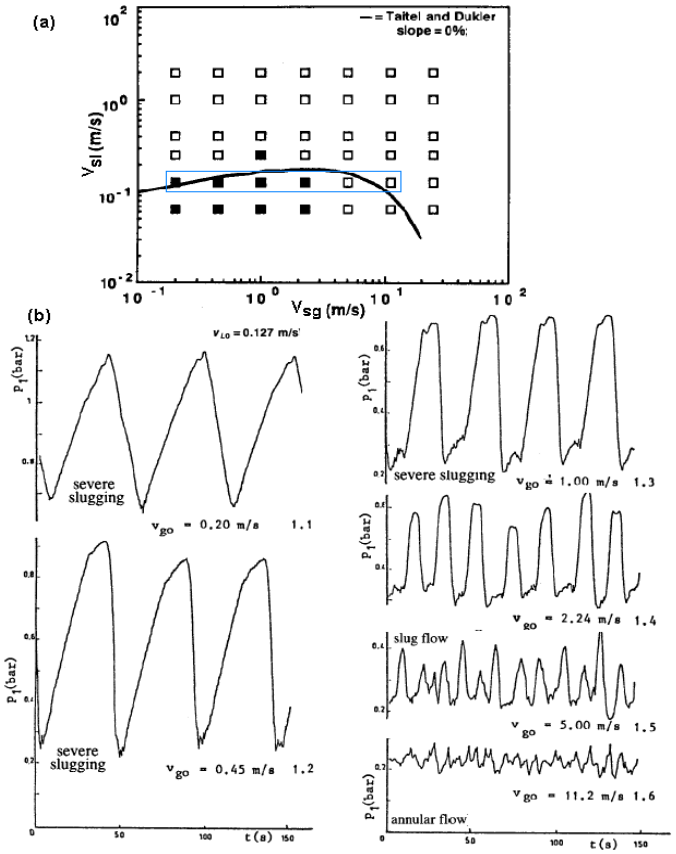

Figure 2.21 (a) Fabre *et al.* (1990) experimental data points on Taitel and Dukler flow regime map (b) flowline pressure response in horizontal flowline-vertical riser system.

Chapter 3

Experimental Facility, Instrumentation and Data Acquisition

This chapter describes the general features of the newly build large diameter riser experimental facility. Its also outlines the instrumentation used, data acquisition, processing and calibration. Finally, the details of the experimental campaign are presented.

3.1 Cranfield University's Large Diameter Experimental Facility

The large diameter vertical riser facility is built in Department of Process and Systems Engineering's laboratory in School of Engineering, Cranfield University.

The large diameter riser facility comprises of water supply circuit and an air supply circuit, vertical/horizontal pipe run before test section, vertical riser test section, upper plenum consisting of overhead/return tank, downcomer and a return line to sump. A schematic of the large diameter riser facility is depicted in Figure 3.1.

3.1.1 Water supply circuit

The water to the rig is supplied from a single phase (water) loop connected to an existing sump in the laboratory area using a Gridlestone 55YA-VLS sump pump (P3) that can produce a maximum flow rate of 546m^3/hr. The flow to the riser is controlled via valve (VW1) and a bypass valve (VW2), downstream of the pump. The water from sump is measured by electromagnetic flow meter (WFM1). The water then passes through a long heavy duty PVC pipeline of 152.4 mm diameter with the different elevations from the ground before finally entering to a 254mm nominal diameter schedule-40 stainless steel pipe at the ground level (near VA5). The further route of water is through a horizontal flowline into the vertical riser, upper plenum, overhead tank, downcomer and back to sump. The detailed photographic views of the whole facility can be viewed in appendix A.

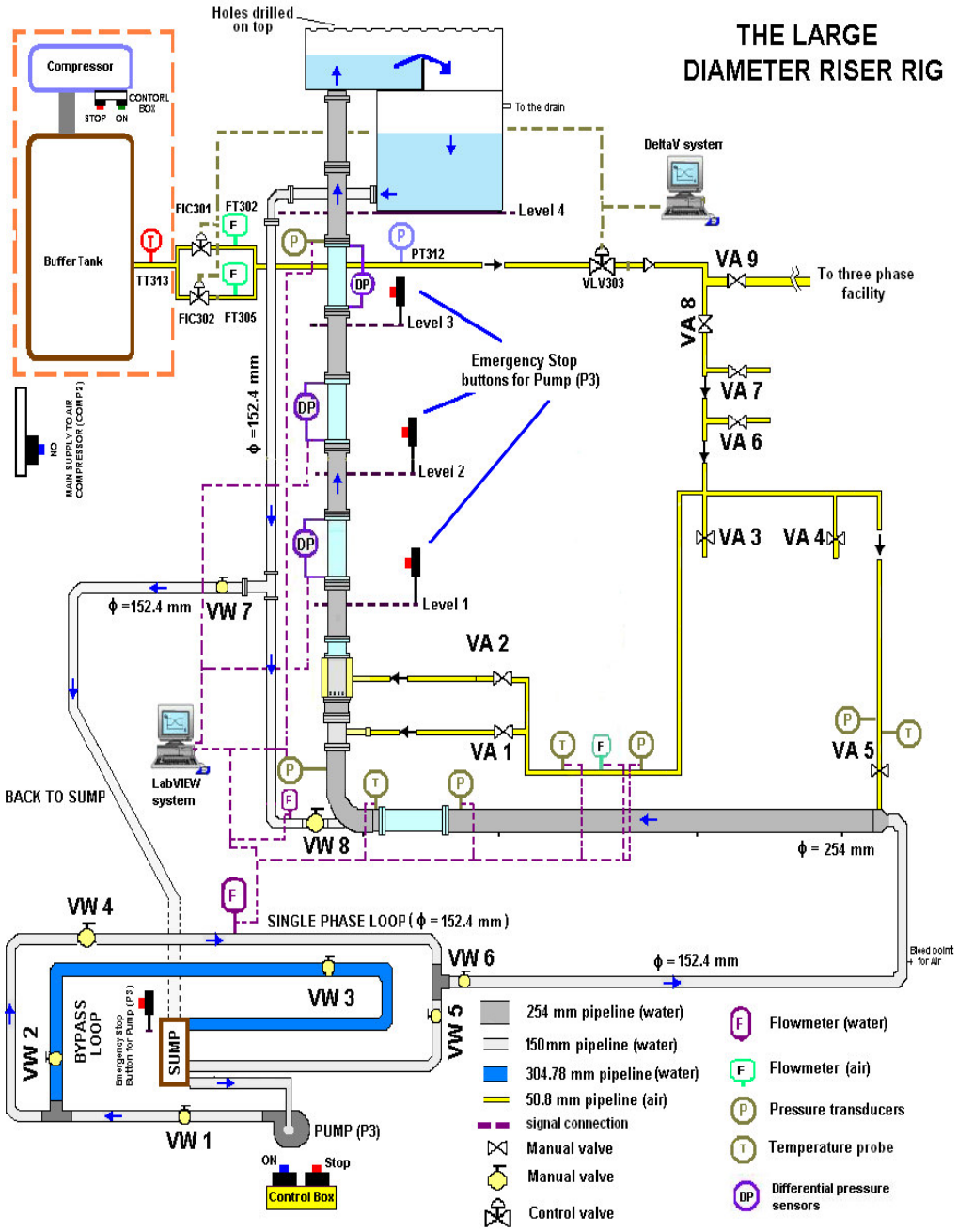

Figure 3.1 Schematic of the large diameter riser facility.

3.1.2 Air supply circuit

The air to the large diameter riser rig is supplied from the compressor of the existing Multiphase flow test Facility. The Atlas Copco Electonikon GA75 compressor delivers air at the maximum flow rate of 1275m^3/hr free air delivery at upto 7 barg. The air from compressor is stored in a 2.54 m^3 buffer (receiver) tank to minimise the pressure pulsations from the compressor. The air flow from the buffer tank is measured by two massprobar flowmeters (FT302 & FT305). The flow to meters is controlled by means of control valves (FIC301 & FIC302) situated upstream from the flow meters. The control valves are managed by DeltaV digital automation system. Air after metering passes through either the 12.7mm (0-100 Sm^3/hr) or 25.4mm (95-1275 Sm^3/hr) pipeline and is delivered to large diameter facility via 50.8mm pipe either near the riser base or at the inlet to horizontal flowline. The valve (VA8) separates the air supply of the Multiphase flow test facility from large diameter riser facility (refer to Figure 3.1).

3.1.3 Test section

The actual test section consists of two parts (a) vertical riser test section, 12.2m in height and (b) a horizontal flowline, 36m in length. Both these sections are 254 mm in diameter. The whole test section is made of combination of schedule-40 stainless steel pipe sections and the clear Perspex sections (see Figure 3.1). The horizontal flowline has one (1) Perspex section installed at approximately 2m before the base of the riser. This transparent section helps in visual observation of the air-water flow exiting the flowline and entering in the riser. The vertical riser section has four (4) transparent Perspex sections installed at different heights for viewing the flow.

3.1.4 Gas injectors

The air to vertical riser is supplied by two air injection devices installed near the riser base namely a Tee and an Annular sleeve injector, see Figure 3.2. The standard Tee injector is a simple 50.8mm diameter pipe attached at 90º to the riser pipe. In comparison to above, the newly design Annular sleeve injector is a 406.4mm diameter injector that act as an encasing to the riser section (254mm pipe) in the centre. The injector's inner core section of 254mm diameter consists of eight (8) holes of 38mm each around the circumference for air entry. This orientation of holes reduces the average liquid level in the encasing when the injection gas is not flowing and ensures that the liquid in sleeve is in motion to avoid erosion. Both the injectors are installed at 1100 and 1460mm from the ground level, refer to Figure 3.3. Apart from above two air entrance points, provision is also made for the air injection at the start of 36m long horizontal flowline, see Figure 3.4 to study the behaviour of two phase flow entering the riser base.

3.1.5 Overhead tank & Downcomer

The air travelling from the riser section is vented to the atmosphere from the upper plenum while water flows from the side of the upper plenum into the overhead tank and than to the downcomer. The upper plenum is simple rectangular tank (height = 0.6m) attached to the riser top to facilitate the air-water separation and to avoid the vortex formation. The downcomer is made up of a 162.5 mm diameter heavy duty PVC pipe offering a flow path either to the sump or recirculating back to the riser at the base via gate valve (VW8). Former is achieved by closing valve VW8 and keeping VW7 opened while in latter, VW7 is kept close and VW8 is opened. In the latter strategy the water flow coming from the downcomer is also measured.

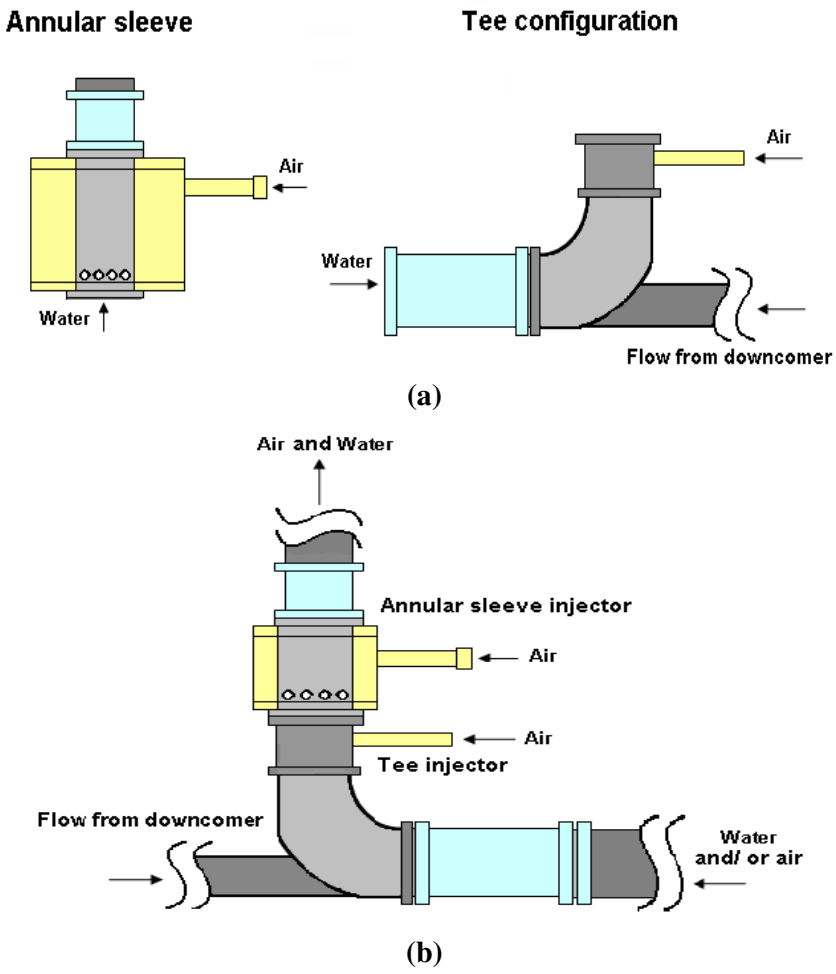

Figure 3.2 (a) The schematic of individual air injectors and (b) the schematic of combined air injectors above the riser base

(a)

(b)

(c)

Figure 3.3 The photographic view of the two gas injectors (a) a simple Tee, (b) newly designed Annular sleeve and (c) the arrangement in the riser section.

(a) (b)

Figure 3.4 The photographic views of (a) the air injection at the upstream of pipeline and (b) Perspex section downstream before riser base for observation

3.2 Instrumentation

This section outlines the details of the instrumentation used to carry out the experimental work. All the instruments along with their ranges and uncertainty are summarized in Table 3.1.

3.2.1 Flowmeters

Two electromagnetic flowmeters were used to measure the water flow rates. The main flow at the inlet to large diameter setup from the sump was measured by Bailey Fischer & Porter XM-2000 series electromagnetic flowmeter that has an accuracy of ±0.5% with minimum and maximum range of 10 to 200 m^3/hr. The water inflow to the riser base from the downcomer path was measured by the ABB MagMaster series electromagnetic flow meter with an accuracy of ±0.2% with minimum and maximum range of 0.50 to14.21 m^3/hr (refer to Figure 3.1 for the arrangements of flowmeters). The later flow meter is connected with serial port of the PC using serial communication RS 232 protocol and serially communicated with the data acquisition system.

Air flow to the large diameter riser rig is measured using two Fischer-Rosemount Mass Probar flow meters. Both the meters provide the volumetric flowrate with an accuracy of ± 1.3% with minimum and maximum ranges of 79 to 4250Sm3/hr and 6 to 100Sm3/hr. The required air flowrate can be set and controlled by flow controllers in DeltaV system through two separate flowlines; low flowrate line and high flowrate line. Apart from the above two gas flowmeters another flowmeter is also installed. This flowmeter is an Endress and Hauser Vortex flow meter with accuracy of ±0.25%. This flowmeter measures the gas flow rate entering in the riser by any of the two

injectors. At this point of gas flow metering, temperature and pressure of gas are also measured.

3.2.2 Pressure Transducers

In all there are three pressure transducers installed in pipeline-riser system. The pressure in the vertical riser test section is monitored through two DRUCK PMP-1400 pressure transducers. The riser base transducer is installed on the test section at 0.88m height from the ground. The top transducer was placed about 1m lower then the exit in order to avoid the exit effects. These transducers are flush mounted, so they do not interfere with the flow. The measurement ranges are 0-2 barg with an accuracy of ±0.15%. Another pressure transducer model no. 249 from RS components Ltd. with the range of 0-6 barg and accuracy ±0.25% is installed near the exit of the horizontal flowline section (near Perspex section) before the riser base to monitor the behaviour of incoming two phase flow in the riser base.

3.2.3 Differential Pressure Transducers

Two DRUCK PMP-4110 differential pressure transducers are also placed in the vertical riser across two of the Perspex sections in the riser. Placement of the differential pressure transducer downstream of the injectors on the Perspex sections allowed visual observation of the flow pattern along with the measured differential pressure. These transducers are placed at approximately 5m and 8m from the ground level. Both the differential pressure transducers have 0-700mbard range with ±0.04% accuracy. Regular flushing from the tappings was performed before each run to prevent the ingress of air and hence affecting the hydrostatic head. Readings of these differential pressure transducers (DP1 & DP2) were used to deduce the void fraction.

3.2.4 Temperature Probes

The temperature of the working fluid (air-water) was also monitored before entering into the vertical riser section. The temperature of the incoming water and air into the riser was measured by digital display temperature Sensor (T0 & T1) & Temperature sensor (T2) of RS components Ltd., having range of 0-100ºC (accuracy of ± 0.5ºC).

3.2.5 Miscellaneous

There were also some miscellaneous instruments like level indicator, pressure gauge and manometer installed at the various locations of the rig. The water level indicator was installed on the top overhead tank while BOSS™ pressure gauge (0-14 bar) was installed at the air inlet to the horizontal flowline. The two manometer tappings were placed across the last Perspex section of vertical riser at approximately10m height.

Table 3.1 Instrumentation ranges and uncertainty

Signal Type	Manufacturer	Range	Accuracy
Volumetric flow rate : water	Bailey Fischer & Porter XM-2000 series electromagnetic flowmeter	25 to 180 m^3/hr	±0.5%
	ABB MagMaster series electromagnetic flow	0.50 to 14.21 m^3/hr	±0.2%
Volumetric flow rate : air	Fischer-Rosemount Mass Probar (1")	79 to 4250 Sm3/hr	± 1.3%
	Fischer-Rosemount Mass Probar (0.5")	0 to 100 Sm3/h	± 1.3%
	Endress and Hauser Vortex flow meter		±0.25%
Pressure Transducers	DRUCK PMP-1400 pressure transducers	0-2 barg	±0.15%
	RS components Ltd. pressure transducer (model no. 249)	0-6 barg	±0.25%
Differential Pressure Transducers	DRUCK PMP-4110 differential pressure transducers	0-0.7 bard	±0.04%
Pressure Gauge	BOSS pressure gauge (model no. BS 80012290)	0-14 bar	± 1.4%
Temperature probes	RS components Ltd thermocouple including digital display	0-100ºC	±0.5%
Video Images & Movies	Fuji FinePix Digital video camera & Webcam	640 x 480 pixels	-

3.3 Data Acquisition

The data signals were acquired through two separate data acquisition systems using two separate PC's namely; DeltaV and LABVIEW. The DeltaV plant automation system was used to obtain the air flow rates delivered from the compressor. The DeltaV system consisted of automatic controllers (FIC301 & FIC302) that controls the air flowrate to the desired flowrate when selected in the DeltaV front panel. Figure 3.5 presents the graphical user interface of DeltaV system. In the figure, the process line coded orange colour indicates the setup path for air flow from compressor to the test facility.

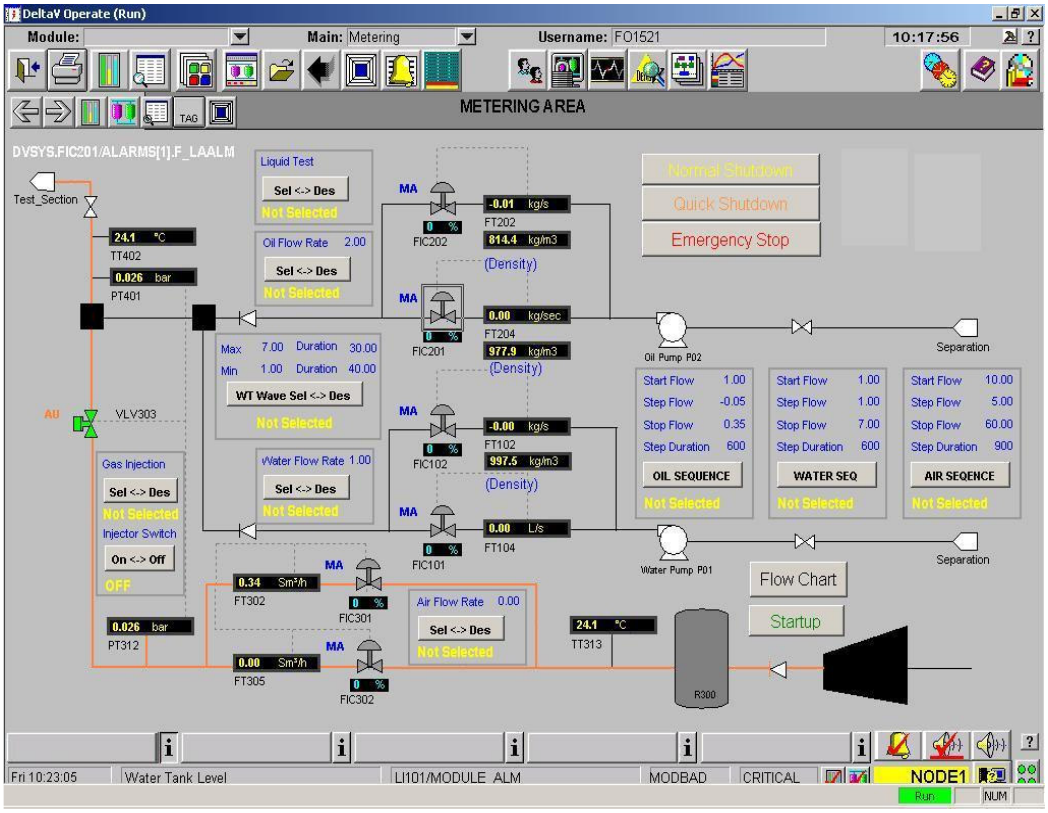

Figure 3.5 DeltaV plant automation system's GUI.

The signals obtained from the electromagnetic water flow meters, vortex gas flow meter, pressure transducers and differential pressure transducers were acquired through National instruments, E-series PCI-MIO-16E-4 data acquisition board. This board is a multifunction data acquisition board with 16 single ended or 8 differential analog input channels. Each channel has 12-bit resolution with a total maximum sampling rate of 500 kHz. The connection between sensors and the DAQ board was achieved by the National instruments BNC-2090 shielded, rack-mountable connector. All the data acquisition, processing and saving is performed through specifically build LABVIEW program (Qazi and Yeung, 2006) installed on Pentium-IV personnel computer. See Figure 3.6 for the front panel of this LABVIEW program while refer to appendix A for the block diagram of the backend panel. The program is subdivided into three stages:

1. ***Data Acquisition*** - sequential acquiring/reading data from the channels and converting the output sensor voltages into corresponding engineering units. Prior to this, all the sensing devices were calibrated, in order to obtain the gain and zeros of the individual sensors.

$$k = \frac{X}{e - e_o} \qquad 3.1$$

Where, X is Physical variable being measured (e.g. flow rate).
e_o is the value of the voltage measured at zero value of physical variable.
e is the final voltage being measured by the sensing device.
And k is the slope or the gain.

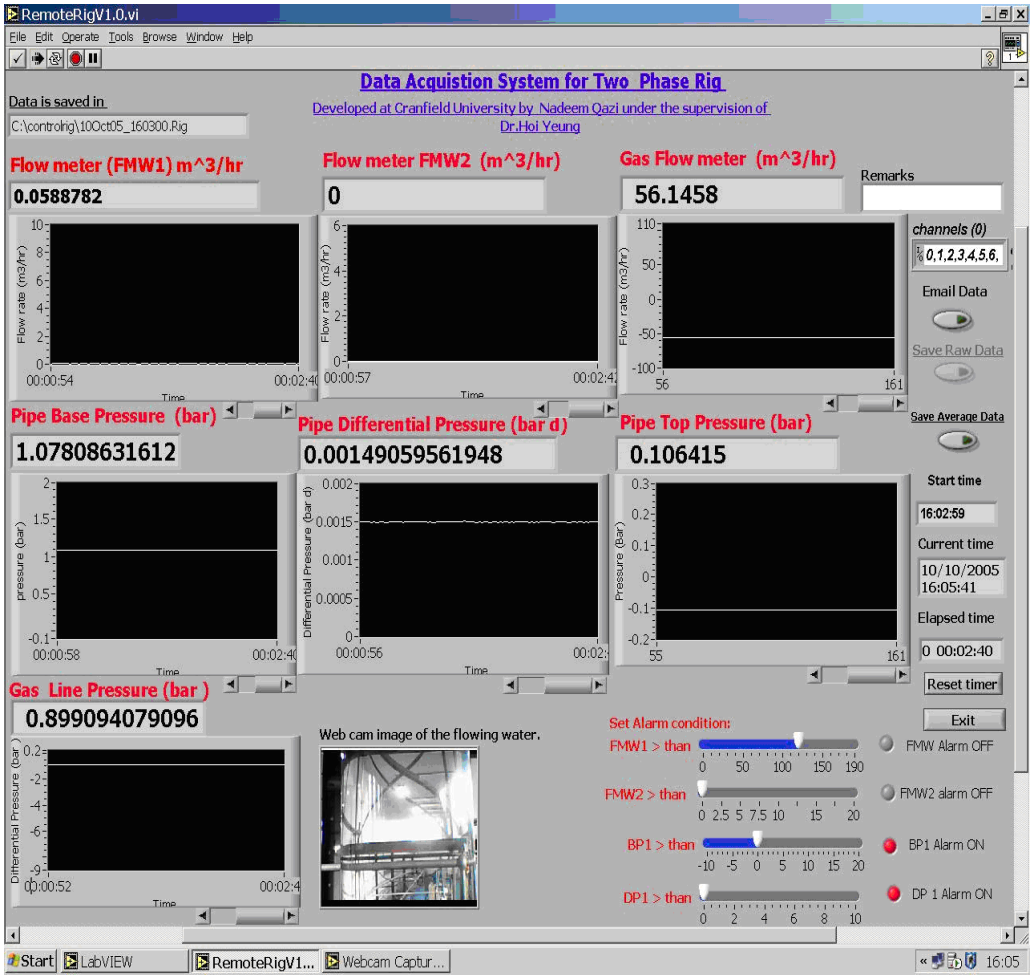

Figure 3.6 A snapshot of the LabVIEW front panel.

2. ***Data Viewing*** - the data acquired is displayed in real time on the computer monitor both numerically as well as graphically.
3. ***Data Storing*** - the data is written and saved in two (2) separate text files. The

first file saves the data at the specified sampling frequency. While the second file takes the data after engineering conversion but averages the data over the specified time period from the main program. The two saved files can then either be analyzed within LabVIEW or can be exported to Microsoft Excel or MATLAB for further analysis.

4. ***Image capturing*** - the above program also employs an image capturing application where webcam images captured from the vertical riser section during the experimental runs are processed and then displayed in real time in GUI.

3.4 Experiments

3.4.1 Experimental configurations

The facility was operated in two different modes namely:

i. Natural lift

ii. Forced lift

From above conditions, not only the performances of both the injectors could be evaluated but also the entrance effect on two phase flow regimes and their transitions can be studied in large diameter vertical riser, a topic that has not been dealt previously.

Natural lift - The natural lift experiments aimed at systematic study of the effect of the injectors on the liquid production, therefore the source of the water is an overhead tank with air injection in near riser base. Under this mode the flow is gravity driven between the upward gas lift flow in the vertical riser and returning single phase flow from the downcomer. The strategy establishes the gravity driven force available from gas lift only. When operating in this manner, the downcomer is connected to the riser in the base via gate valve (VW8) while keeping the (VW7) valve closed to disconnect the circuit from the return sump path.

In ***forced lift***, the water and/or air-water is delivered to the riser base by pumping. When the rig operates in forced circulation mode gate valve (VW8) between riser and downcomer is fully closed and another valve (VW7) is fully opened to allow the return of the water back to the sump. This strategy was intended for three purposes; to establish the precise boundary between the flow regimes i.e. through investigating combinations of the air and water velocities, study the effect of upstream conditions on the flow patterns in vertical riser and to verify the injector's ability to stabilize the unstable flows at the riser base.

Above aspects were achieved in forced experiments in three (3) configurations called ***near riser base air injection (or airlift experiments), upstream air injection*** and ***combine airlift-flowline-riser experiments***. In the former, single phase water was

pumped to riser base through flowline via pump and air is injected near the riser base while in the latter two cases the air and water (two phase flow) was made to flow through the horizontal flowline in order to develop stable and unstable two phase flow at the entrance of the base of riser with/without additional air injection near the base. Figure 3.7 illustrate the above different experimental configurations, while below are the brief descriptions:

1. When the incoming water at the riser base is single phase water from the overhead tank through the downcomer and air is injected through anyone of the two injectors near the riser base, see Figure 3.7a (designated as **NA** and **NT** in later chapters).

2. When the incoming water at the riser base is through flowline pumped from the sump and air is injected through anyone of the two injectors near the riser base, see Figure 3.7b (designated as **RA** and **RT**).

3. When incoming fluid at the riser base is two phase (air-water) flow from horizontal flowline and there is no air injection in the riser base vicinity, see Figure 3.7c (designated as **H**) and,

4. When incoming fluid at the riser base is two phase (air-water) flow from horizontal flowline with air injection in the riser base vicinity by any one of the two injectors, see Figure 3.7d (designated as **HRT** and **HRA**).

It is to be noted that the option (3) and (4) were performed for limited data set only. This was due to two technical difficulties encountered:

(a) During the option (3) experiments, the complete riser platform experienced large cyclic pressure surges due to high velocity air bubbles in slug flow moving in from the flowline into the riser. Thus limiting the experimental runs for two water superficial velocities only. However, it is of interest that most of the flow instabilities are usually encountered at low gas-liquid superficial velocities; hence the data set obtained was considered sufficient for analysis to examine the unstable flow phenomena.

(b) The air supply from the Multiphase flow rig was manually controlled at the entry points to the large diameter facility. Severe difficulties were encountered in controlling the flow conditions constant in option (4) as controlling the one inlet resulted in disturbance of other inlet's set point. Hence the effect of gas injection on liquid slug dissipation or stability characteristics could not be fully studied. Therefore, one of the future recommendations is that the manual valves should either be replaced by more sophisticated control valves or two separate air sources should be employed.

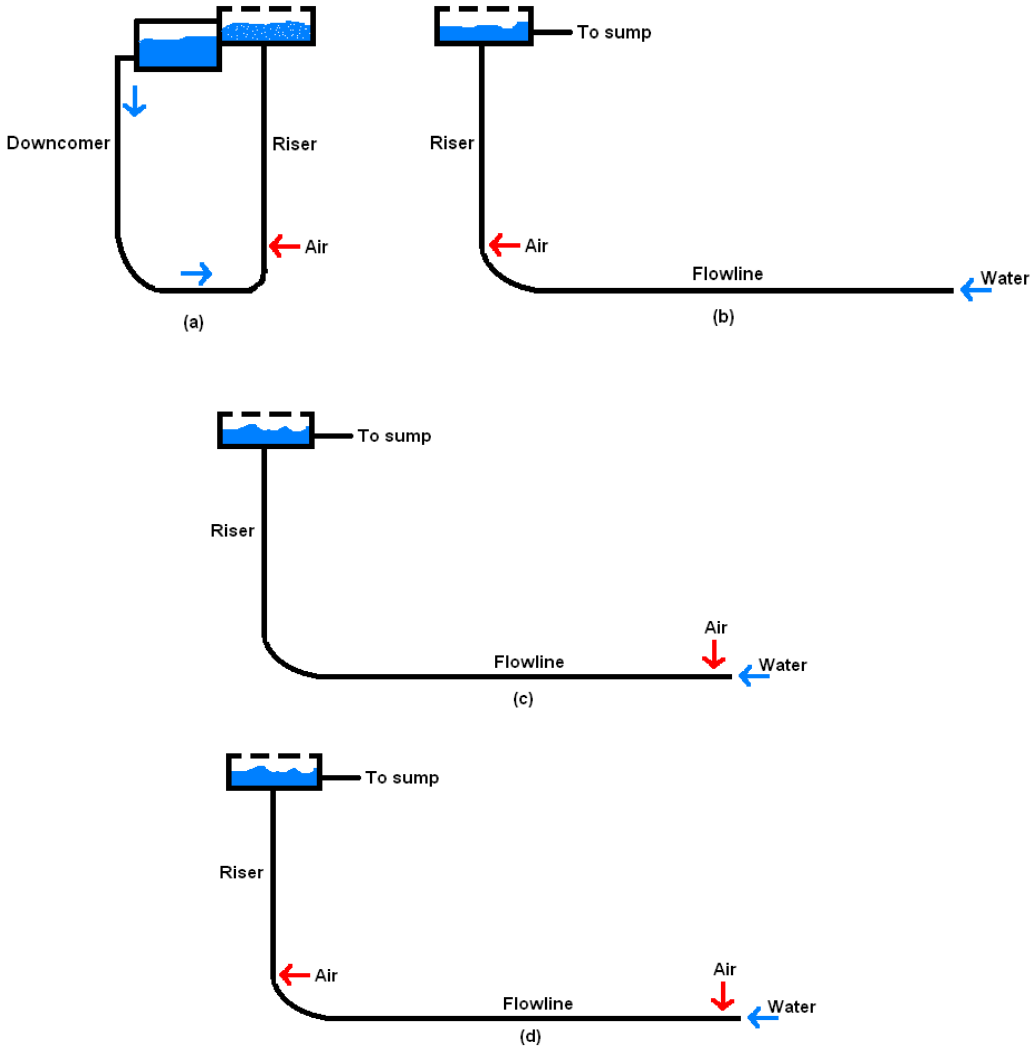

Figure 3.7 Flow loop configurations: (a) Natural lift, (b) Forced lift - air injection near riser base, (c) Forced lift – upstream air injection, and (d) Forced lift – combine flowline - near the riser base air injection.

3.4.2 Test Matrix

Series of tests were performed with configurations mentioned in the earlier section. The matrix of experiments covers the range that is typical of operating conditions in various industries. Table 3.2 provides the summary of the ranges of the experimental parameters covered. At the start of each experimental run, the electrical connections from the sensors were checked along with inspection of pressure tappings, level gauges and temperature probes. After performing the checks, the pump was started and water from single phase rig was supplied at a constant rate with help of bypass

valve into the large diameter flowline-riser setup. Meanwhile air compressor was started and 10-15minutes were allowed for filling of the buffer tank to its capacity. Next air flow in the riser test section was started with the help of the DeltaV® distributed control system using controllers to settle air injection at predefined values. The two phase flow conditions were given and the system was allowed to reach steady state. The further details of the operating procedures can be found in Ali (2005). The real time graphical display of DeltaV and LABVIEW® systems allowed the user to closely monitor the parameters until they reached the targeted values.

With each experimental run, a waiting time of 10 minutes was established in order to obtain steady state readings after which the data acquisition was started. All the parameters were continuously logged for the specified time period 5-8 minutes. The size of facility and the extent of the manual valve control involved along with the data acquisition limited the size of the time period for individual run. However the repeatability of the runs was also performed frequently during the tests and they are in good agreement with the initial runs. During the experiments frequent sensor checkups and re-calibration were also performed especially the pressure sensors, all were calibrated against a certified calibrator.

Table 3.2 Experimental range covered.

Experimental Parameter	Range covered
Gas	Air
Liquid	Water
Water superficial velocities (Natural), m/s	0.18 - 1.1
Air superficial velocities, m/s	0.18 - 2.23
Water temperature, ºC	19 -24ºC
Air temperature, ºC	18-22ºC

Most of the work was performed in four stages. The preliminary stage experiments conducted were for smaller air-water superficial velocity range aimed to determine the liquid production and flow regimes only. From this phase, preliminary results were achieved and the problems concerning the design of the test facility and data acquisition software were identified. In the light of above mentioned the quantitative analysis of the results were limited. However, the conclusions of this phase had an important qualitative meaning. Therefore they have been discussed where appropriate along with subsequent phases of experiments. In the later stages of experiments, series of two-phase (air and water) experiments were performed. In these experiments the problems identified in early phase were removed. These subsequent generations of experiments not only extended the range of air superficial velocities but also covered the movie and still photography under different conditions, liquid production,

riser base and flowline pressures, void fractions and stability characteristics of the two phase flow.

3.4.3 Deduction of Parameters

3.4.3.1 Water and Air superficial velocities

The water flow rate (Q_w) was supplied from the water circuit via pipe that was filled with water all the time; here water metering was performed by electromagnetic flow meter before entering the large diameter test section. Hence water superficial velocity can be calculated as:

$$j_w = \frac{Q_w}{A} = \frac{\dot{m}_w}{\rho_w \cdot A} = \frac{G_w}{\rho_w} \qquad 3.2$$

Where m_w is the mass flowrate, Q_w is the water flowrate, G_w is the mass flux, ρ_w is the water density, j_w is the water superficial velocity and A is the area of the test section.

The air flow rate was measured at standard conditions at three locations with two mass Probar flowmeters and a vortex flowmeter before it entered the test section. Measurements of the pressure and temperature before and in test section were also performed. For the air volumetric flow rates in the test section, the effect of the local pressure has been considered and the air is treated as an ideal gas. The air superficial velocity in test section was then calculated as:

$$\dot{m}_a = \left(\rho_{a,t} \cdot Q_{a,t}\right)_{test\ section} = \left(\rho_{a,r} \cdot Q_{a,r}\right)_{ref} \qquad 3.3$$

$$\rho_a = \frac{M_a}{R} \cdot \frac{P}{T} \qquad 3.4$$

$$m_a = \frac{M_a}{R} \cdot \frac{P_{ref}}{T_{ref}} \cdot Q_{a,ref} \qquad 3.5$$

$$Q_{a,t} = \frac{T_t}{P_t} \cdot \frac{P_{ref}}{T_{ref}} \cdot Q_{a,ref} \qquad 3.6$$

$$Q_{a,t} = A \cdot j_a \qquad 3.7$$

$$j_a = \frac{Q_{a,t}}{A} = \frac{T_t}{P_t} \cdot \frac{P_{ref}}{T_{ref}} \cdot \frac{Q_{a,ref}}{A} \qquad 3.8$$

In above set of equations m_a is the mass flow rate of air, $Q_{a,ref}$ and $Q_{a,t}$ is the air volume flow rate at reference and test section conditions, $\rho_{a,ref}$ and $\rho_{a,t}$ is the density of air at reference conditions and in test section, T_{ref} and T_t is the reference and test section temperatures, P_{ref} and P_t is the reference and test section pressures, M_a is the molecular weight of air, j_a is the air superficial velocity and A is the area of the test section.

3.4.3.2 Void fraction and Flow regime determination

Void fraction is one the most important parameter in determining the hydrodynamic behaviour of two phase flow system. Several methods are available for determination of void fraction. However in this work differential pressure measurement technique was applied on the vertical test section. Void fraction determination by differential pressure measurement is the most simple and economical method. This technique has been employed by various researchers to determine and/or compare their local void fraction measurements from other methods (Fordham *et al.,* 1999; Guet *et al.*, 2003; Hirao *et al.*, 1990; Ma *et al.*, 1991, Ohnuki and Akimoto, 2000).

The technique assumes that the average differential pressure measurement in a vertical test section being equal to the sum of hydrostatic, acceleration, and frictional loss terms. In most cases at low liquid velocities the acceleration and frictional terms can be neglected. However in cases were there are not they need to be evaluated. Generally in air-water flows the acceleration term is neglected while the frictional component can be accounted for if the values of loss are available from the experimental data or from any model prediction (Ohnuki and Akimoto, 2000). Under such cases the resultant differential pressure measurement between two pressure taps is the sum of gravitational component and frictional component.

In current setup the placement of differential pressure transducers allowed the measurement of two phase pressure drop across two different locations in the test section. Each differential pressure transducer was connected to test section via two pressure tappings axially separated by a distance h (h=3.5D) filled with water at height of 5m and 8m approximately. However this scheme requires a continuous monitoring (purging) of the pressure tapping lines so that they are filled with one of the phases (water) only. An easy penetration of second phase (air) often taken place and may cause a major source of error. Therefore a bleed system accompanied so that the air can be purge out regularly to ensure the lines were filled with only water all the time. Figure 3.8 indicates the differential pressure setup used for evaluation of void fraction (holdup) in the test section. Below are the mathematical equations used:

$$\alpha = \frac{\Delta P_{cell} + F}{(\rho_w - \rho_a) \cdot L \cdot g} \qquad 3.9$$

Where ΔP_{cell} is the measured differential pressure, L is the distance between the tappings i.e. $L = h_2 - h_1$, g is the acceleration due to the gravity, ρ_a and ρ_w is the air

and water density, α is the void fraction and F represents a frictional pressure loss term. In above equation F can be predicted from any pressure drop model. In a trail attempt homogenous flow approach was used to calculate the frictional contribution to the total pressure drop. This estimated friction drop (less than 2.5%) was used to determine the static component. It is to be noted that because of the minimal contribution of frictional component to total pressure drop, neglection of this term will not produce significant error. Under current case for each flow condition investigated, F was neglected as all the two phase runs were dominated by hydrostatic head. Consequently the effect of increased diameter (D) is the reduction of the magnitude of F proportionately; hence the assumption of negligible frictional losses is valid. Moreover single phase experiments conducted indicated that the frictional pressure drop was smaller even than the order of milli-bars for highest water flowrate, hence the frictional pressure loss is small in comparison to hydrostatic pressure in the riser. Void fraction was also calculated from the differential pressure between two heights in the vertical test section by using pressure transducers, assuming the losses terms are negligible in comparison to hydrostatic term. The void fraction calculated in this manner is in good agreement with values calculated from above measurements.

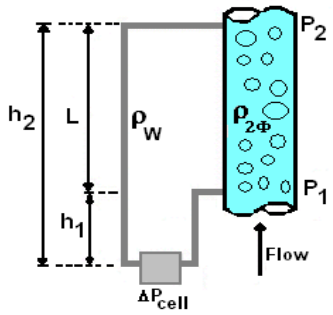

Figure 3.8 A detailed schematic of the differential pressure method arrangement.

3.4.3.4 Analysis of all Pressure traces

Work on pressure trace analysis is scarce and no such literature contribution is available on vertical pipe upflow. Thus the analysis of pressure time series was also performed where appropriate. In this case pressure traces were recorded simultaneously with three pressure sensors. These traces were used to determine the pipeline, riser base and riser top response to air injection. The pipeline pressure trace was monitored before the inlet to vertical riser; riser base pressure while riser top pressure was observed a meter before the exit section. The significance of these traces lies in indicating the hydrostatic variation and the liquid inventory in the riser, flowline response to upstream slugs and liquid film fallback and, riser top pressure will provide the sustaining trends of slugging cycle. Additionally with pressure transducer-time series, differential pressure time series, analysis was also performed to extract more information through statistical analysis.

3.4.3.5 Still Images and Videoing

During all the experimental runs flow pattern observations were also made through clear Perspex sections in the whole pipeline-riser system. A high quality Fuji Fine Fix digital camera cum video was used to record video and images in these observations. The digital camera was used for videoing at the first Perspex section installed above the injectors in the riser and it was also used to record the video of flow patterns in horizontal flowline near the riser base. Spotlights were mounted near injectors and at Perspex sections of the pipeline-riser to ensure good lightening and proper filming of flow regimes. In addition to above, a USB web cam was also used for capturing the videos of the two phase flow at the second floor Perspex section installed at height of 8m approximately in the riser section in conjunction with the data acquisition.

3.5 Summary

This chapter has presented the details of the large diameter horizontal flowline-vertical riser facility. The facility is designed to perform investigations of hydrodynamic behaviour in 254mm diameter vertical riser. The air and water was used as working fluids for this purpose. In section 3.1 details of air and water supply circuits along with details of test section were outlined. The test section itself is equipped with special high pressure Perspex sight glasses to observe the flow pattern occurring in horizontal pipeline and vertical riser sections. Next, the details of instrumentation used were reviewed in section 3.2 while data acquisition was presented in section 3.3. The signals from the instrumentation installed at various locations in the setup were acquired through dedicated LABVIEW software for further analysis in LabVIEW itself, Microsoft Excel and MATLAB softwares.

Lastly in section 3.4 methodology adopted to perform experiments were discussed in detail, operating ranges were defined and various parameter deduction techniques used in later chapters were summarized.

Chapter 4

Experimental Results

The current chapter discusses the various results obtained from the large diameter horizontal flowline vertical riser facility. The first part examines the performance of a novel design gas injector in comparison to the conventional design. The second part details the predictions of the flow patterns and their transitions in the large diameter vertical riser. The effect of upstream conditions on the flow pattern in the riser is presented next. The comparison of the flow patterns, transitions with other maps/models is discussed. Lastly, the experimental void fraction characteristics are discussed and compared with other studies.

Part I – Gas Injectors Characteristics

The objective of the first part of this chapter is to report the experimental investigation of a hydrodynamic performance of a newly designed gas injector against a standard one. Both the injectors are intended for deep offshore riser base setup that heavily utilizes the gas lift concept due to its two-fold benefits of enhancing production and stabilizing the unstable flows. While the annular sleeve injector was a novel design, the latter standard gas injector called Tee injector was being previously used in the offshore oil industry for riser base gas lift. Although efficient performance, the concerns were expressed that the later design (Tee) might result in gas jetting through the inlet onto the opposite wall of the riser in later production life as observed in small diameter risers; therefore its application to large diameter risers will be crucial in terms of CAPEX and OPEX. Thus the former, a novel injector design has been developed to eliminate/minimize this effect on the walls of the riser. As the novel design is specifically intended for deep offshore applications, and before being installed in the field, its hydrodynamic behaviour needs to be predicted and compared with conventional Tee design.

In order to simulate the conditions of riser base gas lift and evaluate the hydrodynamic performances of the above injectors, a typical flowline-riser system was needed along with sources producing gas and liquid, with top facility for gas-liquid separation. The large diameter vertical riser facility used in this work is accordingly designed to simulate such conditions where the injector performance can be evaluated with respect to liquid production and stabilization of the flow. The strategies used for evaluation of the performances of the injectors are called natural and forced lift and has been explained in detail in the earlier chapter (section 3.4).

The results obtained from the experiments conducted with these gas injectors and their comparison in this section are new as it looks into the performance of gas injectors in 254mm diameter vertical pipe in terms of (i) Visual flow pattern characterization, (ii) Lifted liquid flow characteristics, (iii) Pressure gradient characteristics, (iv) Void fraction characteristics, (v) Flow regime transitions, (vi) Riser base pressure characteristics and (vii) ability to stabilize the unstable (cyclic) two phase flow. Moreover the results obtained with the current setup are of significant importance as they are more representative to the actual diameter used in the field.

4.1 Gas Injectors Results

4.1.1 Visual flow pattern characterization of the injectors

Although the details of the flow patterns, representative for this diameter pipe will be presented in later sections, a brief visual observation of the main flows encountered in vertical riser is presented in order to facilitate the results presented in this part of the thesis.

In the experimental range conducted it was observed that the flow pattern generally remained bubbly flow at lower air superficial velocities with the exception of few data points at higher water velocities (j_l = 0.7 - 1m/s) and lowest air superficial velocity, where a slightly ***dispersed bubbly flow*** was observed. This was the consequence of low gas fraction present as small discrete spherical bubbles, uniformly distributed in continuous water phase. However, at lower air-water velocities ($j_w < 0.7$ and $0 < j_a < 0.3$ m/s) the flow remained mainly bubbly flow. This ***bubbly flow*** consisted of bubbles of approximately same size, closely packed in the liquid phase with some occasional coalescence of bubbles in the core. However, with increase in air superficial velocities, the frequency of coalescence of bubbles increased in the core and the flow although still bubbly but also possessed agitation in the liquid phase due to the coalescing bubbles in the core. This flow was not been observed previously and was unlike the slug flow observed under similar velocity range in small diameter pipes. Although the flow initially exhibited less coalescence of bubbles in the core, thus more visible, their formation frequency rapidly increased with air superficial velocities. This new type of the bubbly flow was refereed as ***agitated bubbly flow*** that continued to exist at the intermediate range of air superficial velocities (j_a = 0.35 to 1.4m/s). The flow regime consisted of the large distribution of bubble sizes with distorted surfaces formed due to the coalescence/bubble clustering taking place in the core. The distorted bubble clusters flowed with high velocity with producing zigzag movements in the core region. During this process, the liquid at the side walls were seen flowing up and down randomly or more like recirculation. There were also many small bubbles in the liquid region between the coalescent bubbles and the wall. Further details on this flow will be discussed in later sections.

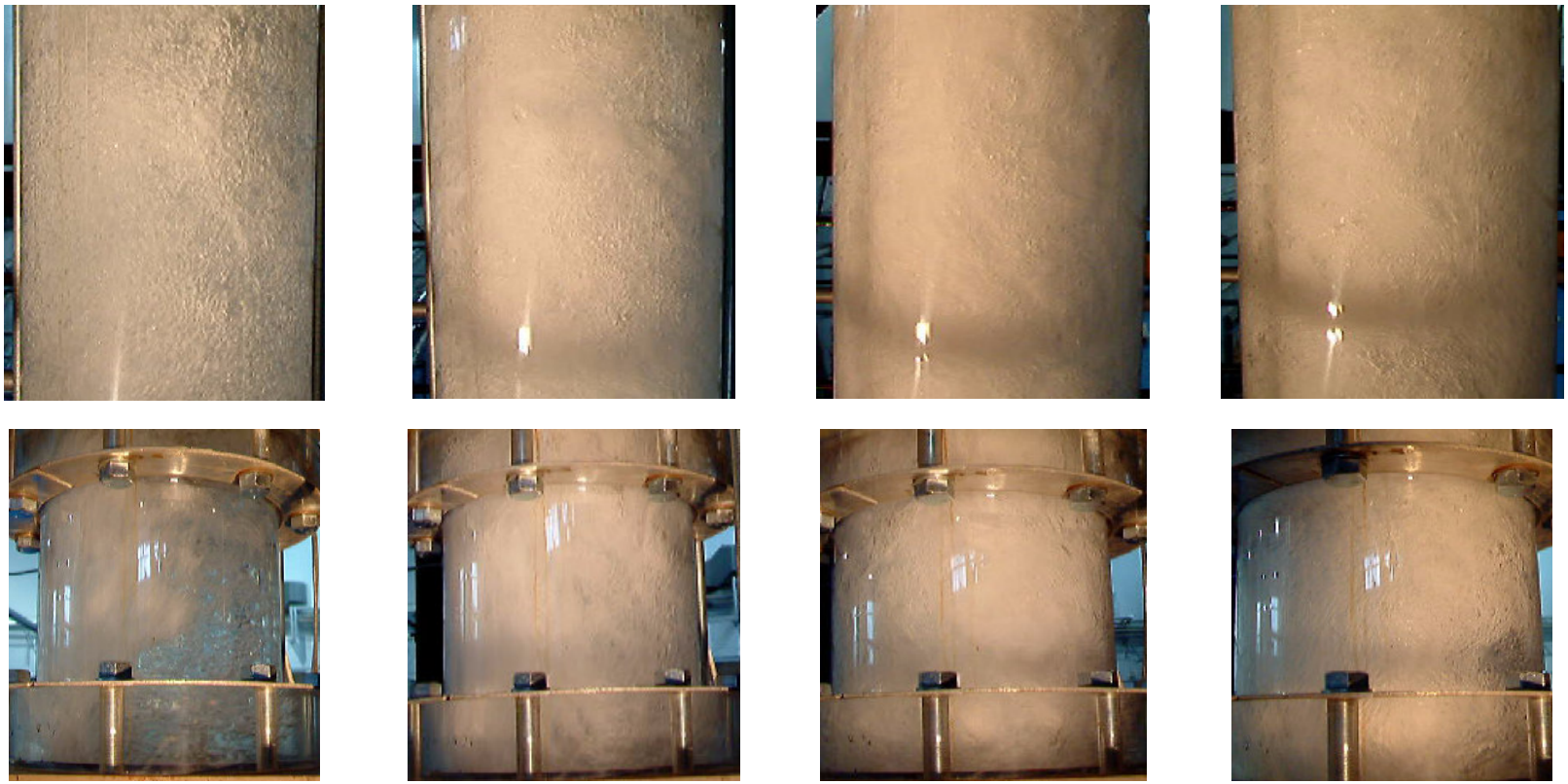

j_a = 0.09m/s | j_a = 0.82m/s | j_a = 1.52m/s | j_a = 2.26m/s

Figure 4.1 **The pair of above photographs shows the flow pattern occurring in the riser with Tee injector near injection vicinity (below) and at 4.8m height from the injector (top) for j_l = 0.25m/s.**

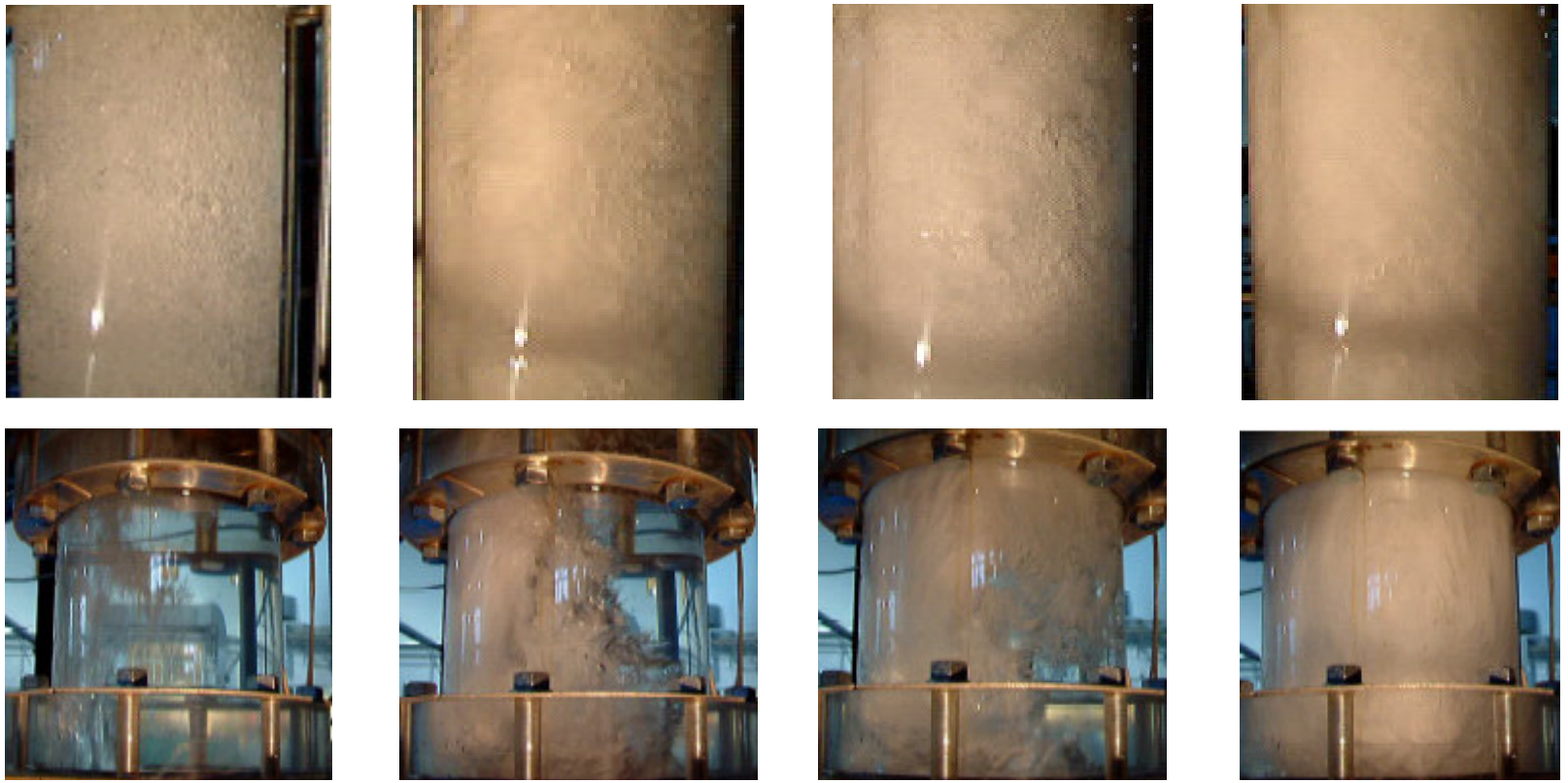

j_a = 0.09m/s | j_a = 0.78m/s | j_a = 0.1.45m/s | j_a = 2.26m/s

Figure 4.2 The pair of above photographs shows the flow pattern occurring in the riser with Tee injector near injection vicinity (below) and at 4.8m height from the injector (top) for j_l= 0.60m/s.

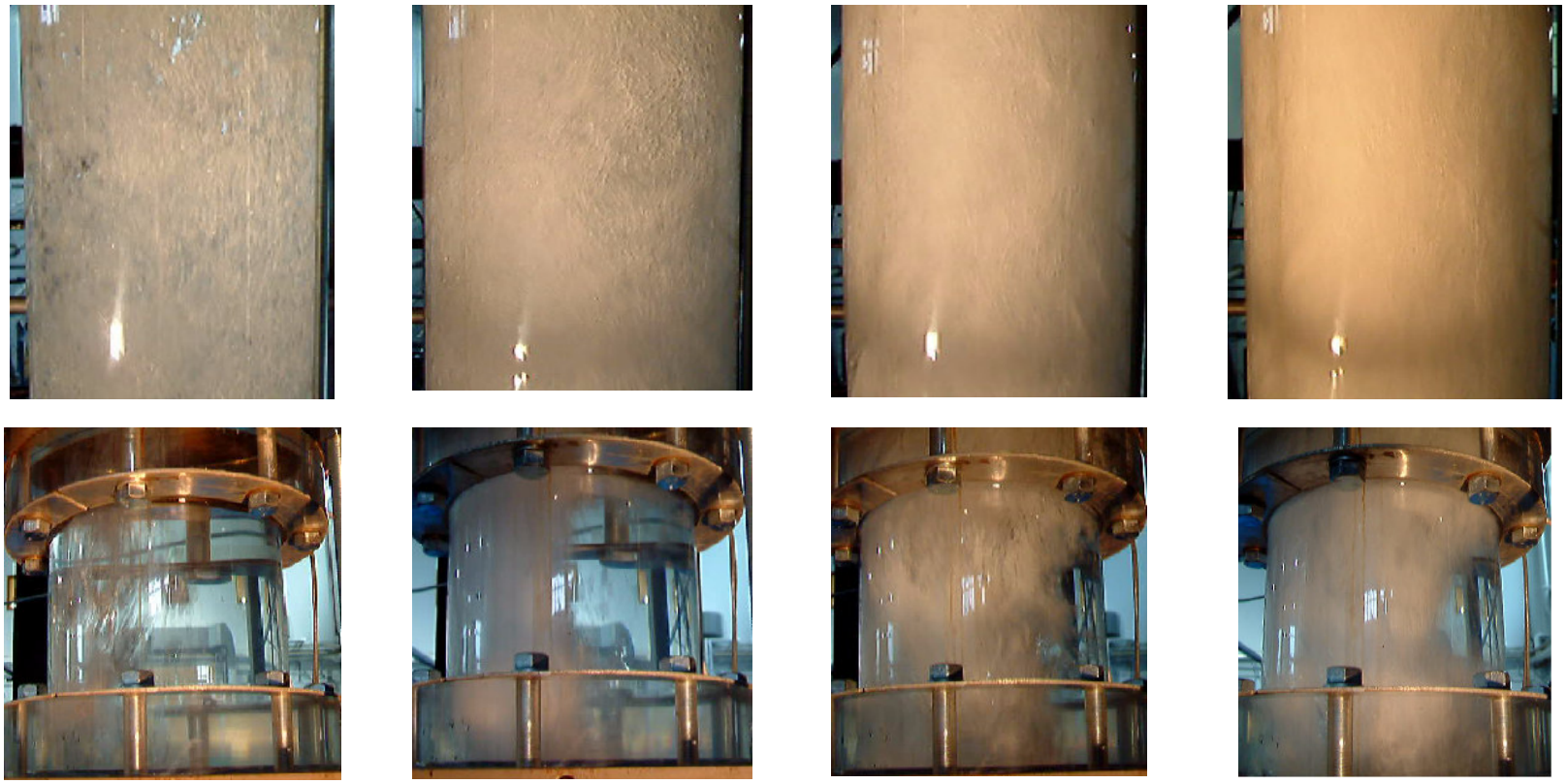

j_a = 0.09m/s | j_a = 0.77m/s | j_a = 1.44m/s | j_a = 2.21m/s

Figure 4.3 The pair of above photographs shows the flow pattern occurring in the riser with Tee injector near injection vicinity (below) and at 4.8m height from the injector (top) for $j_l \approx 1$m/s.

The experiments at the higher air superficial velocity range (j_a > 1.7m/s) allowed the presence of ***churn/froth flow***. In churn/froth flow, the overall flow became increasingly unstable and oscillatory with large irregular bubble clusters churning upward. As the air superficial velocity was increased, these irregular distorted bubble clusters became more frothy with liquid film at the wall either moving upward with their upward flowing or flowing downward when these high velocity distorted bubble have passed with liquid fall back.

The major emphasis of this section is to present the flow behaviour visualization study performed to evaluate the performances of the injectors. This was achieved by using photographs and video observation through transparent Perspex sections specifically installed in the riser just above the gas injectors and then at approximately 5m, 8 and 9.5m heights in the riser.

Figure 4.1 to Figure 4.6 presents the selected photographs of the hydrodynamic flow behaviour during the experiments with both the injectors. The emphasis of these photographs was to visually observe the injectors behaviour near the point of entry in the riser. In all the figures, photographs are taken from near the injector's vicinity (below) and at about 5m height (top) from the injectors. The Figures 4.1 to 4.3 are for Tee injector and Figure 4.4 to 4.6 are for Annular sleeve injector at three different water superficial velocities (j_l = 0.25, 0.61 and 0.96m/s).

In Figure 4.1a, for the Tee gas injector, at lowest air-water superficial velocities, non-symmetric air distribution by virtue of its design is dominant. However, while this effect persists for higher water superficial velocities (Figure 4.2 and 4.3), it does not remain dominant for long in cases of increasing air superficial velocities and soon the flow becomes chaotic and frothy. It is to be noted also that in each figure the top perspex section does not indicate any influence of injector design and flow appears to be uniform across the diameter. The results of visual observation further indicated that while for Tee injector at low gas superficial velocities a wide distribution of sizes was produced, at higher gas superficial velocities, the break-up and coalescence of bubble predominated near the injection vicinity. There was also slowing down of upcoming riser base water flow near the point of injection due to the air injection perpendicular to the flow. The phenomenon was more visible at higher liquid superficial velocities with a non symmetric distribution of wide range of bubbles along with large scale recirculation in the core region near the transparent area (see Figure 4.1 to 4.3). However, the above large scale recirculation decayed and spread across as it moves up the riser, and at 3 to 4m above the injection point, the flow appeared uniformly distributed across the riser diameter. The Tee injector was observed to inject air in bursts at regular short intervals at lower air velocities increasing into a continuous manner with increase air superficial velocities. However frequently, a small temporary liquid block on the opposite side of the riser was seen that even the highest air superficial velocities. This phenomenon in forced lift experiments became more and more obvious at higher water velocities. It was observed that there was no air jetting to the opposite wall of the riser in the whole experimental range reducing the concerns of jetting and the resulting erosion from it.

Figure 4.4 to Figure 4.6 shows the flow behaviour of Annular sleeve injector, it can be noted that at lowest air superficial velocity (j_a = 0.09m/s) the injector influence is dominant. The air-bubbles are seen emerging in form of continuous bubble chain from all around the periphery. Similar to Tee injector, with continuous increase in air superficial velocities at lowest water superficial velocity (j_l = 0.25m/s), the flow became more chaotic with disappearance of this injector effect. However at highest water superficial velocity, this remained dominant but unlike the chain of air bubbles, it was more like continuous air column emerging all along the periphery, see Figure 4.5 and 4.6. In general, the visual observation in annular sleeve injector experiments indicated almost similar flow patterns as the Tee injector. However it was noted, at low air superficial velocity, smaller air bubbles flowing uniformly from all around the periphery of the annular sleeve injector injected. Unlike, the Tee injector, there was no air recirculation in form of plume in the near vicinity of the injection point and rising bubbles from the injector appeared to flow upward along with water in continuous manner near the wall of the riser. Similar to Tee injector above, no air jetting on the opposite wall of the riser was observed under all flowrates studied in the experimental campaign for annular sleeve injector.

From the visual results presented above, the most noticeable difference between the two injectors was air distribution i.e. a non symmetric and symmetric air distribution in the initial section of the riser (at low air-water superficial velocities). However, with the upward flow path, it spread out to opposite side. Thus the flow in the riser ahead, at around 5m showed no sign of dependence on flow injector with flow from both injectors appearing almost alike. Since the inlet or gas injector influence on the overall flow disappears at about 4m ($z > 20D$) from the injector the flow can be assumed to be quasi developed and the flow behaviour after this region is unaffected by upstream conditions. Similar observation of two phase flow pattern showing no sign of injector design after certain length is reported by Herringe and Davis (1976) and Liu (1993) in their 50.8mm ($z > 108D$) and 57.2mm ($z > 30D$) diameters vertical pipe upflow experiments respectively.

It is emphasised that during the visual investigation no large coalescent bubbles like smooth bullet shaped Taylor bubble (occurring in slug flow) were observed either in the injector vicinity or ahead in the test section for all air superficial velocities by both the injectors. Occasionally, some large spherical cap bubbles were produced, when gas valves were opened. These large spherical caps bubbles were found to disintegrate while travelling upwards.

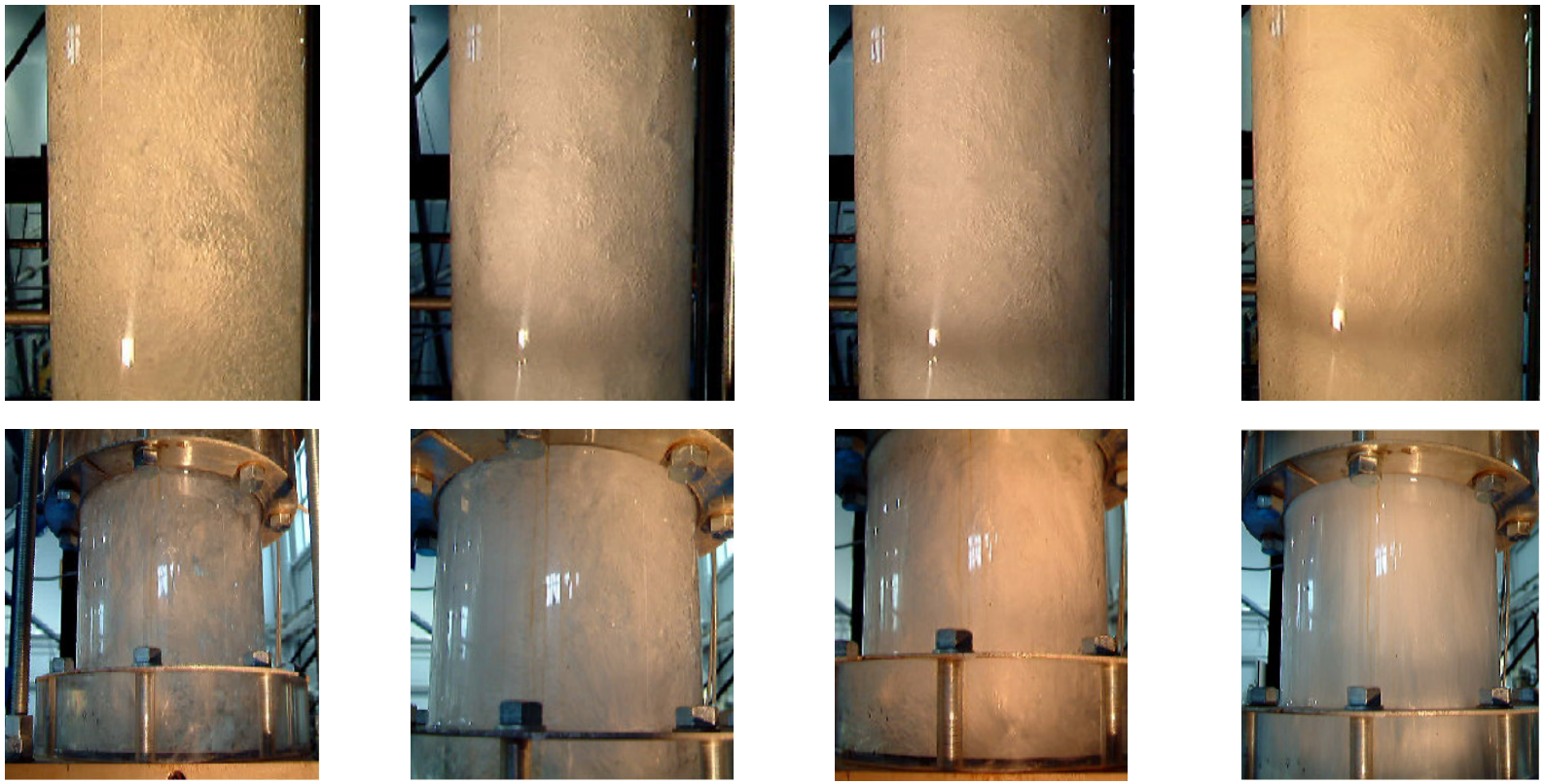

j_a = 0.09m/s | j_a = 0.81m/s | j_a = 1.51m/s | j_a = 2.27m/s

Figure 4.4 The pair of above photographs shows the flow pattern occurring in the riser with annular sleeve injector near injection vicinity (below) and at 4.8m height from the injector (top), for j_l= 0.25m/s.

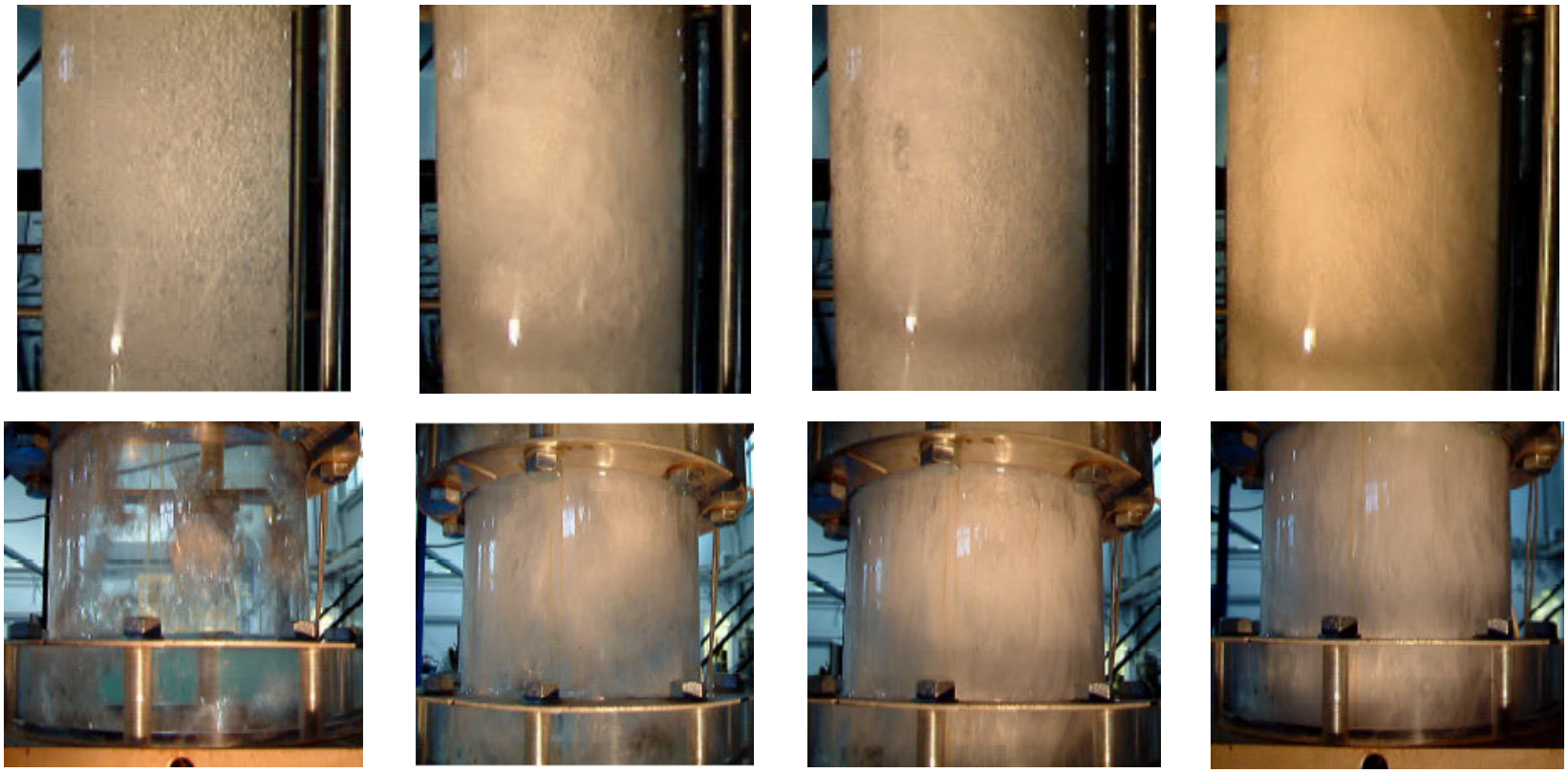

j_a = 0.09m/s **j_a = 0.80m/s** **j_a = 1.50m/s** **j_a = 2.24m/s**

Figure 4.5 The pair of above photographs shows the flow pattern occurring in the riser with annular sleeve injector near injection vicinity (below) and at 4.8m height from the injector (top) for j_l= 0.60m/s.

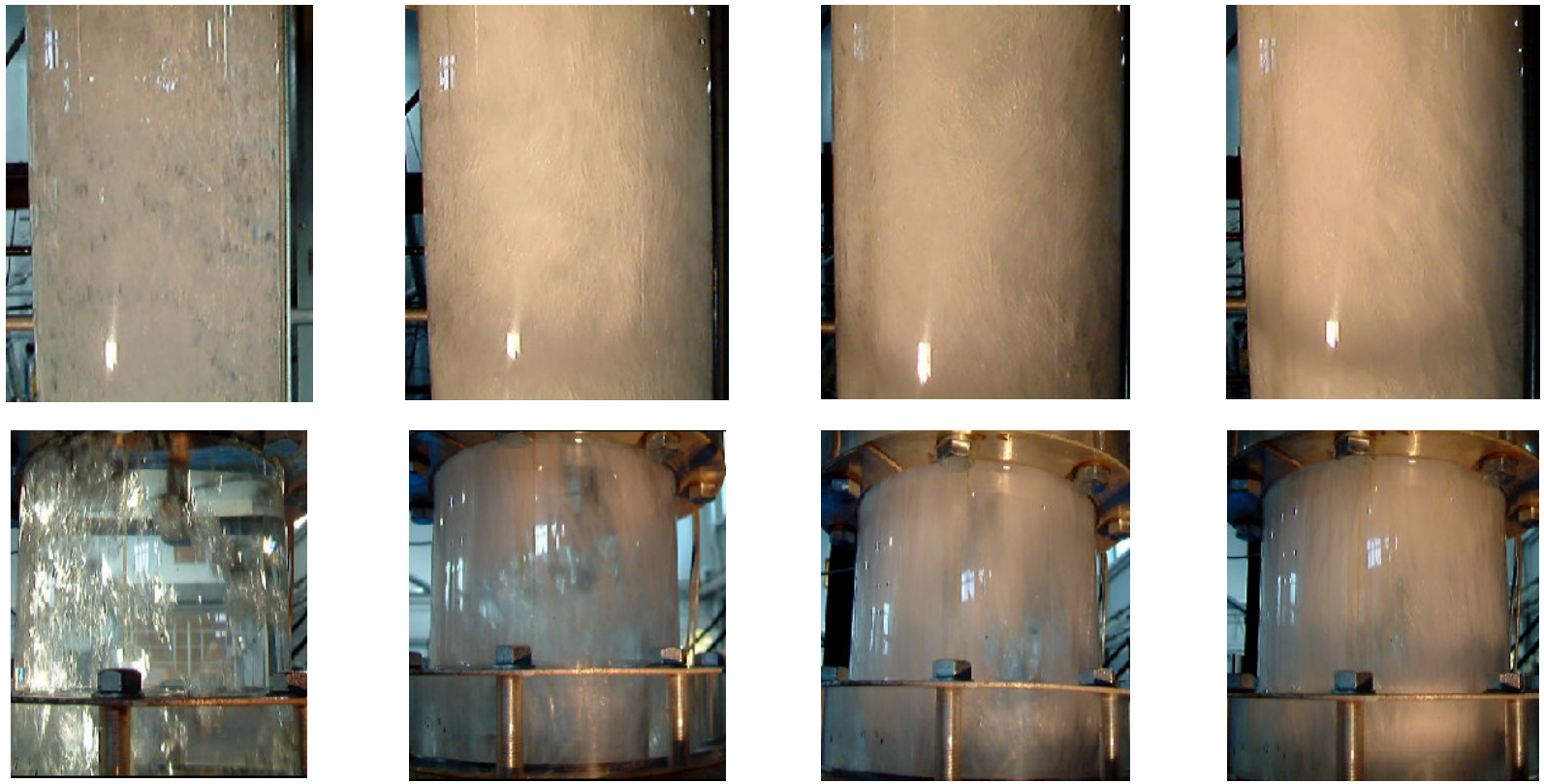

j_a = 0.09m/s | j_a = 0.78m/s | j_a = 1.45m/s | j_a = 2.26m/s

Figure 4.6 The pair of above photographs shows the flow pattern occurring in the riser with Annular sleeve injector near injection vicinity (below) and at 4.8m height from the injector (top) for $j_l \approx 1$m/s.

4.1.2 Lifted liquid flow characteristics

To determine the effect of individual gas lift by the injectors, the experiments were conducted with natural lift with no external power applied. In this case the injection of gas phase in the riser resulted in increase of the volume (due to mixture) causing the liquid level to increase and flow from upper plenum to overhead tank. In the overhead tank the two phases separated via gravity i.e. the liquid flowed through the downcomer while air escaped from the open top. To ensure accuracy, tank water level was kept constant. The water was recirculated back to the base of the riser and the mixture flows to top till the time equilibrium establishes. The liquid productions during the experimental runs were recorded for different gas injection rates.

In preliminary experiments conducted in smaller air superficial velocity range, it was observed that annular sleeve injector was lifting slightly more water (see appendix B). However Figure 4.7, reports the liquid production trends as function of the air superficial velocities for both the Tee and Annular sleeve injectors for a larger range of air superficial velocities. In general, both the injectors indicate a common pattern of variation i.e. the lifted flow increased with an increase in the air superficial velocities due to increase in the buoyancy driving force. The increase in buoyancy force occurs due to the bubble frequency increase in the bubbly flow regime (the initial part of the liquid production vs. gas superficial velocity curve is linear). However, as the bubble population increased, the lift still increases, but this increase was also accompanied by an increase in coalescence of bubbles that occurred also more frequently. This latter process influenced the rate of increase to the extent that the void fraction-gas superficial velocity linear relationship broke down. At higher air superficial velocities, the trends suggests that for both injectors the increase in buoyancy force is compensated by a corresponding increase in the frictional force leaving the lifting capacity to level off.

The Figure 4.7 further indicates that indeed there was an increase in liquid production by annular sleeve injector; however it was limited for low air superficial velocity range only, as observed in preliminary experiments. The figure also demonstrates the performance of the two injectors by virtue of their designs; the liquid production at the lower end of the air superficial velocity range for a specific air superficial velocity is different for both the injectors. In other words to produce a similar magnitude lift, Tee injector requires slightly larger air superficial velocity than annular sleeve injector, almost a magnitude more as that of annular sleeve injector. This result indicates that the annular sleeve injector was lifting more liquid at the same gas superficial velocity. This increase in lift of the annular sleeve injector was due to the production of the smaller air bubbles in the riser that resulted in lowering the average density of the mixture and hence larger production in comparison to the Tee injector. The Tee injector on the other hand, at the same gas superficial velocity produced relatively larger size bubbles with higher rise velocity that promoted further coalescence. The presence of these coalescence bubble in the core and rising up with high velocity resulted in more non uniform void fraction and the lower liquid production. This assertion also supported by the differential pressure sensor response

that indicated that under the same gas superficial velocity, the amplitude of the pressure fluctuation is slightly smaller for annular sleeve injector than Tee injector signifying that slightly smaller bubbles were generated from the former in comparison to the latter (refer appendix B for sensor response).

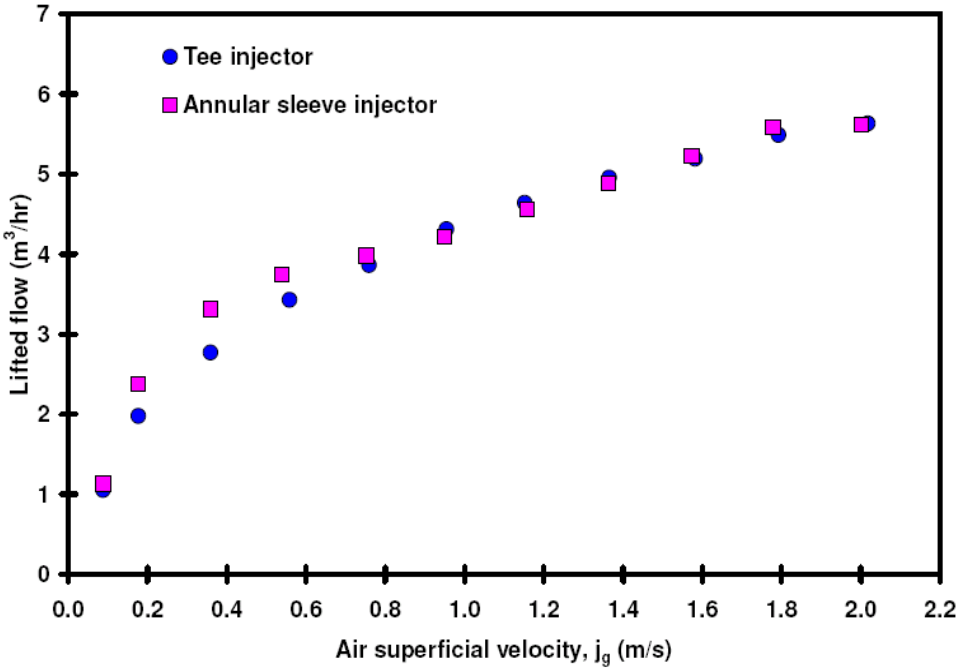

Figure 4.7 The comparison of the liquid production from the two gas injectors.

It is to be noted that although both the injectors showed bubbly flow at lower air superficial velocity range, the Tee injector showed an evolution of agitation in the flow due to the bubble clustering in the core region in comparison to the annular sleeve injector. These rising clustered bubble promoted further coalescence in their wake region along with rapid agitation in the surrounding liquid phase (bubble induce turbulence) with increase in air superficial velocities. The agitation in the liquid phase increased as the bubble clustering got wider in the core region. It was this bubble clustering in Tee injector experiments that resulted in reducing the lift in comparison to annular sleeve. At same air superficial velocity, annular sleeve injector void fraction distribution was still higher due to uniform peripheral distribution, smaller size, and slightly less non-coalescence of the bubbles. However, at higher air superficial velocities, both the injector displays similar lift characteristics. This was because at these superficial velocities the effect of injectors became less pronounced due to increase in coalescence and breakage phenomena of bubbles within the riser. This later mechanism resulted in an intense interaction of bubbles and the liquid

production in this region levelled off due to coupled effect of increase frictional losses and corresponding decrease in hydrostatic head.

It can further be noted in Figure 4.7, there are no obvious slope changes in the lifted flow contrarily to that indicated by Guet *et al.* (2003). Typically this change in slope was used to identify the regime transition from bubbly flow to slug by Guet *et al.* (2003) as it was found to coincide with the visual observation of the first slug bubble. In current set of experiments, it is seen that this transition criterion of monitoring the time-averaged behaviour of the variable is not valid as there is no obvious drop in lifted flow that can mark the flow regime transition. In context of current set of experiments, it is proposed that this behaviour is attributed to the larger bubble sizes formed by the current injectors along with the diameter effect. For the latter case, it is asserted that the large diameter offers a greater degree of freedom of liquid phase movement. This latter effect produces a stabilizing effect due to the liquid recirculations making the influence of the gas injector less pronounced in comparison to smaller diameter vertical upflow condition. The above assertion is also supported by the observation of non-presence of the Taylor bubble in the riser during the entire experimental campaign. Since no Taylor bubble of slug flow was formed, a more gradual transition from bubbly to agitated bubbly flow took place that was still bubbly in nature although accompanied by liquid phase agitation/ recirculation.

Besides the natural lift experiments stated above for determining the lift characteristic of the two injectors, the forced lift experiments were also performed. The experiments were performed with an aim to establish the precise boundary of bubbly/dispersed flow regime transitions under various combinations of liquid superficial velocities at constant air superficial velocity. The Figure 4.8 indicates the experimental matrix with water superficial velocities marked as R1, R2 …R7. The figure also shows the flow regime transitions obtained visually observed and verified from the signal sensor responses (discussed in later sections). For the purpose of determining the area of optimum gas lift by the gas injectors, the demarcation of the transition from bubbly flow /dispersed bubbly is important. From the natural lift experiments results, it is already cleared that the larger lifting of liquid is achieved in bubbly flow only due to the small bubbles uniformly distributed in the liquid phase. This is due to the decrease of the mixture density and hence increases in gas lift rate whereas in agitated bubbly flow due to the larger bubbles the lift is smaller owing to the differences in the relative phase velocity.

Based on the visual and the sensors information, it is concluded that both the injectors do not indicate any significant differences in flow regime transitions from bubbly to agitated bubbly flow. The reasons for this being the small difference of injection holes of the two injectors producing variety of bubble distribution (i.e. eight 38mm holes in annular sleeve in comparison to 50mm single entry of Tee injector) with both the injector injecting gaseous phase perpendicular to the flow.

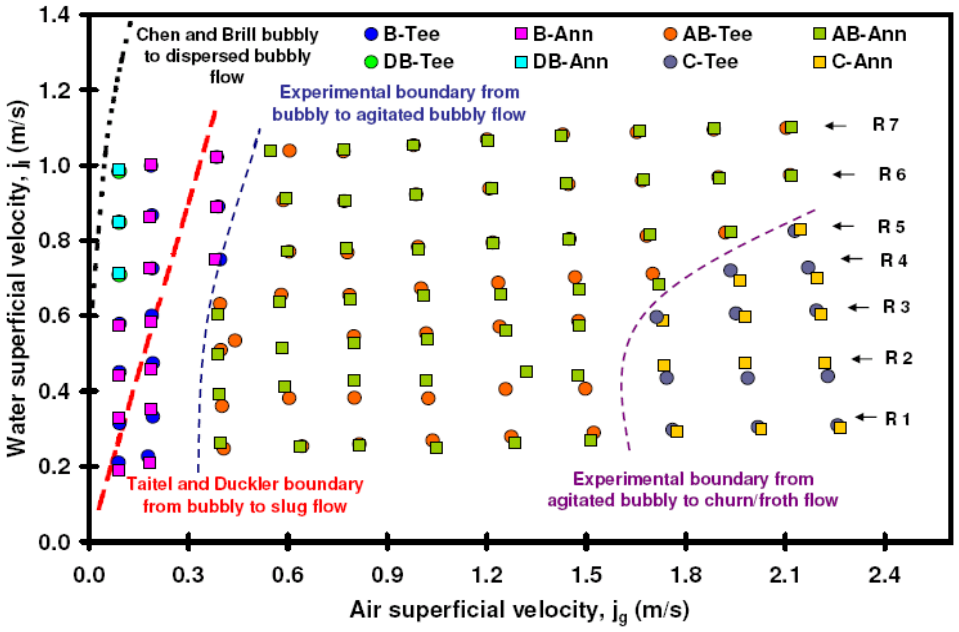

Figure 4.8 The forced lift experiments conducted with combination of air-water superficial velocities showing transition boundary between (a) the bubbly to agitated bubbly flow and (b) agitated bubbly to churn/froth flow for the two injectors.

It is to be noted that at $j_a = 0.09$m/s (with $j_l > 0.7$m/s), a slight dispersed nature bubbly flow was observed in forced lift experiments (see Figures 4.3a and 4.6a). The presence of this dispersed bubbly flow was the consequence of low gas fraction present as small discrete spherical bubbles with large separation distances between them in continuous water phase than the low liquid input bubbly flow. For low air-water superficial velocities the flow was mainly bubbly moving upwards and uniformly distributed across the diameter, however there was some infrequent coalescence in the core. At around, 0.4 m/s when gas superficial velocity is comparatively higher with larger bubbles sizes, an increase in bubble coalescence and their irregular movements is observed producing a rapid agitation in surrounding water phase. This intensity of the bubble agglomeration and irregular movements quickly increased with gas superficial velocity, with some larger bubble clusters appearing within the core that travelled upward with higher velocity. Somewhere around air superficial velocity of 1.4m/s, these oscillations were so highly chaotic that whole riser appeared to operating like column with large highly distorted frothy gaseous structures moving within the core followed by rapid frothy film fall back. From this observation we conclude that there exist two possible flow regime transitions with air superficial velocities in the vicinity of 0.5m/s and 1.4m/s. It is emphasised here that the experimental transition boundaries indicated are not a definitive demarcation line but rather an indicative of the experimental results and like any flow regime map, the transition between flow regimes is a gradual process.

The Figure 4.8 shows the results of the above delineation exercise for the two injectors under the forced flow conditions water-air superficial velocities (refer to appendix B for preliminary results).

In the above results, it is striking to observe the presence of the dispersed bubbly flow at such low liquid velocities, as the traditional flow maps such as Taitel *et al.* (1980) map shows that this flow occurs at higher liquid velocities (j_w > 3m/s). In order to clarify the observation, Chen *et al.* (1997) transition criterion from bubbly to dispersed bubbly was used. From the results obtained, it was found that the experimental data points representing dispersed bubbly flow are indeed close to the boundary define by their model, see Figure 4.8. From the model prediction of Chen *et al.* (1997), it is also clear that bubble breakup from turbulent forces are dominant in near vicinity of j_w > 0.7m/s at j_a = 0.09m/s (since dispersed bubbly flow is observed at these combination of water superficial values). This means at the low air-water superficial velocities, the bubbly flow seen is due to the influence of bubble injectors. It is to be noted here that the Taitel *et al.* (1980) transition criteria from bubbly to dispersed bubbly flow indicated a higher transition (not in the figure).

The Figure 4.8 also indicates the flow regime transition from bubbly to new type of bubbly flow called agitated bubbly flow. Since this new flow was not found in smaller diameter pipe, no model yet exists to characterize this flow transition on flow pattern map. The transition criterion from bubbly to slug flow was used to see the effects. From the Figure 4.8, it is observed that the Taitel *et al.* (1980) transition criterion of bubbly to slug flow (i.e. the transition occurs at α_c = 0.25) is not in agreement with the experimental results at lower water superficial velocities but does come close at higher water superficial velocities. The observed trend is due to the constant critical void fraction employed for bubbly to slug flow transition for all pipe sizes. The failure of the agreement between the experimental and model predictions implies that basis of the modelling of above relation (α_c=0.25) is not applicable in large diameter risers. This topic will further be discussed in section 4.4.

4.1.3 Total pressure gradient characteristics

Figure 4.9 to 4.10 shows the total pressure gradients across the riser for various air injection rates by Tee and Annular sleeve injector respectively under forced and natural lift modes. In both the figures, annular sleeve injector shows slightly lower values under all cases, hence more efficient in reducing the hydrostatic head, although the difference is not significant and only limited to low air-water superficial velocity range. From the trends exhibited by the pressure gradient curves it can be noted that they show a decrease in the pressure gradient with decreasing liquid flow rate. At higher air superficial velocities (j_a > 1.2m/s), although the pressure gradient still decreases but the rate of decreased is less rapid. Note that this region corresponds to the transition from agitated bubbly to churn/froth flow where frictional losses are higher in comparison to the agitated bubbly flow.

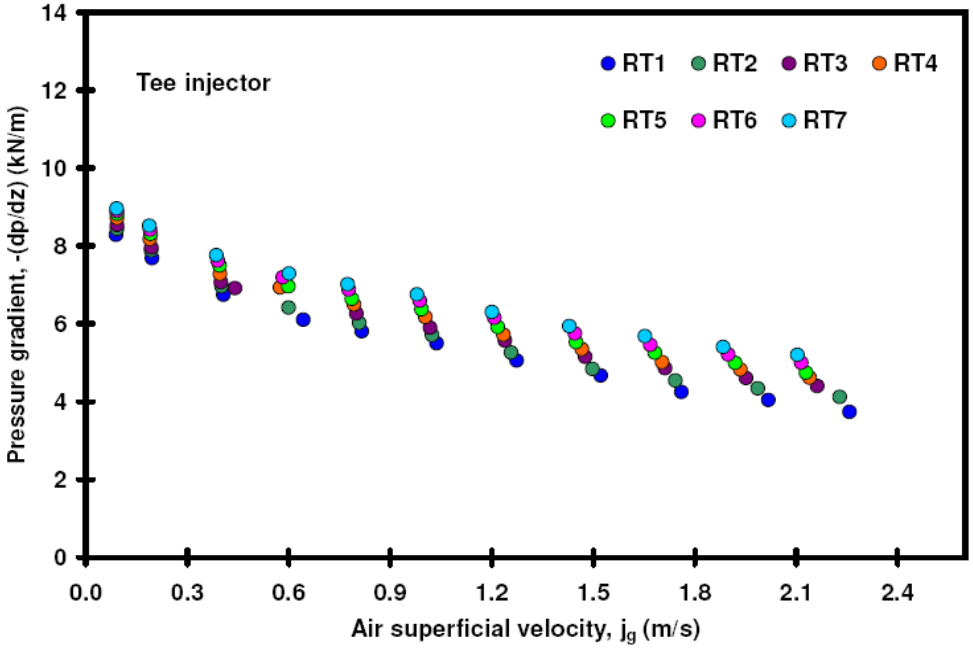

(a)

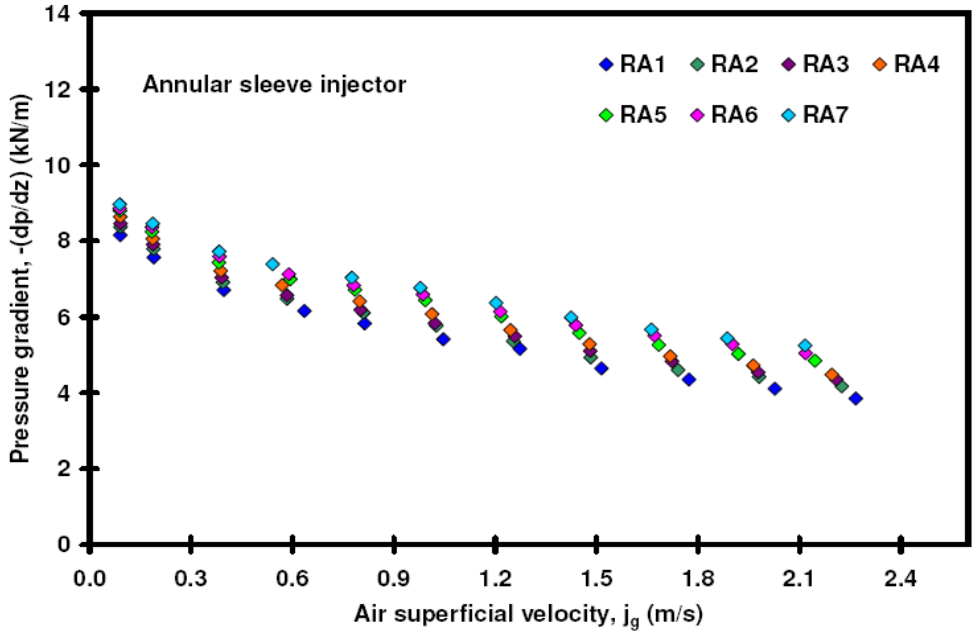

(b)

Figure 4.9 Measured pressure gradient as a function of air superficial velocity for (a) Tee and (b) Annular sleeve injectors under forced lift mode.

It is interesting to note that this rate of decrease occurs at higher water rates. These trends obtained signify that as the air superficial velocity is increased, the total pressure gradient is influenced by two competing factors gravitational and frictional components (acceleration component being negligible). With an increase in the air superficial velocities, the void fraction steadily increases (holdup reduces) causing gravitational component to decrease. In response to this the pressure gradient curve also decreases (and may go to a minimum for any further increase in air superficial velocity-not tested). This is consequence of higher two phase hydrostatic contribution than frictional component, which is still a minor component to influence the total pressure gradient.

The above aspects clearly demonstrates that as the liquid superficial velocity increases the reduction in hydrostatic component becomes less due to the lower void fraction achieved and simultaneous frictional component increase. However, note in the figures that the reduction (in hydrostatic component) is still higher than frictional component hence still influences the total pressure gradient curve. It is emphasized that as the liquid superficial velocity will increase (in the range not tested here), the corresponding the frictional component will also increase and at some critical superficial velocity, this the frictional component will become larger than hydrostatic component causing the total pressure gradient curve to follow the trend as indicated by frictional component of the pressure gradient.

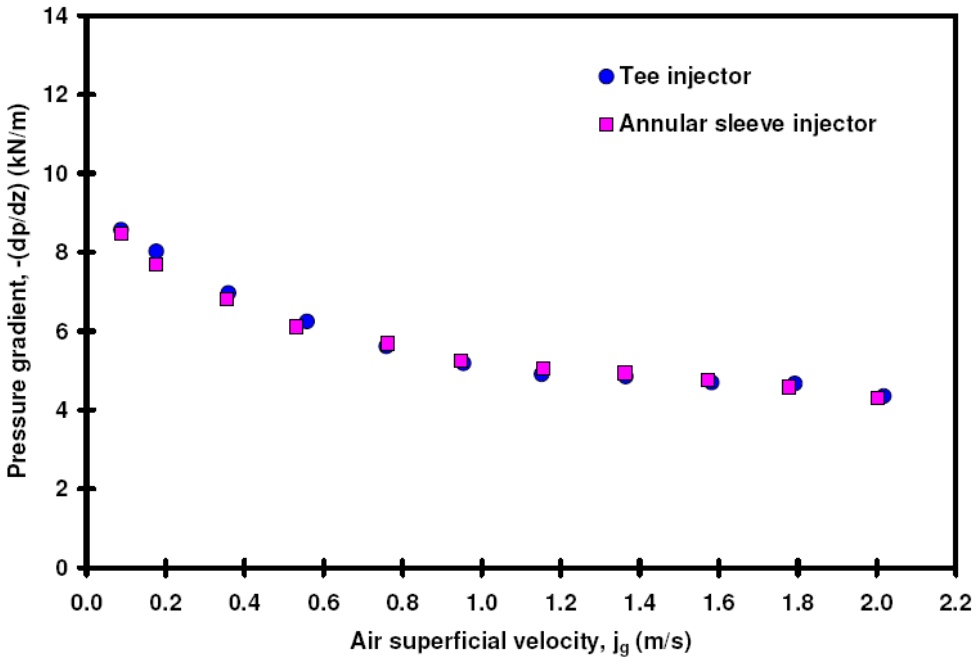

Figure 4.10 Measured pressure gradient as a function of air superficial velocity under natural lift condition for Annular sleeve and Tee injectors.

Above is generally the case in two phase vertical flow experiments where the pipe sizes are small and the velocity ranges tested are in the region where frictional component dominates. However, for given gas-liquid superficial velocities, the contribution of hydrostatic component increases with pipe size. Therefore significant diameter effect becomes evident particularly at lower end of the gas superficial velocities with high liquid flow rates. In present work, it was not possible to fully demonstrate the above nature of the gravitational and frictional components contributing oppositely.

4.1.4 Void fraction characteristics

The third aspect considered in evaluating the performances of the gas injectors is the void fraction distribution. It is important as the sizes of the bubble formed influences the void fraction distribution and hence gaslift technique Guet *et al.* (2003).

Figures 4.11 illustrate the time averaged void fraction distribution in the riser under the natural lift mode. It can be noted that at low air-water superficial velocities the void fraction increases almost linearly, indicating the presence of small uniformly distributed bubbles. As the air superficial velocity is increased the void fraction continues to increase due to increase in bubble population; however this increase in bubble population is also accompanied by coalescing of bubbles which also increases till the point where the flow regime transition to agitated bubbly flow takes place. The overall trend observed is similar to the one seen in liquid production (figure 4.7), i.e. a slightly higher average void fraction distribution in the riser for the annular sleeve injector in comparison to Tee injector at low air superficial velocities only. This is due to the smaller air bubbles injected in the riser from the annular sleeve periphery holes (38mm) than with Tee injector. However at higher air superficial velocities ($j_a >$ 1m/s), the average void fraction distribution under both the injector are almost similar due to the similar flow regime prevailing, indicating that this flow is independent of injector design. Also it could be seen in the figure, that there are no changes in slope of the void fraction trends of the two injectors that demonstrate a flow regime transition. This behaviour further corroborates the observation of gradual transition from bubbly to agitated clustered bubbly flow.

The Figure 4.12 shows the results for forced lift mode with a similar response as natural lift. The estimated void fraction increased with an increase in air superficial velocities while it decreases with an increase of the incoming (pumped) water flow rates. This is due to the increase in the total content of the pipe causing the decrease in void fraction (increase in holdup). The figure further indicates that void fraction values of annular sleeve injector are only marginally higher than Tee injector in bubbly flow (at low void fraction values). This is due to the initial smaller bubble size and the better mixing of injected air all around periphery of the riser. Similar to natural lift case, at the higher superficial velocities void fraction distribution in the riser are almost same due to the same flow regimes occurrence.

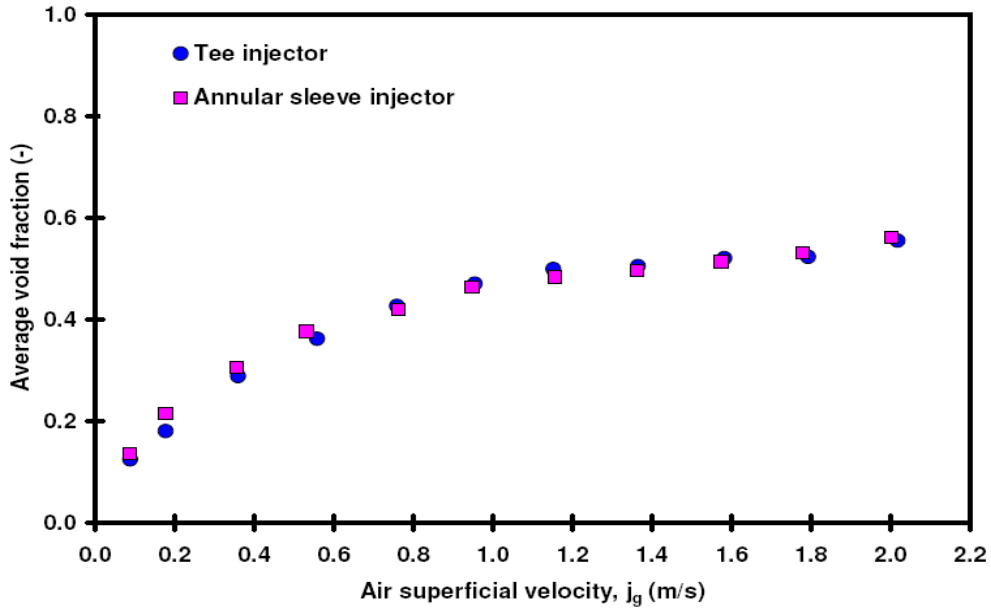

Figure 4.11 The estimated average void fraction in the riser under natural lift condition for Annular sleeve and Tee injectors.

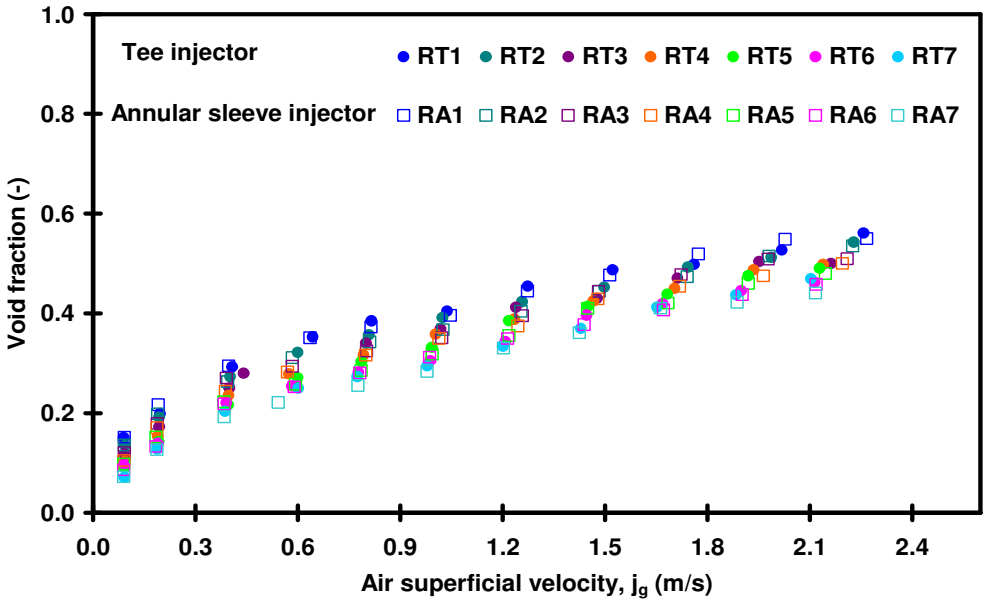

Figure 4.12 The estimated average void fraction in the riser under forced lift condition for Annular sleeve and Tee injectors.

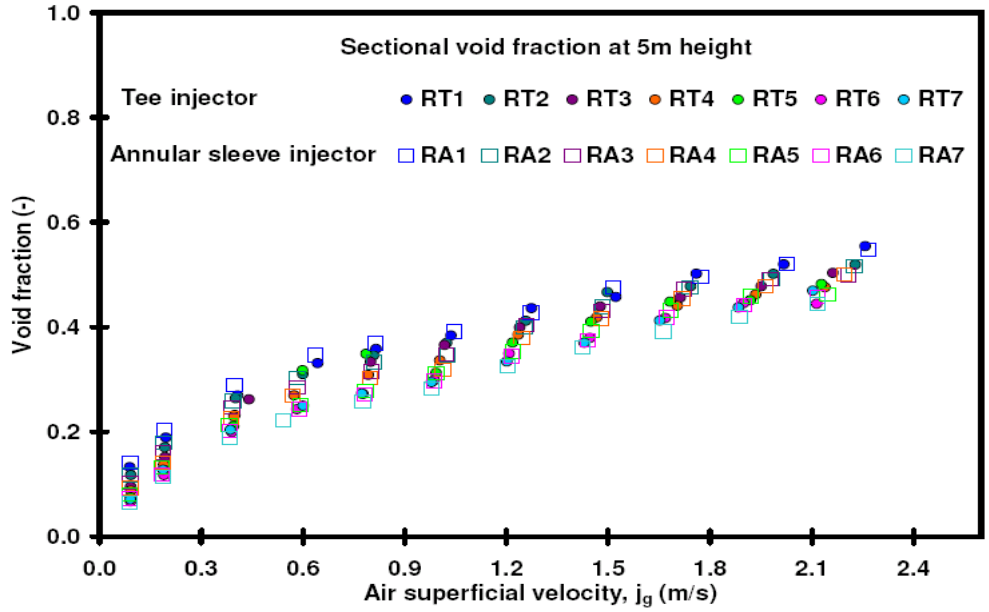

(a)

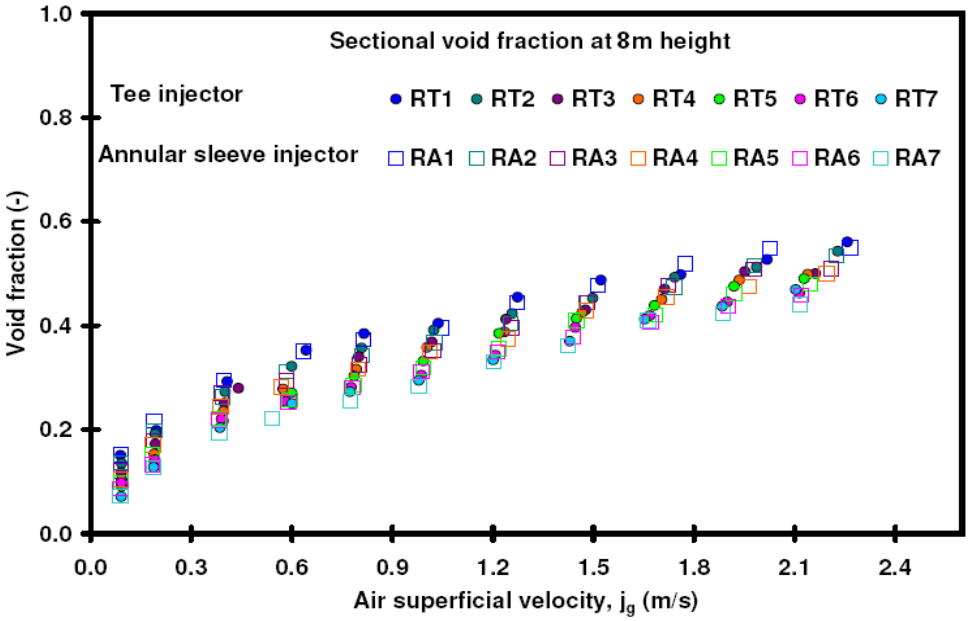

(b)

Figure 4.13 The sectional average void fraction at 5m (top) and 8m (below) height in the riser under forced lift condition.

In order to further investigate the flow behaviour by the two injectors, along side of above average void fraction results, the sectional void fraction distribution in the riser at approximately 5 and 8m height for both the injectors under natural and forced lift modes were also analysed.

Figure 4.13(a-b) illustrates the results of sectional void fraction under forced lift condition for range of water superficial velocities. The figure indicates the combine results of Annular sleeve and Tee injector at 5 and 8m heights. The higher void fraction distribution of annular sleeve injector is obvious for low air superficial velocity range at both heights but diminishes at higher air superficial velocities. This also means that at higher air superficial velocities both the injectors' performances are similar in nature.

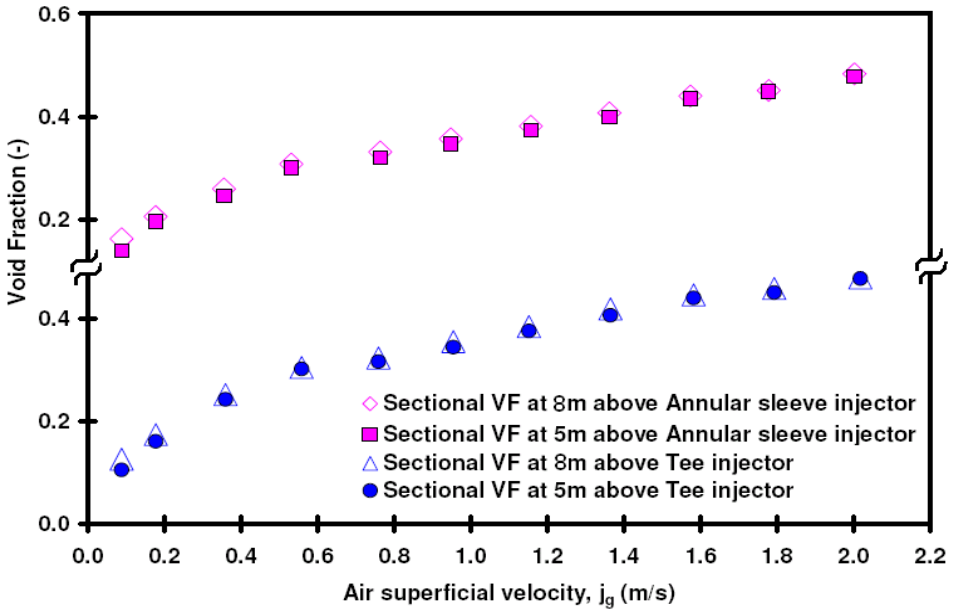

Figure 4.14 The sectional average void fraction at 5m and 8m height in the riser under natural lift condition.

Figure 4.14 depicts the sectional average void fraction for both the injectors under natural lift mode for the both the injector's separately. The overall result shows the increasing effect of void fraction with an increase in air superficial velocities. There is a slight increase in sectional void fraction at 8m than at 5m height for both the injectors, at lower superficial velocities only i.e. in bubbly flow regime. However, at the higher air superficial velocities, the sectional void fraction at the two heights (almost 3m apart) are almost the same. Since the magnitude of sectional void fraction does not change significantly along the pipe, this may approximately represent that the flow is quasi-fully developed. It is to be noted that in usual practice if the bubble size distribution and radial profiles at particular and subsequent locations are

equivalent then a fully developed flow is reached. The results for the forced lift also support the above observation of natural lift mode.

Although in the figures presented earlier (Figure 4.11 to 4.15) annular sleeve values are slightly higher than Tee injector at low air superficial velocities, the difference between the performances of the two injectors are not clearly visible. Thus Figure 4.15(a & b) presents the results in terms of the ratios of Annular sleeve and Tee injector void fraction under forced lift. In Figure 4.15(a), the ratio of time average void fraction across the riser height is given, the trends associated with injectors substantiate the higher liquid production results for annular sleeve injector at lower volumetric fluxes. Similar results are obvious for sectional void fraction distribution in Figure 4.15(b). This has been attributed to the smaller bubble size and uniform distribution from annular sleeve injector. The figure also demonstrates that the influence of the injectors on the measured void fraction distribution proved to be weak at higher volumetric fluxes as indicated by the previous results. In fact the Tee injector performance was marginally higher in this region. This later effect was attributed to the breakage of the large bubbles dominant in case of the Tee injector while coalescence is still prevailing for Annular sleeve injector in this region.

4.1.5 Riser base pressure characteristics

The factor considered for the performances of the injectors is the riser base pressure. The parameter is an important factor but has not been previously considered in lift performance. It was employed to represent the characteristics of the injectors for two reasons:

(1) The trends of the time-averaged values of riser base pressure for different gas superficial velocities will represent the behaviour of individual injector. This is important as the reduction in its magnitude will increase the liquid inflow from the upstream.

(2) The time series riser base pressure variations can be used to characterize the nature of the flow entering the riser from the flowline, consequently the effect of injectors on the behaviour of this flow could be studied.

Figure 4.16 and 4.17 presents the experimental results of the near riser base pressure versus air superficial velocity for both the injectors in forced and natural circulation mode.

In Figure 4.16 for the forced lift case, both the injectors indicate a similar trend i.e. decrease in riser base pressure with the increasing air superficial velocity. This is due to the increase in void fraction with the air superficial velocity. However the rate of pressure decrease was lower for higher water flow rates, this was due to buoyancy force compensated by a corresponding increase in the frictional force leaving the reduction capacity to level off. The riser base pressures were especially higher for the lowest air injection rates because these values were unable to provide an optimum lift, nevertheless with an increase in air superficial velocities, the riser base pressure decreases.

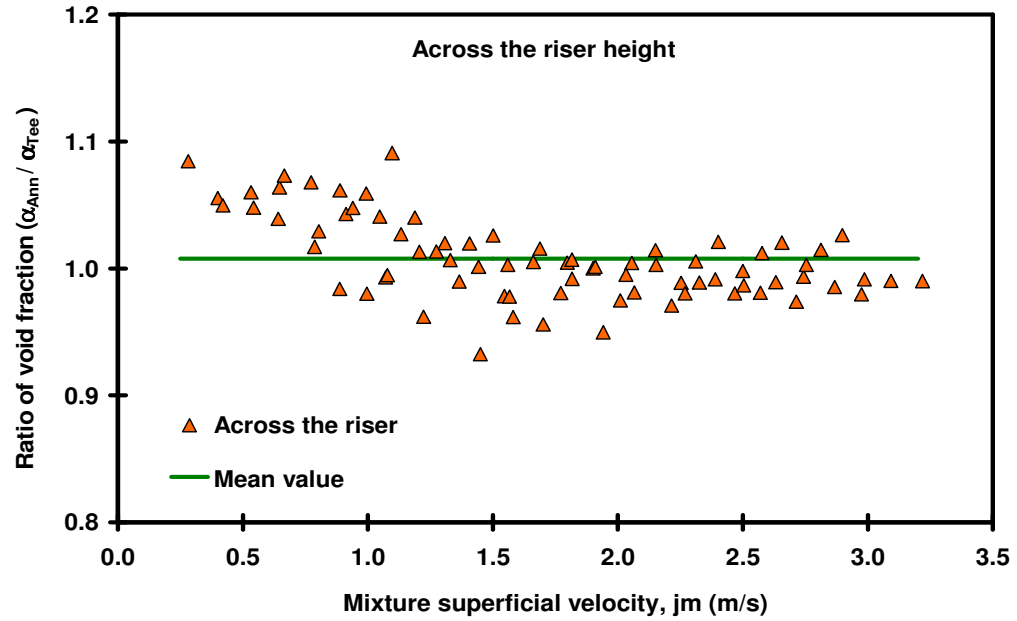

(a)

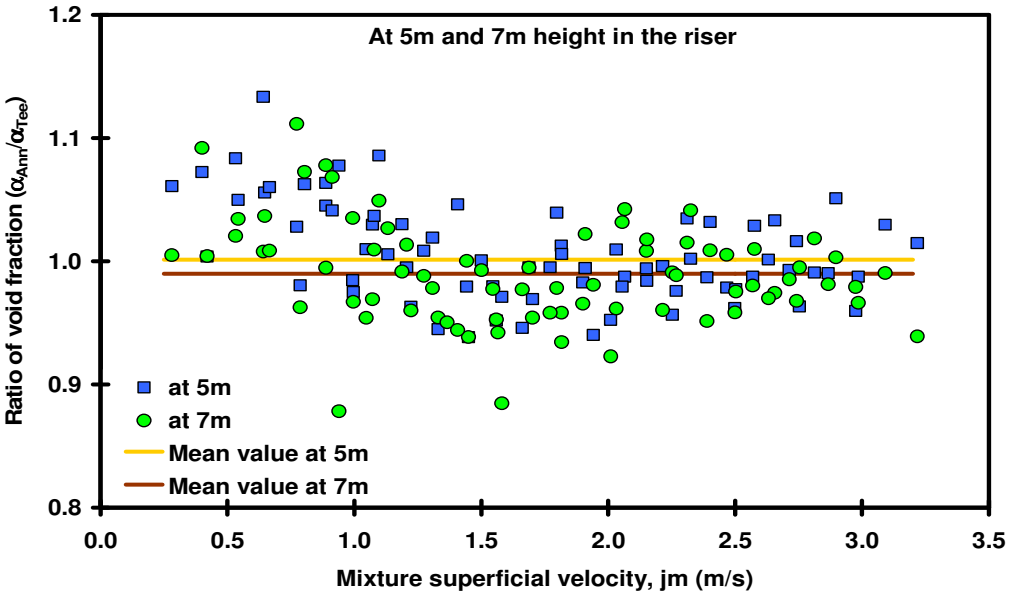

(b)

Figure 4.15 Ratio of void fraction values α_{ANN} / α_{TEE} across the riser height for all the riser injection tests.

The figure also indicates the values of the single phase riser base pressures for comparison with those of air-water mixture. The single phase has higher riser base pressures than that with gas lift. The figure illustrates that the riser base pressures were higher for the Tee injector at lower air superficial velocities in case of forced/pumped flow. This was related to two observations: firstly, due to the large bubble sizes rising at higher velocities, secondly, the slowing down of upcoming water from the upstream due to the air injection perpendicular to the flow. The later aspect as explained earlier caused the incoming riser base water flow to slow down near the point of injection (see Figure 4.1 also). In comparison to above, the annular sleeve injector riser base pressures, in Figure 4.16 are lower than Tee gas injector in the same air superficial velocity range. This was due to the symmetrical distribution all around the periphery of the riser. This allows the upcoming water flow to mix up well in the injector area with air, thus reducing the riser base pressure more than Tee injector. At higher air superficial velocities the behaviour of the two injectors are similar. The riser base pressure trends in the Figure 4.17 for natural lift mode indicated the similar trends as observed in the above forced lift condition that the air superficial velocity increase caused the riser base pressure to decrease.

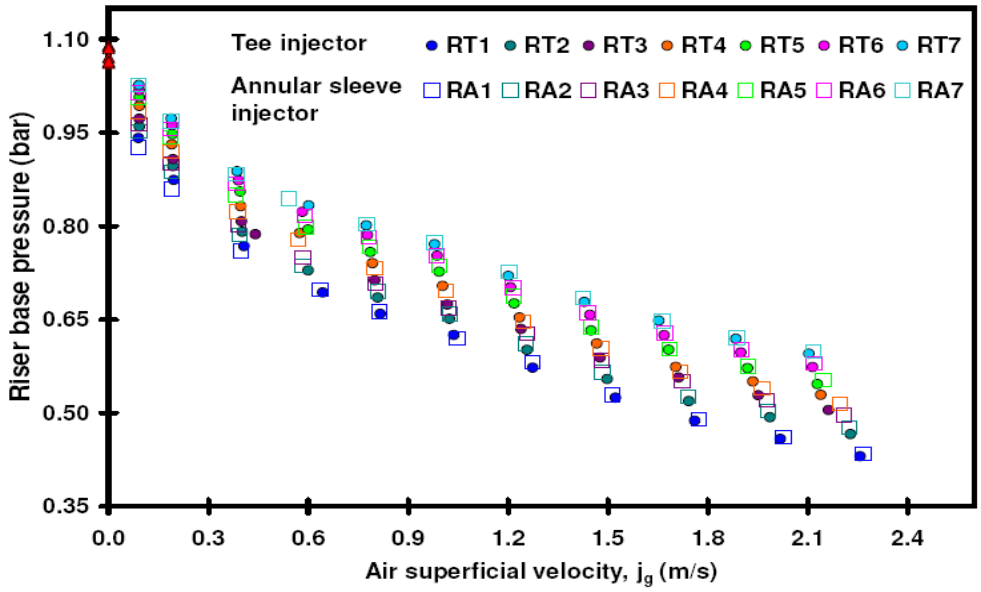

Figure 4.16 The riser base pressure trends under forced lift condition for Annular sleeve and Tee injectors.

4.1.6 Stability characteristics

The final factor considered in evaluating the performances of the injectors is the flow stability. This was needed in order to verify the injector's ability to stabilize the

unstable flows. In actual field conditions the flow instabilities are likely to arise at low gas-liquid superficial velocities due to the conditions such as configuration of the riser base (downward inclined or undulating pipe or complex riser shape) and production flow hydrodynamics like at start-up of the system or at the end of the well life. These flow instabilities results in cyclic production of long liquid slugs that are much longer than steady state slug. The gas injectors are used to mitigate these flow instabilities.

In this work since the simplified horizontal flowline-riser topology is used so the severe slugging is not expected to occur. Therefore, the slug flow (also called hydrodynamic slug flow) encountered in the horizontal flowline was tested to see the gas injectors response. It is to be noted that unlike the severe slugging that occurs at low gas-liquid superficial velocities, the slug flow is encountered at higher gas-liquid superficial velocities. It is also worth mentioning that the slug flow from the horizontal flowline was compounded to more vigorous type of slug flow due to liquid fall back from the riser top. However, this type of flow is as important as severe slugging because in certain cases, such as large and very long flowlines, liquid slugs can be longer than expected from hydrodynamic slugging or transition to slugging (Brill *et al.*, 1981).

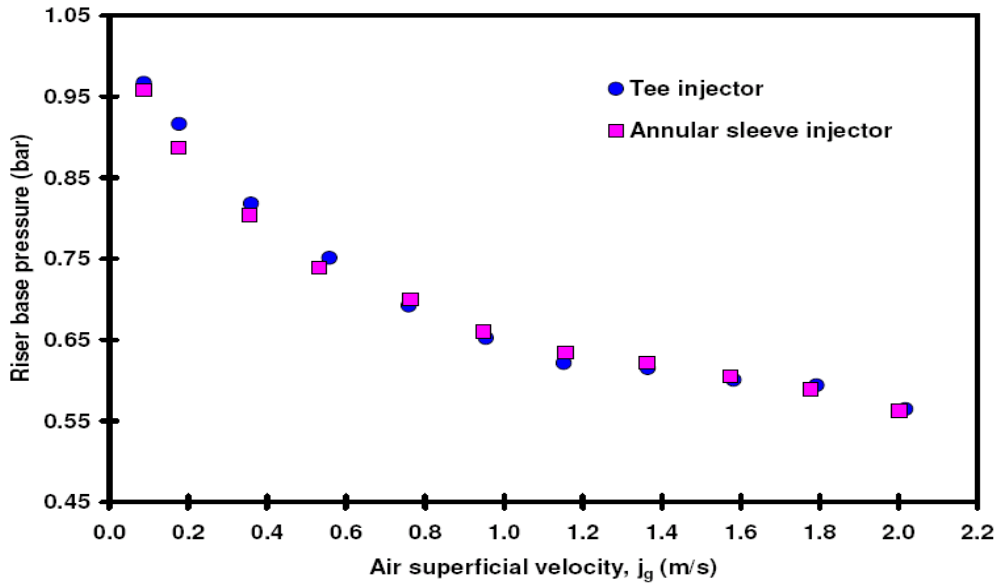

Figure 4.17 The riser base pressure trends under natural lift condition for Annular sleeve and Tee injectors.

In order to evaluate the stability characteristics, combined near riser base-upstream gas injection experiments were performed (refer to chapter 3, Figure 3.7c-d). The results from the near riser base-upstream gas injection cases were compared with the

simple upstream gas injection experiments. For the cases discussed later i.e. the upstream gas injection, the slug flow was imposed before the entrance to the riser.

The Figure 4.18 below shows the time varying flow behaviour at the exit of the flowline and near riser base for the three conditions, (a) when upstream gas injection is performed, (b) near riser base air injection with Tee injector, and (c) near riser base air injection with annular sleeve injector.

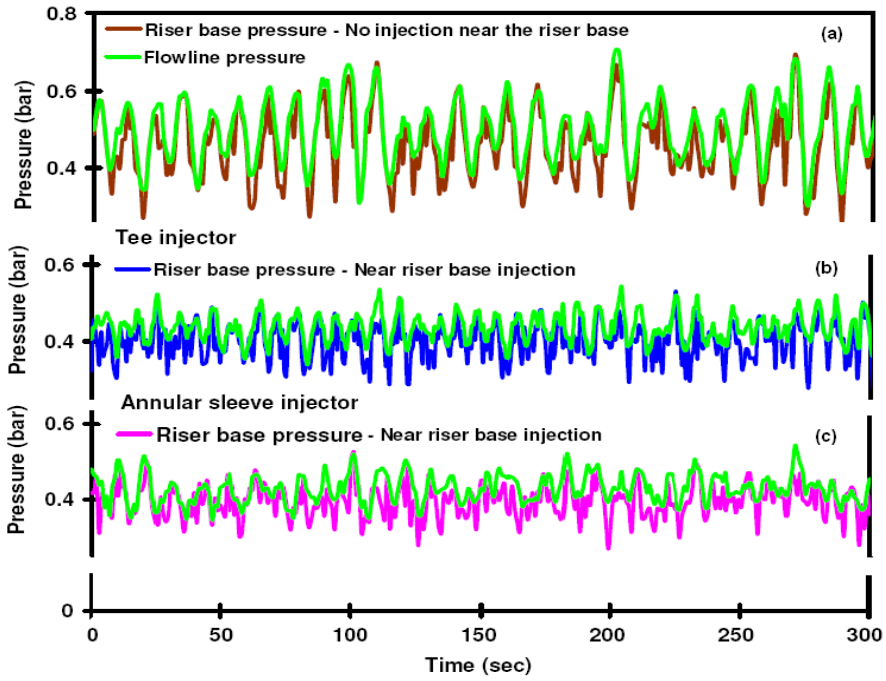

Figure 4.18 The flowline exit and near riser base pressure trends for (a) upstream injection, (b) by Tee and (c) by Annular sleeve injector at j_w =0.3m/s, j_a =1.71m/s and $j_{a,inj}$ =0.45m/s.

The first case in Figure 4.18(a) represents the upstream gas injection having air-water superficial velocity of 1.70 and 0.31m/s respectively. For this case, the flowline flow regime is typically in the range where actual field conditions experiences flow related issues. The trends in the Figure 4.18(a) suggested that the two phase flow (air and water) in the flowline and near the vicinity of the riser base was slug flow. The flow was regular slug flow where the peaks indicate the slug frequencies and their magnitudes indicating the size of the slugs. It can be noted that the slugs formed were regular but of slightly different sizes. In fact this particular flow was a continuation of intermittent flow that had started occurring at slightly lower gas velocities (see Appendix B). The maximum and minimum riser base pressures were around 0.71 and 0.19bars respectively. Visual evidence suggests that these slugs formed in flowline and the riser base areas were pushed up in the riser by the available gas drive, where

they dissipated naturally to some extent. This is due to the high air superficial velocity entering the riser, rapidly accelerating and penetrating into the liquid slug ahead causing the liquid slug to break and fall back on incoming flow that further distorts and successively fall backs. On the conventional horizontal flow regime map under these air-water superficial velocities, stratified flow was expected to occur. However, the liquids slugs were already formed at these low water velocities. In context of current experiments, these slugs were formed due to the downstream topology of the riser i.e. the 90º connection of the flowline to the riser or upstream eccentric expander (or combine effect). It postulated that this terrain influence allows slugs to be present for the flow conditions which normally would result in stratified flow. This configuration caused the accumulation of liquid in the flowline due to slowing down of the water near the flowline-riser base vicinity and thereby initiating the slug formation from upstream. This notion is further supported by Bendiksen and Malnes (1987) work who have reported that there exist strong effects of upstream and downstream conditions on the stratified-slug transition.

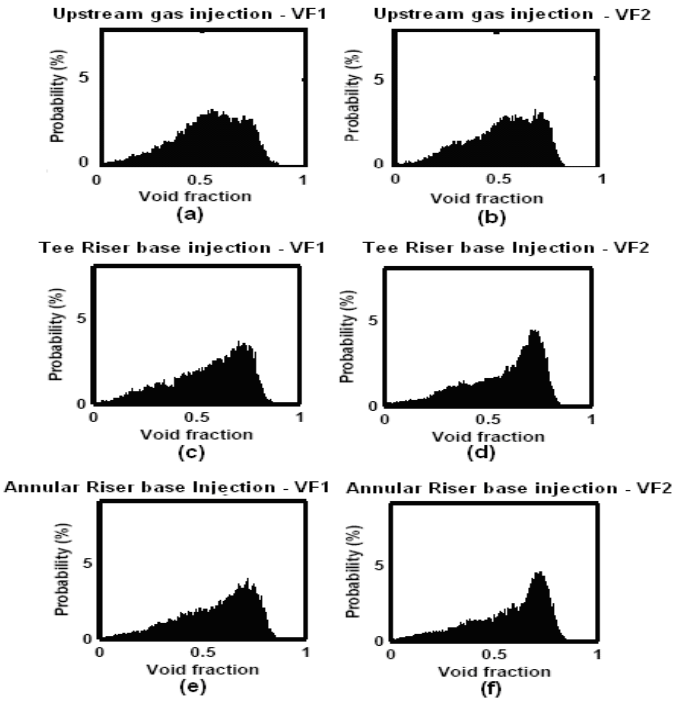

Figure 4.19 The void fraction probability mass function plots taken at the height of 5 and 8m for (a) Upstream injection, (b) by Tee and (c) by Annular sleeve injector at j_w =0.3m/s, j_a =1.71m/s and $j_{a,\,inj}$ =0.45m/s.

Figure 4.18(b & c) presents the results obtained under the condition of near riser base air injection by the two injectors. For Tee injector the test conditions are j_w = 0.3m/s with j_a = 1.71m/s and $j_{a,inj}$ = 0.44m/s. For annular sleeve injection, j_a = 1.55m/s and $j_{a,inj}$ = 0.50m/s respectively. The cases illustrate the effect of gas injection, the overall

near riser base and flowline pressures has decreased and flow pattern is much more stabilised in the near riser base vicinity, in comparison to the upstream gas injection. The injection in the base vicinity has cause the reduction in flowline pressure thus flowline slugs to shrink. In fact the gas injection has affected the flow pattern in flowline to the extent that the flow became more of roll waves with small irregular slugs entering in the riser base. In the of case near riser base injection with Tee injector, the maximum and minimum riser base pressure values observed are 0.529bar and 0.237bar while that for annular sleeve injector are 0.526 and 0.249bar respectively. The results presented above along with visual observations suggest that the gas injection from both the injectors in the near riser base vicinity had effectively dissipated the slugs formed with little difference in performances.

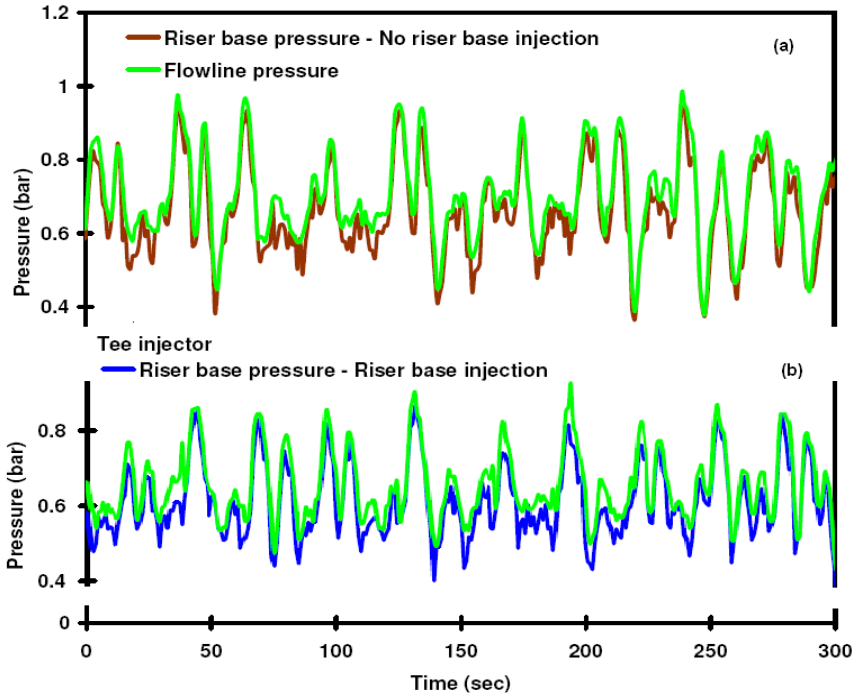

Figure 4.20 The flowline exit and near riser base pressure trends for (a) Upstream injection and (b) by Tee injector at j_w =0.57m/s, j_a =0.98m/s and $j_{a,inj}$ =0.45m/s.

The performances of the gas injectors flow behaviour ahead in the riser was confirmed by the use of the void fraction probability mass function plots. Such plots have been used previously by many investigators (Costigan and Whalley, 1997 and Cheng *et al.*, 1998) to determine the flow pattern occurring in pipes.

The Figure 4.19 shows the void fraction PMF plots of flow behaviour ahead in the riser at approximately 5 and 8m height for all the above three cases; upstream gas injection and gas injection by the Tee and Annular sleeve injectors in the base vicinity. While the upstream gas injection does indicate some survived liquid slugs

(indicated by the broader distribution and thick tail), both the injectors indicated a more uniform distribution, refer to Figure 4.19(c-f). The addition of gas injection in the riser aerated the riser to the extent that the flow is more of churn/froth flow and the incoming slugs are diluted. This demonstrates that the gas injection increases the stability of the flow by the changing the flow pattern in the riser. This result further verifies the visual results presented in section 4.1.1, i.e. showing no sign of injector design on the type of flow pattern occurring in the riser.

Although the technical difficulties limited the experimental runs at higher water superficial velocities restricting the water velocity to approximately 0.61m/s, this range still allowed the limited runs within the slug flow regime so that slugging behaviour could further be exploited. The Figure 4.20 presents the results of case that is showing the beginning of hydrodynamic slugging in the flowline where the incoming slugs from the downstream of the flowline became longer and more regular.

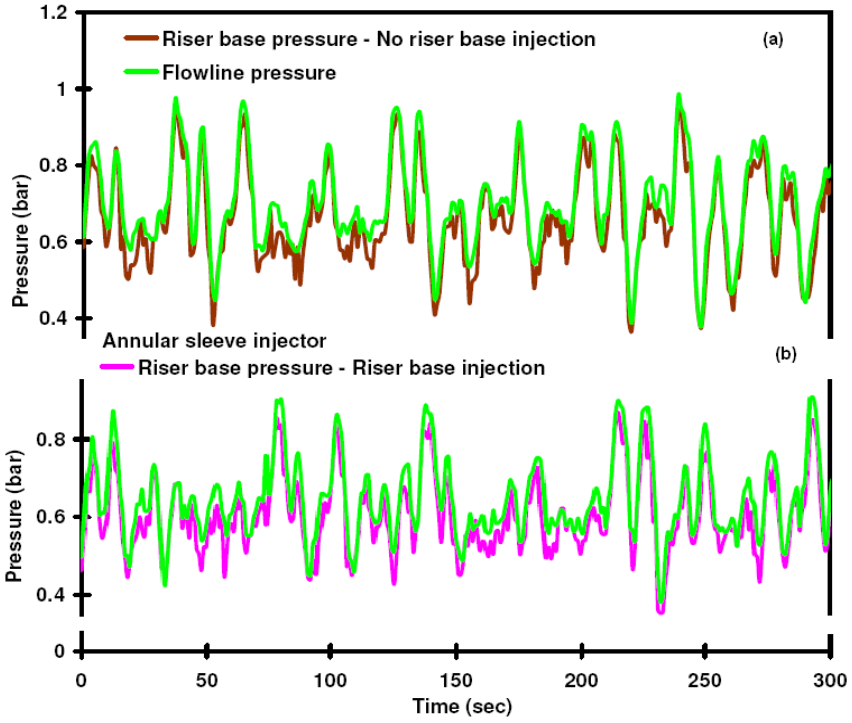

Figure 4.21 The flowline exit and near riser base pressure trends for (a) Upstream injection and (b) by Annular sleeve injector at j_w =0.57m/s, j_a =0.98m/s and $j_{a,inj}$ =0.35m/s.

The test case conditions are j_w = 0.57m/s with j_a = 0.98m/s with air injection superficial velocity of 0.4m/s respectively. The Figure 4.20(a) shows the flowline exit and near riser base flow behaviour with upstream gas injection. The increase in the liquid inventory in comparison to the former case is evident, causing larger slugs.

Along with upstream gas injection, Figure 4.20(b) and Figure 4.21(b) illustrates the gas injection effect of the two injectors. Both the figures, clearly shows that both average and peak riser base and flowline pressures are reduced (slug size is reduced) at only (50%) of the inlet superficial velocities. Thus gas injection in the near base vicinity has caused the liquid slugs to break into smaller segments. However, these injected velocities are not high enough to completely break the riser base blockage, hence the flowline was still slugging because of the compressional effect produced by the water accumulated in the riser base vicinity. Note that the total air velocity still corresponds to a value lying in region of hydrodynamic slugging thus, in order to eliminate slugging, considerably higher air superficial velocities are required to change the flow pattern to annular flow.

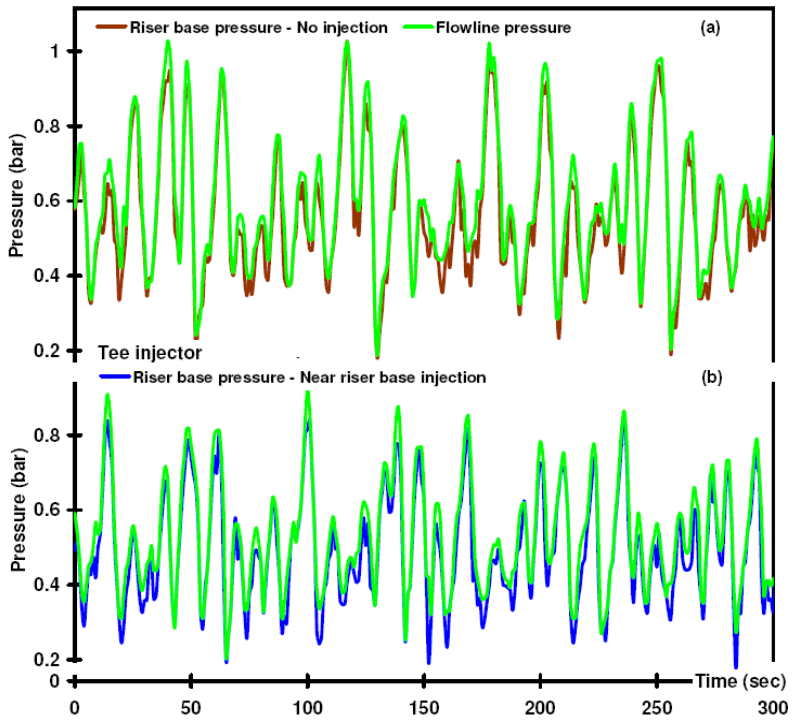

Figure 4.22 The flowline exit and near riser base pressure trends for Upstream injection and by Tee injector at j_w =0.61m/s, j_g =1.68m/s and $j_{g,inj}$ =0.5m/s.

The Figures 4.22 and 4.23 illustrates the case of intense slugging in the flowline (j_w = 0.61 m/s and j_a = 1.68m/s). The mean riser base pressure was quite high due to the high liquid inventory with maximum and minimum near riser base pressure value 1.019 and 0.234bar respectively. The minimum pressure represents that substantial amount of water remains in the riser post-blowdown. However from the Figures 4.22(a) and 4.23(a), the flow behaviour observed was not that of typical slug flow but rather a more excursive and irregular pressure cycling representing different size

slugs due uneven gas penetration from the flowline. This nature of the flow suggested that hydrodynamic slugging had been compounded by some other influence. The close observation suggests that hydrodynamic slugging in flowline was compounded by liquid accumulation in the riser base. This is well indicated in Figures 4.22(a) and 4.23(a) by one or two small slugs followed by a longer slug. Small slugs are formed due to continuous liquid fall back and accumulation in base area and longer slugs corresponds to incoming slug from the flowline. Similar to previous cases observations, the slugs formed were seen to dissipate naturally to some extent (refer to Figure 4.46(g-h)). This is the consequence of the diameter of the riser, because as the gas from flowline entered the riser, it accelerated and rapidly breaks through the small liquid slug ahead. The falling frothy mixture over the preceding gas or slugs made the whole riser appear as an oscillating column moving upward with frothy flow or falling downward with froth flow. In some cases gas could not penetrate the whole liquid slug and some slug structure survive this gas penetration and travelled ahead. It is emphasized here again that due to the horizontal topology of the flowline, the flowline slugs were only few meters in length. Hence this case was of unstable flow rather severe slugging where the liquid slug lengths are expected to be equivalent length or greater in length to riser height.

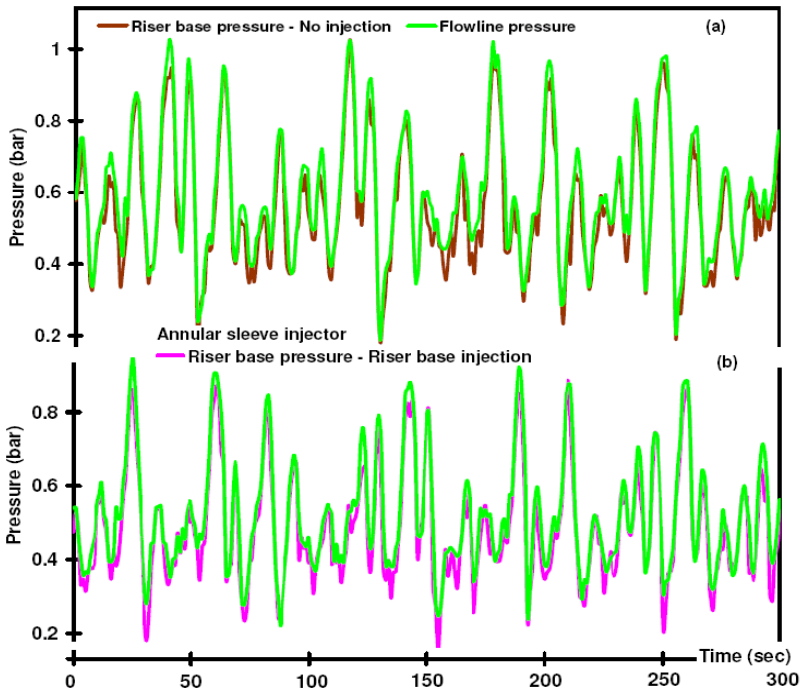

Figure 4.23 The flowline exit and near riser base pressure trends for Upstream injection and by Annular sleeve injector at j_w =0.61m/s, j_a =1.68m/s and $j_{a,inj}$ =0.5 m/s.

The Figure 4.22(b) and Figure 4.23(b) presents the results of gas injection in the base vicinity by the Tee and annular sleeve injector respectively. The injected gas in both

cases is about 0.5m/s. Technical difficulties restricted the air injection superficial velocity in the base, only allowing partial stabilization effect. The figure shows that although the mean riser base and flowline pressures have decreased, typical slug characteristic still persists; this is because the injection gas superficial velocity (approximately 40% of the inlet) was not sufficient to free the flowline from liquid accumulation. However, note that average and peak riser base pressures of both the injectors (blue and pink legend) have reduced. This was an indication that the gas injection in the base vicinity has caused more liquid to be removed in comparison to the no injection case where substantial amount of liquid remain in the riser causing longer slugs. Thus due to the aeration of the base vicinity, the maximum riser base pressure was now around 0.86bars for Tee injector and 0.88 for annular sleeve injector.

Two important aspect inferred from above behaviour are, firstly, it was found that the riser base pressure cyclical behaviour observed was more influenced by the flowline conditions or the flow regime prevailing in the flowline. Hence the near riser base injection does not influence the flowline to the extent that a complete removal of the accumulated liquid can be achieved while freeing the base vicinity. Secondly, the gas lift does provide a stabilizing effect to the unstable flow; however a full stabilization required the increase in gas superficial velocity to bring the riser flow regime into the annular flow.

The Figure 4.24 provides the void fraction PMFs of the flow behaviour in the riser (at 5 and 8m height) for upstream gas injection, Tee riser base injection and Annular sleeve riser base injection. The Figure 4.24(a) shows that while few of slugs dissipated naturally, some of the liquid slugs survived, however, the Figure 4.24(b) shows twin peaks of same height. The twin peaks have almost similar heights representing the simultaneous decay of liquid slugs and coalescence of gas phase in the core region. This behaviour indeed verifies that liquid slugs were naturally dissipated while travelling up in the riser. In comparison to above, Figure 4.24(c) of Tee riser base gas injection clearly indicates that air injection has caused some of the liquid slugs to dissipate while travelling upward. There is a weak liquid peak and a prominent gas peak due to the coalescent of gas phase and liquid fall back. From the Figure 4.24(d), it can be noted that the peak at the higher void fraction is not only higher than rest of the distribution but also broader indicating that the gas structures are longer and distorted. Figure 4.24(e) illustrates the flow behaviour for annular sleeve injector case. There is slight variation in comparison to Tee injector, here a more subtle and gradual transition is approached with Figure 4.24(f) showing a more uniform transition towards churn. This further verifies our earlier results of annular sleeve showing more uniform air distribution all around the periphery of the riser. However, due to limited gas injection rate, there is also long thick tail extending towards lower void fraction indicating some of the survived aerated slugs, typical characteristic of intermittent/transitional flows.

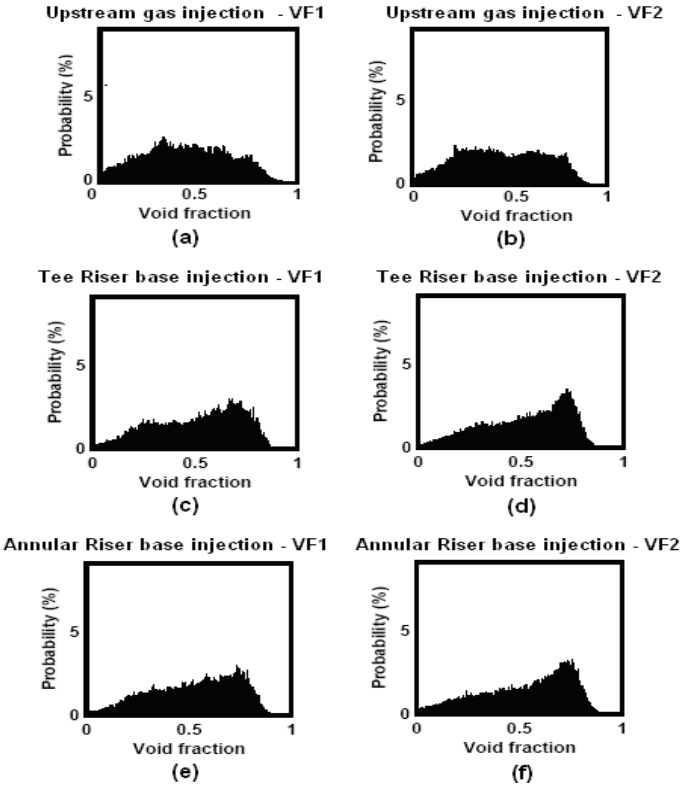

Figure 4.24 The void fraction probability mass function plots taken at the height of 5 and 8m for (a) Upstream injection, (b) by Tee and (c) by Annular sleeve injector at j_w =0.61m/s, j_a =1.68m/s and $j_{a,inj}$ =0.5 m/s.

4.1.7 Interim Summary

In this section of the chapter, a major investigation of the hydrodynamic performances of a conventional Tee gas injector and a novel design Annular sleeve gas injector was undertaken. The large diameter horizontal flowline-vertical riser facility was used in four (4) different flow loop configurations (refer to Figure 3.7) to examine the hydrodynamic characteristics in details. The above mentioned flow loop configurations facilitated the experiments by mimicking the actual flow conditions such as low pressure wells; flowline-riser experiencing flow instabilities and RBGL application to stabilize the unstable/cyclic flows. Many hydrodynamic variables including visual flow observation, lifted liquid flow, pressure gradient, void fraction, riser base pressure and stability of the flow were invesitaged and compared.

The experiental results demonstrated that the Annular sleeve gas injector should be the preferential choice over the conventional Tee gas injector. This is because the Tee gas injector performed well only at high air superficial velocities, while the novel Annular sleeve by virtue of its versatile design was able to perform equally well at both the ends of the air superficial velocity range. At low air superficial velocities it

provided more liquid lift, so could be utilized for smooth production, while at the higher air superficial velocities its performance is equivalent to that of Tee gas injector. In fact, the gas lift stabilization produced by annular sleeve is much smoother and gradual. Additionally, due to its design, no potential concerns of gas jetting on opposite wall are possible.

Part II – Flow Pattern Characterization

4.2 Flow Regime

The aim of almost all the two phase flow research has been with the prediction of flow regimes so that the basic characteristic of those flow regimes can be established. Thus the most important aspect of this work was the determination of the flow behaviour by analysing the flow patterns. Although the existing flow patterns have been briefly discussed earlier, below is the detail study conducted on the flow patterns in large diameter vertical riser set up.

4.2.1 Flow regimes classification

The flow behaviour identification was performed by visual observation through the transparent perspex sections installed specifically for this purpose at the four different heights in the riser i.e. just above the gas injectors and then at approximately at 5, 8 and 10m height. However, other sensors time varying responses (pressure/differential pressure signals) for the identification of the flow patterns and their transition in conjunction with the photography and high-speed videoing of the individual runs were also undertaken to avoid any subjectivity. These will be discussed in later sections.

Ohnuki and Akimoto (2000) defined five types of flow in their experiments in 200mm diameter vertical pipe as undisturbed bubbly, agitated bubbly, churn bubbly, churn/slug and churn/froth flow. Nevertheless, in the present analysis a simplified classification is employed to avoid any subjectivity by considering the flow regimes in large diameter vertical pipe air-water upflow to be consisting of following flow regimes namely:

- ***Dispersed Bubbly Flow***
- ***Bubbly Flow***
- ***Agitated Bubbly Flow***
- ***Churn/Froth Flow and***
- ***Unstable slug flow*** as a special case i.e. consequence of inlet configuration.

Note that the present flow pattern classification of agitated bubbly and churn/froth flow includes all the variation of churn flow defined by Ohnuki and Akimoto (2000).

This is been done intentionally as we planned to clear out the above delineation more clearly in later sections. Below section described the main features of the flow regimes along with their illustrations:

4.2.2 Visual observations

4.2.2.1 Dispersed bubbly flow: In this flow regime the bubbles formed were small, spherical and uniformly distributed by sufficient distance. No bubble to bubble interaction existed due to the high liquid rate turbulence, sufficient to break up the large bubbles as well as suppress coalescence (Taitel *et al.*, 1980; Barnea *et al.*, 1986). The differential pressure time varying record showed small amplitude random fluctuations, see Figure 4.25(a-c). This flow regime appeared in few experimental runs only at high water and low air superficial velocities (j_g =0.06-0.1m/s and j_l >0.7m/s) i.e. at a very low void fraction. Figure 4.25(b & d) shows the video image of the flow with both Annular sleeve and Tee injector

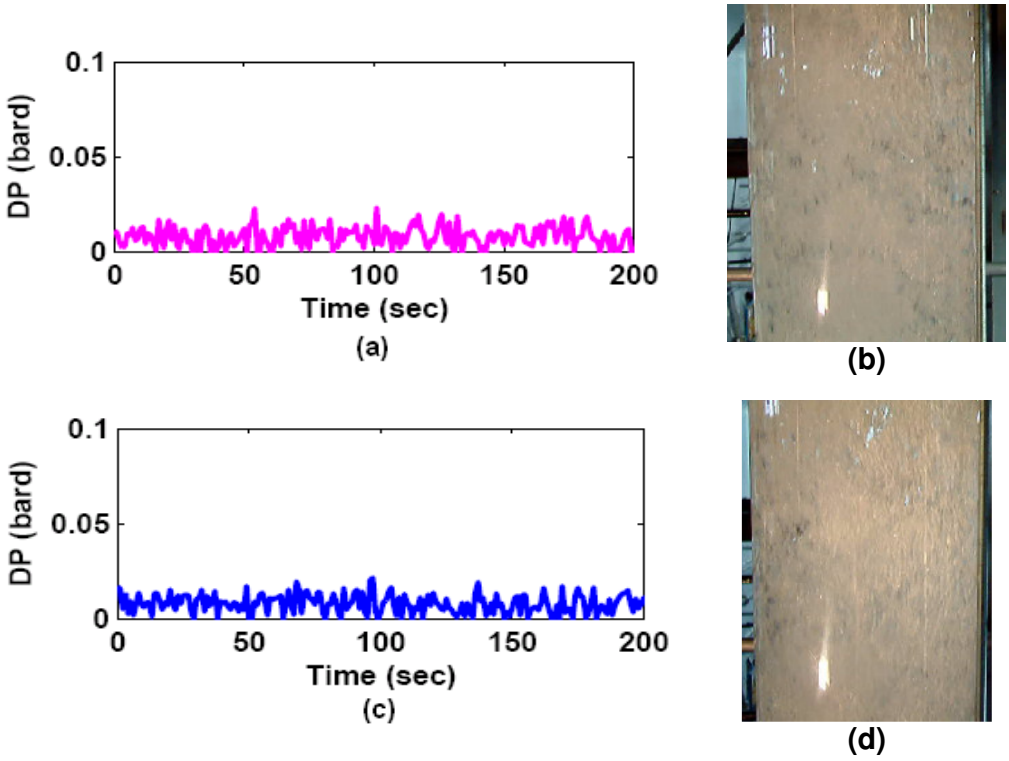

Figure 4.25 Dispersed Bubbly Flow, $j_l \approx 1$m/s and $j_g = 0.09$ m/s, showing: (a) & (b) time trace and flow image for Annular injector and (c) & (d) time trace and flow image for Tee injector.

4.2.2.2 Bubbly flow: This flow pattern was obtained under low air-water superficial velocities. While many researchers have not made any distinction in above dispersed bubbly flow and this bubbly flow also referred as non-dispersed bubble flow (Hewitt and Roberts, 1969; Weisman and Kang, 1981; Mishima and Ishii, 1984), others have classified this flow as low-liquid-input bubbly flow or non dispersed bubbly flow (Taitel *et al.*, 1980; Weisman and Kang, 1981; McQuillan and Whalley, 1985; Brauner and Barnea, 1986; Barnea 1987). In this flow regime, the bubbles were of distorted spheres shapes in large population having very small separation distances. Bubbles in the core region were occasionally coalescing to form larger ones during their upward flow, see Figure 4.26(b-d). However, there was no obvious secondary flow near the wall. The differential pressure vs. time record indicated slightly higher amplitude random fluctuations than observed with dispersed bubbly flow, refer to Figure 4.26(a-c) occurring in the range of j_g = 0.18 – 0.45m/s air superficial velocities. It can be noted that the fluctuations are more rapid and dense due to the interactions of large bubble population.

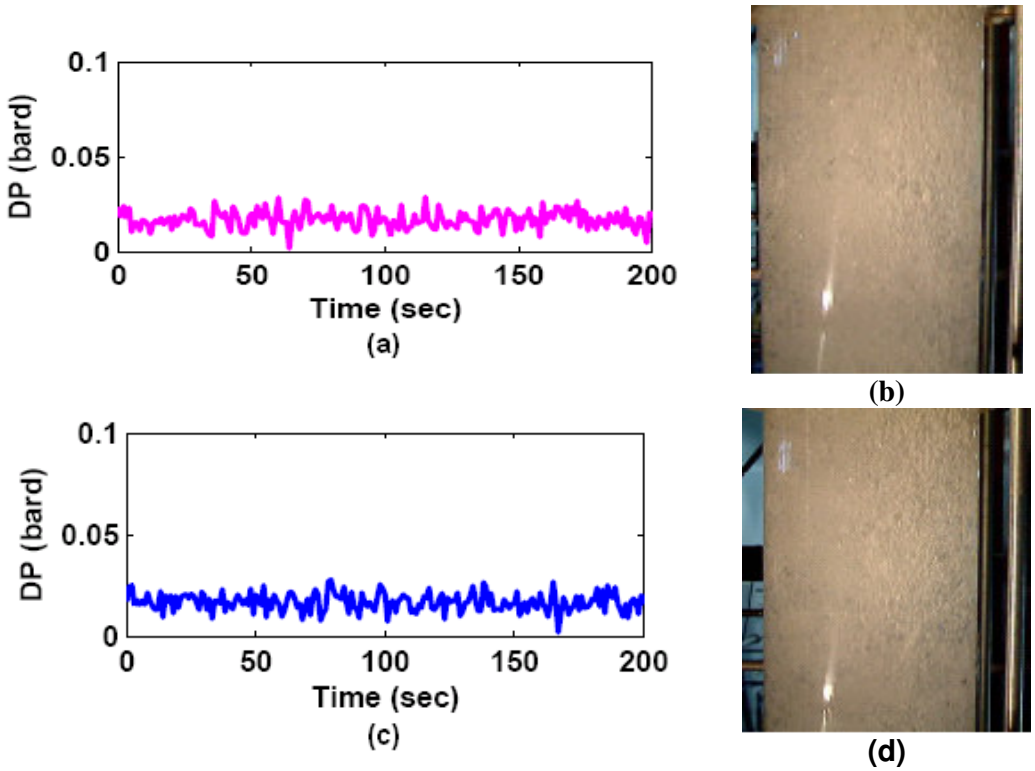

Figure 4.26 Bubbly Flow, $j_l \approx 0.25$m/s and $j_g = 0.09$ m/s, showing: (a) & (b) time trace and flow image for Annular injector and (c) & (d) time trace and flow image for Tee injector.

4.2.2.3 Agitated Bubbly: This type of the flow was not observed previously in small diameter vertical pipes. Most of the earlier work on large diameter classified this flow as transitional flow having visual characteristics of both bubbly and churn/froth flow. However, no existing work explains about the detail characteristics of this flow except for the visual differences and/or similarity between this and the two neighbouring flows. Ohnuki and Akimoto (2000) visually classified this flow region according to the gas phase distribution into churn-bubbly and churn-slug while others simply considered this as transitional region between bubbly and churn turbulent flow. In this work time varying signals of this flow were statistically exploited in an attempt to determine the detail characteristics of this flow. This will be further dealt in later sections; here the visual observation of this flow is outlined.

This flow was obtained under the medium air superficial velocities ($0.45 < j_g \leq 1.6$m/s) and was found to be the most dominant flow throughout the large diameter vertical upflow experiments, prevailing in the same region where slug flow occurs in smaller diameter vertical upflow. It is to be noted here that this flow also did not had any resemblance with typical slug flow found in conventional pipes, in fact no large smooth bullet shaped bubbles like Taylor bubble (occurring in slug flow) were observed under this range of air-water superficial velocities either in the injector vicinity or ahead in the test section, although a coalescence and breakup was visible. The visual observation made during the above air-water superficial velocities, corroborates the general consensus of non existence of slug flow in large diameter vertical upflow condition.

The visual observation made of this flow indicated both bubble breaking up as well as clustering. Visually, at the lower end of superficial velocities small bubbles clustering into larger ones was dominant and it was seen that the clustering grew into large distorted surface bubbles flowing in the core. The rising clustered bubbles were seen to produce a rapid agitation causing circulatory type of motion in the vicinity. This agitation was seen to increase with the increase in gas superficial velocities. However, it was also noticed that during the upward flow of these cluster bubbles, bubbles were also seen to shear off from its surfaces. The Figure 4.27(b) for annular sleeve and 4.28(b) for Tee injector shows the video image of this flow, both the flow apparently looked the same. The differential pressure vs. time record under both gas injectors indicated large amplitude random fluctuations; refer to Figure 4.27(a) and 4.28(a).

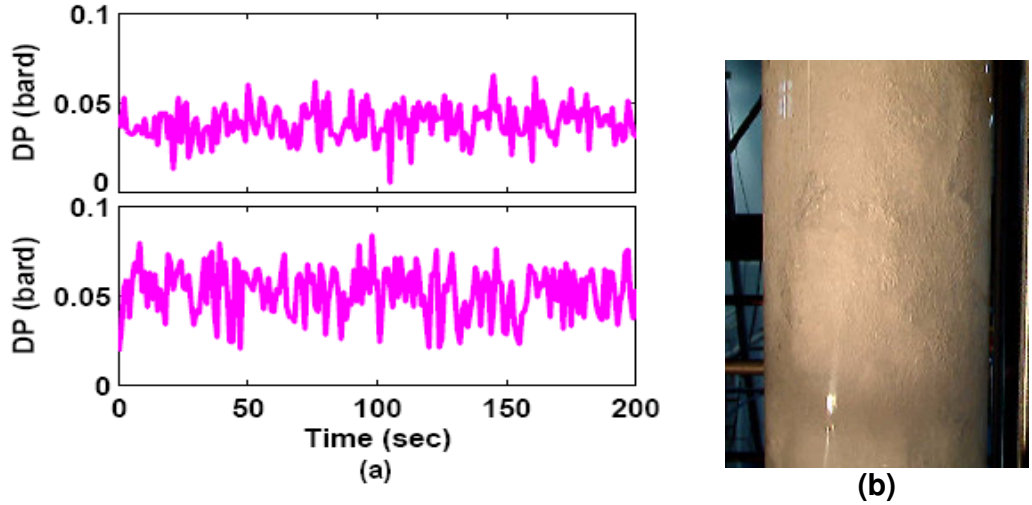

Figure 4.27 **Agitated Bubbly Flow, $j_l \approx 0.3$m/s and $j_g = 0.81$ & 1.51m/s, showing: (a) time traces and (b) flow image for Annular injector.**

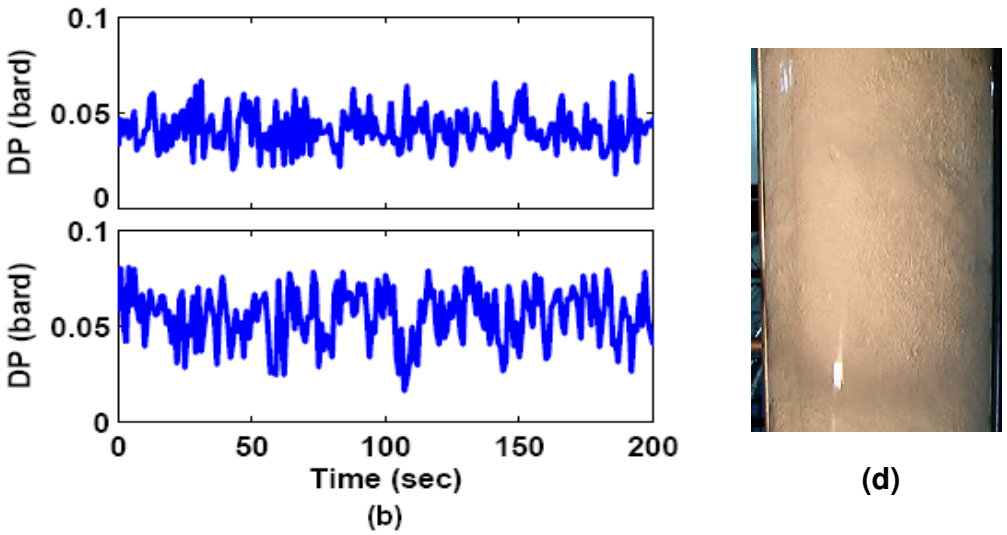

Figure 4.28 **Agitated Bubbly Flow, $j_l \approx 0.3$m/s and $j_g = 0.82$ & 1.51m/s, showing: (a) time traces and (b) flow image for Tee injector.**

It was noted that with the increase in air superficial velocities ($j_g > 1.0$m/s), the flow did have some similarity with churn/froth flow as it appeared to be increasingly consisting of multiple turning and twisting distorted gas clusters, however they remained in the core and still lacked the vigour and intensity of the churn flow. The statistical characteristics of this flow (dealt in later section) were found to be different from those of low input bubbly or churn/froth flow, so they have been classified separately from the former two.

4.2.2.4 Churn/froth flow: This flow existed at higher air superficial velocities when $j_g \geq 1.6$m/s ($j_w \leq 0.8$m/s) and although originated from large group of bubbly clustering and agglomeration was unlike the agitated bubbly flow because of its "frothy" appearance and highly oscillatory characteristics. During the flow observation it was observed that within the core region large highly distorted frothy gaseous structures of axial lengths much greater than the diameter of pipe were flowing upwards in the core section of the pipe accompanied by falling and upward moving liquid film around the periphery. The flow was extremely chaotic and whole riser content appeared to be oscillating with these distorted large gaseous structures. Figure 4.29 shows the frothy nature of the flow along with the differential pressure vs. time record but however does not convey the dynamic information of large highly distorted frothy gaseous structures and their oscillatory characteristics.

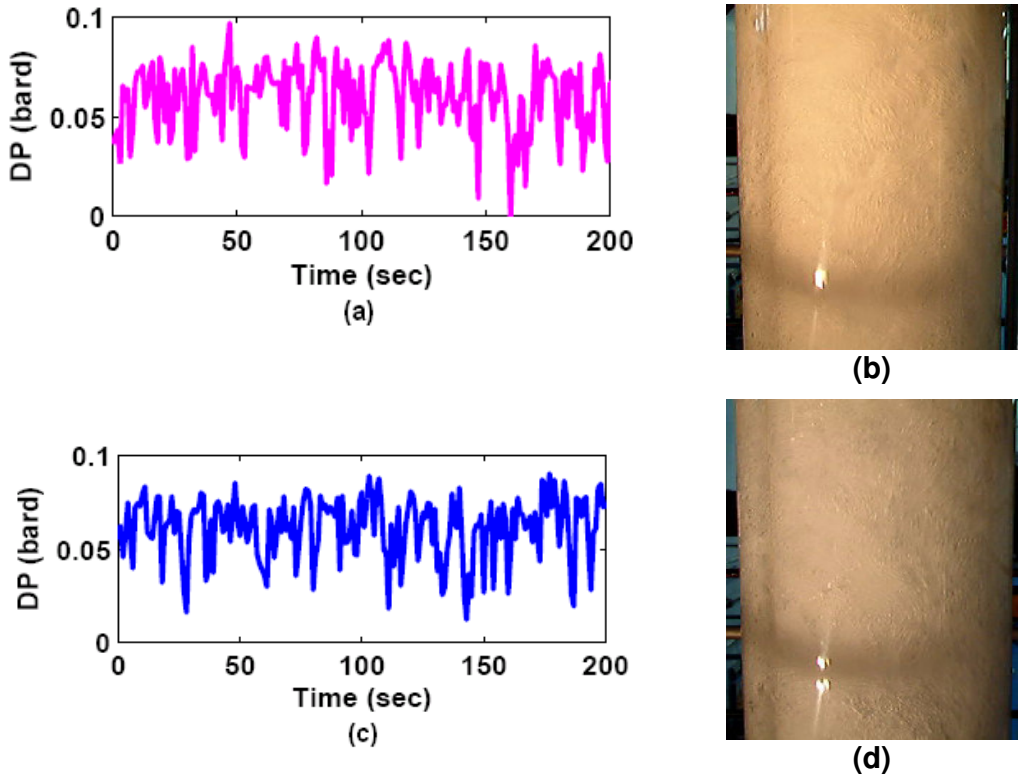

Figure 4.29 Churn/Froth Flow, $j_l \approx 0.3$m/s and $j_g \approx 2.26$m/s, showing: (a) time traces and (b) flow image for Tee injector.

4.2.2.5 Unstable slug flow: Apart from above flow regimes, another unique flow regime encountered was the ***unstable slug flow***; this flow was encountered only in some runs under air-water mixture flow through the flowline-vertical riser configuration between air-water superficial velocity range of (j_g =1.2-1.63 m/s at j_w =

0.58 m/s). The flow regime was detected in the riser when the horizontal flowline was under intense slugging, see Figure 4.30(a). Visual observation indicates that the gas bubble in the flowline behind the liquid slug after being compressed, it pushes up the liquid slug in riser, rapidly break through it, and then appears as a collapsing frothy interface that mixes up with incoming liquid slug or distorted gas bubble near the riser base. Here it also emphasised that exiting bullet shaped gas bubble from flowline reappeared in the first perspex section of the riser as large highly distorted clustered bubbles. This observation corroborates with the our earlier observation and of Kataoka and Ishii (1987), Ohnuki and Akimoto (1996), Ohnuki and Akimoto (2000) that found that smooth bullet shaped bubble also referred as Taylor bubble cannot be sustained in large diameter vertical upflow condition due to the interfacial instability.

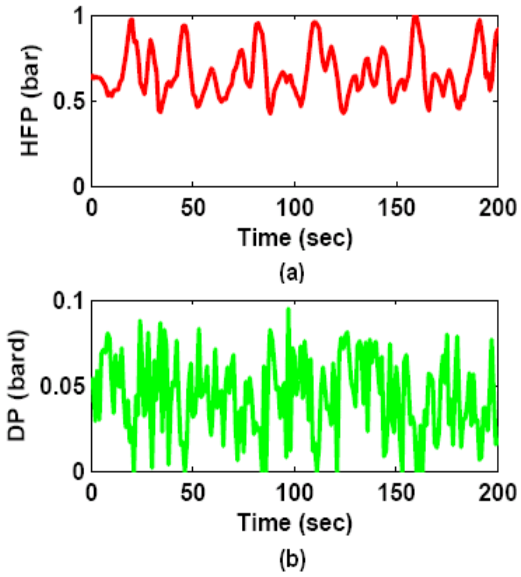

Figure 4.30 Unstable slug Flow, $j_l \approx 0.6$m/s and $j_g = 1.2$ m/s, showing time traces: (a) horizontal flowline pressure and (b) differential pressure up in the riser.

In the Figure 4.30(b) the differential pressure profile from the riser of this flow appears to be more excursive than churn/froth flow defined above although visually the flow was not very different than the churn/froth flow as it was highly chaotic/ oscillating except with some visible small areas of liquid bridging. Thus the above flow name derives from the fact that it exhibited some decaying characteristics of the slug flow from the horizontal flowline and churn/froth flow of the riser. Based on the above observation, it appears to be more of 'Churn-Slug' flow of third kind defined by Jayanti and Hewitt (1992), a transitional region between slug flow and annular. It is to be noted here that in the forced gas-lift experiments when gas injection was only performed near the riser base, this phenomenon was not observed for the entire set of experiments. Based on the observation it is concluded that this particular flow regime

in the vertical riser section was encountered as consequence of slugging in the horizontal flowline.

At the end of the visual observation of flow patterns, it is stated that although the last two visual observation of near riser base injection and upstream flowline injection for $j_g \geq 1.6$m/s ($j_w \leq 0.55$m/s) did suggest that some large deformed coalescent bubble clusters were present within the riser with their diameters close to the riser diameter and the axial length larger than pipe diameter. These were not clearly captured in the videos due to the near wall upward flowing small bubbles and falling film close to the pipe wall. However, some very interesting features of these highly deformed large coalescent bubble clusters under the upstream flowline injection condition were revealed in the videos, by successive still frame that can qualitatively convey the dynamic information on them. Photographs in Figure 4.31 are taken at approximately 5m height in the riser section, the images (a, b and c) are taken where the highly deformed fast moving bubble cluster is entering, penetrating and breaking the slow moving pure liquid slug ahead while the image (d) is when the liquid slug collapses and fallback due to above process.

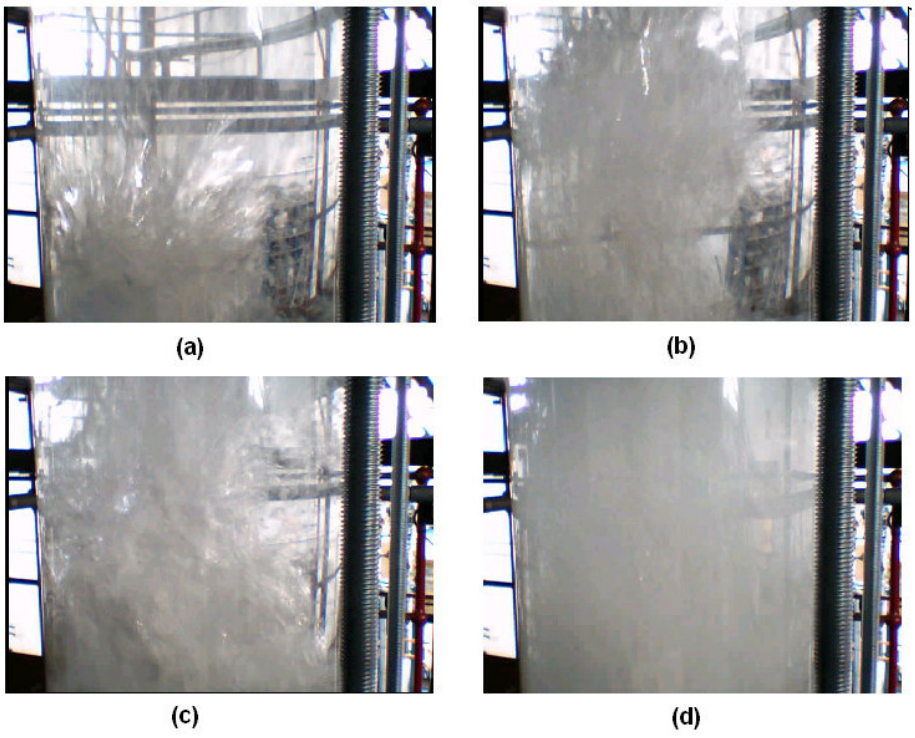

Figure 4.31 Unstable slug Flow, $j_l \approx 0.6$m/s and $j_g = 1.2$ m/s, showing time traces: (a) horizontal flowline pressure and (b) differential pressure up in the riser.

Note that the images (a, b and c) reveal the internal flow structure of the deformed bubble clearly as the view is now not obstructed due to the continuous falling film and small bubbles close to the pipe wall as seen in earlier case. This highly deformed gas coalescent bubble as can be observed (image c) is of closer diameter to the pipe with length less than a meter (as the total perspex section height is about 1m) and has a great resemblance to the large deformed coalescent bubble clusters observed from near perspex section in the earlier case.

Above interpretation of the large deformed bubble size and length from current experiments is also supported by the large diameter vertical pipe upflow work of Prasser *et al.* (2002) for air-water and Omebere-Iyari *et al.* (2008) for steam-water. All these works conducted on 200mm pipes indicates presence of highly deformed large bubbles in the core region under churn flow with their size and number increasing with growing air flow rate.

4.2.3 Statistical analysis

Often the visual identification of the gas-liquid flow patterns are found to be subjective and this results in large discrepancies between the reported data's. So in order to clarify any unintentional subjectivity in current work, the flow regime identification was also performed using statistical analysis on the data collected from the differential pressure sensors. Many earlier researchers have used the statistical procedures especially probability function plots of the void fraction fluctuations to delineate the characteristics of two-phase flow. The probability function plots are found to be the characteristic of the individual flow pattern (Hubbard and Dukler, 1966; Jones and Zuber, 1975; Matsui, 1984; Costigan and Whalley, 1997 and Cheng *et al*., 1998).

Below are the statistical results of the same cases as presented in visual observation section above, however the complete results of all the cases can be found in Appendix B(i).

4.2.3.1 Dispersed bubbly flow: The time trace of this flow presented earlier indicated small amplitude random fluctuations, while the PMF plot of this flow indicated a thin distinct single peak at low void fraction. This peak is different than indicated by bubbly flow as the latter was typically encountered when mean void fraction was greater than 0.16. Another unique feature of this flow was a higher and more pointed peak showing probability of pure liquid which was almost the minimum for bubbly flow. As this flow was encountered at higher liquid rates and lowest superficial velocities, the flow was confined to few cases only. Figure 4.32(a-b) presents the PMF plots results of dispersed bubbly flow under both the Annular sleeve and Tee injector respectively, taken from 5m (VF1) and 8m (VF2) height.

4.2.3.2 Bubbly flow: The analysis of the void fraction fluctuations showed that at the low air-water superficial velocities, the flow was mainly bubbly with PMF showing a distinct peak under both injectors, see Figure 4.33. However, it can be

noted that this peak is different than indicated by dispersed bubbly flow as the single peak is displaced from the near origin and slightly broaden; this type of the flow is defined as low liquid input bubbly flow (Taitel *et al.*, 1980). Moreover, the PMF's from higher height are also broader than from lower height indicating a wider distribution of bubble sizes due to breakup.

4.2.3.3 Agitated Bubbly: Upon increase in gas superficial velocities, the bubbly flow transformed to agitated bubbly or clustered bubbly flow as there was wide distribution of bubble sizes. Coalescence and clustering was observed visually accompanied by a developing agitation in the surrounding due to the movement of clustered bubbles in the centre of the core. This wide distribution of bubble sizes with clustering and coalescence is well indicated in the PMF's in Figure 4.34 and 4.35 for Annular sleeve and Tee injector respectively. From the probability mass function plots of this flow some unique features of this flow were identified.

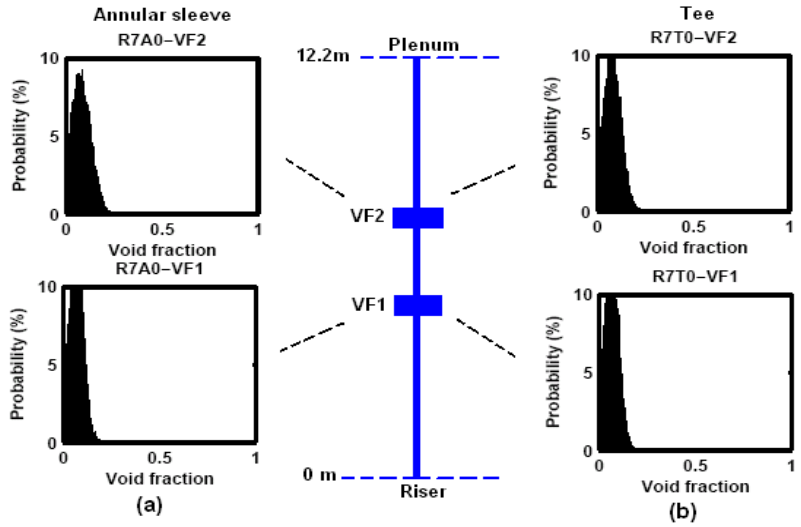

Figure 4.32 Dispersed Bubbly Flow, $j_l \approx 1$m/s and $j_g = 0.09$ m/s, showing: (a) PMF for Annular injector & (b) PMF for Tee injector.

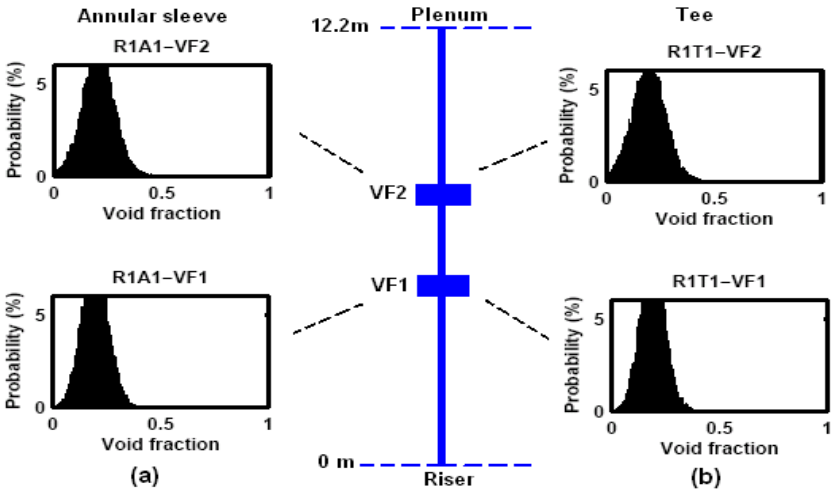

Figure 4.33 Bubbly Flow, $j_l \approx 0.25$m/s and $j_g = 0.09$ m/s, showing: (a) PMF for Annular injector & (b) PMF for Tee injector.

From the behaviour of the PMFs given in Figure 4.33 and higher air superficial velocity cases (refer to appendix B), it was found that the distinct single peak at low void fraction (bubbly flow) progressively shift toward higher void fraction with increase in air superficial velocity. This gradual shift of the distribution from low air superficial velocities to higher velocities without showing any significant changes to its shape also verifies the visual observation of the gradual and smooth transition from bubbly to agitated bubbly flow. This shifting of the distribution was also accompanied by broadening of its distribution as well as reduction in its height.

The Figure 4.34 and Figure 4.35 show flow behaviour for two different air superficial velocities for Annular sleeve and Tee injectors respectively. This broadening and reduction of height suggests that bubble size distribution was increasing by break up and reduction suggesting a further coalescence. Since more breakups of bubbles will result in more bubbles and hence more coalescence, therefore equilibrium between coalescence and breakup existed and the overall PMF shape remain uniform. From the PMFs plots taken from the two successive heights (see in figure) for two different air superficial velocities, it can be noted the peakness of the curve reduces and broadness increases, this implies that bubble were breaking up while moving up the riser and since their population was increasing their coalesce probability was increasing hence the uniform curve suggests that breakup and coalescence were almost in equilibrium.

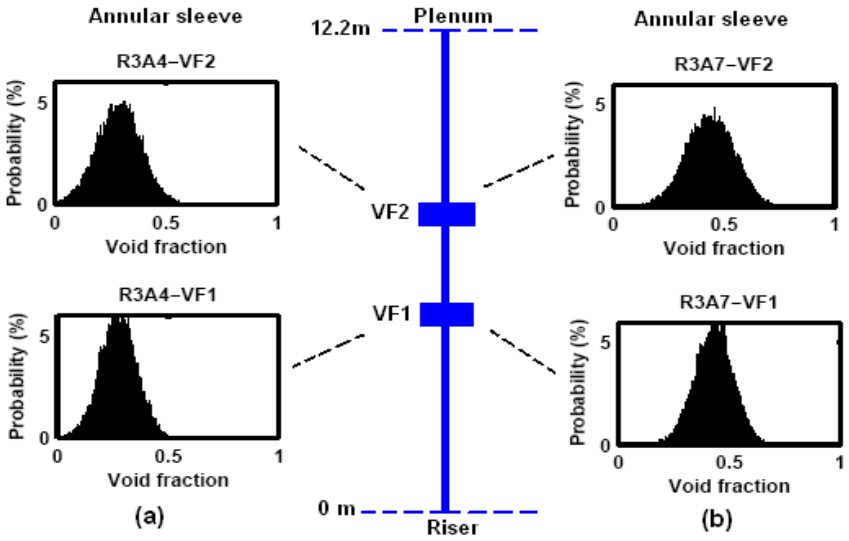

Figure 4.34 Agitated Bubbly Flow, $j_l \approx 0.3$m/s and $j_g = 0.81$ & 1.51m/s, showing PMF for Annular injector.

4.2.3.4 Churn/froth flow: Churn flow was observed in these experiments at the highest air superficial velocities when the flow gradually transformed from agitated /clustered bubbly flow. Visually this flow was identified at experimental run where oscillatory motion was observed within the riser section. At this stage, the flow behaviour was highly chaotic and liquid film at the wall was seen as oscillating up and down rapidly with high velocity large gaseous structure within the core. The PMF in Figure 4.36 of churn flow exhibited a peak (mean value between 0.55-0.65) like bubbly and clustered bubbly flow but was not a normal distribution and possessed a thick tail extending towards the lower void fractions. This long thick tail towards lower void fraction indicated some of the survived liquid slugs and frothy air-water mixture which is typical characteristic of transitional flows. The broad peak at the higher void fraction represents the gas structures that are long and distorted in nature. Note in the Figure 4.36(a) that in case of Annular sleeve a more smoother curve, representing a more uniform distribution is obtained (see the minimum value also), in comparison to Tee injector. In the latter case, a thick tail extends to as low as near zero void fraction along with a prominent high peak of gas structures at higher void fraction. The former aspect further indicates that some liquid bridging existed in Tee injector cases which were not present in Annular sleeve injector due uniform distribution of gas phase.

4.2.3.5 Unstable slug flow: Unlike any of the above flow, this flow possessed a single prominent broad peak at intermediate void fraction along with a thick tail extending towards the higher void fraction; see Figure 4.37(a-b). This flow is considered to be the consequence of flowline slugging, that when entered into the riser became highly distorted and penetrated the liquid slug ahead making the slug

unstable, collapsing and falling back into the lower section of the riser. Thus the PMF's in Figure 4.37 appears more flatten with much wider void fraction distribution.

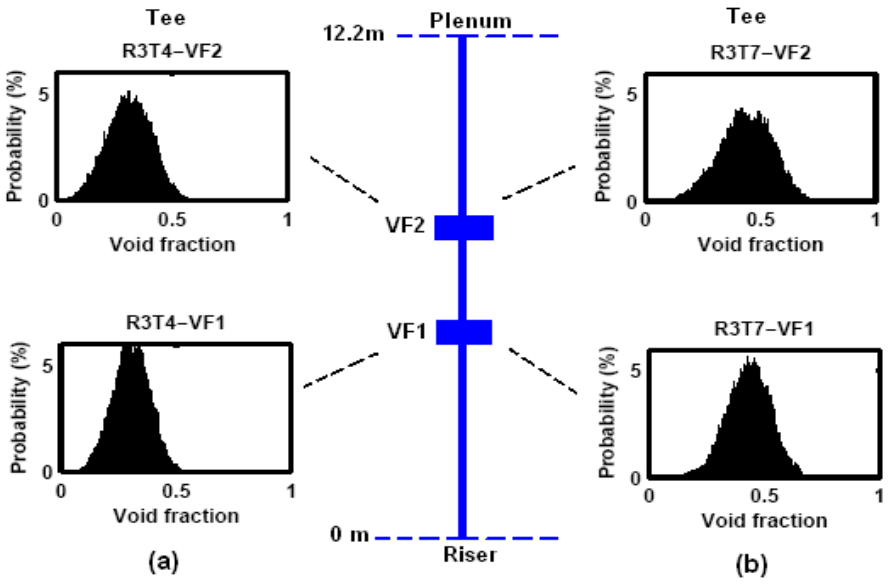

Figure 4.35 Agitated Bubbly Flow, $j_l \approx 0.3$m/s and $j_g = 0.82$ & 1.51m/s, showing PMF for Tee injector.

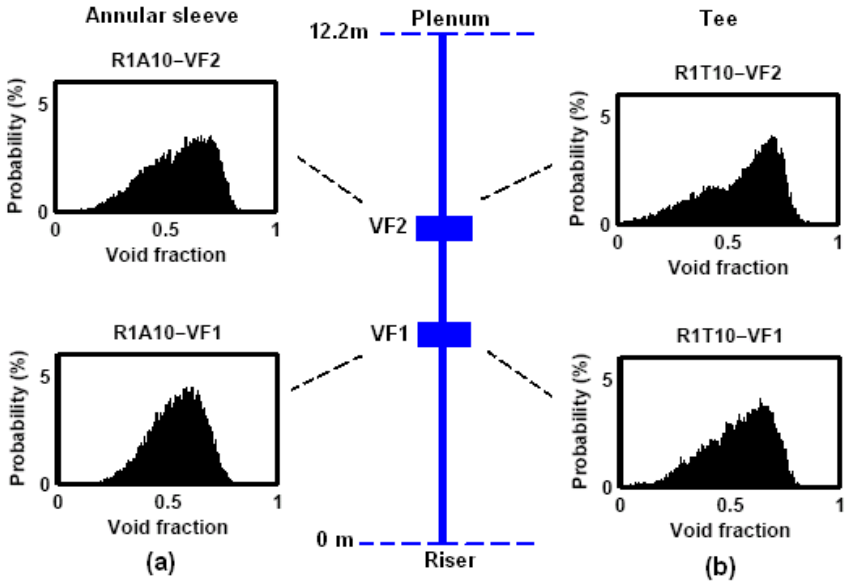

Figure 4.36 Churn/Froth Flow, $j_l \approx 0.3$m/s and $j_g \approx 2.26$m/s, showing: (a) PMF for Annular injector & (b) PMF for Tee injector.

In figure it can also be observed that the PMF from 5m height (VF1) does not contain a clear peak in the distribution but the second PMF from the higher location (VF2) in the riser indicates a progressive development of another peak at higher void fractions. The twin peaks have almost similar heights representing the simultaneous decay of liquid slugs and coalescence of gas bubbles in the core region. With further increase in air superficial velocity, the weak slug peak tends to disappear and gas dominant peak moves to further right turning into churn/froth flow. It is emphasized here that this PMF is not the one that is typically observed in conventional slug flow representing liquid slug and Taylor bubble (Cheng *et al.*, 1998; Costigan and Whalley, 1997; Hubbard and Dukler, 1966; Jones and Zuber, 1975 and Matsui, 1984). However many previous researchers did encountered similar type of flow in conventional pipe and referred it as a transitional flow between conventional slug and churn/froth flow (Costigan and Whalley, 1997; Watson and Hewitt, 1999).

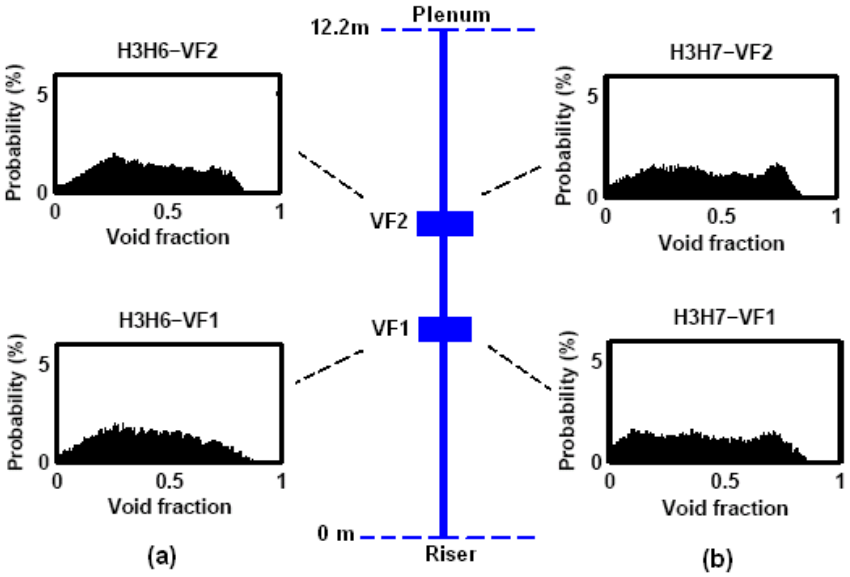

Figure 4.37 Unstable slug Flow, $j_l \approx 0.6$m/s and $j_g = 1.2$ and 1.7m/s, showing PMF plots under flowline-vertical riser configuration.

Based on the above set of cases along with other cases (in appendix B), an important issue of multiphase flow research is cleared. It is reported that no slug flow was envisaged in the riser during all the conducted experimental runs, further it can be also be verified from the non existence of the bimodal peak associated with it in probability function plots. Hence this work confirms the non existence of typical slug flow in large diameter vertical riser.

After the detail statistical investigation of the flow patterns, it is clear that the overall results of the PMF's obtained in current experiments for both the injectors are in good agreement with preceding research works in conventional size pipe. However,

agitated bubbly flow not encountered in conventional pipes sizes needed further investigation as the shape of the PMF remained Gaussian in intermediate air-water superficial velocities range, therefore some discrimination criterion was needed to identify between bubble-agitated bubbly and agitated bubbly-churn flow regimes.

4.2.4 Flow regime transitions characteristics

The detection of flow regime transitions in two phase flows are important because with change in flow regime, significant changes in hydrodynamic characteristics results. Over the years many experimental methods for the flow transition have been suggested, however among all of them two still widely used are visual observation or by measurements of an instantaneous value of either the void fraction (Jones and Zuber, 1975; Costigan and Whalley, 1997 and Cheng *et al.*, 1998) or another suitable hydrodynamic parameter (e.g. the dynamic fluctuations of pressure or differential pressure signal, Tutu, 1982; Matsui, 1984; Annuziato and Girardi, 1984; Lin and Hanratty, 1987) which is closely related to the prevailing flow regime. Traditionally flow patterns have been identified by visual observation or by using high speed photography through transparent channels (Hewitt and Roberts, 1969). However the method is quite subjective as the flow transition take place gradually and it requires the wall of the pipe to be transparent, this is also the main cause of large discrepancies between the investigations.

It was seen in earlier sections that the Guet *et al.* (2003) criterion of the change in slope of global average void fraction to identify the transition (from bubble to slug flow) was not valid in current work. Hence in this work we adopted the approach of Vince and Lahey (1982) who suggested that the nature of the process can be explained by its statistical content. Statistical moments are employed to exploit this information. Thus the four moments of the distributions; Mean, the Variance, the Skewness and Kurtosis were also extracted from the time-varying void fraction signals to establish the characteristic parameters of individual flow pattern. Firstly, the standard deviation was explored as this shows how far the signal fluctuates from the mean (Smith, 1999). The parameter could be used for flow pattern determination because for bubbly and annular flows, it is expected to be small (as data points lie close to mean), while it should assume larger values (data points are far from the mean) for intermittent flows because of the presence of the large distorted bubbles and highly chaotic liquid phase. Thus the standard deviation of the time varying void fraction signal was employed to extract information about the flow regime transitions.

The standard deviations of the void fraction fluctuations extracted from the both injectors experiments for various air-water superficial velocities range are shown in Figure 4.38(a) against mean void fraction. Note the general trends of the void fraction, three clear regions becomes evident. At very low mean void fractions (typically $\alpha \leq 0.12$), the standard deviation is slightly constant, these few data points corresponds to dispersed bubbly flow. The standard deviation then quickly increases with an increase in mean void fraction (due to j_a increase) till $\alpha \approx 0.23$, after which it

stays almost constant till the $\alpha \approx 0.40$ and then again rapidly increase within the current range of experiments.

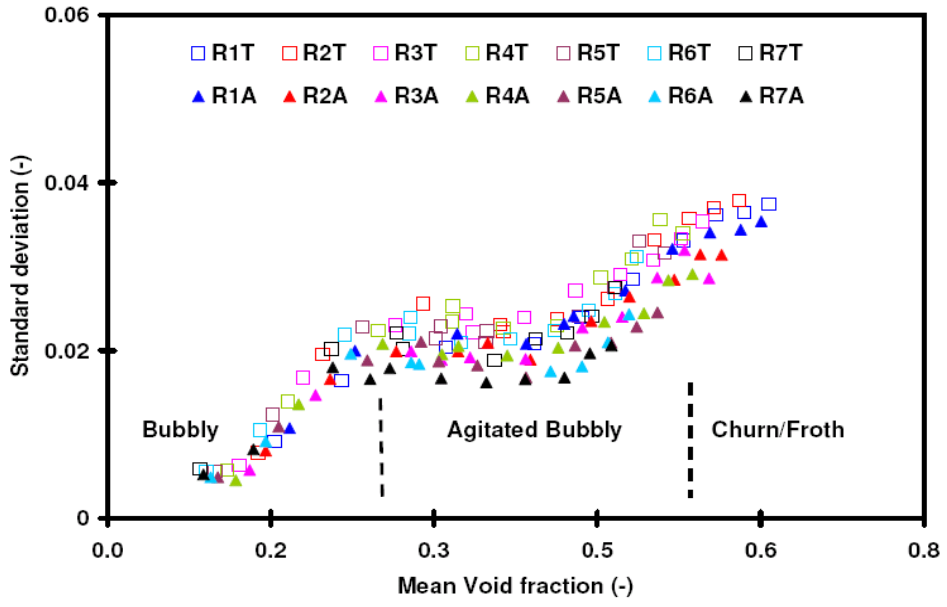

(a)

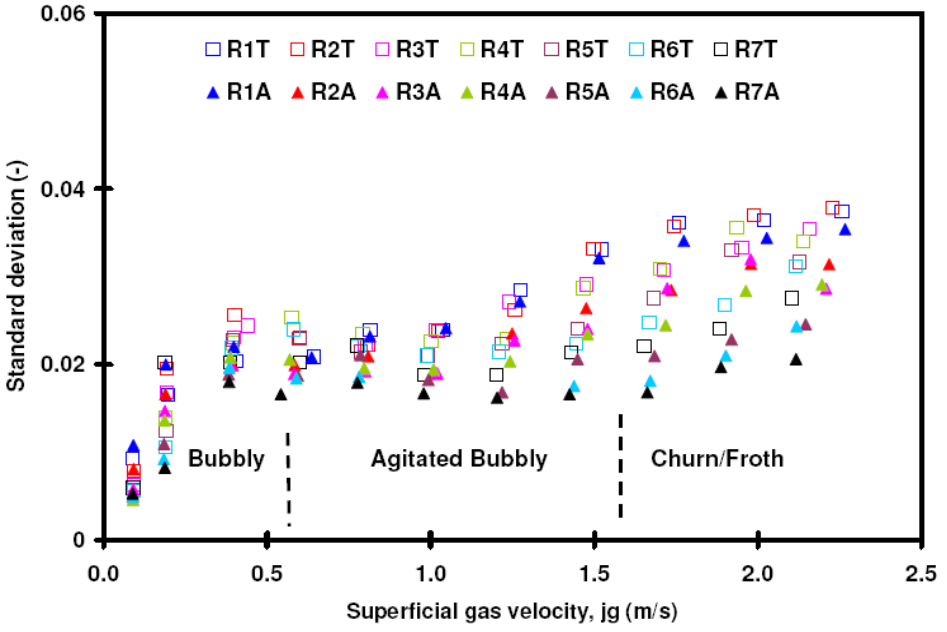

(b)

Figure 4.38 Flow regime transition identification using standard deviation of average void fraction with both the injectors.

On the comparison of this results with the visual observations and probability mass functions plots (refer to appendix B), it is revealed that the first low void fraction region with almost small constant standard deviation is the one where dispersed bubbly flow was observed. In the region of $0.13< \alpha \leq 0.23$ where standard deviation increased, bubbly flow with occasional coalescing was observed while in the region of $\alpha > 0.40$, a highly chaotic and oscillating churn/froth flow was seen with falling liquid film near the wall and rapid upward movement of gaseous structure within the core. The region corresponding to $0.23 < \alpha \leq 0.40$, where the standard deviation was almost constant is the same region where PMF's plots remain Gaussian shape (refer to dataset in appendix B). The visual observation of this region showed that in this region bubble coalescing and breakup to be dominant with strong liquid recirculation in near wall area. It is postulated that the nearly constant standard deviation region is representing the bubble to bubble interaction i.e. coalescence and breakup behaviour of the bubble with further smoothening provided by strong liquid recirculations. However with an increase in mean void fraction (due to increase in air superficial velocity), the local liquid recirculation are damped out promoting bubble coalesce and again a gradual flow transition from agitated bubbly to churn/froth flow. Hence, the changes of slope of standard deviation with an increase in mean void fraction are representing the region of the flow regimes transitions.

An explanation of above may further be found if the same standard deviation is plotted against air superficial velocity, see Figure 4.38(b). The figure illustrates the similar trend as observed in earlier case, three separate regions with respect to increasing air superficial velocities. It is also to be noted that with an increase in water superficial velocities the standard deviation seems to decrease which is in accordance to the visual observation (and PMF's plots) that indicated that the flow remained agitated bubbly for $j_l > 0.7$m/s due to increase liquid inventory and suppression of bubble induced turbulence. Both the figure also shows that the results obtained with both injectors are closer to each other, with tee injector values slightly higher than the annular sleeve due to single orifice opening of 50.8mm in comparison to eight, 38mm orifice openings. Similar results are obtained (refer to appendix B) for natural lift experiments presented in section 4.1.

Figure 4.39(a) and 4.39(b) shows the sectional void fraction standard deviation in forced lift experiments while refer to appendix B for natural lift results. The trends presented with standard deviation of sectional void fraction correspond to the results presented in Figure 4.38(a) and 4.38(b). Similar to above, standard deviation increases with air superficial velocity for a given water superficial velocity and decreases with j_l for a j_a. The standard deviation results are consistent with flow observation i.e. small for bubbly flow, almost constant in the region of coalescence and breakup and large for highly unstable and oscillating churn/froth flow.

The Figure 4.40 indicates an alternate criterion for flow pattern identification presented by Hatakeyama and Masuyama (1994). The plot is of kurtosis vs. skewness of void fluctuations. The number of data points corresponds to the data acquired in entire forced lift and selected natural lift experimental campaign.

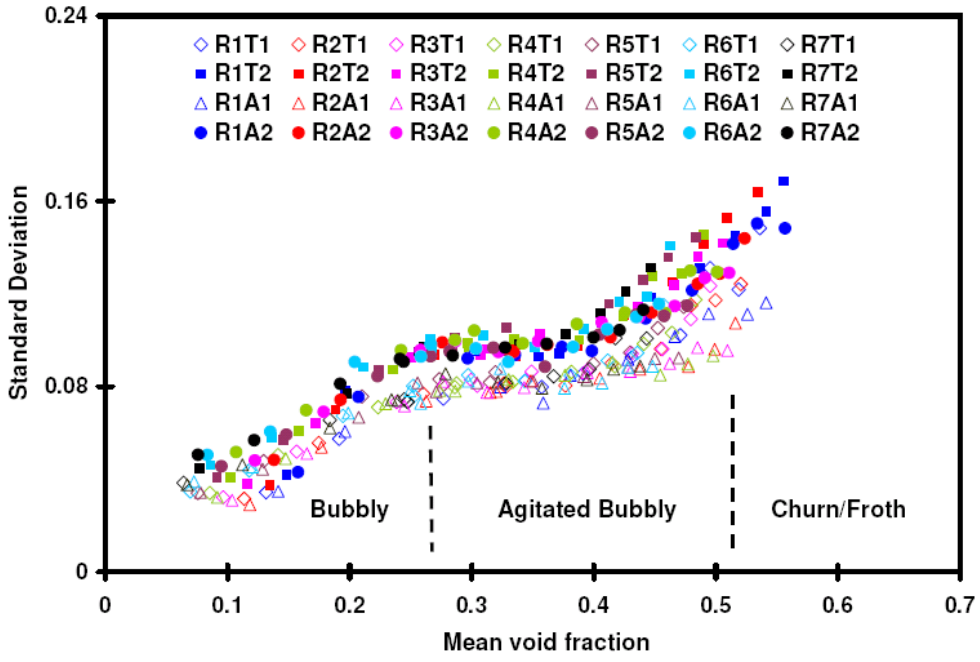

(a)

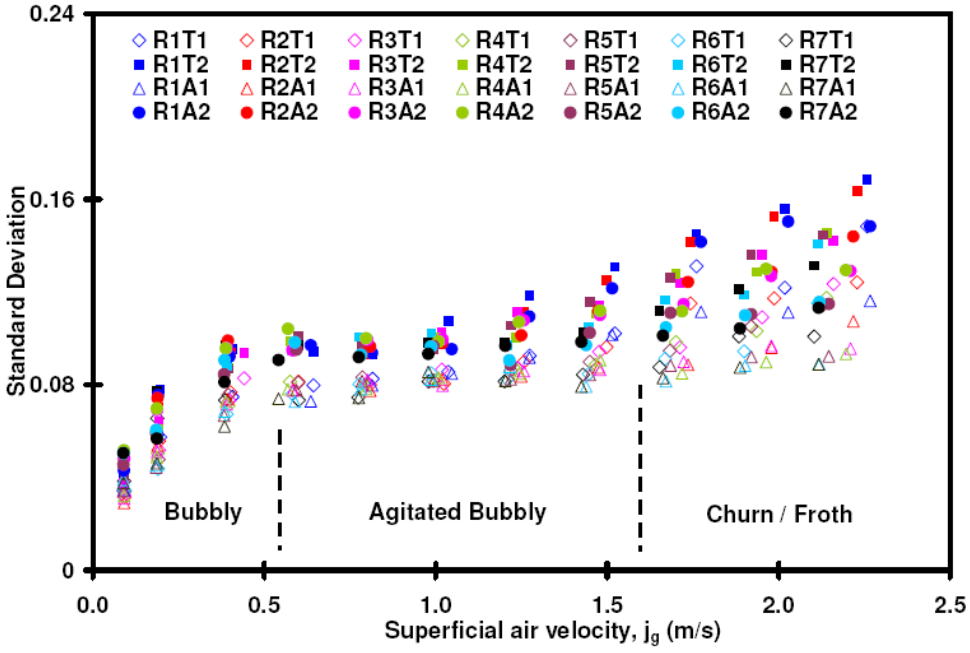

(b)

Figure 4.39 Flow regime transition identification using standard deviation of average void fraction with both the injectors.

The figure also contains two limiting lines (red and blue); these boundaries were developed by in order to classify the data points. The upper boundary (red line) gives the boundary between the intermittent flow and bubbly/annular flow while lower boundary (blue) gives the lower bound for the intermittent flows. Majority of this data is concentrated in the region of -0.2 to 0.2 range of the skewness and 2.8-3.2 of the kurtosis value, where a value of zero skewness represents a perfectly symmetric distribution and a value of 3 for kurtosis indicating a normal distribution. The data lying in this vicinity is for, agitated bubbly flow and verifies the observed trend of the bubble to bubble interaction resulting in the bubble coalescence and breakup along with the stabilizing effect of liquid recirculation. This is indeed a distinct feature in comparison to that of bubbly and churn/froth flow.

The data lying in the region of positive value of skewness are for bubbly flows while those lying beyond negative (-0.2) skewness represents the intermittent flow (typically churn/froth flow). Note that few of the near riser base injection data points (see left side of the figure) lay close to the boundary of the intermittent and bubbly flow especially the data point (solid blue legend) lying on the boundary corresponds to the Tee injector PMF's in Figure 4.36(b) that indicates a gas dominant peak with thick tail towards left, further validating our visual and sensor trends.

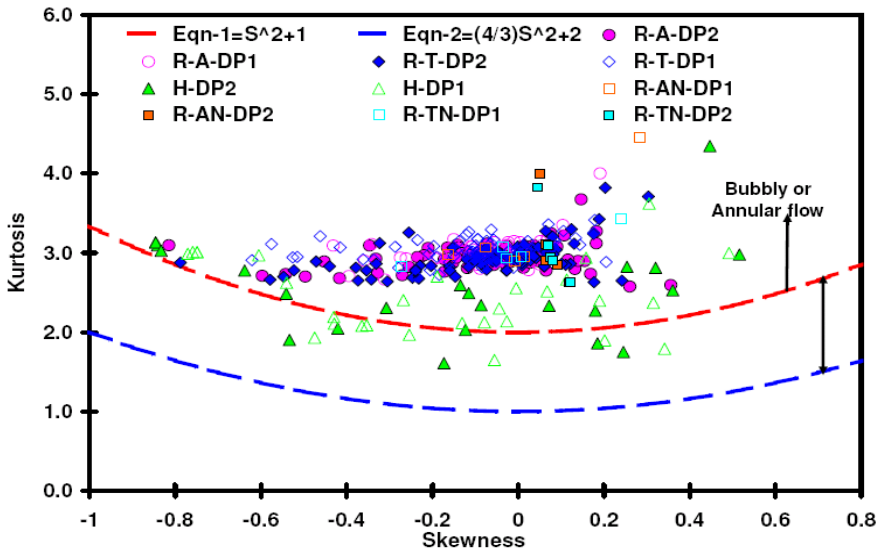

Figure 4.40 Relationship between Skewness and Kurtosis for all the experimental data with both the injectors.

Also note that in the above Figure 4.40, almost all the near riser base injection (both forced and natural lift) experimental data lay above or near the upper boundary which is consistent with the single peak PMF results with non existence of the pure slug flow. The data lying near the intermittent and bubble/annular flow boundary and

inside the intermittent region are for the upstream (combine) flowline-gaslift experiments with few data points of churn flow of the near riser base injection. Under inlet condition of the two phase flow entering the base of the vertical riser without gas injection in the base, the riser is under the influence of the flow occurring in the flowline (intense slugging). The data points lying inside the intermittent region represents those cases of unstable slug and churn/froth flows.

4.2.5 Interim Summary

In this section of the thesis, the flow patterns during two phase air-water flow in a 254mm nominal diameter vertical riser (using both Tee and annular sleeve injector) have been identified using visual observation and statistical analysis of sectional void fraction. The time-varying sectional void fraction signals have been analyzed by probability mass function plots in a manner similar to Costigan and Whalley (1997). The plots provided a good indication of the prevailing flow regimes. Four basic flow patterns were characterized namely; *dispersed bubbly flow*, *bubbly flow or low liquid input bubbly flow*, a*gitated bubbly flow* and c*hurn/froth flow*. Also a special case of u*nstable slug flow* was presented which was found as a consequence of inlet configuration. In was found that in contrast to the slug flow in smaller diameter pipes (D<100mm), agitated bubby flow is found to dominate this (slug flow) region in current experiments. Thus this work reports the absence of conventional slug flow in large diameter vertical riser as the slug flow is not observed neither the bimodal peak associated with it in probability plots. The agitated bubbly flow consisted of irregular bubble clusters that while moving upward, induced liquid recirculation in the vicinity that further promoted coalescence. The probability mass function plots of this (agitated bubbly) flow remained Gaussian in nature and thus required additional quantification. Statistical moments (standard deviation, skewness and kurtosis) were exploited to extract additional information on its characteristics. These moments were further examined to identify the transition boundaries between flow patterns. Based on the observed changes of standard deviation of void fraction fluctuations, the flow regime transition from bubbly to agitated bubbly and from agitated bubbly to churn/froth flow were identified as it was found that this value changes slope at the beginning of the transition to another flow regime.

4.3 Effect of Upstream Conditions on Flow Patterns in Vertical Riser Section

The objective of this part of the thesis was to examine the effect of inlet conditions on flow patterns occurring in the large diameter vertical riser. The experiments were performed with two different inlet conditions namely; (a) near riser base gas injection with conventional tee injector and (b) the upstream horizontal flowline gas injection. The former represents the gas-liquid introduction in the near riser base area while the latter corresponds to the gas-liquid introduction at the inlet of the flowline prior to the riser base. From these inlet conditions, the entrance effect on the two phase flow regimes in the riser was studied. The experiments were conducted in the range of air

superficial velocities of 0.18-2.2 m/s for water superficial velocities of 0.25 and 0.55m/s respectively. Here selected results of the experiments under two different inlet conditions are reported.

4.3.1 Near riser base gas injection

In above riser conditions for the near riser base air injection, the observed flow regimes were bubbly, agitated bubbly or churn/froth flow (see Figure 4.33 - 4.36). Bubbly flow pattern was observed at low gas superficial velocities (jg < 0.2m/s) with gas phase distributed as distorted bubbles in water and flowing upward along with the liquid. For medium gas superficial velocities (0.3 <j_g< 1.6 m/s) the riser flow pattern was mainly agitated bubbly. In fact the agitated bubbly flow regime with bubble coalescence/break-up and rapid agitation dominated the region of the slug flow regime of the conventional flow pattern maps. For the higher gas superficial velocities (j_g > 1.8m/s) the flow transformed to churn/froth flow within the riser with highly visible chaotic oscillations by frothy mixture. It is emphasised here that for near riser base air injection no slug flow was envisaged in the riser during all the conducted experimental runs, refer to section 4.2.2 also.

Figures 4.41 contains the probability mass function plots taken from approximately 5m and 8m height in the riser under the near riser base air injection condition for air superficial velocities of 0.18, 0.54, 1.2, 1.7 and 2.08 m/s. As expected, the void fraction distribution shifts towards higher values with an increase in the gas superficial velocity exhibiting bubbly, agitated bubbly and churn/froth flow. At lowest air superficial velocity, see Figure 4.41(a-e), a thin distinct peaks at lower void fractions values implies the presence of the smaller quantity of gaseous phase or bubbly flow. Upon increase in the air superficial velocities, plots still yields a single peak probability mass function but with a much broader in distribution than observed in previous case of bubbly flow, refer to Figure 4.41(b, c, f & g). The broad peak represents the wider bubble sizes due to the transition of flow from bubbly to agitated bubbly flow regime. The two apparent distinctions among the two flow regimes is the difference in the mean void fraction values, broadening of the distribution due to large bubble sizes and visually a rapid increase in agitation with increase in gas superficial velocities. Further increase in air superficial velocities transforms the flow to highly chaotic and oscillating churn/froth flow with high velocity long irregular gas bubble clusters travelling upwards within the core and the liquid film surrounding it travelling upwards and/or falling downward. The PMF plots are still single peaked but there is a clear shift in the distribution towards higher void fraction with tick tail extending towards the lower void fraction; see Figure 4.41(d). The presence of the large broad tail towards left of the distribution indicates the frothy nature of the flow with some liquid bridging between the irregular gas bubble clusters. However with increase in water superficial velocity, it was observed that this broad tail towards left subsided and more single peaked probability mass function plot is observed, see Figure 4.41h.

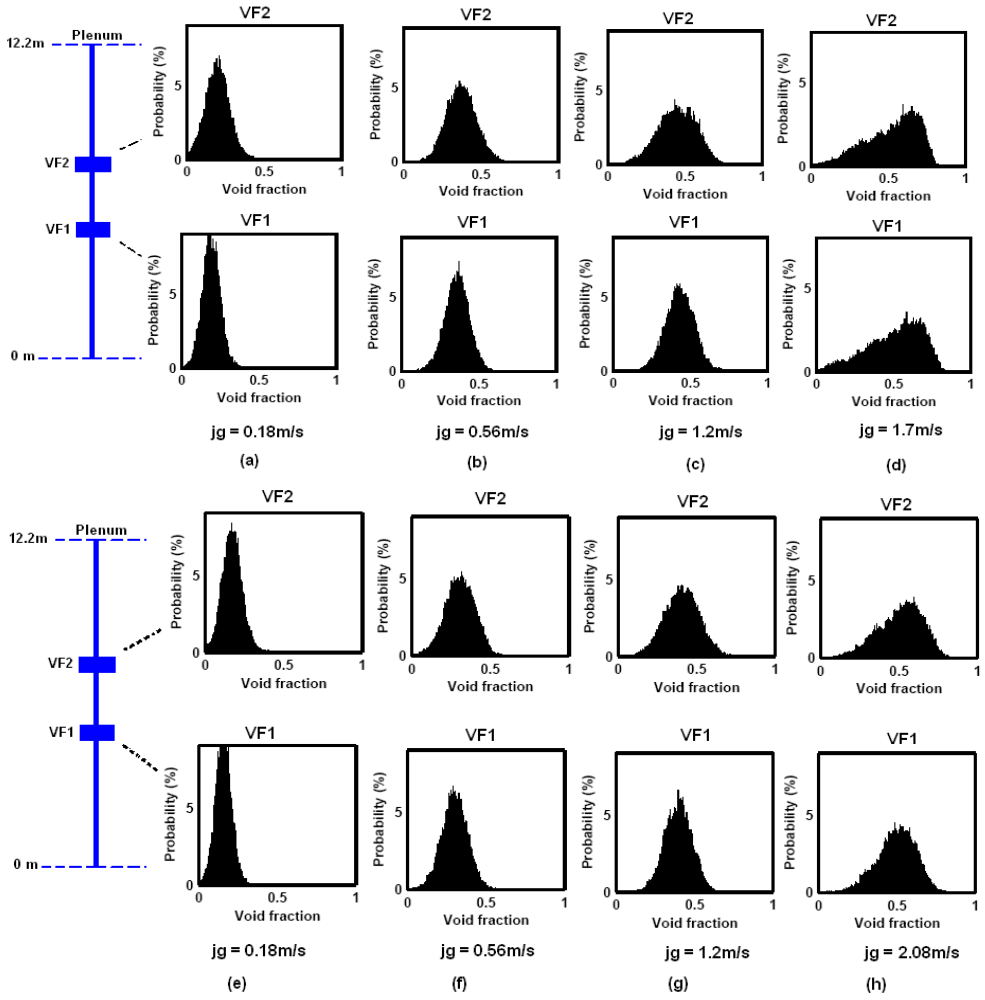

Figure 4.41 Near riser base air injection: (a to d) water superficial velocity of 0.25 m/s and (e to h) water superficial velocity of 0.55 m/s.

Similar trends of PMF's were also obtained from annular sleeve injector under same air-water superficial velocity range conducted above (see appendix B9, Figure 33), hence both the injection methods results in similar downstream characteristics. Also the resulting flow patterns from the above cases and others analysed in near riser base gas injection conditions proves that in this 254mm nominal diameter vertical pipe, no Taylor bubble or liquid slug existed, instead agitated bubbly flow regime with irregular bubble coalescence/break-up and churn/froth flow dominates. The statistical analysis presented further proves that no bi-modal or twin peak representing the liquid slug and Taylor bubble is observed under these experiments validating the earlier observations.

4.3.2 Upstream flowline gas injection

For the air injection at the upstream of the riser base i.e. at the inlet of the horizontal flowline four typical flow regimes have been characterized in the riser section namely bubbly, agitated bubbly, unstable slug and churn/froth flow with stratified, elongated bubble and slug flow in the flowline, see Figure 4.42. Similar to near riser base gas injection, bubbly and agitated bubbly flow regimes prevailed in the riser when the flow was stratified and elongated bubble in flowline at low to medium gas superficial velocities.

At higher gas superficial velocities (j_a>1.2m/s with j_l≥0.25m/s), there was a gradual slowing down of water and accumulation in the base area. This is attributed to the downstream/upstream topology of the flowline i.e. the 90 degree elbow connecting flowline to the riser and an upstream eccentric expander (or combine effect, see Figure 4.43 that initiated the slugging from the upstream in the flowline. It is to be noted that Bendiksen and Malnes (1987) also reported a strong effect of upstream and downstream conditions on the stratified-slug flow transition. As this liquid pool was pushed up in the riser by incoming air bubble a more cyclic frothy type of the flow was observed in the riser due to gas bubble penetration within liquid slug and liquid fall back. Based on the visual observation it is proposed that the gas phase bubble flowing behind the liquid slug in the flowline attains high enough inertia due to compression (by preceding slug), so that when it enters the riser, it rapidly expands and break through the liquid slug preceding it (Figure 4.44a-b). Once the air penetrated the liquid slug, the air-water interface was no longer clearly identifiable except for a collapsing frothy interface (Figure 4.44c-d). The collapsing interface was mixed up with incoming liquid slug or distorted air bubble.

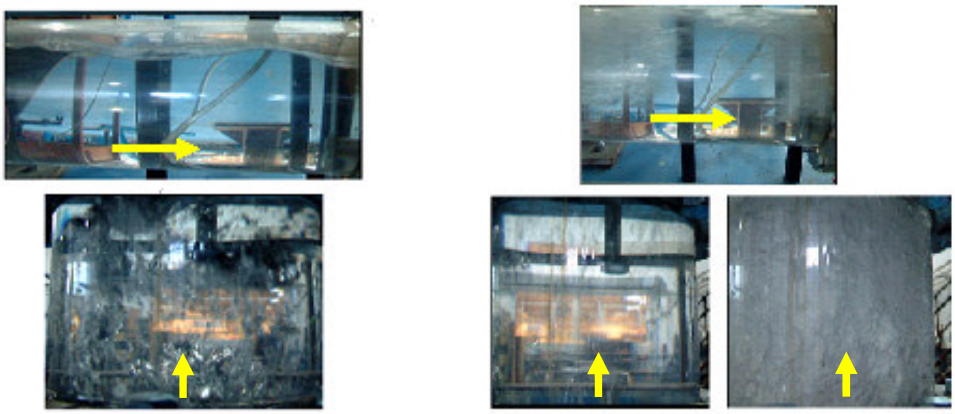

(a) **(b)**

Figure 4.42 Flow regimes in horizontal flowline-vertical riser (a) stratified (top) with agitated bubbly in vertical riser (below) and (b) short slug followed by gas bubble (top) with liquid slug and distorted gas bubble in riser (below) – (arrows are indicating flow direction).

Figure 4.43 Flowline inlet and outlet configurations.

Attention is drawn to the aspect of the fall back of the mixture near the base. Figure 4.45 shows the fall back at ground level near the flowline exit which appeared similar to the fall back and liquid accumulation seen in smaller diameter riser (Fabre *et al.*, 1990). This again compressed the incoming flow from the flowline there by initiating a new cycle of high velocity incoming bubble and accompanied liquid slug in the flowline. It is emphasised here that in some cases, some of the structure of liquid slug survived this penetration of the gaseous phase and travelled ahead as a short aerated slug (typically around ~0.4m length). The cases in which some of the liquid slug structure did survive were called unstable slug flow. It is to be noted here that in the near riser base gas injection experiments this unstable slug flow, where some liquid slug survived was not observed for the entire set of experiments. From above, it can be concluded that this particular flow in riser section was encountered as consequence of slugging in the flowline. With further increase in air superficial velocities the flow became highly chaotic/oscillating in nature in the riser due to collapsing gas-liquid interface, fall back and frequent arrival of longer gas bubble/liquid slugs resembling churn/froth type of flow in the whole riser. However the intensity of this churn/froth flow was quite severe in comparison to the churn/froth observed in near riser base injection.

In comparison to inlet condition of near riser base air injection (in the earlier section), Figure 4.46 illustrates the flowline air injection cases. These figures also accompany the pressure profiles near the exit of the flowline to demonstrate the nature of the flow entering the riser base. It is to be noted that to study the effect of the inlet conditions, air-water superficial velocities studied in both the inlet configurations are kept same.

Similar to near riser base injection, Figure 4.46(a-e) shows a distinct unimodal peak at lower values of void fraction representing the bubbly flow in the riser. The accompanied flowline pressure profiles are typical for the stable stratified flow condition. However unlike the near riser base injection, the probability function plots, these are broader in distribution indication a wide range of bubble sizes. This may be

due to the air phase entering the riser base from the inner corner of the 90º elbow and than dispersing in riser while flowing upward.

During the intermediate air superficial velocities ($0.4 < j_g < 1$m/s) when flowline was experiencing wavy stratified flow, the flow pattern in the riser essentially remained agitated bubbly with single peak, broad distribution like near riser base gas injection. However for air superficial velocities ($j_g > 1$m/s), there appears to be flow transition from agitated bubbly flow as the single peak distribution became skewed towards higher void fraction indicating the presence of various sizes of bubbles in the riser test section. Note the difference between Figure 4.41(b) and Figure 4.46(b), the heights of plots are reduced and there is much broader and even void fraction distribution for flowline gas injection inlet condition. However while the near base gas injection (Figure 4.41c) still indicates the agitated bubbly flow regime, Figure 4.46(c) indicates the flow transition from agitated bubbly flow regime.

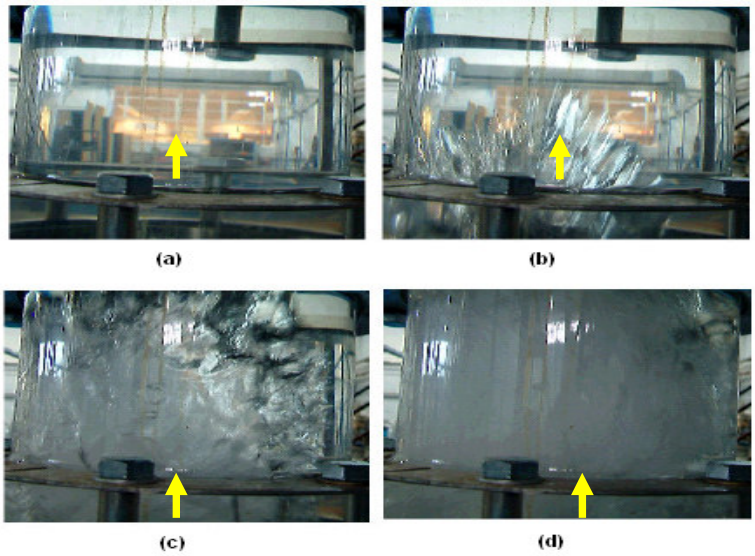

Figure 4.44 Liquid slug dissipation in the riser (a) liquid slug (b) distorted bubble entering the liquid slug (c) distorted bubble penetrating in the liquid slug and (d) fall back of the liquid film.

In cases from and after Figure 4.46(c) pressure profiles, a gradual appearance of slow moving slugs appeared as there was slowing down and liquid accumulation near the base, see the pressure time trace of flowline for case (c). This presence of slug flow at water superficial velocities has been discussed earlier. Figure 4.46(d) indicates the pressure sensor response and probability mass function plots when the flow is transformed to cyclic slugging in the near riser base vicinity. The strength of this pressure cycling increases with an increase in air superficial velocities with the

pressure sensor near the flowline exit indicating almost periodic/cyclic frequency of slugs having cycle of 10s.

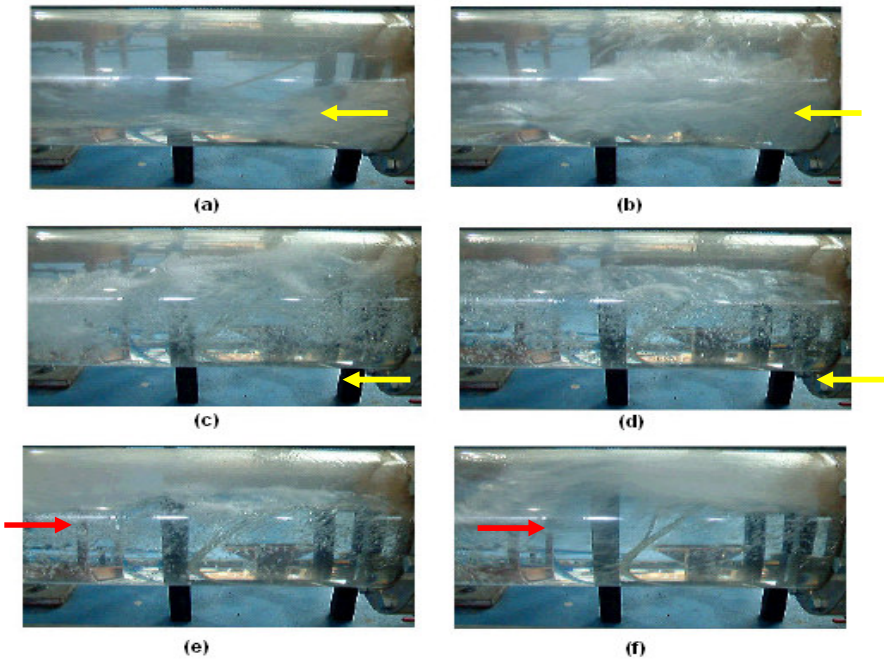

Figure 4.45 (a-d) Frothy mixture fall back near the base in the flowline and (e-f) compressional effect on the gaseous phase – (yellow arrows indicating fall back while red indicating flow direction).

These pressure profiles are similar to that observed by (Fabre *et al.*, 1990 and Schmidt, *et al.*, 1980) in small diameter horizontal flowline-vertical riser configuration. However unlike their observation, it was noted that (1) the bullet shaped slug bubbles from the flowline when reappeared in the vertical riser section were highly distorted and moving with high velocity, (2) the liquid slugs entering the vertical riser were disintegrating while moving up in the riser because the high velocity distorted gas structures penetrated through them and liquid slug collapsed and fell back on incoming flow. The first observation of the high distortion of the large coalescent bubble cluster in vertical riser is due to the action of turbulence on gas-liquid interface (Kataoka and Ishii, 1987; Prasser, 2002). The second observation of liquid slug dissipation is related to the high drift velocity of these deformed bubbles that is ascribed to the increase in diameter along with the influence of physical properties of liquid and gas (Kataoka and Ishii, 1987). However at low water velocities, the liquid fallback and the accumulation from disintegration of the liquid slugs is not enough to completely block the riser base and there is continuous gas penetration as suggested by the constant pressure variation in the flowline. The comparison between both inlet conditions i.e. Figure 4.41(d), and Figure 4.46(d)

indicates the similar trend i.e. a more churn/frothy flow in the riser not the conventional slug flow or its characteristic bi-modal peak.

Figure 4.46(e to h) represents the cases under the slow moving long elongated bubble and slug flow conditions in the flowline. The increase in the liquid inventory has resulted in more distinct single peak in PMF's representing bubbly flow regime in the riser initially while Figure 4.46(f, g and h) are essentially when highly cyclic unstable and chaotic flow in the riser was observed, see the flowline pressure profiles in Figure 4.46(f, g and h). From the figures one can observe that in the experiments; the hydrodynamic slugging from flowline, the uneven gas penetration in the riser base and the liquid accumulation in the riser base due to liquid fall back from the riser top, has compounded the whole process. Thus, the pressure time trace is irregular and periodicity is less straightforward. This behaviour can be attributed to the flowline slugs (hydrodynamic slugs) that are comparatively larger then the slugs formed due to the liquid fall back (smaller peaks). The small slugs are either ejected from the riser base by the gas drive from flowline or commingle with incoming slug to make a temporary but complete blockage. This is indicated well in the pressure profiles by the one or two small slugs followed by a longer slug in the figures. However, both type of slugs dissipated completely or partially by highly distorted air bubble within the riser. Thus the probability mass function plots for cases appear more flatten with much wider void fraction distribution marching towards the right (higher void fraction end).

In Figure 4.46(g), the first plot (VF1) does not contain a clear peak in the distribution but the second (VF2) from the higher location in the riser indicates a progressive development of another peak at higher void fractions. The twin peaks have almost similar heights representing the simultaneous decay/dissipation of the liquid slugs and coalescence of gas bubbles in the core region. However, with further increase in air superficial velocities, the weak slug peak disappeared and air dominate peak moved further to right with increase in height. It is emphasized here that this probability mass function plots is not the one that is typically observed in conventional slug flow representing liquid slug and Taylor bubble. Previous researchers (Costigan and Whalley, 1997; Watson and Hewitt, 1999) have referred this flow as a transitional flow encountered between conventional slug and churn/froth flow.

In Figure 4.46(h) represents the highly unstable and chaotic flow in the riser. The pressure measurements are cyclic representing the frequent slug's arrival to the riser base area. The liquid build up in Figure 4.46(h) is due to the rise in the liquid level within the flowline and base vicinity. The rise in the liquid level results from the accumulation of the incoming liquid slug and/or thick film of liquid with distorted bubble and from the fall back of the frothy mixture. In the latter case (fall back), the liquid accumulation shown by smaller peaks, see Figure 4.46(h) causes partial blockage to the gas passage that then accelerates towards the riser and scoop through the short slug in base area while in former case semi-penetrates into the longer slug while travelling ahead.

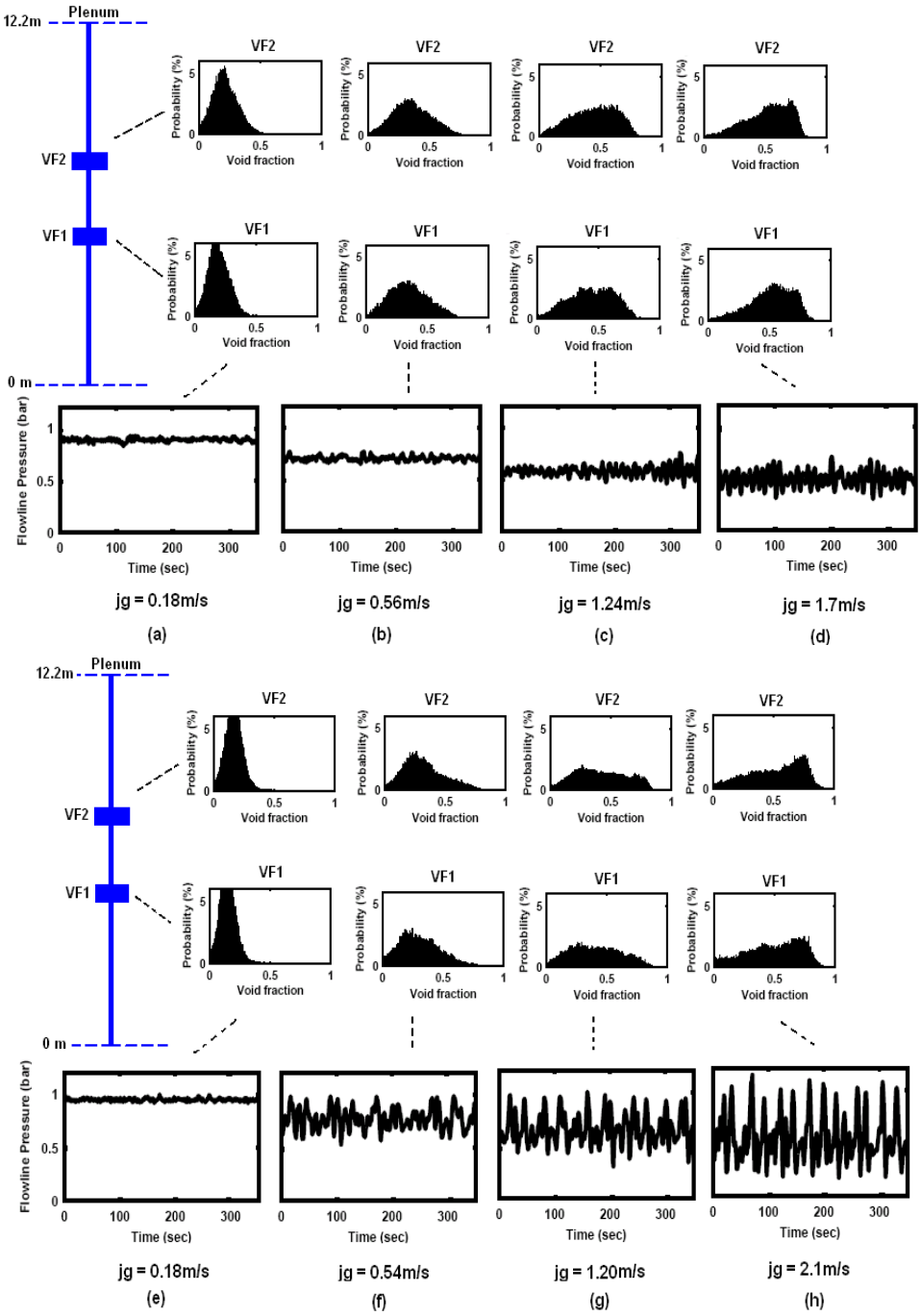

Figure 4.46 **Flowline air injection: (a to d) water superficial velocity of 0.25 m/s and (e to h) water superficial velocity of 0.55 m/s.**

The flowline pressure in Figure 4.46(h) does not correspond to a completely filled riser but the pressure trend indicates that the flow in the riser and base vicinity is cyclic and unstable in nature. However, this is not the severe slugging indicated by many authors (Schmidt *et al.*, 1980; Bendiksen *et al.*, 1991; Sarica and Shoham, 1991; Tin, 1991; Yeung and Montgomery, 2001; Yeung *et al.*, 2003). This because the pressure measurements in current experiments do not indicates a slug production period indicating the temporary nature of the liquid build up in the base, no liquid backup in the flowline after the liquid slug formed in the base is pushed into the riser by the gas (see Figure 4.45a-b), no individually identifiable gas penetration in the base and liquid slug sloshing out of the riser (in Figure 4.46) and no liquid slugs equivalent or larger in length than the riser height, which are typical characteristics of severe slugging. Instead the trends produced are akin to that obtained by Fabre *et al.* (1990) for horizontal flowline-vertical riser topology of 53mm diameter. Fabre *et al.* (1990) defined such flow condition as long period instabilities set forth due to the unstable process in the flowline-riser system.

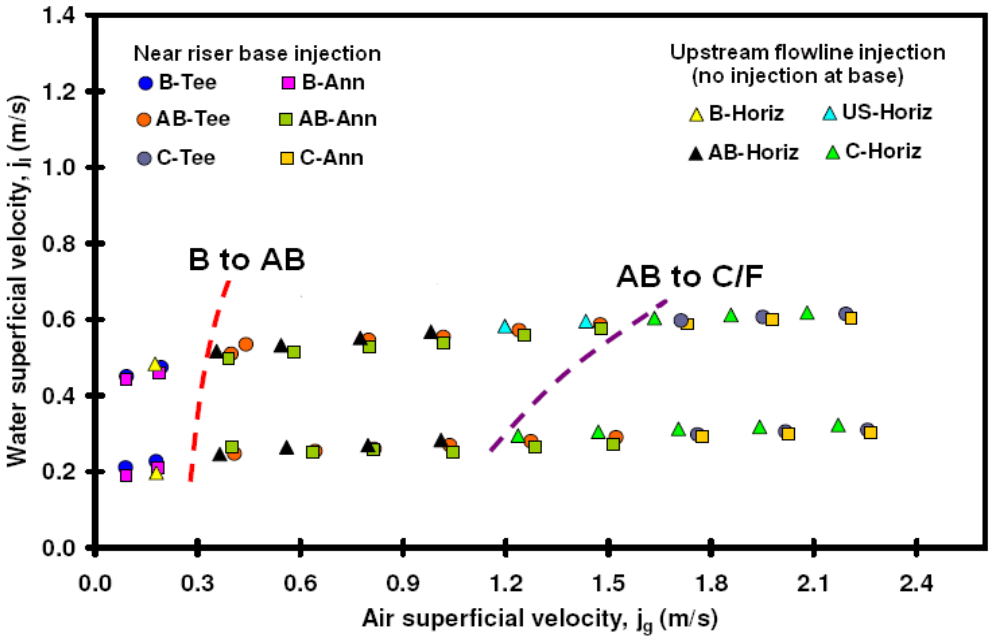

Figure 4.47 The experimental flow regime classification in the riser for the near riser base injection-with both the injectors and upstream flowline injection – no riser base injection.

The Figure 4.47 indicates the flow regime classification for both, the near riser base injection and upstream flowline injection (no injection in the riser base) on a flow pattern map. It is observed that under low liquid velocities (see R1-with $0.18 < j_a <$ 1.0m/s), the flow patterns observed are in conformity to the ones observed at inlet condition of near riser base gas injection. However, at higher air superficial velocity

an earlier churn/froth flow is observed in riser due to the occurrence of slug flow in horizontal flowline. This later aspect signifies that smaller slugs formed in flowline dissipated once entering the riser. At water superficial velocity (see R3) though the general agreement between the two conditions still exist some disagreement is observed in the range of $1.2 < j_a < 1.63$ m/s. This range consisted of unstable slug/flow regime of collapsing slugs with the probability mass function plots not containing clear bi-modal peaks. However with any further increase in air superficial velocities (j_a >1.7m/s), the flow regime transformed to churn/froth type of flow as seen in near riser base injection. This churn froth flow observed at lower water superficial velocity and at this water superficial velocity was more vigorous and chaotic than visually observed in near riser base injection cases.

4.3.3 Interim Summary

The precise inlet configuration at the entry of the test section is often not reported, although it may have a pronounced effect on the flow occurring in the test section and ahead. Thus in this part of the chapter, the entrance effect on the two phase flow in the large diameter vertical riser was investigated by varying inlet configuration, which to the authors' knowledge has not been previously reported. The set of experiments were performed with two different inlet configuration namely; (a) near riser base gas injection with both the injectors and (b) the upstream horizontal flowline gas injection. The former represents the gas-liquid introduction in the near riser base area while the latter corresponds to the gas-liquid introduction at the inlet of the flowline prior to the riser base.

In near riser base gas injection with both the injectors, under the air-water superficial velocity range covered, three different flow patterns were observed in the vertical riser namely bubbly, agitated bubbly and churn/froth flow. While in upstream horizontal flowline gas injection bubbly, agitated bubbly, unstable slug and churn/froth flows were observed. Unstable slug was detected in some runs between air superficial velocity range of $1.2 < U_{sg} < 1.63$ m/s only. This can be considered as the flow regime where the flow exhibited the remains of slug flow structure (from the flowline) but was less stable as the flow transformed into churn/froth flow upon increase in air superficial velocity.

With both the gas injectors i.e. the Tee and Annular sleeve injectors, similar downstream flow characteristics were observed in near riser base gas injection.

No effect of inlet conditions (i.e. near riser base injection with both the injectors and upstream flowline injection) is observed at low air superficial velocities as the similar mean void fractions (and flow pattern) are achieved in all the cases. However, at higher air and water superficial velocities it was observed that the two inlet configurations although exhibited some similarity in flow patterns like agitated bubbly and churn/froth flow, the overall intensity of the flow was more chaotic in the flowline injection. This was due to the intermittent flow behavior in flowline

influencing the riser flow pattern characteristics and thereby controlling the riser dynamics.

It was further found as the air superficial velocity increased at the low water flowrate, a periodic instability set in. This was due to the small liquid slugs in the flowline decelerating in the base vicinity but these liquid slugs dissipated completely while moving up the riser. This is due to the highly distorted trailing slug bubble penetration, therefore flow in the riser was more of churn/froth nature. However when water superficial velocity was increased (under same air superficial velocity as above), this periodic instability was taken over by more chaotic instability within the riser, the severity of which increased with air superficial velocity because of the increase in holdup within the riser base and flowline, thus compounding the whole process. It is to be noted that above instability is not the severe slugging indicated by many authors (Schmidt *et al.*, 1980; Bendiksen *et al.*, 1991; Sarica and Shoham, 1991; Tin, 1991; Yeung and Montgomery, 2001; Yeung *et al.*, 2003) but does possess similarity to unstable flow process defined by Fabre *et al.* (1990) in small diameter horizontal flowline-vertical riser configuration set forth due to the unstable process in the flowline-riser system.

4.4 Flow Regime Maps/ models

4.4.1 Comparison of experimental results with theoretical flow regime maps/ models

Figure 4.48 present the flow regime results for the large diameter (254.5mm) vertical upflow condition employing air-water as working fluid. The map is obtained for water superficial velocity range of 0.18-1.1m/s and air superficial velocity of 0.09-2.2m/s. In the figure the flow patterns observed namely; dispersed bubbly (DB), low liquid input bubbly (B), agitated bubbly (AB) and churn/froth flow (C) are shown at their respective locations.

Dispersed bubbly flow is observed at high liquid velocities only where coalescence seems to be suppressed by the liquid turbulence and bubbles flowed upward without any interaction with one another. Bubbly flow prevailed at low liquid input where bubbles though close in separation distance than dispersed bubbly with occasional coalescing travelled upward without any distortion or secondary motion. The Figure 4.48 indicates that the conventional slug flow pattern has vanished from the flow map. Instead, agitated bubbly prevailed in addition to churn/froth flow. In agitated bubbly flow bubble coalescence and breakup was visible along with secondary motion due to this coalesce and breakup processes. Frequent bubble clusters in the centre of core were visible. The agitated bubbly prevailed for most of condition tested in this work.

Above finding of transition from bubbly to agitated bubbly flow is inline with the observation of Ohnuki and Akimoto (2000) and Omebere-Iyari *et al.* (2008) but in contradiction with Omebere-Iyari *et al.* (2007). In case of former(s) work, transition

from bubbly (variation of bubbly flow included) to churn flow is observed with air-water and steam-water data, while for latter an intermittent flow was observed between bubble and semi-annular flow with nitrogen-naphtha data (see Figure 2.14). The flow pattern trends described as intermittent flow by Ombere-Iyari (2007) i.e. the PDF plot of flow pattern showing higher peak at lower void fraction and smaller peak at higher void fraction is representing highly aerated slugs and some large coalescing bubbles. Since the transition from bubbly flow cannot be delayed even at elevated pressures, it is postulated that the higher PDF peak indicates the smaller bubbles contribution in the slugs while the small peak at higher void fraction values represents the contribution of large bubbles. Hence even at higher pressures, although a transition from bubbly flow has been achieved, yet the contribution of small size bubbles is still larger due to the liquid phase properties. This is also supported by the work of Schäfer *et al.* (2002) on bubble size distributions in a bubble column for N_2/water, N_2/cyclohexane and N_2/ethanol for pressures up to 50 bars that the coalescence is almost unaffected by elevated pressures but breakage is increased thus the mean bubble size decreases with increasing pressure.

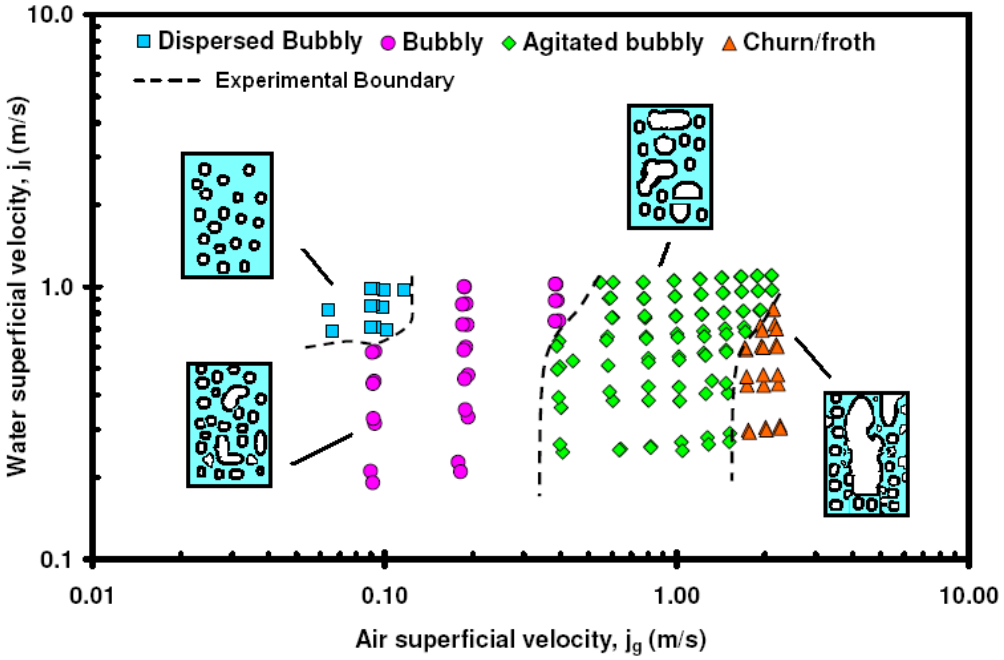

Figure 4.48 Experimental flow regime map for 254mm nominal diameter vertical pipe.

Churn flow occurred at relatively high air superficial velocities, the flow was highly chaotic with large gaseous structures travelling in the core region and liquid film travelling upward and downward along the periphery of the wall. The above flow

regimes and their transitions observed in large diameter vertical upflow condition were compared with the predictions of some well known flow regime maps like Taitel *et al.* (1980), Weisman and Kang, (1981), Mishima and ishii (1984), McQuillan and Whalley (1985), Brauner and Barnea (1986), Jayanti and Hewitt (1992), Chen *et al.* (1997) and Tengesdal *et al.* (1999). Further details of these models can be found in section 2.1.5.

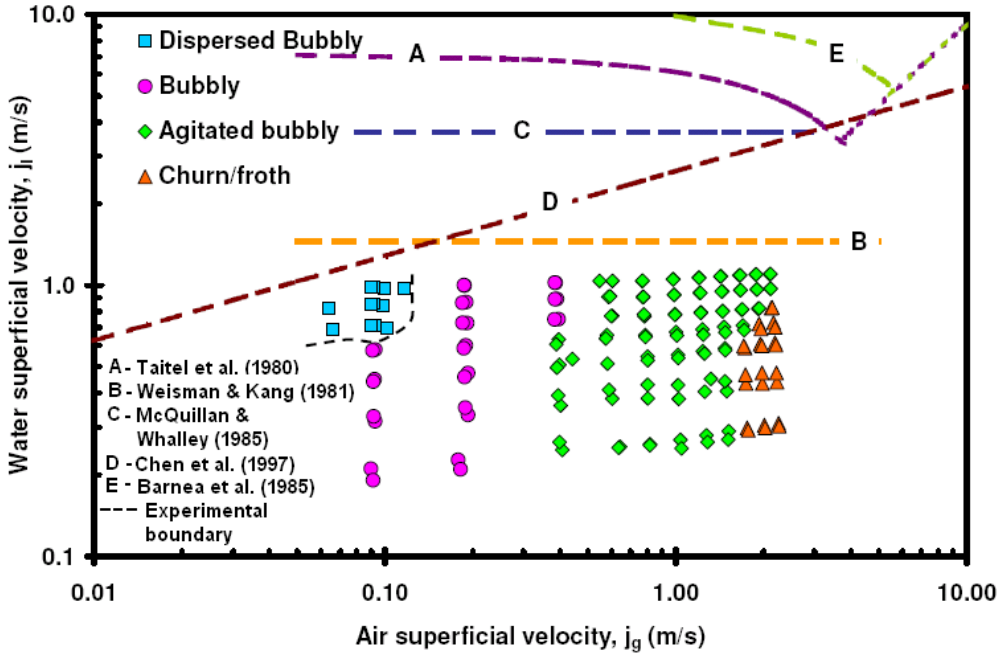

Figure 4.49 Comparison of Bubble-Dispersed bubble transition models for 254mm nominal diameter vertical pipe.

The purpose of this comparison was to determine the validity of the existing flow pattern maps against the experimental flow regimes observed. It is also emphasised that in the plots, the transition model predictions are for general trends.

The flow regime map in Figure 4.49 illustrates the results for the comparison between experimental and various model predicted transitions from bubbly to dispersed bubbly flow. In present work, the dispersed bubbly flow not only occurred at lower air superficial velocities but also at slightly lower liquid velocity than predicted by some models. In fact the predictions of Taitel *et al.* (1980) and Brauner and Barnea (1986) models occurred at a water superficial velocity of approximately one order of magnitude higher than experimentally observed transitions. It is be noted here that Costigan and Whalley (1997) in 32mm diameter vertical upflow experiments also found this transition boundary to be 15 times higher than observed in their experiments. The McQuillan and Whalley (1985) flow regime map for vertical flow

also could not predict the dispersed bubbly flow observed in the experiments. Only Weisman and Kang (1981) and Chen *et al.* (1997) predictions did came closer to predicting the boundary between bubble and dispersed bubbly flow. Weisman and Kang (1981) suggested that this transition to be independent of gas superficial velocity and only depends upon the liquid superficial velocity, fluid properties and diameter of the pipe. It is to be noted that our results observed are also consistent with the observation of Chen *et al.* (1997). Hence at low air superficial velocity range this transition will also be at lower values of liquid superficial velocity unlike the trends suggested by Taitel *et al.* (1980) and Brauner and Barnea (1986).

The Figure 4.50 illustrates the results for the bubbly to slug flow transition. It is interesting to note from the experimental results that for large diameter pipes bubbly flow region became larger compared with conventional size pipes. Taitel *et al.* (1980) and Mishima and Ishii (1984) models underestimated this transition to be occurring at lower gas superficial velocities. However both the above transition models are closer to actual transition at higher liquid velocities only. While both the above models predict an early transition to slug flow from bubbly, experiments results indicate that there is NO slug flow instead there is direct transition from bubbly flow to its variation agitated bubbly flow where a coalescence and break up process is clearly visible along with the local random liquid film movement at the wall. The deviation of the Taitel *et al.* (1980) and Mishima and Ishii (1984) models is due to the use of the constant critical void fraction (α_c = 0.25 and 0.3) value at which transition is expected to occur. Moreover, both the models also do not take into account of diameter of the conduit. This is in contradiction to various studies (Song *et al.*, 1995, Cheng *et al.*, 1998 and Guet *et al.*, 2003) done in past where this transition is found to be dependent upon the initial bubble size and diameter. Moreover Ombere-Iyari *et al.* (2007) mentions that this critical void fraction increases with pipe diameter assuming a constant bubble size.

Comparison with other existing flow regime models e.g. Weisman and Kang (1981) yields the predictions that are closer to the experimental results at lower gas superficial velocities but over predicts at higher gas-liquid superficial velocities than the former models. The actual relation is empirical and is based on the Froude numbers of gas and total volumetric flux alone. Note that Weisman and Kang (1981) did not define slug flow in vertical flow condition but rather referred the region between bubbly flow and annular flow as intermittent flow (consisting of plug, slug and churn flow).

An interesting observation related to bubble-to-slug transition is that all the models prediction are closer to experimental results at higher liquid velocities only and deviates at the low liquid velocities. These trends suggest that while constant critical void fraction approach is able to predict closer actual behaviour, the approach is limited to higher liquid velocities only, and at lower liquid superficial velocity some other mechanism individually or combine with critical void fraction approach seems to be responsible for this transition. This finding is consistent with the work of Omebere-Iyari *et al.* (2008) for pipe size of 194mm for which case the Taitel *et al.*

(1980) bubble to slug transition model, predicted the similar trend as observed in this work. The above observation will be further discussed in later next section.

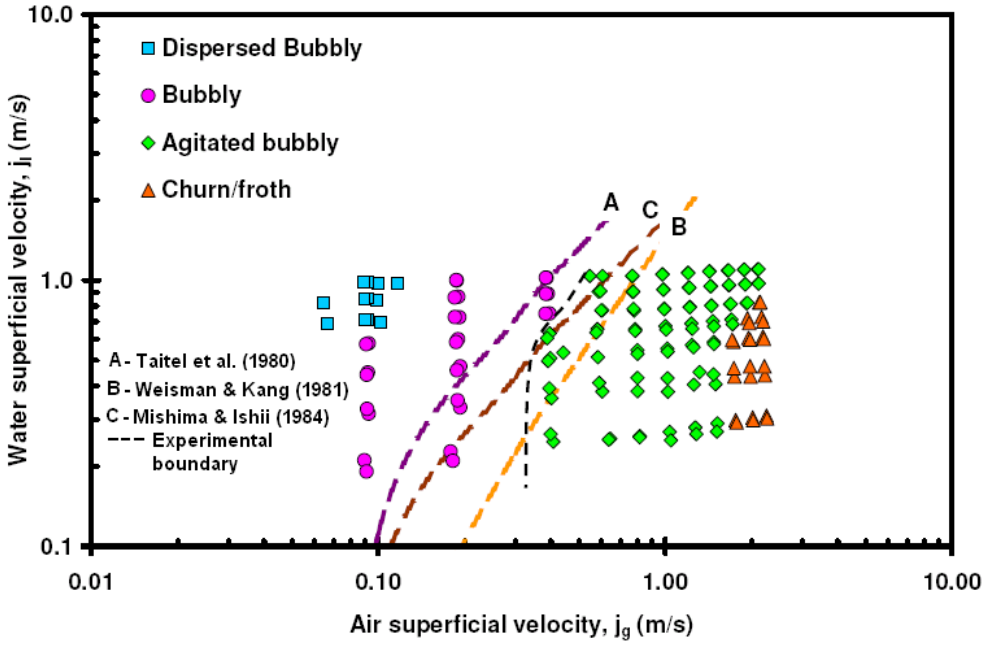

Figure 4.50 Comparison of Bubble-Slug transition models for 254mm nominal diameter vertical pipe.

The Figure 4.51 indicates the experimental results and the performances of the various existing slug to churn flow transition models (Taitel *et al.*, 1980; Mishima and Ishii, 1984; McQuillan and Whalley, 1985; Brauner and Barnea, 1986 and Tengesdal *et al.*, 1999). The experimental result indicates a gradual shift from agitated bubbly to churn flow. The trend shows an increase in liquid superficial velocity with increase in gas superficial velocity near the transition region. The trends predicted by Taitel *et al.* (1980), McQuillan and Whalley (1985) and Brauner and Barnea (1986) are all in contradiction to the experimental trends. It is to be noted that in all the above models, the transition curves terminate at slug to bubble transition boundary (α_c=0.25 or 0.3) as below these values only bubbly flow is predicted. While the general trend of current experimental boundary is consistent to Mishima and Ishii (1984) and Tengesdal *et al.* (1999) slug-churn boundary, it appears at lower gas superficial velocities than predicted by above models. This means that both the models predict a higher slug to churn transition upon increase in diameter. It is to be noted that the current experimental observation is also supported by the work of Ohnuki and Akimoto (2000) with 200mm vertical pipe experiments, who found that this transition occurred earlier than predicted with Mishima and Ishii (1984).

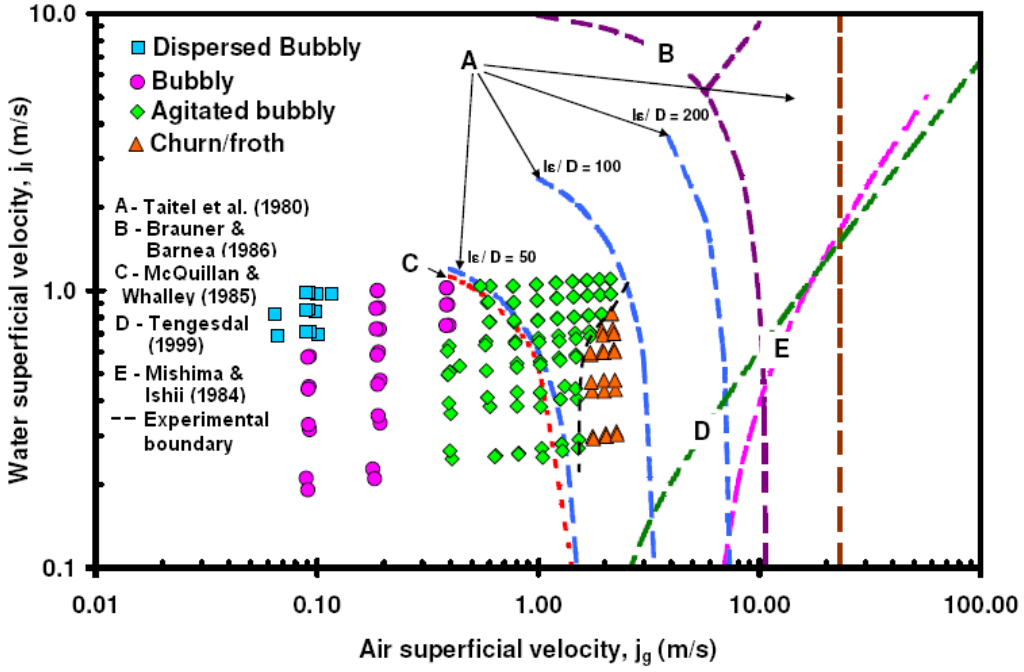

Figure 4.51 Comparison of Slug-Churn transition models for 254mm nominal diameter vertical pipe.

To further support the assertion that some of the presently used models/codes give questionable predictions of flow patterns in large diameter vertical upflow conditions, an effort was made to compare current results with some commercial methods/codes used in oil production systems. Generally in all the commercial methods/models, flow regime identification is performed first and then a set of momentum, mass and energy conservation equations are solved with the help of closure laws which are flow regime dependent. The main predictions obtained from such models are the flow regimes, pressure drops and the liquid hold-up. Unfortunately, due to propriety nature commercial methods/codes, only OLGA code could be explored. However, most of the other codes especially the steady state codes like (PIPESIM and PIPSYS) are mostly based on the traditional empirical methods and software vendors have modified them over the years. Hence two famous models namely Beggs & Brill and Duns & Ros (Brill and Beggs, 1991) that forms core of such steady state codes were used to predict the flow regimes that were compared with the experimental results.

It is to be noted that while the above OLGA code is based on data collected in the 189mm SINTEF flow loop, Beggs and Brill is set of correlations, developed for 25.4 to 38.1 mm diameter pipes at all inclinations (-90º to +90º). The method identify the flow regimes (segregated, transition, intermittent and distributed) first and then liquid hold up for horizontal orientation which is corrected for actual pipe inclination. Duns

and Ros (1963) correlations are specifically developed for vertical flow of gas-liquid mixtures in wells with experimental data of pipe diameters of 32.0 to 142.24mm. This method is based on extensive dimensional analysis to validate the model for different sets of fluids. The model recognizes bubbly, slug and mist flow with transition region between slug and mist flow.

Finally in the last, the flow regime predictions from a more recent 1-dimensional flow pattern dependent mechanistic model of Oliemans & Pots (2006) are also presented. This scheme proposes the determination of flow patterns for gas-liquid flow in tubes followed by the calculation of pressure gradient for individual flow regime.

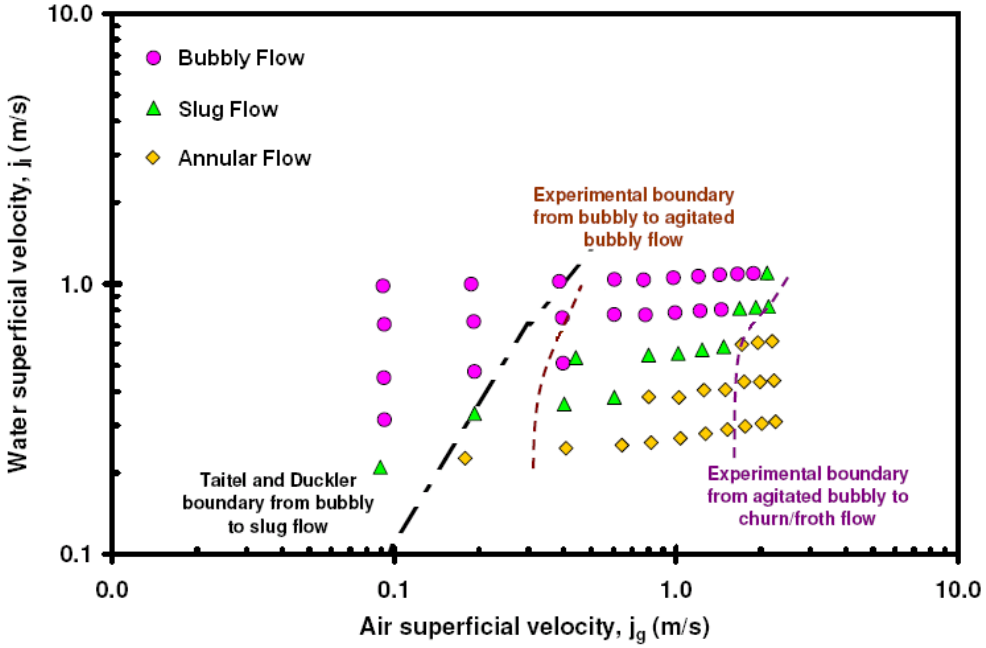

Figure 4.52 Data points corresponds to OLGA steady state flow regime predictions for riser base injection configuration, figure also shows the experimental transitions boundaries and Taitel *et al.* (1980) bubble to slug transition boundary.

The Figure 4.52 above shows the results of flow regime predictions from the leading transient multiphase simulator OLGA ver5.1. The results presented are the data points from the steady state predictions of the code to demonstrate the predictions of the code in comparison to the experimental transition boundaries results obtained. The detailed results can be found in Appendix B. It is to be noted that the agitated bubbly and churn/froth flows are not recognized by code due to its strict classification (bubbly, slug and annular flow under vertical flows). In the results the code predicted some experimental runs of bubbly flow correctly mainly at higher liquid velocities while at the low liquid velocities, the data points were incorrectly identified as slug flow. The agitated bubbly flow was completely unidentified by the code as it was

predicted as bubbly flow at higher liquid velocities (j_w > 0.6m/s), slug flow at intermediate liquid velocities and annular flow as lowest liquid velocities.

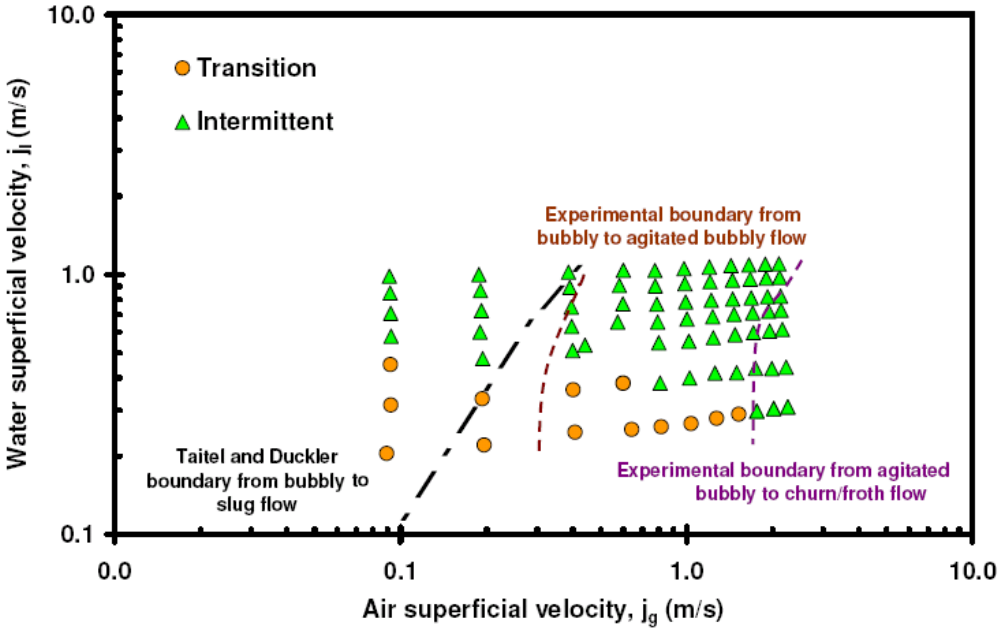

(a)

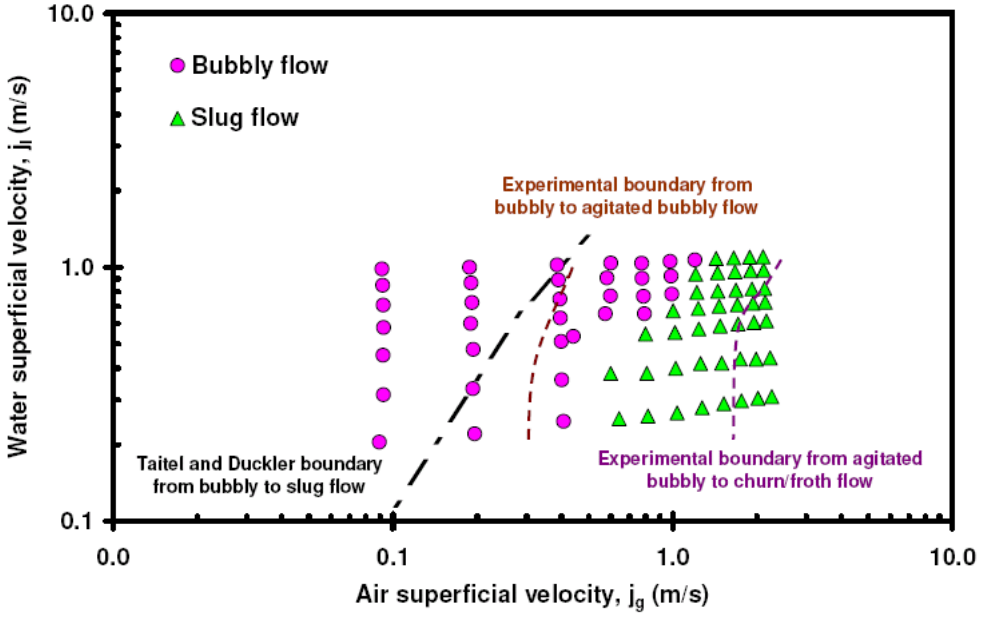

(b)

Figure 4.53 Flow regime predictions by Beggs & Brill (1973) (top) and Duns & Ros models (1963) (below).

The churn/froth flow regime was also predicted as annular flow by the code. This discrepancy highlights that the code's flow regime mechanism is not able to distinguish between the agitated bubbly flow and slug flow and churn/froth and annular flow pattern, thus classifying them as bubbly/slug and annular flow respectively. The inability of the code to predict the correct flow regime is signifying the differences of the database used (due to different physical properties of the working fluids) or the flow loop geometrical configuration in developing the flow regime prediction mechanism.

The Figure 4.53(a) presents the flow regime predictions comparison for Beggs and Brill model (1973) and Duns and Ros model (1963). For the set of data points used, Beggs and Brill model, only predicted either transition or intermittent flow regimes. The intermittent flow regime in model encompasses plug and slug flow. The figure speaks for itself, i.e. none of the flow regime transitions are respected, in fact the model predicts all dispersed bubbly, bubbly and agitated bubbly flows as intermittent at $j_w > 0.4$m/s. Nevertheless the pressure gradient predictions by the model (presented in the later chapter) were satisfactory even the flow regime predictions were not correct. The Figure 4.53(b) indicates the results of Duns and Ros model (1963), in comparison to the previous model, this model predicts all the flow regimes either as bubbly flow or as slug flow. All the experimentally determined dispersed bubbly, bubbly and agitated bubbly flows are all predicted as bubbly flow while some of agitated bubbly and all of the churn/froth flow are predicted as slug flow. Note that the Duns and Ros (1963) transition from bubbly to slug flow lies near to the experimental transition from agitated bubbly to churn/froth flow at higher liquid superficial velocities.

Lastly in the Figure 4.54, the flow regime predictions by the Oliemans and Pots (2006) mechanistic scheme are presented. Similar to above results, this method is also a pressure gradient calculation method and employs flow regime predictions as a first step towards the calculation of pressure gradient (also refer to section 5.6.6). However, unlike above empirically based methods, this scheme is based on phenomenological/mechanistic modeling. Note in the figure that some of the flow regime predictions by this model are correct especially when flow was either dispersed bubbly or churn/froth flow. However, at intermediate air-water superficial velocity range, the bubbly and agitated bubbly flow experimental runs were incorrectly predicted as dispersed bubbly flow by the method. The churn/froth flow transition is also close to the flow regime predictions by the model. It is worth mentioning that the scheme identifies dispersed bubbly, intermittent (encompasses slug and churn/froth flow) and annular flows for vertical upflow condition. It is interesting to note that the results obtained by this method are close to experimental results than predictions of OLGA or Beggs & Brill (1973). The closeness of results could be attributed to the sub-models used that are although empirically based but encompasses the description of actual physical processes.

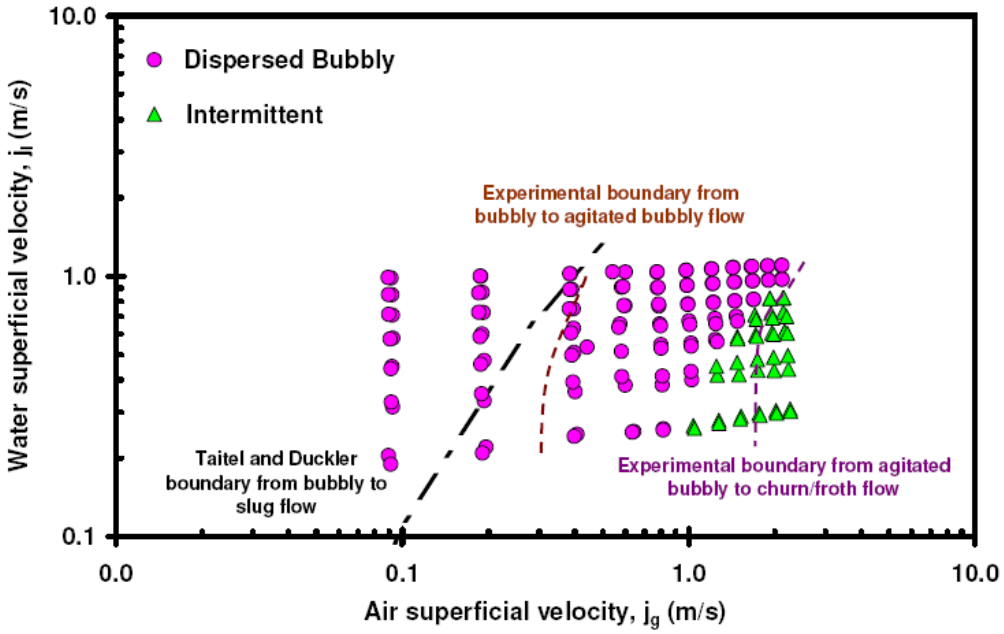

Figure 4.54 Flow regime predictions by the Oliemans and Pots (2006). The data points corresponds to flow regime predictions, the figure also shows the experimental transitions boundaries and Taitel *et al.* (1980) bubble to slug transition boundary.

4.4.2 Comparison of flow pattern results with other experimental studies conducted in large diameter vertical pipe

It is difficult to make a quantitative comparison between the flow patterns and their transitions of present and previous experimental results on large diameter vertical upflow studies as all most all the previous work is confined to pipe diameter ≤ 200mm and no work has been reported for this diameter and L/D to that considered in this study. Here it is also worth mentioning that the few studies like Shipley (1984) for 457mm diameter pipe, Hashemi *et al.* (1986) for 305mm and Ohnuki *et al.* (1995) for 489mm has been performed, however they were mostly for L/D within 12. In such cases the flow structure would still be evolving and flow regime would not represent the actual conditions in larger L/D. Moreover it also emphasised that in many of above studies, although the flow pattern observed were mentioned they were never compared with existing flow regime maps. This leave us with studies (Ohnuki and Akimoto, 2000; Shoukri *et al.*, 2000; Ombere-Iyari *et al.*, 2007 and Omebere-Iyari *et al.*, 2008) conducted on 200mm diameter pipe. Even in former two studies (Ohnuki and Akimoto, 2000 and Shoukri *et al.*, 2000), the flow was confined to the visual observation and determination of local phase distribution and interfacial area concentration, hence could only be used in qualitative sense.

Ohnuki and Akimoto (2000) study based on air-water experiments identified five flow regimes namely undisturbed bubbly, agitated bubbly, churn bubbly, churn slug and churn froth flow. It is observed that the dispersed bubbly flow in present work almost lie at the similar location where undisturbed bubbly flow was observed by them. However the differences arises in the region where existing work show bubbly and agitated bubbly flow, the previous work refer the flow patterns in this range as agitated bubbly, churn bubbly and churn slug. It is emphasised that the previous work is based on visual observation and looking into detail it seems very likely that this discrepancy is due to semantic rather than actual flow behaviour. Interestingly, their results of void phase distribution, validates the flow pattern classification presented here, contrary to five flow regimes defines by them. It also mentioned that it is very likely that this detail classification arises due to the fact that their churn bubbly and churn slug flow were separated well by Mishima and Ishii (1984) transition model. Overall, it can be concluded that there exist a reasonable agreement between their and our results.

Similar to above, Shoukri *et al*. (2000) reported three flow patterns namely bubbly, churn and annular flow in 200mm diameter vertical pipe experiments. The flow patterns were determined by high speed camera as well as signals of optical probes. It is to be noted that they did not classify the bubbly and dispersed bubbly flow and also regarded the current agitated bubbly and churn/froth flow regime as churn flow. Looking at their work without the classification of bubbly/dispersed bubbly flow and agitated bubbly and churn/froth flow a satisfactory agreement exist. However, they like Ohnuki and Akimoto (2000) also reported well predicted trends of Taitel *et al.* (1980) and Mishima & Ishii (1984) model with their experimental work.

Omebere-Iyari *et al.* (2007) employed nitrogen-naphtha as working fluid at high pressure condition of 20 and 90 bars while Omebere-Iyari *et al.* (2008) work is based on 194mm diameter 46.4 bar saturated steam-water vertical upflow experiments (refer to section 2.2). A direct comparison of these work is not possible as the physical properties especially gas density, viscosity, surface tension are affected by operating pressure and they further affect the two phase flow behaviour especially the flow pattern transition e.g. the effect of increased gas density is to move the flow pattern transitions to higher gas superficial velocity (Krishna *et al.*, 1991). Thus the higher pressure are likely to reduce the gas phase coalescence rate and increase the breakup rates so the smaller bubbles are formed that increases the overall void fraction and thus delay the transition from bubbly flow. This is what has been seen in Omebere-Iyari *et al.* (2007) work (at 20 and 90 bar), where bubbly flow is seen till the critical void fraction of 0.68. Although the annular flow was not encountered in current work and in Ombere-Iyari *et al.* (2008) but semi-annular and annular flow were detected by Omebere-Iyari *et al.* (2007) in the region currently predicted as slug to churn transition. No slug or churn flow is observed in their work in the range of current experiments as well as in the range of Ombere-Iyari *et al.* (2008), the only intermittent character flow observed was at very low liquid and gas flowrates. Omebere-Iyari *et al.* (2008) observed bubbly and churn turbulent flow in the range where current work shows the bubbly and agitated bubbly. While an agreement exist for bubbly flow region, the discrepancies arise for the flow designated as churn

turbulent flow. It is perceived that their churn turbulent flow observed is similar to the agitated bubbly flow in current study and their transition from bubble to churn turbulent are not much different from our observation of bubbly to agitated bubbly flow results. It is to be noted that in current work churn/froth flow occurs at j_g > 1.5m/s with probability mass function plots indicating a negatively skewed distribution with distinct peak associated with churn/froth flows. Whereas the churn turbulent flow in former case (Omebere-Iyari *et al.*, 2008) is more Gaussian type distribution similar to those observed in our agitated bubbly flow with positively skewed distribution. It may be that the definition of churn turbulent flow used by them is taken from the two phase flow in bubble columns where flow regime (in column diameter D> 100mm) are based on two types namely; homogenous flow (also referred as bubbly flow) and heterogeneous flow (also called churn turbulent) (Shah *et al.*, 1982). However, even in bubble column application, the two flow regimes are separated by a region considered as transition regime. This transition zone is considered to be the region where visible bubble coalescence, breakup and minor oscillations exist, which might be considered synonymous with agitated bubbly flow encountered in this work. Nevertheless the flow transition trends obtained in both the above mentioned work performed at the high pressures in comparison to Taitel *et al.*, (1980) flow transition models especially for bubble to slug transition are similar to the ones obtained in this work i.e. an earlier transition indicated by the model then observed in large diameter vertical upflow experiments; also the deviation is smaller at higher liquid flow rates than at lower rates.

4.4.3 Modification to Taitel et al. (1980) bubble to slug transition model for large diameter application

In last section, it was found that the Taitel *et al.* (1980) bubble to slug transition model yielded closer predictions to experimental results at higher liquid superficial velocities and deviated at the low velocities (refer to Figure 4.50). Although the effect of this deviation is not clear in current work due to limited water superficial velocity range, this finding was found to be consistent with the work of Omebere-Iyari *et al.* (2008) for pipe size of 194mm. The Taitel *et al.* (1980) bubble to slug transition expression also completely deviates from the results of the Omebere-Iyari *et al.* (2007) for pipe size of 189mm. In this section an attempt is made to discuss this effect in detail for current and Omebere-Iyari *et al.* (2008) work.

The Figure 4.55 shows the Omebere-Iyari *et al.* (2008) steam-water data at elevated pressure of 46.4bar, the bubbly to slug flow transition model of Taitel *et al*. (1980) (at α_c = 0.25) is unable to predict the transition. However based on experimental modification of Omebere-Iyari *et al.* (2007), the Taitel *et al.* (1980) bubbly to slug flow transition criteria was adjusted with the critical void fraction found from the experiments at near the flow transition. In order to show the transition obtained after modification to the original model, the modified critical void fraction (α_c = 0.38) from the experiment is also plotted. From the figure it is evident that the use of experimentally observed critical void fraction is able to produce a slightly better

agreement at j_l > 0.1m/s but still deviates in the region of low liquid superficial velocities for Omebere-Iyari *et al.* (2008) (see Figure 4.50 also for current work).

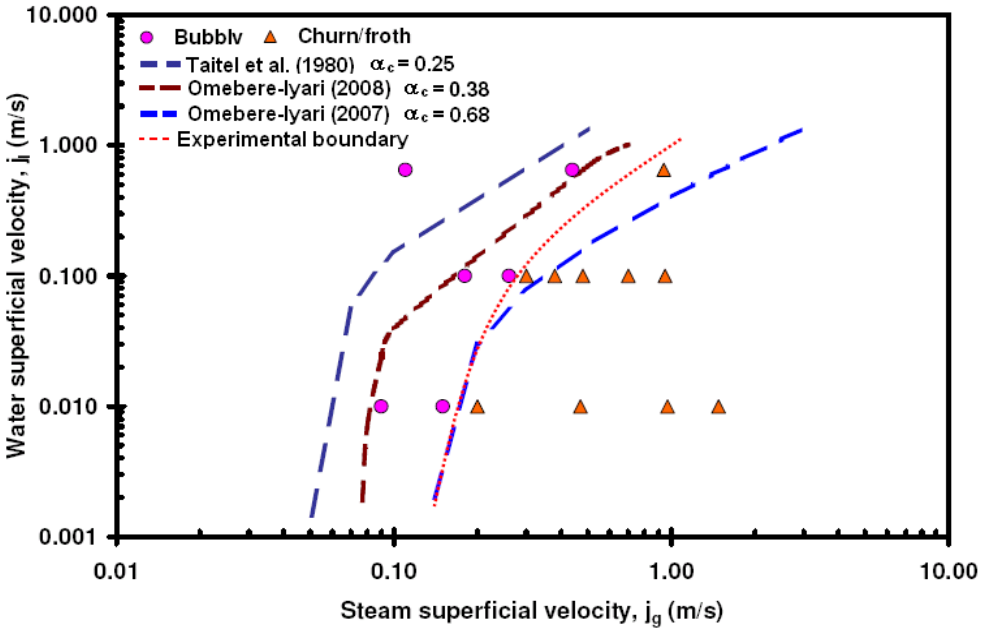

Figure 4.55 Comparison of the bubbly to slug flow transition boundary of Taitel *et al.* (1980) with Modified critical void fraction Omebere-Iyari *et al.* (2008) at 46.4 bar (water-steam) and Modified critical void fraction Omebere-Iyari *et al.* (2007).

A closer examination at the Taitel *et al.* (1980) bubble to slug transition expression (see equation 2.4a) reveals that the first term of the expression is dependent upon the value of critical void fraction and indirectly represents the non uniformity of phase distribution while the second term in the model represents the local relative velocity effect of the two phases. At higher liquid superficial velocities, the first term of Taitel *et al.* (1980) bubble to slug transition dominates as it is controlled by liquid phase properties (i.e. the void fraction being function of liquid phase properties), whereas the second term is negligible in this region. However at lower superficial liquid velocities the second term of the model i.e. the local slip between the gas and liquid phases dominates, and as it is not predicting the local slip in the above mentioned experiments correctly, the results still deviates at lower superficial velocity range.

In the experiments conducted at lower liquid superficial velocities, the local slip is large due to the presence of larger bubbles distributions with higher velocities and due to the greater degree of freedom offered by the larger diameter. However, contrary to the explanation given, the second term of Taitel *et al.* (1980) bubble to slug expression consisting of Harmathy (1960) bubble rise velocity expression does not take into account of this higher velocity. In fact, this term of the expression is

further reduced by the liquid holdup fraction and hence predicts lower slip between gas-liquid phases contrarily to seen in experiments and thus still deviates. It is to be noted that Taitel *et al.* (1980) employed this expression in its model due to its independency of bubble diameter and dependency upon liquid properties alone. All the other bubble rise velocity expressions in this region requires information of equivalent bubble diameter in order to take into account the wall effect of the conduit on the bubble. The expression was derived for ellipsoidal bubble in an infinite media and is restricted within the range $1 < Eö < 40$ (or $1.8 < d_b < 11.3$mm for steam-water and $2.7 < d_b < 17.2$mm for air-water). Hence the above expression cannot be applied for the cases if the bubbles sizes higher than above exist, as logically their presence will impart higher movement to liquid and smaller bubbles in the vicinity. In view of the characteristic differences described for the current work and Omebere-Iyari *et al.* (2008), a modification in the Taitel *et al.* (1980) model is proposed.

It is to be noted that due to the water as liquid phase in both the current and Omebere-Iyari *et al.* (2008) works, a larger bubble size distribution exists. In context of current work, initially this coalescence was occasionally observed in bubbly flow and remained restricted within the core region where these distorted bubble clusters once formed travelled upward with high velocity producing agitation in the region below. These cluster bubbles were observed to shed smaller bubbles from the top rim while moving upward. However, near the transition vicinity this coalescence in the core region not only increased but their size increased too with further multiple coalescences following in the wake regions of these large coalescent bubble clusters. It is to be noted that the small bubble population was still high in near wall vicinity but now due to the higher velocity movement of these large coalescent bubble clusters in the core the small bubbles were randomly moving. From the results of the time varying average void fraction and their probability mass function plots of all the individual runs before and after the flow transition in current work, the best estimate of average void fraction was around 0.27-0.31. This may be because at lower values the formed coalescent bubble clusters while rapidly moving upward were seen to disintegrate after travelling to a short distance. Although the bubble size distribution was not measured in current work but the presence of the large coalescent bubble clusters of equivalent diameter greater than 50mm at steam superficial velocities of 0.47, 0.94 and 1.48 m/s at the lowest water superficial velocity of 0.01m/s with bubble size distribution average around 10mm in Omebere-Iyari *et al.* (2008) supports the above visual observation in current work. The surface tension in above work was one third of the current experiments supporting our assertion that bubbles of larger diameters than above are expected to exist in current work under similar velocities range.

There are no reported large bubble rise velocity correlations available in the literature other than spherical cap, also referred as Taylor bubble (Davies and Taylor, 1950). According to Clift *et al.* (1978), the large bubble (ideally as spherical cap) is the one for which $Eö > 40$. On its basis, for the air-water system, the criterion $Eö > 40$ is met by the bubbles larger than 17mm in diameter (for steam-water it is larger than 12mm). Harmathy (1960) also has theoretically verified that for the spherical cap region ($Eö > 40$), the terminal rise velocity is independent of size and could be related

to of spheroid bubble. No further information was provided but it was stated that their results were in agreement with that of Davies and Taylor (1950).

Following the information of Harmathy in deriving the equation and further using the information provided by Clift *et al.* (1978) and data of current work, Omebere-Iyari *et al.* (2008) and Ohnuki and Akimoto (2000), below, is the theoretical expression derived, where the equivalent diameter of bubble is required:

$$U_o = 0.411 \times U_{s\infty} \tag{4.1}$$

$$U_{s\infty} = 1.74 \times \sqrt{\frac{g \cdot \Delta\rho \cdot d_b}{\rho_l}} \tag{4.2}$$

$$U_o = 0.715 \times \sqrt{\frac{g \cdot \Delta\rho \cdot d_b}{\rho_l}} \tag{4.3}$$

The equation (4.1-4.2) is the result presented by Harmathy. In above equation, U_o is the terminal bubble rise velocity, $U_{s\infty}$ is bubble rise velocity in the infinite media, d_b is the equivalent diameter of the large bubble, $\Delta\rho$ is the difference of ρ_l and ρ_g, the liquid and gas densities, and g is the acceleration due to gravity. Note that the resultant equation (4.3) is same as derived by Davies-Taylor (1950). In order to use equation (4.3), the bubble diameter needs to be determined, which is usually not available.

Wallis (1969) suggested that a correction factor (η) to be introduced into the above classical relation (equation 4.3) taking into account of the wall effect (see Clift *et al.*, 1978). In equation (4.4), the U_t is the corrected bubble rise velocity, $\eta$is the wall correction factor of Wallis (1969), D is the diameter of the pipe, d_b is the equivalent diameter of the large bubble and g is the acceleration due to gravity. The equations (4.3 & 4.5) are valid for large bubbles (or Eö > 40) only.

$$U_t = U_o \cdot \eta \tag{4.4}$$

Where $$\eta = 1.13 \exp\left(-\frac{d_b}{D}\right) \quad \text{for } d_b/D > 0.125 \tag{4.5}$$

At water-steam superficial velocities of 0.01 and 0.091m/s, Omebere-Iyari *et al.* (2008) has reported average bubble size to be around 10mm with large bubbles of 40-50mm in diameter also present. It is to be noted that according to Clift *et al.* (1978), the large bubble (ideally as spherical cap) is the one for which Eö > 40, which for steam-water is equivalent diameter of 12mm. Also the large bubble values are before the transition that took place at j_g = 0.2m/s, hence the bubbles larger than above sizes are suppose to exist in near vicinity of transition gas superficial velocity. Moreover, the visualization study from wire mesh tomography of Omebere-Iyari *et al.* (2008) steam-water work indicates that large bubble clusters with more than half the pipe

diameter in size and with axial length greater than pipe diameter are present at j_g = 0.2m/s (see figure 12, pp 470 of above work). Hence if it assumed that the diameter of such distorted bubble cluster is half the diameter of pipe (i.e. $d_b = D/2$) and using equation (4.3) and (4.4-4.5), the terminal rise velocity of such bubble cluster could be:

$$U_t = 0.715 \times 1.13 \exp\left(-\frac{D}{2D}\right) \times \sqrt{\frac{g \cdot \Delta\rho}{\rho_l} \cdot \left(\frac{D}{2}\right)} \qquad 4.6a$$

$$U_t = 0.346 \times \sqrt{\frac{g \cdot \Delta\rho \cdot D}{\rho_l}} \qquad 4.6b$$

Note that the constant term on the right of above equation (4.6b) is similar as forwarded by Dumitrescu (1943). For any $d_b/D > 0.25$ approximately, the wall effect will influence the bubble rise velocity and in that case, the value of constant approaches 0.35 or the bubble velocity given by Dumitrescu (1943) expression. Upon substitution of above equation (4.6b) in equation (2.4a) makes the transition model from bubbly to intermittent flow as:

$$j_l = \left(\frac{1-\alpha_c}{\alpha_c}\right) \times j_g - (1-\alpha_c) \times 0.346 \times \sqrt{\frac{g \cdot \Delta\rho \cdot D}{\rho_l}} \qquad 4.7$$

The resulting transition boundary from the use of above expression (4.7) is indicated in Figure 4.56(a) for Omebere-Iyari *et al.* (2008). The modified critical void fraction model for the bubbly to slug flow transition is also provided for comparison with above equation. The bubbly flow can be seen to exist on the left of this transition. This further highlights that the presence of coalescent bubbles within the core and the rapid agitation produced by them causes significant changes in the flow field and hence affect the smaller bubble rise velocities. By using the same equation (4.7) for current work, the resultant transition boundary can be seen in Figure 4.56(b). Indeed the predicted transition is seen to lie close to experimental transition in above works than predicted by the original Taitel *et al.* (1980) model and modified critical void fraction model by Omebere-Iyari *et al*. (2007).

Lastly, the Figure 4.58 below presents the results of the equation (4.7) for Ohnuki and Akimoto (2000) work. The critical void fraction with equation (4.7) was taken as 0.27 as it provided the best fit. This value is also close to the value taken by them (α_c = 0.3, see Figure 4.58). The results are indeed satisfactory than predicted by Mishima and Ishii (1984) bubble to slug transition model. The results presented above in Figure 4.58 further shows that discrepancy between current and their work is due to the semantic rather than actual flow behaviour. This is also supported by Ohnuki and Akimoto (2000) that " *….and in the slug flow region of the Mishima and Ishii (1984) map, large coalescent bubbles existed and the flow pattern is changed to a churn froth flow via a churn bubbly and/or a churn slug flow with* j_g".

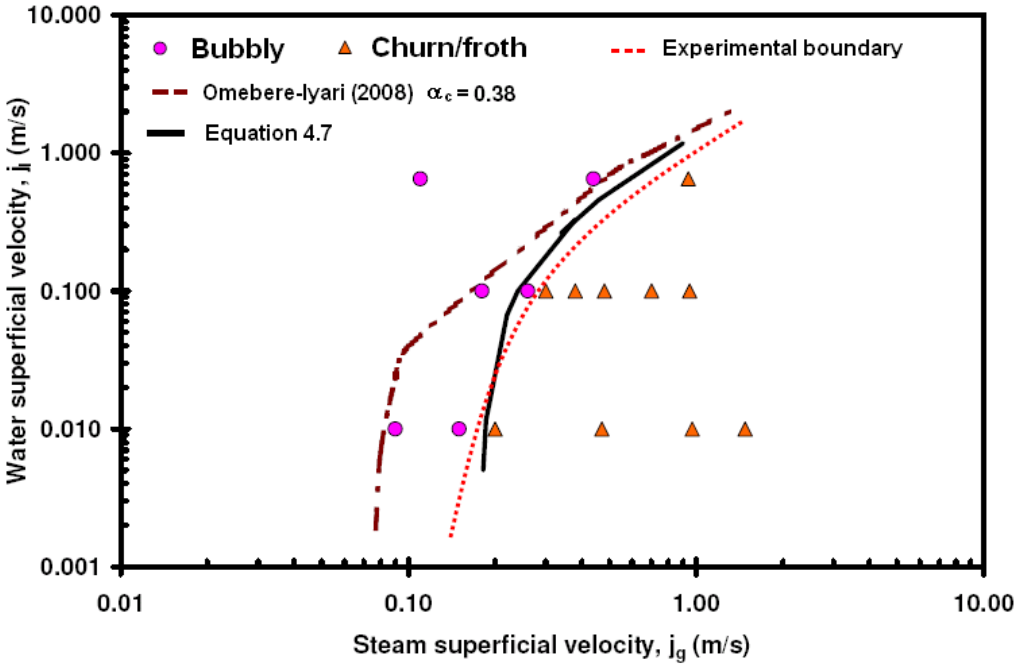

(a)

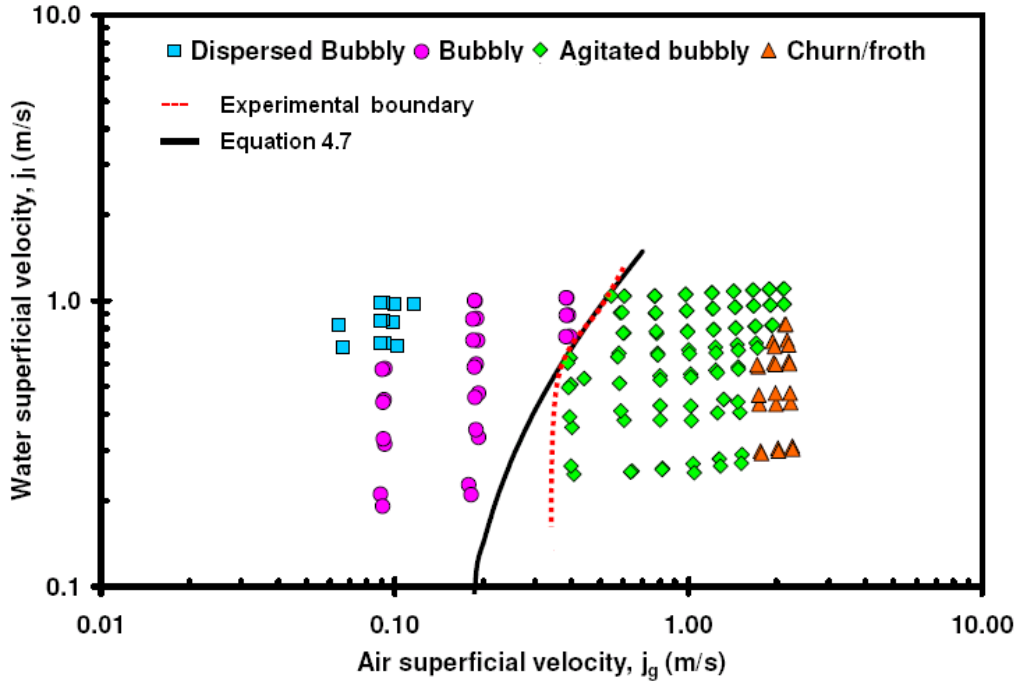

(b)

Figure 4.57 The proposed modification of the bubbly to slug flow transition boundary of Taitel *et al.* (1980) (a) for Omebere-Iyari *et al.* (2008) work (b) for current work.

The latter region classified as churn bubbly and/or churn slug flow is the same region (referred as here agitated bubbly flow) where large coalescent bubble clusters were observed in present work.

It is to be noted that the use of equations (4.7) was not attempted for Omebere-Iyari *et al.* (2007) due the different working fluids resulting in different bubble size distribution, critical void fraction and hence different relative velocity. However, it is anticipated that the equation (4.7) can provide reasonably accurate results for the fluids where more of large coalescent bubbles exist.

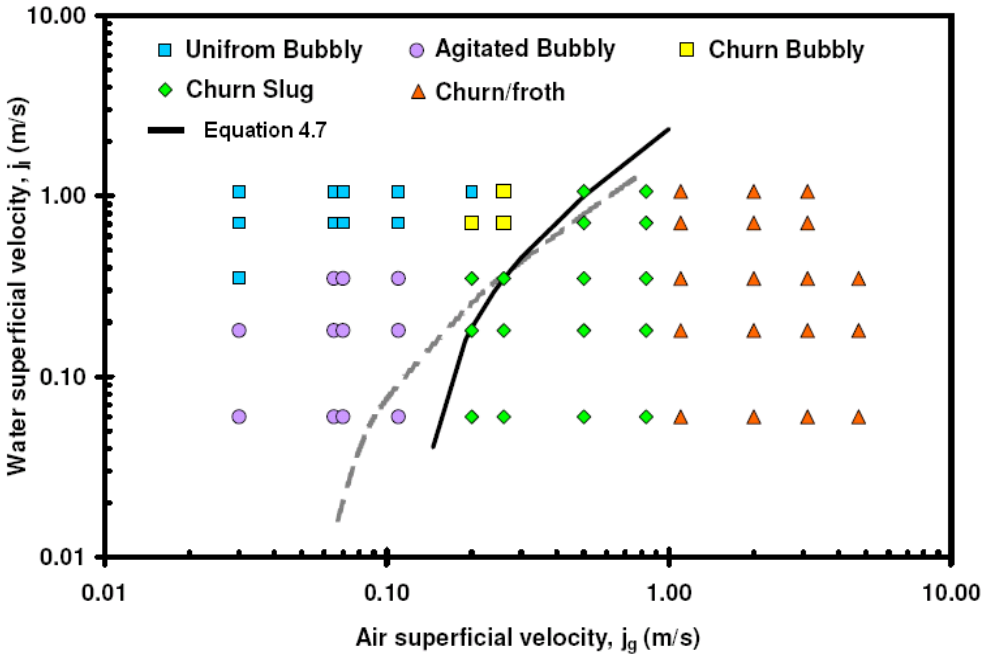

Figure 4.58 The results of the proposed modification of the bubbly to slug flow transition boundary of Taitel *et al.* (1980) for Ohnuki and Akimoto (2000).

4.4.4 Interim Summary

The experimental flow pattern map was developed based on the identification of the flow type by the probability mass function plots in a similar manner to Costigan and Whalley (1997).

From the above comparison presented, it was seen that most of the models: Taitel *et al.* (1980), Mishima and Ishii (1984), McQuillan and Whalley (1985), Brauner and Barnea (1986) were unable to predict the dispersed bubbly-to-bubbly boundary. Only Chen *et al.* (1997) and Weisman and Kang (1981) models came close to predicting above transition boundary. However, while the Chen *et al.* (1997) transition boundary

was developed in the light of poor predictions from Taitel *et al.* (1980) bubble-to-dispersed bubble boundary with some phenomenological basis, Weisman and Kang (1981) uses the modified empirical correlation of Taitel and Dukler (1976) based on negligible slip between the phases.

Taitel *et al.* (1980), Weisman and Kang (1981), Mishima and Ishii (1984) and McQuillan and Whalley (1985) transition models from bubble to slug were used. All the above models, except the Weisman and Kang (1981) are based on the assumption that slug flow transition occurs at a constant critical void fraction. These models report the interesting observation of closer prediction at higher liquid superficial velocities and deviation at lower liquid velocities not only in current work but also in other work conducted in large diameter vertical pipe upflow (Ohnuki and Akimoto, 2000; Omebere-Iyari *et al.*, 2008). The later model (Weisman and Kang, 1981) relates the Froude number of gas and the Froude number of total volumetric flow, although no physical property effect are included yet this transition criterion did yield closer prediction at lower liquid velocities in comparison to above models, due to the inclusion of the diameter in the correlation for the region where the flow pattern being dominated by bubble clusters having high rise velocity.

Slug to churn transition boundary of Mishima and Ishii (1984) and Tengesdal *et al.* (1999) showed a consistent trend as seen in current work, however both predicted a delayed transition. All the other models (Taitel *et al.*, 1980; McQuillan and Whalley, 1985; Brauner and Barnea, 1986) did not adequately predict this transition boundary.

It is clear from above analysis that none of the flow regime transition models are adequate for predicting the flow regimes in large diameter vertical risers as a whole and it is only through understanding of mechanisms involved in individual transition that can provide an appropriate model.

It has been found that the Taitel *et al.* (1980) bubble to slug transition model does not yield satisfactory results for large diameter vertical upflow condition. It was further noted that the discrepancy is due to the Harmathy (1960) expression of the rise velocity of moderately distorted ellipsoidal shape bubble in an infinite media. In view of above mentioned an attempt is made in section 4.4.3 to understand the transition mechanism involved from bubbly flow in large diameter vertical upflow condition. Based on the physical understanding of the process, the deviation of Taitel *et al.* (1980) model in case of large diameter vertical upflow is explained and mathematically modified for the conditions of air-water/steam-water generally. The results obtained by the application of the modified model are in satisfactory agreement with the experimental results.

The comparison of experimental flow patterns results with other work on large diameter vertical pipe especially with air-water as working fluid indicates a close agreement.

Part III - Void Fraction Characterization

This part of the thesis deals with the comparison of the void fraction results with existing work on large diameter vertical pipe upflow condition.

4.5 Void Fraction

4.5.1 Drift flux model

The drift flux model is a widely used model due to its simplicity and applicability in two phase flows (Hibiki and Ishii, 2003). The model is found to predict the two phase characteristics like void fraction. Due to the considerable importance of drift flux model in predicting the two phase flow characteristics, the drift flux parameter i.e. the distribution parameter (C_o) and drift velocity (U_{gj}) were calculated for the current experimental data.

The Figure 4.59 and 4.60 illustrates the current results for individual flow regime in terms of j_g/α vs. j_m. Since both the parameters i.e. distribution parameters (C_o) and drift flux velocity (U_{gj}) are flow regime dependent, hence data is plotted for each of these according to the specified flow regime determined from visual as well as time varying probability mass function plots defined earlier. In the figures, the intercept of the line represents the drift velocity (U_{gj}) while the slope represents the distribution parameter (C_o). Note that the distribution parameter (C_o) is used to quantify the degree of flow uniformity as it represents the global effect due radial non-uniform void and velocity profiles where as the drift flux velocity (U_{gj}) represents the local relative velocity effect.

From the Figure 4.59, it is obvious that for bubbly flow the data presented does not lie on the straight line; also note that slightly similar trend is seen at the lower j for agitated bubbly flow in Figure 4.60a. This behaviour is consistent with results of Hibiki and Ishii (2003) for their 102mm diameter vertical pipe experiments under low mixture volumetric flux. They suggested the scatter in the data is due to the bubble induce turbulence being dominant and hence influencing the flow field. The later effect is also dominant in 254mm diameter pipe for vertical upflow condition and seems to decay out with increase in gas superficial velocity as the shear induce turbulence comes into play. Hence at higher and intermediate mixture volumetric fluxes i.e. near transition from agitated bubbly flow the data converges towards the straight line. This collapse of data on the straight line is also observed in smaller diameter pipes (D< 100mm) where all the data points tend to lie on the straight line regardless of the flow regime due to the insignificant recirculation and similar drift velocity among all the flow regimes (Hibiki and Ishii, 2003). Figure 4.60b shows the results for churn/ froth flow i.e. at highest mixture volumetric fluxes the data lie on the straight line. This indicates a total suppression of localized recirculation with increase in gas superficial velocity.

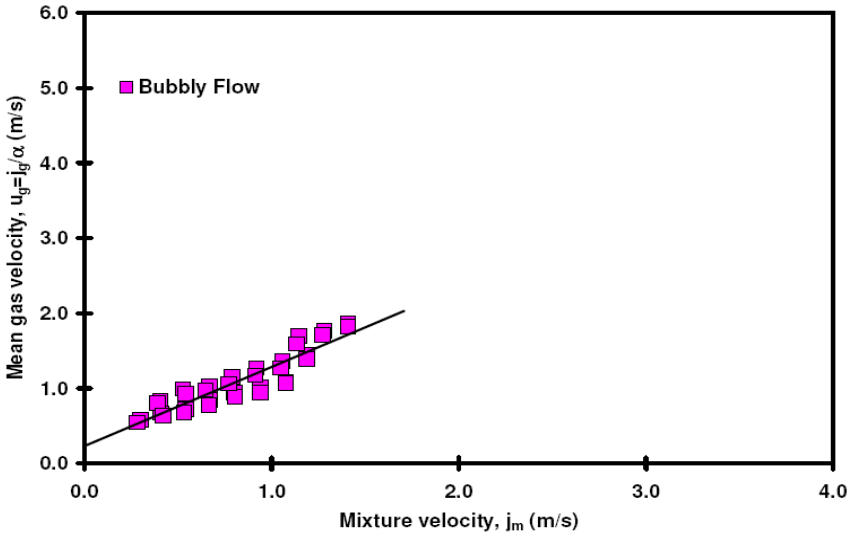

Figure 4.59 The experimental drift flux relationship in bubbly flow regime.

The values of the distribution parameters (C_o) and drift flux velocity (U_{gj}) obtained from the Figure 4.59 and 4.60 are also presented in Table 4.1 for the individual flow regimes. The values obtained from the above figure suggest that a parabolic profile or core peaking profile exist in agitated bubbly and churn/froth flow case ($C_o > 1$) where as for bubbly flow the profile appears to be more uniform. This also means that a bubble migration towards the center of pipe had already started at low values of volumetric fluxes. Thus the drift velocity in the center of the pipe is higher than near the wall and this causes the gas velocity to rise. This is not surprising as in bubbly flow there was occasional coalescing in the core region while for agitated bubbly and churn/froth flow large bubble clusters and gas structures were seen.

It is to be noted that in above results, dispersed bubble flow is not differentiated from the bubbly flow (due to few data points of DB) and, if this was the case then C_o and U_{gj} for dispersed bubbly flow are 0.605 and 0.23 and 1.119 and 0.42 for non-dispersed bubbly flow. The former result represents that that the liquid phase turbulence is dominant and hence the small bubbles are pushed towards the wall leaving a smaller distribution in the pipe center. It is to be noted the more closer this C_o value is to unity a more uniformly distributed void fraction across the diameter exist and hence a flatter peak. However, if $C_o < 1$, then a wall peak void phase profile exist. Various investigators (Guet *et al.*, 2003; Hibiki and Ishii, 2002 and Hibiki and Ishii, 2003) have reported typical values of $C_o < 1$ for a wall peak phase profile, $C_o \approx$ 0.95-1 for uniform phase profile and $C_o \geq 1.2$ for a core peak phase distribution of void fraction.

While the current results of bubbly and dispersed bubbly flow are in fully agreement with conventional size pipes, the distribution parameter results under the agitated

bubbly flow are in agreement with the results of Hills (1976) and Ohnuki and Akimoto (1996) who found similar flow with liquid recirculation at the intermediate superficial gas velocity range. Guet *et al.* (2004) also reported large values of distribution parameter as consequence of the downward liquid flow in the near-wall region. Thus the experimental value of distribution parameter (C_o) = 1.275, shows that the phase distribution in the experiments was indeed the agitated bubbly flow. The distribution parameter (C_o) for churn/froth flow is slightly lower than agitated bubbly flow this due the intermittent character of the flow where some high velocity gas structure were see to rip away the core with a thick liquid film falling downward with some temporary irregular liquid bridging. This later effect resulted in slight decrease in overall void profile.

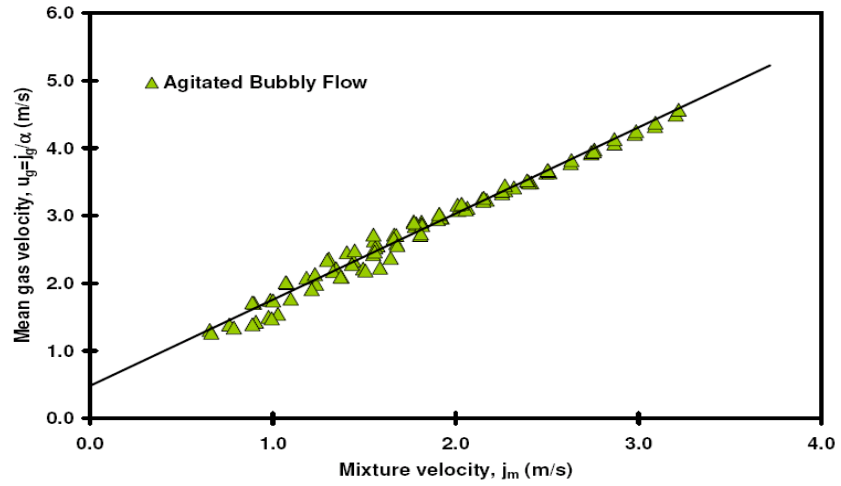

(a)

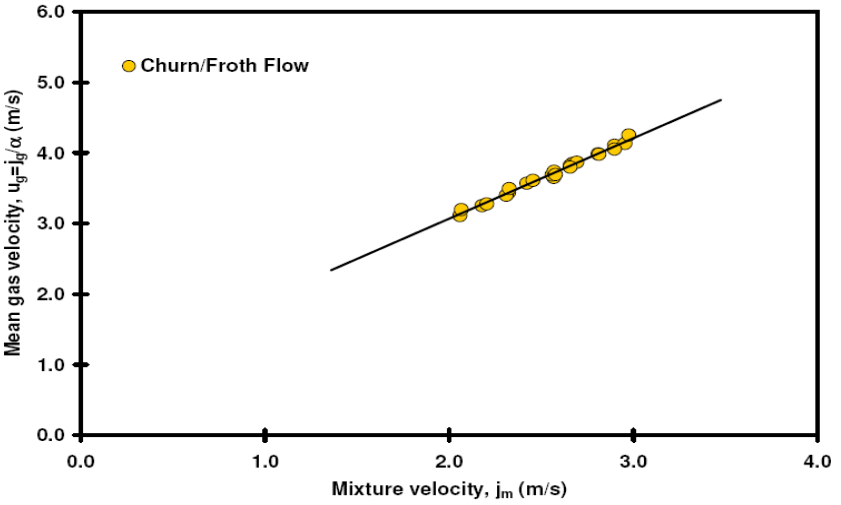

(b)

Figure 4.60 The experimental drift flux relationship in (a) agitated bubbly flow regime and (b) churn/froth flow.

The results of the drift flux velocity are also concurrent to the distribution parameter as this represents the gravitational forces that give a bubble a tendency to rise, hence with increase in gas superficial velocity and enlargement of bubble sizes the drift velocity also increases with flow regime. For agitated bubbly and churn/froth flow the drift velocity is large compared to bubbly flow due to the fast-rising coalesce bubble clusters in agitated bubbly flow and then large distorted structures in churn/froth flow. From the results obtained it can be observed that the distribution parameter values and the drift velocity values are in agreement with those values in the literature.

Table 4.1 The experimental drift flux parameters obtained in different flow regimes

Flow Regime	Bubbly Flow	Agitated Bubbly Flow	Churn/Froth Flow
Distribution Parameter, C_o (-)	1.054	1.275	1.140
Drift velocity, U_{gj} (m/s)	0.237	0.481	0.790

Table 4.2 shows the mean value results of all the data in comparison to the existing distribution concentration parameter and drift flux correlations along with experimental results on large diameter. It is be emphasised here that each flow regime has its own drift velocity and distribution parameter, however in order to compare the overall trends, an average value of all the data are usually computed (Ohnuki and Akimoto, 2000; Shoukri *et al.*, 2000 and Omebere-Iyari *et al.*, 2007). It is seen that the pool correlation of Kataoka and Ishii (1987) slightly over predicts the distribution parameter and under predicts the drift velocity in comparison the experimental value while Hibiki and Ishii (2003) correlation is fairly good agreement with experimental results. It is to be noted that while Kataoka and Ishii (1987) uses the similar expression for distribution parameter as original Ishii model (1977) for all flow regimes while Hibiki and Ishii (2003) distribution parameter is specifically developed for large diameter at low flow rates. Thus in latter set of correlations an effect of inlet condition to vertical upflow is also included in comparison to the former. At higher mixture fluxes, Hibiki and Ishii (2003) recommended the use of similar expression of Ishii (1977) with explanation that liquid recirculation found at low fluxes in large diameter pipes are suppressed hence the correlation of Ishii is applicable at high j_m.

The results of present work were also compared with the previous studies conducted on large diameter pipes (D>100mm), see Table 4.2 column no 3-6. Hills (1976) distribution parameter for 150mm column is in good agreement with current work; however the drift velocity is under predicted. This is due the systematic error in their experiments that has affected the slope of the drift flux equation. However when drift flux parameters are calculated for Hills (1993) data, the values obtained are

satisfactory. Shoukri *et al.* (2000) work from 200mm diameter pipes also yielded close prediction for drift flux but slightly under predicted the distribution parameter. Omebere-Iyari *et al.* (2007) work at 90bar high pressure predicted closer values of distribution parameter than at 20bar. The low 20bar value suggests a more uniform distribution of void across the diameter. Their drift velocity values are very low in comparison to the current work at both pressures, however these small values of drift velocity suggests more homogenous phases. Kataoka and Ishii (1987) from their experimental data have identified that drift velocities could take different values even at same pressure due to the difference in physical properties of the liquid phase. Hence the low drift values observed in Ombere-Iyari *et al.* (2007) work are due to the difference of physical properties of the naphtha. This argument is also supported by the fact that many investigators working with organic compounds in bubble columns have also reported that hydrocarbon liquids tend to increase the void fraction by promoting a bubblier flow. Naphtha used by Omebere-Iyari *et al.* (2007) is a liquid mixture of 66 hydrocarbon chemicals, to model liquids produced from wells, hence the low drift values are due to the fact that in bubbly flow the drift velocity are low and hence results in higher void fraction than non-organic compounds. Above argument is further supported by the fact that for all the flow conditions especially at low liquid input their absolute drift velocity $|U_{gj}|$ mostly varies between negative value to 0.014m/s which are of the same order of $\sqrt{2}[\sigma g(\rho_l-\rho_g)/\rho_l^2](1-\alpha)^{1.75}$, the correlation of drift velocity for bubbly flow given by Ishii (1977). From the results obtained, it can be concluded that the drift rise velocity of bubbles in air-water is larger than nitrogen-naphtha case where the rise velocity will be low due to smaller size and bubblier flow. Omebere-Iyari *et al.* (2008) work with steam-water is also in reasonable agreement for the drift velocity while distribution parameter value is not available.

Figure 4.61 illustrates the effect of diameter on drift velocity; the trends obtained with various large diameter vertical upflow studies are consistent to that found by Kataoka and Ishii (1987) that the drift velocity (U_{gj}) is function of vessel diameter up to about 100mm and then almost stays constant for a vessel diameter greater than 100mm. The figure includes the slug flow drift velocity equation and churn turbulent flow drift velocity equation of Ishii (1977) for the small diameter pipe as well as the Ishii and Kocamustafaogullari (1984) correlations for drift velocity for cap bubble and maximum cap bubble flow in large diameter pipes. All the data plotted are for large diameter vertical upflow conditions and it can be noted that in each case the predicted drift velocity (U_{gj}) is higher than defined by churn turbulent equation of Ishii (1977) for conventional pipe sizes. Only in one case the data lies below where the air injection effect through porous sinter wall is dominant because of small L/D (L/D ≈ 4). However under similar conditions as that of porous sinter wall injection but with nozzle type injector, the drift velocity again lies in the region of maximum cap bubble (Ohnuki and Akimoto, 1996). Thus the figure validates (i) neither the slug flow drift velocity nor the churn turbulent drift velocity equation, can accurately predict the large diameter experimental data and (ii) the current work also shows the consistent trends as obtained by other studies on large diameter vertical upflow conditions.

Table 4.2 The comparison of the drift flux parameters.

	Kataoka & Ishii (1987) †	Hibiki & Ishii (2003) †	Hills (1976) & (1993)	Shoukri *et al.* (2000)	Ombere-Iyari *et al.* (2007)	Ombere-Iyari *et al.* (2008)	Present work
Nominal Diameter (mm)	254	254	150	200	200 (189)	200 (194)	254
Fluid	various	various	air/water	air/water	nitrogen/ naphtha	steam/ water	air/water
Distribution Parameter, C_o (-)	1.196	1.174	1.16 (1.103)	1.015	1.08 @20bar 1.15 @90bar	Not available	1.156
Drift velocity, U_{gj} (m/s)	0.455	0.437	0.36(0.40)	0.49	0.07 @20bar 0.09 @90bar	0.44 @ 46.4 bar 0.1m/s	0.503

† *indicates the drift flux correlations of Kataoka and Ishii (1987) and Hibiki and Ishii (2003).*

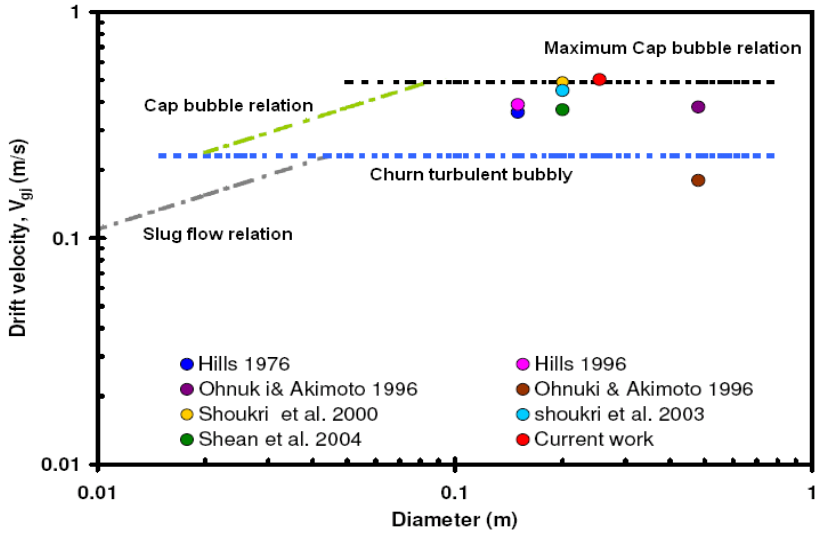

Figure 4.61 Effect of pipe diameter on drift velocity obtained from air-water data.

4.5.2 Void fraction phase distribution

The knowledge of spatial variation of void fraction i.e. void phase distribution is important as it plays major role in scale-up process. The radial void distribution directly affects the pressure field and thus is a cause of liquid recirculation (Hibiki and Ishii, 2003). The liquid recirculation is found to play an important role in large diameter vertical pipe upflow condition, as it greatly affects the mass and heat transfer properties. It been explained in earlier sections that there is fundamental difference in flow behaviour between conventional and large diameter pipe sizes due to the differences in the flow structures. In case of large diameter pipe, the flow structure is more complex as the degree of freedom for liquid movement has increased. This aspect also influences the void phase distribution, velocity distribution and bubble sizes, hence it is necessary to understand the flow structure accurately.

Although no local flow properties like void phase distribution, bubble sizes etc. were measured, however, some inferences using the existing data and its results can be drawn in comparison to existing large diameter work. The phase profile of the void fraction phase distribution has been reported by many previous investigations (Serizawa *et al.*, 1975; Herringe and Davis, 1976 and Liu, 1993) and is found to depend upon on many factors like superficial gas velocity, bubble size distribution, gas injection, pipe diameter, nature of gas-liquid systems and operating conditions. Current comparison is also undertaken due to the fact that majority of data in the Table 4.3 is mostly for air-water in vertical pipe of diameter range 150 to 480mm. Hence all these work can be used to support the present work, especially through the flow regimes predictions and by drift flux analysis performed in earlier section. From the works presented, it can be deduced that in large diameter vertical pipe depending on the flow rate, the void phase distribution can be categorize into either wall peak or the core peak and crossover from these phase distribution represents the change of flow pattern. Additionally in the large vertical pipe, the wall peak is observed under the dispersed bubbly flow only where there is no bubble interaction and the mean void fraction is very low. Ohnuki and Akimoto (2000) found that in the large diameter vertical pipe, the wall peak is lower than observed in smaller diameter pipes due to the "lower radial velocity gradient of water and the larger turbulent dispersion force".

The Table 4.3 above provides the quantitative details of the experimental investigations conducted on phase distributions in large diameter pipes (D≥ 150mm). Generally, a core peak phase distribution was reported and the wall peak was only found at high liquid and very low gas superficial velocities. In latter case i.e. when a wall peak phase distribution was found, the flow was mainly dispersed bubbly while in former the reported flow regimes varied from bubbly, agitated bubbly, churn bubbly, churn slug to churn/froth.

In current investigation, void phase distribution and bubble sizes were not measured, but from both the air inlet configuration i.e. Tee (50.8mm) and Annular sleeve (8×38mm holes) injectors, large size bubble generation is expected, in comparison to the porous sinter plate used in most of the experimental work. However a detailed

analysis on flow regime was performed backed up by the visual observation; based on this, the flow regimes were classified by their time varying void fraction traces, their corresponding probability mass distributions and visual observation into dispersed bubbly, bubbly, agitated bubbly and churn/froth flow. Under bubbly flow although the bubbles were distributed uniformly across the diameter but there was some bubble coalescence in the core region at low air-water superficial velocities, it is likely that void phase distribution was either already a core peak or near to transition under the developing coalescence bubbles. With increase in air superficial velocities, more and more bubble coalescence took place and flow turned to agitated bubbly and then to more chaotic churn/froth flow. It is due to this intense bubble to bubble interaction that the core peak phase distribution starts to occur and becomes more prominent as the flow transition occurs to churn/froth flow. Hence, in the light of tabulated results the agitated bubbly flow and churn/froth flow encountered should be of core peak distribution. In contrast to above, no coalescence was observed at low air and high water superficial velocities when the flow was mainly dispersed bubbly. The visual observation supports the hypothesis that a wall peak ought to exist under the above conditions.

Verification for phase distribution behaviour could also be inferred from the drift flux analysis performed in the earlier section. Figure 4.59-4.60 presented earlier shows the present experimental drift flux results plotted in terms of j_g/α vs. j_m, under the different flow regimes with important characteristic of phase distributions (Table 4.1). The reported values of distribution parameter are C_o = 0.605 for dispersed bubbly flow, C_o =1.054 for bubbly flow, C_o =1.275 under agitated bubbly flow and 1.140 in churn/froth flow. The significance of the above mentioned distribution parameter values (C_o) are that for core peak void phase distribution, the value of distribution is always larger than unity, where as for the wall peak void phase distribution, the value of distribution parameter is always smaller than unity. The later characteristic is attributed to the decrease in the distribution parameter (due to the steep wall peak). Additionally, if the phase distribution is uniform/flat across the diameter; the value of distribution parameter is near unity. Thus above description implies that indeed the dispersed bubbly flow had a wall peak distribution while the experimental runs of agitated bubbly and churn/froth flow were certainly the core peak. As for the bubbly flow since the C_o value lies close to unity, it suggests a uniform phase distribution or near to transition to core peak.

Table 4.3 The comparison of void phase distribution with other studies on large diameter vertical pipe upflow.

	Working fluid	D (mm)	L/D	Flow pattern*	Water superficial velocity, j_l (m/s)	Air superficial velocity, j_g (m/s)	Phase Profile
Hills (1993)	Air-Water	150	27	-	0.26	0.06	Core peak
Ohnuki & Akimoto (1996)	Air-Water	480	3.82	DB	0.18	0.017	Flat/uniform
				AB	0.18	0.131	Core peak
				CB	0.18	0.825	Core peak
Ohnuki & Akimoto (2000)	Air-Water	200	60	CS/CF	1.06	0.83	Core peak
				CB	1.06	0.26	Core peak
				AB	0.18	0.11	Core peak
				DB	1.06	0.11	Wall peak
Shoukri *et al.* (2000 and 2003)	Air-Water	200	43	B	0.4	0.07	Core peak
				DB	0.75	0.032	Wall peak
Shen *et al.* (2005 & 2006)	Air-Water	200	43	CB	0.035	0.0311	Core peak
				DB	0.277	0.0311	Wall peak
				DB	1.12	0.063	Wall peak
Prasser *et al.* (2007)	Air-Water	195.3	40	C	1.02	0.035	Core peak
				B	1.02	0.0094	Wall peak
Omebere-Iyari *et al.* (2007)	Nitrogen-Naphtha	189	157	B	0.01	0.1	Flat
				I	0.1	0.4 -0.5	Flat
				B	0.65	1.0	Flat
				SA	0.1	0.64 -1.0	-
Omebere-Iyari *et al.* (2008)	Steam-Water	194	40	B	0.01	0.09	Core peak
				C	0.65	0.94	Core peak
Current work	Air-Water	254	47	CF	0.2-0.8	>1.6	Core peak
				AB	> 0.2	0.3-1.5	Core peak
				B	< 0.5	0.09 – 0.2	Uniform
				DB	> 0.71	0.09	Wall peak

** B=Bubbly, C=churn, I=Intermittent, AB=Agitated bubbly, CB=Churn bubbly, DB=Dispersed bubbly, CS=Churn Slug, CF=Churn Froth and SA= Semi Annular.*

Although numerous phase distribution studies have been performed in conventional as well as on large diameter vertical pipes but no quantitative relationship were presented to differentiate between the void fraction phase distributions. Similar to Vince and Lahey (1982), Shen *et al.* (2005) suggested to exploit the time varying void fraction signals to analyze the two-phase flow void phase distribution patterns. The idea of monitoring the coefficient of skewness (normalized skewness or "γ",) was employed to classify the phase distribution into wall and core peak. It was proposed that negative value for "γ" implies the core peak phase distribution and a positive value of "γ" means wall peak. The absolute value of the coefficient of skewness $|\gamma|$ represents the broader or sharper the wall or core peak phase distribution i.e. the large negative value of skewness indicates a broader core peak while higher positive skewness indicates sharper wall peak. Uniform phase distribution is achieved when $|\gamma| = 0$.

The Figure 4.62 presents the void fraction skewness results obtained at $z/D \approx 28$ plotted against the superficial gas velocity for all the superficial liquid velocities. Several important aspects can be noted in the figure, e.g. the skewness increases with an increase in liquid superficial velocity with corresponding phase distribution becoming more wall peak and less core peak. Alternatively, at very low liquid superficial velocities, phase distribution can be a core peak even at low gas superficial velocities. It can be further noted that γ varies between +0.38 to -0.82, the significance of this is that for all the flow conditions investigated the phase distribution varied from the wall to core peak as the gas superficial velocity was increased. This could further be explained by the fact that at low air-water superficial velocities ($j_g < 0.3$m/s and $j_l < 0.65$m/s), the γ value are positive but more near zero implying that a more uniform phase distribution existed, while at low air and high water superficial velocities ($j_g < 0.3$m/s and $j_l \geq 0.65$m/s), the γ values are still positive but comparatively higher to earlier situation and hence clearly signifying that a wall peak was present. It should also be noted that for the latter case γ values are not very high ($\gamma_{max} = 0.36$), confirming the Ohnuki and Akimoto (2000) observation that in large diameter vertical pipes the wall peak is less pronounced due to the smaller velocity gradients of water and the larger turbulent dispersion force. On the other hand at $j_g \geq 1.5$ m/s, the γ values are negative and the $|\gamma|$ is greater than 0.7 which implies that in comparison to the wall peak, a broader or sharper core peak exists. In the region of $0.4 \leq jg \leq 1.5$ m/s, skewness has small near zero values corresponding to the region after the transition from bubbly flow where intense bubble to bubble interaction (coalescence and breakup) existed. The statistical identification performed earlier for flow regime transition identification indicated that within this air superficial velocity range, the flow was agitated bubbly flow and the standard deviation of void fraction was like skewness almost constant. It is postulated that the low skewness values in this region are obtained due the intense bubble to bubble interaction and liquid recirculation that further promotes gas phase clustering/agglomeration.

By comparing Shen *et al.* (2005) work on 200 mm diameters vertical pipe, it is found that the $|\gamma|$ values obtained in current work are smaller, both in core and wall peak

distribution regions. While values are still close for core region, the values are noticeably less for wall peak. Form this observation; it is proposed that this is the consequence of larger diameter pipe in current work offering more degree of freedom for liquid movement and hence lower radial velocity gradient.

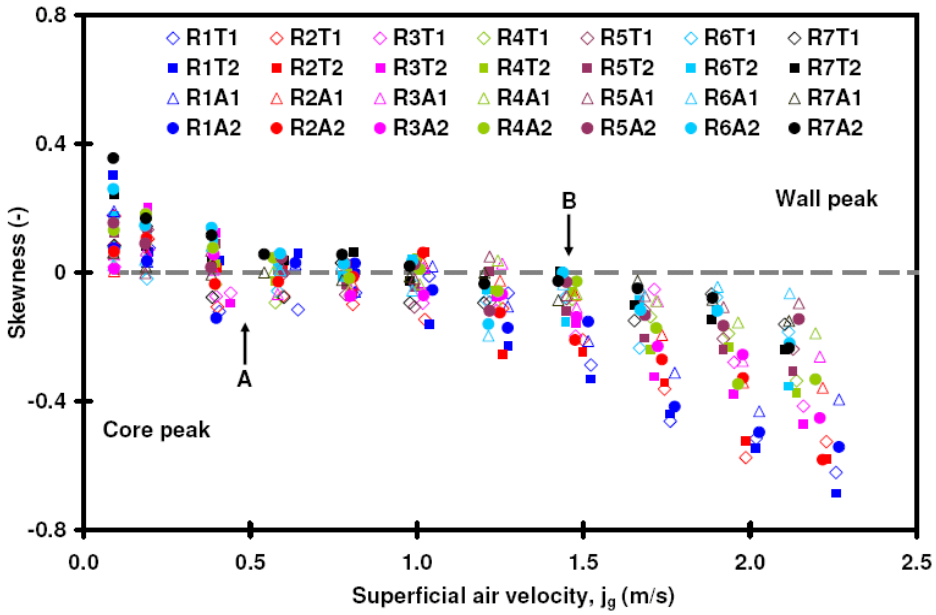

Figure 4.62 The void fraction skewness for phase distribution of the two injectors.

The work presented above supports our conclusion that the phase distribution in current investigation was core peak void phase distribution in most of the cases, where agitated bubbly and churn/froth flow regime prevailed while uniform distribution for bubbly flow and the dispersed bubbly flow in current work was by nature a wall peak. From above discussion and comparison presented, it can be concluded that the predicted void fraction profiles in present investigation are in fairly good agreement with previous studies.

It should also be noted that all the work presented are consistent with each other except for nitrogen/naphtha data of Omebere-Iyari *et al.* (2007). The flat phase distribution obtained in that work could be attributed to use of low surface tension liquid and higher gas density, effects of which are further enhanced at elevated pressures. Thus resulting in lower bubble rising velocities and weak liquid recirculation (due to bubble induce) in comparison to air-water system.

4.5.3 Comparison of experimental results with other studies on large diameter vertical pipe

The Figure 4.63 and 4.64 presents the comparison of the average void fraction from current work along with other studies conducted in large diameter vertical pipes (D=150 to 480mm) for gas-liquid two phase flow under similar velocity range ($j_l \approx$ 0.2, 0.6 and 1m/s). Seven sets of average void fraction data including the air-water, steam-water and nitrogen-naphtha systems (Hills, 1993; Ohnuki and Akimoto, 1996; Ohnuki and Akimoto, 2000; Shoukri *et al.*, 2000; Shen *et al.*, 2004; Omebere-Iyari *et al.*, 2007; Omebere-Iyari *et al.*, 2008) were plotted along with the present data.

The data presented in Figure 4.63, are all of air-water in pipe diameter range of 189-254mm except for Omebere-Iyari *et al.* (2007) for nitrogen-naphtha. Notwithstanding the difference between the current diameter and rest of the work, it can be noted that for liquid superficial velocities of $j_l \approx$ 1.0m/s, there exist a reasonable agreement between the current work and various other work done on large diameter vertical pipes.

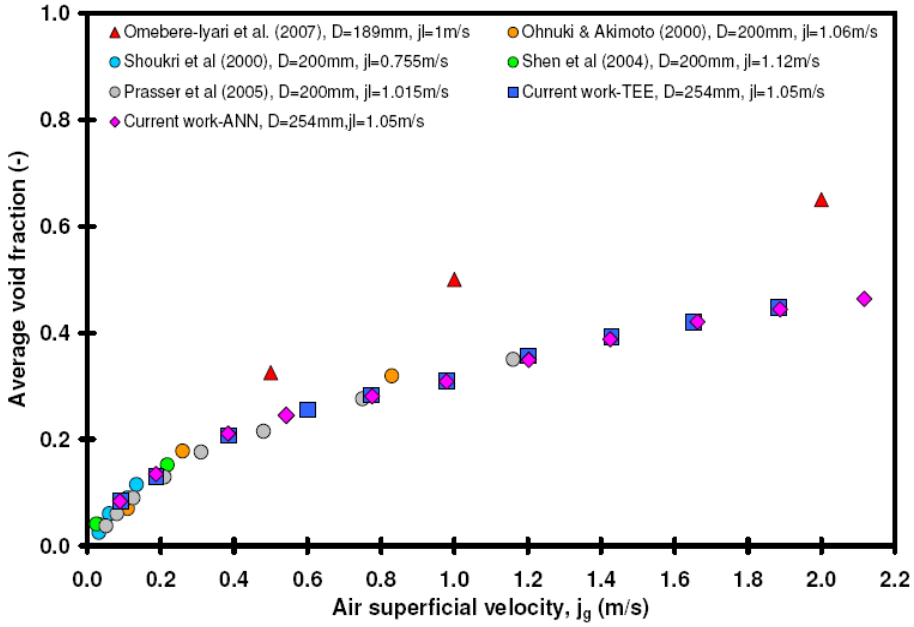

Figure 4.63 Comparison of average void fraction with other works, $j_l \approx 1.0$ m/s.

Similar observation as in Figure 4.63 is made for $j_l \approx$ 0.6m/s, Figure 4.64(a), although the two data sets of Omebere-Iyari *et al.* (2007) and Omebere-Iyari *et al.* (2008), showing higher average void fraction are for nitrogen-naphtha and steam-water respectively. Figure 4.64(b) illustrate the case for $j_l \approx$ 0.2m/s, similar to above two

cases of liquid superficial velocities, the data sets of air-water are lying closing to each other. However a strong discrepancy is observed with data of Omebere-Iyari et *al.* (2007) and Omebere-Iyari *et al.* (2008), similar to seen in Figure 4.63 and 4.64(a). This could be attributed to the effects of increased system pressure and physical properties which are not represented in figures. Both the works uses different working fluids (for nitrogen-naphtha and steam-water respectively) as well as the system pressures (20bar & 30ºC, 46.4bar & 259.3ºC) but the gas density and viscosity are equal with liquid density, surface tension and liquid viscosity for the former case 1.2, 1.3 and 0.3 times that employed in steam-water.

As shown in both the Figures 4.63 and 4.6, the time average void fractions reported by Ombere-Iyari *et al.* (2007) are higher than the data of this study. Higher void fraction can be attributed to the smaller bubble sizes due to higher gas density and reduce surface tension. This was confirmed by comparison with the data obtained by other literature studies (Omebere-Iyari *et al.*, 2008). As shown in Figure 4.64, the void fraction obtained by Omebere-Iyari *et al.*, (2008) are very similar to the data of current study, in both cases; water was used as the liquid phase.

Although not much experimental work is available with two phase gas-liquid flows in D>100mm vertical pipes with varying physical properties and diameter effect to explain above discrepancy at low liquid velocities, some conclusions can be drawn based on the work of large diameter bubble columns. In the light of review conducted, the higher average holdup obtained by Ombere-Iyari *et al.* (2007 and 2008) is partially attributed to the elevated pressure and partly to the physical properties of the liquid. In detail, the increase in pressure causes a shift from a large bubble size distribution to smaller bubble sizes with bubble size distribution becoming narrower along with reduction in bubble rise velocities. This occurs because at elevated pressures, reduction in surface tension occurs that further reduces the initial bubble size and suppresses the coalescence tendency of the bubbles and thus small bubbles are preserved within the flow subsequently increasing the void fraction to steeply high values. The effect of increase gas density is more pronounced at higher pressures, gases with higher molecular weight will lead to higher gas holdup due to enhance bubble breakup and inhibition of bubble coalescence which further promotes the formation of smaller bubbles, leading to higher void fraction globally (Wilkinson, 1991; Letzel *et al.*, 1997; Lin *et al.*, 1998; Schäfer *et al.*, 2002).

Considering that the gas densities are same in both the Ombere-Iyari *et al.* (2007) and (2008) experiments, the only other factor contributing to this higher void fraction could be related to the characteristics of the liquid phase. The surface tension of air-water is much larger than steam-water (almost 3x) and (almost 4x) nitrogen-naphtha and thus in later cases a reduce surface tension results in reduction in initial bubble size and maximum stable bubble size, and inhibition of bubble coalescence. Thus it can be concluded that the resulting discrepancy of the void fraction is due to the naphtha being a mixture of hydrocarbons with a complex longer carbon chain structure.

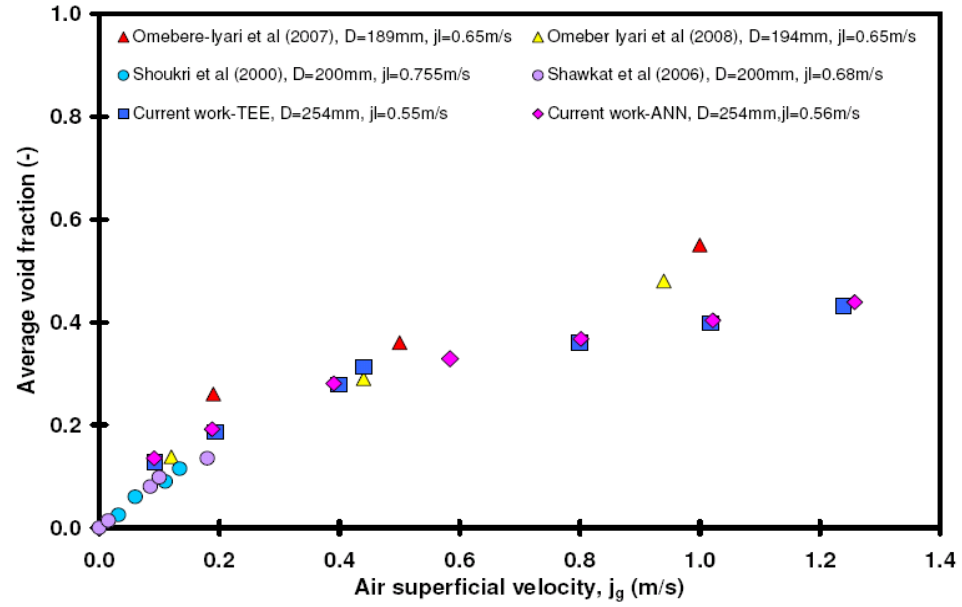

(a)

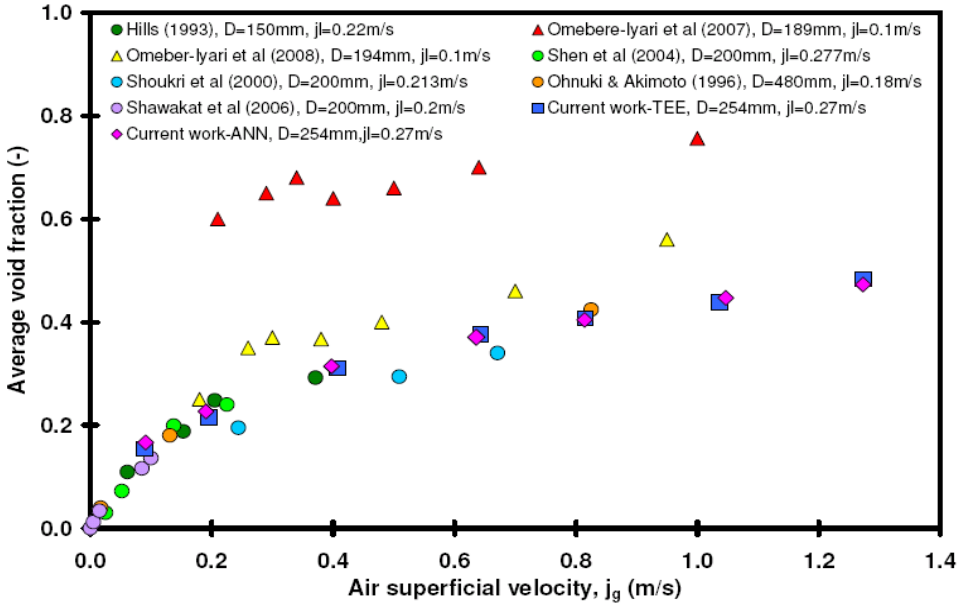

(b)

Figure 4.64 Comparison of average void fraction with other works for (a) $j_l \approx$ 0.6m/s and (b) $j_l \approx$ 0.2m/s.

In Ombere-Iyari *et al.* (2008) experiments water was used as liquid phase and it can be seen that due to similar liquid phase as in current experiments (although a pressure effect also exist), the void fraction values obtained are closer in agreement then the

naphtha as working fluid. Prasser *et al.* (2007) work also support our notion above that at high pressure steam-water flow, the developed bubble sizes are smaller, hence exhibit slightly higher void fractions then to the air-water flow under ambient conditions

Above aspect also highlights an important aspect i.e. the differences in the predictions are smaller at higher liquid superficial velocities, suggesting that the liquid phase properties do not significantly influence the void fraction in this range, however the effect become prominent at lower liquid superficial velocities.

4.6 Conclusion

Based on the experimental work presented in this chapter, the following conclusions are drawn:

Part –I

In the first part of this thesis, a major experimental investigation was undertaken to evaluate the basic hydrodynamic performances of a novel design and a conventional gas injector. It was demonstrated that:

- No gas jetting was observed from either of the gas injectors in the experimental air-water superficial velocity range. However, from the flow behaviour of the novel gas injector, it is expected that even at the very high gas flowrates beyond those considered in this work, the arrayed orifices in riser pipe (of novel annular sleeve injector) will counter act any jetting that might arise.
- The lift provided by novel design is higher at lower end of the gas superficial velocity range in comparison to conventional Tee gas injector. However, at higher gas superficial velocities, the performances of the two gas injectors are equivalent.
- The total pressure gradient, mean void fraction and riser base pressure characteristics, all corroborates the efficient performance of the novel design.
- It was demonstrated that the novel gas injector has more stabilizing effect on the unstable flows, as a more subtle and gradual transition takes place owing to the symmetrical and peripheral gas injection.

The overall results presented shows that annular sleeve gas injector is a more appropriate choice than the conventional Tee gas injector.

Part –II

(i) Flow patterns, transitions and flow pattern map:

- The identification of flow patterns and its transitions was an important aspect of the work. The experimental data collected was exploited to uncover the features of the flow patterns encountered in this size of pipe supplemented by visual

observations.

- The flow development issue was resolved by establishing that the flow had reached a quasi developed state at about 20D, this was to ensure that the flow pattern determined are not influenced by the any developing effects. Based on the probability mass function characteristics and the visual observations the flow in the vertical riser was classified into four basic flow patterns as *dispersed bubbly flow*, *bubbly flow*, a*gitated bubbly flow* and c*hurn/froth flow*. Also a special case of u*nstable slug flow* was found as a consequence of flowline inlet configuration.

- From the visual evidences, it was clear that there were large coalescent bubbles in the riser with diameter close to that of riser and axial length greater than their diameter, but no large coalescent bubble like smooth bullet shaped Taylor bubble (occurring in slug flow) was observed for all air-water superficial velocities in 254mm diameter vertical riser neither the bimodal peak associated with slug flow was found in PMFs.

- While the PMFs obtained for other flows such as dispersed bubbly, bubbly and churn/froth flow are in agreement with small diameter works, new and interesting features were found for agitated bubbly flow. Through the use of statically extracted information it was found that bubbly to agitated bubbly transition is smooth and gradual. Unlike the former transition, as the transition from agitated bubbly to churn/froth is approached, the distribution became more negatively skewed due the presence of large gaseous structures present within the core.

- The PMFs of agitated bubbly flow at intermediate air-water superficial velocities remained Gaussian in nature and thus required additional quantification. Through the statistical analysis, and it was found the characteristic standard deviation of the void fraction fluctuation for this flow were distinct than those from bubbly and churn/froth flow. It is proposed that the observed characteristic standard deviation of the void fraction fluctuation for agitated bubbly flow was due to the intense bubble to bubble interaction resulting in breakup and simultaneous coalescence. Based on the observed changes of this standard deviation of void fraction fluctuations, the flow regime transition from bubbly to agitated bubbly and from agitated bubbly to churn/froth flow were identified. The above behaviour clarifies the ambiguity regarding the prevailing flow regimes in large diameter vertical riser to a large extent, where on one hand, flow pattern classification as large as 5 different flow patterns (Agitated bubbly, churn bubbly, churn slug and churn froth) were found from visual observations and on another hand overly simplified into just bubbly and churn/turbulent flows.

- From the PMFs taken from the two successive heights in the riser under agitated bubbly flow, it is found that the peakness of the distribution was reducing and broadness was increasing, this implies that bubble were breaking up while

moving up the riser and since their population was increasing their coalesce probability was increasing hence the uniform curve suggests that breakup and coalescence were almost in equilibrium. This further verifies the observed characteristic standard deviation of the void fraction fluctuation for this flow.

- The experimental flow pattern map was developed based on the probability mass function plots supplemented by the visual observations. The developed experimental flow regime map was compared with published vertical flow regime maps/models, many discrepancies were noted, and generally a poor agreement was found.

- The comparison of the experimental results with other work on large diameter vertical pipe especially with air-water as working fluid indicates a close agreement while differences were observed with studies employing different gas-liquid as working fluid.

- The Taitel *et al*. (1980) bubble to slug transition model does not yield satisfactory results for large diameter vertical upflow condition. It was further noted that the discrepancy is due to the Harmathy (1960) expression of the rise velocity of moderately distorted ellipsoidal shape bubble in an infinite media. Hence the Taitel *et al.* (1980) model has been successfully modified for large diameter vertical upflow conditions, based on the physical mechanism observed. The general trends of modified criteria agreed well with the current and other large diameter experimental results.

(ii) Effect of upstream conditions on the two phase flow in the large diameter vertical riser:

In offshore oil industry, there is a clear trend toward use of larger diameter vertical risers. This increases the importance of determining the flow behaviour in the riser, especially the impact of the upstream conditions on it. The study investigated the effects of two different inlet configurations on the flow regimes and void distributions namely, (i) near riser base gas injection and (ii) upstream flowline gas injection. The former represents the air-water introduction in the riser base area while the latter corresponds to the air-water introduction at the inlet of the flowline prior to the riser base. From these inlet conditions, the entrance effect on the two-phase flow regimes in the riser was studied.

- It was found that under similar phase velocities, the void fraction distributions (PMFs) along the riser is almost similar without any significant distinguishable features for the both gas injectors in near riser base injection. Hence, both gas injectors result in similar downstream two phase flow characteristics. Thus in the large diameter vertical upflow conditions, the influence of gas injector design ahead in the riser is less pronounced.
- No effect of inlet conditions (i.e. near riser base injection and upstream flowline injection) is observed in the riser flow behaviour at low air-water superficial velocities as the mean void fractions achieved are similar in all the cases.

However, at high air-water superficial velocities, it was found that the overall intensity of the riser flow was more chaotic in the upstream flowline gas injection. This is due to the intermittent flow behavior in flowline influencing the riser flow pattern characteristics and thereby controlling the riser dynamics.

- Some differences in flow behaviour were also found in the limited range of higher air-water superficial velocities (j_w = 0.59m/s and 1.2 < j_a < 1.63 m/s) under upstream flowline injection, where some unstable slug flow is detected in the riser. This flow exhibited some decaying characteristics of the slug flow from the horizontal flowline and churn/froth flow of the riser. Hence, this flow was found as a consequence flowline inlet configuration. The PMFs of this flow were flatter (in comparison to the near riser base injection), with twin peaks having almost similar heights representing the simultaneous decay of liquid slugs and coalescence of gas bubbles in the core region. In the both the above flow cases i.e. unstable slug and churn/froth flow, the mean void fraction obtained is less than the near riser base injection due to the presence of some survived liquid slugs in the riser.
- From the visual observation and as well as through PMFs, it is found that the liquid slug do dissipates in the riser to a certain extent. It is postulated that three forces namely compressional forces of succeeding bubble from the liquid slug (from the flowline), gravitational force and turbulent forces associated with two phase are responsible for the liquid slug collapse in large diameter pipes.
- It is found that as the air superficial velocity increases at the low water flowrate, periodic instability sets in. However, when water superficial velocity increases this periodic instability is taken over by more chaotic instability within the riser, the severity of which increases with air superficial velocity because of the increase in holdup within the riser base and flowline. It is to be noted that above instability is not the severe slugging indicated by many authors (Schmidt *et al.*, 1980; Bendiksen *et al.*, 1991; Sarica and Shoham, 1991; Tin, 1991; Yeung and Montgomery, 2001; Yeung *et al.*, 2003) but does possess similarity to unstable flow process defined by Fabre *et al.* (1990) and Schmidt *et al.* (1980) in small diameter horizontal flowline-vertical riser configuration.

Part - III

The comparison of the experimental results with other work on large diameter vertical pipe:

- From the drift flux analysis results, it found that the values of distribution parameter in bubbly (C_o = 1.054), agitated bubbly (C_o = 1.275) and churn/froth (C_o = 1.14) flow are in good agreement with the values obtained in the literature. Similar to above, the drift velocity results are also in agreement with values in the literature.
- By a employing a simple statistical technique, the void fraction phase distribution profiles were qualitatively characterized. The current experimental phase distribution profiles compared well with the general trends associated with

the work on large diameter vertical pipe upflow.

- The result of the comparison between the present experimental time average void fraction and those of other studies conducted on large diameter vertical pipe upflow under similar phase velocities, showed fairly good agreement with each other, except for the Nitrogen/Naphtha data of Omebere-Iyari *et al.* (2007).The later discrepancy is found to be related to the affects of increase pressure on liquid properties (Wilkinson, 1991; Letzel *et al.*, 1997; Lin *et al.*, 1998; Schäfer *et al.*, 2002).

Chapter 5

The performance assessment study of the existing void fraction correlations and pressure gradient models

Analytical predictions of the void fraction and the pressure gradient in two phase flow are potentially valuable aid for design and analysis of the system. However due to the scarcity of data on large diameter vertical upflow, there exists a large uncertainty in the application of the correlations/models for predicting void fraction, and pressure gradient. This chapter evaluates some of the commonly employed void fraction correlations and pressure gradient methods against the experimental data to increase the confidence on the existing two phase flow prediction methods. The assessment was initially carried out for the void fraction correlations. After identifying the satisfactory void fraction correlations they were employed in the assessment of pressure gradient models along with other commonly applied models.

5.1 Introduction

Prediction of void fraction in two phase flows is highly significant as it plays a fundamental role in characterizing the distribution of the phases within the system, especially in the determination of the amount of liquid phase (holdup) retained in a system. With void fraction predictions further important parameters like two phase density and viscosity are evaluated that are required by the existing models for predicting the flow regime transitions, pressure drops, and heat transfer capabilities. In addition to the above, the void fraction (or holdup) predictions are also important for the calculation of the total pressure gradient. Generally a designer needs a void fraction correlation and pressure gradient methods as a closure relation to predict the two phase flow system behaviour before designing the actual system and/or simulating scenario related to that system. Thus the designing and/or reliability of any two phase flow model is dependent upon the prudent choice of the void fraction correlation and pressure gradient methods used.

Because of the fundamental importance of larger diameter vertical pipes, current chapter of the thesis presents the assessment of void fraction (holdup) correlations and application of some of the successful correlations to determine the pressure gradients. This assessment is taken with a need to determine whether the existing void fraction correlations/ pressure gradient models employed in different fields of multiphase flow are capable in predicting the satisfactory behaviour in large diameter

vertical pipe upflow where it is found to be different then the traditional small diameter vertical pipe upflow.

5.2 Previous Assessments on Void Fraction Correlations and Pressure Gradient Models

Though assessments of void fraction correlations have been done in past, they are still comparatively few in number with evaluation confined either to orientation or specific application (Dukler *et al.*, 1964; Vohra *et al.*, 1975; Friedel, 1980; Simpson *et al.*, 1987; Diener and Friedel, 1994; Chexal *et al.*, 1991; Maier and Coddington, 1997; Vijayan *et al.*, 2000; Manera *et al.*, 2005 and Ghajar, 2006). The recommendations of these assessments are summarised next.

Dukler et al. (1964) performed detailed horizontal pipe flow comparison, by comparing five (5) pressure drop models and three (3) holdup ($H_L = 1-\alpha$) correlations. Out of the three void fraction correlations (Lockhart-Martinelli, 1949; Hoogendoorn, 1959 and Hughmark, 1962) used, only Hughmark (1962) correlation performed satisfactorily in the middle range of hold-ups. None of the void fraction correlations was found to perform adequately at low holdups. Lockhart-Martinelli (1949) correlation best predicted the pressure drop data. ***Weisman and Choe (1976)*** assessed the various homogeneous models and found that McAdams (1942) and Dukler *et al.* (1964) gave better results in the homogeneous flow regime. Interestingly, the homogeneous model by Dukler (1964) gave consistently good results for all flow regimes except the separated (stratified) flow regime (TECDOC, 2001). ***Friedel (1979)*** derived two phase friction pressure drop correlations for horizontal, vertical upflow and downflow based on his own databank. The developed correlation was found to perform better than the Chisholm (1973) and DIF-2 correlations. ***Friedel (1980)*** compared eighteen (18) different void fraction correlations using 9009 data points and 14 pressure drop correlations using 12868 data points of circular and rectangular channels. No distinction was made in assessment as regard to orientation of flow (horizontal or vertical) or type of fluid used. The result indicated that the void fraction correlations of Hughmark (1962), Rouhani I & II (1969) and Chisholm (1973) and Lombardi-Pedocchi (1972) (now referred as CESNEF) predicted the experimental results satisfactorily than the other correlations. ***Beattie and Whalley (1982)*** compared 12 pressure drop correlations including five (5) homogeneous models using the HTFS (Heat transfer and fluid flow services) databank of 13500 adiabatic data points for steam-water and non-steam water mixtures (about 5100 vertical flow and 8400 horizontal flow data points). The homogenous model performance was equally satisfactory along with other models. ***Simpson et al. (1987)*** compared six pressure drop correlations with data from large diameter (127 and 216 mm) horizontal pipes. None of the pressure gradient correlations predicted the measured value accurately.

Chexal et al. (1991) carried out a detail assessment of eight (8) void fraction models using 1500 data points for vertical configurations. The data used was the

representative of the BWR pipes and PWR fuel assemblies of upto 457mm in diameter. The results indicated that Chexal and Lellocuhe (1986) along with GE Ramp (1970) and Dix (1971) correlations gave satisfactorily prediction of all void fraction data very well. In the same paper, assessment for explicit diameter dependences with three different sets of database with 115 data points also indicated Chexal and Lellocuhe (1986) to perform well in comparison to all others. ***Diener and Friedel (1994)*** also made an assessment of void fraction correlations with data consisting of air-water and refrigerant R-12. Twenty six (26) commonly used void fraction correlations were evaluated. The results indicated that only thirteen (13) correlations reproduced the data with a rather acceptable accuracy. However correlations of Rouhani-I (1970) and HTFS-Alpha (propriety correlation) were recommended by authors. ***Vijayan et al. (2000)*** performed an assessment in connection with natural circulation loops. The assessment consisted of thirty-three (33) often cited void fraction correlations. Only few correlations were found to perform satisfactorily with Chexal *et al.* (1996) void fraction performing the best. ***Maier and Coddington (1997)*** carried out a detail assessment of thirteen (13) wide range void correlations using PWR and BWR fuel assemblies/rod bundle void fraction data (362 steam-water data points). The databank was based on wide range of pressure and mass fluxes (0.1 to 15 MPa and 1 to 2000 kg/m^2-s). The five (5) best correlations with minimum of scatter and mean error were Dix (1971), Chexal and Lellocuhe (1992), Bestion (1985), Inoue (1993) and Coddington and Maier (1997).

An assessment of fourteen (14) drift-flux void-fraction correlations was also performed by ***Manera et al. (2005)*** in conjunction with stationary and transient flashing flows in vertical pipes (D = 47mm). The correlations compared showed GE-Ramp (1970) and Dix (1971) void fraction correlations to perform well in the whole range of measured void fractions while Nabizadeh (1977), Takeuchi (1992) and modified Sonnenburg (1994) relations also gave satisfactory predictions in certain regions. ***Ghajar et al. (2006)*** based on the data set of 2845 data points, covering wide range of horizontal and upward inclined pipe flows assessed sixty-eight (68) void fraction correlations. The study concluded that majority of the developed correlations were restricted in their application to a wide variety of data sets. A universal void fraction correlation was proposed, valid for all inclination angles and flow patterns.

To the best of the author's knowledge, almost all the previous reported assessments are for smaller diameter pipe flow except for Chexal *et al.* (1991) and Simpson *et al.* (1987). The former was for vertical large diameter pipe in connection to primary coolant system component of nuclear reactor and the latter was for horizontal large diameter pipes. With such limited assessments mostly confined to void fraction correlations derived from smaller diameter vertical pipe experiments brings in much uncertainty. This calls for a thorough assessment of the predictive capability of void fraction correlations as no study has so far included the assessment of void fraction correlations with respect to their applicability to large diameter vertical pipe upflow. The assessment is also important in order to determine the implications of the different flow patterns occurring in the large diameter and the conventional small diameter vertical pipe.

5.3 Void Fraction Correlations

Broadly void fraction correlations can be classified by one of the following categories:

i. Homogenous void fraction model
ii. Separate flow model using
    a. Slip ratio (s)
    b. Models based on Lockhart and Martinelli parameter (X_{tt})
    c. Mass flux (G) dependent models
    d. Drift flux model (a special case of Separate flow model)

There are a few empirical/specific flow regime correlations which do not specifically belong to either of the above categories, they are listed as;

iii. Miscellaneous correlations.

5.3.1 Homogenous void fraction model: Homogenous void fraction model (HVFM) assumes that both the two phases are well mixed and therefore the two phases (liquid-gas) travel at same velocities ($s = u_g/u_l = 1$). Mathematically they are represented as:

$$\langle \alpha \rangle = \frac{1}{1 + \left(\frac{1 - x}{x} \right) s \frac{\rho_g}{\rho_l}} = \frac{Q_g}{s \cdot Q_l + Q_g} \tag{5.1}$$

$$\langle \alpha \rangle = \frac{1}{1 + \left(\frac{1 - x}{x} \right) \frac{\rho_g}{\rho_l}} = \langle \beta \rangle \tag{5.2}$$

Where "β" is called volumetric gas fraction, j_g, j_l and j are superficial gas, liquid and total mixture velocities. The best agreement of this model is usually obtained for dispersed bubbly and dispersed droplet or mist flows where the two phases have nearly same velocity.

There exist a special case for Homogenous equilibrium model called "**Kβ models**". In this model, the void fraction (α) is calculated by multiplying the homogeneous volumetric gas fraction β by a constant K.

$$\alpha = K\beta \tag{5.3}$$

If K = 1, the expression reverts back to equation (5.2). The relations of Armand (1946), Armand and Treschev (1959), Bankoff (1960), Hughmark (1962) all belong to the "Kβ" forms (Todreas and Kazimi, 1990).

5.3.2 Separate flow model: Contrarily to above, in separate flow model, the two phases travel with two different mean velocities and hence separate. In such cases a term called ***slip*** is defined:

$$s = \frac{u_g}{u_l} \tag{5.4}$$

This represents the ratio of the relative mean velocities of two phases that coexist. Hence if this slip velocity ratio is 1, then void fraction is redefined by homogenous model while for separate flow model in uphill (downhill) flows this ratio is always greater than 1 (less than 1) as the gas(liquid) will move faster than liquid (gas) phase. The void fraction correlation using separate flow concept essentially specifies an empirical equation for the slip ratio (s). The void fraction can then be calculated by the equation (5.1). Some commonly used slip ratio relations are of Levy (1960), Zivi (1963), Smith (1969), Premoli *et al.* (1971), Chisholm (1972), Spedding and Chen (1984), Huq and Loth analytical expression (1990) and Modified Smith (1992). There are some other analytical correlations also based on separate flow model, they include the models that are based on ***Lockhart and Martinelli parameter*** (X_{tt}), models encompassing the mass velocity effects and correlations derived from ***dimension analysis***.

$$\frac{1-\alpha}{\alpha} = f(X) \tag{5.5}$$

$$\alpha = f(x, G, \rho_l, \rho_g, \mu_l, \mu_g, \sigma_l, Q_l, Q_g) \tag{5.6}$$

Some of the example of Lockhart and Martinelli parameter includes Lockhart and Martinelli (1949), Chisholm and Laird (1958), Chisholm (1963), Thom (1967), Chisholm and Baroczy (1966). While for the later examples include Guzhov *et al.* (1967) and Premoli *et al.* (1971).

There also exist another special case of separate flow model called "**Drift Flux Model**" and it accounts not only for relative motion of the two phases but incorporate the radial distributions of local void fraction. The model correlates the actual gas velocity (u_g) and the mixture velocity j, using distribution parameter (C_o) and drift flux velocity (U_{gj}). As different relative velocity exists between the two phases for every flow patterns; the parameters C_o and U_{gj} are different for every flow regime. The model was first presented by Zuber and Findlay (1965) and later on modified by Wallis (1969) and then by Ishii (1977) and many more. General expression for the drift flux formula for void fraction can be expressed as:

$$\{\alpha\} = \frac{\{j_g\}}{C_o \cdot \{j\} + U_{gj}} \tag{5.7a}$$

$$\{\alpha\} = \frac{1}{C_o \cdot \left(1 + \frac{1 - x}{x} \cdot \frac{\rho_g}{\rho_l}\right) + \frac{U_{gj} \cdot \rho_g}{x \cdot G}} \tag{5.7b}$$

Here U_{gj} is the drift velocity ($U_{gj} = u_g - j$), j is the volumetric flux/mixture velocity ($j = j_g + j_l$) and C_o is the distribution parameter that represents the global effect due radial non-uniform void and velocity profiles. Majority of the correlations used for void fraction prediction belong to this group. Most of the transient multi-fluid models belonging to nuclear thermal-hydraulic codes also use void fraction prediction correlations belonging to this class. TACITE, a popular code in oil and gas industry also uses this model for void fraction prediction. Some of the popular drift flux correlations of this class are: Zuber and Findlay (1965), Dix (1971), Rouhani-I & II (1969), Hills (1976), Ishii (1977), Ishii and Kocamustafagoullari (1985), Hirao *et al.* (1986), Kataoka and Ishii (1987), Moorka *et al.* (1989), Hibiki and Ishii (2003).

5.3.3 Miscellaneous correlations: Apart from above correlations another class of correlations commonly employed are empirical correlations that have either been infer and/or validated from large data sets of experimental observations. Some often cited and commonly used empirical void fraction correlations include Levy (1960), Wilson *et al.* (1961), Spedding and Chen (1981), Spedding and Chen (1984) and Neal and Bankoff (1965).

Some of the popular oil and gas industry void fraction correlations also belongs to this class. These include Hagedorn and Brown (1959), Duns and Ros (1963), Beggs and Brill (1973), Gray *et al.* (1978) and Mukherjee and Brill (1985). All of the above oil and gas industry correlations are in actual pressure gradient methods however they also have void fraction correlations included in them for prediction of elevation, friction and acceleration component of total pressure gradient. Finally, this assessment also compares the experimental results with the steady state simulations performed in ***OLGA***, a popular oil and gas industry transient multi-fluid code.

This assessment study presents the results of the evaluation conducted on a 45 wide range correlations popular in their respective fields along with steady state predictions from OLGA simulation code. The correlations assessed in this study include: HVFM, Armand (1950), Armand and Treschev (1950), Bankoff (1960), Lockhart and Martinelli (1949), Baroczy (1966), Levy (1960), Thom (1964), Zivi (1963), Neal and Bankoff (1965), Guzhov *et al.* (1967), Smith (1969), Premoli *et al.* (1971), Chisholm (1973), Butterworth (1975), Spedding and Chen-I (1984), Spedding and Chen-II (1984), Chen-I (1986), Chen-II (1986), Spedding and Chen (1998), Modified Smith (1992), Huq and Loth (1992), Wilson *et al.* (1961), Nicklin (1962), Zuber and Findlay (1965), Rouhani-I (1969), Rouhani-II (1969), GE-Ramp (1970), Rouhani and Axelsson (1970), Dix (1971), Bonnecaze *et al.* (1971), Hills (1976), Kocamustafagoullari and Ishii (1985), Bestion (1985), Liao, Parlos and Griffith (1985), Hirao *et al.* (1986), Kataoka and Ishii (1987), El Boher *et al.* (1988), Morooka *et al.* (1989), Inoue *et al.* (1993), Chexal and Lellouche (1996), Hibiki and Ishii

(2003), Ghajar *et al.* (2006), Hagedorn and Brown (1959), Duns and Ros (1963), Beggs and Brill (1973) and Gray *et al.* (1974), Mukherjee and Brill (1985) and OLGAS. The correlations are not presented here, for the sake of brevity and can be found in appendix C.

5.4 Pressure Gradient Correlations

Similar to void fraction correlations, large number of pressure gradient models can be found in literature. However, they can be classified as following:

i. Correlations based on the homogeneous mixture model.
ii. Correlations based on the two-phase friction multiplier concept.
iii. Correlations based on Flow pattern specific models.

5.4.1 Based on Homogenous mixture model: In homogenous pressure drop model the mixture is treated as single fluid and averages of the properties of liquid and gas phase are used. Void fraction determines the static and momentum components while frictional component requires the evaluation of mixture viscosity that can be chosen from any of the following; Owens (1961), McAdams (1942), Chicchitti *et al.* (1960), Dukler *et al.* (1964) and Beattie and Whalley (1982). The equation representing the total pressure gradient can be found in chapter 2, section 2.1.2. Since acceleration term can be ignored for adiabatic flows, hence two terms to be evaluated are hydrostatic term and frictional term. The frictional term used is defined as below which requires the two phase viscosity term.

$$\left(\frac{\mathrm{dp}}{\mathrm{dz}}\right)_{\mathrm{e}}^{\mathrm{TP}} = \rho_{TP}\cdot \mathrm{g}\cdot\sin\theta \qquad Where\ \rho_{TP} = \rho_m \qquad \text{(5.8 and 5.9)}$$

$$\left(\frac{\mathrm{dp}}{\mathrm{dz}}\right)_{\mathrm{fric}}^{\mathrm{TP}} = \frac{\mathrm{f_{TP}}}{\mathrm{D_e}}\left(\frac{G_m^2}{2\rho_m}\right) \qquad Where \qquad \frac{f_{TP}}{f_{SP}} = \frac{C_1 \big/ \mathrm{Re}_{TP}^n}{C_1 \big/ \mathrm{Re}_{SP}^n} = \left(\frac{\mu_{TP}}{\mu_{SP}}\right)^n \qquad (5.10)$$

5.4.2 Based on Two phase friction multiplier concept: These models generally based on separate flow of the phases and use the friction multiplier concept where two phase flow frictional gradient is related to single phase of either liquid or gas by multiplying this friction multiplier. This multiplier can further be classified as either all mixture as liquid (or gas) or liquid component flows alone (or gas component flows alone). The category includes famous Lockhart and Martinelli friction model, Baroczy frictional model (modified by Chisholm, also called Chisholm-B coefficient model), and Friedel (1979).

$$\left(\frac{dp}{dz}\right)_e^{TP} = \rho_{TP} \cdot g \cdot \sin\theta \qquad Where \rho_{TP} = \rho_l(1-\alpha) + \alpha\rho_g \tag{5.11}$$

$$\left(\frac{\mathrm{dp}}{\mathrm{dz}}\right)_{\mathrm{fric}}^{\mathrm{TP}} = \Phi_{lo}^2\left(\frac{dp}{dz}\right)_{fric}^{lo} = \Phi_{go}^2\left(\frac{dp}{dz}\right)_{fric}^{go} \qquad or \qquad \left(\frac{dp}{dz}\right)_{fric}^{TP} = \Phi_l^2\left(\frac{dp}{dz}\right)_{fric}^{l} = \Phi_{fric}^g\left(\frac{dp}{dz}\right)_{fric}^{g} \tag{5.12 & 5.13}$$

Note, the models like Friedel (1979) and CESNEF-2 (1992) employ, the friction multiplier concept but specify the use of gravitational and acceleration equations of HEM for calculation (Vijayan *et al.*, 2000).

5.4.3 Based on Empirical models: The last of the pressure gradient models include some popular models of oil and gas production and transportation industry. Most of these approaches have flow regime specific void fraction correlations and pressure gradient models. They include Duns and Ros (1963), Hagedorn and Brown (1965) and Beggs and Brill (1973). In above pressure gradient models, the Hagedorn and Brown (1965) is not flow regime specific. It is to be noted that all the above models are empirically derived. However unlike above, the recent approach to determine the pressure gradient in gas-liquid flows is the use of phenomenological models. In these models, firstly the specific flow pattern is identified and then the relevant physical phenomenon of this flow is modelled. This approach is expected to give much improved predictions than the purely empirical correlations. The examples of this approach are the models presented by Holt *et al.* (1999) and Oliemans and Pots (2006). The former approach is restricted to the prediction of pressure gradient in small channels sizes typically of that in conventional shell and tube heat exchanger or in compact heat exchangers (Holt *et al.*, 1999) while latter is now commonly being employed in the oil-gas industry for variety of sizes. In the later approach, Oliemans and Pots (2006) have provided a flow pattern dependent two phase gas-liquid pressure gradient calculation scheme in pipes. In this scheme, the flow pattern is identified first and then pressure gradient is calculated next.

In an attempt to further assess the experimental values, the Oliemans and Pots (2006) scheme was also compared in this assessment.

5.5 Experimental Data

The experimental data used to assess the predictive capability of the void fraction correlations is taken for wide ranges of air-water superficial velocities covered in earlier chapter (refer to Figure 4. 8 and Figure 4.47). All the void fraction data used has been analyzed statistically as well as visually for various flow regimes identification (refer to chapter 4). The data points obtained corresponds to dispersed

bubbly (DB), bubbly (B), agitated bubbly (AB), unstable slug (US) and churn/froth (C) flow regimes. Unfortunately the existing set up did not allow for the experiments in annular flow regime.

The overall void fraction measurements are estimated under the assumption that the pressure drop equals to static head by neglecting accelerative and frictional losses. Both these later terms oppositely contribute to the pressure drop hence the void fraction values obtained are slightly higher then true values (and pressure gradient slightly less), thus providing the upper limit of void fraction attainable.

The major contributor to two phase pressure gradient and hence pressure drop in vertical pipe upflow is hydrostatic component (80-95%) with frictional component not contributing more than 5-20% of the total (Brill and Beggs, 1991). In dealing with pressure gradient discussed here, acceleration term is neglected and it is assumed that total pressure gradient consists of hydrostatic and frictional terms only.

For pressure gradient methods assessment, two approaches were followed. In the first, the pressure gradient models consisting of both hold-up and frictional pressure gradient correlations were evaluated e.g. Hagedorn and Brown (1959), Duns and Ros (1963) and Beg and Brill (1973). This category further includes the pairing of the homogeneous correlations for frictional pressure gradient combined with homogeneous correlations for gravitational pressure gradient e.g. HEM and Bankoff (1960). Similarly, Lockhart and Martinelli based frictional correlation paired with Lockhart and Martinelli based void fraction correlation e.g. Lockhart and Martinelli model (1949), and Chisholm-Baroczy model.

In second approach a particular void fraction correlation that exhibited a satisfactory prediction in comparison to the measured value (by void fraction correlation assessment) was paired against independently developed Friedel (1979) frictional pressure gradient model. Similar approach has been adopted by Friedel (1979 & 1980). The Friedel (1979) frictional pressure gradient was used in this later approach as several studies have found this correlation to yield satisfactory results (Vijayan *et al.*, 2000; Thom, 2004; Ribeiro *et al.* 2006 and Shannak, 2008). The correlation was developed using an enhanced databank of about 25,000 data points.

The accuracy of the void fraction correlations compared in this work is evaluated in terms of average percent errors and standard deviation. While assessing the pressure gradient, the mean error was calculated based on the total pressure gradient. The results are also represented graphically by using “cross plots”, where predicted values versus actual data points are plotted.

5.6 Results and Discussion

5.6.1 Correlation based on Homogenous void fraction model:

Homogenous equilibrium model is known to give satisfactorily results

either when flow is dispersed bubbly or dispersed droplet or mist flows where the two phases have nearly same velocity. Under current experimental conditions where flow regimes encountered were bubbly, agitated bubbly, unstable slug and churn flow regimes, the model exhibits greater accuracy at very low void fraction only i.e. when the flow regime was bubbly and dispersed flow. However once the transition from bubbly flow starts to agitated bubbly, the predicted void fraction values deviates as the flow after transition is no more well mixed, thus the predicted values show high mean percentage error, refer to Figure 5.1(a). It is to be noted that the model is independent of the diameter of the conduit and thus can be applied easily to conditions of two phase flows (of different fluid properties) as a starting point where dispersed bubbly or dispersed droplets (or mist flows) are likely to be encountered.

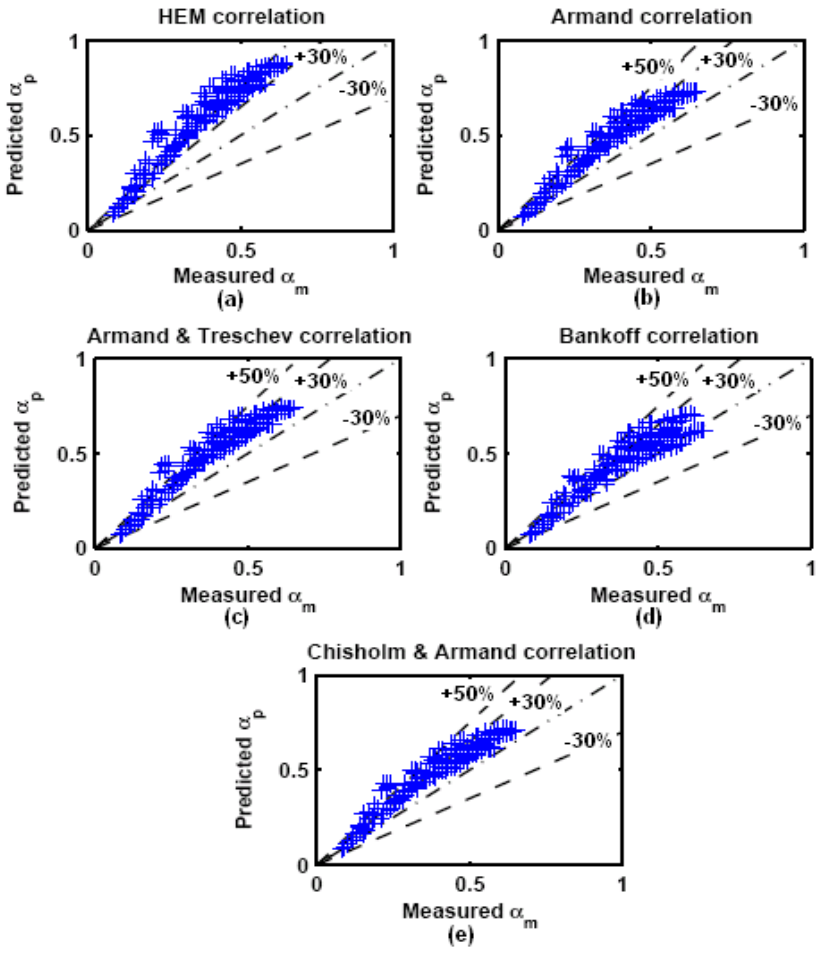

Figure 5.1 The comparison of the measured and the predicted void fraction using correlations based on Homogenous equilibrium mixture assumption.

Armand correlation (1946) is an example of "Kβ" model where the homogenous void fraction (β) is multiplied by the constant, called Armand coefficient ($\alpha=K_A\beta$). Armand coefficient is function of pressure only and neglects the effect of flow velocity. Similar to above correlation, ***Armand and Treschev*** (1959) correlation for rough pipes of 25.5-56mm in diameter at 1.0 to 18 MPa pressures was also tested. Both the correlations show similar trends in comparison with experimental data, however, the results scatter has been reduced in comparison to HVFM with most of data points now lying between 0 to 30%, see Figure 5.1(b-c).

Similar to above two "Kβ" category correlations, ***Bankoff*** (1960) model suggests that under local slip the constant (K) is function of pressure. The correlation attempts to correct the influence of pressure (on fluid properties) on radial distribution of void fraction as well takes into account of flow velocities through the flow parameter (K) (Zuber, 1960). From the comparison of the predicted values with experimental values, improvement in mean percentage errors can be seen (see Figure 5.1d). It is to be noted that the "Kβ" models seems to improve the HVFM results by accounting the radial non uniformity of void fraction and velocity between the two phases by considering the density ratio. For such cases Bankoff (1960) was found to give more reasonable prediction with pressure correction term included then Armand correlation. Dukler *et al.* (1964) also found that Bankoff correlation predictions improve with increasing pressures.

In 1983 ***Chisholm*** modified the Armand (1946) "Kβ" correlation (***Chisholm-Armand***) by including the effect of liquid and gas densities ratio (ρ_l/ρ_g) in the Armand constant (K). This factor accounts for the fact that void distribution can vary across the channel while flowing ahead. The effect of this modification indicated that an improved void fraction prediction (25.64%) with experimental data especially in unstable slug and churn turbulent flow regimes in comparison to original Armand correlation (see Figure 5.1e).

In all the above correlations discussed, the effects of diameter do not appear directly. However in different diameter pipes yet at same pressure, it is expected to indirectly influence the constant K.

5.6.2 Void fraction correlations based Separate flow model

(a) Void fraction correlations based on slip ratio: Correlations based on separate flow model using slip equation shows mixed results, see Figure 5.2 for Smith (1969) and Chisholm (1973) results with only analytical slip expression of Huq and Loth (1990) giving prediction within +20%.

Smith (1969) correlation is based on the equal momentum fluxes of the two phases. This correlations overall over predicts the void fraction (+21%). The deviation is largest for bubbly flow regime and progressively decreases for agitated bubbly,

unstable slug and churn turbulent flow regimes. The Mochizuki and Ishii (1992) modified the above Smith correlation (referred as ***Modified Smith***), however, this correlation severely under predicts in all flow regimes then the original correlation. Next is an analytical correlation of ***Chisholm*** (1972) for the velocity ratio (slip) and is applicable to any fluid. Current results indicate an overall an under prediction (-28%) of the void fraction with largest deviation with bubbly and agitated bubbly flow regimes.

The analytical slip expression of ***Huq and Loth*** (1990) does not contain any empirical constants and predicts the void fraction as a function of quality and pressure alone. In current analysis the expression over predicts the void fraction (within +20%) but higher over prediction is mainly at intermediate void fraction (agitated bubbly flow regime) only. Interestingly correlation converges with lesser deviation towards measured values at higher void fraction values for intermittent flow regimes.

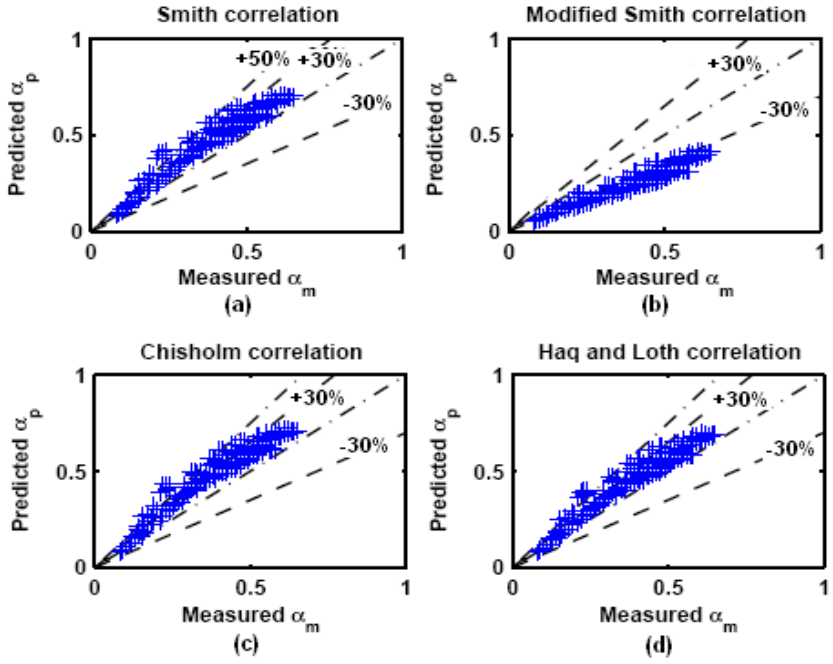

Figure 5.2 The comparison of the measured and the predicted void fraction using correlations based on slip ratio.

(b) Void fraction correlations based on Lockhart and Martinelli parameter (X): Correlations involving Martinelli parameter showed most wide variation in results, see Figure 5.3. Almost all the correlations involving Martinelli parameter did not perform well except for original Lockhart and Martinelli (1949)

model and Chen (1986) I and II with mean error (-24% and ±17%) lying close to maximum allowable limit.

The Lockhart and Martinelli (1949) comparison of the predicted void fraction with the measured values indicates an under prediction, with all data lying between -10 to -32%. The model gives lower mean percentage error prediction for bubbly flows and increasingly deviates for higher void fractions (agitated bubbly, unstable slug and churn flow).

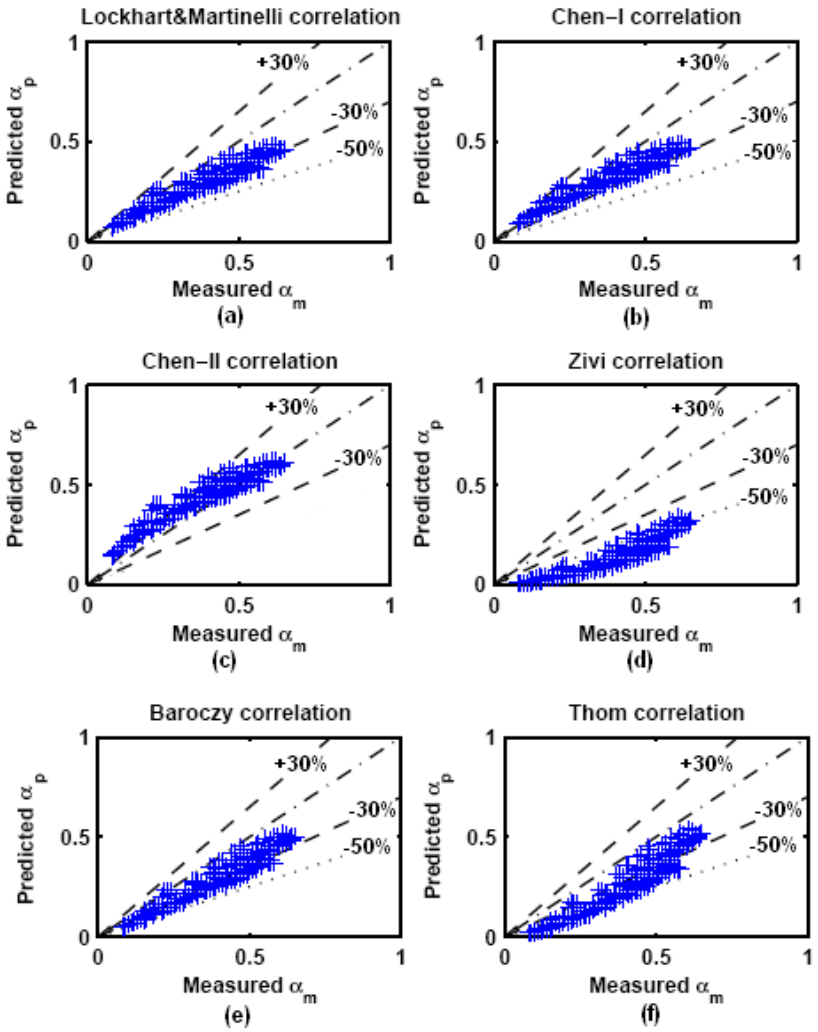

Figure 5.3 The comparison of the measured and the predicted void fraction using correlations based on Lockhart and Martinelli parameter (X).

Perhaps among this class, the most successful correlations are of ***Chen*** (1986) I and II, see Figure 5.3(b-c), which are modified form of the Spedding and Chen (1981) correlation. Note the original correlation did not perform well in the assessment. The correlation based on Martinelli parameter was modified by incorporating an empirical factor (k) which was allowed to vary with the system pressure and a number of parameters including the pipe size. With the modification in k values, the predicted void fraction values were within ±17% in comparison to the original equation (1981).

Another similar correlation of ***Zivi*** (1963) severely unpredicted the void fraction data. The void fraction prediction by Zivi correlation is among one of the largest under prediction (deviation) shown by any of the correlations (-69%), see Figure 5.3(d). ***Baroczy*** (1963) correlated the void fraction data graphically using Martinelli parameter (X) and various property ratios (called property index). Butterworth (1975) transformed these graphs in form of equations. The comparison of this transformed correlation with the experimental data indicates the similar trend as observed with Lockhart and Martinelli correlation with most the prediction data lying within -30%, see Figure 5.3(e).

Similarly to Baroczy (1963), ***Thom (1964)*** correlation greatly underestimates the void fraction. This may be due to the steam/water database used instead of air-water where steam slip being dependent on quality, and slip factor (γ) that was function of pressure. In almost all the above correlations, an under prediction from experimental data was observed (Lockhart & Martinelli correlation (1949), Chen (1986)-I, Baroczy (1963), Zivi, 1963; and Thom, 1964). Among this class, the only satisfactory correlation with large diameter vertical pipe upflow data is of Chen (1986).

(c) Void fraction correlations based on mass flux: Mass-flux-dependent void fraction models are typically correlated to the mass flux by Reynolds number and/or Froude number. The examples of this category include the Guzhov *et al*. (1967) and a Premoli *et al.* (1970) correlations. Both the correlations takes into account of mass velocity and are found to perform superiorly than ones taking account of physical properties only.

Guzhov et al. (1967) correlation was developed for transportation of gas-liquid systems in inclined uphill flows. The correlation defines the holdup and no slip ratio dependence on Froude number which in turn based upon mixture volumetric flux and diameter. The correlation shows an overall mean error of +4%, with successful application in bubbly flow and a slight over prediction for other flows, see Figure 5.4(a). Another correlation of this class is by ***Premoli et al. (1970)***, also known as CISE correlation. The correlation is considered to be valid for wide range of data and uses a slip ratio, $s = f(x, G, \rho_l, \rho_g, \mu_l, \mu_g, \sigma, Q_l/Q_g)$ (Hetsroni, 1982). With the current experimental data this void fraction correlation performed satisfactorily with overall mean error of performance of +10%. The correlation yields closest in intermediate void fraction than at low and higher void fraction, see Figure 5.4(b).

(d) Void fraction correlations based on Drift flux model: Among all the above approaches used for prediction of void fraction, the most successful is the drift flux modelling. The model correlates the actual gas velocity (u_g) and the mixture velocity j, using distribution parameter (C_o) and drift flux velocity (U_{gj}). With the C_o and U_{gj} known along with superficial velocities, the void fraction can be calculated.

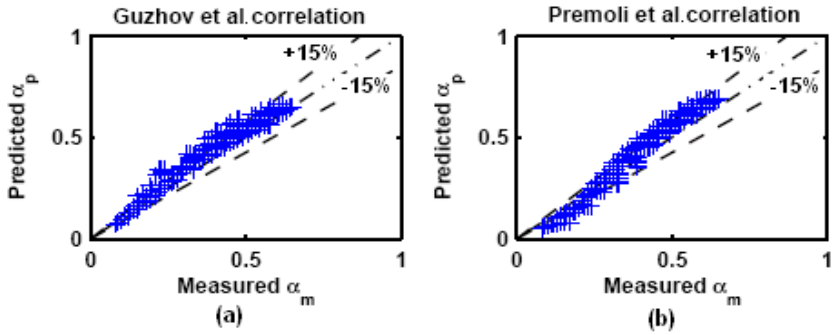

Figure 5.4 The comparison of the measured and the predicted void fraction using correlations based on mass flux effect.

As different relative velocity exists between the two phases for every flow patterns; the parameters C_o and U_{gj} are different for every flow regime. The trends obtained from this set of correlations yielded a closer prediction to measured values over the whole range of void fractions then any other category. However this modelling technique requires careful prediction of flow patterns for its successful application which is usually subjective. As it was found out that most complexities in current analysis arise because of the agitated bubbly flow which is not found in conventional small diameter pipe.

Nicklin et al. (1962) extended the Wallis approach for bubble and slug flow and gave a semi-drift flux void fraction correlation for vertical upflow in tubes. The correlation uses the diameter of the vertical tubes along with total volumetric flux and superficial velocity of gas phase. The overall results of void fraction prediction are -5% with closer prediction in agitated bubbly, unstable slug and churn turbulent flow regimes, see Figure 5.5(a).

Next ***Zuber and Findlay*** (1965) correlation results are presented with the drift velocity expressions for bubbly flow and churn-turbulent flow. Results indicates an under prediction at low void fraction while an over prediction of void fraction at higher void fraction, however the overall mean error is 11.2%, refer to Figure 5.5(b). These findings are inline with Manera *et al.* (2005) assessment, where an over-estimation of the void fraction at low pressures was observed. In 1969 ***Rouhani*** presented two void fraction correlations; Rouhani-I and Rouhani-II. The Rouhani-II correlation gives closer prediction of void fraction (+11.62%) in comparison to Rouhani-I (19.9%) for large diameter void fraction prediction. This finding for

Rouhani-II correlations is similar to finding of Simpson *et al.* (1987) for large diameter horizontal pipe flow assessment where the same correlation equally well predicted the trends (Figure 5.5c-d). In 1970, ***Rouhani and Axelsson*** developed another correlation. This correlation includes the effects of mass flux and surface tension by using two different distribution parameter values. Results indicate a slight overestimation of the void fraction (21.25%) with correlation yielding lower error at low void fraction, see Figure 5.5(e). The ***GE-Ramp*** (1970) correlation is of proprietary nature and has been extensively validated using large databank. The correlation is applicable to all vertical flow conditions (Chexal *et al.*, 1991) with both drift velocity and distribution parameter function of void fraction. Similar to Chexal *et al.* (1991) and Manera *et al.* (2005) assessments in this analysis also, the predicted values are close to measured void fraction with mean error of +5%, see Figure 5.5(f). The correlations slightly overestimate the agitated bubbly, unstable slug and churn/ froth flows.

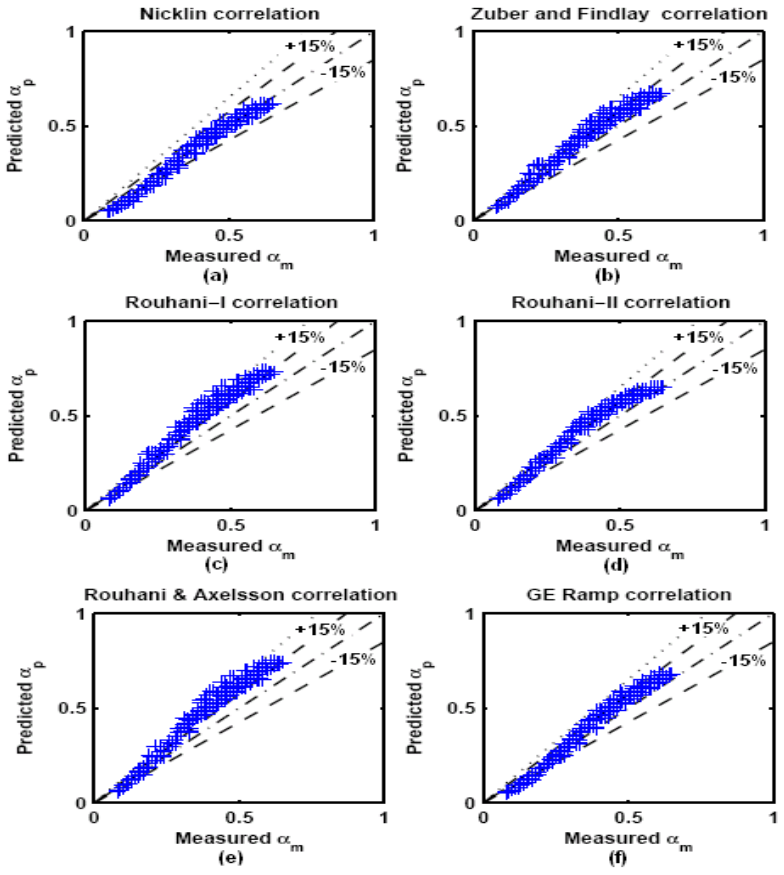

Figure 5.5 The comparison of the measured and the predicted void fraction using correlations based on the drift flux approach.

Dix (1971) correlation was developed for LWR applications and is based on the extensive measurements of the local void fractions (Todreas and Kazimi, 1990). The correlation allows for a radial distribution of void and velocity, which is valid for all the flow regimes. The distribution parameter C_o is function of gas volumetric fraction and pressure. Over all Dix correlation over predicts the void fraction by mean error of +7%, however this under prediction is for unstable slug flow regime in comparison to bubbly, agitated bubbly and churn turbulent flow regimes, see Figure 5.6(a).

Bonnecaze et al. (1971) also extended the work of Wallis *et al.* (1961) proposing a correlation for hold-up in two phase slug flow in inclined pipes. Their correlation indicates a mean percentage error of -5% with applicability in agitated bubbly, unstable slug and churn/froth flows only, with highest deviation in bubbly flow regime, see Figure 5.6(b). Note that the correlation uses drift velocity relation based on diameter of pipe. ***Hills*** (1976) suggested two equations having same form as Zuber and Findlay drift flux correlations. With mean percent error of 1.96% predicted void fraction and measured void fraction shows a good agreement for agitated bubbly flow regime, unstable slug and churn turbulent flow regimes (Figure 5.6c). Present agreement of the measured and predicted void fraction can be attributed to the similar velocity ranges, closer dimension of the geometry and similar working fluid as of the original data of Hills. In year 1977 ***Nabizadeh*** also proposed a drift flux correlation with the distribution parameter as a function of pressure, diameter, mass flux and quality. An overall under prediction is obtained by the correlation (-29%) in comparison to the measured values with lowest deviation in churn turbulent regime (Figure 5.6d). The latter observation is similar to Manera *et al.* (2005) assessments. ***Jowitt et al.*** (1981) correlation was developed from high pressure experiments and the drift flux expression is a function of pressure. A strong under prediction is seen at low void fractions (bubbly flow) which decreases with increasing of void fraction (churn turbulent) with over all mean error between predicted and measured to be around -28%, see Figure 5.6(e).

From the work of earlier researchers (after 1977) it was establish that expression of drift flux model (Ishii, 1977) needed modification for its application to large diameter pipes because of the formation of cap bubbles instead of conventional Taylor bubble slug flow. ***Ishii and Kocamustafagoullari*** (1985) proposed a drift velocity correlation for the cap bubble flow. Except for the drift velocity equation for cap bubble all other equations of Ishii (1977) drift flux model were recommended. All the predicted void fraction values lie within +5% of the measured values indicating agitated bubbly (AB) flow regime and unstable slug (US) flow regime observed can be satisfactorily modelled by this correlation (Figure 5.6f).

Liao, Parlos & Griffith (1985) also developed a drift flux correlation specifically to predict void fraction in vertical upflow (Chexal *et al.*, 1991). In current analysis the correlation strongly under predicts the void fraction values in all flow regimes of large diameter vertical upflow conditions. Similar observations were made by Manera *et al.* (2005) and Coddington and Macian (2002) assessments for low pressures, see Figure 5.7(a). ***Hirao et al.*** (1986) correlation is the result of database using 102.3mm

diameter pipe. Their proposed empirical drift flux correlation takes into account the effects of pressure and pipe diameter on drift flux parameters (C_o and V_{gj}). The set of correlations is not based on flow regimes identification but according to mixture volumetric flux (j) range. The correlation underestimates the value (-15%) within bubbly flow (Figure 5.7b). However, the deviation seems to reduce with increasing void fraction. ***Kataoka and Ishii (1987)*** developed the drift flux correlation for large diameter vessels. The set of correlations is a function of hydraulic diameter, density ratio and viscosity number. The modelled equations are for cap bubbly flow and the use of Ishii (1977) drift flux model for bubbly and churn turbulent regime is recommended. The result of predicted values of void fraction vs. measured values shows good agreement with an overall mean error of about 1.55%, refer to Figure 5.7(c).

El-Boher and Lesin (1988) void fraction correlation was specifically developed with upflow data from an air-water, steam-Hg, Freon-Hg, and N_2-Hg facilities with hydraulic diameter range of 0.016 and 0.203m (Davis, 2001). However in current analysis, the correlation seems to strongly under predicts the void fraction (-27%) with highest deviation in unstable slug and churn flows (Figure 5.7d).

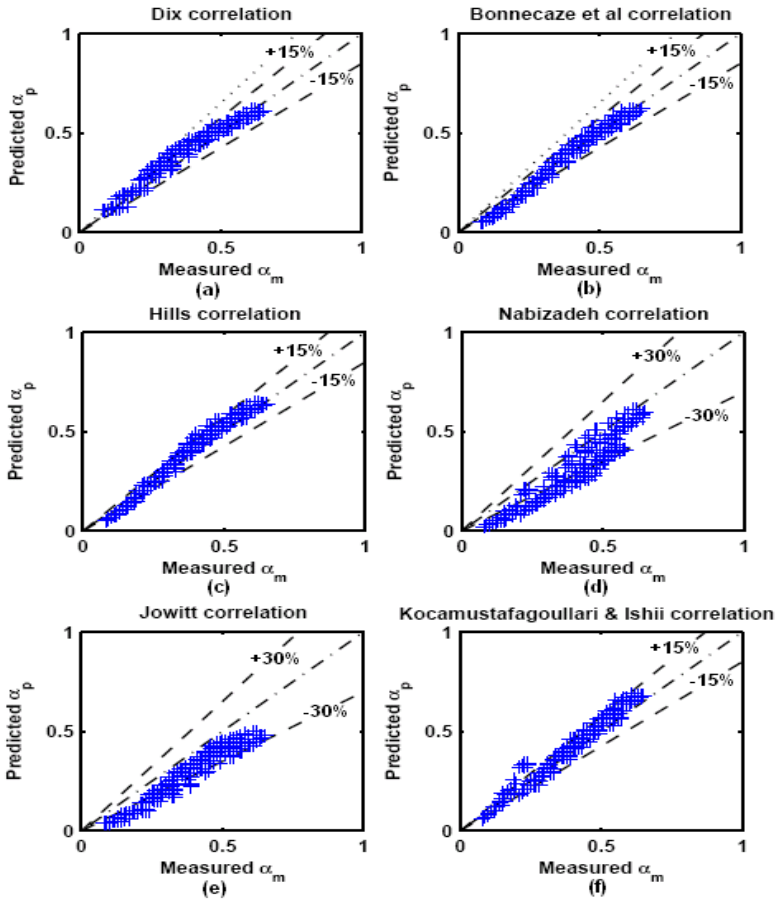

Figure 5.6 The comparison of the measured and the predicted void fraction using correlations based on the drift flux approach.

Morooka et al. (1989) presented a correlation from least square fit to boiling water reactor data (also known as ***Toshiba*** correlation). Though the correlation is applicable to BWR fuel geometry, the prediction of void fraction is agreeable with experimental data of large diameter pipe (+7.6%), see Figure 5.8(a). This closeness can be attributed to the large databank of various hydraulic diameters used for the development of the correlation. The correlation consists of two constant values i.e. distribution parameter (C_o) and drift flux velocity (U_{gj}).

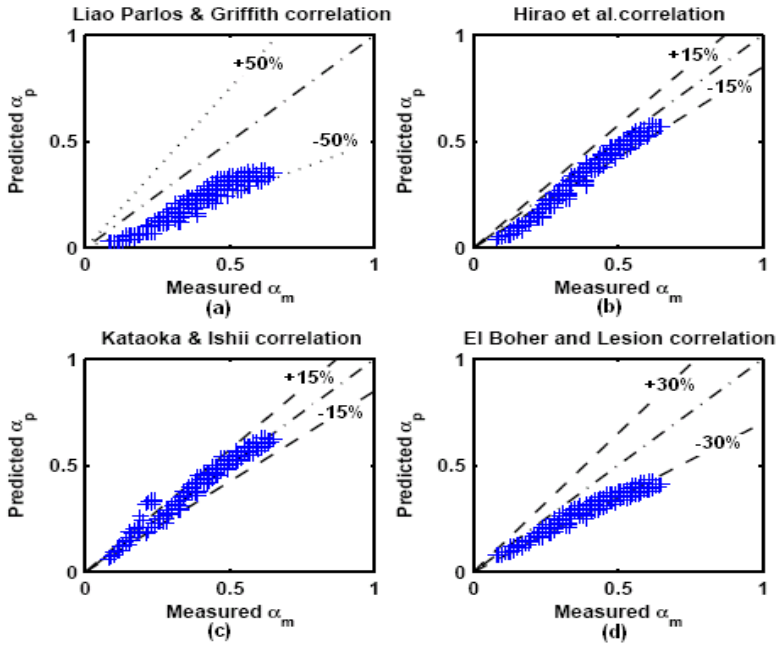

Figure 5.7 The comparison of the measured and the predicted void fraction using correlations based on the drift flux approach.

The ***Chexal and Lellouche*** (1992) proposed a versatile correlation, applicable to all orientation flows. The correlation is applicable to all flow regimes with steam-water, air-water, and refrigerant two-phase flows. The correlation is validated against large data bank consisting of full range of pressures (1-145bars), mass fluxes (0.01-5500kg/m^2-s), void fractions (0.01-0.99) and various diameters (0.005-0.456m). The void fraction predictions of this correlation for large diameter are within -5%, (Figure 5.8b) with an under prediction at low void fractions. Similar results of under

prediction have been obtained by other assessments (Vijayan *et al.*, 2000; Coddington and Macian, 2002; Manera *et al*., 2005).

Inoue et al. (1993) drift flux correlation included the mass flux and pressure influence in drift velocity expression. The correlation was specifically developed for boiling water reactors and strongly under predicts the void fraction (-37%) with maximum deviation in bubbly flow regime (Figure 5.8c). ***Maier and Coddington*** (1997) correlation is result of curve fitting on the data obtained from nine (9) experimental facilities around the world. Their drift flux correlation has eight fitting constants (2 for C_o and 6 for U_{gj}) with pressure dependency. The correlation under predicts the void fraction values with higher deviation for bubbly flow regime that progressively decreases for agitated bubbly, unstable slug and churn turbulent flow regime, see Figure 5.8(d).

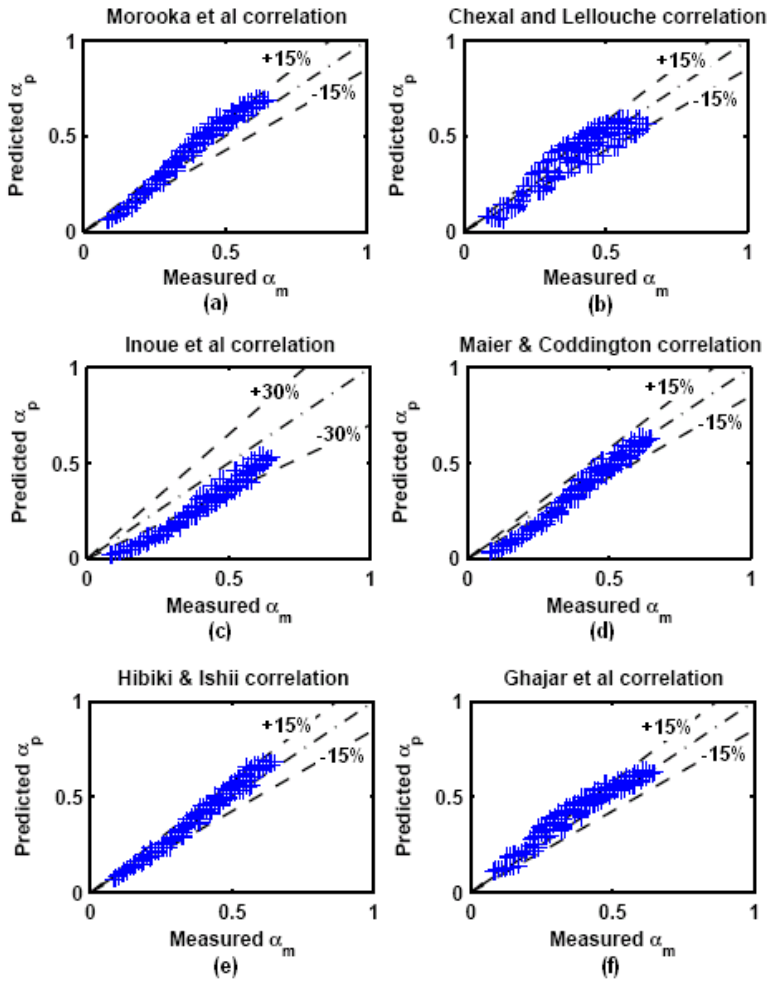

Figure 5.8 The comparison of the measured and the predicted void fraction using

correlations based on the drift flux approach.

Perhaps the most detailed and comprehensive study on drift flux modelling of large diameter pipe after Ishii (1977, 1986, 1987) has been performed by ***Hibiki and Ishii*** (2003). Two inlet flow-regime (bubbly/cap bubbly at inlet or dispersed bubbly at inlet) based correlations were developed for large diameter pipe at low mixture volumetric flux. For higher mixture volumetric fluxes, the use of Ishii (1977) and Ishii and Kataoka (1987) correlation are recommended. Excellent predictions are obtained by these correlations in comparison to other the correlations used, see Figure 5.8(e). It is to be noted that this correlation was able to predict the bubbly flow regime very well, a feature not exhibited by many other correlations.

Recently ***Ghajar et al. (2006)*** presented a universal drift flux correlation applicable to all flow patterns and inclination angles. The correlation is a modification of the Dix (1971) correlation by introducing a correction factor for pressure effects in the drift velocity expression. In current assessment the correlation has performed quite well with mean error of 12.54 % though the original Dix expression proved to be more accurate for large diameter void fraction predictions, refer Figure 5.8(f). The correction suggested by Ghajar *et al.* (2006) improved only the higher void fraction region ($\alpha > 0.4$) for their assessment, this void fraction region which is churn turbulent and unstable slug flow in current work is also predicted quite well. However, the correlation did not improve the prediction at low void fraction region neither in their assessment nor for the large diameter vertical pipe.

5.6.3 Miscellaneous void fraction correlation

Surprisingly some often cited and commonly used empirical void fraction correlations of ***Wilson et al.*** (1961), ***Spedding and Chen*** (1984) and ***Spedding & Chen*** (1998) performed very well also in this analysis.

Wilson et al. (1961) correlation developed with experimental data of pipe diameters of 102-480mm and the pressure of range 1.03-4.14MPa, yielded an overall mean error within -4% with closely predicting all four flows (i.e. bubbly, agitated bubbly and churn flow). ***Spedding and Chen*** (1984) correlation-I indicated a closer prediction of void fraction from the measured values in all flow regimes with low mean errors then the ***Spedding and Chen*** (1984)-II and ***Spedding and Chen*** (1981) correlation based on Lockhart & Martinelli model. Both ***Spedding and Chen*** (1984) correlations are based on the modification of Armand equation and accounts for radial variation of velocity. The correlations consists of holdup ratios and volume flow rate ratio of liquid phase to that of gas phase with various ratios of physical properties been summed up in the constant. The empirical correlation developed for N_2-Hg flows by ***Neal and Bankoff*** (1965) overall under predicts the values of void fraction by mean error of -22% with largest deviation in bubbly flow regime.

The next group of empirical correlations (Hagedorn and Brown, 1965; Duns and Ros, 1963; Gray *et al.*, 1978; Beggs and Brill, 1973 and Mukherjee and Brill, 1985) is widely applied in Oil and Gas industries. In above methods except for Hagedorn and Brown (1959), Duns and Ros (1965), Beggs and Brill (1973) and Mukherjee and Brill (1999) are all flow regime specific model.

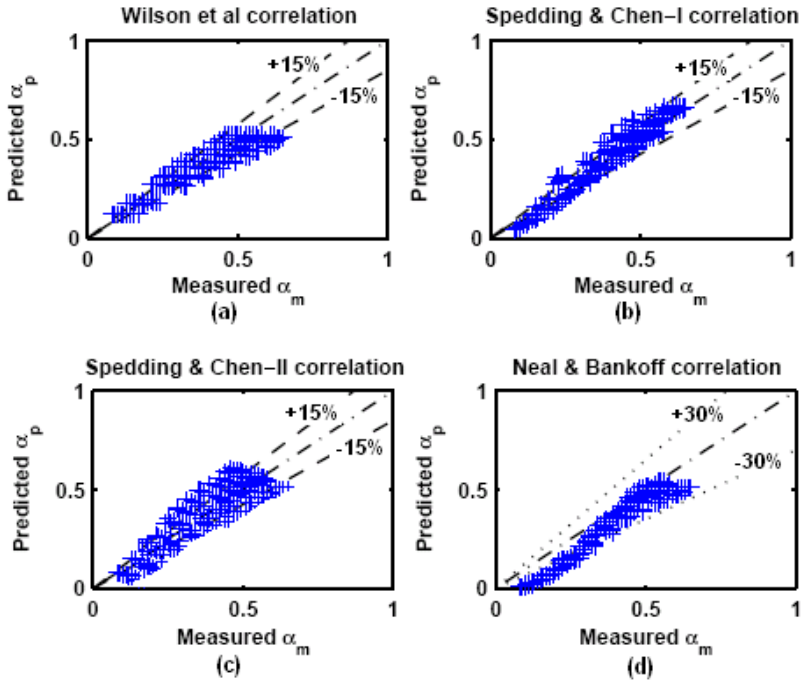

Figure 5.9 The comparison of the measured and the predicted void fraction using correlations based on the empirical approach.

Hagedorn and Brown (1965) method indicated large inconsistencies with an over prediction of the void fraction values in all cases very strongly (+50%), refer to Figure 5.10(a). These values are very similar to HVF signifying the basis of its development. The mean percentage error and standard deviation were obtained after applying the modifications suggested by Hagedorn (Mukherjee and Brill, 1999).

The ***Duns and Ros*** (1963) correlation is very popular in industry and is specifically developed for gas-liquid vertical flow mixtures in wells. The set of correlations initially predicts the flow regime and calculates slippage and friction separately for each flow regime. In current assessment a slight under prediction at lower void fraction (bubbly flow) was observed however for increasing gas superficial velocity an over prediction of the void fraction is seen. The method predicted some cases of bubbly flow regime correctly while in rest of the cases agitated bubbly, churn-turbulent and unstable slug flow are all identified as slug flow (also refer to Figure

4.53b for selected data points). With an overall mean error +15% (Figure 5.10b), the results can be considered to be satisfactory in comparison to the other methods of this class. ***Beggs and Brill*** (1973) pressure gradient set of correlations is the only method that can be applied for any inclination. The method calculates pressure gradient but first identify the flow regimes (segregated, transition, intermittent and distributed) and then liquid hold up for horizontal orientation which is corrected for actual pipe inclination. The method predicted the bubbly and some cases of agitated bubbly flow as transition flow while the cases of churn and unstable slug were identified as intermittent flow (refer to Figure 4.53b). The scatter seen in the Figure 5.10(c) is due to incorrect flow regime predictions. The set of correlations overall over predicts the void fraction with mean error percent of 21.4%. Similar over prediction has been reported for pipe diameters larger than the correlations were developed by Mukherjee and Brill (1999).

Mukherjee and Brill (1985) presented the modification of Beggs and Brill (1973) method, in order to overcome the limitation of earlier method. The method uses new correlations for flow regime identification and liquid hold. The predicted results of void fraction of this method in comparison to original model are much improved with over all mean error reduced to 16.54%, see Figure 5.10(d). Similar to above two methods, Mukherjee and Brill (1985) only identified some cases of bubbly flow regime and all the rest cases (agitated bubbly, churn/froth, and unstable slug flow) were identified as slug flow.

OLGA is an extensively used multiphase simulation tool of oil and gas industries that has been specifically developed for large diameter risers with validation from the SINTEF flow loop of 189mm inner diameter and 50m high riser In current analysis the OLGA steady state model was used, the values indicated are average void fraction in the vertical riser test section. The inlet and outlet sections of the vertical riser geometry were excluded (to minimize the effects of adjoining node) from the calculation of average void fraction to present a more fair assessment. The comparison of the experimental and OLGA results clearly indicates the differences. The results are around +30% in mean error. The over prediction of void fraction indicates a lower pressure drop prediction than true value which is quite an offset from designing point of view. Note that the flow regime predictions in the riser section are also in contradiction with experimental results (refer to Figure 4.52).

According to the Brill and Beggs (1991), in order to perform a meaningful and unbiased comparison of the performances of the existing pressure gradient methods, the methods should be compared against actual data. In an attempt to compare the experimental data further, the data was also compared to the existing pressure gradient methods. The experimental result presented in earlier chapter has indicated that a decreasing relationship is obtained with negative slope signifying that the riser section is dominated by the void fraction enhancement.

The result obtained from the void fraction correlations assessment has indicated that few empirical correlations have predicted the measured void fraction very closely. Thus the use of these correlations values in conjunction with commonly used pressure

gradient methods should yield values close to experimental data. Also the methods that incorporate the void fraction (or holdup) evaluation term can be assessed accordingly.

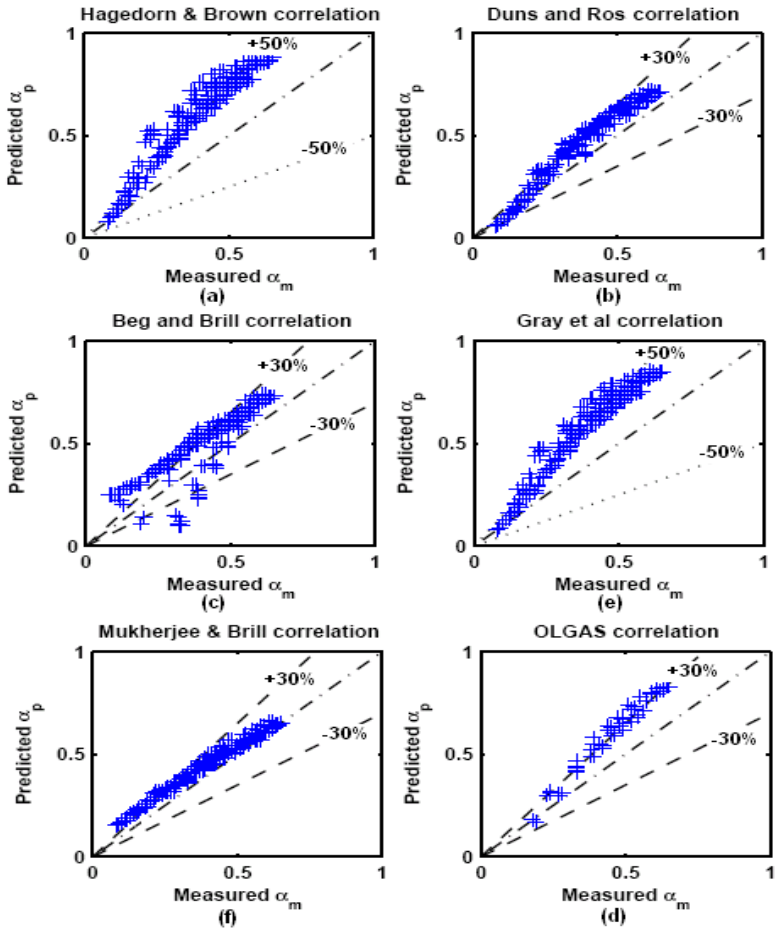

Figure 5.10 The comparison of the measured and the predicted void fraction using correlations based on the flow regime specific approach.

5.6.4 Pressure gradient methods based on Homogenous mixture model

Figure 5.11 show the comparative results of the predicted total pressure gradient with experimental two-phase data.

It can be seen in Figure 5.11(a), the ***homogenous pressure gradient method*** using a total mixture flux and mixture fictional factor shows severe under prediction (-37.58%). This is the consequences of an over prediction of void fraction. Similar to earlier assessment of void fraction, the results shows a closer agreement at higher hydrostatic head (low void fraction) only when the gas phase is uniformly distributed in liquid phase. As the uniformity is lost due to flow regime transition from bubbly flow, the model progressively deviates from the measured data because the gas phase is no longer mixed up as in bubbly flow. It is to be noted that for calculation of two phase homogenous mixture viscosity term in frictional pressure gradient, different correlations i.e. of Chicchitti *et al.* (1960), Dukler *et al.* (1964) and Beattie and Whalley (1982) were made. However here only Chicchitti *et al.* (1960) relation is presented as the same conclusions can be drawn from the other correlations.

Figure 5.11(b) illustrates the results of ***Bankoff (1960)*** model, an extension of homogenous mixture approach. The hydrostatic pressure gradient term uses the Bankoff (1960) void fraction correlation but unlike the homogenous mixture model above, the frictional pressure gradient term uses two phase frictional multiplier. The frictional multiplier term is further function of quality and densities of the two phases. The results show an effect of hydrostatic (void fraction) term clearly as the frictional component calculated was less than 1.5% of the hydrostatic term. The result has improved in comparison to the homogenous model. Next in Figure 5.11(c), the result of CESNEF-2 or Lombardi-Carsana (1992) model is presented. Although the model is empirical in nature and is directly expressed in terms of mass flux, mixture density, equivalent diameter etc., it specifies the use of homogenous hydrostatic pressure gradient for calculation of total pressure gradient (Vijayan *et al.*, 2000). The results obtained are very much similar to homogenous mixture model due to the calculated frictional component term, although slightly larger in magnitude from homogenous but still not dominant to influence the total pressure gradient.

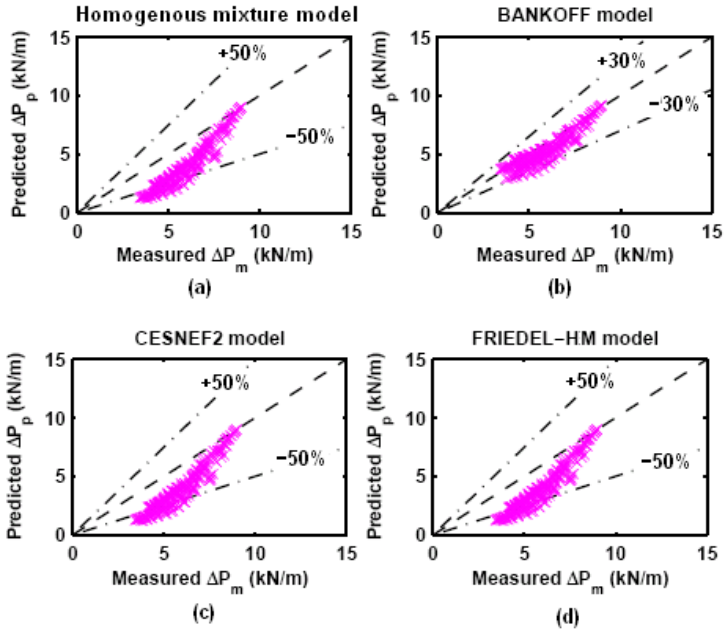

Figure 5.11 The comparison of the measured and the predicted total pressure gradient using the homogenous mixture approach.

Friedel (1979) frictional pressure gradient term, like Bankoff (1960) uses the frictional multiplier concept. Several previous works regards this model as the most appropriate model yielding satisfactory results. Vijayan *et al.* (2000) recommends the use of homogenous hydrostatic term with this frictional model. The Figure 5.11(d) shows the influence of this later statement.

It can be seen that all the models utilizing the concept of homogenous mixture also uses the homogenous hydrostatic term. Since this term is over predicted due to over prediction of void fraction (earlier assessment), severe under prediction of total pressure gradient is seen. Only the Bankoff model due to the use of Bankoff void fraction correlation yielded the results within the usual allowable ±30% range.

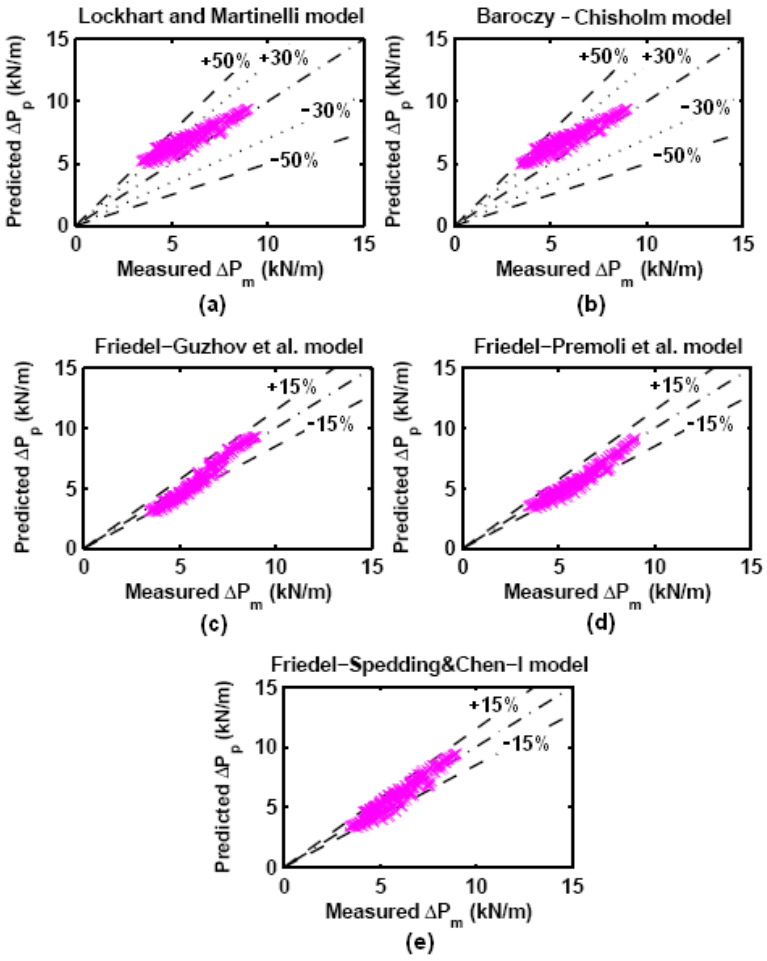

Figure 5.12 The comparison of the measured and the predicted total pressure gradient using the frictional multiplier approach.

5.6.5 Pressure gradient methods based on friction multiplier concept

In this method all the model utilizes the concept of frictional multiplier using separated flow model. The method was originally presented by the Lockhart and Martinelli (1949) for prediction of two-phase frictional pressure drop based on a two-phase multiplier for the liquid phase or the gaseous phase respectively. The Figure 5.12(a) shows the results of ***Lockhart and Martinelli (1949)*** model. The model overall over predicts the total pressure gradient by 22%. Figure 5.12(b) shows the results of modified Baroczy model by Chisholm (1973), also known as the ***Baroczy-Chisholm model***. In this model, the friction multiplier is the complex function of mass flow rate, quality and friction pressure gradient for liquid and gas phases. It is to

be noted that the results by the model are similar to the Lockhart and Martinelli (1949) model.

Next Figure 5.12(c, d and e) illustrates the results of total pressure gradients based on Friedel frictional pressure gradient model. The ***Friedel model*** predictions are combined with the hydrostatic term calculated from selective empirical void fraction correlations. These void fraction correlations namely Guzhov *et al.* (1967), Premoli *et al.* (1971) and Spedding and Chen (1984)-I were selected due to their satisfactory prediction of void fraction in comparison to the measured values. The correlation of Friedel with combination of above void correlations provided the overall best agreement with the experimental results. This further implies that the predicted friction component by this method was also smaller to the extent that it does not influence the total pressure gradient that is dominated by the hydrostatic head.

5.6.6 Pressure gradient methods based on empirical approach

Lastly, the pressure gradients calculations were performed to illustrate the variability of predictions from the oil industry models against the experimental data. Three well known pressure gradient models Hagedorn and Brown (1965), Duns and Ros (1963) Beggs and Brill (1973) were compared along with a more recent Oliemans and Pots (2006) mechanistic pressure gradient scheme.

The Figure 5.13(a) shows the results of ***Hagedorn and Brown (1965) model***. The results obtained by this model shows a severe underprediction (-37.63%) due to the over prediction of the hydrostatic term. ***Duns and Ros (1963)*** method showed more satisfactory results (-15.07%) in comparison to the earlier method, see Figure 5.13(b). The results are closer to measured value at low gas superficial velocities or for bubbly flow (-7.17%) than for agitated bubbly and churn/froth flow (-18%). The results of ***Beggs and Brill (1973)*** model in Figure 5.13(c) were calculated after applying the correction factors suggested by Payne *et al.* (Brill and Mukherjee, 1999). The over all results are within -19%, the scatters obtained are for bubbly flow data points. The experimental bubbly flow data points were identified as transitional flow by this model (9.19%) where as agitated bubbly and churn flow were found to be intermittent flow (-16.70%).

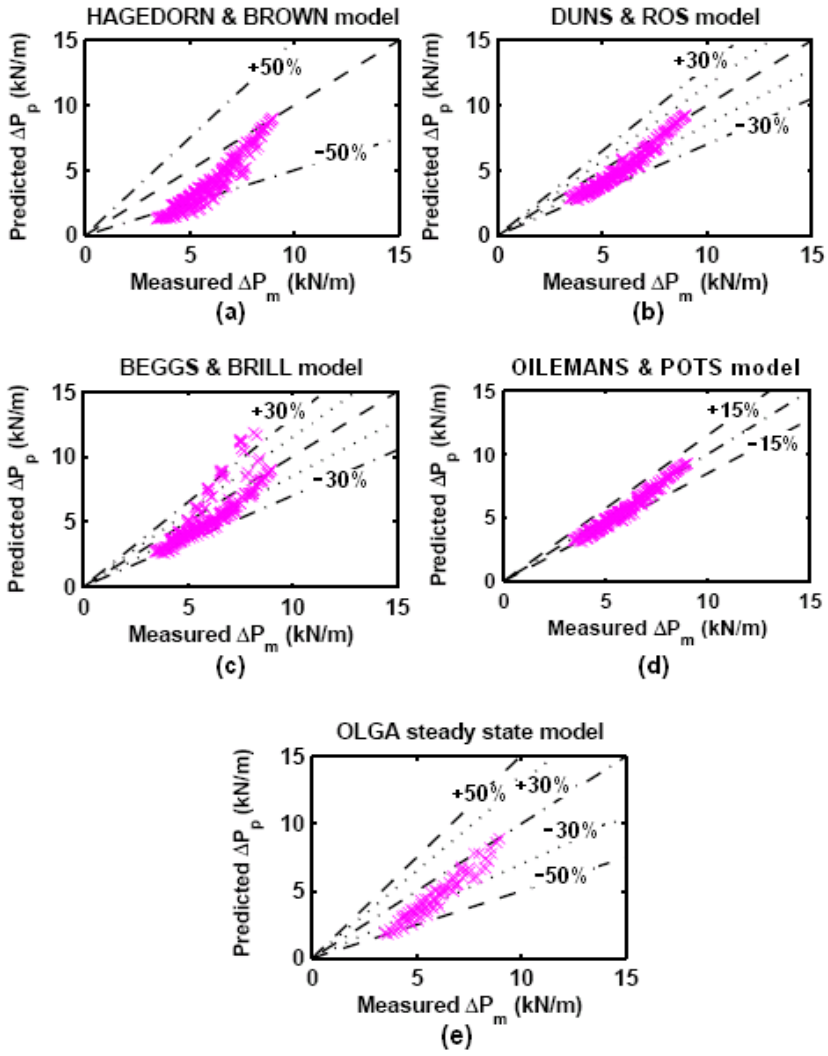

Figure 5.13 The comparison of the measured and the predicted total pressure gradient using the miscellaneous approaches.

The Figure 5.13(d) shows the results of ***Oliemans and Pots (2006)*** model. It is interesting to note that although this approach under predicts, it still yield close results (-5.88%) even though the flow regime were predicted incorrectly i.e. all the bubbly and agitated bubbly flow data points were predicted as dispersed bubbly and remaining data points corresponding to churn/froth were predicted as intermittent flow (also see Figure 4.53 for selected data points). It is emphasized that the flow pattern scheme of Oliemans and Pots (2006) only classify the vertical flow patterns as dispersed bubbly, intermittent flow and annular flow. The scheme further subdivides intermittent flow into elongated bubble, slug and churn/froth flow. However, the pressure gradient scheme calculates the pressure gradient for slug flow only. Hence in

this assessment of pressure gradient in large diameter vertical test section, the slug pressure gradient model was applied on all the data points identified as intermittent flow. From the analysis, it was observed that individually the flow regime identified as dispersed bubbly by the model yielded mean error of -3.65% while flow regime indentified as intermittent and solved as slug flow showed -10%. This indicates that the performance of the drift flux based bubbly flow model is more successful in predicting the performance than the slug flow model used for churn/froth flow. However, the experimental data is dominated by gravity term and so is the calculated term signifying that the liquid holdup (or void fraction) in the above term is the major factor. The predicted values show that this term is close to actual values for bubbly flow only and the deviation increases as the flow progresses from bubbly to agitated bubbly and from agitated bubbly to churn/froth flow. This later aspect signifies that the liquid holdup closure relation used in unit slug modelling approach is not able to accurately predict the churn/froth flow encountered in these experiments.

Lastly, the steady state results of ***OLGA multiphase code*** are presented in Figure 5.13(e). The results presented are for the total pressure gradient calculated by the code for the whole flowline-riser system. An over prediction in void fraction has resulted in the under prediction of pressure gradient, however the code is predicting within the range of ±30% as asserted by the code developers (also refer to Figure 4.52).

Overall, the results of oil industry models are within the range of ±30%, however due to underprediction of the pressure gradient, production losses are expected hence more work is needed to establish accurate methods.

5.7 Summary

In this chapter an extensive assessment of some of the often cited and commonly used void fraction (holdup) correlations and pressure gradients methods from different fields of application was performed. The results of the void fraction assessment study presented in Table 5.1 indicates that many of the published correlations are not appropriate to characterize the void fraction in large diameter vertical pipes and only few have potential to perform satisfactorily within the range (±30%).

Under the flow conditions of the current experiments, total pressure gradient was dominated by hydrostatic head. This implies that in the experiments friction component was smaller to extent that it does not influence the total pressure gradient. For such conditions, it was found that the choice of two-phase void fraction correlation is of major significance in determining the hydrostatic pressure gradient. The void fraction correlations based on the homogenous mixture model gave satisfactorily results for bubbly flow only and progressively deviated with flow regime transition. In general, the pressure gradient model including Friedel and CESNEF2 frictional model with homogenous gravitational pressure gradient showed large deviation. Similar to void fraction correlations, the pressure gradient model and

its combination are valid for flow flows like dispersed bubbly or annular mist where the two phases are expected to travel at similar phase velocities.

All the "Kβ" models seem to improve the homogenous mixture model results by taking into account of radial non uniformity of void fraction and velocity between the two phases. Bankoff frictional model along with its void fraction correlation perform satisfactorily, and should therefore be considered.

The void correlations based on separate flow model using slip equation, mass flux term or Martinelli parameter showed wide variation in results. Satisfactory accuracy was indicated in cases of Spedding and Chen, Guzhov *et al.* and Premoli *et al.* It is to be noted that whenever approximate averages are required or for conditions where the flow type may not be known, Spedding and Chen (1984)-I, Guzhov *et al.* (1967) and Premoli *et al.* (1971) void fraction correlations are recommended on the basis of their simplicity and closer prediction for the experimental data analyzed. Friedel frictional pressure gradient model in combination of Guzhov *et al.* (1967), Premoli *et al.* (1971) and Spedding and Chen-I (1984) correlations calculated gravitational pressure gradient components yielded the overall closest predictions. This is due to the use of the gravitational component (from assessed void fraction correlation) rather than any frictional specific effects.

Some of the void correlations based on separate flow model using Martinelli parameter showed to be inaccurate with deviation from experimental results being very high (Zivi, Thom and Levy). However, the pressure gradient model predictions were much improved with Lockhart and Martinelli (1949), Chisholm and Baroczy (1973), and Friedel (1979), all predicting within ±30% range. This is primarily due to experiments dominated by gravitational regime or the results of void fraction correlation of Lockhart and Martinelli (1949) and Chisholm and Baroczy rather than satisfactory calculation of frictional component.

Overall the drift flux based void fraction correlations were more successful in predicting the closer results to the experimental values. Almost all the drift flux correlations indicated satisfactorily performances (within ±20%), however following predicted values within ±10%; Nicklin *et al.* (1962), GE-Ramp (1970), Dix (1971), Bonnecaze *et al.* (1971), Hills (1976), Ishii and Kocamustafagoullari (1985), Kataoka and Ishii (1987), Morooka *et al.* (1989), Chexal and Lellouche (1992) and Hibiki and Ishii (2003).

Table 5.1 The comparison of various void fraction correlations using large diameter vertical upflow data.

Category	Correlation	References	Mean % error	Standard Deviation (%)
Homogenous void fraction model ($\alpha=\beta$)	HEM model	Neil & Kazimi (1989)	52.67	19.59
The "$\alpha=K\beta$" forms.	Armand (1950)	Spedding *et al.* (1998)	27.17	16.32
	Armand &Treschev (1950)	Neil & Kazimi (1989)	29.8	16.8
	Bankoff (1960)	Neil & Kazimi (1989)	16.46	16.52
Some commonly used slip ratio (S) relations.	Chisholm (1972)	Thom (2004)	-27.5	9.89
	Smith (1969)	Thom (2004)	21.38	14.30
	Premoli *et al.* (1971)	Hewitt (1982)	10.11	10.54
	Guzhov *et al.* (1967)	Garcia *et al.* (2005)	3.13	16.82
	Huq & Loth (1992)	Huq & Loth (1992)	17.63	13.60
	Modified Smith (1992)	TECDOC-1203	-37.94	6.68
Based on Lockhart and Martinelli parameter (X).	Lockhart & Martinelli (1949)	Butterworth (1975)	-24.07	9.66
	Levy (1960)	Thom (2004)	-30.06	10.21
	Thom (1964)	Thom (2004)	-40.93	15.74
	Zivi (1964)	Butterworth (1975)	-68.93	10.49
	Baroczy (1966)	Butterworth (1975)	-28.39	9.37
	Chen (1986) I & II	Spedding & Spence (1989)	-17.11 & 16.54	12.38 & 22.17
Based on empirical correlations.	Wilson *et al.* (1961)	Kataoka & Ishii (1987)	-3.98	14.57
	Neal & Bankoff (1965)	Spedding & Spence (1989)	-22.48	21.79
	Spedding & Chen (1981)	Spedding & Spence (1989)	-34.94	8.76
	Spedding & Chen (1984) - I & II	Spedding & Chen (1984)	-2.59 & -8.54	16.19 & 25.37
	Nicklin (1962)	Nicklin (1962)	-5.41	11.93

Based on drift flux model, mostly from Nuclear industry.	Zuber & Findlay (1965)	Thom (2004)	11.19	9.27
	Rouhani (1969) - I & II	Spedding & Spence (1989)	19.93 & 11.62	11.53 & 10.08
	Rouhani & Axelsson (1970)	Thom (2004)	21.25	11.96
	GE Ramp (1970)	Tecdoc-1203	4.79	12.81
	Dix (1971)	Neil & Kazimi (1989)	-6.90	19.34
	Bonnecaze *et al.* (1971)	Spedding *et al.* (1998)	-5.40	11.93
	Nabizadeh (1979)	TECDOC-1203	-29.0	17.42
	Hills (1976)	Hills (1976)	1.96	10.81
	Jowitt (1981)	TECDOC-1203	-27.73	13.79
	Kocamustafagoullari & Ishii (1985)	Hibiki & Ishii (2003)	4.45	10.85
	Liao Parlos & Griffith (1985)	Maier & Coddington (1997)	-47.37	11.21
	Hirao *et al.* (1986)	Hirao *et al.* (1986)	-14.86	13.34
	Kataoka & Ishii (1987)	Kataoka & Ishii (1987)	1.55	10.40
	El-Boher and Lesion (1988)	MIT report (2000)	-26.57	7.10
	Morooka *et al.* or Toshiba (1989)	Morooka *et al.* (1989)	7.63	13.29
	Chexal and Lellouche (1992)	Chexal & Lellouche (1992)	-4.53	19.62
	Inoue *et al* (1993)	Coddington *et al.* (2002)	-36.98	14.82
	Maier & Coddington (1997)	Coddington *et al.* (2002)	-15.38	15.47
	Hibiki & Ishii (2003)	Hibiki & Ishii (2003)	1.75	8.78
	Ghajar *et al.* (2007)	Ghajar *et al.* (2006)	12.54	11.06
Based on popular Oil & Gas industry.	Hagedorn & Brown (1959)	Brill & Mukherjee (1999)	52.63	19.61
	Duns & Ros (1963)	Brill & Mukherjee (1999)	15.62	13.86
	Beg & Brill (1973)	Brill & Mukherjee (1999)	21.42	50.73
	Mukherjee & Brill (1985)	Brill & Mukherjee (1999)	16.54	17.18
Two fluid model	OLGA-S	Scandpower (2000)	30.26	11.51

It is to be noted that in the above correlations Ishii and Kocamustafagoullari (1985), Kataoka and Ishii (1987), Hibiki and Ishii (2003) and Hills (1976) are specifically for large diameter application. It can further be noted that with lowest mean percent error Kataoka and Ishii (1987) outperforms other empirical correlations while on the basis of standard deviation, the figures clearly shows that the Hibiki and Ishii (2003) correlation performs the best. Although the drift flux correlations are found to closely predict the experimental data, three (3) constraints are met by them (i) expressions are flow regime dependent hence are not continuous and this might give rise to numerical instabilities during computation (ii) because the models are sensitive to prediction of flow patterns, any inappropriate choice of flow pattern would increase the variance of the whole model and, (iii) many of the above correlations are iterative in nature which inhibits their frequent use in comparison to simpler correlations.

The empirical based void fraction correlation/pressure gradient methods of the oil industry showed inconsistencies excluding the Duns and Ros (1963). The results of the Duns & Ros (1963) can be considered to be satisfactory in comparison to the other methods of this class. Hagedorn and Brown (1965) known to perform satisfactorily in the field showed large mean errors, with Beggs and Brill (1973) also showing large percentage errors in void fraction calculation. The latter may be due to the empirical correlations incorrectly predicting flow regimes. However, it is also worth mentioning that the void fraction correlations belonging to nuclear industry are closer in prediction than the oil industry correlations. In this respect the OLGA model results are worth referring where over prediction of void fraction led to a lower pressure gradient prediction, this can be quite an offset from designing point of view.

Overall, the results of the pressure gradient models used in oil industry are within the range of ±30% except for Hagedorn and Brown (1959). In this regard, it also worth mentioning that the Oliemans and Pots (2006) mechanistic pressure gradient scheme based on the individual flow regime has also been successful in predicting the total pressure gradient. The results obtained from this flow regime specific model are close to that indicated by models where the combination of Friedel frictional component with gravitational component determined from Guzhov *et al.* (1967), Premoli *et al.* (1971) and Spedding and Chen (1984) were combined.

Thus the important implication of this assessment then is that two phase flow void fraction prediction should be based on flow regime prediction. The correlations taking into account of this fact are closer to experimental trends with exception of few empirical correlations. It was noted that most of the correlations performed well in some of the flow regimes and their performance deteriorated in the other thus none of the correlation was able to predict all the flow regimes accurately (see Table 5.2). Most of the successful correlations, at the maximum predicted three flow regimes. It was found that correlations that successfully predicted the three flows AB, US and C, did not predicted the bubbly flow accurately while those predicting bubbly flow showed acceptable trend for agitated bubbly but did not predicted US and C flows satisfactorily. This trend highlights the difference in the flow structure variation behind the bubbly and rest of the flows.

Table 5.2 The recommended void fraction correlations according to flow regimes.

Flow regime	Recommended Correlation	Correlation Type	Mean % error	Standard Deviation	Influencing parameter	Working Fluid
Bubbly flow (B)	Hibiki & Ishii (2003)	Drift Flux	-5.24	3.15	C_o and U_{gj}	Steam-water / Air-water / N_2-water
	Duns & Ros (1963)	Empirical	-7.17	7.13	D, P, j_g & j_l	Oil-gas mixtures with varying water cuts
	Chen-I (1986)	Empirical	5.98	9.62	D, P, velocity profile	Steam-water
	Rouhani-II (1969)	Drift Flux	-3.49	13.61	C_o and U_{gj}	Steam-water
	Dix (1971)	Drift Flux	6.29	13.80	C_o and U_{gj}	Steam-water
	Rouhani & Axelsson-I (1970)	Drift Flux	1.38	14.60	C_o and U_{gj}	Steam-water
	Zuber & Findlay (1965)	Empirical	-7.30	15.07	C_o and U_{gj}	Steam-water & R-22
	Rouhani-I (1969)	Drift Flux	4.20	18.05	C_o and U_{gj}	Steam-water
	Wilson *et al.* (1961)	Drift Flux	1.84	21.24	D & P	Steam-water
Agitated bubbly flow (AB)	Bonnecaze (1971)	Drift Flux	-1.60	7.52	C_o and U_{gj}	-
	Nicklin (1961)	Drift Flux	-1.61	7.53	C_o and U_{gj}	Air-water
	Kataoka & Ishii (1987)	Drift Flux	0.94	7.72	C_o and U_{gj}	Steam-water / Air-water/ Air-glycerine
	Hibiki & Ishii (2003)	Drift Flux	0.99	7.77	C_o and U_{gj}	Air-water/Steam-water / N_2-water
	Ishii & Kocamustafagoullari (1985)	Drift Flux	1.53	8.07	C_o and U_{gj}	Air-water/Steam-water
	Hills (1976)	Drift Flux	5.68	7.58	C_o and U_{gj}	Air-water
	GE Ramp (1970)	Drift Flux	9.01	8.1	C_o and U_{gj}	Steam-water
	Chen & Spedding-I (1984)	Empirical	-0.91	8.36	Q_g & Q_l	Steam-water/ Air-water
	Wilson *et al.* (1961)	Empirical	-2.09	14.10	D, P & j_g	Steam-water
	Chexal and Lellouche (1992)	Drift Flux	0.39	17.91	C_o and U_{gj}	Air-water/Steam-water/Refrigerant
	Guzhov *et al.* (1967)	Slip ratio	8.04	11.17	D & j_g	Oil-gas
	Chen & Spedding-II (1984)	Empirical	-2.94	25.51	Q_g & Q_l	Steam-water/ Air-water
Unstable slug flow (US)	Nicklin (1962)	Drift Flux	-2.92	1.90	C_o and U_{gj}	Air-water
	Bonnecaze (1971)	Drift Flux	2.89	1.96	C_o and U_{gj}	-
	Hills (1976)	Drift Flux	1.50	2.02	C_o and U_{gj}	Air-water
	Kataoka & Ishii (1987)	Drift Flux	-1.39	2.13	C_o and U_{gj}	Steam-water/ Air-water/ Air-glycerine

	GE Ramp (1970)	Drift Flux	2.1	7.02	C_o and U_{gj}	Steam-water
	Guzhov *et al.* (1967)	Slip ratio	8.52	2.15	D & j_g	Oil-gas
	Toshiba (1989)	Drift Flux	9.60	2.18	C_o and U_{gj}	Steam-water
	Premoli *et al.* (1971)	Slip ratio	1.82	2.26	G, P, Q_l and Q_g	Air-water/Steam-water/Refrigerant
	Ishii & Kocamustafagoullari (1985)	Drift Flux	7.80	2.42	C_o and U_{gj}	Air-water/Steam-water
	Hibiki & Ishii (2003)	Drift Flux	7.80	2.42	C_o and U_{gj}	Steam-water/ Air-water / N_2-water
	Bankoff (1960)	Kβ	-0.47	2.75	β and P	Steam-water
	Huq & Loth (1992)	Slip ratio	6.54	2.85	x and P	Air-water/Steam-water/
	Maier & Coddington (1997)	Drift Flux	-6.70	3.04	C_o and U_{gj}	Steam-water
	Chen-II (1986)	Empirical	-5.03	3.08	D, P etc.	Air-water
	Dix (1972)	Drift Flux	-1.43	3.16	C_o and U_{gj}	Steam-water
	Chen & Spedding-I (1984)	Empirical	-8.69	3.61	Q_g & Q_l	Steam-water/ Air-water
	Rouhani – II (1969)	Drift Flux	7.60	4.25	C_o and U_{gj}	Steam-water
	Chen & Spedding-II (1984)	Empirical	-1.62	3.96	Q_g & Q_l	Steam-water/ Air-water
	Chexal & Lellouche (1992)	Drift Flux	-3.61	6.91	C_o and $U_{gj.}$	Air-water/Steam-water/Refrigerant
Churn/ froth flow (C)	Nicklin (1962)	Drift Flux	2.48	1.24	C_o and U_{gj}	Air-water
	Bonnecaze (1971)	Drift Flux	2.49	1.24	C_o and U_{gj}	-
	Kataoka & Ishii (1987)	Drift Flux	3.35	1.25	C_o and U_{gj}	Steam-water/ Air-water/ Air-glycerine
	Dix (1972)	Drift Flux	3.25	1.41	C_o and U_{gj}	Steam-water
	Hills (1976)	Drift Flux	6.93	1.47	C_o and U_{gj}	Air-water
	Premoli *et al.* (1971)	Slip ratio	7.53	2.59	G, P, Q_l and Q_g	Air-water/Steam-water/Refrigerant
	Maier & Coddington (1997)	Drift Flux	-2.06	3.91	C_o and U_{gj}	Steam-water
	Hirao *et al.* (1985)	Drift Flux	-4.43	3.89	C_o and U_{gj}	Steam-water
	Chexal and Lellouche (1992)	Drift Flux	3.86	5.31	C_o and U_{gj}	Air-water/Steam-water/Refrigerant
	Chen & Spedding-I	Empirical	-3.86	5.56	Q_g & Q_l	Steam-water/ Air-water
	Wilson *et al.* (1961)	Empirical	-7.64	5.57	D, P & j_g	Steam-water
	Chen & Spedding-II	Empirical	3.89	6.02	Q_g & Q_l	Steam-water/ Air-water
	Chen-II (1986)	Empirical	5.55	6.04	D, P etc.	Air-water
	Neal & Bankoff (1965)	Empirical	-6.30	6.21	D, P, Q_g & Q_l	N_2-Hg

Based on the assessment results of the void fraction correlations, a set of table is developed; refer to Table 5.2. This table recommends correlations based on their performances in the individual flow regimes i.e. B, AB, US and C encountered in current experiments. It also mentions the influencing variable in the correlation and the working fluid used in validating the developed correlation. Thus in the conditions where the prevailing flow pattern of the two phase flow is known, prior to design/simulation stage, the selection of the appropriate void fraction prediction will be closer to the true value then the value of randomly selected.

From the pressure gradient results obtained, it is seen that the successful predictions of pressure gradients methods are due to the flow dominated by hydrostatic head and thus influenced by the assessed void fraction (or holdup) correlation. In this regard, the hybrid models of Friedel frictional pressure gradient with combination of Guzhov *et al.* (1967), Premoli *et al.* (1971) and Spedding and Chen (1984) have been successful in predicting the pressure gradient. However, it is the flow regime specific approach that is again successful similar to void fraction assessment, with Oliemans and Pots (2006) mechanistic pressure gradient scheme giving far closer results to experimental values than conventional methods. The other flow regime specific models such as Duns and Ros (1963) and Beggs and Brill (1973) also yielded satisfactory results, refer to Table 5.3 for overall results.

Table 5.3 The comparison of various pressure gradient models.

Category	Model	Mean % error	Standard Deviation (%)
Based on the Homogenous equilibrium model	HEM model	-37.58	17.28
	Bankoff (1960)	-9.69	9.65
Based on the two-phase friction multiplier concept	Lockhart & Martinelli (1949)	21.23	13.04
	Chisholm -Baroczy (1973)	21.09	12.29
Empirical models	Friedel-HEVM	-37.17	17.23
	CESNEF2-HEVM	-36.94	17.15
	Friedel-Guzhov *et al.*	-5.32	7.8
	Friedel-Premoli *et al.*	-5.42	5.54
	Friedel-Spedding & Chen-I	1.35	8.06
Based on popular Oil & Gas industry.	Hagedorn & Brown (1959)	-37.63	17.23
	Duns & Ros (1963)	-15.07	8.29
	Beggs & Brill (1973)	-18.67	16.50
	Oliemans & Pots (2006)	-5.88	5.60
Two fluid model	OLGA-S	-25.22	12.94

Chapter 6

Numerical simulation of the large diameter horizontal flowline-vertical riser system

In this chapter, large diameter horizontal flowline-vertical riser system has been numerically simulated. A major commercial simulator OLGA has been explored for computing hydrodynamic characteristics with an aim to increase the confidence on the existing modelling tools.

6.1 Introduction

A significant proportion of the available oil and gas reserves are in deep offshore waters. Design and operation of the recovery systems in these deep offshore facilities are therefore crucial in terms of CAPEX and OPEX. For such critical application, much optimized designs are needed; therefore the use of the transient multiphase flow simulators plays a vital role. Most of the commercially available transient multiphase flow simulators are based on the empirical data and the phenomenological information derived from small diameter pipe. However, it has been observed that the performances of these simulators deteriorate when applied for the conditions outside their benchmark data especially under the case of large diameter risers. This is mainly due to the scarcity of the experimental and field data.

In view of the aforementioned, the data generated from the horizontal flowline-vertical riser system was used with an intention of identifying the capability of OLGA transient multiphase flow simulator. The idea behind was to explore the predictive capability of OLGA multiphase flow simulator. This is an important aspect of the work as no simulation study in public domain so far has been conducted with respect to large diameter vertical riser flow characteristics.

6.2 Pipeline-Riser Experiments

A set of twenty experiments were carried out to test the capabilities of the simulator. The set of experiments used in current analysis consisted of two air injection configurations, refer to Figure 6.1 for simplified configurations.

6.2.1 Parameters simulated

The parameters investigated in the simulations were flow regime, flowline/riser base pressure characteristics and holdup. However, the main distinguishable feature of the stable and unstable flow is the variation in pressure so near riser base pressure was used as a prime means of assessing the simulation. All previous researchers have used this parameter for classifying the unstable flows e.g. severe slugging (Schmidt *et al.*, 1980; Tin, 1991; Yeung and Montgomery, 2001 and Yeung and Montgomery, 2002) and in identifying the amplitude of unstable flow in different topology pipeline-riser systems. Validation of simulations was carried out by comparing the above variables with experimentally determined values.

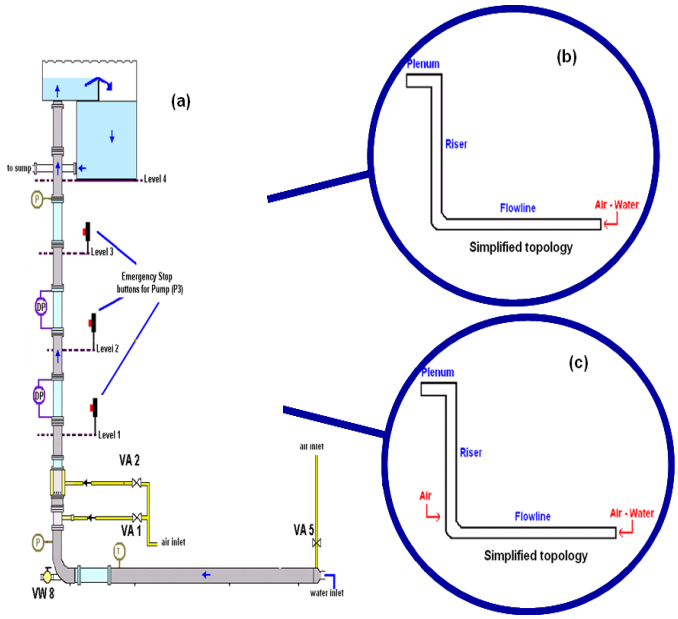

Figure 6.1 (a) The schematic of the large diameter riser along with simplified configurations (b) air injection in the flowline prior to riser base and (c) air injection in the flowline along with air injection in the near riser base area.

It is emphasized here that following measurements were not available during these experiments; local liquid holdup measurement in the flowline/riser base, pressure drop in the flowline and gas-liquid production in the overhead tank. While the non availability of the former two measurements was deemed acceptable at the time (because the focus was the measurements in the riser), the latter measurement (gas-liquid production) was not possible because the level indicator in the top tank highly fluctuated during the intermittent flows.

6.2.2 Test matrix description

The gas and liquid superficial velocities were varied over the range of 0.18 - 2.14m/s and 0.20 to 0.62m/s respectively. Figure 6.2 indicates the range of experiments conducted on the horizontal flow pattern map (Taitel and Dukler, 1976). The flow regimes encountered in this particular set of experiments ranges from stable bubble flow to highly intermittent churn/froth flow. Here, the results of only selected cases consisting the bubbly flow, agitated bubbly flow and unstable flows (i.e. unstable slug and churn/froth flow) is presented and labelled as A, B, C, D, E, F and G on Figure 6.2. The Table 6.1 below summarizes the above simulated cases in terms of superficial velocities of air and water. The table also comprises of the different flow regimes encountered in these cases under horizontal and vertical riser section during above velocity ranges.

To make the investigation of the code more meaningful and reliable, the methodology used is to test some stable flow cases along with unstable flow cases. Two cases, A and E were defined under "stable flow cases" as the flow was mainly stratified and plug flow in the flowline with bubbly flow in the riser. The cases B, C, D, F, G, H and I all belonging to the flowline slugging (terrain or combination of terrain/hydrodynamic slugging) with intermittent flow in the riser (agitated bubbly, unstable slug and churn/froth flow) were defined as "unstable flow cases". Thus if the simulation can reflect the stable flow characteristics, then we can have some confidence on the results for unstable flow cases performed by the code. It is also outlined here that "stable" and "unstable" characteristic of flows are judged from the time series of the variables. If the time series tend to develop into cycle, then the flow is unstable. For the sake of brevity, results of only few dynamic cases will be discussed in terms of limitation of the initial model. Here after these cases will be referred as case A1, B1 and C1 where numeral '1' is referring to the first model predictions, '2' to the modifications in the first model and '3' the final model.

6.3 The Model Formulation

6.3.1 Loop Topology

The large diameter riser facility is modelled as a horizontal flowline-vertical riser in OLGA (see Figure 6.1) with the simplified topology (constant diameter) of the rig. Upstream air and water supply loop are not included in the model and the downstream only consists of a short horizontal pipe as a separator. Three Grids were tested on the above simplified pipeline-riser system to perform two checks; (a) the solution obtained is grid independent and (b) a finer grid size that can capture the characteristic of the flow thus enabling comparison of the flow characteristics. For the three grids implemented, horizontal pipeline of 36m is divided into 40 sections (0.9m each), 20 sections (1.8m each), and 10 sections (3.6m each). The grid sizes for the vertical riser sections are slightly different, these being as 13 sections (0.9m each), 7 sections (1.67m), and 4 sections (2.95m) respectively. The upper tank of experimental

facility is modelled as short horizontal pipe consisting of two sections to avoid numerical instabilities during the numerical simulations.

A plain text version of the model used in the simulations can be found in appendix D, whereas below sections outlines the details of the model.

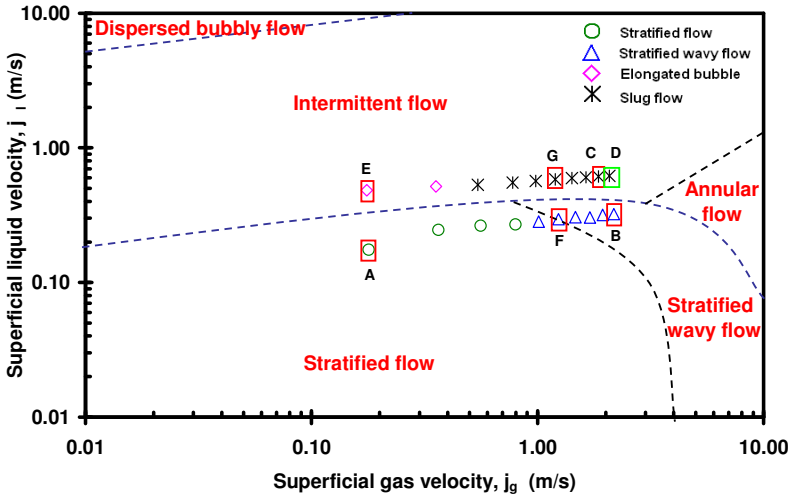

Figure 6.2 The Taitel and Dukler (176) horizontal flow regime map indicating the tested cases.

Table 6.1 The simulated test cases.

Case Name	Superficial Air velocity (j_a)	Superficial Water velocity (j_w)	Experimental Flow regime
	(m/s)	(m/s)	(FL/R) †
A	0.18	0.20	ST/BU
B	2.17	0.32	ST-SL/C
C	1.86	0.61	SL/C
D	2.10	0.62	SL/C
E	0.18	0.50	PL/B
F	1.24	0.29	ST-SL/AB
G	1.20	0.58	SL/US-C
H	2.16	0.31	SL/C
I	2.14	0.62	SL/C

† FL = Flowline, R=Riser, ST=Stratified, PL=Plug, SL=Slug, BU=Bubbly, AB=Agitated bubbly, US= Unstable slug and C=Churn.

6.3.2 Piping material

The whole pipeline-riser system is made of 254mm nominal bore, Schedule 40 carbon steel pipes with properties mentioned in Table 6.2.

Table 6.2 The piping material properties.

Property	Value
Heat capacity	500 J/kg-C
Density	7850 kg/m3
Thermal conductivity	50 W/m-K
Internal diameter	254.5 mm
Thickness	9.25 mm
Roughness	0.035 mm

6.3.3 Assumptions

Some general assumptions used in modelling are defined below:

1. Constant diameter pipe with standard carbon steel properties.
2. The working fluid air-water exists as mixture with standard properties.
3. Air is treated as an ideal gas.
4. No heat and mass transfer between the phases and the environment.
5. Flow rates input remain constant.

Note that this work does not include "Slug tracking module" implementation available in OLGA. Numerical problems were encountered for simulations when slug tracking option was "ON" in the simulations performed, this behaviour is probably due to two factors; firstly the pipeline ending in a vertical riser and secondly due to the back-flow in the riser.

6.3.4 PVT file description

With help of PVTSim fluid property simulator from CALSEP, a table of temperature and pressure was constructed for the air-water properties. OLGA uses this table to model air-water behaviour in the pipeline-riser. The air is modelled as a mixture of nitrogen and oxygen. The SRK-Peneloux equation of state is used for the calculation of PVT behaviour in all simulations (Lockett, 2007). The range of temperature and pressure was taken as the minimum and maximum allowed by the software. This was done in order to provide greater flexibility for numerical calculation by OLGA as otherwise error of pressure and temperature values beyond the table range can result in halting or stopping the simulation. Thus a range of 0.01-50bara and 5-50ºC was thus used for the formulation of the table.

6.3.5 Run time conditions

OLGA code requires initial conditions like pressure, gas fraction, temperature and total mass flow rates as initial conditions, so all the simulation performed were first simulated as the steady state cases and later ran as dynamic cases, unless specifically mentioned. For dynamic cases a minimum time period of 2 hours (7200 seconds) was used. OLGA has an automatic time step control based on pressure's second order time derivate and the transport criterion of Courant-Friedreich-Levy (CFL) criteria; however user can also force a timestep by using same initial, maximum and minimum value. The time step is increased or reduced according to pressure changes between the minimum and maximum value defined by the user (OLGA, 2000; OLGA, 2007). In all the transient simulations from first model, time step was set to initial value of 10^{-1} s with minimum and maximum limit set to 10^{-3} and 1s. The initial value is used by the code to ensure the convergence of the simulation while minimum value is used to ensure practical simulation times. The maximum value is set to ensure that value selected is below the value of CFL (Courant-Friedrich-Levy) condition preventing the pressure-volume temperature (PVT) table errors (OLGA, 2000; OLGA, 2007).

It is important to outline here that during each simulation run; global volume error in the system was monitored, as the minimization of this variable (VOLGBL) was imposed as convergence criteria. This variable reflects the discrepancy between the volume calculated in code compared with the volume of the pipe section. The acceptable difference between the above two values in field cases is usually a value of less than 0.01, however in current analysis it was under 0.001 by taking small time step. It is to be noted that in previous work with the code (Yeung and Montgomery, 2001; Yeung *et al.*, 2003) do not mention whether this variable has been monitored and its minimum value obtained during the individual simulation to ensure that proper convergence with appropriate timestep has been achieved.

6.3.6 Boundary conditions

Choice of boundary conditions is very important in simulation as the closest to real ones will results is more pragmatic answers. In simulation studies many times simulation model do not incorporate the processing equipment as it may also require a complete separate model for setting it up, in such cases, user has to specify the boundary conditions at the upstream and downstream end of the model. These are generally defined as fixed flow rate or fixed pressures; often it is fixed flow rate at the inlet and fixed pressure at outlet.

The first model created in OLGA for large diameter flowline-vertical riser system consisted of separate sources for air and water each with both of them entering in the first section of the pipeline. The plenum is modelled as a short horizontal section and is the outlet node of the entire flowline-riser model. Earlier work with OLGA have acknowledged (Montgomery, 2002; Mehrdad *et al.*, 2006; OLGA, 2007) that this addition of the horizontal section at the end of the riser is to prevent liquid fall back into the pipeline during the blowdown stage and high back pressure thus avoiding

numerical instability introduced in model during calculation. Since pressure at the outlet of the riser i.e. in the plenum during the experiments was atmospheric, the outlet is modelled as a constant pressure boundary. The important parameter set here, at the outlet node is the gas fraction that helps in determination of liquid gradient at the final cell boundary. Thus the gas fraction node value i.e. the fictitious cell is set equal to 1 (i.e. to prevent liquid fall back into the riser during the blowdown stage). It is to be noted that this is the usual practice employed in the development of the model in OLGA. Rest of all the data used for the input file for above inlet and outlet conditions were the averaged steady state values taken from the experimental measurements, refer to Figure 6.3(a).

The above model was also applied with similar boundary conditions for the two cases of riser base gas injection (discussed in later sections), where the pipeline inlet is modelled as the two separate mass sources along with the air injection in the riser base as a third mass source with specified air flow rate, refer to Figure 6.3(b).

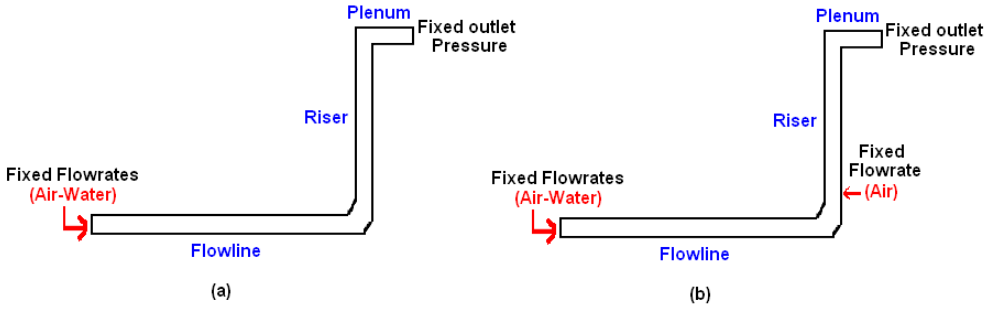

Figure 6.3 The boundary condition used in OLGA simulations.

6.4 Results – from First Model

This set of the results constitute the initialization of the cases as steady state and followed by the transient simulation performed in OLGA using first model developed. The model was first tested with respect to the flow regimes in the flowline-riser. In OLGA-ver5.1, a command called "Steady State pre-processor" exists that utilizes the point equation model and is used for generating the initial values for transient simulations. Since the steady state simulations were not computationally intensive, many cases were simulated for the wide range of experimental flow rates, refer to appendix D that summarizes all the cases with horizontal flowline-vertical riser experimental results. The Figure 6.4 below shows the flow regime prediction in the riser by steady state pre-processor when two phase air-water flows from the upstream of horizontal flowline. The data points correspond to the flow regimes predicted by the pre-processor (OLGAS). The code predicts the cases as bubbly, slug and annular flow according to its flow regime classification for

vertical flows. The code prediction are contrary to that observed in experiments, where under similar conditions of air-water superficial velocities bubbly, agitated bubbly and churn/froth flows were observed.

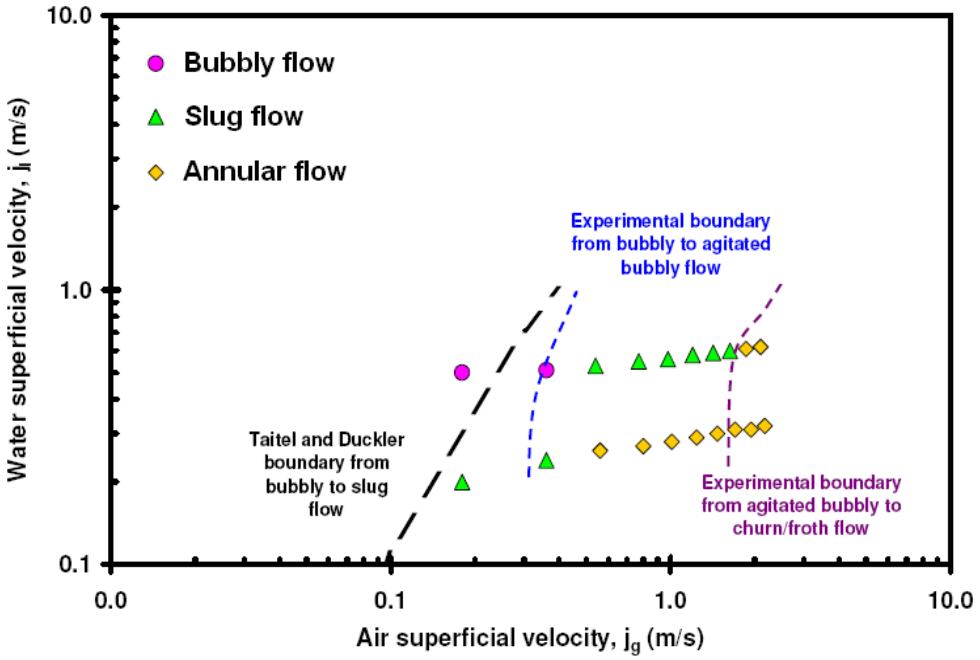

Figure 6.4 The steady state flow regime prediction in the riser for upstream flowline two phase air-water flow.

6.4.1 Case A1

For the first example, the case considered is of the lowest air-water superficial velocities (j_w = 0.18 m/s and j_a = 0.20m/s). The flow regime determined indicated that under above air-water superficial velocity range, the flowline was under stratified flow while riser indicated bubbly flow. In comparison to above, the code steady state and dynamic simulation both predicts the stratified flow in the flowline and in the near riser base vicinity with the slug flow occurring in the remaining riser sections. The predicted flows agrees with the experimental result for flowline only but does not predict the flow regime riser sections correctly i.e. slug flow is predicted instead of bubbly flow (refer to Figure 4.52 for steady state results or see Appendix D). The Figure 6.5 indicates the experimental pressure profiles from the riser base and the flowline exit (2m downstream) as a function of time along with the simulated results of the OLGA.

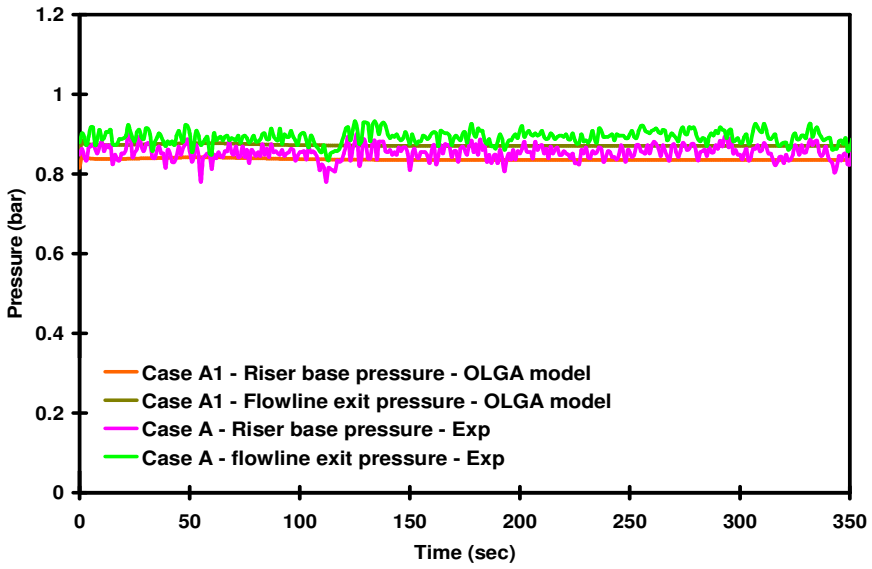

Figure 6.5 The experimental and simulated flowline exit and riser base pressure response for Case A.

The experimental pressure profiles suggest that the fluctuations in the flowline are of smooth stratified flow regime while that of the riser base are for the bubbly flow. It can also be observed from the riser base pressure time traces that the case A1 is a typical bubbly flow with a high riser base pressure due to hydrostatic weight of the liquid column with small void fraction variation. The code predicts the mean near riser base pressure as 0.834 bars in comparison to the actual mean pressure of 0.853 bars. There is a good agreement between the simulated riser base mean pressure and the experimentally observed value of within 2%. It can also be noted in the figure that the OLGA simulates this case as constant average pressure profiles. The constant average pressure profiles are indicating the stable nature of the flow in the flowline as well in the riser base vicinity. This can be attributed to the fact that both the stratified and bubbly flow encountered are considered to be stable flows, hence it is likely that that the code tends to smoothen out small pressure perturbations when using average boundary conditions in comparison to the experiments. The liquid holdup in the flowline and near riser base was not determined in experiments; however liquid holdup was measured at the heights equivalent to that of section 5 and 8 in the code. Figure 6.6 shows the simulated holdup predictions and the experimental average liquid holdups in the riser sections 5 and 8. The predicted liquid holdup values are slightly lower than the experimentally determined values. This under prediction in the liquid holdup is also reflected in the near riser base pressure trends where this under prediction has resulted is slightly lower hydrostatic head.

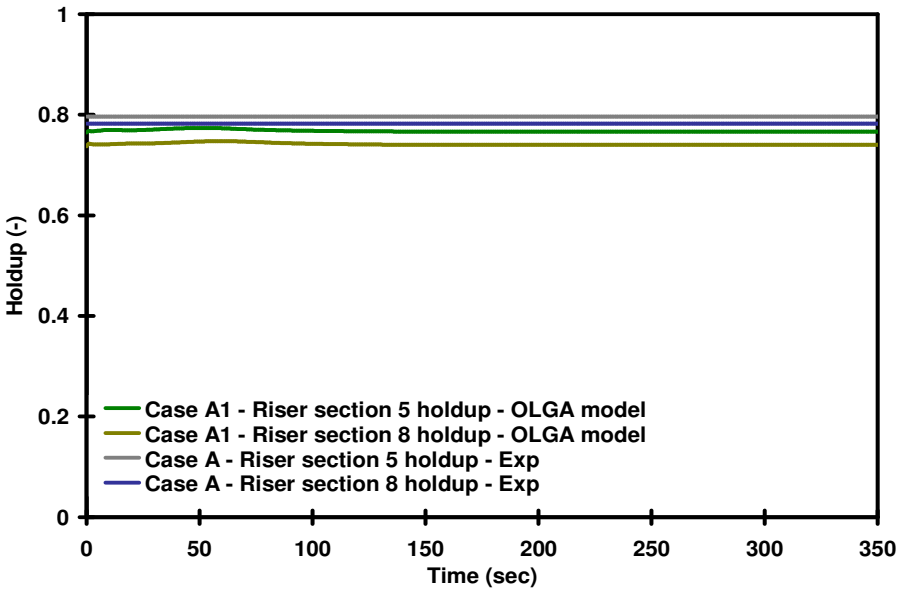

Figure 6.6 The OLGA simulated and average experimental liquid holdup predictions for Case A1.

6.4.2 Case B1

As a second example case B1 was taken (see Figure 6.2), this particular case is chosen to demonstrate the above model's ability to simulate the unstable cyclic nature of the flow as observed in the experimental conditions. The case is for low superficial water velocity with highest superficial air velocity (j_w = 0.32m/s and j_a = 2.17 m/s). In fact this particular flow is a continuation of slugging that had started occurring at slightly lower gas velocities (refer to section 4.3.2, see Figure 4.46d) but for this highest gas flow rate it appeared more periodic.

According to the flow regime map (Taitel *et al.*, 1976), no slug should be present under the flow condition of the case B; however slugs were already formed at these low liquid velocities. In context of current experiments their presence is attributed to the upstream and downstream topology of the flowline i.e. the elbow connecting flowline to the riser (refer to section 4.3.2, see Figure 4.43d). It postulated that this terrain influence allows slugs to be present for the flow conditions which normally would result in stratified flow. This configuration caused the accumulation of liquid due to slowing down of the water and thereby initiating slug formation in stratified flow regime. The near riser base pressure response of this flow regime is indicated in Figure 6.7. The figure shows the regular arrival of slug near the exit of the flowline with slugging changing to almost periodic sinusoidal type, regularly varying with minimum and maximum pressure of 0.3 to 0.6 bar and with cycle time of 10-12s. Notice two aspects first; the cyclic behaviour with slug build-up which corresponds to an increase in riser-flowline pressure due to liquid build-up in the vicinity; (however

this liquid build-up is small) and second, there is no slug production period. During this partial build-up, gas in the flowline is being temporarily compressed, moves in towards riser base with high velocity pushing the short accumulated pool ahead in the riser. In this situation since the air superficial velocity is quite high compared to the liquid superficial velocity, consequently the liquid fall back is not enough to block the base completely for long and there is continuous gas penetration as suggested by the constant pressure variation in the flowline.

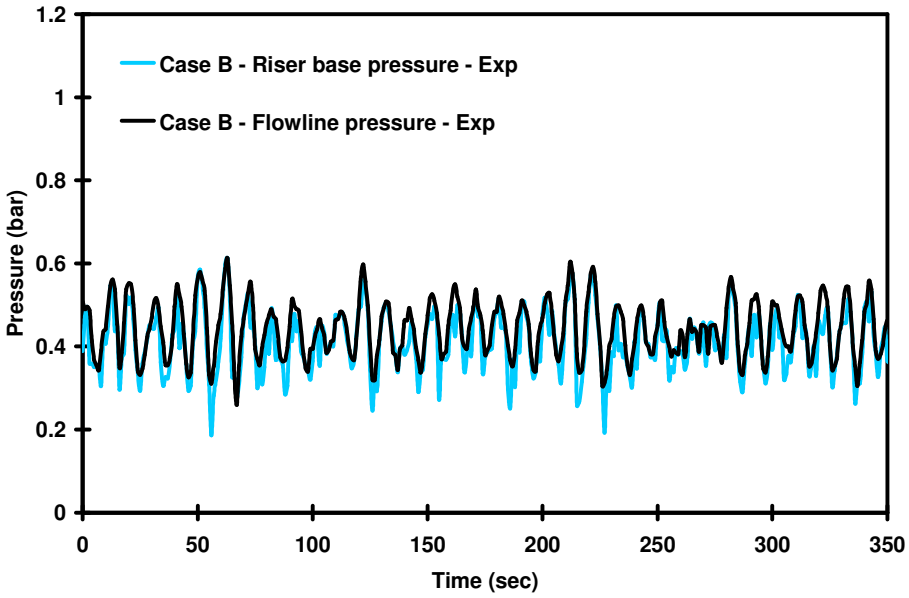

Figure 6.7 The flowline and riser base pressure response for Case B1 from the experiments.

Similar pressure cycling behaviour is also observed by other researchers in smaller diameter horizontal flowline-vertical riser configuration (Schmidt *et al.*, 1980; Fabre *et al.*, 1990). However the unique aspect of this case, in comparison to the earlier work is that liquid slug pushed up by the available gas drive is dissipated completely or partially, turning to churn/froth type of flow in later sections by the highly distorted bubble clusters travelling upward with high velocity. Finally, churn frothy mixture sloshes out of the plenum with some of the liquid falling back on the upcoming flow in the riser.

The Figure 6.8 indicates the OLGA simulated flow regimes IDs in flowline and riser for case B1. The code designates flow regimes as numerals, on the plot they have been displaced slightly upwards by a small offset to aid clarity. The code predicts hydrodynamic slugging in the flowline and annular flow in the riser section.

Above behaviour of the code indicates that in case of the slugging in the flowline, the code is completely dissipating the created liquid slug in the riser base vicinity making annular flow ahead in the later sections. Although situation does corresponds to experiment slightly but slugs formed in the flowline were observed to dissipate while travelling upward in the riser in experiments. This trend further indicates that firstly the code does not distinguish between hydrodynamic slug flow and terrain induced slugging and produces the same slug flow in both cases. Secondly, since the code does not classify churn/froth flow as an individual flow therefore the transition from slug flow is to annular flow.

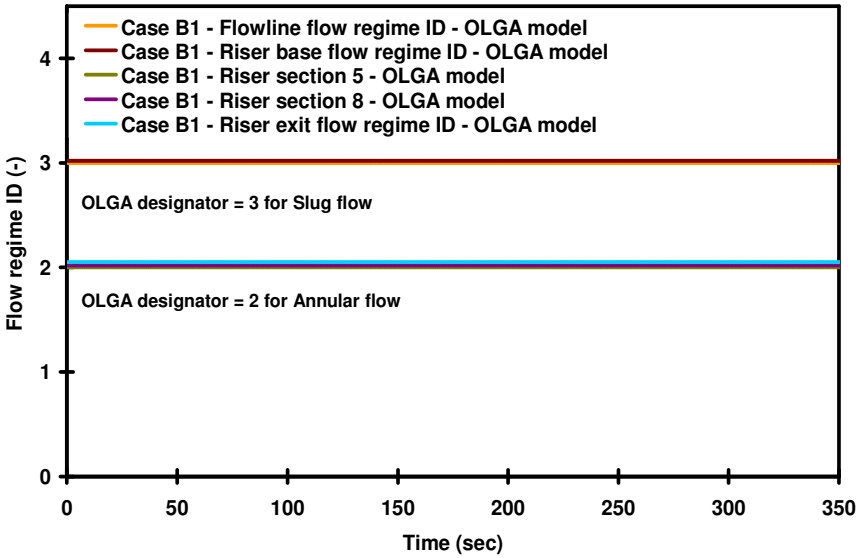

Figure 6.8 The simulated flow regimes by OLGA for Case B1.

The simulated flowline exit and near riser base pressure responses from the code along with the experimental results are shown in the Figure 6.9. In the figure, the pressure profile appears quite stable for both flowline and the riser base. The simulated mean pressure is around 0.208bar in comparison to mean value of 0.413bar from the experiments. It is to be noted that the flow during the experiments remained highly intermittent (0.186 – 0.714bar minimum and maximum) in comparison to simulation. This behaviour is attributed to the incorrect flow regime predictions, where the code predicts the case as annular flow and hence a stable pressure profile. Note the small surges at the start of the simulated profiles (in Figure 6.9) are due to initialization of the case and are decayed down as the solution proceeds towards the stable behaviour. This shows that the model developed must be run for sufficient period of time to ensure the phase behaviour is fully developed in the code.

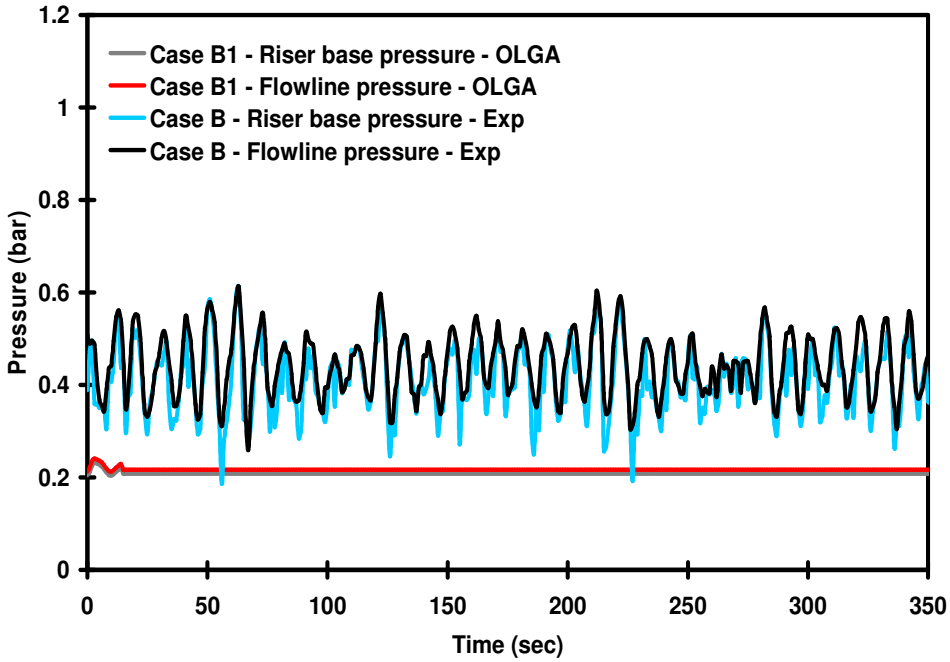

Figure 6.9 The simulated flowline and riser base pressure response for Case B1.

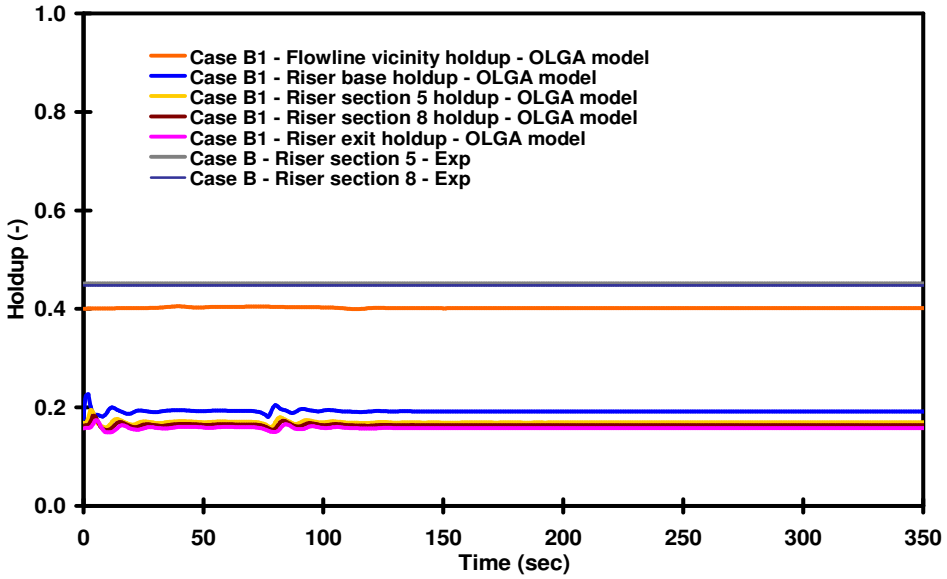

Figure 6.10 The OLGA simulated and average experimental liquid holdup predictions for Case B1.

In Figure 6.10, the model's holdup predictions for this particular case are shown. The figure also shows the experimentally determined steady state average liquid holdup values from section 5 and 8 in the riser. From the figure, the importance of the correct flow regime prediction is highlighted as the liquid holdup predicted is quite lower than the experimentally determined value at section 5 and 8 due to annular flow regime prediction. Note that the simulated liquid inventory is high in flowline in comparison to the liquid hold prediction in the riser. This is due to the code prediction of annular flow with liquid film at the wall flowing downwards and liquid droplets carried up by the gas.

6.4.3 Case C1

The third case tested for this model is the case C1 which is taken at higher liquid and gas superficial velocities (j_w = 0.61 m/s and j_a = 1.86m/s). The flow regime map indicates this case to be in slug flow. The interesting feature of this case is the longer aerated slugs coming from flowline upstream due to increase in liquid inventory. However in comparison to previous case B1 this case indicated higher and more irregular pressure cycling, see Figure 6.11. This is due to the instability of the flow i.e. hydrodynamic slugging alongside the downstream topology (elbow) with the uneven gas penetration in the riser base compounding the whole process, so the pressure cycling is more excursive rather than sinusoidal varying as in case B1. The further details of this case are similar to that explained in Chapter 4 (refer to section 4.3.2, Figure 4.46g-h)

In contrast to above the experimental near riser base and flowline pressure response, Figure 6.12 shows the code simulated near riser base and flowline response. In the simulations for this case, oscillations are reproduced. It should be noted that the code did not show any significant variations within first 100seconds and appeared more or less as a steady. However later, pressure cycling starts to set in slowly, and gradually the amplitude level off and become apparently constant after 211seconds. From this behaviour, it is obvious that the model is not predicting this case accurately. This behaviour of slugging was observed in the experiments at lower gas superficial velocities than shown by the code (see Figure 6.2, case F). The behaviour of the code does indicate an important feature, that the code does not distinguish between hydrodynamic slugging and terrain induced slugging.

To further demonstrate this effect, the case is explained in detail next. Considering the case C in detail, refer to Figure 6.13; from t = 0 to 100s, the code indicates a stable liquid bulk flow at the exit, however at t = 110s there is an increase in liquid bulk flow at the riser exit verifying the arrival/exit of the slug (Figure 6.13). After t =110s onwards, entire riser is experiencing pressure cycling (i.e. slug flow) indicating that the slugs formed are travelling up the riser (Figure 6.14). At t = 211s, a long slug arrives at the riser exit and bulk liquid mean velocity becomes negative, indicating that gas available does not posses enough drag to take the whole liquid slug up in the separator and the some liquid falls back (Figure 6.13). The increase in the immediate riser base holdup cycle verifies this liquid fall back (Figure 6.14). Thus, the next

incoming slug is longer; indicating that incoming slug from flowline and the fall back has compounded this unstable process. From above behaviour, the code may be judged to predict the unstable behaviour in general terms only.

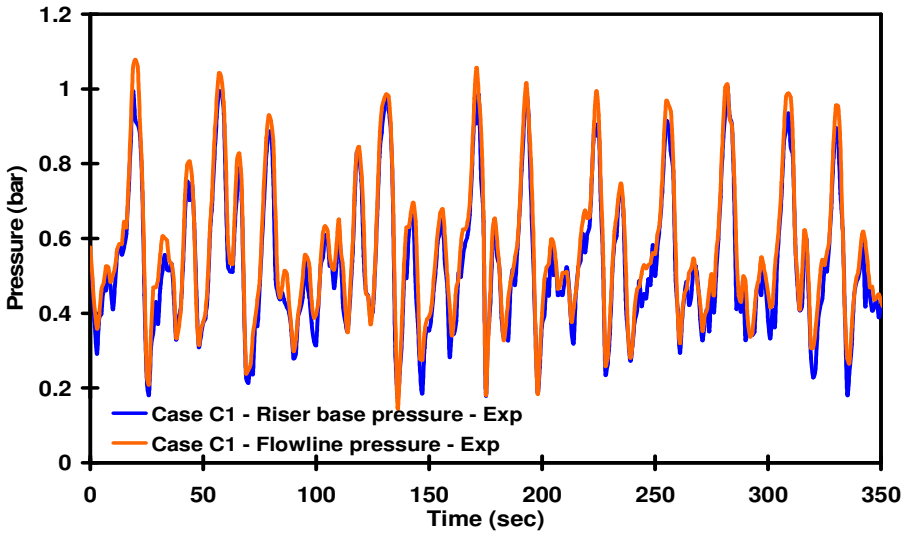

Figure 6.11 The experimental flowline and riser base pressure profile for Case C1.

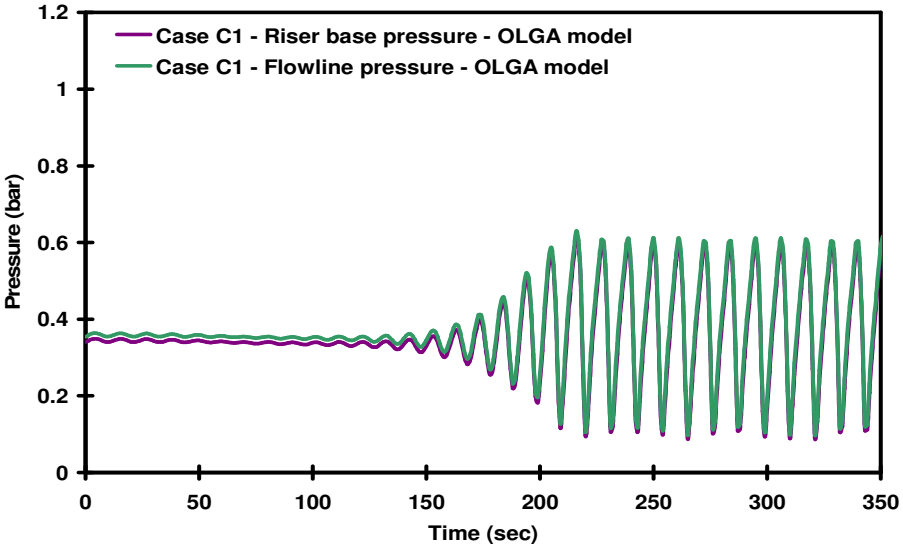

Figure 6.12 The simulated flowline and riser base pressure prediction by OLGA for Case C1.

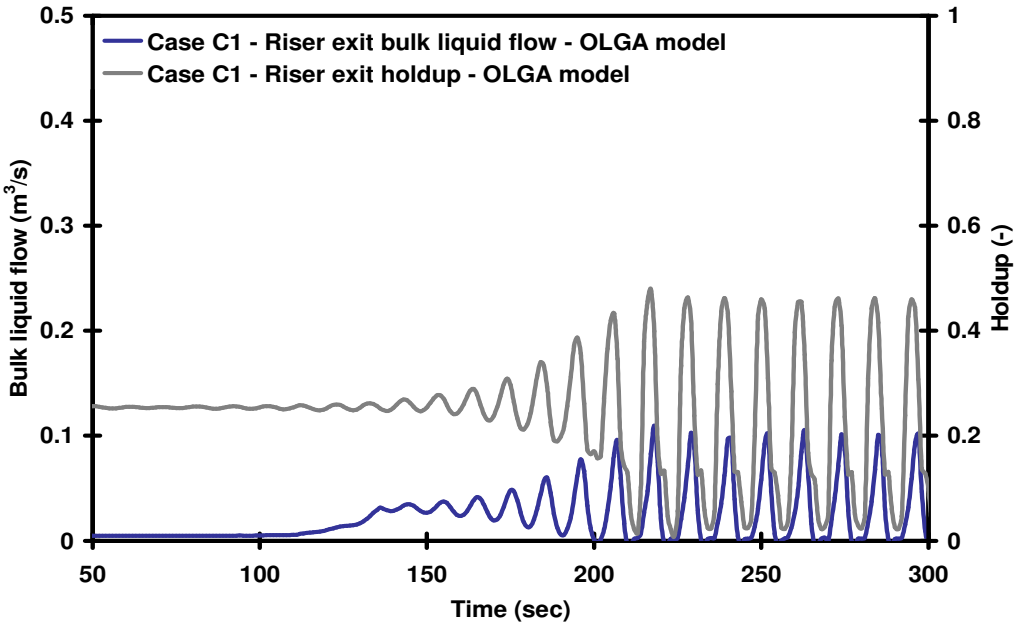

Figure 6.13 The simulated riser exit bulk liquid flow and holdup by OLGA for Case C1.

Although the steady state prediction of the code is slug flow in flowline and annular flow in the riser, an interesting feature between above time period (from t = 211s onwards) in dynamic simulation is flow regime ID flipping between stratified-to-slug in the flowline and bubble-slug-annular in the riser. According to the Montgomery (2002), for conditions where the case lies near the flow regime transition as in this case, some variation in output should be expected. However, this flow regime flipping can be regarded as the non-physical attribute indicated by the code.

From the behaviour defined above case, the code may be judged to predict the unstable behaviour in general terms only, further indicating that the onset of terrain slugging is not represented in the code directly and need to be inferred. Moreover the code under predict the riser base pressure (simulation =0.371bar and experimental = 0.5328bar) for this unstable flow. This is because the code is globally under predicting the liquid holdup (see appendix D). The maximum and minimum pressures (0.611bar and 0.087bar) in the simulations are also lower then actual values of the experiments. This means that the code under predicts the size of the liquid slug as well as the liquid inventory at the base while over predicting the slugging frequency.

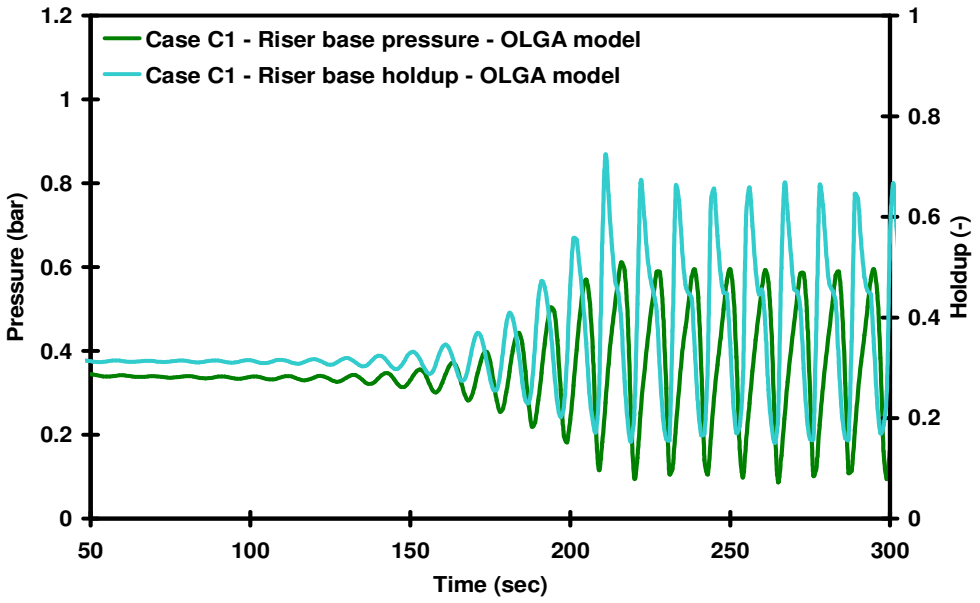

Figure 6.14 The simulated near riser base bulk liquid flow and holdup by OLGA for Case C1.

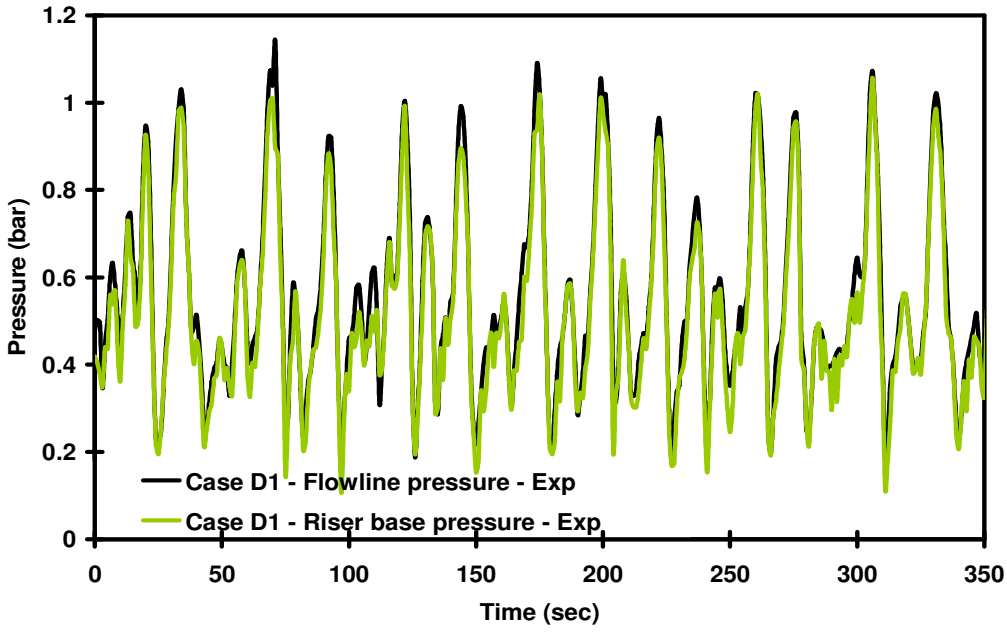

Figure 6.15 The flowline and riser base pressure response for Case D from experiments.

6.4.4 Special Case - D1

The next case tested is the case D which is the highest water-air superficial velocities case (see Figure 6.2). The case is important because in this case, flowline was in highly slugging condition with long air bubbles and liquid slugs. Moreover there was temporary blockage due to the liquid accumulation, with flowline almost being empty after the liquid was pushed up by the comparatively large air pocket in the riser (refer to section 4.3.2, Figure 4.45). Later this air pocket seems to penetrate within liquid slug, dissipating it to churn/froth type of flow (refer to section 4.3.2, Figure 4.44). In comparison to case B and C this case indicated more irregular chaotic pressure cycling, see Figure 6.15 (also refer to section 4.3.2, Figure 4.46g). The simulation results of this case are very important, as well as interesting because they display the weakness of the code and emphasize numerical stability problems. It is reminded here that this particular case was run in OLGA ver5.1 as well as in ver5.2, both indicated similar problem; although the latter version proved to be less stable in comparison to the former.

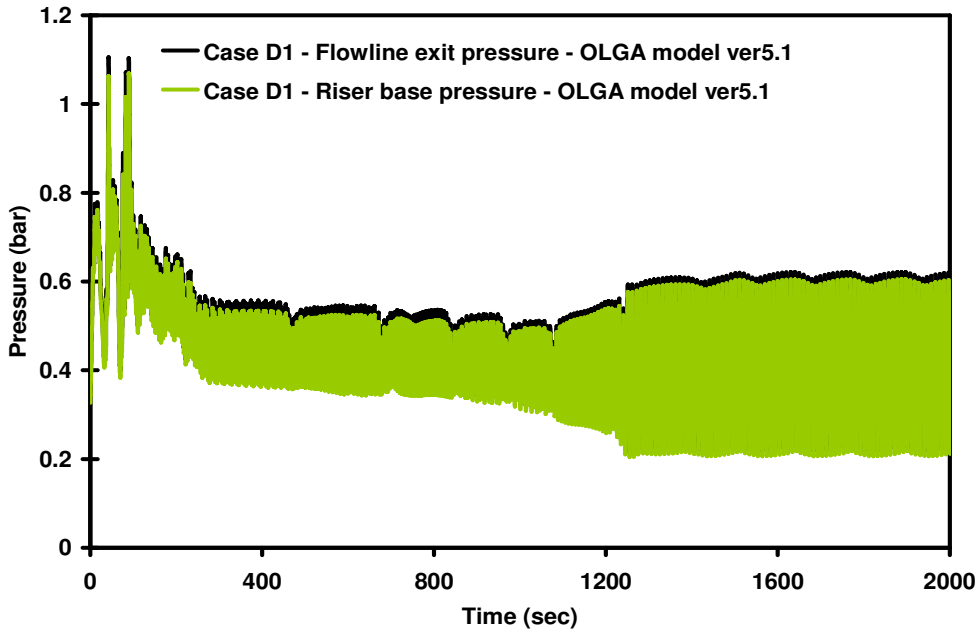

Figure 6.16 The simulated flowline and riser base holdup prediction by OLGA for Case D1.

Similar to earlier case, the code steady state prediction indicates slugging in the flowline and annular flow in the riser but the dynamic run of the case continued to show variety of flows. There is no physical explanation to this behaviour other than it has arisen because of a numerical problem within the code. Figure 6.16 indicates the OLGA simulated flow riser base and flowline exit pressure profile for case D. The

discrepancies between the experimental and code predicted trends are evident. The simulated pressure trends do not follow the measured trends (Figure 6.15). Note that the simulated pressure trend has been reproduced with considerably longer period of the time to demonstrate the nature of the simulated trends. By analyzing the trends in Figure 6.16 in detail, it is noted that there are at lest two states indicated by the code after initial unsteady state (t = 0-300s, at approximately t = 400 - 1200s and t = 1300 - 7200s). This indicates that the initial state and one immediately after this are highly unstable and leaving the last state as the only stable state under above conditions. The new steady state parameters are different from the previous two states; although nothing has been altered in the model i.e. the model still has same boundary conditions.

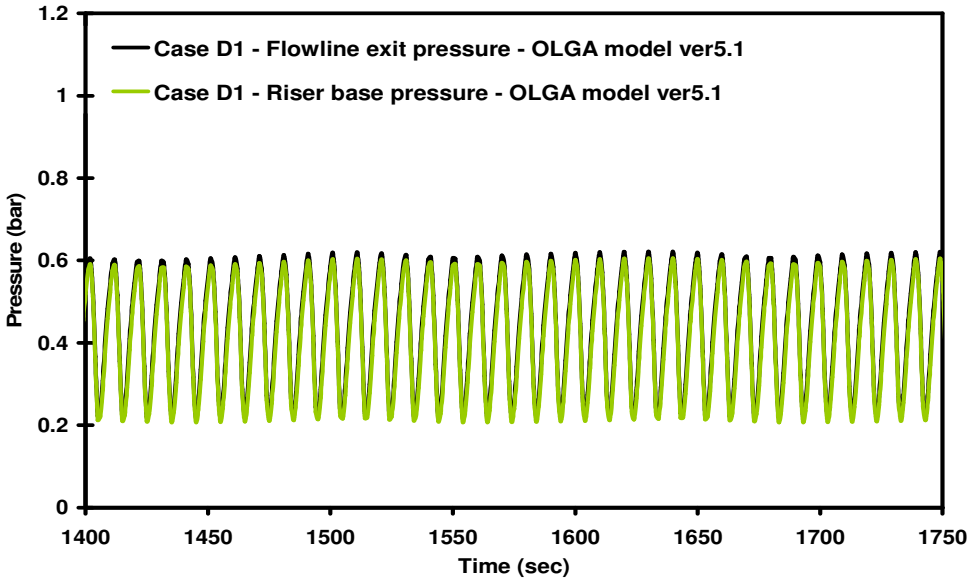

Figure 6.17 The detailed simulated flowline and riser base pressure prediction by OLGA for Case D1.

The Figure 6.17 above shows the details of the part of the stable solution offered by the code. As obvious, the sinusoidal pressure cycling suggests the code is predicting this flow to be unstable; however, note the cyclic trends are of regular amplitudes. This behaviour is in contradiction to the experimental observation as it indicates a more irregular cycle representing an uneven gas penetration in the base. In figure it can also be noted that the maximum pressure is considerably lower while the minimum pressure in the simulation (0.605 and 0.208 bar) is higher then seen in the experiments (1.05 - 0.11bar). This signifies that the stable solution offered by the code is under predicting the liquid slug size and leaving more liquid in the base and flowline vicinity. The slugging frequency indicated in the simulation is also higher in simulation (approx 35 slugs in 350s to 29 in 350s) and more regular then

experimental values. The mean pressure in simulation is around 0.414bar (75% of the experiment, 0.5514bar). This again signifies the under prediction of the liquid holdup.

Above behaviour of the OLGA code is quite unusual; it is revealed that this is an example of the two fluid model yielding multiple roots or non-unique solution (Lockett, 2007). With OLGA, there are some evidences of the code giving multiple roots for conditions such as upward inclination angles, low liquid velocities and low/medium gas velocities (Lockett, 2007). However since the code is of propriety nature not much information is available on its 1D-two fluid model and closure relations, also no available work in public domain on the code has ever reported such a behaviour.

The problem of multiple roots or non-unique solution was first discovered by Baker & Gravestock (1987) when applying the 1-D stratified flow model based on Taitel and Dukler (1976) work. Multiple roots results when the momentum balance equations for separated flow model are solved to determine the liquid height (or liquid holdup). Under the given flow conditions and fluid properties, generally this liquid height has a unique value, however for certain conditions, it exhibits a region in which three solutions for the liquid height in the stratified/wavy flow regime exists. This result has an important bearing as the three values of liquid heights leads to erroneous value for total pressure gradient due to triple value of gravitational pressure gradient. This non uniqueness causes the models to fail as it is unable to determine the unique solution. Multiple roots are generally reported for the cases where the gas-liquid interface is smooth, flow is laminar becoming more evident in the case of upward inclination (Ullmann *et al.*, 2003). Ullmann *et al.* (2003) further states that in general, the multiple roots issue arises due to *"the inherent weakness of the closure laws used for the shear stresses and, in particular, the interfacial shear stress"*. The determination of the interfacial shear stress through interfacial friction factor (f_i) introduces the empiricism in the model. Numbers of empirical correlations for interfacial friction factors have been proposed, however the Taitel and Dukler (1976) model assumes that in the stratified region the interfacial friction factor and gas frictional factor are equal. Generally in most cases of multiple roots, the lowest value is taken as the relevant solution for specified conditions of operations and the highest and intermediate equilibriums are regarded as being unstable (Landman, 1991; Barnea and Taitel, 1992; Oliemans & Pots, 2006). OLGA also uses the similar criteria and selects the root exhibiting minimum holdup (maximum gas volume fraction) as the possible solution. In the code, this stable solution is achieved by changing the initial conditions (Lockett, 2007) discussed further in later sections.

In order to check the non unique solution region of stratified flow in air-water system of 254mm diameter pipe, the original Taitel and Dukler (1976) model was revisited. The model is known to give very accurate results for upto ±10° and reasonable estimates for higher degree inclination (Barnea, 1987). The equivalent curves for the dimensionless liquid height were developed with particular emphasis on the multiple roots region. The original model can be referred in Taitel and Dukler (1976) work. The Figure 6.18 displays the plot of the dimensionless liquid height ($\hat{h}_L = h_L/D$) as a function of the Lockhart-Martinelli parameter (X) for above system. For a 254mm

diameter horizontal or downward inclined pipes ($Y \geq 0$), the Taitel and Dukler model indicates a unique value of liquid height for any value of Lockhart-Martinelli parameter (X). However for upward inclined pipes ($Y < 0$) of similar size, a small multiple roots region can be observed, where there exist three liquid height values for one particular value of Lockhart-Martinelli parameter (X) for the cases of Y = - 4.72 and -6.23. Based on the above, it is obvious that the multiplicity of liquid height is only possible for upward inclined pipes and even a small change of 1° upward from the horizontal can have a major effect on the stratified to non-stratified transition boundary and hence codes based on separate flow model can experience multiple root problem. It can also be noted from the figure that for this size of pipe the multiplicity of roots lie at very low ratios of Lockhart-Martinelli parameter (ratio of liquid to gas flow) which correspond to the region of very low liquid superficial velocity with very high gas superficial velocity.

In current experiments no liquid holdup measurements were made in the near vicinity of horizontal flowline-vertical riser base to confirm the above results obtained. However considering the flowline to be horizontal, no multiple roots region is expected, as shown on the figure. Moreover, the region encompassing the multiplicity is out of the range of the experiments conducted ($10^{-4} \leq j_l \leq 0.01$m/s and $30 \leq j_g \leq 35$m/s). It is not clear why OLGA encountered the multiple roots problem during computation, nonetheless OLGA experiencing the computational problem in the cases of flowline ending at the vertical riser has been documented earlier (OLGA, 2000).

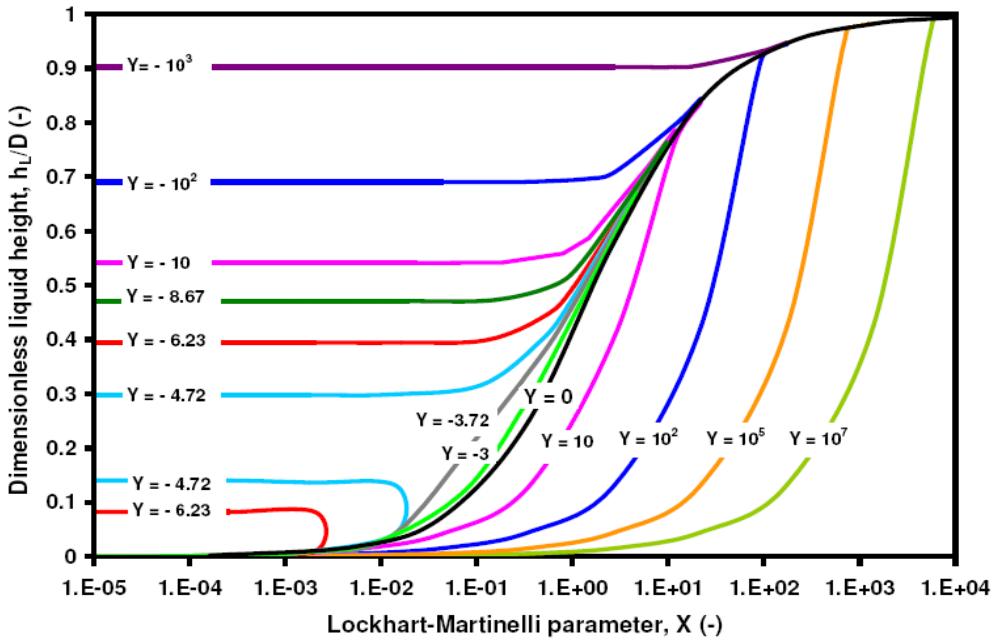

Figure 6.18 The Taitel and Dukler (1976) relation showing liquid height vs. the Lockhart-Martinelli parameter (X) (for D=254mm pipe, turbulent/turbulent flow regime & $f_i / f_{sg} = 1$).

During the writing up of this work, Scandpower has introduced a newer version of the code OLGA 5.3. It has been claimed that the newer version of the code incorporates improve numerical stability. As this particular case has proved to be a tough case for the code (OLGA 5.1 and OLGA 5.2), the case was re-run in the newer version. Below we present the results obtained, in running the simulation in the newer version, no changes has been made to the original model.

The Figure 6.19 presents the simulated riser base and the flowline exit section pressure responses. The difference between the results from the two versions (Figure 6.16 & 6.19) is evident, while the multiple roots existed for older version, newer version does not indicate this problem verifying the numerical stability claim. The code now directly reproduces the most stable root i.e. the minimum liquid holdup (maximum void fraction). Figure 6.20 shows the details of the pressure response where the mean riser base pressure is 0.382bar with minimum and maximum riser base pressure of 0.082 and 0.747bars respectively. The new version has produced identical response as of stable root in the ver5.1. Even the cyclical behaviour is reproduced quite well. However it is to be note that this riser base pressure is still different than observed experimentally. The lower value of the predicted riser base pressure is also indicating a lower value of liquid inventory in the riser i.e. the code is under estimating the slug size, with more liquid left in the system in actual to initiate intense slugging. This highlights that the selection of this stable root could lead to serious implications with respect to the sizing of liquid handling facilities at the downstream.

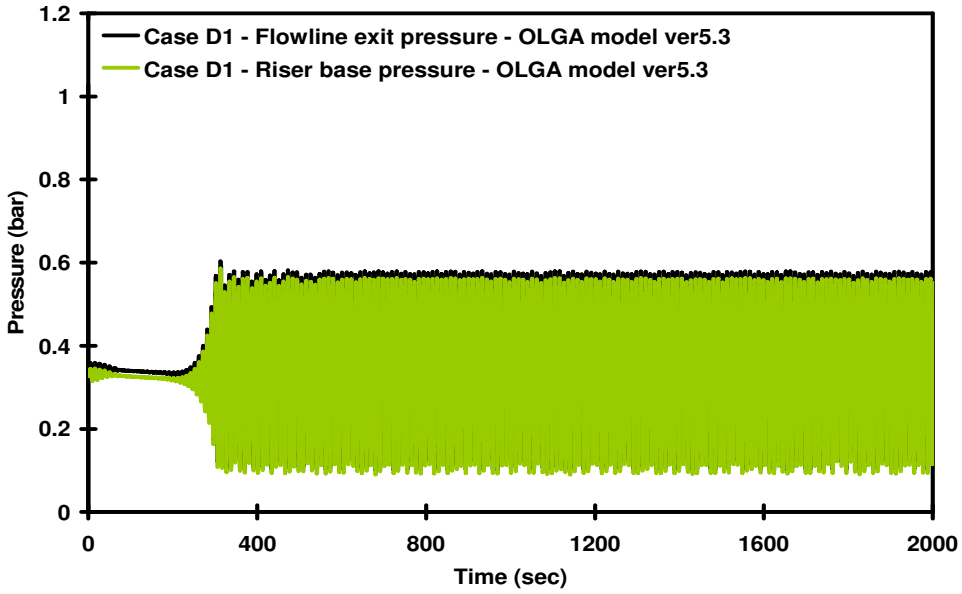

Figure 6.19 The simulated flowline and riser base pressure prediction by OLGA for Case D1 by OLGA ver5.3.

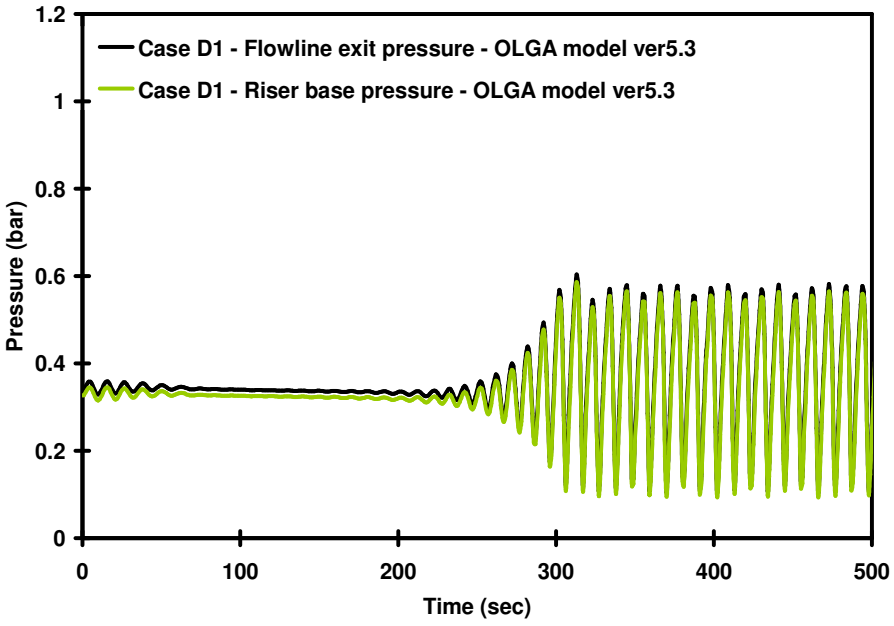

Figure 6.20 The detailed (0 – 500s) simulated flowline and riser base pressure prediction by OLGA for Case D1 by OLGA ver5.3.

6.4.5 Case E1

Under this case, stable plug flow was observed in the flowline whereas pure bubbly flow prevailed in the riser section (also refer to section 4.3.2, Figure 4.46e). The air-water superficial velocity range was j_w = 0.18 and j_a = 0.50m/s respectively. The difference between this case E and case A is of former being at the higher liquid flow rate making more dispersed but bubbly flow at the inlet to the riser in comparison to the case A, where the flow regime at the inlet to riser was possibly more agitated possibly due to the stratified flow in the flowline. In contrast to prevailed flow regimes above, simulated flow regimes by the code for this case is stratified flow in the flowline and in the riser base vicinity with bubbly flow in riser sections ahead. The bubbly flow regime in the riser is simulated by the code in this case correctly where as the code prediction of riser base flow regime appears to be influence by incoming flow from the exit node of the flowline. Figure 6.21 shows the simulated flowline exit and riser base pressure prediction for this case. Like case A, a stable profile is indicated over lying on the experimental trends of a dispersed bubbly flow. The simulation pressure is around 0.907bar in comparison to 0.912bar in the experiments. The results are in good agreement with the experimental results.

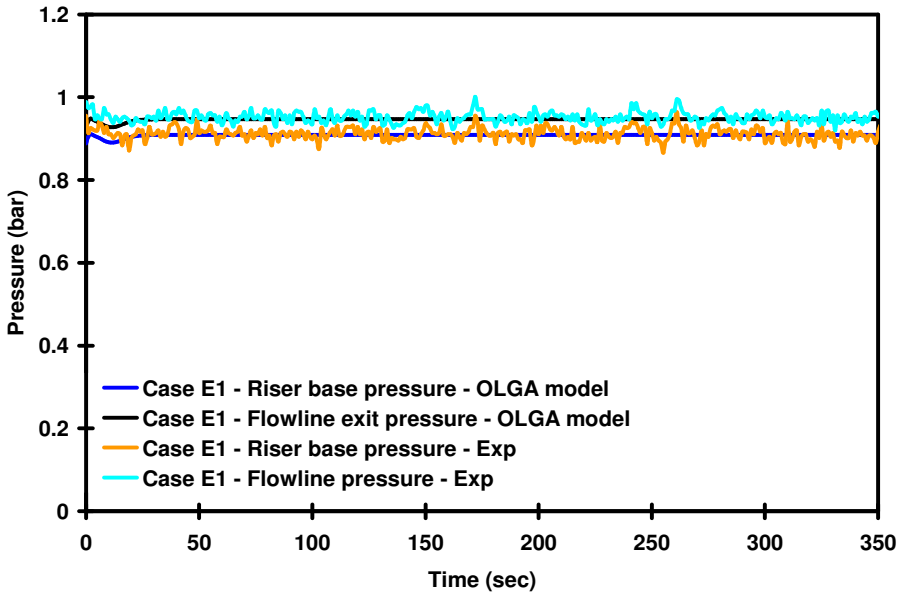

Figure 6.21 The simulated flowline and riser base pressure prediction by OLGA for Case E1.

6.4.6 Discussion on first model predictions

OLGA preliminary model has been applied and the result of the four cases; two dealing with the stable flows and other two related to unstable flows were presented. It is reminded that this model was based on steady state average boundary conditions and the criterion for bench marking was to be able to simulate the flowline and riser base pressure variations and flow regime predictions.

The developed model was first tested with respect to the flow regimes in the flowline-riser. The code accurately predicted flowline flow regime for the cases A and B only and failed to predict the cases C, D and E. For cases A and B, the flowline flow regime was indeed stratified and slug flow in the experiments. For case C, it was intense slugging in experiments which had started occurring at much lower gas superficial velocities, unlike the code prediction of initially stratified flow turning into slug flow. In the experiments, the case E was of plug flow but the code predicted it as stratified flow. The code recognized the bubbly flow in riser section in the case E only but predicted the bubbly flow of case A as slug flow. For cases B, C and D the code did not recognize unstable slug and churn/froth flow. It is pointed out that while agitated bubbly, unstable slug and churn/froth flow are not recognized by code due to

its strict classification (bubble, slug and annular flow for vertical flows), it interesting to note that code predicted bubbly flow as slug flow in case A, churn/froth flow as annular flow (in case B) accompanied by numerical flipping of flow regimes between bubble-slug-annular in cases C and D. This highlights firstly, that the code's flow regime mechanism is not able to distinguish between the agitated bubble and slug flow pattern and churn/froth and annular flow pattern, thus classifying them as slug and annular flow respectively. Secondly, the code also does not distinguish between hydrodynamic slugging and terrain induced slugging and produces the same slug flow ID in both cases. This further indicates that the onset of terrain slugging is not represented in the code.

The simulated riser base pressure by the code for cases A, B and E under steady state average gas-liquid flowrates with constant outlet pressure turned out to be stable. Indeed case A and E are of stable bubbly flow and but cases B, C and D are not. The case B belongs to the churn/froth flow but due to incorrect flow regime (annular flow) predictions, the code predicts the case as stable flow. From the simulated behaviour of the case C, it is suspected that the code does not distinguish between hydrodynamic slugging and terrain induced slugging. In the case D with OLGA ver5.1, multiple roots problem was encountered by the code. It is seen that for this case, not only the pressure disturbances amplify with time but they also move to lower state. This means that that the simulation indicates that this case does not possess an initial stable dynamic state. However, after running simulation for long period of time the amplitudes level off and become apparently constant after 37minutes yielding the minimum stable root. The multiple roots issue was resolved with same model being run in OLGA ver5.3, with code directly yielding the most stable root as the only answer. However, the predicted pressure and liquid inventory was still underestimated.

While the code is in good agreement in stable flow cases A and E, the code globally under predicts average riser base pressure in the unstable flow cases B, C and D. Thus the average, maximum and minimum pressures in latter cases are also lower then actual values in experiments. This implies that the code under predicts the liquid inventory at the base. Based on the results of first model it is obvious that while the code did predict the stable flow cases satisfactorily it was unable to predict the unstable flows accurately. In fact the experimental pressure variations are larger than the code anticipates. The code was only partially able to predict the unstable flow. This later aspect motivated the study presented in the next section whereby some modification techniques are employed to improve the model results for unstable flow cases.

6.5 Modifications to the First Model

Many techniques in the light of the literature survey were investigated to achieve a closer match between the first model predictions and experimental data. They include; (i) tuning with pipe roughness, (ii) modifying outlet gas fraction, (iii) initializing with air filled system and, (iv) varying the separator pressure.

The model was first investigated with respect to geometry lay out. Since the geometry was found in accordance with the actual lay out, this lead us to the conclusion that the simulation differences especially the under estimation of liquid holdup predictions might not have arise from any simplification of the geometry. In order to further confirm that the geometrical effect not being the influencing factor on the global under prediction of liquid holdup, the single phase riser base pressure profiles from the code were plotted against the experimental results (see appendix D). No significant differences between the predicted and experimental values was observed, hence this difference in liquid holdup between the simulation and experiments can solely be attributed to the over prediction of void fraction by the code.

In many of the field studies tuning the model with pipe roughness is performed to match the results (Kashou, 1996; Putra, 2002 and Song and Peoples, 2003). The changes in this parameter additionally, also results in changing the flow regime (Bendiksen *et al.*, 1991) e.g. increase in pipe roughness will result in earlier flow regime transition and vice versa. For current experiments, schedule-40 stainless steel pipe was used, for which generally the pipe roughness is taken as 0.025mm (Miller, 1990). However this value changes, once the pipe is exposed to the working fluids such as tap water during the current experiments. In the first model the average pipe roughness (ε = 0.035mm) obtained from the experiments were used as an input to the model. This value is close to a relatively new pipe.

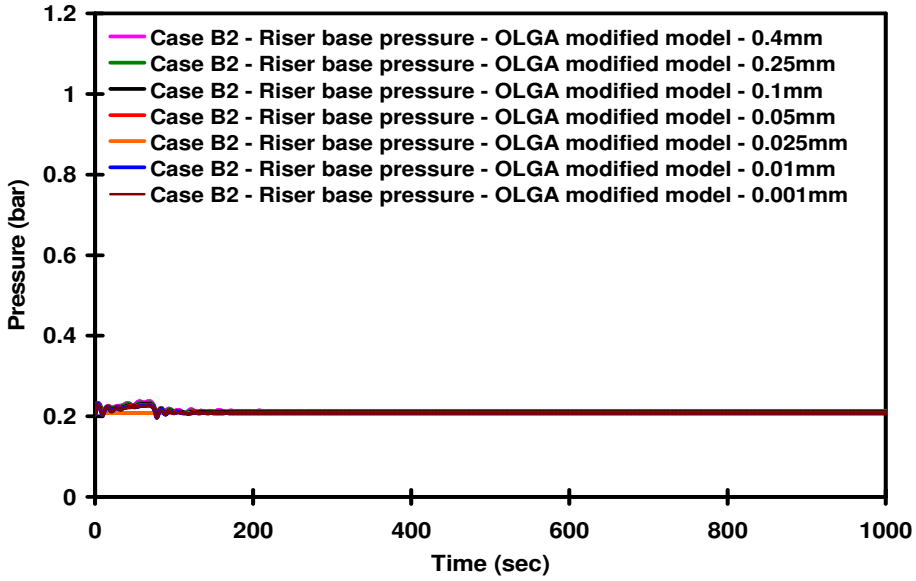

Figure 6.22 The effect of roughness on the riser base pressure profile for Case B.

Based on predictions of the first model with above pipe roughness, a parametric study was executed with roughness values of 0.0001 (very smooth pipe) to 1mm (heavy rust). Although the above exercise did not improve results but the outcome was not irrelevant either. In fact, these modified results demonstrated that the tuning of the roughness within the above applied limits has no considerable effect on the behaviour of these cases (B, C and D) and both pressure magnitude and flow regimes were quite insensitive to it. Figure 6.22 indicates the results for the case B, while for sake of brevity the results of other cases (C and D) are not presented here but are appended in appendix D.

In order to improve the model predictions of the cases, outlet gas fraction was modified. This was carried out on the basis of the steady state solution obtained from OLGA that suggested that the system was gravity dominated. In this technique the value of gas fraction at the outlet boundary node was manipulated. In the OLGA, it is usual practice to set this value equal to 1. As mentioned in the section 6.4.6, in the base model the value of gas fraction was set equal to 1 to avoid the possibility of inadvertently occurring liquid inflow at the outlet boundary. This inflow of the liquid results if the pressure in the last pipe section falls lower than that of the boundary and it may lead to difficulties in obtaining a stable solution. Alternatively the gas fraction on the outlet boundary was set to zero (0) to represent the liquid suck back from the outlet boundary to be possible. The above different treatment of the outlet boundary condition resulted in only slight differences in the period and amplitude of the oscillations in all the cases.

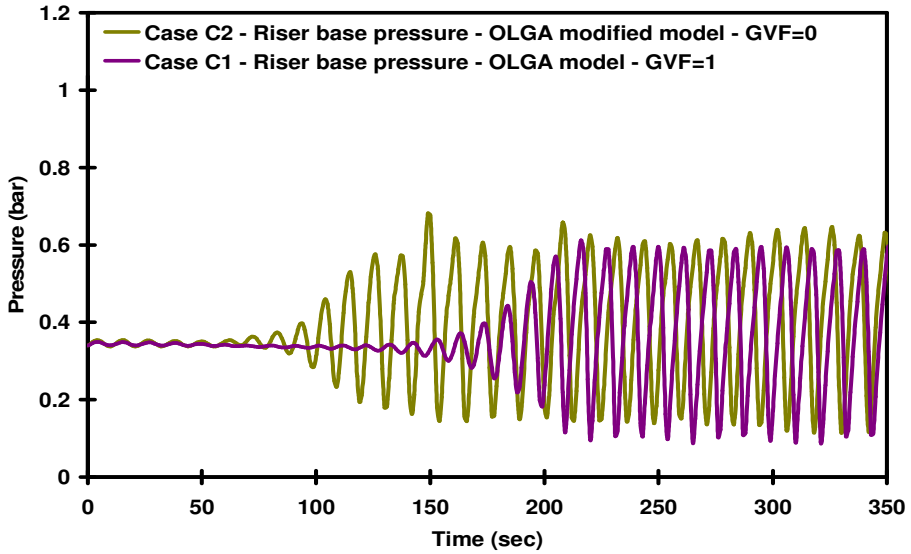

Figure 6.23 The results of the riser base pressure simulation for Case C (GF = 0 & 1).

The Figure 6.23 above shows the comparison between the two models for case C only. Note in the figure that by using GF = 1 at the fictitious cell near the exit, code prevent liquid from going back into the riser while GF = 0 allows the liquid fall back and hence an earlier transition to unstable flow in comparison to the previous condition. However though the GF change resulted in an earlier transition to slug flow, the flow regime ID for this case still predicted a stable annular flow. The modelling of the remaining cases by modifying the GF resulted in only limited success; refer to Appendix D for the cases B and D.

For dynamic modelling, the initial conditions must either be specified from steady state simulation or user must specify, whether the simulation should start with an empty/filled pipe. This technique was applied by initializing the cases differently then the OLGA steady state preprocessor. It was performed because while using transient simulation models, the result obtained by the preprocessor are not necessarily the same as the result obtained by running with constant flow for extended period of the time (Eidsmoen *et al.*, 2005). These differences are usually caused by the terms included in the dynamic model not being in the steady state preprocessor. Thus, the selected cases were initialized with an air filled system. The cases were then run for 6 hours to establish a dynamic steady state. The subsequent simulation in each case is then based on this dynamic steady state. The results of these simulations indicate that the system settles down to the final dynamic steady-state in each case at a different time period. While the case B took 50 seconds, case C took 25 minutes and case D took 22 minutes. Although from this modification, the model predicted the cases as stable or unstable qualitatively in all three cases, yet the overall riser base pressure behaviour was still not predicted correctly. As an example see Figure 6.24, the modified result of the case B which was earlier indicated as stable annular flow (see Figure 6.9) now with gas filled system initialization indicated a typical unstable flow. Note that the simulated riser base pressure trends by the code now predicts the case as typical terrain induced slugging type II, with slug production period, a continuous gas penetration and small slug formed at the base due to liquid fall back. However this behaviour was not observed in the experiments.

It is to be noted here that for the multiple roots issue in the code, initialization from an air filled system was recommended (Lockett, 2007). Therefore, case D was initialized as an air filled system so that the case can reach a dynamic steady-state that is independent of the initial condition of the system. The results of this case are presented in appendix D from running the OLGA ver5.1 as well as OLGA ver5.3. Similar to the simulated results of the first model (Figure 6.16), OLGA ver5.1 results for the gas filled system initialization of the case D confirms that the system is unstable, as predicted experimentally. However the simulation still indicated the multiple roots. The gas filled initialization affect of this case was also studied with OLGA ver5.3; the results obtained are similar to the ones presented in Figure 6.19 i.e. the model yielded the same stable root directly (see appendix D).

Lastly, a numerical study was performed by varying the separator pressure. This study was performed in order to verify whether the effect of boundary condition variations was the cause of the differences between the simulations and the experiments. For the cases simulated, all the input parameters in the model were kept the same (as in 1st model) except that the separator pressure was varied by +5% and +15%. The overall results obtained from +5% variation of separator pressure do not show significant changes from the first model results with riser base pressure trends slightly higher than first model but still under predicting with no changes in the flow regimes under all the cases. For maximum variation of +15%, an overall change in mean pressure is noted. The case C showed a mean pressure of 0.523bar (experimental value = 0.533bar, first model = 0.3711bar) but with an earlier transition, (at t = 100s, before t = 150s) to unstable flow in comparison to the first model results, see Figure 6.25. For case B, +15% variation resulted in an increase of mean riser base pressure to 0.363bar (experimental value =0.413bar, first model results = 0.208bar) but riser base and flowline still indicated a stratified-slug flow with a stable annular flow in the riser sections ahead (refer to appendix D). This result of boundary pressure variation signifies that the outlet boundary condition variation has influenced the experimental results and a controlled outlet pressure is necessary for realistic simulation.

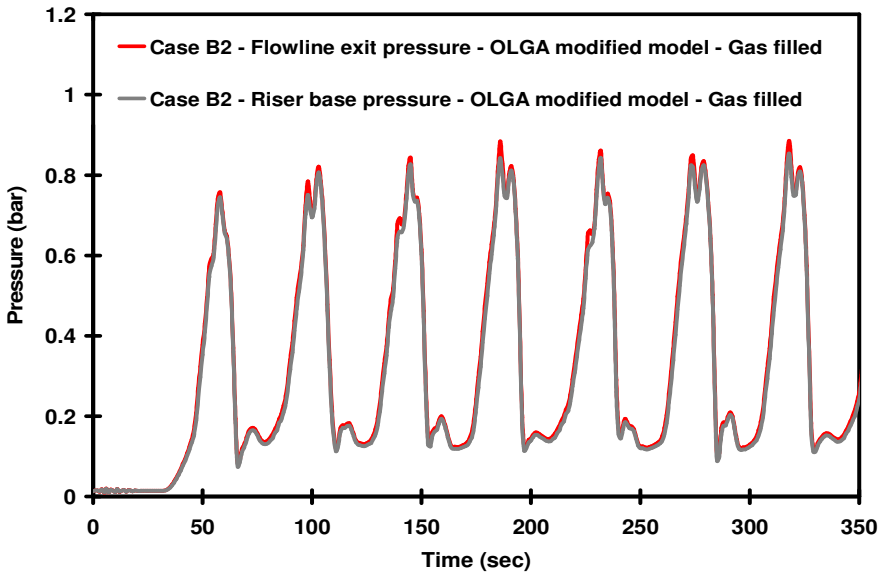

Figure 6.24 The results of the riser base pressure simulation for Case B with gas filled system initialization.

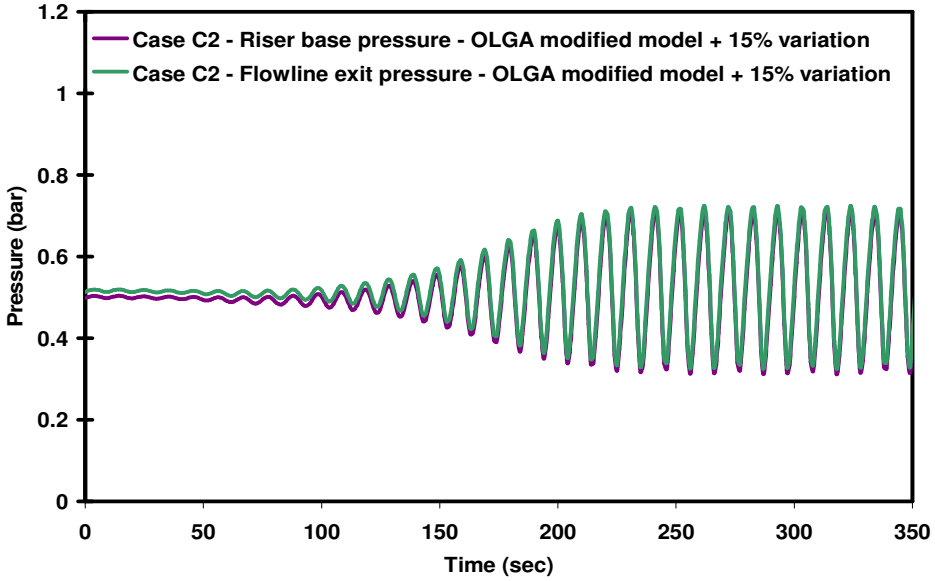

Figure 6.25 The effect of the magnitude of boundary condition variation for Case C – 15% variation.

6.6 Results from the Extended Model

As outlined in earlier section, all the attempts to improve the first model predictions by applying modifications in the above cases did not resulted in any significant improvements. However, the outlet boundary pressure variation did show that this parameter may have influenced the results. Hence, it was concluded that the possible option was to change the boundary condition to more realistic input rather then using steady state average values. This is because during unstable flows, the boundaries of the system are most affected and hence parameters at these boundaries display the similar affect. A satisfactory approach to this was to use the experimental time series input as the boundary conditions for the modified model. In this respect the separator pressure series was the appropriate choice however since the upper plenum was open to atmosphere, it was decided to use the near exit pressure sensor response of the riser instead. In this regard an online application feature of the OLGA code was explored where the real process condition can be picked up from the process in real time and is fed to the model (Lockett, 2007). Consequently the experimentally obtained pressure at the near riser exit is applied as the separator pressure. All other conditions were kept same as mentioned in earlier section (6.4-6.6). Admittedly, this change does bring the mean pressure in the simulation and the riser base closer to each other as a consequence of the head imposed ($\leq$ 0.1bar). However, it has been already demonstrated from steady state and first model results that the code is under predicting the liquid holdup. Therefore even with this alteration at the outlet boundary, the model will be able to mimic the actual conditions encountered during the experiments. Thus if positive results are obtained from the simulations, it at least

indicates that the code is capable of capturing the dynamics of typical unstable flow phenomena in large diameter horizontal flowline-vertical riser.

6.6.1 Case B3

The results from the extended model for the case B are presented in Figure 6.26. The code still incorrectly predicts the flow regimes in flowline-riser, similar to the first model. However, the interesting change in the simulated results was the riser base pressure trend indicating the similar unstable flow behaviour with oscillations as observed in experiments (see Figure 6.26). In comparison to the mean riser base pressure of the first model (0.208bar) and the experimental value (0.413bar) (also see Figure 6.9), the mean riser base pressure predicted by this extended model is 0.272bar. This is the consequence of the head imposed. The predicted slugging frequency in simulation is same as the experimentally observed however slugging cycle is underestimated by the code. This under prediction of the slugging cycle is accompanied by the underestimation of the slugging amplitude. Both the factor can be attributed to the underestimation of the liquid holdup by the code. From the figure one can notice that the simulation indicates that there is continuous large amount of gas penetration in the riser base with stratified flow in the flowline.

6.6.2 Case C3

The steady state model and first model results of this case have identified this flow as the slug flow in flowline and in the riser base while annular flow in riser sections ahead. The extended model still indicates same variety of flow regimes but unlike the first model and its modifications, the application of new boundary condition has resulted in predicting the flow as unstable flow from the beginning of the simulation like observed in experiments. The Figure 6.27 below shows the riser base and flowline exit pressure trends. The mean riser base pressure predicted by the extended model is 0.438bar in comparison to the 0.533 bar observed in experiments. Although the riser base pressure amplitude is still under predicted by the code (see Figure 6.11), the application of the new boundary condition in the model has now reproduced the overall riser base pressure trends at least qualitatively. Some of the slugging cycle/oscillations along with kinks as observed in the experiments are also replicated, as these oscillations and kinks were not simulated before, they can be attributed to the presence of pressure fluctuations due to the newly imposed boundary condition. It is likely that the code tends to smoothen out such surges when using steady state average boundary conditions. Also note that the individual cycle time in the trends are still in error because of the slight time shift between simulation and data set but the reasons of this are unknown, similar time shift is also seen in Yeung *et al.* (2003) work.

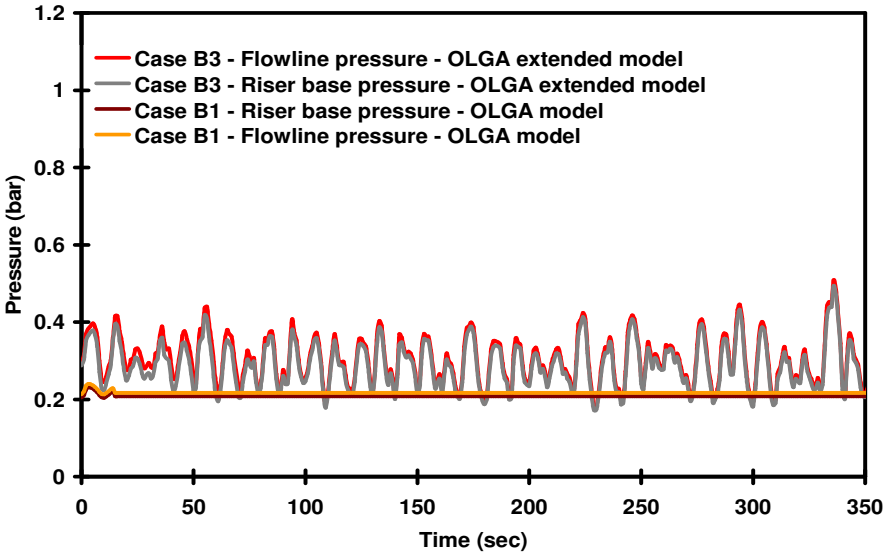

Figure 6.26 The OLGA extended model results of the riser base pressure profile for Case B.

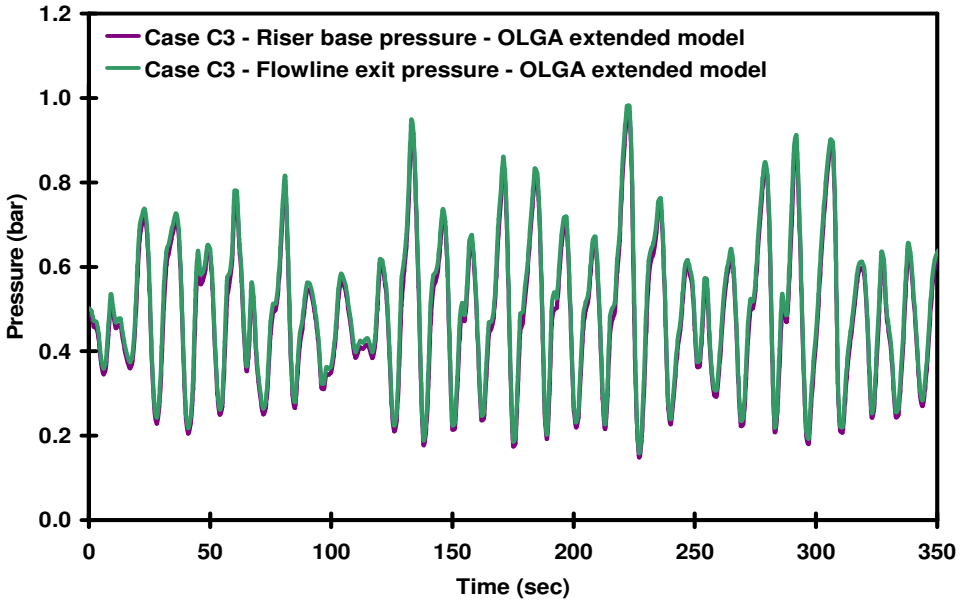

Figure 6.27 The OLGA extended model results of the flowline exit and riser base pressure profile for Case C.

6.6.3 Case D3

This case has proved to be the toughest case for the code as it demonstrated the weakness of the code's two fluid model (refer to section 6.5.4).

Similar to the results of the first model and gas initialization modification, extended model's riser base pressure trends (from OLGA ver5.1) do not follow the experimental observations. By analyzing the extended model response, see Figure 6.28, it can be noted that still there exist the highest unstable root, intermediate partially stable root and lastly, the lowest stable root. It is to be noted that the trends are shifted upward; this is due to the consequences of imposed riser exit pressure time series at the outlet node. Overall the application of the extended model on this particular case in OLGA ver5.1 did not resulted in different response that seen in earlier section. The extended model application in ver5.3 on this case did not resulted in any success with code terminating the run prematurely.

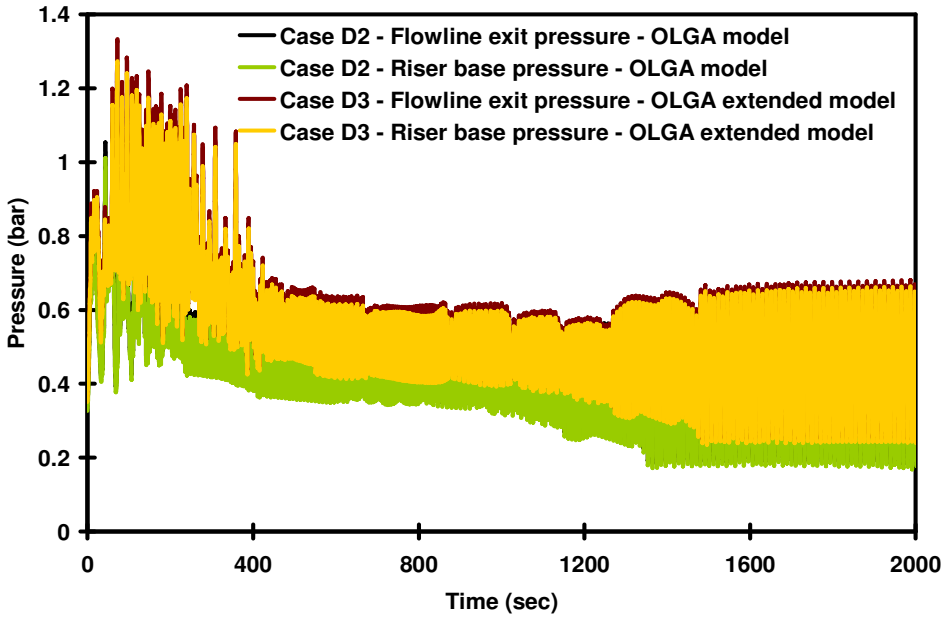

Figure 6.28 The OLGA extended model results of the flowline exit and riser base pressure profile for case D (from OLGA ver5.1).

6.6.4 Case F3

Consider case F next, this case deals with air-water superficial velocities of 1.24 and 0.29m/s respectively. This case demonstrates the code behaviour near transition in flowline as well as in the riser. In the flowline, flow transformed from stratified wavy to slow moving slugs, while in the riser this change brought the transition from

agitated bubbly flow to churn/froth flow. This case can be considered to be exhibiting the initial behaviour that later changed into case B, i.e. more regular slugging in the base vicinity. This flow regime is not previously observed in small diameter vertical pipe where under similar conditions slug flow regime is observed. The flow regime is different then the bubbly flow in riser test section previously stated in case A and E. Current set of experiments have proved that this is indeed the most dominant flow regime in large diameter vertical pipe. With above flow in riser section, flowline flow pattern was highly stratified wavy with waves frequently touching the top of the pipe initially that later changed into small slugs (also refer to section 4.3.2, Figure 4.46c). The Figure 6.29 below show the experimental response of the flowline exit and riser base pressure of this case. It can be noted that initially the flow is more irregular due to wavy/roll waves flow turning into small slug at the end.

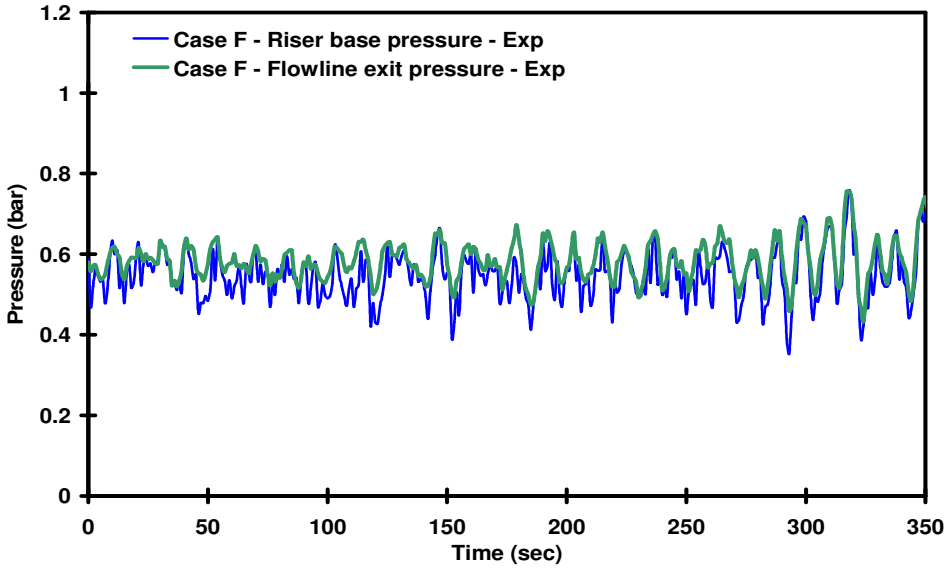

Figure 6.29 The experimental flowline exit and riser base pressure profile of case F.

The steady state flow regime prediction of this case is slug flow in flowline and annular flow in riser sections ahead; however dynamic run shows variety of flows in the riser. The application of the extended model has brought no change in flow regime predictions of this case. Figure 6.30 indicates the simulated behaviour of the code for this case, the figure shows that the code predicts this case to be slugging whereas it is near the transition from stratified to slug flow in the experiments. The application of the extended model (mean riser base pressure = 0.434bar) has qualitatively increase the riser base pressure (first model mean riser base pressure = 0.297bar) but there is still an under prediction of the riser base pressure due to the underestimation of the liquid holdup. Both the first and the extended model in the code underestimated the liquid holdup in comparison to the experimental values. This

also signifies the fact that the underestimation might be due to the incorrect flow regime predictions that are based on the closure relations used.

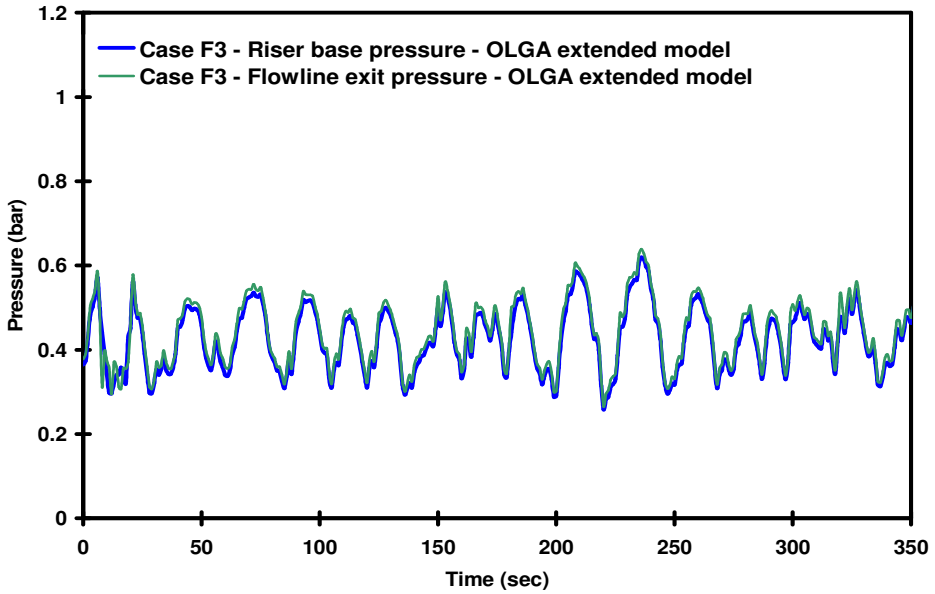

Figure 6.30 The OLGA extended model results of the flowline exit and riser base pressure profile for case F.

6.6.5 Case G3

This case G is of air and water superficial velocities of 1.20 and 0.58m/s respectively. The case is similar to case F above in terms of gas superficial velocity but with higher water velocity. The application of the model in this case can identify the code's ability to predict dissipating characteristic within the riser section. The case belongs to the intense slug flow in the flowline with unstable slug flow in the riser section (refer to Figure 4.46f-g).The unstable slug flow in the riser where the flow exhibited the remains of slug flow structure (from the flowline) but was less stable as the flow was transforming into semi churn/froth flow while travelling up the riser due to the penetration of large distorted gas bubbles. Figure 6.31 indicates the experimental riser base pressure profile for this case; the flow appears to be highly chaotic with frequent slug arrival from the upstream of the flowline along with smaller slugs formed in the base vicinity due to liquid fall back from the riser.

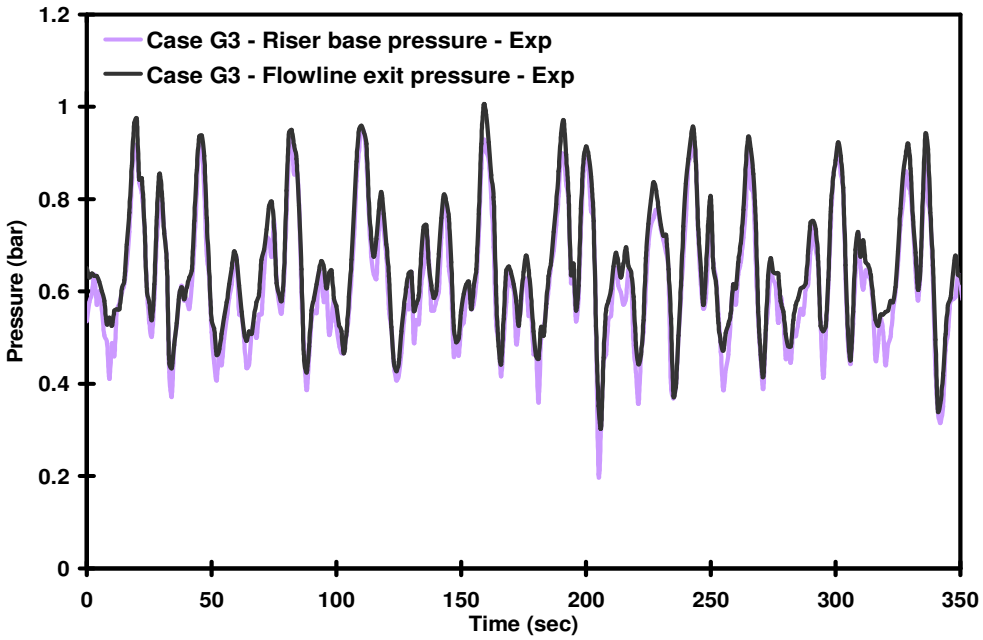

Figure 6.31 The flowline and riser base pressure response for case G from experiments.

The steady state flow regime prediction of this case is correctly predicted by the code as slugging in the flowline but the code also predicts slugging in the riser. This later simulation results does corresponds to the experimental observation slightly as some liquid bridging was seen. Both the first and extended models predicted this flow incorrectly. This means that the application of the new boundary does not affect the code flow regime prediction mechanism in anyway.

In comparison to the experimental results in Figure 6.31, the Figure 6.32 presents the simulated results of the extended model. Note the riser base pressure cycling now has some similarity with the experimental observation, although it appears to be more regular than experiments. The simulated results show 24 regular slugs in 350s in comparison to 30 irregular slugs in the experiments. The codes under prediction of the slugging frequency can be attributed to fact that it did not generate the small slugs formed in the base due to the liquid fall back in the riser base as seen in the experiments; rather it indicates the long flowline slugs only. This means that although the slugging phenomenon in experiments was compounded due to hydrodynamic slugging and terrain effect of elbow at flowline-riser connection, in simulation it's the result of hydrodynamic slugging only.

The minimum and maximum pressure cycling is still under predicted by the code along with the amplitude. This reflects the under prediction of the liquid inventory that also results in less number of slugs formed and overestimation of the gas volume fraction in the system by the code. The overestimation of the gas fraction results in driving the less liquid inventory out more frequently from the riser.

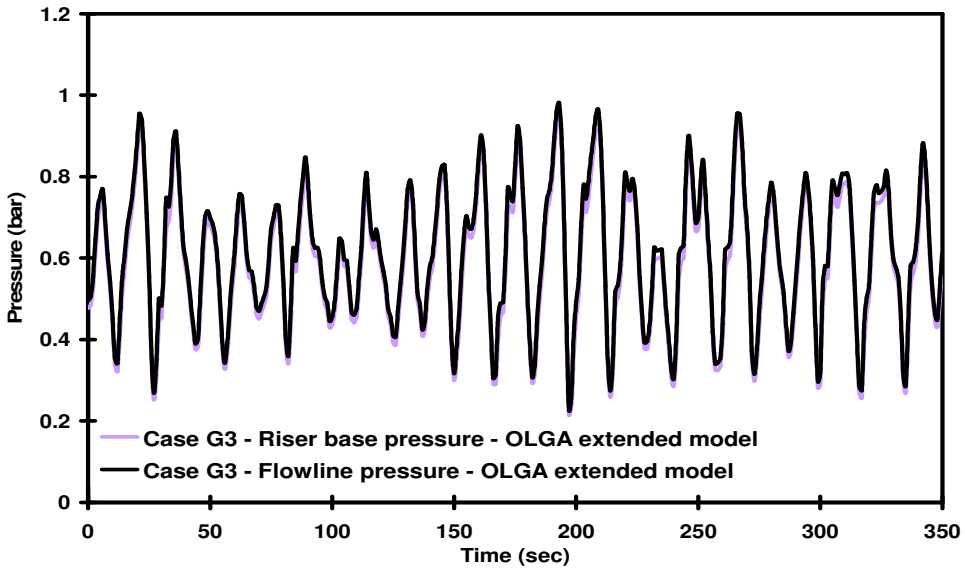

Figure 6.32 The OLGA extended model results of the flowline exit and riser base pressure profile for case G.

6.6.6 Case H3

This case and the following case deals with testing the riser base gas lift capabilities within the code. In both the cases, air injections into the flowline inlet as well as in the riser base were performed. The objective of doing this set of experiments was to verify whether the riser base injection is able to effectively dissipate the liquid slugs originating from the flowline. The case was conducted with the flowline inlet air and injected air superficial velocity equal to 1.70m/s and 0.46m/s respectively. The water superficial velocity was 0.31m/s. As such no changes have been made in the first model or extended model other than the introduction of an air injection source at the riser base section.

The conditions prevailing before the gas injection was performed in this case were typically of regular slugging, also represented in Figure 6.33 with the mean riser base pressure around 0.461bar (max = 0.675bar and min = 0.269bar). The addition of the riser base injection appeared to aid: (a) the slug dissipation mechanism via increasing the aeration in the incoming liquid slug and breaking the liquid slug (see Figure 6.32), (b) reduce the riser base pressure as well as that of the flowline - causing small slugs and thus higher cycle frequency than that of without gas injection and, (c) reduce the cycle time of slugging. Note that the mean riser base pressure has lowered (0.400bar) along with the maximum and minimum values observed (max = 0.529bar and min = 0.237bar).

Figure 6.35 shows the void fraction probability mass function plots taken from the riser section 5 (a-c) and 8 (b-d) for both the above two conditions of this case; (i) before air injection or upstream gas injection only and (ii) riser base injection by the injector. The upstream gas injection condition (Figure 6.35a-b) indicates some survived liquid slugs indicated by the broader distribution and thick tail. The riser base injection shows a more uniform distribution representing a transformation to churn/froth type of flow (Figure 6.35c-d). The addition of the injected gas has aerated the riser to the extent that the flow is more of churn/froth flow and, the incoming slugs are diluted. This demonstrates that gas injection increases the stability of the flow by the changing the flow pattern in the riser.

Although the code's first model results of this case indicated a stable annular flow in the riser, with slugging in the flowline dissipating in riser base (see appendix D), Figure 6.36 shows the case simulated in with extended model. Note that the flow now appears to be qualitatively similar to the one seen in the experiments. In the figure the starting 2-2.5minutes does not include the riser base gas injection hence the flowline is slugging while after the introduction of the riser base gas injection, the slugs breaks up and become aerated hence the flow appears to be more like observed in Figure 6.34. This demonstrates that for this particular case, the injected gas has effectively dissipated the slugs. The mean riser base pressure in simulation is around 80% of the value (0.328bar). This clearly identifies that the liquid holdup prediction mechanism in the code is underestimating the liquid inventory. It is probable that the liquid accumulation due to the fall back before riser base injection is not reproduced with sufficient accuracy in the code. From above simulated case, it is clear that code is able to predict the slug formation and its dissipation via gas injection.

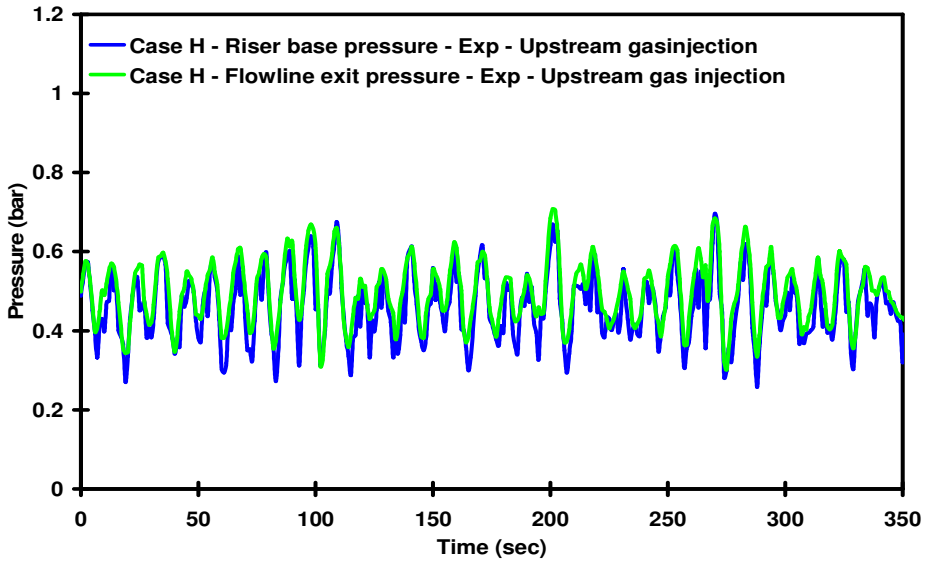

Figure 6.33 The flowline and riser base pressure response for case H from experiments – Upstream gas injection.

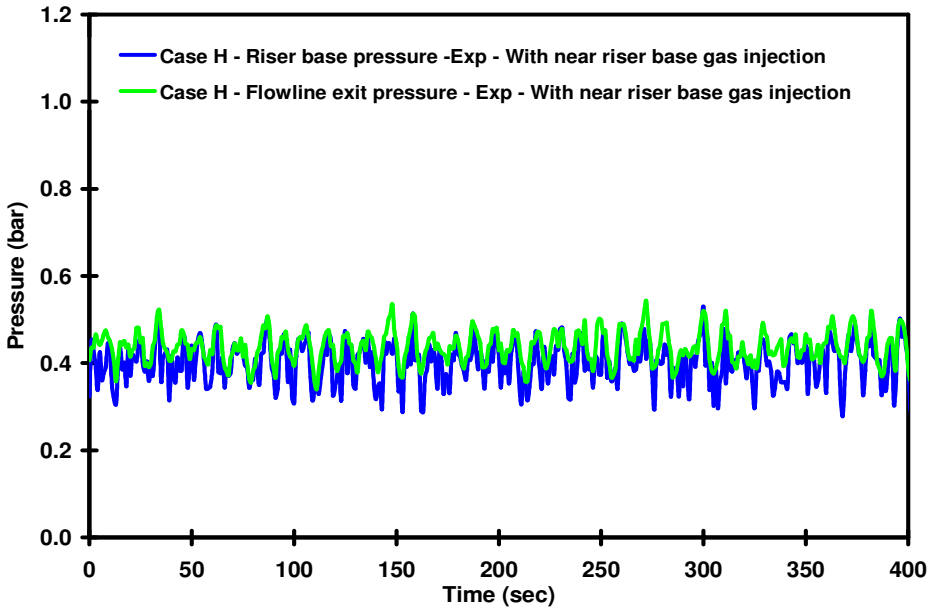

Figure 6.34 The flowline and riser base pressure response for case H from experiments – With near riser base injection.

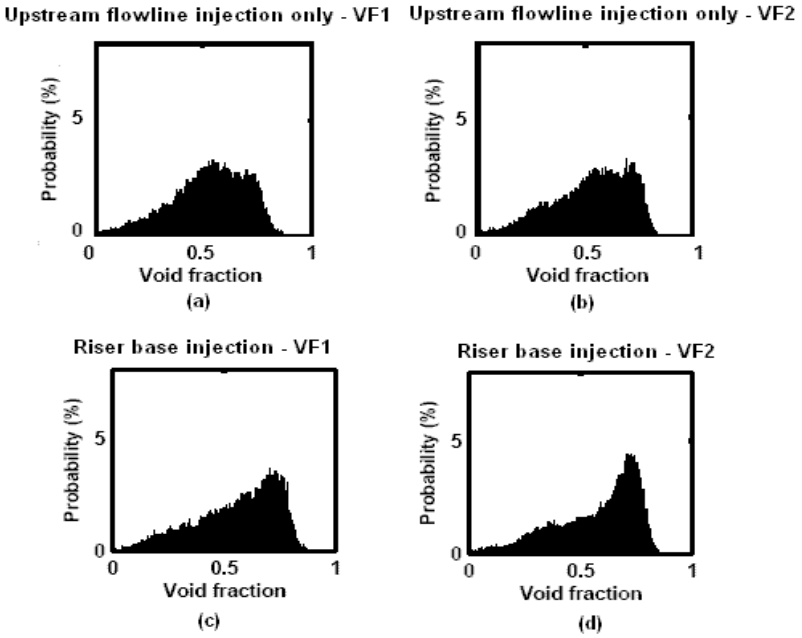

Figure 6.35 Probability mass function plots obtained from riser sections 5 and 8 for case H, (a-b) upstream gas injection only and, (c-d) with near riser base injection.

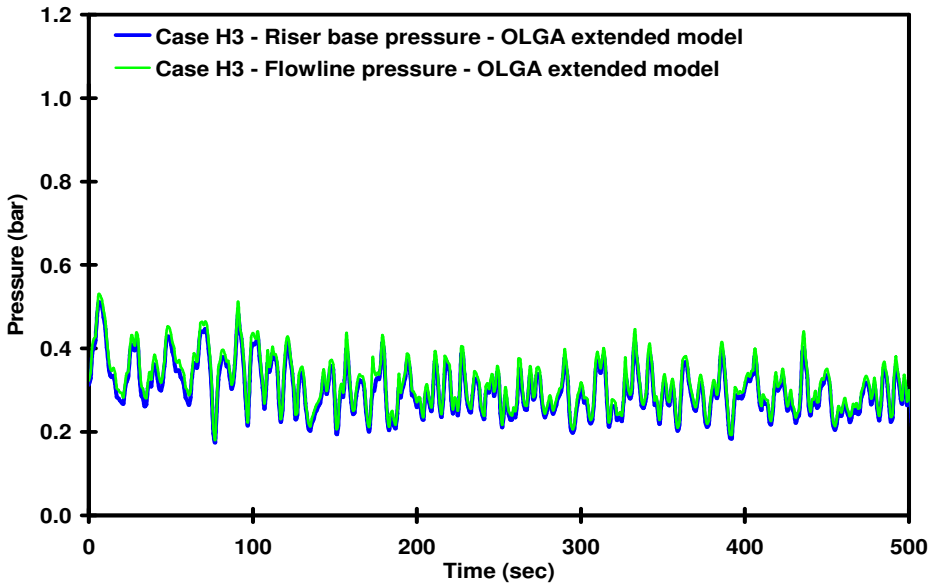

Figure 6.36 The simulated flowline and riser base pressure prediction by OLGA for Case H.

6.6.7 Case I3

The last case discussed is the riser base gas injection case with highest liquid superficial velocity of 0.61m/s, with flowline inlet and injected air superficial velocities equal to 1.68 m/s and 0.46m/s respectively. The condition in this case is maintained within the slugging flow regime (refer to section 4.3.2, Figure 4.22). The objective of doing this set of experiments was to verify whether the riser base injection is able to effectively dissipate the long liquid slugs originating from upstream of the flowline. Simulating such a case will illustrate the code's ability in modelling the slug dissipating effect.

This case belongs to the condition where the complex behaviour of hydrodynamic slugging and elbow terrain effect was seen. Although only partial dissipating effect of the liquid slugs is obtained due to the technical difficulties (see Figure 4.22). The result does provide an indication of the application of gas lift in stabilizing the unstable flow.

The Figure 6.37 shows the experimental riser base and flowline exit pressure response when flowline was under intense slugging with the slug build up and the blow out of aerated liquid. The combine effect of hydrodynamic slugging and terrain are obvious, where the flowline generated slugs are longer in size, the smaller slugs represents the slugs formed due to liquid fall back and accumulation in the base. The

flow regime in the riser during slugging in the flowline without gas injection was churn/froth nature, although some slugs structure remains were also seen to survive, this well represented in the figure. Note, since the gas penetration in the riser is uneven, this causes the smaller slugs to eject sooner than longer slugs from the base. The mean riser base pressure in experiments is quite high (0.599bar) due to the high liquid inventory with maximum and minimum value of 1.019 and 0.234 bar respectively.

Next Figure 6.38 indicates the riser base gas injection response to this slugging. The complete slug dissipation effect is not clear due to limited air injection rate available but it can be noted that aeration of the riser base causes some slugs to break forming similar slug sizes as caused by liquid fall back while partially dissipating the longer slugs to some extent. Due to the aeration of the base vicinity, the mean riser base pressure has reduced (around 0.495bars with maximum and minimum around 0.855 and 0.157bars) but not enough to completely unblock the base, however, the slugging frequency is increase and cycle time has reduced slightly.

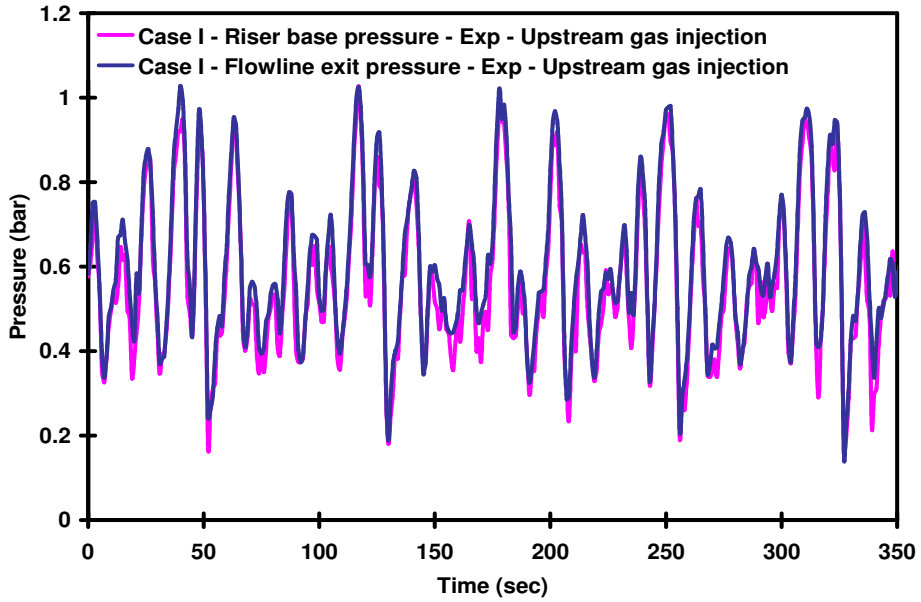

Figure 6.37 The flowline and riser base pressure response for case I from experiments –Upstream gas injection.

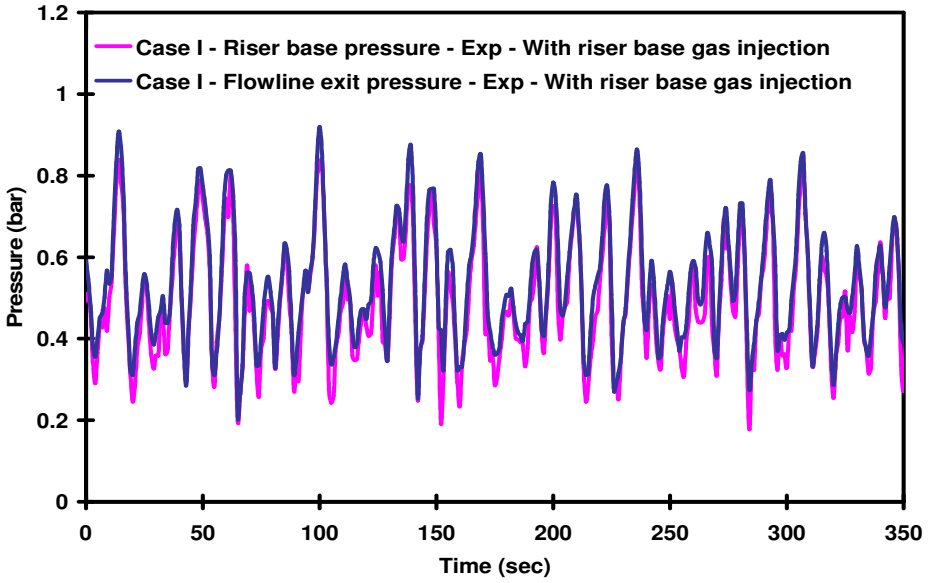

Figure 6.38 The flowline and riser base pressure response for case I from experiments – With near riser base injection.

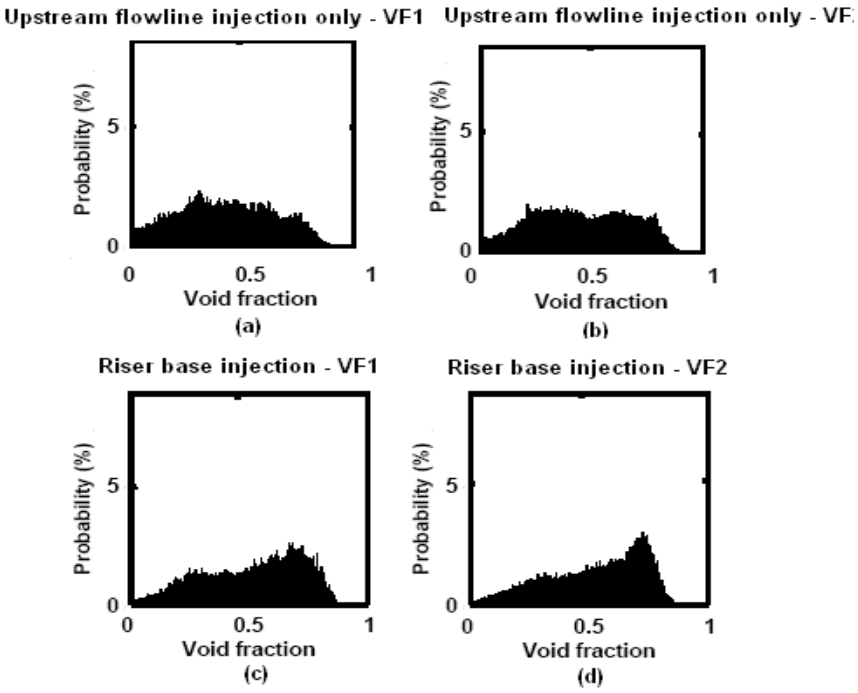

Figure 6.39 Probability mass function plots obtained from riser sections 5 and 8 for case I, (a-b) upstream gas injection only and, (c-d) with near riser base injection.

The Figure 6.39(a-b) shows the probability mass function plots taken from the riser section 5 and 8 with upstream of gas injection while Figure 6.39(c-d) shows the riser section 5 and 8 response with gas injection in the riser base. In Figure 6.39(a), no clear peak in the distribution exists but in the Figure 6.39(b), a slightly flatter void fraction distribution with two peaks is observed. The twin peaks have almost similar heights representing the simultaneous decay of liquid slugs and coalescence of gas bubbles in the core region of the riser. This behaviour indeed verifies that liquid slugs are indeed naturally dissipated while travelling up in the riser to certain extent. It is emphasised here that this PMF plot is not that is typically observed in conventional slug flow representing liquid slug and the Taylor bubble. Previous researchers (Watson and Hewitt, 1999) have referred this flow as a transitional flow encountered between conventional slug and churn/froth flow. In comparison to above, Figure 6.39(c-d) riser base gas injection clearly indicates that the liquid slugs were dissipated while travelling upward, due to long and highly distorted gas bubble clusters that penetrated through them. This can be verified by the appearance of a weak peak at lower void fractions along with strong prominent gaseous phase peak at higher void fractions in the Figure 6.39(c) representing the coalescent of gas phase. From the Figure 6.39(d) it can also be noted that the peak at the higher void fraction is not only higher than rest of the distribution but also broader indicating that the gas bubbles are longer and distorted. There is also long thick tail extending towards lower void fraction indicating some of the survived aerated slugs which is typical characteristic of transitional flows.

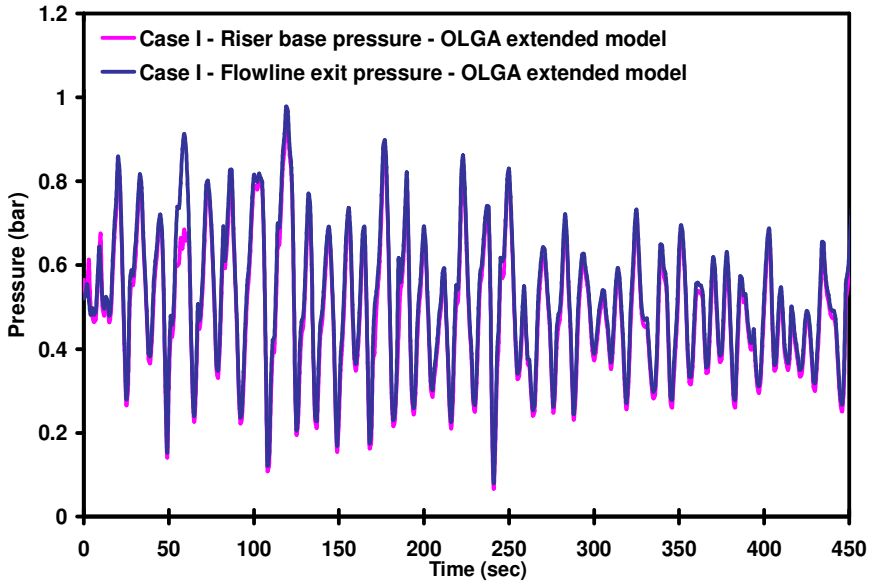

Figure 6.40 The simulated flowline exit and riser base pressures by OLGA for case I.

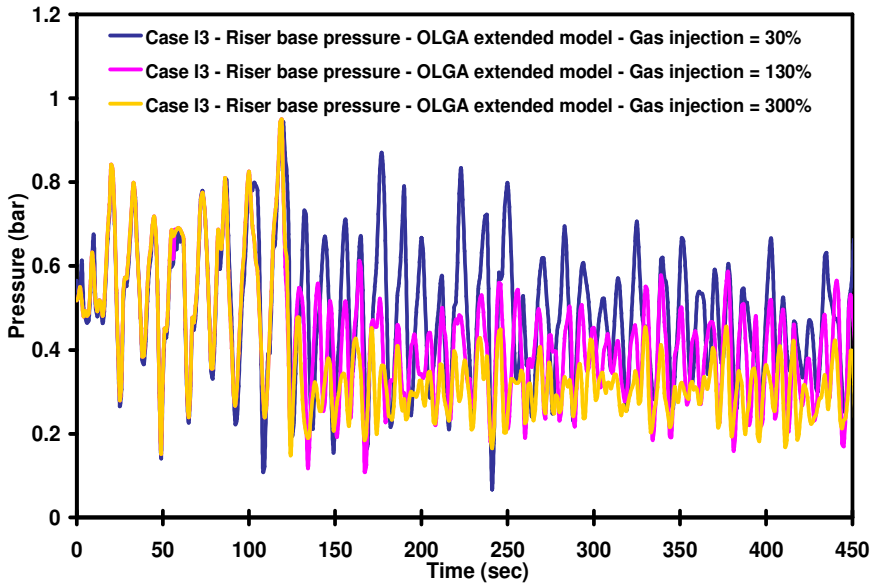

Figure 6.41 The effect of the gas injection rate on the riser base pressure simulated by OLGA.

The OLGA codes prediction from the first model indicates this case as a slugging flowline, with an initial stable annular flow in the riser that later transforms to slugging due to liquid fall back in the base (similar to one seen in case C1). However, the extended model results shows this case to be undergoing slugging right from beginning, see Figure 6.40. The figure initially indicates larger and longer slugs that dissipate to some extent after around 120s slightly and more visibly after 260seconds. It can be seen that with the introduction of the gas injection in the base, the continuous penetration of gas phase in the riser induced a smaller slug cycle (thus high frequency) along with a corresponding reduction in riser base pressure. The mean riser base pressure during gas injection predicted by the code is 0.497bar, less than the mean pressure seen in experiments (mean = 0.578bar). Overall, the results presented above showed that the riser base injection does reduce the severity/intensity of severe slugging to some extent. However, due to the available gas injection rate constraint, it could not fully eliminate the liquid slugs and merely break up the long liquid slugs into smaller ones.

Lastly, a parametric study in OLGA has been made by increasing the gas injection rate in the riser base with constant upstream gas injection in flowline. This study was performed to investigate the amount of gas injection rate needed to stabilize the flow. This aspect is also related to the stability characteristics study performed in chapter 4 (section 4.1.6). The Figure 6.41 provides the simulation results in which the riser base pressures are plotted for three different gas injection rates with all other parameters and boundary conditions kept the same. It can be noted that riser base pressure oscillations amplitude decreases with an increasing gas injection rate along with an

increase in frequency. With only 30% of the upstream gas injection rate, riser base gas injection has slightly dissipated the incoming liquid slugs. At 130%, the gas injection has further dissipated the liquid slugs and with gas injection rate of 300% of upstream, the riser was finally in slightly stable condition. However, even with 300% of upstream gas injection rate, the cyclic behaviour still persists. Any further increase in riser base gas injection will cause liquid slug to breakup more and hence a more continuous and manageable liquid inflow in the separator till the rate at which the flow in the riser is brought into annular flow regime. Note that large amount of gas was required (+300% of the inlet) to bring the riser in more stable state, which in most cases likely to be annular flow.

6.7 Numerical Experiments

This section addresses the numerical experiments conducted to examine the sensitivity of the simulated results on the grid size or the timestep used. In numerical simulation such sensitivity studies are of prime importance in reaching the correct conclusions as in theory the simulated results obtained should not differ with coarsening or refining of the grid or the timestep used.

6.7.1 Effect of Grid density change

It is known that the staggered grid applied in the OLGA code has a tendency of diffusing out the sharp interface (slug fronts and tails) encountered in the slug flow (Straume *et al.*, 1992). Therefore in the resolution of the grid, it was ensured that the section length should be fine enough to capture the important physical phenomena with minimum of diffusion. Also, during the modelling it was also ensured that the cell length between adjacent sections of 2 or less to minimize numerical smearing. To ensure that a grid independent solution was achieved; three different grid sizes ($\Delta x/2$, Δx, and $2\Delta x$) were used in all cases. Table 6.3 shows the grid sensitivity for the time evolution of the riser base pressure simulation, obtained with above grid sizes. Only tabular results are presented here and more details can be found in Appendix D. From the table it can be noted that varying the grid size does produces a slight effect on the predictions especially in unstable flows while in stable flow cases the differences are not significant.

In all the cases presented, the deviation between simulations and experiments are from 2 to 38%. It is to be noted that the larger deviation are for unstable flow cases and can mainly be attributed to the numerical smearing effects of slug fronts. Nevertheless, the increase in the grid density causes the numerical diffusion to decrease to some extent. Comparing the simulated results of increased and decreased grid size with the base case indicates that the results are within ±6%, of each other, confirming that a grid convergence has been achieved.

Table 6.3 The grid sensitivity studies.

Case Name	Experimental Value (bar)	Dx (bar)	Dx/2 (bar)	2Dx (bar)
Case A	0.853	0.834	0.809	0.867
Case B	0.413	0.272	0.269	0.265
Case C	0.533	0.438	0.368	0.447
Case D	0.551	0.506	-	0.469
Case E	0.912	0.907	0.852	0.901
Case F	0.546	0.463	0.429	0.488
Case G	0.617	0.562	0.521	0.564
Case H	0.454	0.289	0.279	0.319
Case I	0.543	0.496	0.469	0.499

From all the simulation results, in terms of flow regime identification, the increasing or decreasing the grid density has no effect. However in riser base pressure trends of unstable flow cases, some effects like higher frequency and mean pressure amplitude are seen with coarsening the grid density. For case D results obtained from the OLGA ver5.1, it was found that the solution multiplicity phenomena obtained is independent of the grid size, as increasing the section length still indicated the similar multiplicity trend while using the smaller section length resulted in crashing the simulation.

From the above grid sensitivity study, it can be said that on the whole there is deterioration in the quality of code predictions with the coarsening of the grid size but it is mainly attributed to the numerical diffusion caused by the use of the staggered grid scheme to define the sharp gas-liquid interface of slug flow. This observation is in corroboration with the work of Montgomery (2002) and Bendiksen *et al.* (1990), where the OLGA code predictions in comparison with the experimental results show large numerical diffusion of the sharp fronts and tails. While the latter study was limited to a single terrain slugging case, the former study included severe slugging type 1, 2 and 3 along with oscillation flow, slug flow and bubbly flow predictions. For the above former study, Montgomery (2002) found some grid sensitivity effects on flow regime predictions, slug sizes and peaks production rates of gas phase. Straume *et al.* (1992) while comparing slug tracking option with standard OLGA code scheme also reported a large deviation of liquid holdup in the riser base of the latter scheme (standard scheme) in comparison to the former (slug tracking).

6.7.2 Effect of Timestep change

When performing unsteady simulations, the size of the time step is another important parameter for the accuracy of the results. So, similar to above grid resolution study a time resolution study was performed. It is known that the convergence behaviour of simulation can deteriorate when selected timestep is too large and does not fulfil the CFL criteria, while smaller timestep will lead to definite convergence due to fulfilment of CFL criteria. This criterion is more strict when using explicit time schemes, but for OLGA semi implicit scheme the conditions are less strict. However, in OLGA simulations it was seen that too large time step resulted in an increase numerical diffusion causing large global volume error and degraded accuracy. So trials were performed with various timesteps and finally the initial timestep of 0.001s was manipulated from $\Delta t/10$, Δt, $10\Delta t$ in order to keep the deviation to the minimum. The predictions are shown in Table 6.4 with above timesteps for comparison. As before, the detailed results of these numerical experiments are given in appendix D.

Similar to grid sensitivity study, the changes is time step has not caused any change in the flow regime predictions of the cases. The riser base pressure trends of stable flow cases A and E do not show any changes. For unstable flow cases, while decreasing the timestep by a factor of 10 did not change the results of the simulations, a slight affect of increasing the timestep was seen (refer to appendix D).

Table 6.4 The timestep sensitivity studies.

Case Name	Experimental Value (bar)	Δt (bar)	$\Delta t/10$ (bar)	$10\Delta t$ (bar)
Case A	0.853	0.834	0.835	0.835
Case B	0.413	0.272	0.273	0.276
Case C	0.533	0.438	0.386	0.443
Case D	0.551	0.506	-	0.508
Case E	0.912	0.907	0.909	0.909
Case F	0.546	0.463	0.457	0.468
Case G	0.617	0.562	0.559	0.563
Case H	0.454	0.289	0.288	0.298
Case I	0.543	0.496	0.494	0.495

In some simulations of typical unstable flow (cases D, G and I), the larger timestep $10\Delta t$ and above resulted in leading to differences in the prediction of the mean amplitudes and frequency signifying numerical diffusion and degraded accuracy. This outlines the importance of analyzing various timestep in order to achieve more realistic results. Similar behaviour in code predictions has been observed in previous work on S-shaped riser also (Montgomery, 2001).

6.8 Summary

In this chapter, a leading multiphase flow simulator (OLGA) has been tested against the selected experimental runs from the large diameter horizontal flowline-vertical riser system. The test cases were divided into two main categories of "stable" and "unstable" flows. Two cases, A and E were defined under stable flows as the flow was mainly stratified and plug flow in the flowline with bubbly flow in the riser. The cases B, C, D, F, G, H and I all belonging to the flowline slugging (terrain or combination of terrain/hydrodynamic slugging) and intermittent flow in the riser (agitated bubbly, unstable slug and churn/froth flow) were defined as unstable flow.

A simple first model was formulated with steady state average boundary conditions (i.e. average air and water flowrates with constant outlet pressure boundary). The results obtained from this numerical model were compared with experimental near riser base pressure in terms of time varying behaviour and the flow regimes in the flowline-riser. The code indicated satisfactory agreement with time varying riser base pressure data, within an average error of less than 3% in the stable flow cases. However, the code only partially predicted the flow regimes especially in the riser. The discrepancies between experiments and simulation were found for unstable flows cases (B, C, D, F, G, H and I). In all these cases, the code globally underestimated the riser base pressure which was also reflected on the liquid inventory as it was also underestimated. The numerical difficulty posed to the code in flow regime prediction for unstable flows was also observed. The results of the case D (from ver5.1 and ver5.2) have provided the strongest evidence so far of the existence of the multiple roots in the code. This issue was resolved with same model being re-run in ver5.3 - a new version, with code directly yielding the most stable root as the answer.

Attempts were made in modifying the first model results, although these modifications did not improve the results, they showed that outlet boundary condition has been influenced in the experiments. As an alternative, real boundary condition were given to the model (extended model) to reduce the deviation seen by the unstable flow cases. The code showed interesting changes in the simulated results of this model by indicating the real flow behaviour for all the unstable flow cases. In general, the simulated cases showed a degree of success in reproducing the nature of the unstable flows that follows well the shapes of the experimental ones. However, this behaviour proved to be qualitative in nature, as there is an offset in numbers from the code and the experiments. This is primarily due to the discrepancies between the flow regimes observed and predicted by the code. Thus the discrepancies between the

above results and experimental data are therefore likely to be related to the incorrect closure relations used based on these flow regimes. Table 6.5 shows the detailed comparison of the results obtained between experiments and the OLGA simulations.

To examine the sensitivity of the simulated results, a set of numerical experiments was also performed by varying the timestep and the grid size. From the results, it was concluded that the sensitivity of the solution as a result of coarsing the grid size as well as the timestep is due to smearing of sharp fronts and tails of the liquid slugs.

6.8.1 General Observations

This section outlines some of the general findings based on the set of the simulations and numerical experiments performed:

- From the results, it is found that the effect of boundary conditions on simulations was indeed substantial. Whilst stable flows have been satisfactorily modelled with steady state average boundary conditions, this practice was insufficient for determining the hydrodynamic behaviour in unstable flows in large diameter horizontal flowline-vertical riser. Especially, as steady state average (i.e. fixed inlet flowrates and constant outlet pressure) boundary conditions assumption caused unrealistic over-simplification of boundary conditions that are dominated by large transient variations as shown in unstable flow cases.
- In certain cases, (mainly in unstable flows), the detailed characteristics were not reproduced by code satisfactorily, as inconsistencies were found in the prediction of flow regimes along with the under prediction of the riser base pressure. These were further reflected on liquid holdup prediction as the code globally under predicts the liquid holdup in all these cases.
- The results of the case D have provided the strongest evidence so far of the existence of the multiple roots in the OLGA code. No available work in public domain on the code has ever reported such behaviour before. Through the Taitel *et al.* (1976) model it was demonstrated that for the horizontal topology flowline multiple roots are not likely to be expected, even if a slight inclination is assumed in real facility then also, the expected multiple roots region lie quite lower to that considered in current experimental range. It is still unknown what happened inside the OLGA code.
- The code was unable to simulate the complex response of the unstable flows, even after applying the various options available to tune it up, thus a new and more creative solution of real time boundary application was found. The technique was partially successful in qualitatively reproducing the trends but the code was still unable to quantitatively predict the unstable flows in large diameter horizontal flowline-vertical riser system.
- Although the real time boundary condition application could not yield the desired results, this feature is promising in terms of predicting more realistic response of the simulated system under transient conditions.

- Numerical experiments conducted have shown the code sensitivity to the coarsing of the grid size as well as the timestep.

6.8.2 Recommendations

This work has shown that the unstable flows can be qualitatively reproduced with OLGA. However, in order to perform a quantitative comparison, the code needs improvements. It is difficult to predict the exact cause of discrepancies between experimental results and the simulations but based on the above observations following hypotheses are plausible, requiring recommendations:

- Generally, most of the two fluid model use the assumption of flat gas-liquid interface in calculating the liquid height. In unstable flows, it was observed that the gas-liquid interface became wavy, allowing liquid to climb up the walls with increasing j_a. It is possible that this curved interface which is actually covered by the liquid is ignored in calculation of liquid holdup, and possibly resulted in reducing the real area occupied by the liquid phase. This reason also explains the over prediction of the void fraction obtained due to the area covered by the gas and not by the liquid film. A further investigation seems necessary in this regard.
- It is also likely that inaccurate flow regime predictions and hence use of different closure relations are responsible for the discrepancy. It is to be noted that the largest discrepancies between the predictions and the data are for the flow identified as the slug flow in the riser by the code whereas these were agitated bubbly and churn/froth flow in actual. The code uses many experimental empirical relations for simulating slug flow. The deviation between the actual and the calculated value by the model may be attributed to the use of such empirical relations (e.g. (i) general parameters including wall and interfacial friction factors and entrainment/deposition rates (ii) slug flow parameters with bubble nose velocity, gas entrained in slug body) for churn/froth flow, that can have a direct impact on the evaluation of the void fraction and liquid holdup in the riser. Thus the flow regime prediction and the related transition mechanism must be investigated in detail in the light of flow patterns found in large diameter vertical risers.

Table 6.5 Summary of the simulated cases.

Case Name	Experimental Value (bar)	Steady State (bar)	1st Model (bar)	Modified model - Roughness (bar)	Modified model – GF (bar)	Modified model -Air Initialization (bar)	Modified model - Separator P +15% variation (bar)	Extended Model
Case A	0.853	0.815	0.834	-	-	-	-	-
Case B	0.413	0.205	0.208	0.214	0.259	0.366	0.363	0.272
Case C	0.533	0.340	0.371	0.409	0.411	0.424	0.523	0.438
Case D *(ver5.1)*	0.551	0.327	0.428	0.428	0.434	0.416	-	0.506
(ver5.3)			0.365	0.379	-	0.357	0.508	-
Case E	0.912	0.888	0.907	-	-	-	-	-
Case F	0.546	0.300	0.297	-	-	-	-	0.463
Case G	0.617	0.432	0.481	-	-	-	-	0.562
Case H	0.454	0.207	0.209	-	-	-	-	0.289
Case I	0.543	0.344	0.353	-	-	-	-	0.497

Chapter 7

Conclusions and Future Work

This chapter presents the summary of the detailed input to the body of knowledge concerning the hydrodynamic characteristics of a large diameter vertical riser and concludes with a discussion of recommendations for future research.

7.1 Summary of the thesis

The work performed in this thesis can roughly divide into three main parts:

1. A literature review on the topics of (a) large diameter vertical upflow studies along with (b) application of the multiphase flow simulator OLGA (Chapter 2).
2. Three major experimental studies (Chapter 4): (a) study of the riser base gas lift performance in large diameter vertical riser with a conventional Tee and a novel design Annular sleeve gas injector, (b) detail investigation of the hydrodynamic flow behaviour in large diameter vertical riser and, (c) examine the effects of the upstream conditions on the flow behaviour in the vertical riser.
3. Compare and analyze the collected data to increase the confidence on the existing two phase flow literature:

(a) By comparing with other experimental studies on large diameter vertical upflow (Chapter 4).

(b) By assessing the predictive capability of void fraction and pressure gradient methods (Chapter 5).

(c) By developing a numerical model of the large diameter horizontal flowline-vertical riser system using multiphase flow simulator OLGA and comparing the results with experimental work (Chapter 6).

7.2 Conclusions

Experimental Results (Part - I)

Considerable economic advantages can be gain in offshore oil industries if the instabilities causing serious detrimental effects such as, reduction in production and damaging the topside facility are minimized. While above factors are important, equally important is the enhanced recovery of the hydrocarbon. Gas lift is often proposed as the solution of the above problems.

In context of the above, a major experimental investigation was undertaken to evaluate the basic hydrodynamic performance of a novel gas injector. The novel gas injector results obtained from the four different loop configurations were compared with the results from a conventional Tee gas injector. The experimental results demonstrated that the novel design Annular sleeve gas injector should be the preferential choice over the conventional Tee gas injector. It was established from the basic hydrodynamic parameters that the Tee gas injector performed well only at high air superficial velocities. In comparison, the novel Annular sleeve by virtue of its versatile design was able to perform equally well at both the ends of the air superficial velocity range. At low air superficial velocities it provided more liquid lift, so could be utilized for smooth production. At the higher end, its performance is equivalent to that of Tee gas injector. In fact, the gas lift stabilization produced by annular sleeve is much smoother and gradual. This later aspect can result in fewer shutdowns with improved regularity for the topside processing facilities. Additionally, due to its design, no potential concerns of gas jetting are expected even at very high gas superficial velocities.

The BP's Angola Block 18 Greater Plutonio project after installing the longest single vertical riser tower in the world has started production in October 2007. It is of interest to note that the vertical riser tower employs a gas lift umbilical all arrayed around the core riser pipe, a slightly modified design of novel annular sleeve injector.

Experimental Results (Part - II)

(i) Flow patterns, transitions and flow pattern map

- The identification of flow patterns and its transitions was an important aspect of the work. The experimental data collected was exploited to uncover the features of the flow patterns encountered in this size of pipe supplemented by visual observations.

- The flow development issue was resolved by establishing that the flow had reached a quasi developed state at about 20D, this ensures that the flow pattern determined are not influenced by the any developing effects. Based on the probability mass function characteristics and the visual observations the flow in the vertical riser was classified into four basic flow patterns as *dispersed bubbly flow*, *bubbly flow*, a*gitated bubbly flow* and c*hurn/froth flow*. Also a special case of u*nstable slug flow* was found as a consequence of flowline inlet configuration.

- From the visual evidences found, it was clear that there were large coalescent bubbles in the riser with diameter close to that of riser and axial length greater than their diameter, but no large coalescent bubble like smooth bullet shaped Taylor bubble (occurring in slug flow) was observed for all air-water superficial velocities. Hence, there is no slug flow in 254mm diameter vertical riser, this was indeed verified from the PMFs as no bimodal peak associated with slug flow was found.

- The statistical information obtained for dispersed bubbly, bubbly and churn/froth flow are in agreement with earlier works, new and interesting features were found for agitated bubbly flow – a flow pattern found in large diameter vertical pipe instead of conventional slug flow.

- The characteristic standard deviation of the void fraction fluctuation for this new agitated bubbly flow is distinct than those from bubbly and churn/froth flow. It is proposed that the above newly found distinct feature for this flow is due to the intense bubble to bubble interaction resulting in breakup and simultaneous coalescence with further smoothening provided by strong liquid recirculations

- The above distinct behaviour clarifies the ambiguity regarding the prevailing flow regimes in large diameter vertical riser to a large extent, where on one hand, flow pattern classification as large as 5 different flow patterns (Agitated bubbly, churn bubbly, churn slug and churn froth) were found from visual observations and on another hand overly simplified into just two (bubbly and churn/turbulent flows).

- From the series of PMFs plot, it was found that bubbly to agitated bubbly transition is smooth and gradual. However, unlike this transition from bubbly flow, as the transition from agitated bubbly to churn/froth is approached, the distribution becomes more negatively skewed due the presence of large gaseous structures present within the core. Although this is a similar characteristic feature synonymous to small diameter churn/froth flow, no previous large diameter studies have found such feature in the experimental range conducted. Instead a typical normal distribution is often reported as the churn/froth flow in these studies (Cheng *et al.*, 1998; Omebere-Iyari *et al.*, 2008).

- Based on the observed changes of this standard deviation of void fraction fluctuations, the flow regime transition from bubbly to agitated bubbly and from agitated bubbly to churn/froth flow were identified. The experimental flow pattern map was developed based on the probability mass function plots supplemented by the visual observations. The developed experimental flow regime map was compared with published vertical flow regime maps/models, discrepancies were noted, and a poor agreement was found.

- From the current work as well as other conducted on large diameter vertical upflow condition, it is obvious that the Taitel *et al.* (1980) bubble to slug transition model does not yield satisfactory results. It was noted that the discrepancy is due to the Harmathy (1960) expression of the bubble rise velocity of moderately distorted ellipsoidal shape bubble in an infinite media. Through the visual observation of current and other large diameter work, it was concluded that it is this expression that is unable to account for the high velocity large coalescent bubbles formed near the bubble to agitated bubbly flow transition. Hence the Taitel *et al.* (1980) model has been modified for large diameter vertical upflow conditions, based on the physical mechanism observed. The general trends of modified criteria agreed well with the current and other large diameter experimental results.

(ii) Effect of upstream conditions on the two phase flow in the large diameter vertical riser

In various industries, there is a clear trend towards the use of larger diameter vertical risers. This increases the importance of determining the flow behaviour in the riser, especially the impact of the upstream conditions on it.

- The study investigated the effects of two different inlet configurations on the flow regimes and void distributions in the large diameter vertical riser namely, (i) near riser base gas injection and (ii) upstream flowline gas injection. The former represents the air-water introduction in the riser base area while the latter corresponds to the air-water introduction at the inlet of the flowline prior to the riser base where a quasi developed flow pattern is made to enter into the riser.
- It was found that under high but similar phase velocities in case of near riser base gas injection, the influence of gas injector design ahead in the riser is less pronounced as both the gas injectors resulted in similar downstream two phase flow characteristics.
- While no effect of inlet conditions (i and ii) was observed in the riser flow behaviour at low air-water superficial velocities, at high air-water superficial velocities, the overall intensity of the riser flow was more chaotic in the upstream flowline gas injection. This is due to the intermittent flow behavior in flowline influencing the riser flow pattern characteristics and thereby controlling the riser dynamics.
- Under a limited range of higher air-water superficial velocities (j_w = 0.59m/s and $1.2 < j_a < 1.63$ m/s) for upstream flowline injection, some unstable slug flow was detected in the riser. This flow exhibited some decaying characteristics of the slug flow from the horizontal flowline and churn/froth flow of the riser. The PMFs of this flow were flatter (in comparison to the near riser base injection), with twin peaks having almost similar heights representing the simultaneous decay of liquid slugs and coalescence of gas bubbles in the core region.
- For both the above flow cases (i.e. unstable slug and churn/froth flow) for upstream flowline injection, the mean void fraction obtained is less than the near riser base injection due to the presence of some survived liquid slugs in the riser.
- From visual observations (as well as through PMFs), it is found that the liquid slug do dissipates in the riser to a certain extent due to the compressional forces of succeeding bubble from the liquid slug (from the flowline), gravitational force and turbulent forces associated with two phases.
- For upstream gas injection at low j_w = 0.25 m/s and high j_a = 2.1m/s, periodic instability is detected with regular slugging in the flowline, however at higher j_w = 0.55m/s and high j_a = 2.1m/s, this periodic instability is taken over by more chaotic instability within the riser, the severity of which increases because of the increase in liquid holdup within the riser base and flowline. It is to be noted that this instability is not the severe slugging indicated by many authors (Schmidt *et al.*, 1980; Bendiksen *et al.*, 1991; Sarica and Shoham, 1991; Tin, 1991; Yeung and Montgomery, 2001) but does possess similarity to unstable flow defined by

Fabre *et al.* (1990) and Schmidt *et al.* (1980) in small diameter horizontal flowline-vertical riser configuration.

Experimental Results (Part - III)

In the last section of the experimental results, a detail comparison of the experimental results with other work on large diameter vertical pipe was performed. The comparison of the experimental results with other work on large diameter vertical pipe especially with air-water as working fluid indicates a close agreement while differences were observed with studies employing different gas-liquid as working fluid.

Performance assessment study of void fraction correlations and pressure gradient methods

For the first time, a comprehensive assessment of a wide range void fraction correlations/pressure gradient methods belonging to different industries was performed. The results of the assessment showed that:

- Except for the few specifically developed correlations for large diameter vertical pipes, none of the compared correlations could predict the satisfactory trends.
- It was found that drift flux modelling approach provided much closer void fraction predictions with experimental data than other methods. It is worth mentioning that more correlations belonging to nuclear industry are closer in prediction while none of the oil industry correlations succeeded in predicting the void fraction under ±10%.
- It was noted that most of the correlations performed well in some of the flow regimes and their performance deteriorated in the other, thus none of the correlation was able to predict all the flow regimes accurately. Most of the successful correlations, at the maximum predicted three flow regimes. It was found that the correlations that successfully predicted the three flows AB, US and C, did not predicted the bubbly flow accurately while those predicting bubbly flow showed acceptable trend for agitated bubbly but did not predicted US and C flows satisfactorily. This trend highlights the difference in the flow structure variation behind the bubbly and rest of the flows.
- The important contribution of this assessment is a set of table developed that recommends the appropriate void fraction correlations based on their performances in the individual flow regimes found in large diameter vertical pipes.
- The pressure gradient methods assessment showed that the successful predictions of the methods are due to the flow dominated by hydrostatic head and thus influenced by the assessed void fraction (or holdup) correlation. The hybrid models of Friedel frictional pressure gradient with combination of Guzhov *et al.* (1967), Premoli *et al.* (1971) and Spedding and Chen (1984) have been successful in predicting the pressure gradient. However, it is the flow

regime specific mechanistic approach that is again successful similar to void fraction assessment, with Oliemans and Pots (2006) mechanistic pressure gradient scheme giving closer results to experimental values than conventional empirical methods.

Numerical modelling with OLGA

With an aim to increase the confidence on the existing modelling tools, the predictive capability of OLGA multiphase flow simulator was explored by comparing the simulation predictions with the experimental results. It has been shown that:

- The effect of boundary conditions on simulations was indeed substantial. Whilst stable flows have been satisfactorily modelled with steady state average boundary conditions, discrepancies were found in simulations under the above boundary conditions. This signifies that the real behaviour of unstable flows was dominated by large transient variations at the boundary.
- The code was unable to simulate the complex response of the unstable flows, even by applying the various options to tune up, thus a more creative solution of real time boundary condition application was applied. The technique was partially successful in qualitatively reproducing the trends but the code was still unable to quantitatively predict the unstable flows in large diameter horizontal flowline-vertical riser system.
- The detailed flow characteristics (mainly in unstable flows) were not reproduced by the code satisfactorily, inconsistencies were found in the prediction of flow regimes along with the under prediction of the riser base pressure. These were further reflected on liquid holdup prediction as the code globally under predicts the liquid holdup in all unstable flow cases.
- The results of the case D have provided the strongest evidence so far of the existence of the multiple roots in the OLGA code. No available work in public domain on the code has ever reported such behaviour before.
- Numerical experiments conducted have shown the code sensitivity to the coarsing of the grid size as well as the timestep.
- The inaccurate flow regime predictions and hence use of different closure relations might be responsible for the discrepancy between the results. Another possible reason can be due to the code's assumption of a flat gas-liquid interface which explains the under prediction of liquid inventory and over prediction of void fraction within the flowline-riser base vicinity.
- The code in its present form does not offer the implementation of user defined equation, which if available could have been explored to account for the differences between the numerical and experimental results.

7.2 Future work

There are a number of areas that can further enhance the experimental work as well as the modelling efforts in future studies. Below they are briefly defined:

7.2.1 Experimental work

Being one of it's kind in the entire UK, several recommendations can be made, as to how this versatile facility can be used more efficiently:

- An experimental investigation on the bubble size distribution and breakup in large diameter vertical upflow condition with special emphasis on "stability of a large bubble".
- The performances of injectors can further be tested by moving the injectors to the upstream of the riser i.e. near the exit to the flow line. This could provide a new opportunity to explore the stability characteristics of unstable flow.
- Air/water mixture flows through the horizontal flowline with larger air-water velocity range could provide more insight especially under the unstable slug flow encountered.
- Due to the limited time available and the length of time required for the top facility modification due to slugging surges, the effect of gas injection on liquid slug dissipation/stability characteristics could not be fully studied. Hence, an addition of a two phase flow horizontal separator and installation of control valves on air supply system is proposed.
- About 2° dip near the riser base in the flowline OR an inclination of the riser by 2° from the vertical can help in studying the effects of inclination on the flow characteristics occurring in a large diameter inclined riser. For the later option, no such experimental work exists in the literature.
- Oil and gas production tends to operate under extreme environments, therefore the need for testing the effects of surfactants, drag reducing agents and corrosion inhibitors is increasing. The current flow loop can provide an excellent opportunity to investigate the effects of above mentioned in large diameter vertical riser. It is emphasised that these topics have not been investigated before in this size of vertical riser.
- Usually the gaslift is applied at the conditions of large water cuts in oil i.e. when the reservoir is towards deletion. Use of low proportions of oil in conjunction with water in existing facility can provide an interesting opportunity to study the non-miscible liquid phase distribution in gas-liquid-liquid flows in large diameter vertical pipes. However, for this study a divertible flow path from top facility to existing three phase gravity separator will be required.
- Lastly, due to the menace of the flow related instabilities in the off-shore environment, novel control strategies are very often proposed. The large

diameter riser facility could also be utilized for testing such novel control strategies.

7.2.2 Numerical work

Considering the interest of the Oil and Gas industry in knowing the simulated behaviour of large diameter risers, OLGA modelling is an important contribution. This is the first time that large diameter vertical riser study has been documented. Obviously much more needs to be done in order to gain more confidence. Therefore, it would be of further benefit to incorporate various below mentioned suggestions in any future work.

- Flow regime identification mechanism and closure laws used in the codes should be examined and the closure relations based on the user defined values should be allowed to be incorporated within the code.
- A full scale hydrodynamic study of the flowline-vertical riser system with a top side separator is needed.
- Additionally above study may also include the tests of various control strategies like effects of separator choking and riser base control.
- Finally, numerical investigation of the hydrodynamic behaviour in large diameter 2º down inclined flowline- vertical riser system or 2º inclination of riser from the vertical (as mentioned above) system could be performed.

REFERENCES

Ali, S. F. (2005) "Large Diameter Riser Rig Operating Procedures along with safety guidelines manual", 2005

Armand, A. A. (1946) "The resistance during the movement of a two-phase system in horizontal pipes", *Izv. Vses. Teplotekh*, Inst. 1, pp. 16-23, AERA-Lib/Trans 828 (Cited in: Neil, E. T. and Kazimi, M. S. (1989). *"Nuclear Systems I: Thermal hydraulics fundamentals"*. Hemisphere Publishing Corporation, USA.)

Armand, A. A., and Treschev, G. G. (1959) "Investigation of the resistance during the movement of steam-water mixtures in heated boiler pipe at high pressure", *AERE Lib/Trans, 81*, (Cited in: Neil, E. T. and Kazimi, M. S. (1989). *"Nuclear Systems I: Thermal hydraulics fundamentals"*. Hemisphere Publishing Corporation, USA.)

Awad, M. and Muzychka, Y. S. (2004) "Bounds on Two Phase Flow – Part I: Frictional Pressure Gradient", ASME International Mechanical Engineering Congress and Exposition, November, 2004.

Annunziato, C. M. and Girardi, G. (1984) "Flow pattern identification by pressure drop and void fraction fluctuations analysis in vertical two phase flow. *Proceedings of European Two Phase Flow Group Meeting*, Rome, June 19-21, 1984.

Bankoff, S. G. (1960) "A variable density single-fluid model for two-phase flow with particular reference to steam-water flow", *Trans. ASME, Journal of Heat Transfer*, Vol. 82, pp. 265-272 (Cited in: Neil, E. T. and Kazimi, M. S. (1989). *"Nuclear Systems I: Thermal hydraulics fundamentals"*. Hemisphere Publishing Corporation, USA)

Barnea, D. (1987) "A unified model for predicting flow pattern transitions for the whole range of pipe inclinations. *International Journal of Multiphase flow*, Volume 13(1), pp. 1-12.

Barnea, D. (1986) "Transitions from annular flow and from dispersed bubble flow – unified models for the whole range of pipe inclinations", *International Journal of Multiphase flow*, Volume 12(5), pp. 733-744.

Baker, O. (1954) "Oil and Gas Journal", Volume (53) (Cited in: Hewitt, G. F. (1982). "Chapter 2: flow regimes and Chapter 10: *Measurement of Two-Phase Flow Parameters*". In: Handbook of Multiphase Systems, Edited by Hetsroni, G. Publisher: Hemisphere/McGraw Hill, Washington.)

Baker, A and Gravestock, N. (1987) "New Correlations for Predicting Pressure Loss and Holdup in Gas/Condensate Pipelines". In the Proceedings of 3rd International Conference on Multiphase Flow, Hague, Netherlands, pp 417-435.

Beattie, D. R. H. and Whalley, P. B. (1982) "A simplified two-phase frictional pressure drop prediction method", *International Journal of Multiphase Flow*, Volume 8, pp 83-87 (Cited in: TECDOC-1203. (2001). Thermohydraulic Relationships for

Advanced Water Cooled Reactors. Report IAEA: International Atomic Energy Agency, Nuclear Power Technology Development Section, Vienna)

Beggs, H. D and Brill, J. P. (1973) "A Study of Two-Phase Flow in Inclined Pipes," *Journal of Petroleum Technology,* Volume 255, pp. 607-17 (Cited in: Brill, J. P., Mukherjee, H. (1999). "Multiphase Flows in Wells", SPE Henry Doherty series: Monograph, volume 17.Society of Petroleum Engineers Inc, Texas.

Bendiksen, K. H. (1984) "An experimental investigation of the motion of long bubbles in inclined tubes". *International Journal of Multiphase Flow,* Volume 10(4), pp 467-483.

Bendiksen, K., Brandt, L., Fuchs, P., Linga, H., Malnes, D. and Moe, R. (1986) "Two-Phase Flow Research at SINTEF and IFE: Some Experimental Results and a Demonstration of the Dynamic Two-phase Flow Simulator OLGA". Presented at The Offshore Northern Seas Conference, Stavanger, Trondheim. (Cited in: Bendiksen, K. H., Malnes, D., Moe, R. and Nuland, S. (1991). "The Dynamic Two-Fluid Model OLGA: Theory and Application". *SPE production engineering*, SPE Paper number 19451, pp. 171-180.)

Bendiksen, K. H. and Malnes, D. (1987) "Experimental data on inlet and outlet effects on the transition from stratified to slug flows in horizontal tubes". *International Journal of Multiphase flow*, Volume (13), pp. 131-135.

Bendiksen, K. H., Malnes, D., Moe, R., and Nuland, S. (1991) "The Dynamic Two-Fluid Model OLGA: Theory and Application". *SPE production engineering*, SPE paper-19451, pp. 171-180.

BP Report: Angola. (2004) BP Angola environmental statement 2004.

(InternetLink:http://www.bp.com/liveassets/bp_internet/globalbp/STAGING/global_assets/downloads/V/verfied_site_reports/Africa_Russia_caspian/Angola_2004.pdf)

Brauner, N. and Barnea, D. (1986) "Slug/Churn Transition Upward Gas-Liquid Flow", *Chemical Engineering Science*, Volume 41, pp. 159-163.

Brennen, C. E. (2005) "Fundamentals of Multiphase Flow".[e-book], Cambridge University Press. Available online: http://resolver.caltech.edu/CaltechBOOK [Accessed on 26th February 2009]

Brill, J. P., Schmidt, Z., Coberly, W. A., Herring, J. D., Moore, D. W. (1981) Analysis of two phase tests in large diameter flowlines in Prudhoe Bay field. Society of Petroleum Engineers Journal, SPE-paper-8305, pp. 363-378.

Brill, J. P., Mukherjee, H. (1999) "Multiphase Flows in Wells", *SPE Henry Doherty series: Monograph,* volume 17.Society of Petroleum Engineers Inc, Texas.

Burke, N.E., Kashou, S.F., Hawker, P.C. (1992) "History matching of a North Sea flowline start up using the OLGA Transient Multiphase Flow Simulator". Presented at 67th Annual Conference and Exhibition of the Society of Petroleum Engineers in Washington, DC, October 4-7, 1992. SPE paper-24789

Burke, N.E. and Kashou, S.F. (1996) "Slug Sizing/Slug Volume Prediction, State of the art review and simulation," *SPE Production and Facilities*, Volume 11(3), SPE paper-30902, pp. 166.

Butterworth D. (1975) A comparison of some void-fraction relationships for co current gas-liquid flow, *International Journal of Multiphase Flow*, Volume (1), pp. 845-850.

Cheng, H., Hills, J. H. and Azzopardi, B. J. (1998) "A study to bubble-to-slug transitions in the vertical gas-liquid flow in columns of different diameter". *International Journal of Multiphase flow*, Volume 24(3), pp. 431-452.

Cheng, H., Hills, J. H. and Azzopardi, B. J. (2002) "Effects of initial bubble size on flow pattern transitions in a 28.9 mm diameter column", *International Journal of Multiphase flow*, Volume 28(6), pp. 1047-1062.

Chen, X. T., Cai, X. D. and Brill, J. P. (1997) "A general model for transition to dispersed bubble flow". *Chemical Engineering Science,* Volume 52(23), pp. 4373-4380.

Chexal, B., Lellouche, G., Horowitz, J. and Healzer, J. (1992) "A void fraction correlation for generalized applications". *Progress in Nuclear Energy,* Volume 27(4), pp 255-295.

Chisholm, D. (1967) "A Theoretical Basis for the Lockhart-Martinelli Correlation for Two-Phase Flow", *International Journal of Heat Mass Transfer*, volume 10, pp. 1767 - 1778. (Cited in: Chisholm, D., 1983, *Two-Phase Flow in pipes and Heat Exchangers*, Longman Inc., New York)

Chisholm, D. (1972) "An equation for velocity ratio in two phase flow". *National Engineering Laboratory report, Number* 535.

Chisholm, D. (1983) "*Two-Phase Flow in pipes and Heat Exchangers"*, Longman Inc., New York.

Clark, N. N. and Flemmer, R. (1986) "The effect of varying gas voidage distributions on average holdup in vertical bubble flow", *International Journal of Multiphase Flow*, Volume 12(2), pp. 299-302.

Clark, N. N., Van Egmont, J. W. and Nebiol, E. P. (1990) "The drift-flux model applied to bubble columns and low velocity flows", *International Journal of Multiphase Flow*, Volume 6(2), pp. 261-279.

Clift, R., Grace, J. R. and Weber, M. E. (1978) "Bubbles, Drops and Particles", Academic Press, New York (1978).

Coddington, P and Macian, R. (2002) "A study of the performance of void fraction correlations used in the context of drift-flux two-phase flow models", *Nuclear Engineering and Design*, Volume 215(3), pp.199-216.

Costigan, G. and Whalley P. B. (1997) Slug flow regime identification from dynamic void fraction measurements in vertical air-water flows. *International Journal of Multiphase flow*, Volume 23(2), pp. 263-282.

Davis, C. B. (2001) "Assessment of the ATHENA Code for Calculating the Void

Fraction of a Lead-Bismuth/Steam Mixture in Vertical Upflow". *Nuclear Technology*, Volume 133 (2), pp.187-193.

Dhulesia, H. and Lopez, D. (1996) "Critical Evaluation of Mechanistic Two-Phase Flow Pipeline and Well Simulation Tools", SPE Annual Technical Conference & Exhibition, Denver, October 6-9, 1996, SPE paper-36611.

Diener, R. and Friedel, L. (1994) Proceeding of German-Japanese Symposium on Multiphase Flow, Karlsruhe, Germany (Cited in: TECDOC-1203. (2001). Thermohydraulic Relationships for Advanced Water Cooled Reactors. Report IAEA: International Atomic Energy Agency, Nuclear Power Technology Development Section, Vienna)

Dix, G. E. (1971) "Vapour void fraction for forced convection with subcooled boiling at low flow rates," Ph.D. Thesis, University of California, Berkeley. (Cited in: Neil, E. T. and Kazimi, M. S. (1989). *"Nuclear Systems I: Thermal hydraulics fundamentals"*. Hemisphere Publishing Corporation, USA.)

Dukler, A. E., Wicks, M. and Cleveland, R. G. (1964) "Frictional pressure drop in two phase flow: a comparison of existing correlations for pressure loss and holdup". *The AIChE Journal*, Volume (10), pp. 38-43.

Dukler, A. E and Taitel, Y. (1977) "Flow regime transitions for vertical upward gas-liquid flow, Paper presented at 70th Annual meeting of AICHE, New York. (Cited in: Weisman, J. and Kang, S. Y. (1981) "Flow pattern transitions in vertical and upwardly inclined lines", *International Journal of Multiphase Flow*, Volume 7(3), pp 271-291)

Duns, H. Jr. and Ros, N. C. J. (1963) "*Vertical Flow of Gas and Liquid Mixtures from Boreholes*," Proceedings of the Sixth World Petroleum Congress, Frankfurt, Section II, 22-PD6. (Cited in: Brill, J. P., Mukherjee, H. (1999). "Multiphase Flows in Wells", SPE Henry Doherty series, Monograph volume 17.Society of Petroleum Engineers Inc, Texas.)

Eidsmoen, H., Roberts, I. and Alana, J. (2005) "Issues relating to proper modelling of the profile of long gas condensate pipelines". In proceedings of Pipeline Simulation Group Conference, San Antonio, November 7-9, 2005.

Ekberg, N.P., Ghiaasiaan, S.M., Abdel-Khalik, S.I., Yoda, M. and Jeter, S.M., (1999) Gas–liquid two-phase flow in narrow horizontal annuli. *Nuclear Engineering Design,* Volume 192, pp. 59-80.

ESDU. (2004) "Pressure gradient in upward adiabatic flows of gas-liquid mixtures in vertical pipes", Engineering Services Data Unit, The Institution of Mechanical Engineers.

Fabre, J., Peresson, L., Corteville, J., Bernicot, M. and Ozon, P. (1990) Severe Slugging in Pipeline /Riser Systems, SPE Production Engineering, pp. 299-305.

Fairhurst, P. (2004) Private communications.

Fordham, E. J., Lenn, C. P, Holmes, A., Simonian, S. and Ramos, R. T. (1999) "Corrections of gradiomanometer data for volume fractions in two-phase flows", *Measurement Science and Technology*, Volume (10), pp. 131-135.

Friedel, L. (1979) "Improved Friction Pressure Drop Correlations for Horizontal and Vertical Two Phase Pipe Flow," *European Two Phase Flow Group Meeting, Ispra, Italy* (Cited in: Thom J. R. (2004). "Wolverine Engineering Data Handbook", edition III, Wolverine Tube Inc. (internet source: www.wlv.com/products/index.html)

Fuchs, P. and Brandt, I. (1989) Liquid Holdup in Slugs: Some Experimental Results from the SINTEF Two-Phase Flow Laboratory". In 4th International Conference on Multiphase Flow, Nice, France, 1989, pp. 41-47.

Ghajar, A. J and Woldesemayat, M. A. (2007) "Comparison of void fraction correlations for different flow patterns in horizontal and upward inclined pipes", *International Journal of Multiphase Flow*, Volume 33(4), pp. 347-370.

Govier, G. W. and Short, W. L. (1958) "The upward vertical flow of air-water mixture – II". *The Canadian Journal of Chemical Engineering (CJChE)*, Volume (36), pp 195-202. (Cited in: Spedding, P. L. and J. J. J. Chen. (1984). "Holdup in two phase flow". *International Journal of Multiphase flow*, Volume 10(3), pp. 307-339)

Guet, S., Ooms, G., Oliemans, R. V. A. and Mudde, R. F. (2003) "Bubble injector effect on the gaslift efficiency". The AIChE Journal, Volume 49(9), pp. 2242-2252.

Guzhov, A., Mamayev, V., Odishariya, G. (1967) A study of transportation in gas–liquid systems. In: 10th International Gas Conference, Hamburg, Germany. (Cited in: Garcia, F., Garcia, R., Joseph D. D. (2005), "Composite power law holdup correlations in horizontal pipes", International Journal of Multiphase Flow, Volume 31, pp 1276-1303)

Hagedorn, A.R. and Brown, K.E. (April 1965) "Experimental Study of Pressure Gradients Occurring During Continuous Two-Phase Flow in Small-Diameter Vertical Conduits," *Journal of Petroleum Technology*; Trans., AIME, 234, pp 475-484. (Cited in: Brill, J. P., Mukherjee, H. (1999). "Multiphase Flows in Wells", SPE Henry Doherty series, Monograph volume 17. SPE Inc, Texas)

Hashemi, A., Kim, J. H., and Sursock, J. P. (1986) "Effect of diameter and geometry on two phase flow regimes and carry over in model PWR hot leg". Proceedings of 8th International Heat Transfer Conference. San Francisco, CA, USA.

Hasanein, H. A., Kawaji, A., Chain M. C, Yoshioka, Y. (1997) "Flow regime identification of steam-water flow in al large vertical pipe at elevated pressures". Proceedings of 1997 ASME Fluids Engineering Division Summer Meeting. ASME. Vancouver, BC, Canada.

Hatakeyama, N. and Masuyama, T. (1994) "Statistical characteristics of void fraction fluctuation and flow regime identification in vertical gas-liquid two phase flow", Japanese Journal of Multiphase flow, Volume 8(1), pp14. (Cited in Hasanein, H. A., Kawaji, A., Chain M. C, Yoshioka, Y. (1997)." Flow regime identification of steam-water flow in al large vertical pipe at elevated pressures". Proceedings of 1997 ASME Fluids Engineering Division Summer Meeting. Vancouver, BC, Canada)

Hedne, P. and Linga, H. (1990) "Suppression of terrain slugging with automatic and manual riser choking". Paper presented at ASME Winter Annual Meeting, Dallas, Texas, November 1990.

Herringe, R. A. and Davis, M. R. (1976) "Structural development of gas -liquid mixture flows". Journal Fluid Mechanics, Volume 73(1), pp. 97-123.

Heskestad, K., L. (2005) "Field Data Analysis Using the Multiphase Simulation Tool OLGA 2000", Diploma Thesis, NTNU, Stavanger, Trondheim, June 2005. Internetsource:www.ipt.ntnu.no/jsg/studenter/diplom/KarlLudvigHeskestad2005.pdf. [Last accessed 3 February 2009]

Hewitt, G. F. (1982). "Chapter 2: flow regimes and Chapter 10: *Measurement of Two-Phase Flow Parameters*". In: Handbook of Multiphase Systems, Edited by Hetsroni, G. Publisher: Hemisphere/McGraw Hill, Washington.

Hewitt, G. F. and Hall-Taylor, N. S. (1970) "Annular Two-Phase Flow", Pergamon, New York (Cited in: Hewitt, G. F. (1982). "Chapter 2: flow regimes and Chapter 10: *Measurement of Two-Phase Flow Parameters*". In: Handbook of Multiphase Systems, Edited by Hetsroni, G. Publisher: Hemisphere/McGraw Hill, Washington)

Hewitt, G. F. and Roberts, D. N. (1969) "Studies of two-phase patterns by simultaneous X-ray and flash photography". Atomic Energy Research Establishment Report AERE-M 2159, Harwell, England. (Hewitt, G. F. (1982). "Chapter 2: flow regimes and Chapter 10: *Measurement of Two-Phase Flow Parameters*". In: Handbook of Multiphase Systems, Edited by Hetsroni, G. Publisher: Hemisphere/McGraw Hill, Washington)

Hibiki, T. and Ishii, M. (2002) "Distribution parameter and drift flux velocity of drift flux model in bubbly flow", *International Journal of Heat and Mass transfer*, Volume 45(4), pp. 707-721.

Hibiki, T. and Ishii, M. (2003) "One dimensional drift flux model for two phase flow in large diameter pipe". *International Journal of Heat and Mass transfer*, Volume 46(7), pp. 1173-1790.

Hill, T. J. (1989) "Riser Base Gas Injection into the S.E Forties Line". Proceedings of 4th International Conference on Multiphase flows, BHRA, pp. 133-148, Nice, France.

Hill, T. J. (1990) "Gas injections at riser base solve slugging flow problems". The Oil & Gas Journal, pp. 88-92.

Hills, T. J. (1976) "The operation of bubble column at high throughputs: Gas hold u-measurements". The Chemical Engineering Journal, Volume 12, pp. 89-99.

Hills, T. J. (1993) "The behaviour of bubble column at high throughputs: Radial voidage profiles". The Chemical Engineering Journal, Volume 53, pp. 115-123.

Hirao, Y., Kawanishi, A., Tsuge, A. and Kohriyama, T. (1986) "Experimental study on drift flux correlation formulas for two phase flow in large diameter tubes". *Proceedings of 2nd International Topical Meeting on Nuclear Power Plant Thermal Hydraulic and Operations Conference*. Tokyo, Japan.

Hollenberg, J. F., Wolf, S., and Meiring, W. J. (1995) "A method to suppress severe slugging in flow line riser systems". *In Proceedings of: 7th International Conference on Multiphase Production*, BHR Group, Cannes, France, 1995.

Holt, A. J., Azzopardi, B. J. and Biddulph, M. W. (1999) "Calculation of two-phase pressure drop for Vertical upflow in narrow passages by means Of a flow pattern specific model", Transaction of IChemE, Part A, Chemical Engineering Research and Design, Volume 77, pp. 7-15.

Hubbard, M. G., and Dukler, A. E. (1966) "The Characterization of Flow Regimes for Horizontal Two-Phase Flow: I. Statistical Analysis of Wall Pressure Fluctuations," *Proceedings of Heat Transfer and Fluid Mechanics Institute*, Stanford University Press, pp. 100-121 (Cited in: Hewitt, G. F. (1982). "Chapter 2: flow regimes and Chapter 10: *Measurement of Two-Phase Flow Parameters*". In: Handbook of Multiphase Systems, Edited by Hetsroni, G. Publisher: Hemisphere/McGraw Hill, Washington)

Hughmark, G. A. (1962) "Holdup in gas-liquid flow." Chemical Engineering Progress, Vol. 58, No. 4, pp. 62-65. (Cited in: Garcia, F., Garcia, R., Joseph D. D. (2005), "Composite power law holdup correlations in horizontal pipes", *International Journal of Multiphase Flow*, Volume (31), pp. 1276–1303)

Huq, R. and Loth, J. L. (1990) "An Analytical Two-Phase Flow Void Prediction Method". In Proceedings of AIAA/ASME 5th Joint Thermophysics and Heat Transfer Conference, June 18-20, 1990, Seattle, WA, USA.

Huq, R. and Loth, J. L. (1992) "Analytical Two-Phase Flow Void Prediction Method," *Journal of Thermophysics*, Volume 6(1), pp. 139-144.

Irfansyah, T. M., Bansal, K.M., Gunarwan, G. and Lopez, D. (2005) "Simulation of multiphase flows in Indonesian Pipelines: Comparison of TACITE and OLGA results". Presented at 12th International Conference on Multiphase Production Technology, Barcelona, Spain, May 25-27, 2005.

Ishii, M., (1977) One-dimensional drift-flux model and constitutive equations for relative motion between phases in various two-phase flow regimes, ANL-77-47, Argonne National Laboratory, Argonne. (Cited in: Neil, E. T. and Kazimi, M. S. (1989) *"Nuclear Systems I: Thermal hydraulics fundamentals"*. Hemisphere Publishing Corporation, USA)

Jayanti, S. and Hewitt, G. F. (1992) "Prediction of the slug-to-churn flow transition in vertical two-phase flow", *International Journal of Multiphase Flow*, Volume18, pp 847-860.

Jansen, F. E. Shoham, O. and Taitel, Y. (1996) "The elimination of severe slugging – experiments and modelling". International Journal of Multiphase Flow, Volume 22(6), pp. 1055-1072.

Jansen, F. E. Shoham, O. (1994) "Methods for eliminating pipeline-riser flow instabilities". Paper presented at Western Regional Meeting, Long Beach, CA, Society of Petroleum Engineers, SPE paper- 27867, pp. 195-204.

Johal, K. S., The, C. E. and Cousins, A. R. (1997) "An alternative economic method to riser base gas lift for deep water subsea oil/gas field developments". Paper presented at 1997 Offshore European Conference, Aberdeen, Scotland, Society of Petroleum Engineers, SPE paper-38541, pp. 487-492.

Jones, O. C. Jr. and Zuber, N. (1975) "The interrelation between void fraction fluctuations and flow patterns in two phase flow". *International Journal of Multiphase Flow*, Volume 2 (3), pp. 273-306.

Kang, C., Vedapuri, D., Gopal, M. and Jepson, W. P. (2000) "The effect of inclination of slug characteristics in three phases, oil/water/gas flow in large diameter pipes". In the Proceedings of 2nd North American Conference on Multiphase Technology, Banff, Canada.

Kashou, S. (1996) Severe Slugging in an S-Shaped or Catenary Riser: OLGA Prediction and Experimental Verification. Paper presented at IBC Technical Services, Advances in Multiphase Technology Conference, Houston, TX, June 24-25, 1996.

Kataoka, I. and Ishii, M. (1987) "Drift flux model for large diameter pipe and new correlations for pool void fraction". *International Journal of Heat and Mass Transfer*, Volume 30(9), pp 1927-1939.

Khartabil, H. F. and Spinks, N. J. (1995) An Experimental Study of a Flashing-driven CANDU Moderator Cooling System, 16th Annual Conference, Canadian Nuclear Society, Saskatoon, Canada.

Klemp, S., Norris III, H.L., Fuchs, P., and Malnes, D. (1985) "Developments in the Simulation and Design of Multiphase Pipeline Systems". In 60th Annual Technical Conference and Exhibition of the Society of Petroleum Engineers held in Lass Vegas, SPE paper-14283, September 22-25, 1985.

Klemp, S. (1988) "Dynamic computer simulation – practical design experience with the OLGA code". Presented at Multiphase Flow - Technology and Consequences for Field Development -1987, paper no. 14.

Kocamustafaogullari, G. and Ishii, M. (1985) Maximum fluid particle size for bubbles and drops. In ASME Winter Annual Meeting, Proceedings of Fundamental Aspects of Gas–Liquid Flow, FED-Volume 29, Florida, USA, pp. 99

Kokal, S. L. and Stanislav, J. F (1989) "An experimental study of two phase flows in slightly inclined pipes: flow patterns". Chemical Engineering Science, Volume 44(3), pp. 665-679.

Krishna, R, Wilkinson, P. M., Van Dierendonck, L. L. (1991) "A model for gas holdup in bubble columns incorporating the influence of gas density on flow regime transitions", *Chemical Engineering Science*, Volume 46(10), 1991, pp. 2491-2496.

Landman, M. J. (1991) "Non-unique holdup and pressure drop in two-phase stratified inclined pipe flow". *International Journal of Multiphase Flow*, Volume 17 (3), pp. 377-394.

Letzel, H.M., Schouten, J.C., Van den Bleek, C. M., Krishna, R. (1997) "Influence of Elevated Pressure on the Stability of Bubbly Flows," Chemical Engineering Science, Vol. 52, pp. 3733-3739.

Lin, P. Y. and Hanratty, T. J. (1987) "Detection of slug flow from pressure measurements", *International Journal of Multiphase Flow*, Volume 13(1), pp.13-21.

Lin, T.-J., Tsuchiya, K., Fan, L. S. (1998) "Bubble Flow Characteristics in Bubble Columns at Elevated Pressure and Temperature". *The AIChE Journal*, Volume44, pp. 545-560.

Liu, T. J. (1993) "Bubble size and entrance length effects on void development in vertical channel", *International Journal of Multiphase flow*, Volume 19(1), pp. 99-113.

Liu, T. J. and Bankoff, S. G. (1993) "Structure of air-water bubbly flow in vertical pipe-II: void fraction, bubble velocity and bubble size distribution". International Journal of Heat and Mass Transfer, Volume 36(4), pp. 1061-1072.

Lockett, T. (2007). Private communications.

Lopez, D. and Duchet-Suchaux, P. (1998) "Performances of Transient Two-Phase Flow Models". Presented at the International Petroleum Conference and Exhibition of Mexico, SPE paper-39858, Villahermosa, March 3-5, 1998.

Ma, P. Y., Chung, N. M., Pei, B. S. (1991) "Two simplified methods to determine void fractions for two phase flows", *Nuclear Technology*, Volume 94, pp. 124-133.

Mandhane, J.M., Gregory, G.A., and Aziz, K. (1974) A flow pattern map for gas--liquid flow in horizontal pipes. *International Journal of Multiphase flow*, Volume 1, pp. 537-553.

Manera, A., Prasser, H-M, Tim, H. J. and Hagen, V J. (2005) "Suitability of Drift-Flux Models, Void-Fraction Evolution, and 3-D Flow Pattern Visualization During Stationary and Transient Flashing Flow in a Vertical Pipe", *Nuclear Technology*, Volume 152 (1), pp. 38-53.

Maier, D. and Coddington, P. (1997) Review of wide rang void correlations against and extensive data base of rod bundle measurements, Proceedings of ICONE-5, Paper no-2434.

Mao, Z. S. and Dukler, A. E. (1993) "The myth of churn flow", International *Journal of Multiphase flow*, Volume (19), pp. 377-383.

Matar, O., Hewitt, G. F., Lawrence, C. J., and Spelt, P. D. M. (2008) Multiphase flow in vertical and deviated pipes. EPSRC Research Contract: EP/F017448/1, UK. (Internet link: http://gow.epsrc.ac.uk/ViewGrant.aspx?GrantRef=EP/F017448/1)

Matsui, G. (1984) Identification of flow regimes in vertical gas-liquid two phase flow using differential pressure fluctuations. *International Journal of Multiphase flow*, Volume 10(6), pp. 711-720.

Matsui, G. (1986). "Automatic identification of flow regimes in vertical two-phase flow using differential pressure fluctuations". *Nuclear Engineering and Design*, Volume 95, pp. 221-231.

McQuillan, K. W. and Whalley, P. B. (1985) "Flow patterns in vertical two phase flow". *International Journal of Multiphase Flow*, Volume 11, pp 161-175

Mehrdad P. F., John-Morten G., and Svein Ivar S. (2006) "Modelling of Severe Slug and Slug Control with OLGA", SPE Production & Operations, Volume 21, Number 3, pp. 381-387.

Miller, D. S. (1990) "Internal Flow Systems", 2nd Edition, BHR Group, Cranfield, UK.

Mishima, K. and Ishii, M. (1984) "*Flow regime transitions criteria for upward two phase flow in vertical tubes*". International Journal of Heat and Mass transfer, Volume 27 (5), pp. 723-737.

MIT report. (2000) Annual Project Status Report: Design of an Actinide Burning, Lead or Lead-Bismuth Cooled Reactor that Produces Low Cost Electricity, MIT-ANP-PR-071, INEEL/EXT-2000-00994, July 2000.

Mokhatab, S. (2007). "Severe Slugging In a Catenary-shaped Riser: Experimental and Simulation Studies". *Petroleum Science and Technology*, Volume 25, pp. 719-740.

Montgomery, J. A. (2002). Severe Slugging and Unstable Flows in an S Shaped Riser. PhD Thesis, Cranfield University, Bedfordshire, UK.

Morooka, S., Ishizuka, T., Isuzu, M., and Yoshimura, K. (1989) "Experimental Study on Void Fraction in a Simulated BWR Fuel Assembly (Evaluation of Cross-Sectional Averaged Void Fraction)", *Nuclear Engineering and Design*, Vol. 114, pp. 91-98.

Neil, E. T. and Kazimi, M. S. (1989) *"Nuclear Systems I: Thermal hydraulics fundamentals"*. Hemisphere Publishing Corporation, USA.

Nicklin, D.J. (1962) Two-phase bubble flow, *Chemical Engineering Science*, Volume 17 (9), pp. 693-702.

Norris III, H.L., Fuchs, P., Malnes, D., Klemp, S. (1985) "Developments in the Simulation and Design of Multiphase Pipeline Systems", In 60th Annual Technical Conference and Exhibition of the Society of Petroleum Engineers held in Lass Vegas, NV. SPE paper-14283, September 22-25, 1985.

Oddie, G., Shi, H., Durlofsky, L. J., Aziz, K., Pfeffer, B. and Holmes, J. A. (2003) "Experimental study of two and three phase flows in large diameter inclined pipes". International Journal of Multiphase Flow, Volume 29(4), pp. 527-720.

Offshore Technology. (2009) *Na Kika Oil and Gas Fields, Gulf of Mexico, USA.* Available: http://www.offshore-technology.com/projects/na_kika/. Last accessed 3 June 2009.

Ohnuki, A. and Akimoto, H. and Sudo, Y. (1995) "Flow pattern and its transitions in gas-liquid two phase flow along as large vertical pipe". Proceedings of the 2nd International Conference on Multiphase, Kyoto, Japan.

Ohnuki, A. and Akimoto, H. (1996) "An experimental study on developing air-water two phase flow along a large vertical pipe: effect of air injection method. *International Journal of Multiphase flow*, Volume 22(6), pp. 1143-1154.

Ohnuki, A. and Akimoto, H. (2000) "Experimental study on transitions of flow pattern and phase distribution in upward air-water two phase flow along a large vertical pipe". *International Journal of Multiphase flow*, Volume 26(3), pp. 367-386.

OLGA (2000) "OLGA 2000 - User Manual".

OLGA (2007) "OLGA - User Manual version 5".

Omebere-Iyari, N. K., Azzopardi, B. J. and Ladam, Y. (2007) "Two-phase flow patterns in large diameter vertical pipes at high pressures", *The AIChE Journal*, Volume 53(10), pp. 2493-2504.

Omebere-Iyari, N. K., Azzopardi, B. J., Lucas, D., Beyer, M. and Prasser, H-M. (2008) "The characteristics of gas/liquid flow in large risers at high pressures". *International Journal of Multiphase Flow*, Volume 34(5), pp. 461-476.

Ouyang, L. B. and Aziz. K. (2002) Solution non-uniqueness for Separated Gas-Liquid Flow in Pipes and Wells – I: Occurrence. *Petroleum Science and Technology*, Volume 20 (1-2), pp 143-171.

Pickering, P. F., Hewitt, G. F., Watson, M. J. and Hale, C. P. (2001). The prediction of flows in production risers - truth & myth. IIR Conference, Aberdeen, UK, June 26-27, 2001.

Postvoll, W., Thaule, S. B., Flaten, G., Urdahl, O., Spiers, R. and Barley, J. (2002) "Huldra: Initial Experiences in Real-Time Multiphase Pipeline Modelling". In proceedings of: 34th Pipeline Simulation Annual meeting, Oregon, US, October 23-25, 2002.

Pots, B. M. F., Bromilow, I. G., and Konijin, M. J. W. F. (1985) "Severe slugging flow in offshore flowline/riser systems". Presented at Middle East Oil Technical Conference and Exhibition, Bahrain, Society of Petroleum Engineers, SPE paper-13723, pp. 347-352.

Prasser, H-M., Boettger, A., Beyer, M., Carl, H., Lucas, D., Schaffrath, A., Schütz, P., Weiss, F. P., and Zschau, J. (2002) "TOPFLOW tests on the structure of the gas-liquid Interface in a large vertical pipe". Forschungszentrum Rossendorf Annual Report-2002, FZR-380.

Prasser, H. M., Beyer, M., Carl, H., Gregor, S., Lucas, D., Schütz, P., and Weiss, F. P. (2005) "Evolution of the structure of a gas-liquid two-phase flow in a large vertical pipe". Presented at: The 11th International Topical Meeting on Nuclear Reactor Thermal-Hydraulics (NURETH-11) Popes Palace Conference Centre, Avignon, France, October 2-6, 2005

Prasser, H-M., Beyer, M., Carl, H., Gregor, S., Lucas, D., Pietruske, H., Schütz, P., Weiss, F-P. (2007) "Evolution of the structure of a gas–liquid two-phase flow in a large vertical pipe". Nuclear Engineering and Design, Volume (237), pp. 1848-1861.

Premoli, A., Francesco, D., and Prina, A. (1970) "An Empirical Correlation for Evaluating Two-Phase Mixture Density under Adiabatic Conditions", European Two-Phase Flow Group Meeting, Milan, Italy (cited in: Hewitt, G. F. (1982). "Chapter 2: flow regimes and Chapter 10: *Measurement of Two-Phase Flow Parameters*". In: Handbook of Multiphase Systems, Edited by Hetsroni, G. Publisher: Hemisphere/McGraw Hill, Washington)

Pushkina, O. L. and Sorokin, L. (1969) "Breakdown of liquid film motion in vertical tubes", Heat Transfer Soviet Res., Volume (1), pp. 56-64 (Cited in: Neil, E. T. and Kazimi, M. S. (1989). *"Nuclear Systems I: Thermal hydraulics*

fundamentals". Hemisphere Publishing Corporation, USA)

Putra, S. A. (2002) "East Java Gas Pipeline Liquid Condensation Study Using Dynamic Multiphase Flow Simulator," presented at the SPE Asia Pacific Oil and Gas Conference and Exhibition in Melbourne, Australia, October 8-10, 2002. SPE paper-77928

Qazi, N. and Yeung, H. (2006) Remote access and monitoring of two phase flow rig using Web/WAP protocol. National Instruments: LabVIEW in the Curriculum Paper Contest, pp. 80-85.

Ribeiro, A. M., Ferreira, V., Campos, J. B. L. M. (2006) On the comparison of new pressure drop and hold-up data for horizontal air–water flow in a square cross-section channel against existing correlations and models. *International Journal of Multiphase Flow,* Volume 32, pp. 1029–1036.

Rouhani, S. Z., and Axelsson, E., (1970) "Calculation of void volume fraction in the subcooled and quality boiling regions," *International Journal of Heat and Mass Transfer*, Volume 13, pp. 383-393. (Cited in: Wolverine Engineering Data Handbook, by Prof. J. R. Thom, edition III, 2004-2006, Wolverine Tube Inc.)

Sarica, C. and Shoham, O. (1991) "A Simplified Transient Model for Pipeline-Riser Systems", *Chemical Engineering Science*, 46, pp. 2167-2179.

Sarica, C. and Tengesdal, J. Ø. (2000)"A new technique to eliminate severe slugging in pipeline/riser systems". Paper presented at 2000 SPE Annual Technical Conference and Exhibition, Dallas, Texas, Society of Petroleum Engineers, SPE e-library; paper number 63185, pp. 633-641.

Scandpower. (2007) Flow assurance with OLGA – Training manual.

Schäfer, R., Merten, C. and Eigenberger, G. (2002) "Bubble size distributions in a bubble column reactor under industrial conditions", *Experimental Thermal and Fluid Science*, Volume (26), pp. 595–604. (2002).

Schmidt, Z. and Beggs, H. D. (1979) "Choking can eliminate severe pipeline slugging", *Oil Gas Journal*, pp. 230-238.

Schmidt, Z., Brill, J.P., Beggs, H.D. (1980) "Experimental study of severe slugging in a two-phase-flow pipeline - riser pipe system". *SPE Journal*, SPE paper- 8306, Volume 20(5), pp407-414.

Schmidt, Z., Brill, J. P. and Beggs, H.D. (1981) "Experimental study of two phase normal slug flow in a pipeline riser pipe system". Journal of Energy Resources Technology, Volume 103, pp. 67-75.

Schmidt, Z., Brill, J. P. and Beggs, H.D. (1980) "Experimental study of severe slugging in two phase flow pipeline riser pipe system". SPE Journal, pp 67-75. Cited in: Bendiksen, K. H., Malnes, D., Moe, R., & Nuland, S. (May 1991). "The dynamic two-fluid model OLGA: Theory and application". SPE production engineering, SPE paper-19451.

Schmidt, Z., Doty, D. R. and Roy, K. D. (1985) "Severe slugging in offshore pipeline riser pipe systems". SPE Journal, Society of Petroleum Engineers. Pp. 27-38.

Sekoguchi, K., Fukui, H. and Sate, Y. (1980) "Two-phase Flow Dynamics", Edited by: A.E. Bergles and S. Ishigai, Japan-US (cited in: Hills, T. J. (1993). "The behaviour of bubble column at high throughputs: Radial voidage profiles". The Chemical Engineering Journal, Volume 53, pp. 115-123)

Serizawa, A., Kataoka, I. and Michiyoshi, I. (1975) "Turbulence structure of air-water bubbly flows-2 Local properties", *International Journal of Multiphase Flow,* Volume 2**,** pp. 235-246.

Serizawa, A., Kataoka, I., Zun, I. and Michiyoshi, I. (1988) "Bubble size effect on phase distribution". Proceedings of the Japan-US Seminar on Two phase flow dynamic. Japan. Pp. 379-400.

Shah, Y. T., Kelkar, B. G., Godbole, S. P. Deckwer, W.D. (1982) Design parameters estimations for bubble columns reactors, *The AIChE Journal*, Volume 28, pp.353-379.

Shannak, B. A. (2008) Frictional pressure drops of gas liquid two-phase flow in pipes, *Nuclear Engineering and Design*, Volume 238(12), pp. 3277-3284.

Shen X, Mishima K, Nakamura H. (2005) "Two-phase phase distribution in a vertical large diameter pipe". *International Journal of Heat Mass Transfer*, Volume (48), pp. 211-225.

Shen, X., Saito, Y., Mishima, K., and Nakamura, H. (2006) "A study on the characteristics of upward air–water two-phase flow in a large diameter pipe", *Experimental Thermal and Fluid Science*, Volume 31, pp. 21-36.

Shipley, D. G. (1984) "Shorter Communications: two phase flow in large diameter pipes". *Chemical Engineering Science*, Volume 39(1), pp. 163-165.

Shoukri, M., Stankovic, B., Hassan, I., Dimmick, J. (2000) "Effect of pipe diameter on flow pattern transitions and void fraction of air-water flow in vertical pipes". Proceedings of ICONE-8, 8th International Conference on Nuclear Engineering, Baltimore, MD, USA.

Shoukri, M., Hassan, I., Gerges, I. (2003) "*Two phase bubbly flow structure in large diameter vertical pipes*", *The Canadian Journal of Chemical Engineering*, Volume 81, pp. 205-211.

Smith, S. W. (1999) The Scientist and Engineer's Guide to Digital Signal Processing, Second Edition, California Technical Publishing, San Diego, CA, US. www.DSPguide.com

Simpson, H. C., Rooney, D. H., Gilchrist, A., Grattan, E. and Callander, T. M. S. (1987). "*An assessment of some two phase pressure gradient, holdup and flow pattern prediction method in current use"*. In proceedings of 3rd BHRA International Conference on Multiphase Flow, The Hague, pp. 23-32.

Smith, S. P., Gregory, G. A. and Yarranton, Harvey W. (2003) *"Experimental investigation of multiple solutions for liquid holdup in upward inclined stratified flow". Journal of Energy Resources Technology*, Volume 125(2), pp.137-144.

Snoek, C. W. and Leung, L. K. H. (1989) A model for predicting diabatic pressure

drops in multi-element fuel channel, *Nuclear Engineering and Design*, Volume110, pp. 299-312.

Song, C. H., No, H. C., and Chung, M. K. (1995) "Investigation of bubble flow developments and its transition based on the instability of void fraction waves", *International Journal of Multiphase Flow*, Volume 21(3), pp. 381-404.

Song, S. and Kouba, G. (2000) "Characterization of Multiphase Flow in Ultra-Deep Subsea Pipeline/Riser System," ETCE/OAME2000 Joint Conference, New Orleans, LA, Feb. 14-17, 2000.

Song, S. and Peoples, K. (2003) "Impacts of transient analysis on Kuito production operations". In proceedings of 2003 Offshore Technology Conference, Houston, Texas, US, OTC paper no. 15186, 5–8 May, 2003.

Spedding, P. L. and Nguyen, T. Van. (1980) "Regimes for air-water two phase flow". Chemical Engineering Science, Volume 35 (4), pp. 779-793.

Spedding, P. L. and Chen, J. J. J. (1984) "An Analysis of Holdup in Horizontal Two-Phase Gas-Liquid Flow", *International Journal of Multiphase flow*, Volume 9(2), pp. 147-159.

Spedding, P. L. and Spence, D. R. (1989) Predicting holdup in two phase flow, *International Journal of Engineering Fluid Mechanics*, Volume 1, pp. 67-82.

Spedding, P., G. S. Woods' R. S. Raghunathan **and** J. K. Watterson. (1998). "Vertical Two-Phase Flow Part II: Experimental Semi-Annular Flow and Hold-Up", *Chemical Engineering Research and Design*, Volume: 76 (A5), Special issue: Oil and Natural Gas Production.

Straume, T., Nordsveen M., and Bendiksen, K. (1992) "Numerical simulation of slugging in pipelines". *ASME 1992 series: Multiphase Flow Wells and Pipeline*, pp. 144.

Subbotin, V. I., PokhvaIov, Yu. E., Mikhailov, L. E., Kronin, I.V. and Leonov, V. A. (1975) Teploenergetika, Volume 22 (4), pp 70-75 (Cited in: Hills, T. J. (1976). "The operation of bubble column at high throughputs: Gas holdup measurements". The Chemical Engineering Journal, Volume 12, pp. 89-99)

Sun, B., Wang, R., Zhao, X. and Dachun, Y. (2002) "The mechanism for the formation of slug flow in vertical gas-liquid two phase flow". Solid State Electronics, Volume 46, pp. 2323-2329.

Sun, X., Smith, T. R., Kim, S., Ishii, M. and Uhle, J. (2003) "Interfacial structure of air-water two phase flow in a relatively large diameter pipe". *Experimental Thermal in Fluids*, Volume 34, pp. 206-219.

Taitel, Y., and Dukler, A. E. (1976) A model for predicting flow regime transitions in horizontal and near horizontal gas- liquid flow", *The AIChE Journal*, Volume 22(1), pp. 47-55.

Taitel, Y., Barnea, D. and Dukler, A. E. (1980) "Modelling flow pattern transitions for steady upward gas-liquid flow in vertical tubes". *The AIChE Journal*, Volume 26(3), pp. 345-354.

Taitel, Y. (1986) "Stability of severe slugging". *International Journal of Multiphase flow*, Volume 12(2), pp. 203-217.

Taitel, Y., Shoham, O. and Brill, J. P. (1989) "Simplified transient solution and simulation of two phase flow in pipelines". *Chemical Engineering Science*, Volume 44 (6), pp 1353-1359.

Taitel, Y., Vierkandt, S., Shoham, O. and Brill, J. P. (1990) "Severe slugging in a riser system: Experiments and modelling", *International Journal of Multiphase Flow*, Volume 16(1), pp. 57-68.

TECDOC-1203. (2001) Thermohydraulic Relationships for Advanced Water Cooled Reactors. Report IAEA: International Atomic Energy Agency, Nuclear Power Technology Development Section, Vienna, Austria.

Tengesdal, J. O., Sarica, C. and Kaya, A. S (1999) "Flow-pattern transition and hydrodynamic modelling of churn flow", SPE Journal, SPE-57756. Volume (4), pp. 342–348.

Tengesdal, J. Ø., Leslie, T., and Sarica, C. (2003) A design approach for self-lifting: method to eliminate severe slugging in offshore production systems. Paper presented at SPE Annual Technical Conference and Exhibition, Denver, Society of Petroleum Engineers, SPE paper- 84227, October 5-8, 2003.

Thom J. R. (2004) "Wolverine Engineering Data Handbook", edition III, Wolverine Tube Inc. (internet source: www.wlv.com/products/index.html)

Tin, V. (1991) "Severe Slugging in Flexible Risers", In Proceedings of 5th International Conference on Multiphase Production, Cannes, France, pp. 507-526.

Tomiyama A. (1998) "Struggle with computational bubble dynamics". In: Proceedings of the Third International Conference on Multiphase Flow, ICMF-98, Lyon, France: June 8-12 (Cited in: Prasser, H-M., Beyer, M., Carl, H., Gregor, S., Lucas, D., Pietruske, H., Schütz, P., Weiss, F-P. (2007). "Evolution of the structure of a gas–liquid two-phase flow in a large vertical pipe". Nuclear Engineering and Design, Volume (237), pp. 1848-1861)

Tutu, N. K. (August 1982) Pressure fluctuations and flow pattern recognition in vertical two phase gas-liquid flows". *International Journal of Multiphase Flow*, Volume 8(4), pp. 443-447.

Ullmann, A., Zamir, M., Gat, S. and Brauner, N. (2003) "Multi-hold-ups in co-current stratified flow in inclined tubes". *International Journal of Multiphase Flow*, Volume 29(10), pp. 1565-1581.

Van der Welle. (1985) "Void fraction, bubbly velocity and bubble size in two phase flow*", International Journal of Multiphase flow*, Volume 11(3), pp. 317-345.

Vigneron, F., Sarica, C. and Brill, J. P. (1995) "Experimental analysis of imposed two-phase flow transients in horizontal pipelines". In: Proceedings of the BHR Group 7th International Conference*, Multiphase'95,* pp. 199-217, 1995.

Vijayan, P. K., Patil, A. P., Pilkhwal, D. S., Saha, D., Venkat R. V. (2000) "An assessment of pressure drop and void fraction correlations with data from two-phase

natural circulation loops", *Journal of Heat and Mass Transfer*, Volume 36(6), pp. 541-548.

Vince, M. A. and Lahey Jr., R. T. (1982) On the development of an objective flow regime indicator", *International Journal of Multiphase Flow*, Volume 8(2), pp. 93-124.

Vohra, I. R., Hernandez, F., Marcano, N., Brill, J.P. (1975) "Comparison of Liquid-holdup and Friction factor correlations for gas-liquid flow", *Journal of Petroleum Technology*, SPE paper-4690, pp. 564-568.

Whalley, P. B. (1996) "Two phase flow and heat transfer". Oxford University Press Inc. New York., USA.

Watson, M. J. and Hewitt, G. F. (1999) Pressure effects on the slug to churn transition. International Journal of Multiphase Flow, Volume 25(6-7), pp. 1225-1241.

Weisman, J., Duncan, D., Gibson, J., and Crawford, T. (1979) "Effects of fluid properties and pie diameter on the two phase flow patterns in horizontal lines". International Journal of Multiphase flow, Volume 5, pp. 437-462.

Weisman, J. and Kang, S. Y. (1981) "Flow pattern transitions in vertical and upwardly inclined lines", *International Journal of Multiphase Flow*, Volume 7(3), pp 271-291.

Weisman, J. and Crawford, T. (1984) "Two phase flow pattern transitions in ducts of non-circular cross-section and under diabatic conditions", *International Journal of Multiphase Flow*, Volume 10(3), pp. 385-391.

Wilkinson, P.M., Van Dierendonck, L.L. (1991) "Pressure and Gas Density Effects on Bubble Break-Up and Gas Hold-Up in Bubble Columns," *Chemical Engineering Science*, Volume 45, pp. 2309-2315.

Xu, Z. G. (1997) "Solutions to Slugging Problems Using Multiphase Simulations", *3rd International Conference of Multiphase Metering*, Aberdeen, United Kingdom, March 12-13, 1997.

Yeung, H. and Montgomery, J. (2001) "Hydrodynamic behaviour of a flexible riser - a comparison of experimental data and three transient code predictions". *In Proceedings of: MULTIPHASE '01, 10th International Multiphase Flow Conference*, Cannes, France, June 13–115, 2001.

Yeung, H. and Montgomery, J. (2002) "The Stability of Fluid Production from a Flexible Riser", *Journal for Energy Resources Technology*, Volume 124, pp. 83-89.

Yeung, H., Tchambak, E. and Montgomery, J. (2003) "Simulating the behaviour of an S-shaped riser". *In Proceedings of: 11th International Conference on Multiphase Flows, MULTIPHASE '03*, BHR Group, San Remo, Italy: June 11-13, 2003.

Yocum, B. T. (1973) "Offshore riser slug flow avoidance: mathematical models for design and optimization". Paper presented at 2nd Annual European Meeting of Society of Petroleum Engineers of AIME, London, SPE paper- 4312.

Zuber, N. (August 1960) On the Variable-Density Single Fluid Model for Two phase

flow, “Trans ASME, *Journal of Heat Transfer*”, Volume 83, pp. 265-272.

Zuber, N. and Findlay, J. A. (1965) “Average volumetric concentration in two-phase flow systems,” *Journal of Heat Transfer*, Volume 87, pp. 453-468. (Cited in: Wolverine Engineering Data Handbook, by Prof. J. R. Thom, edition III, (2004-2006), Wolverine Tube Inc.).

Zun, I. (1988) Transitions from wall void peaking to core void peaking in turbulent bubbly flow. In : Transient Phenomenon in Multiphase Flow, edited by N. H. Afghan, Hemisphere, Washington, DC, pp 225-245. (Cited in: Hibiki, T. and Ishii, M. (2002). Distribution parameter and drift flux velocity of drift flux model in bubbly flow. *International Journal of Heat and Mass transfer*, Volume 45(4), pp. 707-721)

APPENDIX A

Appendix A-1

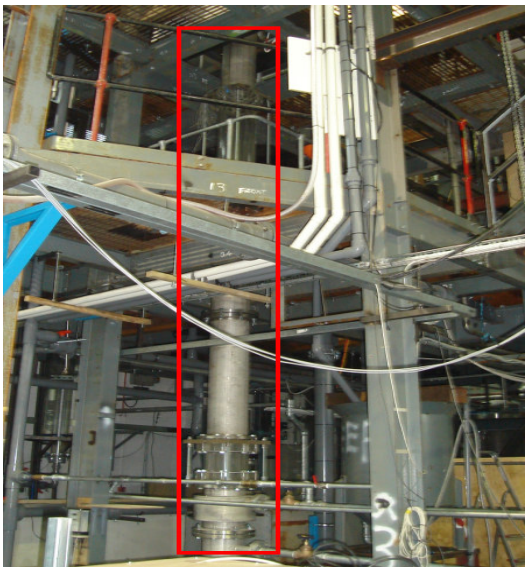

Figure 1. Photographic view of large diameter riser test section.

Figure 2. Photographic view of horizontal pipeline-riser base along with return path to sump and also return path to riser base (downcomer).

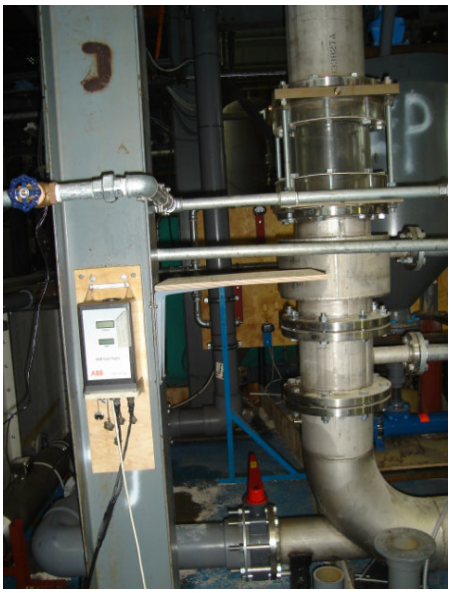

Figure 3. Photographic view of return path to riser base (downcomer).

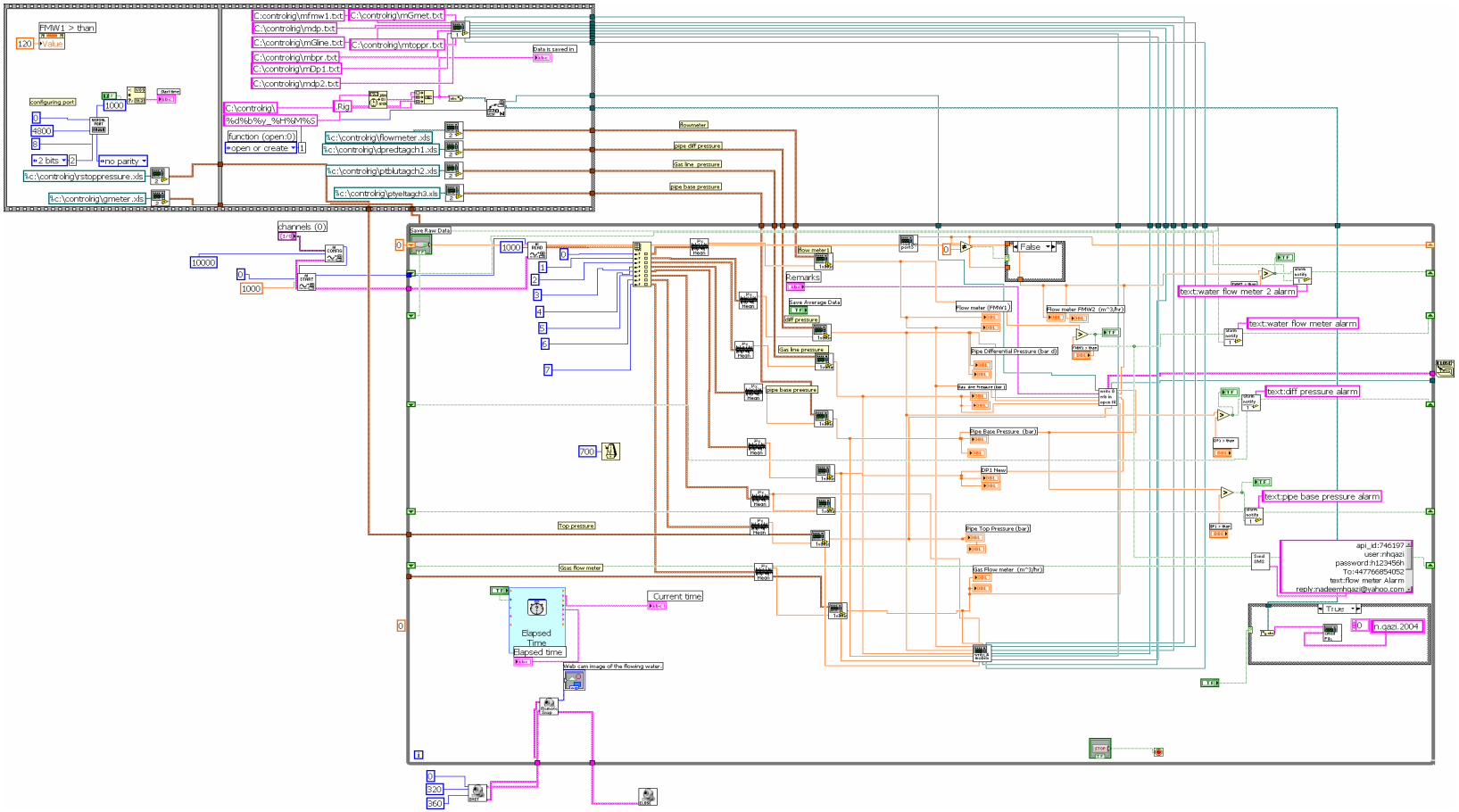

Figure 4. LABVIEW diagram of backend panel indicating all the used VI's (virtual instruments).

Appendix A-2

Single phase experiments

Prior to performing the two phase experiments, single phase experiments were conducted. The objective behind these experiments was to establish the frictional losses and hence friction factor for the input to the numerical simulations. From the experiments the magnitude of frictional loss involved can be determined by:

$$(\Delta P)_{sp,R} = (\Delta P)_s + (\Delta P)_{fric} \quad (2a)$$

$$(\Delta P)_{fric} = (\Delta P)_{sp,R} - (\Delta P)_s \quad (2b)$$

In above equations $(\Delta P)_{sp,R}$, $(\Delta P)_s$, $(\Delta P)_{fric}$ are the total single phase pressure drop in the riser, static and frictional pressure drop respectively. With the help of above, f was calculated for given water velocity according to the Darcy equation:

$$\Delta P_{RL} = 4f \cdot \left(\frac{L}{D}\right) \cdot \frac{\rho_w \cdot U_w^{\,2}}{2} \text{ and } \qquad \mathrm{Re}_w = \frac{\rho_w U_w D_w}{\mu_w} \quad (2d \text{ \& } 2c)$$

In above equation, ΔP_{RL} is measured frictional loss, f is fanning friction factor ($4f = f_D$), L is length of the riser, D is diameter of pipe, U_w is the water velocity and ρ_w is the water density. The Reynolds number for each water velocity was calculated. Where Re_w is the Reynolds number and μ_w is the water viscosity. From measured single phase frictional pressure drop (equation 2d), friction factor were determined and then ε/D by using Nikuradse correlation for rough pipes (Brill and Mukherjee, 1992) for input to numerical simulation. The results are provided below in tabular form:

$$\frac{1}{\sqrt{f}} = 1.74 - 2\log\left(\frac{2\varepsilon}{D}\right) \quad (2c)$$

Case	j_w	ΔP_R	ΔP_{RL}	f	ε
	m/s	**bar**	**mbar**	**-**	**mm**
Single phase - # 1	0.14	0.899	0.034	0.241	0.109
Single phase - # 2	0.27	0.900	0.042	0.077	0.050
Single phase - # 3	0.41	0.901	0.051	0.043	0.027
Single phase - # 4	0.55	0.903	0.075	0.035	0.021
Single phase - # 5	0.69	0.906	0.136	0.031	0.017
Single phase - # 6	0.82	0.907	0.106	0.023	0.011
Single phase - # 7	0.96	0.909	0.135	0.020	0.009
Average				0.067	0.035

Above values of relative roughness (ε) has been used in the numerical simulation and are approximate in nature.

APPENDIX B

B-1. Liquid Production
B-2. Differential pressure profiles
B-3. Visual flow regime transitions
B-4. Sectional void fraction distribution
B-5. Riser base pressure
B-6. Stability analysis
B-7. Statistical analysis
B-9. Effect of inlet conditions (annular sleeve results)
B-10. Steady state results from OLGA for vertical riser base gas injection

B-1. Liquid Production: Preliminary results of Annular sleeve and Tee injectors for different runs under Natural lift mode.

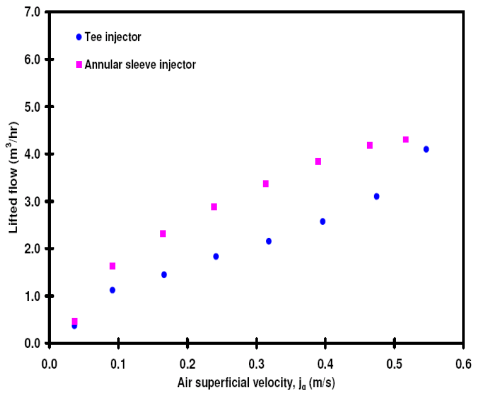

Figure 1. The comparison of the liquid production from the two injectors, phase-I results.

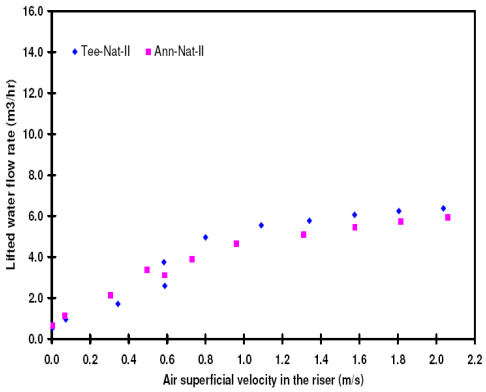

Figure 2. The comparison of the liquid production from the two injectors, phase-II results.

B-2. Differential pressure profiles: from the riser at about 5m height for Annular and Tee injectors under Natural lift for increasing air superficial velocity. Note that in all the figures standard deviations representing the fluctuation magnitude are also mentioned. This serves as rough guide to compare the size of bubbles generated to identify the flow pattern, as suggested by various researchers (Hubbard & Dukler, 1966 etc.).

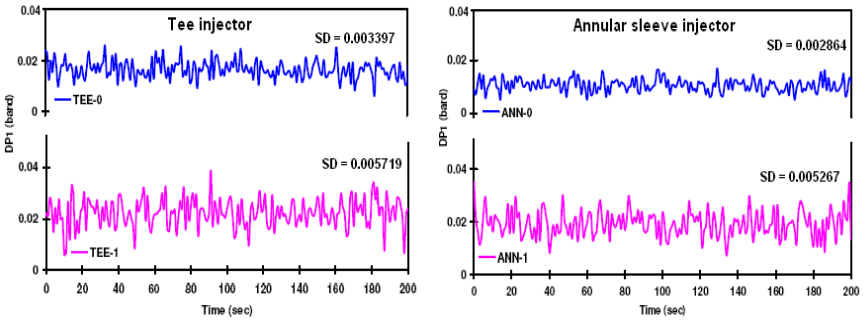

Figure 3. Pressure profile obtained from pressure sensor near the exit of the riser under natural lift mode for Tee and Annular sleeve injectors.

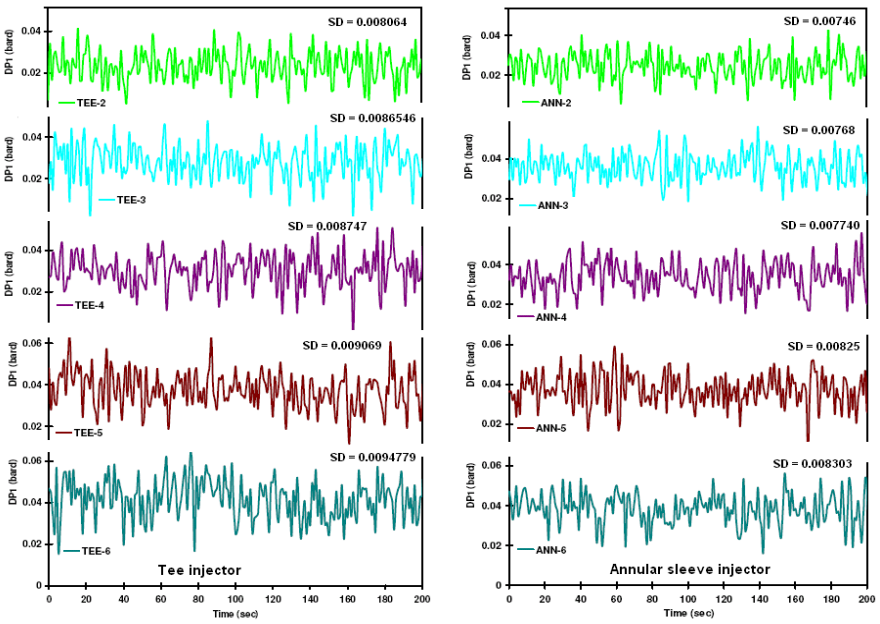

Figure 4. Pressure profile obtained from pressure sensor near the exit of the riser under natural lift mode for Tee and Annular sleeve injectors.

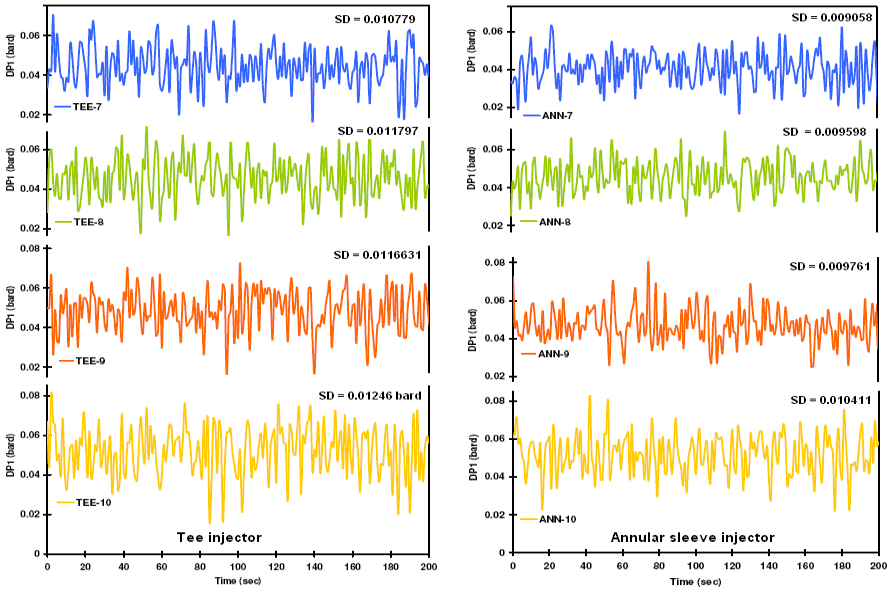

Figure 5. Pressure profile obtained from pressure sensor near the exit of the riser under natural lift mode for Tee and Annular sleeve injectors.

B-3. Visual flow regime transitions: for Annular sleeve and Tee injector obtained under forced lift mode from the preliminary set of experiments.

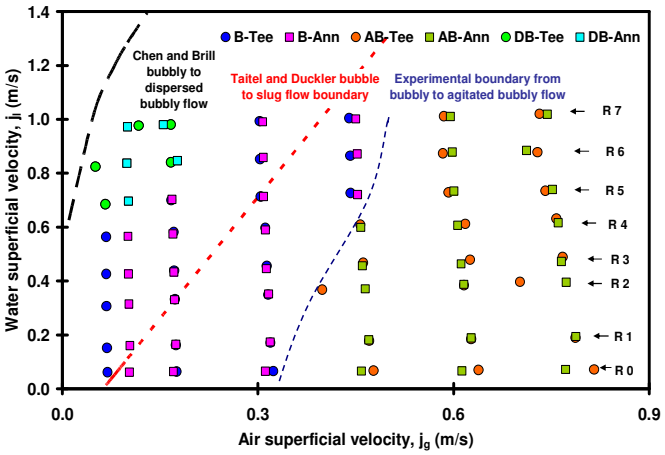

Figure 6. The preliminary forced lift experiments showing transition boundary between (a) the bubbly to agitated bubbly flow and (b) agitated bubbly to churn/froth flow for the two injectors.

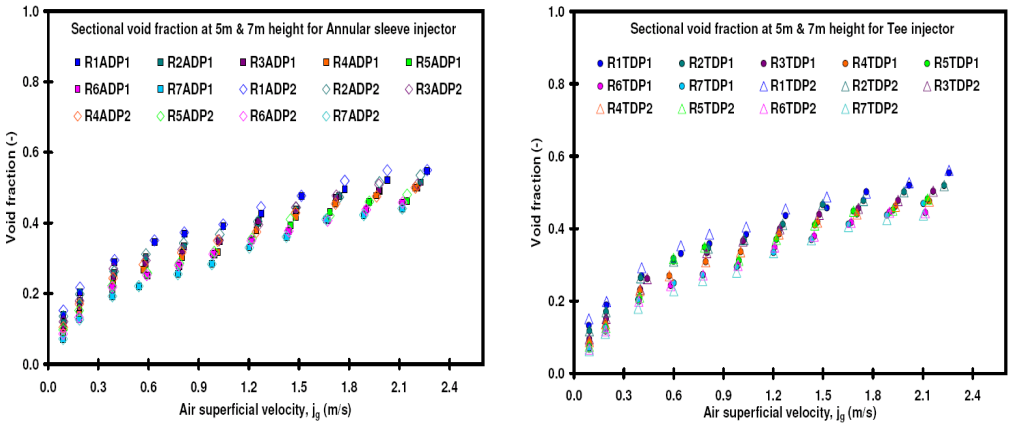

Figure 7. The sectional average void fraction at 5m (top) and 8m (below) height in the riser under forced lift condition for two injectors separately. (Note that dp1 & and dp2 not changing significantly this shows low development)

B-4.Void fraction distribution: for Annular sleeve and Tee injector obtained under natural lift mode.

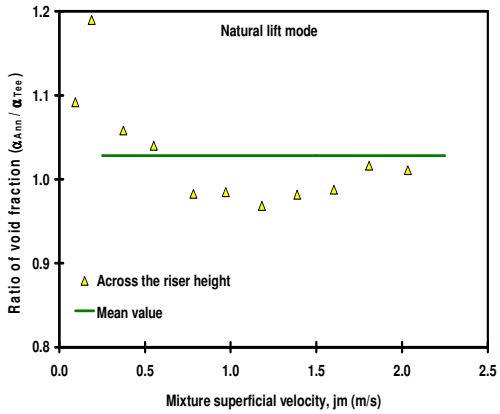

Figure 8. Ratio of average void fraction values α_{ANN} / α_{TEE} across the riser height for all the riser injection tests.

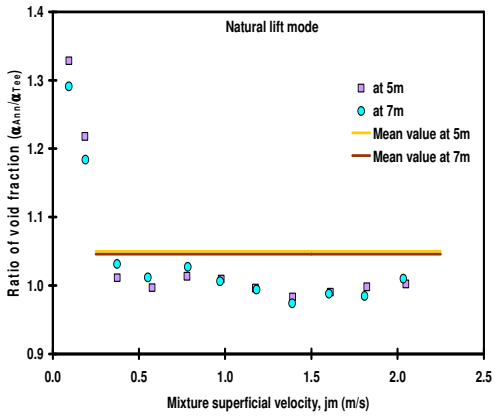

Figure 9. Ratio of sectional void fraction values α_{ANN} / α_{TEE} across the riser height for all the riser injection tests.

B-5. Riser base pressure: for Annular sleeve and Tee injector obtained under forced lift mode from the preliminary set of experiments.

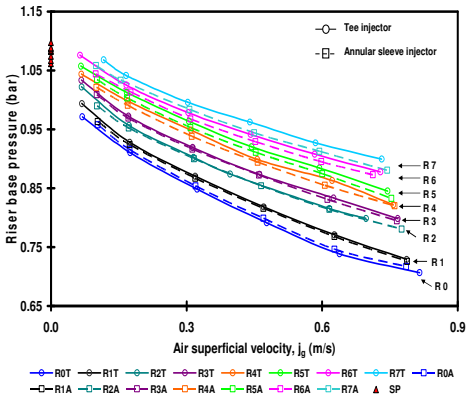

Figure 10. Riser base pressure under forced lift mode for both the injectors, phase-I results.

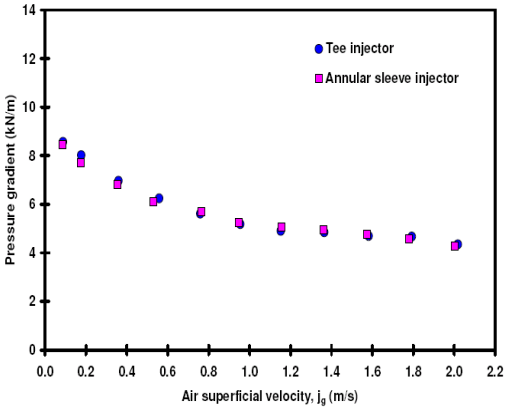

Figure 11. The riser base pressure trends under natural lift for Annular sleeve and Tee injectors, phase-I results.

B-6. Stability analysis: simple flowline-riser experiments vs. combine air lift with tee /annular sleeve injector flowline-riser experiments.

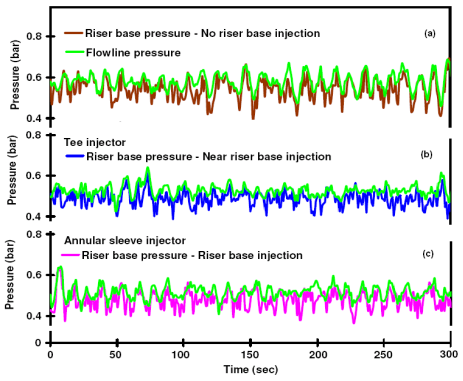

Figure 12. The flowline exit and near riser base pressure trends for Upstream injection, by Tee and by Annular sleeve injector at j_w =0.3m/s, j_g =1.23m/s and $j_{g,inj}$ =0.3m/s.

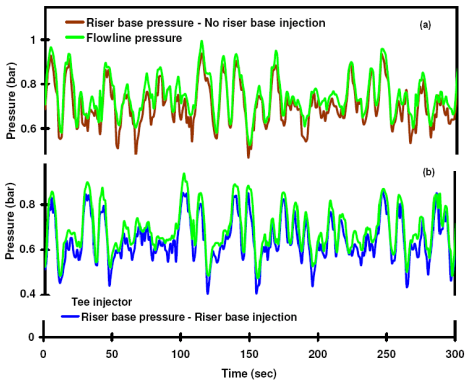

Figure 13. The flowline exit and near riser base pressure trends for Upstream injection and by Tee injector at j_w =0.55m/s, j_g =0.76m/s and $j_{g,inj}$ =0.24m/s.

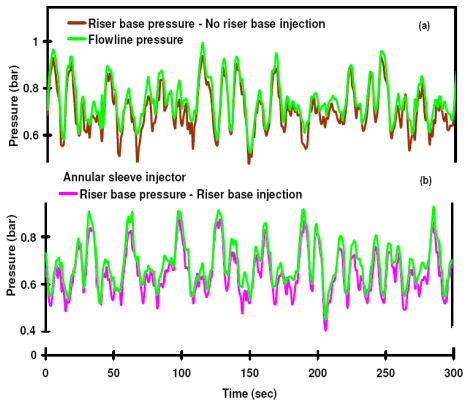

Figure 14. The flowline exit and near riser base pressure trends for Upstream injection and by Annular sleeve injector at j_w =0.55m/s, j_g =0.78m/s and $j_{g,inj}$ =0.2m/s.

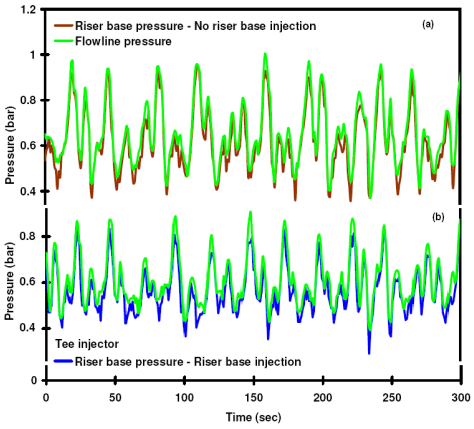

Figure 15. The flowline exit and near riser base pressure trends for Upstream injection and by Tee injector at j_w =0.58m/s, j_g =1.11m/s and $j_{g,inj}$ =0.5m/s.

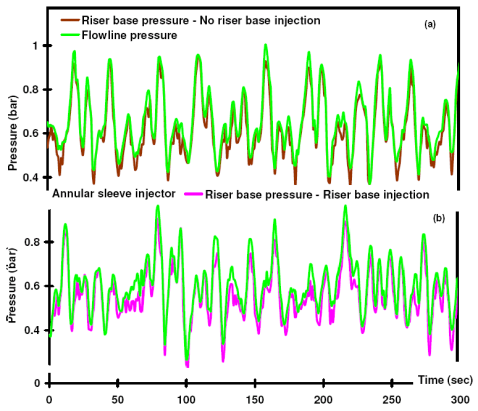

Figure 16. The flowline exit and near riser base pressure trends for No injection and by Annular sleeve injector at j_w =0.58m/s, j_g =1.15m/s and $j_{g,inj}$ =0.48m/s.

B-7. Statistical analysis: Probability mass functions PMF's of all the experiments provided on the flow regime map in section 4.1.2 (Figure 4.8). Note that we have not plotted in the first gas superficial velocity in these figures, they have been plotted in separately in figure 29 & 30 in order to differentiate between bubbly and dispersed bubbly flow.

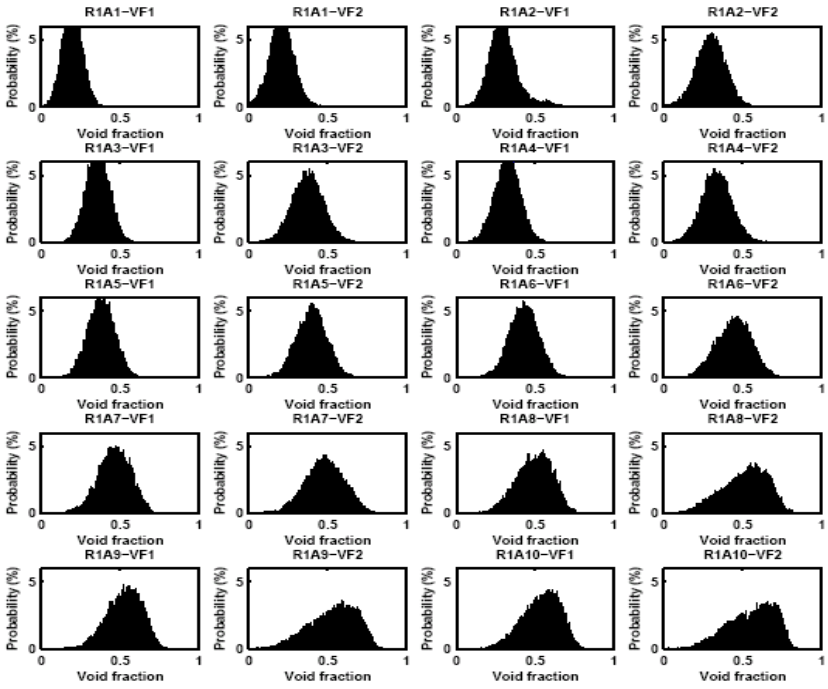

Figure 17. The PMF's plots taken at the height of 5 and 8m for Annular sleeve injector (R1).

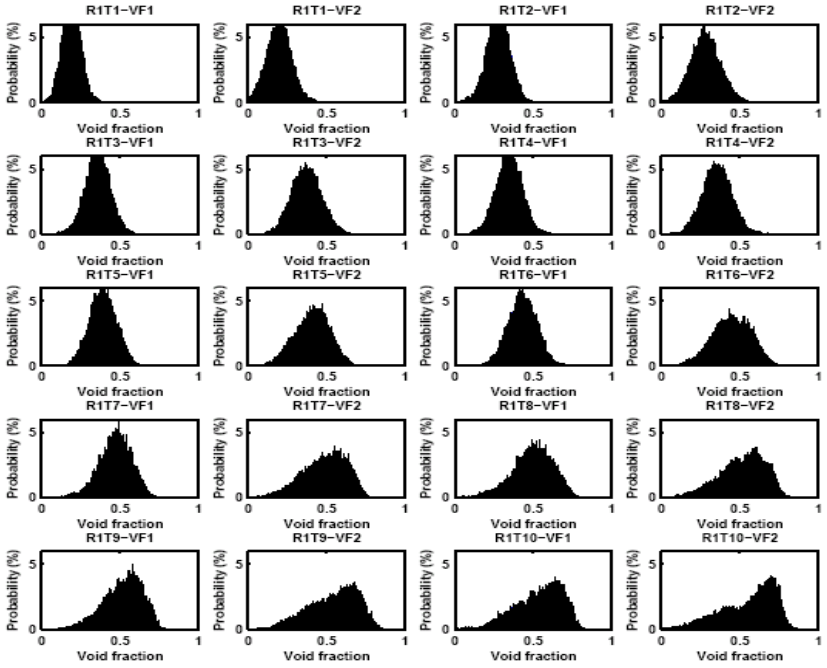

Figure 18. The PMF's plots taken at the height of 5 and 8m for Tee injector (R1).

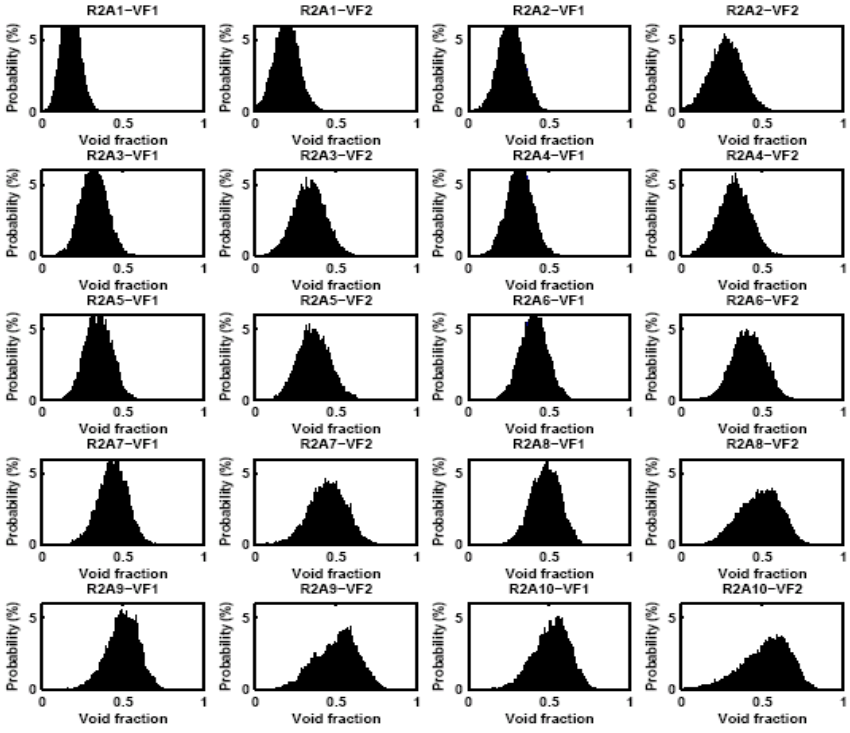

Figure 19. The PMF's plots taken at the height of 5 and 8m for Annular sleeve injector (R2).

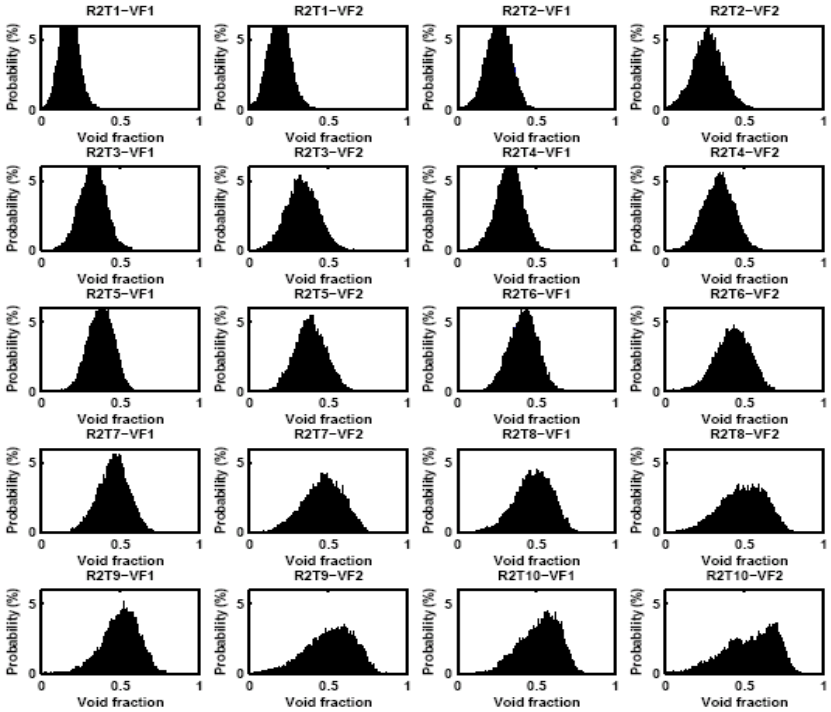

Figure 20. The PMF's plots taken at the height of 5 and 8m for Tee injector (R2).

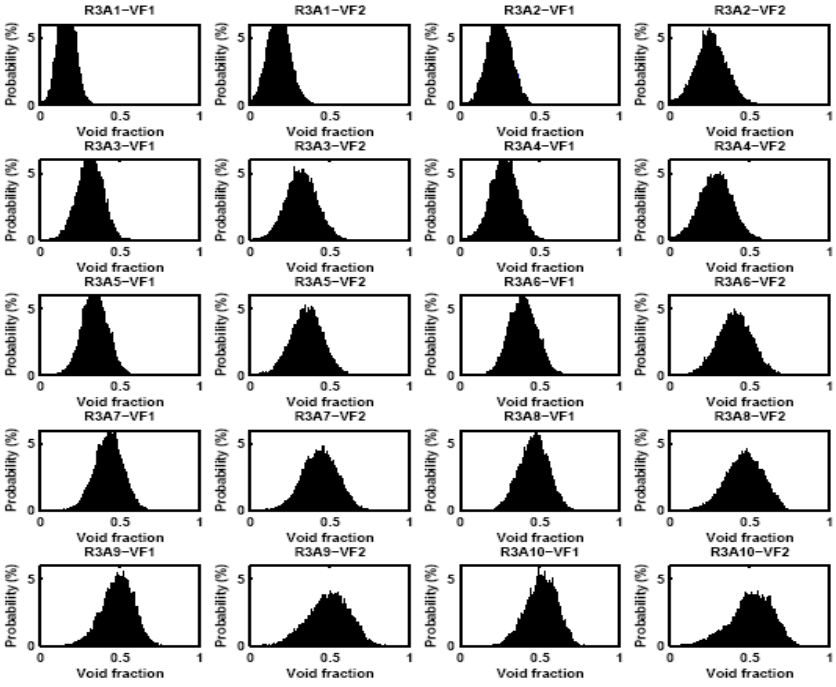

Figure 21. The PMF's plots taken at the height of 5 and 8m for Annular sleeve injector (R3).

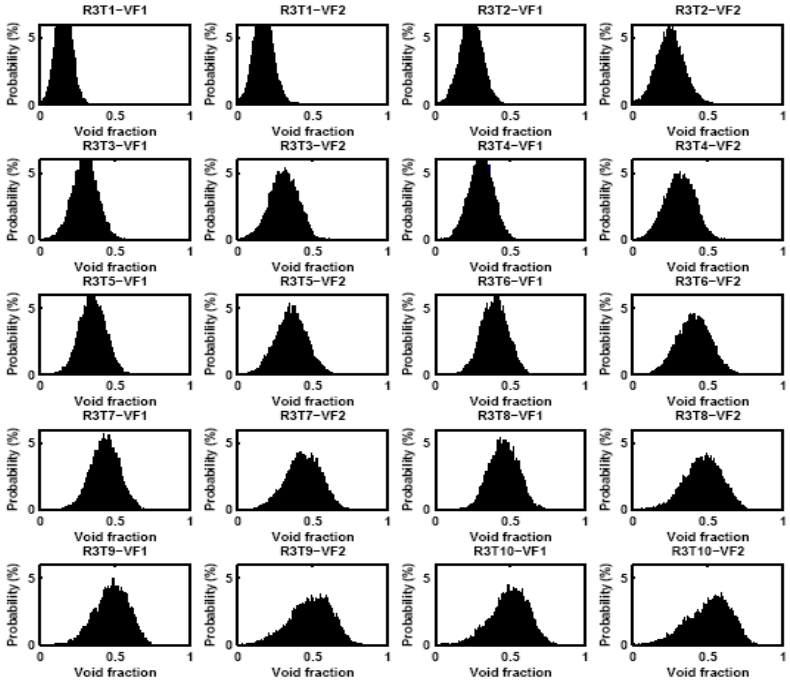

Figure 22. The PMF's plots taken at the height of 5 and 8m for Tee injector (R3).

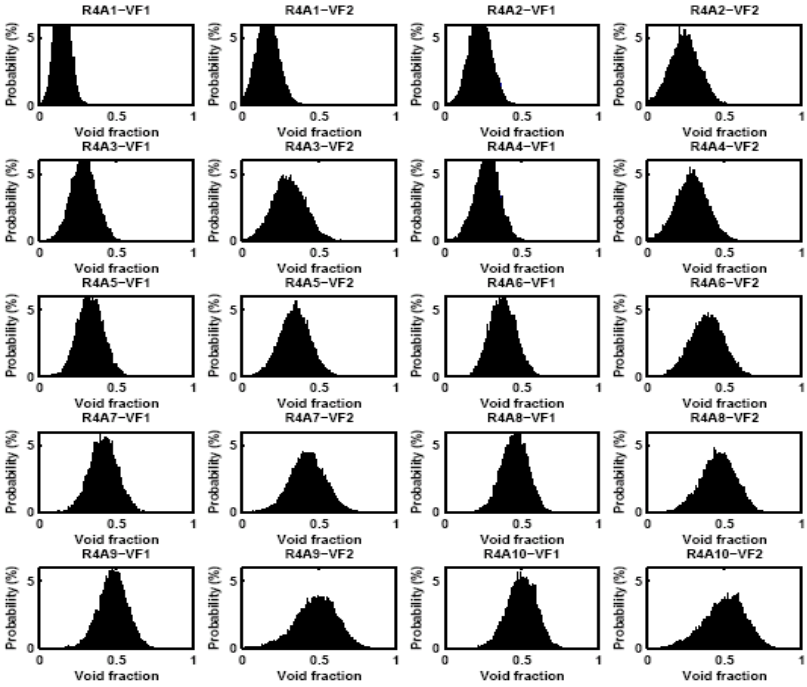

Figure 23. The PMF's plots taken at the height of 5 and 8m for Annular sleeve injector (R4).

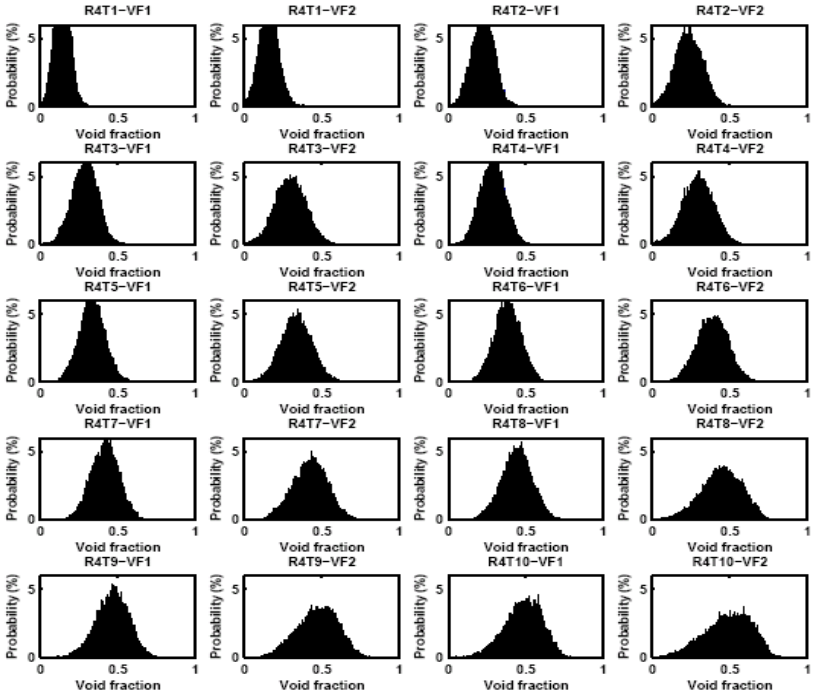

Figure 24. The PMF's plots taken at the height of 5 and 8m for Tee injector (R4).

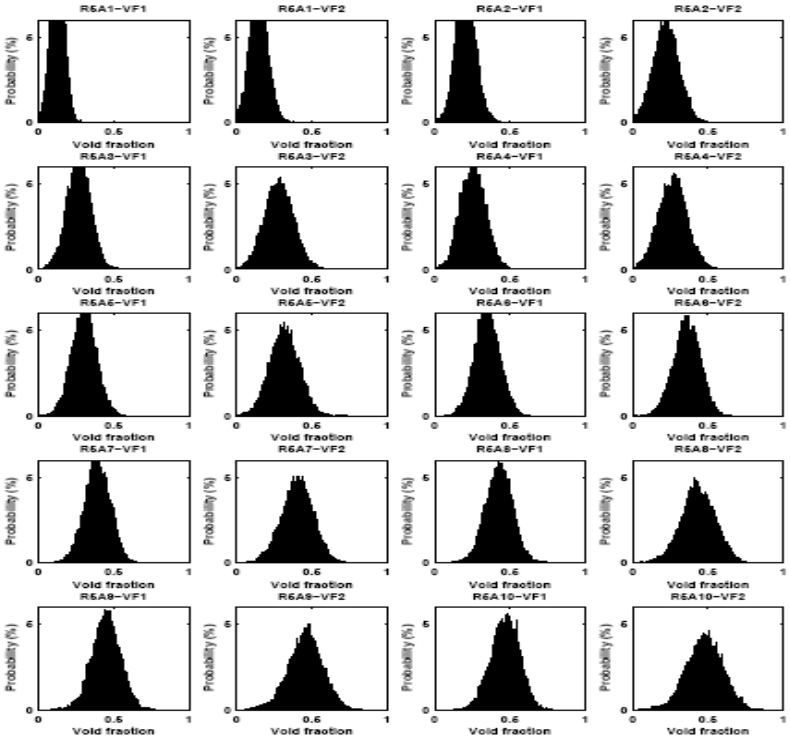

Figure 25. The PMF's plots taken at the height of 5 and 8m for Annular sleeve injector (R6).

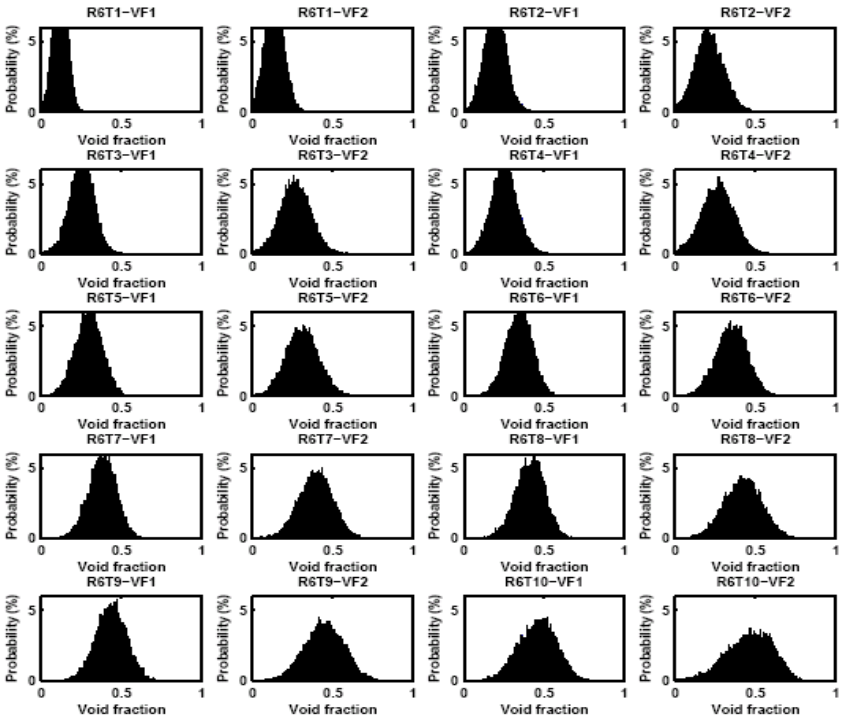

Figure 26. The PMF's plots taken at the height of 5 and 8m for Tee injector (R6).

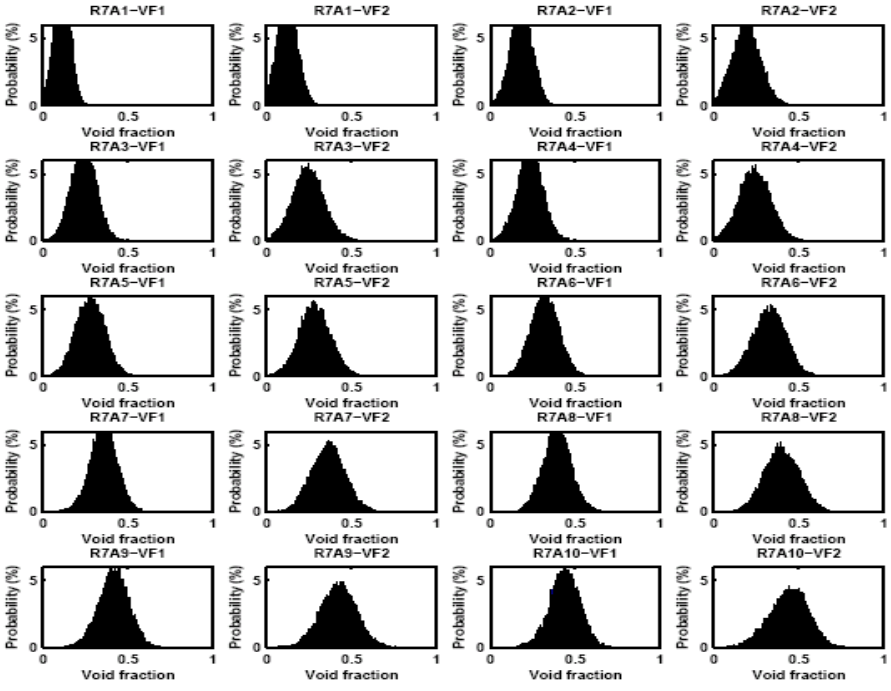

Figure 27. The PMF's plots taken at the height of 5 and 8m for Annular sleeve injector (R7).

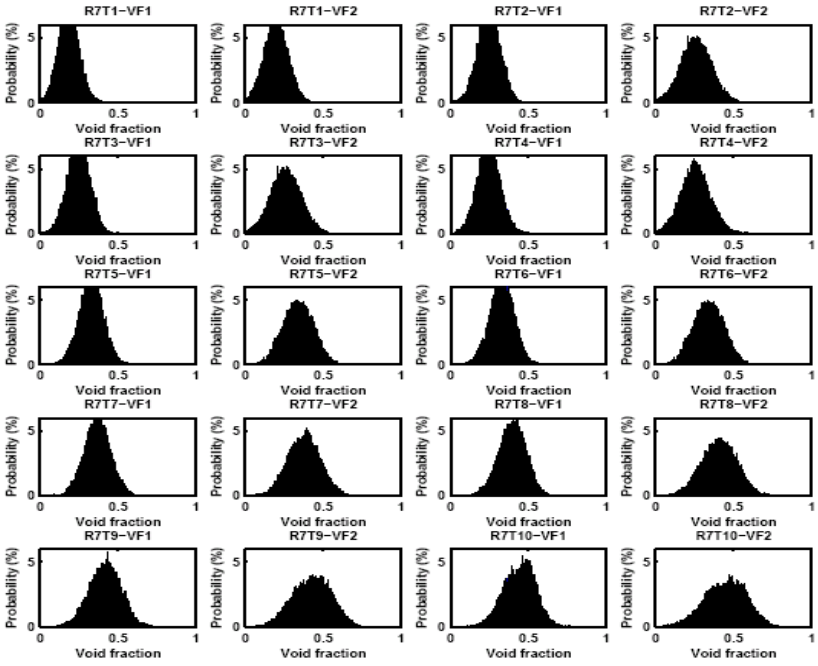

Figure 28. The PMF's plots taken at the height of 5 and 8m for Tee injector (R7).

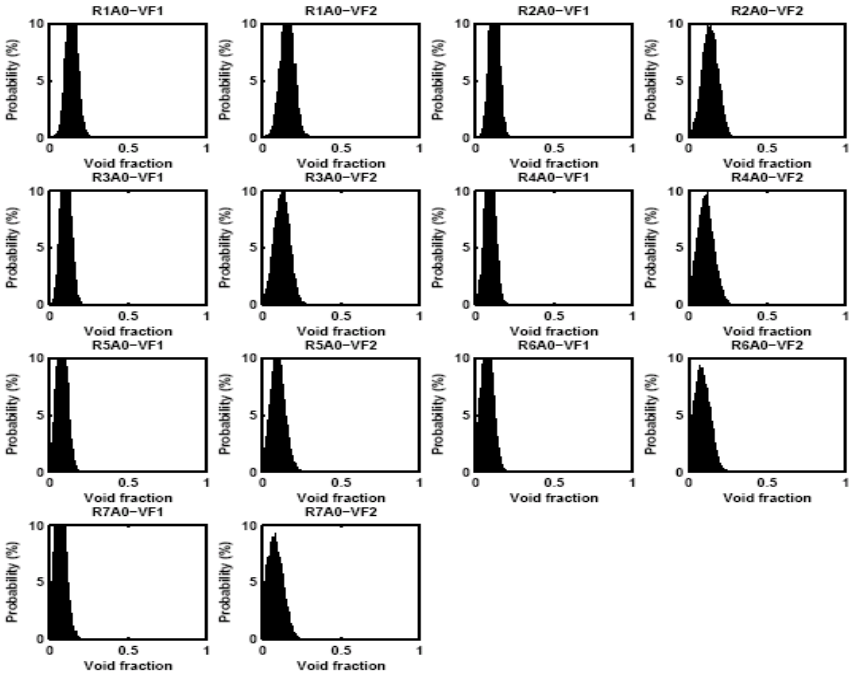

Figure 29. The PMF's plots taken at the height of 5 & 8m for Annular sleeve injector under lowest air superficial velocity.

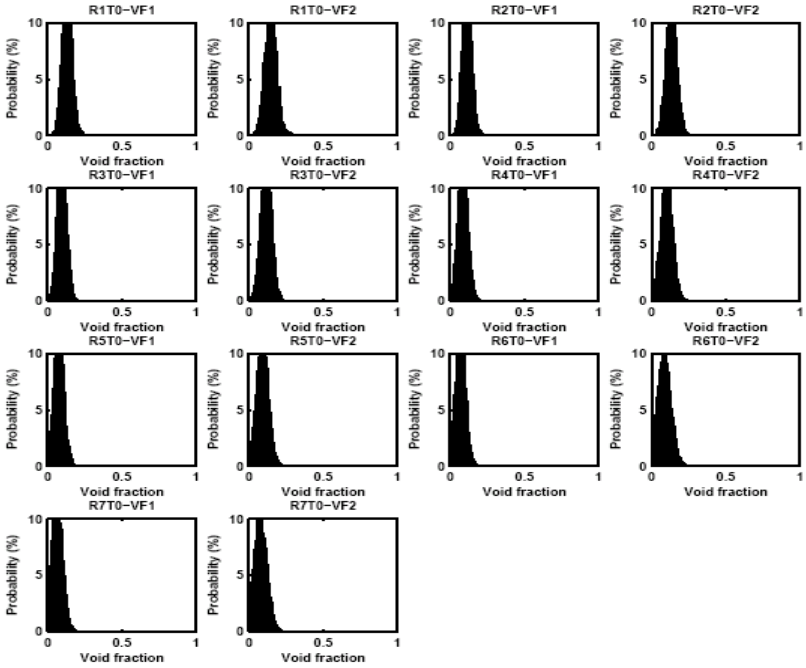

Figure 30. The PMF's plots taken at the height of 5 & 8m for Tee injector under lowest air superficial velocity.

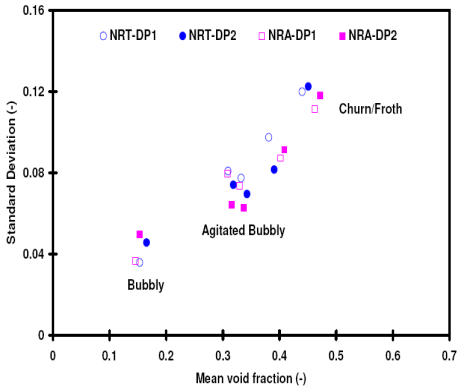

Figure 31. The flow regime transition based on the standard deviation of sectional void fraction at 5m and 7m height in the riser under natural lift condition.

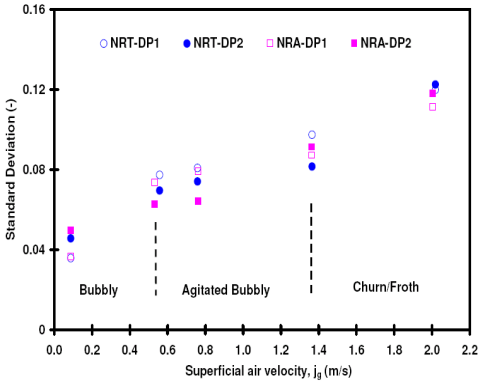

Figure 32. The flow regime transition based on the standard deviation of sectional void fraction at 5m and 7m height in the riser under natural lift condition.

B-9.Effect of inlet conditions (annular sleeve results):

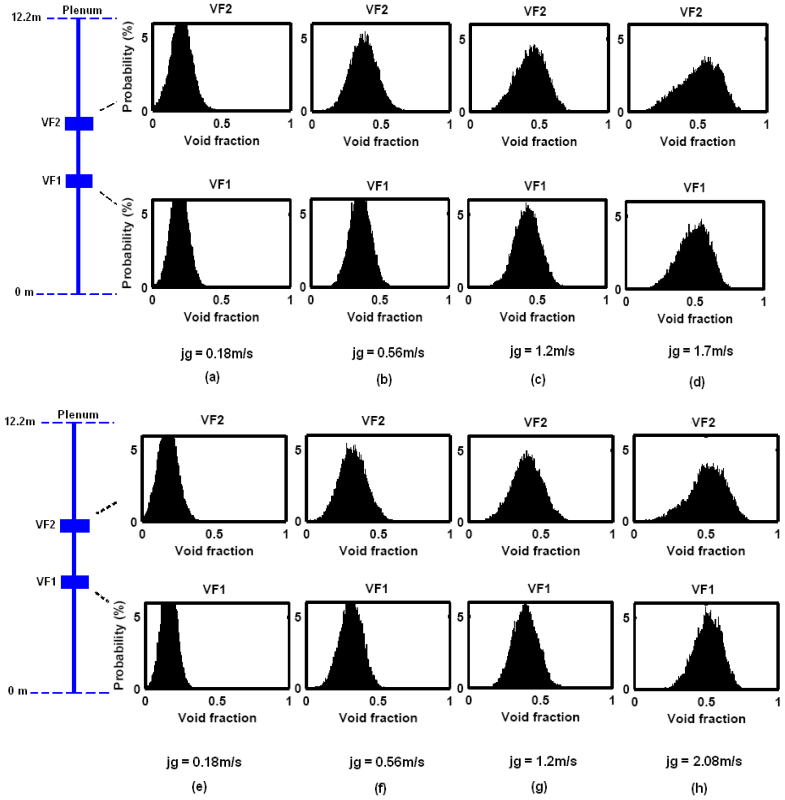

Figure 33. Near riser base injection from the annular sleeve injector (same j_a and j_w as in Fig 4.4).

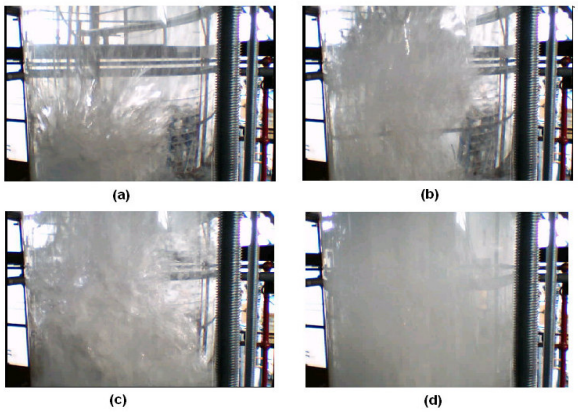

Figure 34. Liquid slug dissipation in the riser at approx. 5m height (a) liquid slug (b) distorted bubble entering the liquid slug (c) distorted bubble penetrating in the liquid slug and (d) fall back of the liquid film.

B-11. Steady state results from OLGA for vertical riser base gas injection only

Table 1. Selected simulated cases in OLGA.

Run	Flow regime by OLGA in riser section	Void Fraction (-)	Pressure Drop (bar)	Run	Flow regime by OLGA in riser section	Void Fraction (-)	Pressure Drop (bar)	Run	Flow regime by OLGA in riser section	Void Fraction (-)	Pressure Drop (bar)
R1T0	SLUG	0.318	0.787	**R3T0**	BUBBLY	0.203	0.916	**R7T0**	BUBBLY	0.1012	1.05
R1T1	ANNULAR	0.426	0.690	**R3T1**	BUBBLY	0.3356	0.778	**R7T1**	BUBBLY	0.1865	0.963
R1T2	ANNULAR	0.523	0.594	**R3T2**	BUBBLY	0.4183	0.706	**R7T2**	BUBBLY	0.2352	0.20.913
R1T3	ANNULAR	0.664	0.452	**R3T3**	SLUG	0.47669	0.649	**R7T3**	BUBBLY	0.349	0.797
R1T4	ANNULAR	0.684	0.431	**R3T4**	SLUG	0.54096	0.579	**R7T4**	BUBBLY	0.390	0.755
R1T5	ANNULAR	0.736	0.375	**R3T5**	SLUG	0.5978	0.517	**R7T5**	BUBBLY	0.455	0.690
R1T6	ANNULAR	0.781	0.329	**R3T6**	SLUG	0.640	0.473	**R7T6**	BUBBLY	0.5108	0.636
R1T7	ANNULAR	0.795	0.314	**R3T7**	SLUG	0.6733	0.445	**R7T7**	BUBBLY	0.5502	0.595
R1T8	ANNULAR	0.822	0.286	**R3T8**	ANNULAR	0.7042	0.420	**R7T8**	BUBBLY	0.5928	0.577
R1T9	ANNULAR	0.843	0.266	**R3T9**	ANNULAR	0.7314	0.398	**R7T9**	BUBBLY	0.6312	0.521
R1T10	ANNULAR	0.8657	0.244	**R3T10**	ANNULAR	0.7627	0.373	**R7T10**	SLUG	0.6475	0.506
R2T0	BUBBLY	0.2662	0.846	**R5T0**	BUBBLY	0.1358	1.01				
R2T1	SLUG	0.3967	0.707	**R5T1**	BUBBLY	0.1403	0.10				
R2T2	SLUG	0.4627	0.652	**R5T2**	BUBBLY	0.293	0.783				
R2T3	SLUG	0.5157	0.603	**R5T3**	BUBBLY	0.4192	0.714				
R2T4	ANNULAR	0.5683	0.553	**R5T4**	BUBBLY	0.4932	0.639				
R2T5	ANNULAR	0.6516	0.468	**R5T5**	BUBBLY	0.534	0.598				
R2T6	ANNULAR	0.7056	0.412	**R5T6**	BUBBLY	0.590	0.592				
R2T7	ANNULAR	0.7202	0.398	**R5T7**	BUBBLY	0.6224	0.512				
R2T8	ANNULAR	0.7479	0.371	**R5T8**	SLUG	0.662	0.472				
R2T9	ANNULAR	0.7786	0.343	**R5T9**	SLUG	0.6931	0.441				
R2T10	ANNULAR	0.7901	0.333	**R5T10**	SLUG	0.706	0.427				

APPENDIX C

C. Void fraction correlations and Pressure gradient methods

C1. Void fraction correlations

Table 1. Void fraction correlations and Pressure gradient methods used in this performance assessment.

Name	Correlation	Reference
1. HEM	$\langle \alpha \rangle = \frac{1}{1 + \left(\frac{1 - x}{x}\right)\frac{\rho_g}{\rho_l}} = \langle \beta \rangle$	Neil and Kazimi (1989)
2. Armand (1946) & Armand & Treschev (1959)	$\alpha = K\beta = \frac{\beta}{1.2} \qquad K = (0.833 + 0.05\ln(10P)) \qquad P = MPa$	Spedding et al (1998)
3. Bankoff (1960)	$\alpha = K\beta = (0.71 + 1.450377 \times 10^{-7}) \cdot Pa$	Neil and Kazimi (1989)
4. Lockhart & Martinelli (1949)	$\alpha = \frac{1}{1 + 0.28\left(\frac{1-x}{x}\right)^{0.64}.\left(\frac{\rho_g}{\rho_l}\right)^{0.36}.\left(\frac{\mu_l}{\mu_g}\right)0.07}$	Butterworth (1975)
5. Baroczy (1966)	$\frac{1-\alpha}{\alpha} = \left(\frac{1-x}{x}\right)^{0.74}.\left(\frac{\rho_g}{\rho_l}\right)^{0.65}.\left(\frac{\mu_l}{\mu_g}\right)^{0.13}$	Butterworth (1975)
6. Levy (1960)	$\alpha = \frac{\phi_l}{\phi_l - 1}$	Thom (2004)
7. Thom (1964)	$\alpha = \frac{1}{1 + \left(\frac{1-x}{x}\right).\left(\frac{\rho_g}{\rho_l}\right)^{0.89}.\left(\frac{\mu_l}{\mu_g}\right)^{0.18}}$	Butterworth (1975)
8. Zivi (1964)	$\alpha = \frac{1}{1 + \left(\frac{1 - x}{x}\right)\left(\frac{\rho_g}{\rho_l}\right)^{2/3}}$	Thom (2004)
9. Neal &Bankoff (1965)	$\alpha = 1.25\left(\frac{Q_g}{Q_l}\right)^{1.88}\left(\frac{j_l^2}{gD}\right)^{0.2}$	Spedding and Spence (1989)
10. Guzhov et al (1967)	$\frac{\alpha}{\beta} = 0.81 \cdot \left[1 - \exp(-2.2 \cdot \sqrt{\mathrm{Fr}})\right] \quad Where \quad Fr = \frac{j_l^2}{gD}$	Vohra et al (1975)

11. Smith (1969)	$S = e + (1 - e) \cdot \left[\frac{\left(\frac{\rho_l}{\rho_g} \right) + e \left(\frac{1 - x}{x} \right)}{\left[1 + e \left(\frac{1 - x}{x} \right) \right]} \right]^{1/2}$ Where $e = 0.4$	Thom (2004)
12. Premoli et al (1971)	$\alpha = \frac{Q_g}{Q_g + S \cdot Q_g}$ $S = 1 + E_1 \left[\frac{y}{1 + E_2} - y E_2 \right]^{1/2}$ $E_1 = 1.578 \cdot Re^{-0.19} \left(\frac{\rho_l}{\rho g} \right)^{0.22}$ $E_2 = 0.0273 \cdot We \cdot Re^{-0.51} \left(\frac{\rho_l}{\rho g} \right)^{0.22}$ $y = \frac{\beta}{1 - \beta} = \frac{Q_g}{Q_l}$ $Re = \frac{DG}{\mu_l}$ $We = \frac{DG^2}{\sigma \rho_l}$	Hewitt (1982)
13. Chisholm (1972)	$S = \frac{u_g}{u_l} = \left(\frac{\rho_l}{\rho_H} \right)^{1/2} = \left[1 - x \cdot \left(1 - \frac{\rho_l}{\rho_g} \right) \right]^{1/2}$	Chisholm (1972)
14. Spedding & Chen (1984) –I and II	$\frac{1 - \alpha}{\alpha} = \frac{1}{\left[0.2 + 2.2 \left(\frac{Q_l}{Q_g} \right) \right]}$ $\frac{1 - \alpha}{\alpha} = \frac{1}{0.2 + j_l^{-1.44} \left(\frac{Q_l}{Q_g} \right)}$	Spedding and Chen (1984)
15. Chen (1986) -I and Chen (1986) -II	$\alpha = \frac{K}{K + \chi^{2/3}}$ $Where K_I = 3.5$ $\alpha = \frac{K}{K + \chi^{2/3}}$ $Where K_{II} = 6.0$	Spedding and Spence (1989)
16. Spedding & Chen (1998)	$\frac{\alpha}{1 - \alpha} = 0.45 \left(\frac{Q_g}{Q_l} \right)^{0.65}$	Spedding and Spence (1989)
17. Modified Smith (1992) (by Mochizuki and Ishii, 1992)	$S = e + (1 - e) \cdot \left[\frac{\left(\frac{\rho_l}{\rho_g} \right) + e \left(\frac{1 - x}{x} \right)}{\left[1 + e \left(\frac{1 - x}{x} \right) \right]} \right]^{1/2}$ $e = 0.95 \tanh(5x + 0.05)$	Tecdoc-1203
18. Huq & Loth (1992)	$\alpha = 1 - \frac{2(1 - x)^2}{1 - 2x + K}$ $Where$ $K = \sqrt{1 + 2 \left((2x(1 - x)) \cdot \left(\frac{\rho_l}{\rho_g} - 1 \right) \right)}$	Huq & Loth (1992)
19. Wilson et al (1961)	$\alpha = 0.56157 \cdot F^{0.62086} \left(\frac{\rho_g}{\rho_l - \rho_g} \right)^{0.0917} \cdot \left(\frac{L}{D} \right)^{0.11033}$ $for F < 2$ $\alpha = 0.68728 \cdot F^{0.41541} \left(\frac{\rho_g}{\rho_l - \rho_g} \right)^{0.10737} \cdot \left(\frac{L}{D} \right)^{0.11033}$ $for F \geq 2$ $F = j_g \left(\frac{\rho_l - \rho_g}{g \sigma} \right)^{1/4}$ $L = \left(\frac{\sigma}{g(\rho_l - \rho_g)} \right)^{1/2}$	Kataoka & Ishii (1987)

20. Nicklin (1962)	$\alpha = \frac{j_g}{1.2\,j + 0.35\sqrt{gD}}$	Nicklin (1962)
21. Zuber & Findlay (1965)	where C_o = 1.0 (bubbly) and 1.2 (Slug/Churn) $U_{gj} = 1.53\left(\frac{g\,\sigma\,\Delta\rho}{\rho_1^{\,2}}\right)^{1/4}$ and $U_{gj} = 0.35\left(\frac{g\,\Delta\rho}{\rho_1}\right)^{1/2}$	Thom (2004)
22. Rouhani (1969) –I	$\alpha = \frac{\frac{x}{\rho_g}}{\left[e_1\left(\frac{x}{\rho_g} + \frac{1-x}{\rho_l}\right) + \frac{V_r}{G_t}\right]}$ *Where* $e_1 = 1 + 0.12\,(1-x)$ $V_r = \frac{1.18}{\sqrt{\rho_l}}\left(g\,\sigma\,(\rho_l - \rho_g)\right)^{1/4}$	Spedding and Spence (1989)
23. Rouhani (1969) -II	*Where* $e_2 = 1 + 0.2(1-x)(gD)^{1/4}/(G_t/\rho_l)^{1/2}$	Spedding and Spence (1989)
24. Rouhani & Axelsson (1970)	$U_{gj} = 1.18 \cdot \left(\frac{g\,\sigma\Delta\rho}{\rho_l^{\,2}}\right)^{1/4}$ where C_o = 1.1 for G > 200 kg/m^2-s and C_o = 1.54 for G < 200 kg/m^2-s	Thom (2004)
25. GE Ramp (1970)	$C_o = 1.1$ for $\alpha \le 0.65$ $C_o = 1 + \frac{0.1(1-\alpha)}{0.35}$ *for* $\alpha > 0.65$ $V_{gj} = R\left[\frac{(\rho_l - \rho_g)\sigma g}{\rho_l^{\,2}}\right]^{1/4}$ *Wher* $R = 2.9$ *for* $\alpha \le 0.65$ & $R = \frac{2.9(1-\alpha)}{0.35}$ *for* $\alpha > 0.65$	Tecdoc-1203
26. Dix (1971)	$C_o = \beta \cdot \left[1 + \left(\frac{1}{\beta} - 1\right)\left(\frac{\rho_g}{\rho_l}\right)^{0.1}\right]$ and $U_{gj} = 2.9 \cdot \left(\frac{g\,\sigma\Delta\rho}{\rho_l^{\,2}}\right)^{1/4}$	Neil and Kazimi (1989)
27. Bonnecaze et al (1971)	$\alpha = \frac{j_g}{1.2\,j + 0.35\sqrt{gD\left(1 - \frac{\rho_g}{\rho_l}\right)}}$	Spedding et al (1998)
28. Hills (1976)	$u_g = 1.2j + 0.24$ for $j_l > 0.3$ m/s $u_g = j + (4\alpha^{172} + 0.24)(1-\alpha)$ for $j_l \le 0.3$ m/s	Hills (1976)
29. Kocamustafagoullari & Ishii (1985)	$D_H^{\,*} = \frac{D_H}{\sqrt{\frac{\sigma}{g\,\Delta\rho}}}$ $U_{gj} = 0.54\sqrt{\frac{gD_H\,\Delta\rho}{\rho_l}}$ for $D_H^{\,*} \le 30$ & $U_{gj} = 3.0\left(\frac{g\,\sigma\Delta\rho}{\rho_l^{\,2}}\right)^{1/4}$ for $D_H^{\,*} \ge 30$	Hibiki & Ishii (2003)
30. Liao Parlos & Griffith (1985)	For Bubbly flow $jl > 2.34 - 1.07\left(\frac{g\,\sigma\Delta\rho}{\rho_l^{\,2}}\right)$ $C_o = 1$ *and* $V_{gj} = 1.53(1-\alpha)^2\left(\frac{g\,\sigma\Delta\rho}{\rho_l^{\,2}}\right)^{1/4}$ For Churn flow	Coddington and Macian (2002)

	$C_o = \left(1.2 - 0.2\sqrt{\frac{\rho_g}{\rho_l}}(1 - \exp(-18\,\alpha))\right)$ *and* $V_{gj} = 0.33\left(\frac{g\,\sigma\,\Delta\rho}{\rho_g^2}\right)^{1/4}$	
31. Hirao et al (1986)	(a) $U_{gj} = \sqrt{2}\left(\frac{gD\,\Delta\rho}{\rho_f}\right)^{1/4}$ at j = 0 m/s (b) $U_{gj} = 0.35\left(\frac{gD\Delta\rho}{\rho_l}\right)$ at j ≥ 0.24 m/s and D ≤ 0.05m $U_{gj} = 0.52\sqrt{\frac{gD\Delta\rho}{\rho_l}}$ at j ≥ 0.24 m/s and D >0.05m, while interpolation in region of 0 ≤ j ≤ 0.24 m/s by equation (a) and (b)	Hirao et al (1986)
32. Kataoka & Ishii (1987) drift flux equations applicable to cap bubble or slug flow regime in large diameter channel;	$N_{\mu l} = \frac{\mu_l}{\left(\sigma\rho_l\sqrt{\frac{\sigma}{g\Delta\rho}}\right)^{1/2}}$ and $U_{gj}^{+} = \frac{U_{gj}}{\left(\frac{g\,\sigma\Delta\rho}{\rho_l^2}\right)^{1/4}}$ For low viscous case $N_{\mu l} \le 2.25\times10^{-3}$ $U_{gj}^{+} = 0.0019 D_H^{*\,0.809}\left(\frac{\rho_g}{\rho_l}\right)^{-0.157} \cdot N_{\mu l}^{-0.562}$ for $D_H^{*} \le 30$ $U_{gj}^{+} = 0.0\,3\left(\frac{\rho_g}{\rho_l}\right)^{-0.157} \cdot N_{\mu l}^{-0.562}$ for $D_H^{*} \ge 30$ For high viscous case $N_{\mu l} > 2.25\times10^{-3}$ $U_{gj}^{+} = 0.92\left(\frac{\rho_g}{\rho_l}\right)^{-0.157}$. for $D_H^{*} \ge 30$	Kataoka & Ishii (1987)
33. El Boher et al (1988)	$\alpha = \frac{1}{\left[1 + 0.27\,Qr^{-0.69} \cdot Fr^{-0.177} \cdot \left(\frac{\mu_l}{\mu_g}\right)^{0.378}\left(\frac{\mathrm{Re}}{We}\right)^{0.067}\right]}$ *Where* $Qr = \frac{x \cdot \rho_l}{[(1-x)\rho_g]} = \frac{j_g}{j_l}$ $Fr = \frac{j_l^2}{gD}$ $\mathrm{Re} = \frac{\rho_l j_l D}{\mu_l}$ $We = \frac{j_l^2 \rho_l D}{\sigma}$	Davis (2001)
34. Morooka et al or Toshiba (1989)	$\alpha = \frac{j_g}{C_o \cdot j + U_{gj}}$ where $C_o = 1.08$ and $Ugj = 0.45$	Morooka et al (1989)

35. Chexal and Lellouche (1992)	$C_o = \frac{L_c}{K + (1 - K)\alpha^r}$ *and* $L_c = \min(1.15\alpha^{0.25}, 1)$ $K = B_1 + (1 - B_1)\left(\frac{\rho_g}{\rho_l}\right)^{1/4}$ $r = \left(\frac{1.0 + 1.57\left(\frac{\rho_g}{\rho_l}\right)}{1 - B_1}\right)$ $B_1 = \min(0.8, A_1)$ *and* $A_1 = \frac{1}{1 + \exp\left(\frac{-\mathrm{Re}_l}{60000}\right)}$ $V_{gj} = 1.41\left[\frac{(\rho_l - \rho_g)\sigma g}{\rho_l^2}\right]^{1/4} C_1 C_2 C_3 C_4$ *where* $C_1 = (1 - \varepsilon)C_{lv}$ $C_{lv} = C_5$ $C_5 = \sqrt{\frac{150}{\rho_l/\rho_g}}$ *If* $C_5 \geq 1$, $C_2 = 1$ *else* $C_2 = 1 - \exp\frac{-C_5}{1 - C_5}$ $C_3 = \max\left(0.5, 2\exp\left(\frac{\mathrm{Re}_l}{300{,}000}\right)\right)$ *If* $C_7 < 1$ $C_4 = \frac{1}{1 - \exp(-C_8)}$ *else* $C_4 = 1$ *Where* $C_7 = \left(\frac{D_r}{D}\right)^{0.6}$ $D_r = 0.09144\ m$ $C_8 = \frac{C_7}{1 - C_7}$	Chexal and Lellouche (1992)
36. Inoune et al. (1993)	$C_o = 6.76 \times 10^{-3} p + 1.026$ $V_{gj} = (5.10 \times 10^{-3} G + 6.91 \times 10^{-2}) + (9.42 \times 10^{-2} p^2 - 1.99 + 12.6)$	
37. Maier & Coddington (1997)	$C_o = C_1 \cdot p + C_2$ $V_{gj} = (v_1 . p + v_2 . p + v_3)G + (v_4 p^2 + v_5 . p + v_6)$ $C_1 = 2.57 \div 10^{-3}$ $C_2 = 1.0062$ $v_1 = 6.73 \times 10^{-7}$ $v_2 = -8.81 \times 10^{-5}$ $v_3 = 1.05 \times 10^{-3}$ $v_4 = 5.63 \times 10^{-3}$ $v_5 = -1.23 \times 10^{-1}$ $v_6 = 8.00 \times 10^{-1}$	Coddington and Macian (2002)
38. Hibiki & Ishii (2003) model for large diameter pipe	Bubbly or cap bubbly flow $\langle\alpha\rangle \leq 0.3$ $C_o = \exp\left\{0.475\left(\frac{\langle j_g^+\rangle}{\langle j^+\rangle}\right)^{1.69}\right\}(1 - \sqrt{\frac{\rho_g}{\rho_1}}) + \sqrt{\frac{\rho_g}{\rho_l}}$ for $0 \leq \langle jg^+\rangle/\langle j^+\rangle \leq 0.9$ Inlet flow regime uniformly distributed bubbly flow $C_o = \left\{-2.88\left(\frac{\langle j_g^+\rangle}{\langle j^+\rangle}\right)^{1.69} + 4.08\right\}(1 - \sqrt{\frac{\rho_g}{\rho_1}}) + \sqrt{\frac{\rho_g}{\rho_l}}$ for $0.9 \leq \langle jg^+\rangle/\langle j^+\rangle \leq 1$ $U_{gj}^+ = U_{gj,B}^+ \exp(-1.39\langle j_g^+\rangle) + U_{gj,P}^+\{1 - \exp(-1.39\langle j_g^+\rangle)\}$ Bubbly or cap bubbly flow $\langle\alpha\rangle > 0.3$ $C_o = 1.2\exp\left\{0.11\langle j^+\rangle^{2.22}\right\}(1 - \sqrt{\frac{\rho_g}{\rho_1}}) + \sqrt{\frac{\rho_g}{\rho_l}}$ for $0 \leq \langle j^+\rangle \leq 1.8$	Hibiki & Ishii (2003)

	Inlet flow regime cap bubbly or slug flow $C_o = [0.61\exp\{-1.2.11(\langle j^+ \rangle - 1.8)\} + 1.2].(1 - \sqrt{\frac{\rho_g}{\rho_1}}) + \sqrt{\frac{\rho_g}{\rho_l}}$ for $1.8 \le <j^+>$and $U_{gj}^{+} = U_{gj,P}^{+}$ For low viscous case $N_{\mu l} \le 2.25 \times 10^{-3}$ $U_{gj}^{+} = 0.0019 D_H^{*0.809} \left(\frac{\rho_g}{\rho_l}\right)^{-0.157} \cdot N_{\mu l}^{-0.562}$ For high viscous case $N_{\mu l} > 2.25 \times 10^{-3}$ for $D_H^{*} \le 30$ $U_{gj}^{+} = 0.03 \left(\frac{\rho_g}{\rho_l}\right)^{-0.157} \cdot N_{\mu l}^{-0.562}$ for $D_H^{*} \ge 30$	
39. Hagedorn & Brown (1959)	1. Check for flow regime $A = 1.071 - \frac{0.2218\,(j_g + j_l)^2}{0.3048^2 \cdot D}$ 2. If A< 0.13 then A=0 $B = \frac{j_g}{j_l + j_g}$ 3. If B-A =+ve or zero, use Hagedorn-Brown correlation, $N_L = \mu_l \left(\frac{g}{\rho_l \sigma}\right)^{0.25}$ $C_{NL} = \frac{0.0019 N_L + 0.0322 N_L - 0.6642 N_L^2 + 4.9951 N_L^3}{1 - 10.0147 N_L + 33.869 N_L^2 + 277.287 N_L^3}$ If N_L<0.002 then C_{NL}=0.0019 or N_L>0.4 then C_{NL}=0.0115 or else (B-A=-ve) use Griffith correlation $H_l = 1 - 0.5\left[1 + \frac{j}{v_s} - \sqrt{(1 + \frac{j}{v_s})^2 - 4\frac{j_g}{v_s}}\right]$ 4. $N_{lv} = jl \left(\frac{\rho_l}{g\sigma}\right)^{0.25}$ $N_{gv} = j_g \left(\frac{\rho_l}{g\sigma}\right)^{0.25}$ $N_d = D\left(\frac{g\rho_l}{\sigma}\right)^{1/2}$ $\phi_1 = \frac{N_{lv}}{N_{gv}} + \left[\frac{P}{14.7}\right]^{0.10} \cdot \left[\frac{C_{NL}}{N_d}\right]$ 5. $\frac{H_l}{\psi} = \frac{0.0047 + 1123.32\phi_1 + 729489\,\phi_1^2}{1 + 1097.01566\,\phi_1 + 722153.97\,\phi_1^2}$ where $\psi = \frac{1.0866 - 69947\phi_2 + 2334.35\phi_2^2 - 128968\phi_2^3}{1 - 15344\phi_2 + 151794\phi_2^2 + 84198.2\phi_2^3}$ 6. $\phi_2 = \frac{N_{lv}^{0.38} \cdot N_{gv}}{N_d}$ 7. $H_l = \frac{H_L}{\psi} \cdot \psi$ *and* $\rho_s = (1 - H_l)\rho_g + H_l \rho_l$	Brill & Mukherjee (1999

	8. $\left(\frac{dP}{dL}\right)_{Total} = \rho_s g \sin\theta + \frac{2 f \rho_\lambda j^2}{D} \cdot \frac{\rho_\lambda}{\rho_s}$ Where f is from Colebrook equation	
40. Duns & Ros (1963)	1. Find flow regimes by: $N_L = \mu_l \left(\frac{g}{\rho_l \sigma}\right)^{0.25}$ $N_{lv} = jl\left(\frac{\rho_l}{g\sigma}\right)^{0.25}$ $N_{gv} = j_g\left(\frac{\rho_l}{g\sigma}\right)^{0.25}$ $N_d = D\left(\frac{g\rho_l}{\sigma}\right)^{1/2}$ 2. $L_s = 50 + 36 N_{lv}$ $L_m = 75 + 84 N_{lv}^{0.75}$ 3. *Bubble* $0 \le N_{gv} \le L_1 + L_2 N_{lv}$ *Slug* $L_1 + L_2 N_{gv} \le N_{gv} \le L_s$ *Transition (mist)* $L_s < N_{gv} < L_m$ 4. For Bubble flow $S_B = F_1 + F_2 . N_{lv} + F_3 ' \left[\frac{N_{gv}}{1 + Nlv}\right]^2$ F_1, F_2, F_3, F_4 *from* *Fig* 4.7 5. For Slug flow $S_S = (1 + F_5) \cdot \left[\frac{N_{gv} + F_6'}{(1 + F_7 N_{lv})^2}\right]$ *where* F_5, F_6, F_7 *from* *Fig* 4.9 6. $v_s = \frac{S_B (or S_S)}{\left(\rho_l / \sigma g\right)^{0.25}}$ 7. $H_l = 1 - 0.5\left[1 + \frac{j}{v_s} - \sqrt{(1 + \frac{j}{v_s})^2 - 4\frac{j_g}{v_s}}\right]$ 8. $\text{Re}_l = \frac{\rho_l j D}{\mu_l}$ $f_m = f_1 \cdot \frac{f_2}{f_3}$ 9. Where f_1 and f_2 from Fig 4.8 10. $\left(\frac{dP}{dL}\right)_{Total} = \rho_s g \sin\theta + \frac{f_m \rho_l jl \cdot j}{2D}$ Where $\rho_s = (1 - H_l)\rho_g + H_l \rho_l$	Brill & Mukherjee (1999
41. Beg & Brill (1973)	1. $j = j_l + j_g$ 2. $\lambda = \frac{j_l}{j_l + j_g}$ 3. $Fr = \frac{j^2}{gD}$ 4. $N_{lv} = jl\left(\frac{\rho_l}{g\sigma}\right)^{0.25}$ 5. $L_1 = 316\ \lambda^{0.302}$ $L_2 = 0.0009252\ \lambda^{-2.4684}$ $L_3 = 0.10\ \lambda^{-1.4516}$ $L4 = 0.5\ \lambda^{-6.738}$	Brill & Mukherjee (1999)

	Segregated $\lambda < 0.01$ *and* $Fr < L_1$ *Transition* $\lambda \geq 0.01$ *and* $L_2 < Fr \leq L_3$ *Intermittent* $0.01 \leq \lambda < 0.4$ *and* $L_3 < Fr \leq L_4$ $\lambda \geq 0.4$ *and* $L_3 < Fr \leq L_4$ *Distributed* $\lambda < 0.4$ *and* $Fr \geq L_1$ $\lambda \geq 0.4$ *and* $L_3 < Fr \leq L_4$ $\lambda \geq 0.01$ *and* $Fr < L_2$ 7. $\lambda_H = \frac{a\lambda^b}{Fr^c}$ where a, b and c are 8. Inclination correction factor, C: $C = (1-\lambda)\ln(d\lambda^e \cdot N_{lv}{}^f \cdot Fr^g)$ 9. $\psi = 1 + C\left[\sin(1.8\theta) - 0.333\ \sin^3(1.8\theta)\right]$ 10. $\lambda_V = \lambda_H \cdot \psi$ 11. $\lambda = a\lambda_S + (1-a)\lambda_I$ $a = \frac{L_3 - Fr}{L_3 - L_2}$ For Transition flows 12. $\frac{f_{TP}}{f_\lambda} = e^S$ $S = \ln(2.2y - 1.2)$ 13. $\mathrm{Re}_\lambda = \frac{\rho_\lambda jD}{\mu_\lambda}$ $f_{TP} = f_\lambda \cdot \frac{f_{TP}}{f_\lambda}$ 14. $\left(\frac{dP}{dL}\right)_{Total} = \rho_\lambda g \sin\theta + \frac{2 f_{TP} \rho_\lambda j^2}{D}$	
42. Bankoff, 1960	$\left(\frac{dp}{dz}\right)_{frict} = \left(\frac{dp}{dz}\right)_L \Phi_{Bf}^{\frac{7}{4}}$ $\Phi_{Bf} = \frac{1}{1-x}\left[1-\gamma\left(1-\frac{\rho_G}{\rho_L}\right)\right]^{\frac{3}{7}}\left[1+x\left(\frac{\rho_L}{\rho_G}-1\right)\right]$	Thom (2004)

	$\gamma = \frac{.71 + 2.35\left(\frac{\rho_G}{\rho_L}\right)}{1 + \left(\frac{1-x}{x}\right)\left(\frac{\rho_G}{\rho_L}\right)}$	
43. Friedel, 1979	$\Delta p_{frict} = \Delta p_L \Phi_{fr}^2 \qquad \Delta p_L = 4 f_L (L/d_i) \dot{m}_{total}^2 (1/2\rho_L) \; f = \frac{.079}{\mathrm{Re}^{0.25}} \qquad \mathrm{Re} = \frac{\dot{m}_{total} d_i}{\mu}$ $\phi_{fr}^2 = E + \frac{3.24 FH}{Fr_H^{0.045} We_L^{0.035}}$ $Fr_H = \frac{\dot{m}_{total}^2}{g d_i \rho_H^2} \quad E = (1-x)^2 + x^2 \frac{\rho_L f_G}{\rho_G f_L} \qquad We_L = \frac{r h_{total}^2 d_i}{\sigma \rho_H}$ $F = x^{0.78}(1-x)^{0.224} \;\&\; H = \left(\frac{\rho_L}{\rho_G}\right)^{0.91}\left(\frac{\mu_G}{\mu_L}\right)^{0.19}\left(1-\frac{\mu_G}{\mu_L}\right)^{0.7} \qquad \rho_H = \left(\frac{x}{\rho_G} + \frac{1-x}{\rho_L}\right)^{-1}$	Thom (2004)
44. Lockhart & Martinelli, 1949	$\Delta p_{frict} = \phi_{Ltt}^2 \Delta p_L \qquad \Delta p_{frict} = \phi_{Gtt}^2 \Delta p_G \qquad \Delta p_G = 4 f_G (L/d_i) \dot{m}_{total}^2 x^2 (1/2\rho_G)$ *C = 20 for Li quid =Turbulent & gas = Turbulent* $\Phi_{Ltt}^2 = 1 + \frac{C}{X_{tt}} + \frac{1}{X_{tt}^2}$, *for* $\mathrm{Re}_L > 4000 \qquad \Phi_{Gtt}^2 = 1 + CX_{tt} + X_{tt}^2$ *for* $\mathrm{Re}_L < 4000$ $X_{tt} = \left(\frac{1-x}{x}\right)^{0,9}\left(\frac{\rho_G}{\rho_L}\right)^{0.5}\left(\frac{\mu_L}{\mu_G}\right)^{0.1}$	Thom (2004)
45. Chisholm, 1973	$\left(\frac{dp}{dz}\right)_{frict} = \left(\frac{dp}{dz}\right)_L \Phi_{Ch}^2 \qquad \left(\frac{dp}{dz}\right)_L = f_L \frac{2\dot{m}_{total}^2}{d_i \rho_L} \qquad \left(\frac{dp}{dz}\right)_G = f_G \frac{2\dot{m}_{total}^2}{d_i \rho_G}$ $Y^2 = \frac{(dp/dz)_G}{(dp/dz)_L}$, $\Phi_{Ch}^2 = 1 + (Y^2 - 1)\left\lfloor Bx^{(2-n)/2}(1-x)^{(2-n)/2} + x^{2-n}\right\rfloor$ n = 0.25 Blasius value *For 0 < Y < 9.5, then B is* $B = \frac{55}{\dot{m}_{total}^{1/2}}$ *for* $\dot{m}_{total} \geq 1900 \; kg/m^2 s \qquad B = \frac{2400}{\dot{m}_{total}}$ *for* $500 < \dot{m}_{total} < 1900 \; kg/m^2 s$ $B = 4.8$ *for* $\dot{m}_{total} < 500 \; kg/m^2 s$ *For 9.5 < Y < 2.8, then B is*	

	$B = \frac{520}{Y\dot{m}_{total}^{1/2}}$ *for* $\dot{m}_{total} \leq 600\ kg/m^2 s$ $\quad$ $B = \frac{21}{Y}$ *for* $\dot{m}_{total} > 600\ kg/m^2 s$ *For Y > 2.8 then B is* $B = \frac{15000}{Y^2 \dot{m}_{total}^{1/2}}$	

APPENDIX D

D-1. Steady state processor results from OLGA
D-2. Comparison of the single phase riser base pressure profiles
D-3. Modifications in the first model
D-4. Selected cases results of the First model
D-5. Sensitivity studies of extended model
D-6. Simulated model

D-1. Steady state processor results from OLGA

Table 1. Steady State Results of the simulated cases in OLGA.

	j_a(m/s)	j_w(m/s)	Experimental flow regime in riser section	Flow regime by OLGA in riser section	Flow regime in FL/R/P	Pressure Drop in pipeline-riser(bar)	AL(-)
H1H1	0.18	0.20	Bubbly	Slug	ST/SL/ST	0.75	0.32
H1H2	0.36	0.24	Agitated bubbly	Slug	ST/SL/ST	0.66	0.41
H1H3	0.56	0.26	Agitated bubbly	Annular	ST/AN/SL	0.48	0.58
H1H4	0.80	0.27	Agitated bubbly	Annular	SL/AN/SL	0.41	0.64
H1H5	1.01	0.28	Agitated bubbly	Annular	SL/AN/SL	0.37	0.68
H1H6	1.24	0.29	Agitated bubbly	Annular	SL/AN/SL	0.30	0.74
H1H7	1.47	0.30	Agitated bubbly	Annular	SL/AN/SL	0.26	0.78
H1H8	1.70	0.31	Churn/froth	Annular	SL/AN/SL	0.24	0.80
H1H9	1.94	0.31	Churn/froth	Annular	SL/AN/SL	0.22	0.82
H1H10	2.17	0.32	Churn/froth	Annular	SL/AN/SL	0.21	0.83
H3H1	0.18	0.50	Bubbly	Bubble	ST/BU/ST	0.92	0.18
H3H2	0.36	0.51	Agitated bubbly	Bubble	ST/BU/SL	0.78	0.30
H3H3	0.54	0.53	Agitated bubbly	Slug	SL/SL/SL	0.61	0.47
H3H4	0.77	0.55	Agitated bubbly	Slug	SL/SL/SL	0.56	0.52
H3H5	0.98	0.56	Agitated bubbly	Slug	SL/SL/SL	0.52	0.55
H3H6	1.20	0.58	Unstable slug/churn	Slug	SL/SL/SL	0.45	0.62
H3H7	1.42	0.59	Unstable slug/churn	Slug	SL/SL/SL	0.42	0.64
H3H8	1.63	0.60	Churn/froth	Slug	SL/SL/SL	0.38	0.68
H3H9	1.86	0.61	Churn/froth	Annular	SL/AN/SL	0.35	0.72
H3H10	2.10	0.62	Churn/froth	Annular	SL/AN/SL	0.34	0.73
H1R10	2.16	0.31	Churn/froth	Annular	SL/AN/SL	0.22	0.83
H3R10	2.14	0.62	Churn/froth	Annular	SL/AN/SL	0.37	0.73

D-2. Single phase riser base pressure profiles:

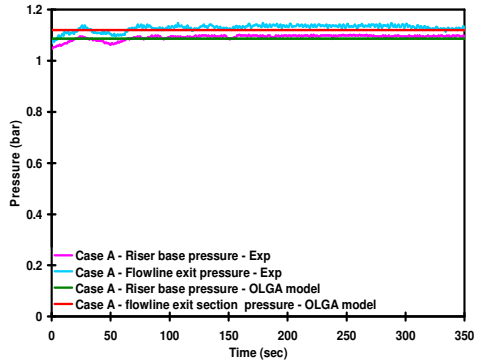

Figure 1. Single phase simulated & experimental near riser base pressure for Case A.

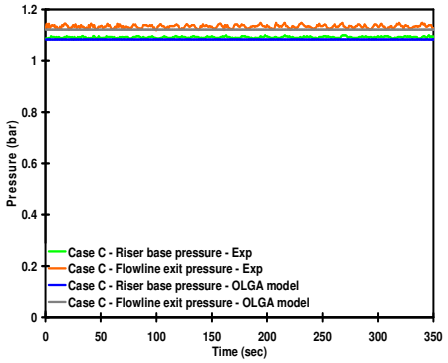

Figure 2. Single phase simulated & experimental near riser base pressure for Case C.

D-3. Modifications in the first model

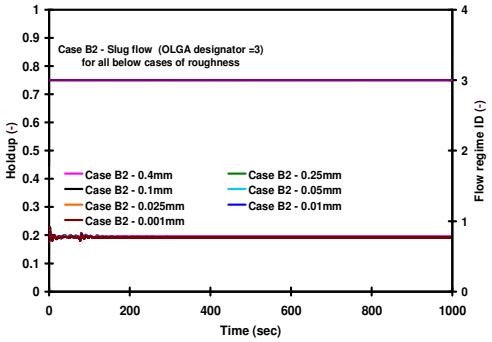

Figure 3. Effect of roughness on the riser base holdup and flow regime for Case B.

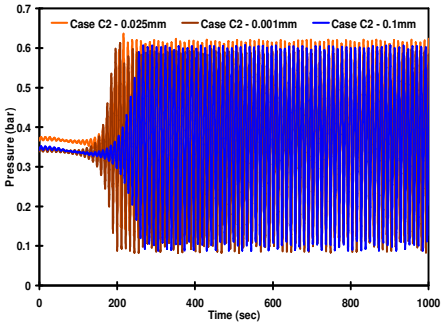

Figure 4. Effect of roughness on the riser base pressure for Case C.

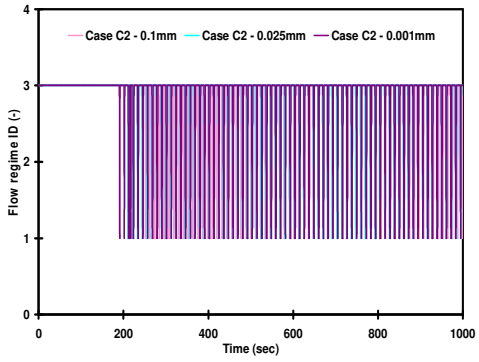

Figure 5. Effect of roughness on the riser base flow regime for Case C

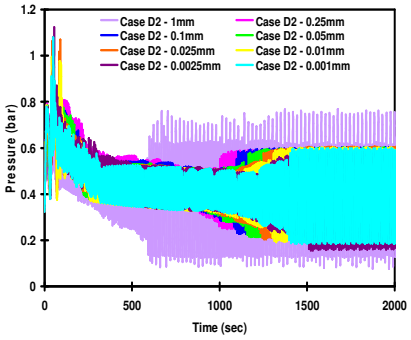

Figure 6. Effect of roughness on the riser base pressure for Case D.

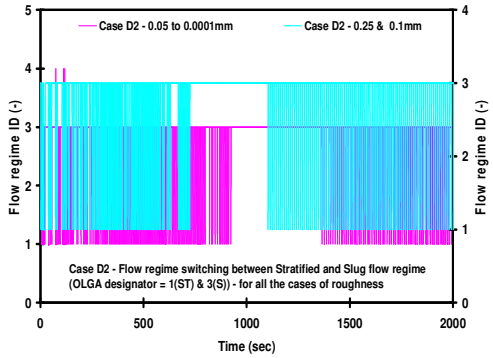

Figure 7. Effect of roughness on the riser base flow regime for Case D.

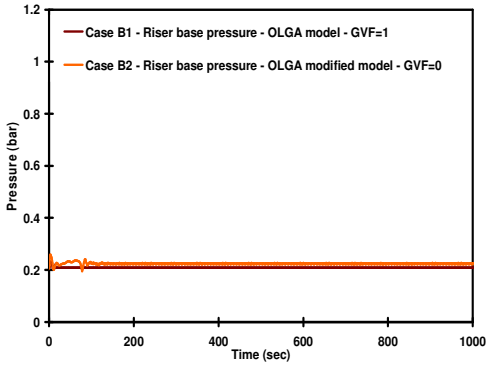

Figure 8. Riser base pressure simulation for Case B (when GF=0 and 1).

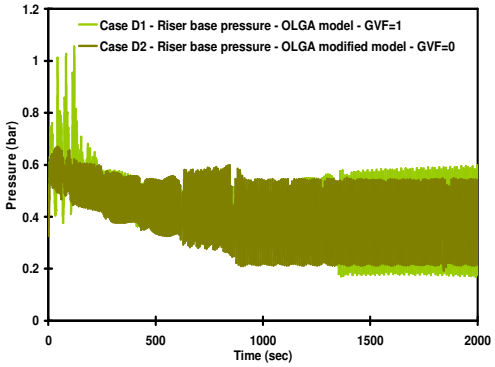

Figure 9. Riser base pressure simulation for Case D (when GF=0).

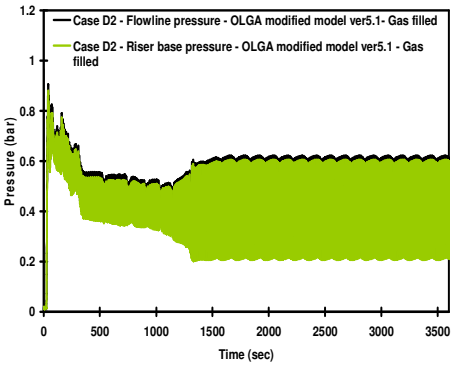

Figure 10. Riser base pressure simulation via gas filled system initialization for Case D.

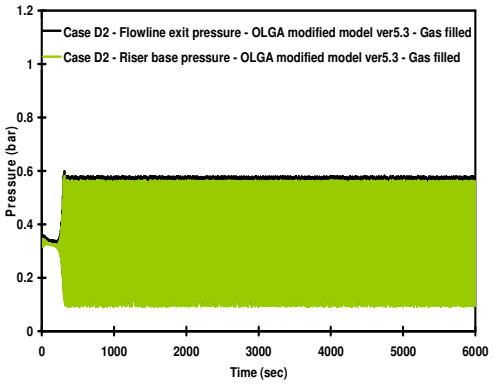

Figure 11. Riser base pressure simulation via gas filled system initialization for Case D.

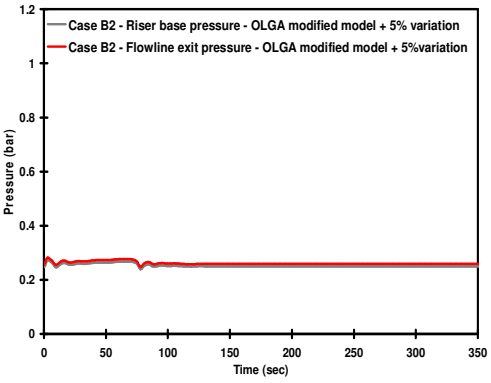

Figure 12. Effect of magnitude of boundary variation in case B.

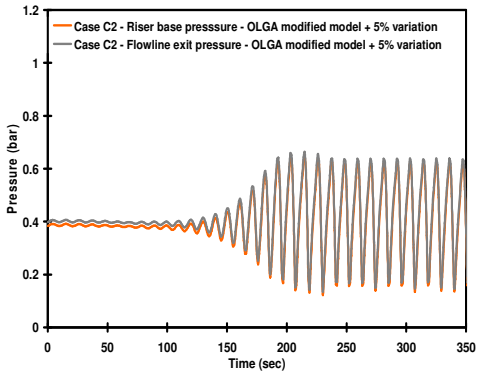

Figure 13. Effect of magnitude of boundary variation in case C

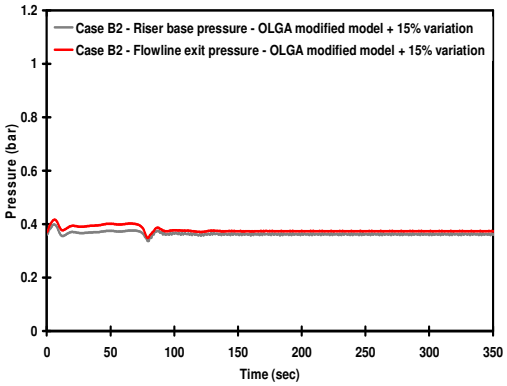

Figure 14. Effect of magnitude of boundary variation in case B.

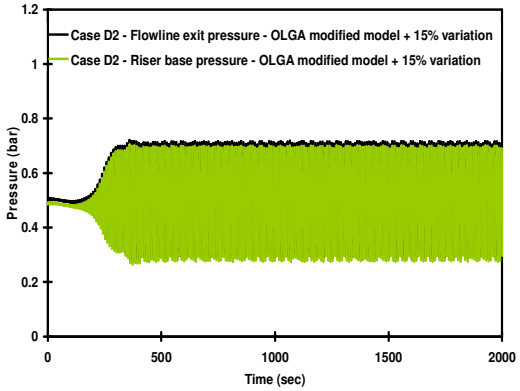

Figure 15. Effect of magnitude of boundary variation in case D.

D-4. Results of Selected cases the First model

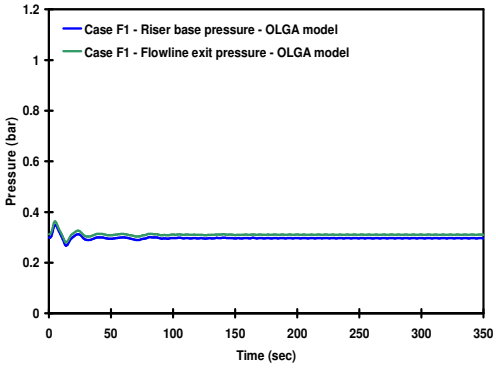

Figure 16. The simulated riser base and flowline exit pressure from the first model for case F.

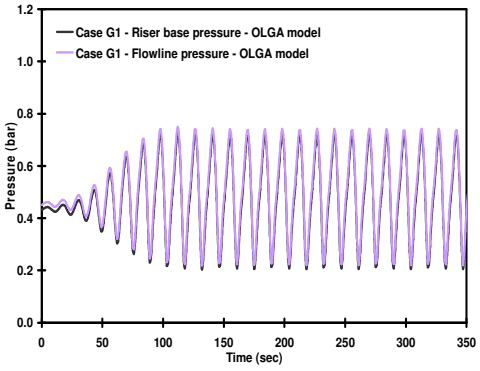

Figure 17. The simulated riser base and flowline exit pressure response from the model for case G.

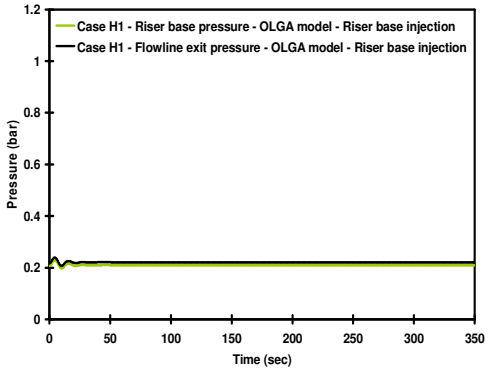

Figure 18. The simulated riser base and flowline exit pressure from the first model for case H.

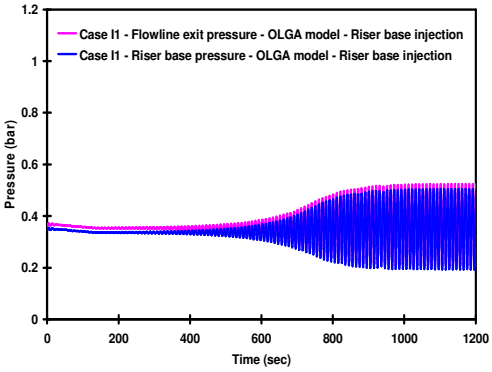

Figure 19. The simulated riser base and flowline exit pressure from the first model for case I.

D-5. Sensitivity studies of extended model

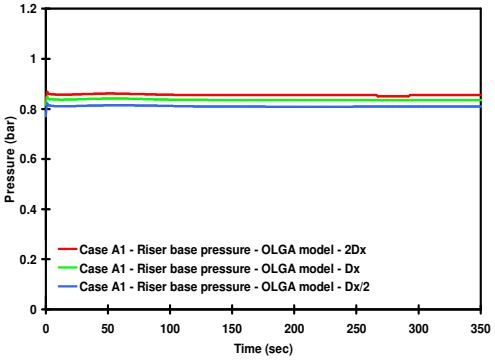

Figure 20. Effect of grid size on the time evolution of the riser base pressure for case A.

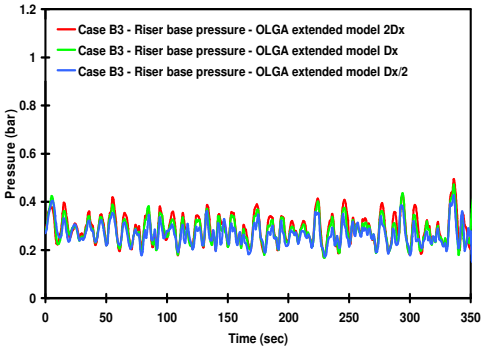

Figure 21. Effect of grid size on the time evolution of the riser base pressure for case B.

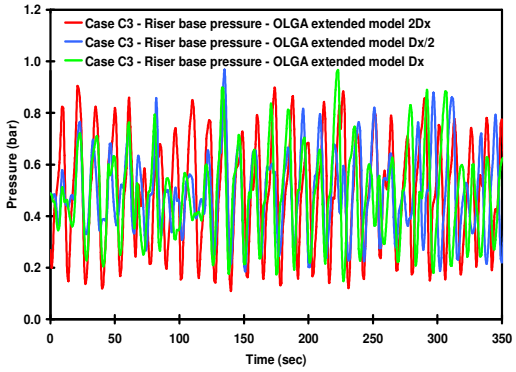

Figure 22. Effect of grid size on the time evolution of the riser base pressure for case C.

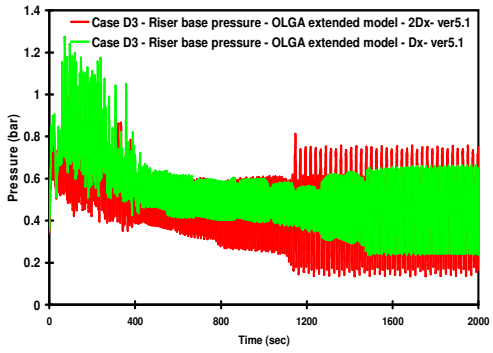

Figure 23. Effect of grid on the time evolution of the riser base pressure for case D.

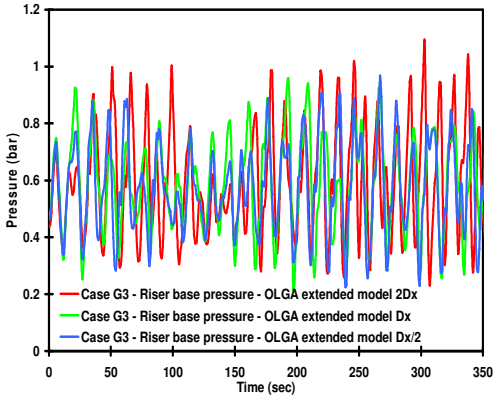

Figure 24. Effect of grid size on the time evolution of the riser base pressure for case G.

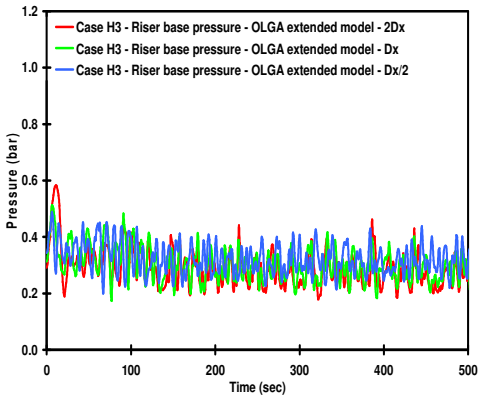

Figure 25. Effect of grid size on the time evolution of the riser base pressure for case H.

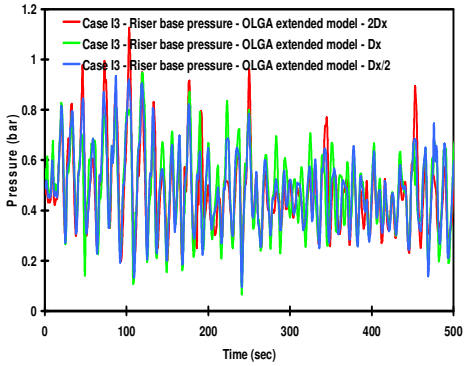

Figure 26. Effect of grid size on the time evolution of the riser base pressure for case I.

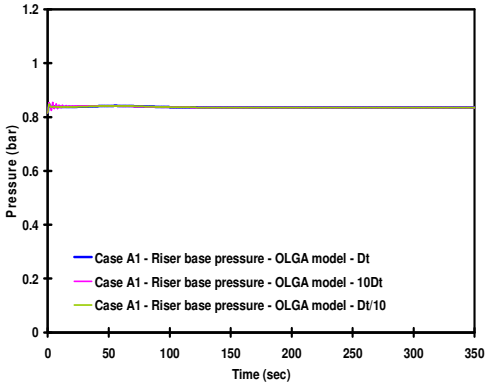

Figure 27. Effect of timestep on the time evolution of the riser base pressure for case A.

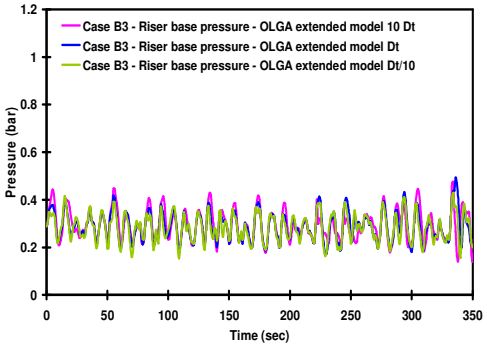

Figure 28. Effect of timestep on the time evolution of the riser base pressure for case B.

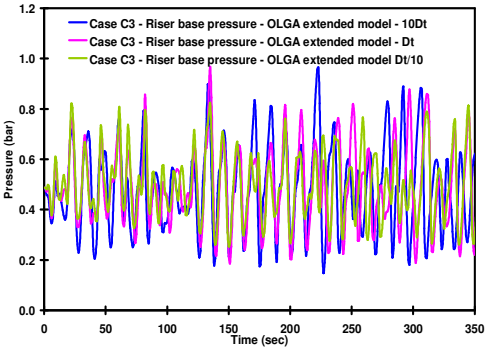

Figure 29. Effect of timestep on the time evolution of the riser base pressure for case C.

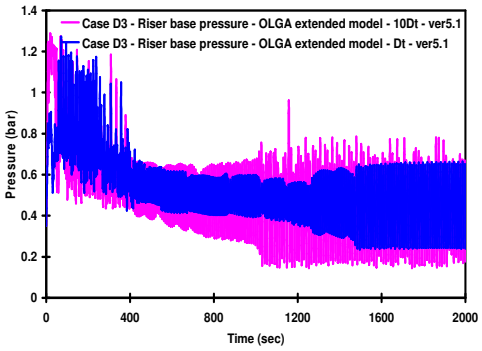

Figure 30. Effect of timestep size on the time evolution of the riser base pressure for case D.

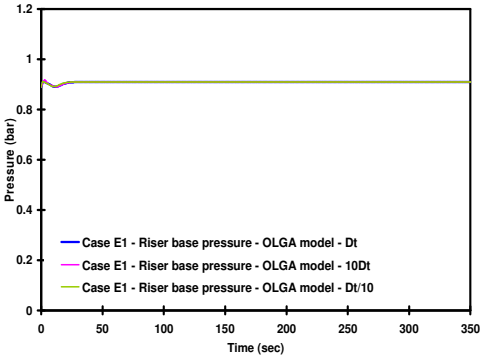

Figure 31. Effect of timestep on the time evolution of the riser base pressure for case E.

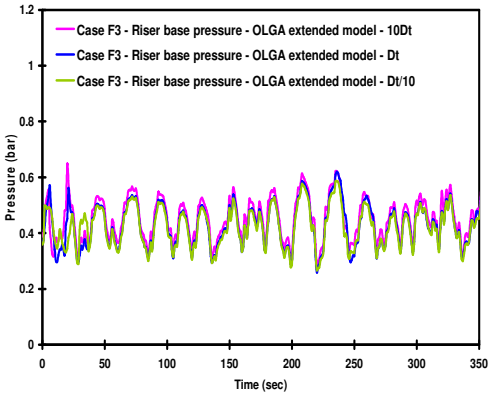

Figure 32. Effect of timestep on the time evolution of the riser base pressure for case F.

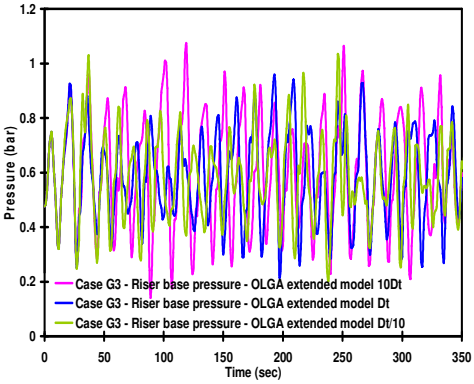

Figure 33. Effect of timestep on the time evolution of the riser base pressure for case G.

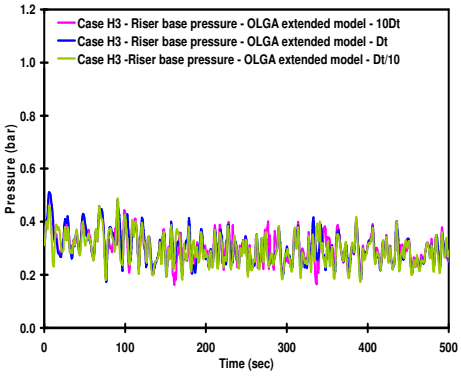

Figure 34. Effect of timestep on the time evolution of the riser base pressure for case H.

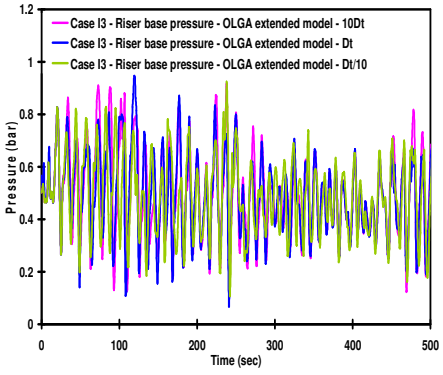

Figure 35. Effect of timestep on the time evolution of the riser base pressure for case I.

D-6. OLGA Simulated model

```
!*****************************************************************************
!        CASE
!*****************************************************************************
CASE AUTHOR="XYZ", \
DATE="12/18/2007", \
INFO="My file", \
PROJECT="LD-Rig", \
TITLE="CaseY"
!*****************************************************************************
!        OPTIONS
!*****************************************************************************
OPTIONS DEBUG=LIMITED, PHASE=TWO, SLUGVOID=AIR, TEMPERATURE=ADIABATIC
!*****************************************************************************
!        FILES
!*****************************************************************************
FILES PVTFILE="../../../PVTSimdatabase/rigfluid.tab"
!*****************************************************************************
!        INTEGRATION
!*****************************************************************************
INTEGRATION DTSTART=0.01 s, ENDTIME=1 h, MAXDT=1 s, MINDT=0.001 s, STARTTIME=0 S
!*****************************************************************************
!        MATERIAL
!*****************************************************************************
MATERIAL LABEL=Steel, CAPACITY=500 J/kg-C, CONDUCTIVITY=50 W/m-K, DENSITY=7850 kg/m3
!*****************************************************************************
!        WALL
!*****************************************************************************
WALL LABEL=ALLWALLS, THICKNESS=0.009 m, MATERIAL=Steel
!*****************************************************************************
!        GEOMETRY
!*****************************************************************************
GEOMETRY LABEL=Geo1, XSTART=0 M, YSTART=-11.7 M, ZSTART=0 M
PIPE LABEL=Pipeline, ROUGHNESS=3.5E-05 M, XEND=36 M, YEND=-11.7 M, DIAMETER=0.2545 M,\
 NSEGMENT=40, LSEGMENT=(0.9, 0.9, 0.9, 0.9, 0.9, 0.9, 0.9, 0.9, 0.9, 0.9, 0.9,
0.9, 0.9, 0.9, 0.9, 0.9, 0.9, 0.9, 0.9, 0.9, 0.9, 0.9, 0.9, 0.9, 0.9, 0.9, 0.9,
0.9,0.9, 0.9, 0.9, 0.9, 0.9, 0.9, 0.9, 0.9, 0.9, 0.9, 0.9) M
PIPE LABEL=Riser, ROUGHNESS=3.5E-05 M, XEND=36 M, YEND=0 M, DIAMETER=0.2545 M,
NSEGMENT=13,\
 LSEGMENT=(0.9, 0.9, 0.9, 0.9, 0.9, 0.9, 0.9, 0.9, 0.9, 0.9, 0.9, 0.9, 0.9) M
PIPE LABEL=Pleum, ROUGHNESS=3.5E-05 M, XEND=37 M, YEND=0 M, DIAMETER=0.2545 M,
NSEGMENT=2,\
 LSEGMENT=(0.5,0.5) M
!*****************************************************************************
!        NODE
!*****************************************************************************
NODE LABEL=Inlet, TYPE=TERMINAL, Y=-11.77 m
NODE LABEL=Outlet, TYPE=TERMINAL, X=37 m
!*****************************************************************************
!        BRANCH
!*****************************************************************************
BRANCH LABEL=PipelineRiser, FROM=Inlet, TO=Outlet, GEOMETRY=Geo1, FLUID="fluid"
!*****************************************************************************
!        BOUNDARY
!*****************************************************************************
BOUNDARY NODE=Inlet, TYPE=CLOSED
BOUNDARY NODE=Outlet, TYPE=PRESSURE, TEMPERATURE=20.2 C, PRESSURE=1.013bara,
GASFRACTION=1
!*****************************************************************************
!        CONTROLLER
!*****************************************************************************
!
!*****************************************************************************
!        SOURCE
!*****************************************************************************
SOURCE LABEL=WATER, TIME=0 s, TEMPERATURE=20.2 C, BRANCH=PipelineRiser,
PIPE=Pipeline,\ SECTION=1, MASSFLOW=16.34 kg/s, GASFRACTION=0, WATERFRACTION=1
SOURCE LABEL=Air, TIME=0 s, TEMPERATURE=20.2 C, BRANCH=PipelineRiser, PIPE=Pipeline,\
 SECTION=1, MASSFLOW=0.14 kg/s, GASFRACTION=1
!*****************************************************************************
```

```
!        OUTPUT
!************************************************************************
OUTPUT DTOUT=10 M
OUTPUT BRANCH=PipelineRiser, VARIABLE=(AL, HOL, PT, TM)
OUTPUT BRANCH=PipelineRiser, VARIABLE=ID
OUTPUT BRANCH=PipelineRiser, VARIABLE=(GLT, GT, QG, QGST, QLST, QLT)
OUTPUT BRANCH=PipelineRiser, VARIABLE=(DPZA, DPZF, DPZG)
!************************************************************************
!        TREND
!************************************************************************
TREND DTPLOT=1 s
TREND VARIABLE=VOLGBL
TREND BRANCH=PipelineRiser, VARIABLE=(HOL, PT, ROG, ROL, ROWT, TM), PIPE=Pipeline,\
 SECTION=1
TREND BRANCH=PipelineRiser, VARIABLE=(HOL, PT, ROG, ROL, ROWT, TM), PIPE=Pleum,
SECTION=2
TREND BRANCH=PipelineRiser, VARIABLE=(ACCGAG, ACCGAQ, ACCLIG, ACCLIQ, GG, GL, GLT,\
 GT, QG, QL, QLT), PIPE=Pleum, SECTION=2
TREND BRANCH=PipelineRiser, VARIABLE=(GASC, GASCNS, LIQC, LIQCNS)
TREND BRANCH=PipelineRiser, VARIABLE=(DPZA, DPZF, DPZG, ID), PIPE=Pipeline, SECTION=40
TREND BRANCH=PipelineRiser, VARIABLE=(DPZA, DPZF, DPZG, GG, GL, GLT, GT, ID, QG, QL,\
 QLT, QT), PIPE=Riser, SECTION=13
TREND BRANCH=PipelineRiser, VARIABLE=(DPZA, DPZF, DPZG, ID), PIPE=Pleum, SECTION=2
TREND BRANCH=PipelineRiser, VARIABLE=(ACCDPZA, ACCDPZF, ACCDPZG, HOL, PT),
PIPE=Pipeline,\
 SECTION=40
TREND BRANCH=PipelineRiser, VARIABLE=(ACCDPZA, ACCDPZF, ACCDPZG, PT), PIPE=Riser,
SECTION=13
TREND BRANCH=PipelineRiser, VARIABLE=(ACCDPZA, ACCDPZF, ACCDPZG), PIPE=Pleum,
SECTION=2
TREND BRANCH=PipelineRiser, VARIABLE=(GGSOUR, GLSOUR, QGSTSOUR, QLSTSOUR)
TREND BRANCH=PipelineRiser, VARIABLE=(DPT, HOL, PT, PTMAX, PTMIN, TM), PIPE=Riser,\
SECTION=1
TREND BRANCH=PipelineRiser, VARIABLE=(GG, GL, GLT, GT, ID, QG, QL, QLT, UG, UL, USG,\
 USL), PIPE=Pipeline, SECTION=39
TREND BRANCH=PipelineRiser, VARIABLE=(GG, GL, GLT, GT, ID, QG, QL, QLT, USG, USL),\
 PIPE=Riser, SECTION=1
TREND BRANCH=PipelineRiser, VARIABLE=(DPZA, DPZF, DPZG, ID, USG, USL), PIPE=Riser,\
 SECTION=13
TREND BRANCH=PipelineRiser, VARIABLE=(DPZA, DPZF, DPZG, ID), PIPE=Riser, SECTION=5
TREND BRANCH=PipelineRiser, VARIABLE=(DPZA, DPZF, DPZG, ID), PIPE=Riser, SECTION=8
TREND BRANCH=PipelineRiser, VARIABLE=(AL, HOL, PT), PIPE=Riser, SECTION=8
TREND BRANCH=PipelineRiser, VARIABLE=(AL, HOL, PT), PIPE=Riser, SECTION=5
TREND BRANCH=PipelineRiser, VARIABLE=(DPT, HOL, PT, PTMAX, PTMIN, TM), PIPE=Riser,
 SECTION=11
TREND BRANCH=PipelineRiser, VARIABLE=(DPT, HOL, PT, PTMAX, PTMIN, TM), PIPE=Pipeline,\
 SECTION=39
TREND BRANCH=PipelineRiser, VARIABLE=(ACCDPZA, ACCDPZF, ACCDPZG, AL, DPT, HOL, PT,\
 PTMAX, PTMIN, TM), PIPE=Riser, SECTION=1
TREND BRANCH=PipelineRiser, VARIABLE=(ACCGAG, ACCGAQ, ACCLIG, ACCLIQ, GG, GL, GLT,\
 GT, ID, QG, QL, QLT, QT, USG, USL), PIPE=Riser, SECTION=1
TREND BRANCH=PipelineRiser, VARIABLE=(ACCDPZA, ACCDPZF, ACCDPZG, AL, DPT, HOL, PT,\
 PTMAX, PTMIN, TM), PIPE=Riser, SECTION=2
TREND BRANCH=PipelineRiser, VARIABLE=(ACCGAG, ACCGAQ, ACCLIG, ACCLIQ, GG, GL, GLT, GT,
ID, QG, QL, QLT, QT, UG, UL, USG, USL), PIPE=Riser, SECTION=2
TREND BRANCH=PipelineRiser, VARIABLE=(DPT, HOL, PT, PTMAX, PTMIN, TM), PIPE=Pipeline,\
 SECTION=40
TREND BRANCH=PipelineRiser, VARIABLE=(GG, GL, GLT, GT, ID, QG, QL, QLT, UG, UL, USG,\
 USL), PIPE=Pipeline, SECTION=40
!************************************************************************
!        PROFILE
!************************************************************************
PROFILE DTPLOT=2 s
PROFILE BRANCH=PipelineRiser, VARIABLE=(AL, HOL, HOLWT, ID, PT, QLT, TM)
PROFILE BRANCH=PipelineRiser, VARIABLE=(DPZA, DPZF, DPZG)
!************************************************************************
!        PLOT
!************************************************************************
PLOT DTPLOT=1 s, VARIABLE=(ACCDPZF, ACCDPZG, AL, HOL, PT, QLT, QT)

ENDCASE
```